Report No. CCEER-04-06

Seismic Performance of RC Bridge Columns Reinforced with Two Interlocking Spirals

Juan F. Correal
M. Saiid Saiidi
David H. Sanders

A Report to the California Department of Transportation

Center for Civil Engineering Earthquake Research
Department of Civil Engineering/258
University of Nevada, Reno
Reno, Nevada 89557

August 2004

Acknowledgements

The California Department of Transportation (Caltrans) funded this study. However, the opinions, findings and conclusions presented in this reported are those of the authors and do not necessarily represents the views of Caltrans.

The authors would like to express their appreciation for the support and many helpful comments in the course of this study to Saad El-Azazy of Caltrans. Thanks are also due to Patrick Laplace, Jesus Pedroarena, Paul Lucas, and the staff of the Civil Engineering Department for their help and support.

This report is based on a Ph.D. dissertation by the first author supervised by the other authors.

Abstract

Interlocking spirals are used in bridge columns not only because they provide more effective confinement than rectangular hoops but also because interlocking spirals simplify the column fabrication. The behavior of columns with interlocking spirals has been studied only to a limited extent. A study was conducted at University of Nevada, Reno, on the seismic behavior of double interlocking spirals columns to determine the effect of some of the more critical parameters.

Experimental and analytical studies were conducted on six large scale concrete columns with double interlocking spirals. The primary test variables were the levels shear stress and the limits of the horizontal distance between the centers of the spirals. The specimens were tested under increasing amplitudes of the Sylmar record from the 1994 Northridge Earthquake, in the strong direction of the columns until failure. The tests revealed that the Caltrans upper spirals spacing limit of 1.5 times the radius is satisfactory even under high shear. However, supplementary cross ties are needed to prevent premature vertical shear cracking.

The analytical studies included push-over analysis, development of a plastic shear stiffness model, and development of design recommendation for cross ties. The proposed shear stiffness model improved the calculated shear deformation.

Table of Contents

List of Tables

List of Figures

Chapter 1. Introduction

1.1. Introductory Remarks

New design strategies have been investigated during the last decade in an effort to improve the general performance of structures and elements under earthquake loading. The current seismic design philosophy is based on ductility capacity of the structural members. The confinement provided by the transversal steel has an important role in improving the ductility capacity and the strength of reinforced concrete members. Confinement reinforcement in bridge columns usually consists of spirals in columns with circular shape and ties in columns with square or rectangular cross sections. Past experience has shown that circular spirals confine concrete much more effectively than rectangular or square hoops. In addition, circular spirals are often easier to construct and require fewer amounts of transverse steel than tied columns. Thus, interlocking spirals have been used as transverse reinforcement in bridge columns, especially in large rectangular cross sections that would normally be detailed as tied columns.

The California Department of Transportation (Caltrans) Bridge Design Specifications (BDS)[6] and Seismic Design Criteria Version (SDC)[7] are the only codes in the United States that include provisions for the design of columns with interlocking spirals. Due to a lack of research on interlocking spirals, the provisions are driven mainly by those of single spirals and constructability considerations. Previous studies[4,5,30] have being conducted on the effect of several design parameters, including a comparison between interlocking spirals and ties, horizontal spacing between centers of the spirals, quantity of transverse reinforcement, variation of the axial load ratios, appropriate size and spacing of longitudinal bars in the interlocking region, variation in flexural detailing, and cross section shape. Those studies concluded that the performance of interlocking spirals was satisfactory and the flexural and shear capacities can be conservatively calculated using current procedures. Nevertheless, none of previous studies addressed the Caltrans upper limit on spiral spacing in detail and none used dynamic testing.

In order to refine or possibly revise the current Caltrans design provisions, Caltrans funded this study on the seismic performance of interlocking spirals columns. Based on past research important design parameters in RC column with interlocking spirals were: the level of average shear stress, the limits of the horizontal distance between the centers of the spirals, d_i, as a function of the radius of the spirals, R, rectangular columns cross sections versus oblong cross section, two versus three interlocking spirals, presence of flare, number and position of longitudinal bars within the interlocking spirals, presence of cross ties connecting the spirals, column aspect ratio, and longitudinal steel ratio. The last two-design parameters are inter-related to the first parameter. The level of average shear stress and the limits of the horizontal distance between the centers of the spirals, d_i as a function of the radius of the spirals, R, were investigated in this study because they were considered by Caltrans designers to be of the highest priority. Two additional variables, one an intermediate level of d_i and the other supplementary cross ties were studied based on the test results of the first columns.

The purpose of the present study was to assess the seismic performance of reinforced concrete bridge columns with interlocking spirals using shake table simulation of earthquake loads, including the effect of the above mentioned design parameters.

1.2. Previous Studies

An extensive literature review on previous research was conducted. Only a few previous studies had been reported on columns reinforced with interlocking spirals. All of those were performed on specimens subjected to static loading. Because dynamic testing was used in the present study, a brief review of the shake table testing of circular columns is first presented.

The following discussion on past research includes shake table testing of circular columns and the performance of columns with interlocking spirals subjected to static-cyclic loading, monotonic loading, and concentric axial loads.

1.2.1. Shake Table Testing of Circular Column

Laplace et al.[16] tested two 1/3- scale circular reinforced concrete bridge columns with identical properties on the shake table system. The columns were 406 mm (16 in) in diameter and 1829 mm (72 in) in height and they were designed based on 1992 Caltrans design provisions. All the columns had an axial index of 10% with a longitudinal and transverse steel ratio of 2% and 1%, respectively. The scale of the columns was chosen based on the models of the prototype column used in standard-cyclic studies concluded at the National Institute of Standards and Technology (NIST)[2]. Two different earthquake loading scenarios to compare the effect of load history on the two columns were done.

Based on the test results, the author concluded that the columns subjected to a high amplitude motion in an undamaged state exhibited a slightly higher capacity than a column subjected to incrementally increasing amplitudes as is usually used in shake table testing. The author also concluded that as displacement increase the difference between test results of high amplitude motion and incrementally increasing amplitudes becomes less. Comparing the slow cyclic testing performed at NIST[2] with the experimental results, an increase of 7% in a column capacity was estimated due to the strain rate effect on the material properties. In addition, ductility and drift levels under dynamic excitation were greater than those achieved in the slow cyclic testing.

1.2.2. Static-cyclic Load Testing

Important details of the specimens in previous are shown in Table 1.1. The level of shear stress was determined by the shear index. The average shear stress was calculated as the maximum measured shear force divided by 0.8 times the gross area.

The shear index is found by dividing the average shear stress by $0.083\sqrt{f'c}$ [MPa] or $\sqrt{f'c}$ [psi].

Tanaka and Park[30] performed the first test on columns with interlocking spirals. Three columns with interlocking spiral were tested and, for comparison, one column with rectangular hoops and cross ties was tested as well. The columns were designed using provisions for columns with single spirals in the New Zealand concrete design code. The objective of the research was to assess a series of methods to evaluate effectiveness of interlocking spirals as shear and lateral confining reinforcement.

The test results showed similar satisfactory performance for the interlocking spirals and tied columns, however the tied columns had almost double volumetric ratio for the transverse reinforcement. The measured lateral load displacement hysteresis loops showed very good energy dissipation and limited reduction in strength. All tested columns exceeded a displacement ductility of 10. Yielding of interlocking spirals occurred at a displacement ductility of 3 to 4 in all columns. The measured shear deformation accounted for 10% to 30% of the column deflection.

Based on an analytical study, the authors concluded that the amount of transverse reinforcement required for the confinement of the core concrete in the potential plastic hinge region of a column can be reduced considerably by using interlocking spirals instead of rectangular hoops and cross ties. The spiral reinforcement required for confinement of columns with interlocking spirals could be designed using the provisions for single spirals columns. A proposed method that considered the interlocking spirals as an equivalent transverse reinforcement can be used to calculate the shear carried by the interlocking spirals. In order to provide sufficient area of interlocking for adequate shear transfer, the spacing between center to center of the spirals was limited to 1.2 times the spiral radius according to that study. It was further recommended that, to insure adequate shear transfer between the interlocking spirals, at least four bars should be placed inside the interlocking area of the spirals.

A study conducted at the Washington State University by Buckingham et al.[5], compared the behavior of columns with interlocking spirals under shear, flexural and torsional loading. Six 1/5-scale specimens with interlocking spirals and two with conventional ties were tested. Design parameters investigated included spacing between center to center of the spirals, size of longitudinal bars in the interlocking area, variations in flexural detailing of interlocking spirals, column cross-sectional shape, and performance of columns with interlocking spirals was compared with tied columns.

According to the test results, the specimens reinforced with interlocking spirals performed as well as or better than the ones with ties under both shear and flexural loading, despite 50 % less content of transverse reinforcement steel. The specimens loaded to failure in shear with spacing between center to center of the spirals equal to 1.2 times the spiral radius demonstrated less strength degradation than similar specimens with spacing between center to center of spirals equal to 1.5 times the spiral radius.

Higher degradation was found using small-diameter (nominal) longitudinal bars in the interlocking zone compared with the similar specimen with the same size of longitudinal bars in the interlocking zone as that used for the main column reinforcement. According to the author, the degradation was due to the separation of the spiral cages resulting from severe deformation of the interlock bars. Current procedures can be used in order to obtain a reasonable estimate of shear and flexural capacities of columns with interlocking spirals. A conservative torsional capacity can be predicted using an approach adapted from current design equations for the torsional capacity of rectangular beams. Nevertheless, further investigation was recommended on this topic. The authors also recommend more research in columns with more than two interlocking spirals.

The Aristotle University Thessaloniki in Greece study by Tsitotas and Tegos[32] on seismic behavior of columns and beams with interlocking spirals was reviewed. One column with interlocking spirals was tested under cyclic lateral loading and constant axial load. Experimental results showed that columns with interlocking spirals have an excellent performance from a mechanical stand point. The influence of slippage of the reinforcement is negligible, since no hysteresis loop pinching was observed in the load displacement diagram of the specimen. Thus, the cyclic shear had no deteriorating influence upon the interlock of the two spirals. The spiral spacing of 35 mm (1.38 in) satisfies the minimum required spacing in the Greek Concrete Code of at least 20 % of the diameter of the circular core section.

Four 1/4-scale shear-critical rectangular reinforcement concrete columns with interlocking spirals were tested in a study by Benzoni et al.[4] at the University of California, San Diego (UCSD). The purpose of the study was to investigate the behaviors of shear dominated interlocking spirals columns, under different axial load ratios (P/f'_cA_g). Ratios of 0.0, 0.35, and -0.1 were used in the first three specimens tested in double curvature. Vertical loads varying as function of the applied horizontal loads from axial load ratios of –0.1 to 0.35 were applied to the last specimen. Most of the research was focused on analysis of the shear strength of the columns with interlocking spirals for the case of variable axial load. Different approaches of the shear capacity for interlocking spirals were compared with the experimental results. The formulation proposed by the authors was adequate to predict the shear capacity of the columns with interlocking spirals. The shear capacity used took into account the effect of the neutral axis depth. Differential slippage was experienced between the two spirally reinforced sections. The authors suggested further investigation mainly on the extent of the interlocking zone and its content of reinforcement.

Mizugami[19] studied the performance of columns with interlocking spirals under cyclic lateral loading in single bending. Three columns with interlocking spirals were loaded in the strong axis of the cross section and three more in the weak axis. For comparison, one conventional column with rectangular hoops and cross ties was tested in the weak axis. Different volumetric confinement steel ratios were used in all the columns. The author concluded that the flexural strength and the deformation capacity of the interlocking spirals were the same as conventional rectangular columns with 300 %

higher volumetric ratio than columns with interlocking spirals. The columns tested in the strong direction with different volumetric ratios showed different failure mode corresponding to the amount of the reinforcement. Nevertheless, no of the columns exhibited brittle shear failure. Both flexural strength and deformation capacity of interlocking spirals can be accurately predicted using conventional procedures. The shear strength of the interlocking spirals can be conservatively estimated taking into account the core area of the cross section as an effective shear area and the shear resistance of two spirals. Based on ductility response of interlocking spirals columns, the volumetric confinement ratio of at least 0.3% is recommended. In addition, a shear deformation of at least 20% of the total deformation needs to be estimated in order to predict the columns deformation.

1.2.3. Monotonic Load Testing

Tsitotas and Tegos[32] tested two columns, one with interlocking spirals and one with a single spiral. The interlocking column was 2000 mm (78.7 in) in height with an oblong cross section 300 mm (11.81 in) in width and 205 mm (8.07 in) in depth and with spacing between the centers of spirals equal to 1.0 times the spiral radius. The longitudinal and transverse steel ratios were 4.0% and 1.4 %, respectively. The single spiral column had a diameter of 205 m (8.07 in) with longitudinal and transverse steel ratio of 3.7% and 1.4 %, respectively. The columns were subjected to monotonic loading as simply supported beams. The shear span-to depth ratios were 3.0 for the interlocking spiral column and 3.5 for single the spirals column.

According to the tests results, flexural and shear cracks appeared on either side of the load points with typical shear cracks at a 45° degree inclination toward the support points around the element axis. In the case of the interlocking spirals uniform cracking was observed without any signs of separation of the interlocking spirals at any point in the span length under the ultimate load. Maximum capacities of 350 kN (78.7 kips) and 220 kN (49.4 kips) were recorded for the interlocking spirals column and the single spiral column, respectively.

The concept of a substitute section was introduced in this study. Rectangular and circular envelope sections are proposed as the substitute section to estimate the section resistance to shear with bending or bending only, respectively. Good agreement was found between the values calculated using the substitute section and the experimental results.

1.2.4. Concentric Axial Load Testing

A study by Kim and Park[13] at Korea Advance Institute of Science and Technology, South Korea, investigated the strength and the deformability of specimens with interlocking spirals subjected to concentric axial load. For this purpose, 108 specimens with interlocking spirals were tested. The main test variables were concrete

strength, spacing of spirals or pitch, yield strength of spirals and the spacing between center to center of the spirals. The compressive strengths of concrete was 27 MPa (3916 psi), 62 MPa (8992 psi), and 81 (11748 psi) MPa. Six spacing of spirals 120 mm (4.72 in), 60mm (2.36 in), 40 mm (1.57 in), 30mm (1.18 in), 25mm (1 in) and 20mm (0.78 in)) were used. Steel yield strength of the spirals was 451 MPa (65 ksi) and 1375 MPa (200 ksi). The spacing between center to center of spirals equal to 0.5, 1.0 and 1.5 times the spiral radius were selected. On the basis of the experimental study, the authors concluded that the spiral strain decreased with the increasing of the concrete strength for the same details of reinforcement and with the increasing of the spacing of spirals for the same concrete strength. In addition, they found that increasing the yield strength of spirals improved the strength and the ductility of specimens with interlocking spirals. Model equations for prediction of the strength and the axial strain at the peak stress of specimens with interlocking spirals were proposed.

1.3. Objectives and Scope

The primary objective of this research was to study the seismic performance of bridge columns with interlocking spirals subjected to earthquake excitation on a shake table and to assess the most critical design parameters that were of interest to Caltrans designers. The level of average shear stress, the horizontal distance between the centers of the spirals, d_i as a function of the radius of the spirals, R, and supplementary horizontal cross ties were the design parameters included in this study.

Six large-scale columns reinforced with interlocking spirals were built based on the current Caltrans design provisions. Two 1/4-scale specimens with d_i of 1.0R and 1.5R subjected to low level of average shear stress (shear index of 3) and two 1/5-scale specimens with d_i of 1.0R and 1.5R subjected to high level of average shear stress (shear index of 7) were tested in order to study the effect of the first two design parameters mentioned above. Two additional variables, one an intermediate level of d_i and the other with supplementary cross ties and d_i of 1.5R were studied after observed vertical cracks in one of the high shear columns tested with the maximum horizontal spacing between center to center of the spirals (d_i of 1.5R). All the specimens were designed to fail in a ductile mode and they were subjected to increasing amplitude of the Sylmar record from the 1994 Northridge earthquake. The specimens were tested at James E. Rogers and Louis Wiener Large-Scale Structures Laboratory at the University of Nevada, Reno. Only in-plane response of the columns was studied with axial load index of 10%.

Based on the data and analyses in this and other studies, a new model to estimate the post yield shear stiffness was developed and recommendations were made for possible adoption by Caltrans.

Chapter 2. Design of the Specimens and Preliminary Analysis

2.1. Introduction

Reinforced concrete columns with double interlocking spirals were designed based on the current Caltrans design provisions. The scales of the specimens were based on the capacity of the shake table system. Typical steel ratios were chosen for the longitudinal reinforcement. The transverse steel ratios were selected based on target displacement ductility of 5 as well as the limitations of Caltrans provisions. Moment-curvature analysis was performed for all the columns using the program SPMC[34], developed at the University of Nevada, Reno. An idealized elasto-plastic force and displacement was used to perform a nonlinear response history of the columns in order to select the input record used in the shake table tests. This chapter describes the design as well as the preliminary analysis of the test specimens.

2.2. Average Shear Stress Index

The average shear stress is calculated as the lateral load over the effective shear area. The effective shear area is equal to 80% of the gross area. The shear stress index is found by dividing the average shear stress by $0.083\sqrt{f'c}$ [MPa] or $\sqrt{f'c}$ [psi]. This index is used to determine the level of shear stress in the column. In this project, two level of shear were selected. Low index equal to 3 and high index equal to 7 were chosen. Columns with a low shear index are called ISL1.0 and ISL1.5 and columns with a high shear index are ISH1.0, ISH1.25, ISH1.5 and ISH1.5T.

2.3. Test Variable

The primary test variables in the experimental studies were the shear index and the horizontal distance between the centers of the spirals, d_i. Based on the test results of the first two high shear columns, two additional variables, one an intermediate level of d_i and the other supplementary cross ties were added to the high shear models. Three alphabetical characters followed by a number were used to identify the test specimens. The initial I and S were for interlocking and spirals, respectively. The third initial L or H was for the shear index of low or high, respectively. The number was the d_i used in the specimen. For the last specimen an additional initial (T) was used at the end in order to identify the addition of the supplementary cross ties. A summary of the test variable in the specimens is listed in Table 2-1.

2.4. Current Design Guidelines for Columns Reinforced with Interlocking Spirals

RC Columns reinforced with interlocking spirals have been implemented in New Zealand (Tanaka and Park[30] and NZS 3101[29]), Japan (JRA[12]) and other countries. Caltrans is the only code in the United States that has provisions for columns reinforced with interlocking spirals. These provisions are based on the requirements of single spiral

reinforced column. Two different provisions of Caltrans, Seismic Design Criteria (SDC)[7] and Bridge Design Specifications (BDS)[6], were followed in order to design columns specimens reinforced with interlocking spirals. Next is the description of the current guidelines used in the design of the six specimens.

2.4.1. Horizontal Distance between Centers of the Spirals, d_i

The BDS[6], Section 8.18.1.4, requires that when more than one cage is used to confine an oblong column core, the spirals must be interlocked or the seismic design must be modeled as having multiple single columns. A maximum limitation of 0.75 times the spiral diameter (1.5 times the radius of the spirals, R, is measured to outside of the spiral) for the horizontal spacing of the spirals measured center-to-center of the spirals, d_i, is established by a geometrical relationship for stability normal to the bent (Fig. 2-1). A minimum spacing of 0.50 times the spiral diameter (1.0R) is recommended to avoid overlaps of more than two spirals. In addition, BDS[6] suggests to revise the column shape, size, number of columns, etc, to avoid a closer spacing.

In this research, two specimens were designed with d_i of 1.0R, one specimen with d_i of 1.25R, and three with d_i of 1.5R.

2.4.2. Longitudinal Reinforcement

Section 3.7 in SDC[7] specifies a maximum and minimum area of the longitudinal reinforcement for compression members as $0.04A_g$ and $0.01A_g$, respectively. Longitudinal reinforcement area of $0.02xA_g$ and $0.028xA_g$ were selected for the specimens with low shear (ISL1.0 and ISL1.5) and high shear (ISH1.0, ISH1.25, ISH1.5 and ISH1.5T), respectively. These values were chosen because they are typical. In addition according to BDS[6], Section 8.18.1.4 a minimum distance between adjacent bars should be 20.32 mm (8 in). Taking into the account the scale factor (see Section 2.8) and in order to meet BDS[6], Section 8.18.1.4, 9.5 mm diameter (#3) longitudinal reinforcing bars were used in all the specimens.

2.4.3. Minimum Vertical Reinforcement in Interlocking Portion

Section 3.6.5.3 in SDC[7], specifies the minimum vertical reinforcement in the interlocking portion. The interlocking portion is defined as the transverse area within the interlocking of the spirals. According to SDC[7], the longitudinal bars in the interlocking portion of the column shall have a maximum spacing of 203mm (8 in) and need not be anchored in the footing or the bent cap unless deemed necessary for the flexural capacity of the column. The longitudinal bar size in the interlocking portion depends on the size of the bars outside the interlocking portion as listed in Table 2-2.

In this project four bars of the same size as those of the bars outside the interlocking portion were used in the interlocking region. This selection was made based on previous research (Tanaka and Park[30] and Buckingham et al[5]) also because SDC[5]

Section 3.6.5.3 was not available when the design of the first 4 specimens were being designed. These bars were anchored to the footing and they were taken into account in the calculations of the flexural capacity of the columns (M-ϕ analysis, Section 2.12.1).

2.4.4. Nominal Shear Capacity

Section 3.6.1 in SDC[7], state the shear capacity for ductile concrete members shall be conservatively based on the nominal material strengths as follows

$$\phi V_n \geq V_o \tag{2-1}$$

Where

V_o = Plastic shear associated with the overstrength moment, M_o
ϕ = Strength reduction factor = 0.85
V_n = Nominal shear strength = $V_c + V_s$
V_c = Nominal shear capacity provided by concrete
V_s = Nominal shear capacity provided by shear reinforcement

According to SDC[7], Section 3.6.2, the concrete shear capacity (V_c) of members designed for ductility shall consider the effects of flexure and axial load as specified in the following equation

$$V_c = \nu_c x A_e \tag{2-2}$$

Where

ν_c = Permissible shear stress carried by concrete defined in the Equations 2.5 and 2.6, for regions inside the plastic hinge zone and outside the plastic hinge zone, respectively. For members whose net axial load is in tension, $\nu_c = 0$.

A_e = Effective shear area = $0.8 x A_g$
A_g = Gross cross section area

ν_c for inside of the plastic hinge can be found according to the following equation

$$\nu_c = F1 x F2 x \sqrt{f'_c} \leq 0.33\sqrt{f'_c}\,(MPa) = 4\sqrt{f'_c}\,(psi) \tag{2-3}$$

ν_c for outside of the plastic hinge can be found according to the following equation

$$\nu_c = 0.25 x F2 x \sqrt{f'_c} \leq 0.33\sqrt{f'_c}\,(MPa) \tag{2-4a}$$

$$\nu_c = 3 x F2 x \sqrt{f'_c} \leq 4\sqrt{f'_c}\,(psi) \tag{2-4b}$$

Where

f'_c = Compressive strength of unconfined concrete

F1 is given by

$$F1 = 0.025 \le \frac{\rho_s f_{yh}}{12.5} + 0.305 - 0.083\mu_d < 0.25(MPa) \quad (2\text{-}5a)$$

$$F1 = 0.3 \le \frac{\rho_s f_{yh}}{150} + 3.67 - \mu_d < 3(psi) \quad (2\text{-}5b)$$

Where

ρ_s = Ratio of volume of spiral or hoop reinforcement to the core volume confined by the spiral or hoop reinforcement (measured out-to-out), for columns with circular or interlocking core sections, defined by Equation 2-8.
f_{yh} = Nominal yield stress of transverse column reinforcement (MPa, ksi)

μ_d = is defined as the local displacement ductility demand. However, SDC[7] specifies that the global displacement ductility demand μ_D shall be used in the determination of the F1 provided a significant portion of the global displacement is attributed to the deformation of the column or pier. In all other cases a local displacement ductility demand μ_d shall be used in F1.

ρ_s can be found according to the following equation

$$\rho_s = \frac{4A_b}{D's} \quad (2\text{-}6)$$

Where

A_b = Area of individual reinforcing steel bar (mm², in²)
D' = Cross-sectional dimension of confined concrete core measured between the centerline of the peripheral hoop or spiral
s = Spacing of transverse reinforcement measured along the longitudinal axis of the structural member (mm, in)

F2 is given by

$$1 + \frac{P_c}{13.8xA_g} < 1.5(\text{MPa}) \quad (2\text{-}7a)$$

$$1 + \frac{P_c}{2000xA_g} < 1.5(\text{psi}) \quad (2\text{-}7b)$$

Where

P_c = The column axial force including the effects of the overturning
A_g = Gross cross section area (mm², in²)

According to SDC[7], Section 3.6.3, the shear reinforcement capacity (V_s) for confined circular or interlocking core sections is defined as follows

$$V_s = \frac{A_v f_{yh} D'}{s} \tag{2-8}$$

Where

A_v = Total area of shear reinforcement = $n\left(\frac{\pi}{2}\right)A_b$ (2-9)

n = number of individual interlocking spirals or hoop core sections
A_b = Area of individual reinforcing steel bar (mm², in²)

According to SDC[7], Section 3.6.5.1, the shear strength V_s provided by the reinforcement steel shall be not be taken greater than:

$$0.67x\sqrt{f'_c}\,A_e(MPa) \tag{2-10a}$$

$$8x\sqrt{f'_c}\,A_e(psi) \tag{2-10b}$$

In addition, SDC[7] Section 3.6.5.2 specifies that the shear reinforcement for each individual core of columns confined by interlocking spirals or hoops shall be greater than the area required by the following equation

$$A_v \geq 0.17x\frac{D's}{f_{yh}}(mm^2) \tag{2-11a}$$

$$A_v \geq 0.025x\frac{D's}{f_{yh}}(in^2) \tag{2-11b}$$

2.4.5. Confinement Reinforcement

According to SDC[7], Section 3.8.1, the volumetric ratio, provided inside the plastic hinge length and defined by Equation 2.6 shall be sufficient to ensure the column meets the performance requirements of SDC[7], Section 4.1, which establish that the displacement capacity should be greater than the displacement demand. In addition SDC[7], Section 3.8.2 determine that the lateral reinforcement inside the plastic hinge region shall meet the requirements of nominal shear capacity described above (Section 2.4.4) as well as the maximum spacing requirement of SDC[7], Section 8.2.5, listed as follows:

- One fifth of the least dimension of the cross-section for columns and one-half of the least cross-section dimension of piers
- Six times the nominal diameter of the longitudinal reinforcement
- 220 millimeter (8 in)

SDC[7], Section 3.8.3 specifies that the volume of the lateral reinforcement required outside of the plastic hinge region, shall not be less than 50% of the amount specified for the lateral reinforcement inside the plastic hinge region (SDC[7], Section 3.8.2) and meet the shear requirements of nominal shear capacity described above (Section 2.4.4).

BDS[6], Section 8.18.2.2, requires that the volumetric ratio, for spiral reinforcement shall be not less than

$$0.45\left(\frac{A_g}{A_c}-1\right)\frac{f'_c}{f_y}\left(0.5+1.25\frac{P_e}{f'_c\,A_g}\right) \tag{2.12}$$

for columns less than 0.9 m (3 ft) in diameter

or

$$0.12\frac{f'_c}{f_y}\left(0.5+1.25\frac{P_e}{f'_c\,A_g}\right) \tag{2-13}$$

for columns larger than 0.9m (3 ft) in diameter

but not less than

$$0.45\left(\frac{A_g}{A_c}-1\right)\frac{f'_c}{f_y} \tag{2-14}$$

Where

A_g = Gross cross section area
A_c = Area of core measured to the outside diameter of the spiral
f'_c = Compressive strength of unconfined concrete
f_y = Specified yield strength of reinforcement (hoops/spirals)
P_e = Design axial load due to gravity and seismic loading

2.5. Cross Ties Reinforcement Specimen ISH1.5T

Currently, there are no design procedures available to design cross ties connecting the interlocking hoops. These cross ties may be needed to reduce and delay vertical cracks in the interlocking region under service load conditions. The specimen ISH1.5T with di equal to 1.5R and high shear index was detailed with cross ties in order to study the effectiveness of the cross ties. A design procedure was developed and it is described in the Chapter 8. As a result, cross ties with the same size of bar as the spirals and spacing of 2.0 times the spacing of the spirals were recommended.

2.6. Material Properties

A concrete compressive strength of 34.5 MPa (5000 psi) was specified for the design of the all specimens. In addition, specified minimum yield strength of 420 MPa (60 ksi) was selected for all the reinforcement used in the design of the specimens.

2.7. Axial Load Index

The axial load index defined as the compressive axial force divide by the product of the cross section area of the column and the concrete compressive strength, typically varies between 5% to 25% for bridge columns. Particularly for this study an axial load index of 10% was selected based on recommendations by Caltrans as being a typical value.

2.8. Scaling Factor

Scale factors of 1/4 for the specimens with low shear and 1/5 for the specimens with high shear were selected based on the typical cross section dimensions of bridge columns. The scale factor was applied in a way that stresses would not be scaled and real concrete and steel could be used. A different test setup for each set of specimens (low shear and high shear) was used (see Section 3.5). The effective weight of the inertial system (mass rig) was constant for all test setups. In order to account for the difference between the applied axial load (Section 2.7) and the effective weight of the inertia system and also the effect of the scale of the specimens, a time scale factor for the earthquake motion of $\sqrt{\frac{w_i}{P} l_r}$ was used, where l_r is the scale factor, w_i is effective weight of the inertia system including the mass rig and P is the applied axial force on the column (see Appendix A for detailed derivation). The model scale factors for different parameters are as listed in Table 2-3.

2.9. Cross Section Area of the Specimens

The cross section areas of the specimens were selected in order to achieve failure of the specimens when they were subjected to dynamic excitations based on the maximum capacity of the shake table system. The shake table specifications are given in Table 2-4. All specimens presented an oval shape cross section with semicircular ends. The cross section is defined by the diameter of the semicircular ends as well as d_i (see Section 2.4.1) (Fig 2-1). The first set of models had a semicircular diameter of 305 mm (12 in) with di of 1.0 R and 1.5 R, where R is the spiral radio equal to 140 mm (5.5 in). The second set had a semicircular diameter of 254 mm (10 in) with di of 1.0R, 1.25R and 1.5R, with R equal to 114 mm (4.5 in). A cover of 127 mm (0.5 in) was selected based on the scale factor. The first and the second sets corresponded to the low and high shear specimens, respectively. The average shear stress was defined in the Section 2.2.

2.10. Displacement Based Design

Section 3.1.4.1 in SDC[7] states that each ductile member shall have a minimum local displacement ductility capacity of 3 to ensure dependable rotational capacity in the plastic hinge regions regardless of the displacement demand imparted to that member. Particularly for this study, Caltrans recommended a target displacement ductility capacity of 5 for the design of the specimens.

The provisions in SDC[7], Section 3.1.3 were used in order to design the specimens with a target displacement ductility capacity of 5. According to this section the displacement ductility capacity is defined as

$$\mu_c = \frac{\Delta_c}{\Delta_y^{col}} \tag{2-15}$$

Where

Δ_c = Member displacement capacity = $\Delta_y^{col} + \Delta_p$

Δ_y^{col} = Idealized effective yield displacement of the column at the formation of the plastic hinge = $\frac{L^2}{3}\phi_y$

L = Distance from the point of maximum moment to the point of contra-flexure

ϕ_y = Idealized yield curvature defined by an elastic-plastic representation of the cross section M-ϕ curve, see Section 2.13.1.

Δ_p = Idealized plastic displacement of the column at the formation of the plastic hinge= $\theta_p\left(L - \frac{L_p}{2}\right)$

L_p = Plastic hinge length

= $0.08L+0.022\, f_{ye}\, d_{bl} \geq 0.044\, f_{ye}\, d_{bl}$ (MPa) or

= $0.08L+0.15\, f_{ye}\, d_{bl} \geq 0.3\, f_{ye}\, d_{bl}$ (ksi)

θ_p = Plastic rotation capacity = $L_p(\phi_p)$

ϕ_p = Idealized plastic curvature capacity (assumed constant over L_p) = $\phi_u - \phi_y$

ϕ_u = Ultimate curvature capacity, defined as the curvature when the concrete strain reaching ε_{cu} or the confinement reinforcing steel reaching the reduced ultimate strain ε_{su}^R , from M-ϕ analysis, see Section 2.13.1.

In order to calculate the height of the specimens, a target shear force was first calculated. The target shear force was defined as the average shear stress (Section 2.2) multiplied by 0.8 times the area gross. The heights of the specimens were calculated based on the test setup (Section 3.5) for both specimens with low (single curvature) and high shear (double curvature). For the specimens with low shear the height was determined as the ratio of the idealized plastic moment capacity and the target shear force and for the specimens with high shear the height was found as two times the ratio of the idealized plastic moment capacity and the target shear force.

An iterative approach was used in order to obtain a displacement ductility capacity of 5. The vertical spacing of the spirals (pitch) was varied while the longitudinal steel, material properties, axial load and the cross section dimension were kept constant. The spirals were made of plain wire W2.9 and W2.0 for columns with low and high shear, respectively. An initial value of the lesser of the values from the provisions described in Section 2.3.4 and 2.3.5 was selected. The M–ϕ analyses were performed until a displacement capacity of at least 5 was achieved and the provisions described in the Section 2.3.4 and 2.3.5 were met. Table 2-5 shows a summary of the final values of the last iteration for all specimens, based on the details given in the next section.

2.11. Description of the Specimens

The dimensions of the cross section with the reinforcement detail and the elevations of the specimens are shown in Figs. 2-2 and 2-3. The spirals were continuous with constant pitch, through the height of the specimen. The spirals were extended along the whole height of the footing and top loading head. The longitudinal reinforcement was continuous and detailed at the ends with 90° degree standard hooks. The height of the specimens with low shear (ISL1.0 and ISL1.5) was taken from the top of the footing to the center of the application of the lateral load and for the high shear specimens (ISH1.0, ISH1.25, ISH1.5 and ISH1.5T) was taken as the clear height between the top of the footing and the bottom of the loading head. It is due to the double curvature produced by the dual link configuration. A summary of the most relevant design parameters are presented in Table 2-6. The design of the footing as well as the loading head will be describe in the following section.

2.12. Footing and Loading Head Design

The footings were designed to be rigidly attached to the shake table deck. Fourteen steel rods were used in order to prevent uplift and sliding of the footing. The steel rods were threaded and inserted into the strong holes in the shake table deck distributed on a 30.48 cm (12 in) grid spacing. Based on the number and location of the strong holes, a footing cross section dimension of 1.52 m x 1.52 m (5 ft x 5 ft) square was selected. Fourteen PVC 7.62 cm (3 in) diameter duct were placed through the height of the footing in order to provide a hole that allow the passage of the rods. The clamping load used in each rod was about 111.2 kN (25 kips). The height of the footing was selected in such way that the height of the column plus the height of the footing plus 3.81 cm (1.5 in) thickness grout match the distance between the shake table deck and the sets of holes of the mass rig plate. The Table 2-7 shows the height of the footing for all the specimens. Overturning moment, bearing, punching shear as well as one way shear checks were made in the design of the footing. Based on the flexural bending analysis, the minimum longitudinal steel ratio controlled the design. As a result two mats of steel reinforcement, top and bottom in both directions, were needed in order to resist the applied bending moments. Figure 2-4 illustrated a typical plan and profile views of the footing with the distribution of the reinforcement steel. Number 4 footing longitudinal

bars were used in the vicinity of the column in order to allow the bars to pass through the column and # 8 bars were used elsewhere. The # 8 bars were detailed with a 90° crossties standard hook at the ends while the # 4 bars where detailed straight bars for construction purpose. The concrete cover on all sides was 5.08 cm (2 in). Number 3 crossties, located at the intersection of the mats in both directions, were used in the footing to provide shear reinforcement. The detail of the cross ties is shown in Fig. 2-4. Number 10 lift bars were designed and added to the footing for transportation purpose.

Figures 2-5 and 2-6 show plan and section views of the loading head for the specimens with low and high shear, respectively. Minimum reinforcement was used in the head for the low shear specimens due to small level of stress to which it was subjected. Number 4 bars were placed in all of the direction of the faces of the head to provide confinement (see Fig. 2-5). Four PVC pipes 5.08 cm (2 in) diameter were cast in the column head to provide holes for the bolts in order to attach the head to the link assembly load. The top head for the specimens with high shear was designed in order to prevent separation of the vertical connecting plate which was post-tensioned to the head using Dywidag bars. The dimensions of the head were controlled by the connecting plate dimensions between the loading head and the dual link assembly. The head width was determined based on the limitation on the edge distance of the post-tensioned bars. The steel reinforcement was provided based on the flexural demand from the dual link couple moment. The steel design details were very similar to the details provided in the footings (see Fig. 2-6).

2.13. Preliminary Analysis

In order to design and predict the seismic performance of the scaled bridge columns reinforced with double interlocking spirals. The program SPMC[34] was used to perform a moment-curvature analysis in order to estimate the lateral load and displacement carrying capacities. Once the capacity was estimated, a dynamic analysis using the program RCShake[16] was done to determine the seismic response of the column specimens with double interlocking spirals under different earthquake ground motions and to select the input record for the shake table test.

2.13.1. Moment-curvature analysis

Program SPMC[34] was used for the cross sectional analysis of the specimens. This program was specially developed for columns with interlocking spiral reinforcement.

The Hognestad model[22] is used for unconfined concrete stress-strain relationship. The Figure 2-7 shows the stress-strain curve. This model consists of two segments. The first segment is an ascending parabolic curve up to the point representing the unconfined concrete and is strength expressed by the following equation

$$f_c = f'_c \left(\frac{2\varepsilon_c}{\varepsilon_0} - \left(\frac{\varepsilon_c}{\varepsilon_0} \right)^2 \right) \quad (2\text{-}16)$$

Where

f_c = concrete stress
f'_c = unconfined concrete compressive strength
ε_o = strain at concrete strength
ε_c = crushing strain of unconfined concrete

The second segment is a descending straight line starting from the peak point connected to the ultimate point with a negative slope equal to $\frac{0.15f'_c}{\varepsilon_u - \varepsilon_o}$ in which ε_u is the ultimate strain.

The Modified Mander et al[17] model was used to model the confined concrete stress-strain relationship (see Fig. 2-8). The equation for the curve is described by the following equation:

$$f_c = \frac{f'_{cc}\, xr}{r - 1 + x^r} \quad (2\text{-}17)$$

Where

$$x = \frac{\varepsilon_c}{\varepsilon'_{cc}}$$

$$r = \frac{E_c}{E_c - E_{sec}}$$

$E_c = 4730\sqrt{f'_c}$ [N/mm²] or $E_c = 57000\sqrt{f'_c}$ [psi]

$$E_{sec} = \frac{f'_{cc}}{\varepsilon'_{cc}}$$

f'_{cc} = confined concrete compressive strength
ε'_{cc} = strain at concrete compressive strength

When the effective confining stress, f'_l, is the same in orthogonal x and y directions of the circular or rectangular section, f'_{cc} is related to the unconfined strength by

$$f'_{cc} = f'_c \left(-1.254 + 2.254\sqrt{1 + \frac{7.95f'_l}{f'_c}} - \frac{2f'_l}{f'_c} \right) \quad (2\text{-}18)$$

Where

$$f'_l = \frac{2A_{sh}f_{yh}}{d_s s_h}$$

f_{yh} = yield strength of the lateral reinforcement
A_{sh} = area of the stirrup or hoop
d_s = distance between centers of the stirrup or hoop legs within each hoop set
s_h = spacing of stirrups or hoops

The strain at concrete compressive strength (ε'_{cc}) and the ultimate compression strain (ε_{cu}) are defined by

$$\varepsilon'_{cc} = 0.002\left(1 + 5\left(\frac{f'_{cc}}{f'_c} - 1\right)\right) \tag{2-19}$$

$$\varepsilon_{cu} = 0.004 + \frac{1.4\rho_s f_{yh}\varepsilon_{sm}}{f'_{cc}} \tag{2-20}$$

Where

ρ_s = volumetric transversal steel ratio (see Equation 2-6)
ε_{sm} = steel strain at maximum tensile stress = 0.09 according to SDC[5], Section 3.2

The parabolic strain hardening model was used to model the stress-strain relationship for the steel. The curve is shown in the Fig. 2-9. The model consists of 3 segments. The first segment represents the elastic range of the steel with a constant modulus of elasticity of steel, E. The second segment (segment 1-2) corresponds to the yield plateau where the strain is constant without increasing of stress. The third segment (segment 2-3) represents the strain hardening curve recommended by Priestley et al.[26] defined as follows

$$f_s = f_y\left(1.5 - 0.5\left(\frac{0.12 - \varepsilon_s}{\varepsilon_{su} - \varepsilon_{sh}}\right)^2\right) \tag{2-21}$$

Where

f_s = steel stress
f_y = steel yield stress
ε_{sh} = strain at beginning of strain hardening
ε_{su} = ultimate tensile strain

Table 2-8 shows the material properties used for the M–ϕ analysis of all the specimens. The values of the strain at concrete strength (ε_o), crushing strain of unconfined concrete (ε_c), strain at beginning of strain hardening (ε_{sh}) and ultimate tensile strain (ε_{su}) were taken according to the recommendations in SDC[7], Section 3.2. Also in this section, a value of the expected steel yield stress of 475 MPa (68 ksi) was

recommend for a specified steel yield stress of 420 MPa (60 ksi). The concrete geometry was defined according to the cross section areas of the specimens shown in the Fig. 2-2. The discrete bars (interactive mode) option in SPMC[34] was used to defined the steel geometry. This was possible because all the longitudinal bars were the same size and properties. Because 4 longitudinal bars were placed in the interlocking portion and because the program places only two bars in that region (where the two spirals intersect), two additional bars were added manually into the input file. Finally a reduction factor of the concrete stress-strain curve of 0.85 was used. The M-ϕ curves were idealized as elasto-plastic models; they are shown in the Fig. 2-10 through Fig. 2-15. According to SDC[7], Section 3.3, the elastic portion of the idealized curve should pass through the M-ϕ point that corresponds to the first reinforcement bar yield. In addition, the idealized plastic moment capacity is obtained by balancing the areas between the actual and the idealized M- ϕ curves beyond the first reinforcing bar yield point. The plastic moment with the idealized yield curvature as well as the ultimate curvature are shown in Table 2-9 for all the specimens.

2.13.2. Dynamic Analysis

Dynamic analysis was performed using the Program RCShake[16]. It is a non-linear single-degree-of-freedom analysis program that was developed in UNR to predict column models response under dynamic excitations using shake table systems. RCShake[16] takes into account the equations of motion for the mass rig system (see Section 3.5), including the P-Delta effect, earthquake amplitudes and other shake table parameters to check if the shake table system limits are exceeded during earthquake simulations.

Program RCShake[16] was used to define the earthquake ground motion record as well as the testing protocol (see Sections 4.2 and 5.2) that were used in the shake table test. In order to use program RCShake[16] the elastic stiffness for each specimen needs to be calculated. The elastic stiffness is defined by the plastic shear divide by idealized yield displacement (see Section 2.10). The plastic shear is defined by the plastic moment divide by the height of the specimen. For specimens with low shear the height was taken as the height shown in the Fig. 2-1 and for specimens with high shear the height was taken as half of the clear height shown in Fig. 2-1 because of the effect of double curvature (see Section 3.5). The plastic shear, the idealized yield displacement and the elastic stiffness are shown in Table 2-10 for all specimens.

Figure 2-16 through Figure 2-18 show the earthquake records used as input motions in the dynamic analysis of the specimens with low shear. The time factor of $\sqrt{\frac{w_i}{P} l_r}$ (see Table 2-3) was applied to these motions in order to take into account the mass and the scale factors. The selection of the earthquake motion for the test was based on the two specimens with low shear, since these were scheduled to be designed and constructed first. A comparison of the dynamic analysis results for the two specimens with low shear is made in the Table 2-11. The Sylmar record was selected based on the

maximum displacement ductility demand. RCShake[16] force-displacement hysteresis curves for specimens ISL1.0 and ISL1.5, subjected to the Sylmar record, are shown in Figs. 2-19 and 2-20, respectively. In order to allow for comparison between specimens with low and high shear, Sylmar record was also selected as the input motion used in the shake table test for specimens with high shear. The testing protocol for the specimens will be discussed in Sections 4.2 and 5.2, for specimens with low and high shear, respectively.

Chapter 3. Construction of the Specimens and Experimental Setup

3.1. Introduction

The experimental study consisted of six scaled columns reinforced with double interlocking spirals subjected to earthquake excitation on a shake table system. Two 1/4-scale specimens with low shear (ISL1.0 and ISL1.5) and four 1/5-scale specimens with high shear (ISH1.0, ISH1.25, ISH1.5 and ISH1.5T) were built, instrumented and tested at James E. Rogers and Louis Wiener Large-Scale Structures Laboratory at the University of Nevada, Reno. The geometric and reinforcement details for all the specimens were discussed in Chapter 2. Standard procedures were used for the construction of the specimens. Concrete cylinders and steel reinforcement samples were tested in order to verify the strength on the day of the test and the stress-strain relationship, respectively. Two different test setups were used for the specimens with low and high shear. The construction procedure, material properties, instrumentation and the test setup are presented in this Chapter.

3.2. Construction of the Test Specimens

All the specimens were constructed at James E. Rogers and Louis Wiener Large-Scale Structures Laboratory at the University of Nevada, Reno. The specimens with low shear were scheduled to be constructed first. After the testing of the specimens with low shear, specimens ISH1.0 and ISH1.5 were build. Specimens ISH1.25 and ISH01.5T were constructed four months after the testing of the first two high shear specimens (ISH1.0 and ISH1.5) and their design was affected by the performance of ISH1.0 and ISH1.5. The construction procedure for all the specimens was the same. The column steel cage was fabricated first. Each spiral cage was fabricated separate and then interlocked with the other cage to form the steel cage of the column (Figs. 3-1 and 3-2). In order to allow the installation of the strain gages in the spirals, the least possible amount of longitudinal bars were used in the steel cage initially (Fig. 3-3). Heat shrink plastic tubing of different diameters were used to protect the strain gages wires during casting of concrete (Fig. 3-4). Once the strain gages were placed on the spirals and the longitudinal bars, the steel cage was completed with the rest of the longitudinal bars. Figure 3-4 shows the steel cage of the column ready to place on the base of the footing. Before setting the column steel cage on the base of the footing, the steel bottom mats in the footing as well as the PVC pipes were placed (Fig. 3-5). The details of the reinforcement as well as the PVC pipe locations were discussed in Sections 2.10 and 2.11. The column was placed in the center of the footing and the rest of the reinforcement of the footing was placed (Figure 3-6). Then the concrete for the footing was poured. The construction of the column form was started at least three days after pouring the concrete in the footing. Wood forms with steel laminates were used to make the oval form of the column (Fig. 3-7). The wood form for the column was reinforced every 30.48 cm (1 ft) in order to ensure the adequate performance of the form under lateral pressure of the concrete (Fig. 3-8). Eight mm (5/16 in) and 4.76 mm (3/16 in) thread rods were placed through the column section and cast integral with the column in order to provide support for the displacements

transducers. The form for the top column head was built and PVC pipes were placed according to Figs. 2-4 and 2-5. Subsequently, the steel reinforcement for the head was placed. Top column head for one of the specimens with high shear is shown in Fig. 3-9. Lateral bracing was provided for the column form to prevent lateral instability. Figure 3-10 shows the final column form for one of the specimens with high shear. Once the head was completed the concrete was poured for the column and head at the same time.

3.3. Material Properties

Local companies supplied the material used in the construction of the test specimens, except for the galvanized plain wire W2.9 and W2.0 that were purchased from Western Steel & Wire INC, San Francisco, CA. The fabrication of the spirals was made by Camblin Steel Service INC, Sacramento, CA. The concrete was designed and distributed by Reno-Sparks Ready Mix. The longitudinal bars # 3 of the column and the steel reinforcement bars used in the footing and the loading head were supplied for Northern Nevada Rebar, Blue Mountain Steel and Reno Iron Works.

The specified concrete compressive strength was 34.5 MPa (5000 psi) with 9.52 mm (3/8 in) maximum aggregate size. In order to verify the concrete strength three concrete cylinders were tested at 7 days, 14 days, 28 days and on the day of column test. Tables 3-1 and 3-2 show the average values of the compressive strength of the concrete cylinders for the footing and column, respectively.

Minimum yield strength of 420 MPa (60ksi) was specified for the steel reinforcement used in the construction of the specimens. Samples of longitudinal bars (#3) as well as wires (W2.9 and W2.0) used in the spirals were tested either a Tinius-Olsen or MTS testing machine. Table 3-3 shows the average values of the yield strength, strain at the beginning of strain hardening, and at ultimate strength, and ultimate tensile strain of the samples for the longitudinal bars for all the specimens. Figure 3-11 shows a typical stress-strain curve for one of the #3 bar samples tested in the MTS machine. Figure 3-12 shows a typical stress-strain relationship for the plain wires. No clear yield point could be found for the wires. The 0.2% offset method described in ASTM A370, Section 13.2.1 was used to determine the effective yield strength (Figure 3.12). Table 3-4 presents the average values of the yield strength, the ultimate strength and the ultimate tensile strain for the samples of the plain wires for all specimens. The same plain wire (W2.0) was used in all the specimens with high shear. Only the ultimate tensile strain of the sample for the specimens with high shear was reported since this wire was tested in the MTS machine that allowed the measurement of strain until failure.

3.4. Instrumentation

Different instruments were placed in the test specimens in order to measure acceleration, axial force, lateral force and lateral displacement, and curvature. Also, strain gages were placed on the longitudinal and transversal steel. In addition, shear

deformation was measured in the specimens with high shear. The following subsections describe the instrumentation used in the test specimens.

3.4.1. Acceleration

A Kinemetrics FBA-11g accelerometer was used to measure the horizontal acceleration at the top of the specimen. It was located at the end of the swiveled link near to the column. In addition, the acceleration of the shake table was recorded by an internal accelerometer.

3.4.2. Lateral and Axial Load

The lateral load was measured by a 667-kN (150-kip) Lebow load cell that was attached to the swiveled links. This load cell captured the lateral force due to the mass rig inertia force and the mass rig P-Δ force due to the overturning effect, but did not capture the inertia mass of the swiveled link between the load cell and the specimen as well as all the mass inertia of the axial load system and the mass of the specimen (top loading head and half of the column). The accelerometer placed at the top of the specimen and the mass of the axial load system and the mass of specimen were used calculated the lateral inertia force not captured by the load cell. Two load cells, Sensotec Model 41 (445 kN-100 kips) and Model 41 (889 kN-200 kips) were used to measure the axial load on the column. The load cells were placed in line with the threaded rods that were prestressed to provide the vertical load.

3.4.3. Lateral Displacement

The absolute lateral displacement was measured by Temposonic (LA-Series 91 cm -36in) displacement transducers. The transducers were attached to the specimen head at the level of the application of the lateral load for the specimens with low shear and to the top and bottom of the specimen head for the columns with high shear. In addition, the table displacement was recorded by an internal displacement transducer. The relative displacement was calculated as the difference between the data from the Temposonic instrumentation and the internal displacement transducer of the shake table.

3.4.4. Strain Gauges

Strain gauge series YFLA-2-5L (rated to measure large post strain) distributed by Texas Measurements were placed on the longitudinal and transverse reinforcement. The adhesive type CN-Y was used to install the gauges. In order to provide the best condition to adhere the gauge, the bar surface was sanded and cleaned with molar hydrochloric acid and base. After attaching the strain gauge with the adhesive, the gauge was covered with at least three layers of electric tape in order to avoid damage during pouring of concrete. In addition a heat shrink plastic tubing of different diameters were used to protect the strain gauges wires at during placing of the concrete (Figure 3-4). The potential plastic hinge region was the location selected for the strain gauges placed on the longitudinal and

transversal reinforcement for the specimens with low shear. Figure 3-13 shows the location of the strain gauges for specimens ISL1.0 and ISL1.5. For the specimen with high shear, the potential plastic hinge region was also selected for the location of the strain gauges placed on the longitudinal reinforcement (Figure 3-14) whereas the strain gauges for the transverse reinforcement were located through the entire height of the specimens. Figures 3-15 through 3-18 illustrate the location of the strain gauges placed on the transversal steel for specimens with high shear. In addition, 22 strain gauges were placed on the cross ties connecting the interlocking hoops in specimen ISH1.5T (Figure 3-19).

3.4.5. Curvature Transducer

Novotecknik TR-50 displacement transducers were used to measured curvature in the potential plastic hinge region. These instruments were attached to 8mm (5/16 in) thread rods on both sides of the column section. The thread rods were continuous through the column section and they were cast integral with the column. For specimens with low shear, the Novotecknik transducers were spanned a nominal distance of 102 mm (4 in) from the top of the footing to a height of 508 mm (20 in). For specimens with high shear the Novotecknik transducers were spanned a nominal distance of 12.7 cm (5 in) at the top and bottom of the column in a region of 508 mm (20 in). Figures 3-20 and 3-21 show the location of the Novotecknik displacement transducers for specimens with low and high shear, respectively.

The strain at each location is calculated from the vertical displacement measured in each Novotecknik transducer divide by the gauge length (Figure 3-22). Once the strain is calculated the average curvature over the gauge length can be calculated as follows:

$$\phi_i = \frac{\varepsilon 1_i - \varepsilon 2_i}{x1_i + D + x2_i} \qquad [3.1]$$

Where

$\varepsilon 1_i$ = strain at side 1 along the gauge length i
$\varepsilon 2_i$ = strain at side 2 along the gauge length i
$x1_i$ = distance from the column surface to the Novotecknik transducer at side 1 for the gauge length i
$x2_i$ = distance from the column surface to the Novotecknik transducer at side 2 for the gauge length i
D = column depth

3.4.6. Panel Instruments

The specimens with high shear were instrumented with fifteen Novotecknik TR-50 displacement transducers forming a panel configuration that allow measurement of total displacement at the corner of each panel (Figure 3-23). One 8mm (5/16 in) thread rod was welded on each side of the 48 mm (3/16 in) thread rods that were cast with the column. Four additional 8 mm (5/16 in) thread rod were bolted to the steel angles and

they were anchored to the head and footing surface to provide support for the Novotecknik transducers. The location of the thread rods used for the panel instrumentation is shown in Figure 3-24. In order to install the Novotecknik transducers to the thread rods, the Novotecknikss were attached to aluminum channel with rod ends (Figure 3-25). Figure 3-26 shows the panel configuration for one of the specimens with high shear.

3.5. Test Setup

An MTS shake table system was used to perform the dynamic tests on the specimens. Each specimen was lifted with a crane and set on the shake table under wood pieces in order to provide a gap of 38 cm (1.5 in) between the bottom of the footing and the top of the table. A 1830 mm x 1830 mm x 102 mm (72 in x 72 in x 4 in) formwork was placed around the footing of the specimen and 380 mm (1.5 in) thickness non-shrink grout was poured. After the grout was dry, the specimen was attached to the shake table deck using 14 steel thread rods connected at the strong holes of the shake table deck.

The axial load system consisted of a steel spreader beam bolted to embedded 19 mm (3/4 in) diameter and 305 mm (12 in) long thread rod at the top of the head. This beam transferred the axial load that was applied through two Enerpac 30 ton (66 kips) hole rams (Figure 3-27). The axial load was kept constant by a Reddick 9.46L (2.5 gallon) accumulator connected to the ramps. Two 22 mm (7/8 in) high strength steel thread rods run from the rams through the footing into strong holes of the shake table deck. Two load cells between the rams and the spread beam were used to monitor the axial load.

The inertia mass system designed by Laplace et al.[16] was used to apply the lateral inertia force to the column. The mass rig is an eight pin frame with concrete blocks placed on its deck. These concrete blocks determine the inertia mass applied to each specimen. Different number of concrete blocks and different swiveled links were used for the specimens with low and high shear, as described in the next sections.

3.5.1. Specimen with Low Shear

The same test setup was used for specimens ISL1.0 and ISL1.5. Four concrete blocks were used with the mass rig as the inertia mass. The total inertia mass was 445 kN (100 kips) that came from the weight of four concrete blocks [89 kN (20 kips)] each and the effective weight of the mass rig itself, also 89 kN (20 kips). The lateral load was applied on the top of the column through one rig swiveled link, testing the specimens as a cantilever member with single curvature. The test setup schematic is shown in Fig. 3-28 and the actual test setup is shown in Fig. 3-29.

3.5.2. Specimen with High Shear

All the specimens with high shear, ISH1.0, ISH1.25, ISH1.5 and ISH1.5T, were tested using the same test setup. The test setup schematic is shown in the Fig. 3-30 and the actual test setup is shown in Fig. 3-31. The total inertia mass was 36289 kg (2487 slug) and it consisted of three concrete blocks each with a weight of 89 kN (20 kips) each plus the mass rig with an effective of weight of 89 kN (20 kips). A double swiveled link system was used to transmit the lateral load from the mass rig to the column. This dual link configuration allows the specimens to be tested in double curvature. A link connector plate was post-tensioned to the specimen top head and bolted to the double links (Fig. 3-32).

Chapter 4. Experimental Results for Specimens with Low Shear

4.1. Introduction

The seismic behavior of six bridge RC column models with double interlocking spirals was studied experimentally using shake table tests. Two of the models were 1/4-scale with low average shear stress (ISL1.0 and ISL1.5). They were tested under increasing amplitudes of the Sylmar record from the 1994 Northridge Earthquake until failure. The observed performance and measured response of the specimens are described in this chapter. This chapter also presents plastic hinge length, the effective force-displacement yield point and the ductility displacement capacity calculated based on the experimental data for each specimen.

4.2. Testing Protocol

The Sylmar record was selected as the input motion for the shake table tests based on the maximum displacement ductility demand (Section 2.13.2). Time compression factor of 0.51 and 0.50 was applied to the input motion for specimens ISL1.0 and ISL1.5, respectively. The testing sequence for each specimen is shown in the Table 4-1. The testing sequence was defined based on the dynamic response obtained from the Program RCShake[15] with the estimated properties of each specimen. A fine-tuning of the shake table with the specimen was done prior to the test in order to minimize the different between the target and the achieved acceleration. Small increments of the Sylmar record were applied to the specimens in order to determine the elastic response as well as to find the effective yield point. Once the effective yield was reached, the amplitude of the input record was increased until failure. Intermittent free vibrations tests were conducted to measure the change in frequency and damping ratio of the columns.

4.3. Observed Performance

A lime and water mixture was applied to the surface of the column in order to make the cracks more visible. Flexural cracks were observed in specimen ISL1.0 during the first three runs (displacement ductility demand, μ_d, between 0.2 and 0.8) and in specimen ISL1.5 during the first six runs (μ_d between 0.1 and 1.5). Most of these cracks were located in the lower third of the column height. Figure 4-1 and 4-2 show the flexural cracks for specimens ISL1.0 and ISL1.5, respectively. First spalling and shear cracks were formed in ISL1.0 at 0.5xSylmar (μ_d = 1.5) and ISL1.5 at 1.25xSylmar (μ_d = 2.4). The shear cracks for specimens ISL1.0 and ISL1.5 are shown in Figs. 4-3 and 4-4, respectively. These cracks were located in the interlocking region in the lower third of the height of the column and they were connected with the flexural cracks. Considerable spalling in the bottom of the column, as well as propagation of flexural and shear cracks was observed after 1.25xSylmar (μ_d = 2.8) in ISL1.0 (Fig. 4-5) and 1.5xSylmar (μ_d = 3.1) in ISL1.5 (Fig. 4-6). Spirals were visible at 1.5xSylmar (μ_d =4.1) and longitudinal bars were exposed at 1.75xSlymar (μ_d = 5.6) in ISL1.0 (Fig. 4-7). Spirals were visible in

ISL1.5 after 1.75xSlymar (μ_d = 4.5) and become clearly exposed at 2.0xSlymar (μ_d = 7.5) (Fig. 4-8). There was no visible core damage in either specimen. Specimens ISL1.0 and ISL1.5 failed during 2.0xSylmar (1.21g PGA and μ_d = 9.6) and 2.125xSylmar (1.29g PGA and μ_d = 10.4), respectively. The failure in both columns was due to rupture of the spirals and buckling of the longitudinal bars at the bottom of the column in the plastic hinge zone. Figures 4-9 and 4-10 show the damage after failure for specimens ISL1.0 and ISL1.5, respectively. The observed performance is summarized in Table 4-2 for specimen ISL1.0 and in Table 4-3 for specimen ISL1.5.

4.4. Target and Measured Acceleration

Even though a fine-tuning of the shake table was performed before the test, some differences between the target accelerations (Sylmar record) and the achieved accelerations by the shake table were noted. Tables 4-4 and 4-5 show the target accelerations and the peak maximum and minimum accelerations achieved for the specimens ISL1.0 and ISL1.5, respectively, at each run. The ratios of achieved and target PGA's are also reported in the tables. The ratios of the maximum value of PGA were constant in most of the motions with an average value of 1.19 for specimen ISL1.0 and 1.30 for specimen ISL1.5. Program Degtra 2000[21] was used to calculate the elastic response spectra for a single degree of freedom. A comparison between the elastic response spectra for target and achieved input motions are shown in Figs. 4-11 through 4-20 for specimen ISL1.0 and in Figs. 4-21 through 4-31 for specimen ISL1.5. Also shown in the figures are the elastic periods of the models during each run. A Fourier analysis of acceleration data, between the last 10 to 15 seconds for the accelerometer attached at the swiveled link, was performed to find the elastic period at each motion. Most of the variation between target and achieved acceleration is at the low period of the spectrum. The impact of these variations is not significant since the potential column response is at higher periods as is shown in the previous figures. Tables 4-6 and 4-7 show the ratios of the achieved and target spectra response for the elastic period of the specimens at each motion. Better agreement was found from this ratio and the table performance was acceptable for the period range of interest.

4.5. Axial Load Variation

Two load cells between the hydraulic jacks and the spreader beam were used to monitor the axial load, as mentioned in Chapter 3. An accumulator connected to the jacks was used to minimize the variation of the axial load. The target axial load was –400 kips (-90 kips) for specimen ISL1.0 and –472 kN (-106 kips) for specimen ISL1.5. The variation of the axial load versus top displacement of the column is shown in the Figures 4-32 and 4-33, for specimen ISL1.0 and ISL1.5, respectively. The axial load fluctuated between –338 kN (-87 kips) and –422 kN (-95 kips) for specimen ISL1.0 and –436 kN (-98 kips) and –472 kN (-106 kips) for specimen ISL1.5. The average value of the axial load variation was -396 kN (-89 kips) for specimen ISL1.0 and -444 kN (-100 kips) for specimen ISL1.5. The performance of the axial load system was satisfactory with a 1% and 6 % difference between target and the average value of the axial load for

specimens ISL1.0 and ISL1.5, respectively. The average value of the axial load variation will be used in the section analysis (M-ϕ) in the Chapter 6.

4.6. Force and Displacement Hysteresis Curves and Envelopes

The lateral force was measured by a load cell attached to the swiveled link. The load cell captured the lateral force due to the mass rig inertia force and the mass rig P-Δ force due to the overturning effect, but did not capture the inertia force due to the mass of the swiveled link between the load cell and the specimen, the mass of the axial load system and the tributary mass of the specimen (top specimen head plus half of the column). In order to calculate the inertia force that was not captured by the load cell, the accelerometer attached at the end of the swiveled link was used. Therefore, the summation of the mass of the swiveled link between the load cell and the specimen, the mass of the axial load system, the mass of the top specimen head and half of the column were multiplied by the acceleration measured by the accelerometer at each time step in order to calculate the additional inertia force. The total lateral force applied at the top of the column was calculated as the summation of the additional inertia force and the force measured by the load cell.

The absolute lateral displacement was measured at the top specimen head at the level of the applied horizontal load. The displacement at the top of the column relative to the footing was calculated as the different between the absolute lateral displacement and the displacement of the shake table.

The measured force-displacement hysteresis curves for different motions are shown in Figs. 4-34 through 4-43 for ISL1.0 and Figs. 4-46 through 4-56 for ISL1.5. An accumulated hysteresis is plotted for all the motions in Figure 4-44 and 4-57 for specimens ISL1.0 and ISL1.5, respectively. The data were low-pass filtered at 80 Hz with analog filters to eliminate high-frequency noise.

The measured peak forces with the corresponding displacements and the peak displacements with the corresponding forces at each motion are shown in Tables 4-8 and 4-9 for ISL1.0 and ISL1.5, respectively. An envelope curve was developed based on the peak forces with corresponding displacements for all the motions before failure. The failure point for the envelope curve was assumed either by the peak displacement with the corresponding force or 80 percent of the maximum force with the corresponding displacement when the force for the peak displacement dropped more than 20 percent of the maximum force. Figures 4-45 and 4-58 show the envelope of accumulated force displacement hysteresis curve for specimens ISL1.0 and ISL1.5, respectively.

4.7. Dynamic Properties

The low level elastic response for each motion was used to calculate the frequency and stiffness of the specimens. The low level elastic response was taken as the response of the accelerometer attached at the end of the swiveled link between last 10

seconds and 15 seconds of each motion. A Fourier spectrum was performed to find the predominate frequencies of each motion, using the Program Degtra 2000[21]. The following equation was used in order to calculate the stiffness of the specimen at each motion:

$$K = M\frac{4\pi^2}{T^2} \tag{4-1}$$

Where

M = inertia mass

T = period

A summary of the dynamic properties are shown in Tables 4-10 and 4-13 for specimens ISL1.0 and ISL1.5, respectively.

A series of snap ramps or free vibration test were performed in order to calculate the frequency and the damping of the specimens. The tests were part of the loading protocol described in Section 4.2. They consisted of free vibration under square pulse at low amplitudes of displacement. Program Degtra[21] was used to compute the frequencies from the Fourier spectrum. Equation 4-1 was used to calculate the stiffness of the specimens. The equivalent viscous damping ratio was calculated using the decrement logarithmic method[9]. The damping ratio ζ is calculated from the following equation:

$$\text{In}\frac{\nu_n}{\nu_{n+m}} = \frac{2m\pi\zeta}{\sqrt{1-\zeta^2}} \tag{4-2}$$

Where

ν_n = peak values of force, displacement or acceleration at the first cycle

ν_{n+m} = peak values of force, displacement or acceleration at the m^{th} successive cycle

Tables 4-11 and 4-14 show the dynamic properties for the specimens ISL1.0 and ISL1.5, respectively, measured from the snap ramp tests.

In addition to low level elastic response and snap ramp test, the peak forces and the corresponding displacements were used to calculate the effective stiffness of the specimens at each motion. The stiffness was calculated as the ratio of the peak force and the corresponding displacement. Tables 4-12 and 4-15 show the force and displacement values used to calculate the stiffness for ISL1.0 and ISL1.5, respectively. The period and the frequency were computed using the Equation 4-1.

Good agreement for the dynamic properties was found between the values for low level elastic response, snap ramp and the peak force and corresponding displacement. In

general, as the specimen degraded and the stiffness reduced and the period and the damping of the specimen increased.

4.8. Curvature Profile

Novotecknik displacement transducers were used to measure curvature in the potential plastic hinge region. The strain on each side of the column is calculated from the vertical displacement measured in each Novotecknik transducer divide by the gauge length. Once the strain is calculated, the average curvature over the gauge length can be computed as the difference of the strains on the sides of the column, divided by the total horizontal distance between the instruments. This procedure assumes that the sections remained plane. The curvature instrumentation details were presented in Section 3.4.5.

The curvature profiles are shown in Figs. 4-59 and 4-60 for specimen ISL1.0 and Figs. 4-61 and 4-62 for specimens ISL1.5. The values of the curvature profiles correspond to the maximum and minimum peak values of lateral force. Due to the asymmetry of Sylmar motion, relatively high curvature were developed when the peak lateral forces were minimum (Figs. 4-60 and 4-62) that correspond to the predominate direction of motion. The high curvature values were measured at the base of the column due to the high moment at the base in both specimens.

4.9. Flexural and Bond Slip Deformation

The curvature profiles were used to calculate the flexural deformation by integrating the curvature using the moment-area method. The curvatures were assumed to be constant over the gauge length. Since no instruments were placed from 609 mm (24 in) above the top of the footing to the top of the column, a straight line connecting the curvature measured at 609mm (24 in) to zero curvature at the top was assumed. Figure 4-63 shows the moment area method and the constant curvature profile. The flexural deformation was calculated only for the peak values of lateral force that correspond to the predominant direction of motion. Figures 4-64 and 4-65 show the lateral force versus flexural deformation for specimens ISL1.0 and ISL1.5, respectively. Additional rotation due to the bond slip is recorded by the curvature instruments. Therefore, the flexural deformation calculated by these instruments present a component from the bond slip effect that can not be uncoupled.

4.10. Shear Deformation

In order to determine the shear deformation of the column, the flexural deformation calculated in the previous section was subtracted from the total displacement at the top of the column (Section 4.6). The shear deformation was computed only for the predominant direction of the motion. The lateral force versus shear deformation for specimens ISL1.0 and ISL1.5 are shown in Figures 4-66 and 4-67, respectively. A bilinear behavior is observed for the lateral force and the shear deformation, in both cases. Tables 4-16 and 4-17 present the flexural and bond slip deformation as percentage

of the total deformation at the top of the columns. The shear deformation was 11% to 14% of the total deformation for specimen ISL1.0 in all the motions. For specimen ISL1.5 the shear deformation was 7% to 39% of the total deformation until 1.25xSylmar and 16 % to 12 % of the total deformation for the last two motions. The relatively large shear deformation in the first motions of specimen ISL1.5 correspond to the relative small flexural deformation at the first motions since the curvatures did not increase particularly at the base of the column. This was in agreement with the observed performance described in Section 4.3.

4.11. Measured Strains

The strain gauges were placed at the potential plastic hinge region for longitudinal and transverse reinforcement. The maximum and minimum strains measured in the longitudinal bars are presented in Tables 4-18 through 4-21 for specimen ISL1.0 and in Tables 4-22 through 4-26 for specimen ISL1.5. Positive strains correspond to tensile strains, while negative strains correspond to compressive strain. The yield strain of 2310 microstrain, for the # 3 longitudinal bars, was calculated based on the yield stress reported in Section 3.3 and a modulus of elasticity of 200 MPa (29000 Ksi). The maximum strains were below yielding in the bars at –152 mm (-6 in) below the top of the footing, for specimen ISL1.0. However in ISL1.5 strains exceeded the yield strain at –152 mm (-6 in) below to the top of the footing. The yield strain was reached at 0.3xSylmar for specimen ISL1.0 with a value of 11,149 microstrains (Table 4-19) in strain gauge #10 at 127 mm (5 in). In ISL1.5 the yield strain was reached at 0.4xSylmar with a value of 18,896 microstrains in strain gauges # 10 at the top of the footing. Strain gauges #4 and #7 measured strain in the longitudinal interlocking bars in both specimens. In ISL1.0 strain gauge # 4 and # 7 yielded at 0.5xSylmar and 1.0xSylmar, respectively (Table 4.18). Strain gauge # 4 yielded at 1.25xSylmar (Table 4-23) while strain gauge # 7 yielded at 1.5xSylmar (Table 4-24), for specimen ISL1.5. The strain profile for strain gauge #1 is presented in the Figures 4-68 and 4-69 for ISL1.0 and ISL1.5, respectively. Higher strains were measured in both specimens at or near the base of the column compared with the other locations through the height of the column. Also note that yielding spread beyond the height of 508 mm (20 in), over which the longitudinal bar gauges had been placed.

Tables 4-27 through 4-31 for specimen ISL1.0 and Tables 4-32 through 4-35 for specimen ISL1.5 show the maximum and minimum strains measured in the spirals. The same convention of signs used in longitudinal bars is used for the tensile strains and compressive strain in the spirals. The spirals yield strain of 2,241 microstrain was calculated based on the yield stress reported in Table 3-4 and a modulus of elasticity of 200 MPa (29000 Ksi). Strain gauge # 2 at the height of 254 mm (10 in) in specimen ISL1.0 (Table 4-30) yielded at 0.5xSylmar with a value of 2,556 microstrains. Strain close to yield was recorded in strain gauge # 1 (Table 4-32) at 1.25xSylmar in specimen ISL1.5. Strain gauges # 2 in specimen ISL1.0 in # 1 for specimen ISL1.5 confirms the formation of the first shear cracks described in the Section 4.3. In most of the locations, strains below yielding were measured until the last motions, in both specimens. The

average maximum spiral strain at each motion was plotted again displacement ductility capacity in Fig. 4-70. This figure shows that average strain was bellow yield in most of the locations for both specimens. In addition, spirals in specimen ISL1.5 were subjected to higher strain compared with the spirals in ISL1.0, particularly toward end of the test. As a result, slight degradation of the load capacity (Figure 4-58) was observed in ISL1.5.

4.12. Idealized Force-Displacement Relationship

The measured envelope curves (Figs. 4-45 and 4-58) were idealized by elasto-plastic curves to quantify the ductility capacity of the specimens. Three methods were used to find the force-displacement point (F_{y1}, D_{y1}) that defines the elastic portion of the idealized curve (Fig. 4-71). The first method consists of taking the force-displacement point that corresponds to the first reinforcement bar yield. In some cases, this point is not on the envelope. In those cases, a different point needs to be chosen in order to force the elastic portion of the idealized curve to pass through the measured curve. The second method can be used in those cases. It consists of taking the force corresponding to the first reinforcement yield and finds the corresponding displacement on the measured envelope using linear interpolation. A third method is to take one-half of the peak force and find the corresponding displacement on the measured curve. This method is useful especially when no strain data are available. Once the elastic portion is defined the yield level is establish by equalizing the area between the measured and the idealized curves (Fig. 4-71). The failure was assumed to occur when the maximum displacement corresponding to the column failure occurred at a force exceeding 80% of the peak force, the actual column failure point was used.

Table 4-36 for specimen ISL1.0 and Table 4-37 for specimen ISL1.5 show a comparison of the idealized force-displacement values obtained using the three methods. A variation of 10 % to 20 % of the displacement ductility capacity was found between the methods. Since strain data are available and the force-displacement point (F_{y1}, D_{y1}) needs to be on the measured curve, the second method was selected to idealize of the measured curve. Figure 4-72 and 4-73 present the elasto-plastic idealization of the response in the predominant direction of motion for ISL1.0 and ISL1.5, respectively.

4.13. Plastic Hinge Length

The plastic rotation θ_p over the equivalent plastic hinge length l_p is defined by

$$\theta_p = (\phi_u - \phi_y) l_p \qquad (4\text{-}3)$$

Where

ϕ_u = Ultimate curvature capacity
ϕ_y = Idealized yield curvature capacity

Equation 4-4 is used to calculate the plastic deformation of the cantilever column when the plastic rotation is assumed to be concentrate at midheight of the plastic hinge.

$$\Delta_p = \theta_p \left(L - \frac{l_p}{2} \right) \tag{4-4}$$

Where

L = Distance from point of maximum moment to the point of contra-flexure

In addition, the ultimate deformation of the column, $\Delta_{u,}$ can be related to the plastic and idealized effective yield displacement, $\Delta_{y,}$ as follows

$$\Delta_u = \Delta_y + \Delta_p \tag{4-5}$$

Substituting Equations 4-3 and 4-4 into Equation 4-5 and solving for l_p and taking the negative root of the quadratic equation, the following equation is found

$$l_p = \frac{\left(\phi_p L - \left(\phi_p \left(\phi_p L^2 - 2\Delta_p \right) \right)^{\frac{1}{2}} \right)}{\phi_p} \tag{4-6}$$

Where

ϕ_P = Plastic curvature capacity = ϕ_u-ϕ_y

Δ_p = Plastic displacement of the column = Δ_u - Δ_y

Equation 4-6 was used to calculate the measured l_p based on the average value of the measured curvatures at 50.8 mm (2 in) and 152.4 mm (6 in). The curvature over a 203 mm (8 in) rather than 101.6 mm (4 in) gauge length was used because the most of plastic deformation was concentrated over that region according to the measured curvature and strain values. The elasto-plastic idealization for the average measured moment-curvature at 50.8 mm (2 in) and 152.4 mm (6 in) is shown in Fig. 4-74 for specimen ISL1.0 and in Fig. 4-75 for ISL1.5. Table 4-38 summarize the values used in Equation 4-6 to calculate the experimental l_p for both specimens. The values of l_p of 0.75 and 0.83 times the total depth of the column were found base on Equation 4-6 for specimens ISL1.0 and ISL1.5, respectively.

Chapter 5. Experimental Results for Specimens with High Shear

5.1. Introduction

Previous chapter described the experimental results for the two specimens with low shear. In this chapter the experimental results of four additional specimens with high shear are presented. Note that specimens were designed to fail with considerable flexural hinging despite their average shear strength. As part of the experimental program, four 1/5-scale specimens (ISH1.0, ISH1.25, ISH1.5 and ISH1.5T) were tested under increasing amplitudes of the Sylmar record until failure. These specimens were loaded in double curvature using the test setup described in Chapter 3. The observed performances of the specimens are described in terms of increments amplitudes of Sylmar and displacement ductility capacities to allow comparisons among specimens. The experimental data from the instruments placed on the specimens and described in Chapter 3 are presented in this Chapter. In addition, measured dynamic properties are reported. The yield point and the displacement ductility capacity for each specimen are calculated based on the experimental data and discussed.

5.2. Testing Protocol

The Sylmar record was selected as the input motion for the shake table tests based on the maximum displacement ductility demand of the specimens with low shear (Section 2.13.2). In order to allow for comparison between specimens with low and high shear, the Sylmar record was used as the input motion in the testing protocol for specimens with high shear. Based on the Section 2.8 a time compression factor of 0.49, 0.46, 0.50 and 0.45 was applied to the input motion for specimens ISH1.0, ISH1.25, ISH1.5 and ISH1.5T, respectively. The testing protocols for each specimen are shown in Table 5-1. The testing protocol was developed based on the dynamic response obtained from the Program RCShake[15] with the estimated properties of the each specimen. A fine-tuning was performed at the beginning of the test in order to minimize the difference between the target and the achieved accelerations. Small increments of Sylmar record were applied to the specimens to determine the elastic response and to find the effective yield point. Once the effective yield point was identified, the amplitude of the input record was increased until failure. Notice that the testing protocol for specimens ISH1.5 and ISH1.5T is the same until the failure of ISH1.5. Free vibrations tests were conducted to measure the change in frequency and damping ratio of the columns.

5.3. Observed Performance

In order to make the cracks more visible, a lime and water mixture was applied to the surface of the column. Flexural cracks were observed during the first three or four runs in ISH1.0 with displacement ductility demand, μ_d, of 0.06 to 0.4, in ISH1.25 with μ_d = 0.1 to 0.6, in ISH1.5 with μ_d = 0.2 to 0.7 and in ISH1.5T with μ_d = 0.1 to 0.6. The flexural cracks were located in the plastic hinge zones at the top and bottom on both sides of the column. This crack pattern was observed in specimens ISH1.0, ISH1.25 and

ISH1.5T and is shown in Figs. 5-1, 5-2 and 5-4, respectively. Figure 5-3 shows the flexural cracks for specimen ISH1.5. These cracks were concentrated mainly at the lower third of the column height. A vertical crack located in the interlocking region going from the top of the column to the mid height of the column was visible after 0.4xSlymar (μ_d = 0.7) in ISH1.5 (Fig. 5-5).

Shear cracks, located in the interlocking region in the plastic hinge zones, were formed in all the specimens. These cracks began to form starting with 0.5xSylmar (μ_d = 0.6) and became pronounced under 0.75xSylmar (μ_d = 0.9) in ISH1.0 (Fig. 5-6) and 1.0xSylmar (μ_d = 1.4) in ISH1.25 (Fig. 5-7). In ISH1.5 shear cracks were visible starting with 0.75xSylmar (μ_d = 1.0) and in ISH1.5T under with 1.0xSylmar (μ_d = 1.2). Figures 5-8 and 5-9 show the shear cracks for ISH1.5 and ISH1.5T, respectively. Localized small vertical cracks were observed in ISH1.5T at 1.0xSylmar (Fig. 5-9).

After 1.0xSylmar (μ_d = 1.4), first spalling at top and bottom of the column was observed in ISH1.0 and ISH1.5, whereas in ISH1.25 (μ_d = 1.6) and ISH1.5T (μ_d = 1.7), first spalling at top and bottom of the column was observed during 1.25xSylmar. Propagation of flexural, shear cracks and increasing of the spalling were observed after 1.5xSylmar (μ_d = 2.5) in ISH1.0 (Fig. 5-10), after 1.75xSylmar (μ_d = 2.2) in ISH1.25 (Fig. 5-11), after 1.25xSylmar (μ_d = 1.7) in ISH1.5 (Fig. 5-12) and after 1.75xSylmar (μ_d = 2.5) in ISH1.5T (Fig. 5-13). The spirals were visible at top and bottom of the column after 2.125xSylmar (μ_d = 2.9) in ISH1.25 (Fig. 5-14). The longitudinal bars were exposed during 1.75xSylmar (μ_d = 3.6) in ISH1.0 (Fig. 5-15), 2.25xSylmar (μ_d = 3.7) in ISH1.25 (Fig. 5-16), 1.5xSylmar (μ_d = 2.2) in ISH1.5 (Fig. 5-17), and 2.0xSylmar (μ_d = 2.8) in specimen ISH1.5T (Fig. 5-18). Specimens ISH1.0 (Fig.5-19) and ISH.125 (Fig.5-20) failed in shear during 2.0xSylmar (μ_d = 4.7) at the bottom and 2.375xSylmar (μ_d = 4.7) at the top, respectively. Damage in the core was observed in ISH1.5 (Fig. 5-21) after 2.125xSlymar (μ_d = 4.7) and in ISH1.5T (Fig. 5-22) after 2.25xSylmar (μ_d = 3.0). Buckling of the longitudinal bars at the bottom of the column was visible after 2.25xSylmar (μ_d = 3.4) in ISH1.5 (Fig. 5-23) and 2.5xSylmar (μ_d = 3.4) in ISH1.5T (Fig. 5-24). Specimen ISH1.5 (Fig. 5-25) and ISH.5T (Fig. 5-26) failed during 2.375xSylmar (μ_d = 4.0) and 2.625xSylmar (μ_d = 3.8), respectively. Failure in ISH1.5 was due to fracture of the spirals and buckle of the longitudinal bars, whereas in ISH1.5T failure was due to fracture of the spirals and one of the longitudinal bars. The observed performance is summarized in Tables 5-2, 5-3, 5-4 and 5-5 for the specimens ISH1.0, ISH1.25, ISH1.5, and ISH1.5T, respectively.

5.4. Target and Measured Acceleration

Tables 5-6, 5-7, 5-8 and 5-9 show the maximum and minimum peak target and peak achieved accelerations for specimens ISH1.0, ISH1.25, ISH1.5 and ISH1.5T respectively, at each run. The ratios of achieved and target PGA's are also reported in tables. The maximum acceleration values correspond to predominant direction of motion. The average values for the ratio of maximum achieved and target PGA's were

1.06, 1.11, 1.05 and 0.96 for specimens ISH1.0, ISH1.25, ISH1.5 and ISH1.5T, respectively. An additional comparison between the target and achieved acceleration were made using the elastic response spectra. Program Degtra 2000[21] was used to calculate the elastic response spectra for the target and achieved acceleration records. The acceleration responses for target and achieved input motions are plotted in Figs. 5-27 through 5-36 for specimen ISH1.0 and in Figs. 5-37 through 5-48 for specimen ISH1.25 Figures 5-49 through 5-61 and Figs. 5-62 through 5-76 show the acceleration responses for target and achieved input motion for specimens ISH1.5 and ISH1.5T, respectively. The variation between target and achieved acceleration depends on the period of the column which changes at each motion. A Fourier spectrum was performed to find the predominate frequencies between last 10 seconds and 15 seconds of each motion, using the Program Degtra 2000[21]. The inverse of the frequencies from the Fourier spectrum were used to find the elastic period at each motion. Tables 5-10, 5-11, 5-12 and 5-13 show the ratios of the achieved and target spectra response for the elastic period for specimens ISH1.0, ISH1.25, ISH1.5 and ISH1.5T, respectively. The maximum values of the ratio of the achieved and target accelerations occurred after the effective yield was reached (around 1.0xSylmar), since the tuning of the shake table was base on the initial stiffness of the specimen. Average values of ratio of the achieved and target acceleration of 0.97, 0.91, 0.98 and 1.10 were found for specimens ISH1.0, ISH1.25, ISH1.5 and ISH1.5T, respectively for all the motions. Base on the comparison between the peak and spectrum accelerations the table performance was acceptable.

5.5. Axial Load Variation

The axial load system was discussed in Section 3.5. The variation of the axial load was controlled by an accumulator connected to the hydraulic jacks. The target axial loads were –275 kN (-62 kips), –300 kN (-67 kips), –259 kN (-58 kips) and –356 kN (-80 kips) for specimens ISH1.0, ISH1.25, ISH1.5 and ISH1.5T, respectively. The variation of the axial load during the test versus top displacement of the column is shown in the Figures 5-77 through 5-80. The variation of the axial load is summarized in Table 5-14 for all the specimens with high shear. The performance of the axial load system was satisfactory with a maximum of 6%, 1%, 3% and 4% difference between target and the average value of the axial load for specimens ISH1.0, ISH1.25, ISH1.5 and ISH1.5T, respectively. The average value of the axial load variation was used in sectional analysis (M-ϕ) discussed in Chapter 6.

5.6. Force and Displacement Hysteresis Curves and Envelopes

The load cell attached to the swiveled links captured the lateral force due to the mass inertia force and the mass rig P-Δ force due to the overturning effect. The load cell did not capture the inertia force due to the mass of the swiveled link between the load cell and the specimen, the mass of the axial load system and the tributary mass of the specimen (loading head plus half of the column). The same procedure used in Section 4.5 was followed in order to calculate the additional inertia force that was not captured by the load cell. The total lateral force applied at the top of the column was calculated as the

summation of the additional inertia force and the force measured by the load cells of the links system.

In the absence of any head rotations, the displacements at the top and bottom of the loading head are the same. However, because a head rotation is expected due to finite element stiffness of the links, the absolute lateral displacement was measured at the top and bottom of the loading head. The head displacement was calculated as the average of the top and bottom displacement measurements. The specimen "top" displacement relative to the footing was calculated as the difference between the average head displacement and the displacement of the shake table.

The measured force-displacement hysteresis curves for different motions are shown in Figs. 5-81 through 5-90 for ISH1.0, Figs. 5-93 through 5-104 for ISH1.25, Figs. 5-107 through 5-119 for ISH1.5 and Figs. 5-122 through 5-136 for ISH1.5T. The accumulated hysteresis curves are plotted for all the motions in Figures 5-91, 5-105, 5-120 and 5-137 for specimens ISH1.0, ISH1.25, ISH1.5 and ISH1.5T, respectively. The data were low-pass filtered at 80 Hz with analog filters to eliminate high-frequency noise.

The measured peak forces with the corresponding displacements and the peak displacements with the corresponding forces at each motion are shown in Table 5-15, 5-16, 5-17 and 5-18 for ISH1.0, ISH1.25, ISH1.5 and ISH1.5T, respectively. An envelope curve was developed based on the peak forces with corresponding displacements for all the motions before failure. The failure point for the envelope curve was assumed either by the peak displacement with the corresponding force or 80 percent of the maximum force with the corresponding displacement when the force for the peak displacement dropped more than 20 percent of the maximum force. Figures 5-92, 5-106, 5-121 and 5-138 show the envelopes of accumulated force displacement hysteresis curve for specimens ISH1.0, ISH1.25, ISH1.5 and ISH1.5T, respectively.

5.7. Moment Demands and Head Rotation

The moment demands at the bottom and top of the column were calculated using the force recorded in the load cell attached at each link and the distances of the individual links to the bottom of the head and to the top of the footing. Figure 5-139 shows the forces of the links and the moment arms used to calculate the moment at top and bottom of the column. The P-Δ effect due to the axial load and the weight of the head were included in the calculation of the moment demands at the bottom of the column. The moment demands were calculated at the same time instance of the values of the forces used in the calculation of the envelope in the predominant direction of motion. Figures 5-140, 5-141, 5-142, and 5-143 show the moment demand at the top and bottom of the column for specimens ISH1.0, ISH1.25, ISH1.5 and ISH1.5T, respectively.

The inflection point for each column was found based on the moment demand at the top and bottom of the column. Table 5-19 summarizes the distance of the inflection point from the top of the columns. A perfect double curvature implies that the inflection

point should be located at the mid height of the column. The figures and the table show the shifting of the inflection point at each motion. A relatively small variation of the inflection point close to the mid height of the column was seen in ISH1.0. Significant variation of the inflection point was noted for ISH1.25, ISH1.5 and ISH1.5T. In general, the inflection point was located above the mid height of the column due to the higher moment demand at the bottom of the column in the first few motions. Once the plastic moment was reached at the bottom of the column, the moment demand was increased at the top and the inflection point was shifted close to the mid height of the column. Under 1.25xSylmar the actual inflection point was within 5 % of one-half of the column clear height in all the specimens.

The difference between the moment demand at the top and bottom of the column was due to the vertical rotation produced at the head of the column. The head rotation was recorded by two displacement transducers placed at top and bottom of the head. Table 5-20, 5-21, 5-22 and 5-23 show the forces and displacements used in the envelope of the force displacement hysteresis curves for the predominant direction of motion with the corresponding rotation of the head. Figure 5-144 compares the head rotation for the predominant direction of motion with the corresponding lateral displacement for the specimens with high shear. Relatively higher rotation was recorded in specimen ISH1.5 and ISH1.5T compared with ISH1.0 and ISH1.25. The head rotation was stabilized after the yielding of one end, which is in agreement with the variation of the moments recorded at top and bottom of the column presented in Figs. 5-140 through 5-143. The rotation of the head is attributed to a rocking movement produced at the contact surface between the plate connection and the column head. The contact surface of the head is not perfectly plane and it can be bulged during the concrete pouring process. The finite stiffness of the dual link system can also be a cause of the head rotation according to Laplace et al[15].

5.8. Dynamic Properties

The low level elastic response, described in Chapter 4.7, was used for each motion to calculate the frequency and stiffness of the specimens. A summary of the dynamic properties are shown in Tables 5-24, 5-27, 5-30 and 5-33 for specimens ISH1.0, ISH1.25, ISH1.5 and ISH1.5T, respectively.

A series of snap ramps, free vibration tests, were performed in order to calculate the frequency and damping of the specimens. The tests were part of the loading protocol described in Section 5.2. They consisted of free vibration caused by a square pulse at low amplitudes of displacement. Program Degtra[21] was used to compute the frequencies from the Fourier spectrum. The stiffness of the specimens was calculated based on the methodology described in Chapter 4.7. The equivalent viscous damping ratio was calculated using the decrement logarithmic method[9]. Tables 5-25, 5-28, 5-31 and 5-34 show the dynamic properties for specimens ISH1.0, ISH1.25, ISH1.5 and ISH1.5T, respectively, measured from the snap ramps tests.

In addition to low level elastic response and snap ramp test, the peak force and the corresponding displacement were used to calculate the chord stiffness of the specimens at each motion. The stiffness was calculated as the ratio of the peak force and the corresponding displacement. Tables 5-26, 5-29, 5-32 and 5-35 show the force and displacement values used to calculate the stiffness for specimens ISH1.0, ISH1.25, ISH1.5 and ISH1.5T, respectively.

Frequencies extracted for low level response are generally higher than snap results. This indicated that snap tests impose larger displacements than the amplitudes considered in the low level response analysis. Frequencies for snap tests are higher than those based on the chord stiffness, except for the initial runs. This is expected because chord stiffness represents the stiffness under high amplitudes whereas the stiffness for snap test stiffness is at relatively low loading. As the motion amplitudes increased, the specimen degraded, the stiffness was reduced, the damping of the specimen increased. This trend is seen in all three data sets for each specimen.

5.9. Curvature Profile

Novotecknik displacement transducers were used to measure curvature in the potential plastic hinge region at the top and bottom of the column. The strain on each side of the column was calculated from the vertical displacement measured each Novotecknik transducer divided by the gauge length. Once the stain is calculated, the average curvature over the gauge length can be computed as the difference of the strains on the sides of the column, divided by the total horizontal distance between the instruments. This procedure assumes that the sections remained plane. The curvature instrumentation details were presented in Section 3.4.5.

The curvature profiles for the predominant direction of motion are shown in Figs. 5-145, 5-146, 5-147 and 5-148 for specimens ISH1.0, ISH1.25, ISH1.5 and ISH1.5T, respectively. Higher values of curvature were observed at the top and bottom of the column due to the double curvature deformation. Slightly higher curvatures were measured at the base of the column compared to the curvature measured at the top of the column due to the head rotation.

5.10. Flexural and Bond Slip Deformation

The curvature profiles were used to calculate the flexural deformation by integrating the curvature using the moment-area method. The curvatures were assumed to be constant over the gauge length. A straight line connecting the curvatures measured at 508 mm (20 in) above the top of the footing and 508 mm (20 in) below the bottom of the head was assumed because no instruments were placed between those locations. Figure 5-149 shows the moment area method and the constant curvature profile. The flexural deformation was calculated only for the peak values of lateral force that correspond to the predominant direction of motion. Figures 5-150, 5-151, 5-152 and 5-153 show the lateral force versus flexural deformation for specimens ISH1.0, ISH1.25,

ISH1.5 and ISH1.5T, respectively. Additional rotation due to the bond slip at the base and top is recorded by the curvature instruments. Therefore, the flexural deformation calculated by these instruments includes a component from the bond slip effect that can not be uncoupled.

5.11. Panel Zone Deformations

The total displacement at the panel configuration nodes was calculated using the relative deformation from the Novotecknik transducers and a kinematic matrix [A] (Mc Guire et al[18]). This procedure was used before by Laplace et al[15]. The kinematic matrix relates the relative deformation $\{\delta\}$ and the total displacement at each node of the panel zone $\{\Delta\}$ as follows:

$$\{\delta\} = [A]\{\Delta\} \qquad [5\text{-}1]$$

Where

$\{\delta\}$= vector of the relative deformation from the Novotecknik transducers
$[A]$ = kinematic matrix
$\{\Delta\}$ = vector of total displacement at each node (Figure 5-154)

The total displacement can be solved as follows:

$$\{\Delta\} = [A]^{-1}\{\delta\} \qquad [5\text{-}2]$$

Fifteen and sixteen row were used in $\{\delta\}$ and $\{\Delta\}$, respectively for all the specimens. The number of rows in $\{\delta\}$ and $\{\Delta\}$ represents the number of Novotecknik transducers used panel configuration and the total vertical and horizontal displacement component at each panel node (Fig. 5-154), respectively.

The total displacement was solved at every time steep for all the data. A Matlab subroutine developed by Laplace et al[15] was used to solve the total displacement using the corresponding kinematic matrix. Tables 5-36, 5-37, 5-38, and 5-39 present a comparison between the deflections at the top panel nodes using Eq. 5-2 and the deflection measured with the displacement transducer located at the bottom of the head for the predominant direction of motion. A good correlation was found between the panel zone deflections and the displacement transducer located at the bottom of the head. Laplace et al[15] also reported a good agreement between the panel zone deflections and the displacement transducer. It confirms the accuracy of the panel zone instruments to measure deformation at the panel nodes.

5.12. Shear Deformation

The flexural deformation at the top of each panel was calculated using the moment area method with average curvature described in Section 5.10. This deformation was subtracted from the corresponding total node panel deformation to obtain the shear deformation at the top of each panel. The shear deformation of individual panels was

calculated as the difference between the average shear deformation of the top nodes and the subsequent nodes. For the lowest panel, the shear deformation was taken as the average shear deformation of the top nodes. Shear deformation was computed only for the predominant direction of motion. Tables 5-40, 5-41, 5-42 and 5-43 present the shear deformation for individual panels in percentage of the total shear deformation measured at the top of the column for ISH1.0, ISH1.25, ISH1.5 and ISH1.5T, respectively. On average, 60% to 70% of the total shear deformation comes from panels 1 and 4 located at the plastic hinge zones of the column. Shear deformation in panels 1 and 4 tend to increase compared with the other two panels in the last five runs. The lateral force versus shear deformation for specimens ISH1.0, ISH1.25, ISH1.5 and ISH1.5T are shown in Figures 5-155, 5-156, 5-157 and 5-158 respectively. A bilinear behavior is observed for the lateral force and the shear deformation, in all the specimens. Tables 5-44, 5-45, 5-46 and 5-47 present the combined flexural and bond slip deformation as percentage of the total deformation at the top of the columns. Shear deformation in specimen ISH1.0 was approximately 40% of the total deformation in the first five motions and 19% to 25% of the total deformation for the last five motions. Shear deformation between 16% to 24%, 13% to 18% and 32% to 37% of the total deformation was measured in specimens ISH1.25, ISH1.5 and ISH1.5T, respectively.

5.13. Measured Strains

Strain gauges were placed at the potential plastic hinge regions for longitudinal steel whereas the strain gauges for the transverse steel they were located through the entire height of the column. The maximum and minimum strains measured in the longitudinal bars are presented in Tables 5-48 through 5-52 for specimen ISH1.0, in Tables 5-53 through 5-57 for specimen ISH1.25, in Tables 5-58 through 5-61 for specimen ISH1.5 and in Tables 5-62 through 5-65 for specimen ISH1.5T. Positive strains indicated tension. The yield strain for the longitudinal bars was 2,207 microstrains for specimens ISH1.0 and ISH1.5 and 2,172 microstrains for specimens ISH1.25 and ISH1.5T. This strain was calculated based on the yield stress reported in Section 3.3 and a modulus of elasticity of 200 MPa (29000 Ksi). Tensile strain penetration was measured in the strain gauges located in to the footing and column head. The yield strain was reached during 0.75xSylmar for ISH1.0 and ISH1.25 and during 0.6xSylmar for ISH1.5 and ISH1.5T for strain gauges located in the footing and during 1.0xSylmar for ISH1.0 and ISH1.5 and during 1.25xSylmar for ISH1.25 and ISH1.5T for strain gauges located in the head. The first yielding of the longitudinal bars was at 0.75xSylmar, 0.5xSylmar, 0.40xSylmar and 0.60xSylmar for specimens ISH1.0, ISH1.25, ISH1.5 and ISH1.5T, respectively. This first yielding was measured in strain gauges #5 and #6 between the base of the column and 127 mm (5 in) above the footing. Strain gauges #3 and #4 measured strain in the longitudinal interlocking bars in all specimens. The longitudinal interlocking bars yielded at 1.0xSylmar in all the specimens in the vicinity of the base of the column. The strain profile for the strain gauge #6 in the predominant direction of motion is presented in the Figures 5-159, 5-160, 5-161 and 5-162 for ISH1.0, ISH1.25, ISH1.5 and ISH1.5T, respectively. Same levels of strains were measured at or near the base and top of the column in specimens ISH1.0 and ISH1.25.

For specimens ISH1.5 and ISH.15T higher strain were measured at the base of the column compared to the strain measured at the top of the column. The strain profiles are in agreement with the moment demand and curvature reported in Section 5.7 and 5.9. A decrease in strain for ISH1.25 and ISH1.5 was measured at 127 mm (5 in) above the base of the column and the base of the column, respectively. This reduction of the strain was measured after the spalling of concrete in ISH1.0 and after the longitudinal bar was visible in ISH1.5. A localize damage, such as spalling of concrete and exposure of longitudinal bar, that coincide with the location of specific gauges can affect their measurements and cause reduction of strain.

Tables 5-66 through 5-70, Tables 5-71 through 5-75, Tables 5-76 through 5-79 and Tables 5-80 through 5-84 show the maximum and minimum strains measured in the spirals for specimens ISH1.0, ISH1.25, ISH1.5 and ISH1.5T, respectively. A positive strain indicates tension. The spirals yield strain of 2,172 microstrains was calculated based on the yield stress reported in Table 3-4 and a modulus of elasticity of 200 MPa (29000 Ksi). The spirals in specimen ISH1.0 did not yield until the last motion. Strain gauge # 2 at 178 mm (7 in) (Table 5-71) and strain gauges # 8 and # 9 at 1422 mm (56 in) (Table 5-75) reached yield at 2.125xSylmar in specimen ISH1.25. The yield strain is reached in strain gauge # 1 at 1.0xSylmar (Table 5-79) in specimen ISH1.5. For specimen ISH1.5T yield strain was reached in strain gauge # 1 at 178 mm (7 in) (Table 5-80) and in strain gauge # 10 at 1753 mm (69in) (Table 5-84) at 2.125xSylmar. The average maximum spiral strain for gauges # 2 and # 5 for specimens ISH1.0 and ISH1.5 and gauges # 2 and # 9 for specimens ISH1.25 and ISH1.5T was plotted again displacement ductility in Fig. 5-163. This figure shows average strains below yielding in most of the locations for all the specimens. In addition this figure shows slightly smaller strains in ISH1.0 compare to the rest of the specimens until the last motion. The average maximum spiral strains in ISH1.25 and ISH1.5T were nearly the same level of strain and the average maximum spiral strain in ISH1.5 was the highest until displacement ductility of about 1.6.

Table 5-85 shows the maximum and minimum strains measured in the cross ties of the specimen ISH1.5T. The yield strain was reached at 1.75xSylmar in gauge # 1 at 1391mm (54.75 in) and at 1562 mm (61.5 in). Strains below yielding were measured in most of the locations along the height of the column.

5.14. Idealized Force-Displacement Relationship

The measured envelopes (Figures 5-92, 5-106, 5-121 and 5-138) were idealized by elasto-plastic curves to quantify the ductility capacity of the specimens. The same three methods described in Chapter 4.12 were used to find the force-displacement point (F_{y1}, D_{y1}) that defines the elastic portion of the idealized curve. The failure was assumed either by the peak displacement with the corresponding force or 80 percent of the maximum force with the corresponding displacement when the force for the peak displacement dropped more than 20 percent of the maximum force at failure.

Tables 5-86, 5-87, 5-88 and 5-89 show a comparison of the idealized force-displacement values obtained using the three methods for specimens ISH1.0, ISH1.25, ISH1.5 and ISH1.5T, respectively. A variation of 3 % to 7 % of the displacement ductility capacity was found among the methods for specimens ISH1.0, ISH1.25 and ISH1.5T. A difference of 250 % was found between first method and the other two methods in specimen ISH1.5. This is because the force-displacement point (F_{y1}, D_{y1}) is not on the measured curve. The second method was selected to idealize of the measured curve since strain data are available and the force-displacement point (F_{y1}, D_{y1}) needs to be on the measured curve. Figure 5-164, 5-165, 5-166 and 5-167 present the elasto-plastic idealization of the response in the predominant direction of motion for ISH1.0, ISH1.25, ISH1.5 and ISH1.5T, respectively.

5.15. Plastic Hinge Length

Two different plastic hinge lengths, at the top and bottom of the column, were developed in the specimens due to the double curvature deformation. The measured plastic hinge lengths could not be calculated using Equation 4-6 defined in Chapter 4.13 because the corresponding ultimate deformation of the column, $\Delta_{u,}$ and idealized effective yield displacement, $\Delta_{y,}$ for the top and bottom plastic hinge length were not measured independently. Equation 5.1 was used in specimens with high shear to calculate the plastic hinge lengths.

$$l_p = -\frac{1}{2}\frac{\left(-\phi_p L + \left(\phi_p\left(\phi_p L^2 - 4\Delta_p\right)\right)^{\frac{1}{2}}\right)}{\phi_p} \qquad (5\text{-}1)$$

Where

ϕ_P = average measured plastic curvature capacity at top and bottom of the column

$= \phi_{u_{avg}} - \phi_{y_{avg}}$

$\phi_{u_{avg}}$ = average measured ultimate curvature at top and bottom of the column

$= \dfrac{\phi_{u_{TOP}} + \phi_{u_{BOT}}}{2}$

$\phi_{y_{avg}}$ = average measured yield curvature at top and bottom of the column

$= \dfrac{\phi_{y_{TOP}} + \phi_{y_{BOT}}}{2}$

$\phi_{u_{TOP}}$ = measured ultimate curvature capacity at the top of the column

$\phi_{u_{BOT}}$ = measured ultimate curvature capacity at the bottom of the column

$\phi_{y_{TOP}}$ = measured idealized yield curvature capacity at the top of the column

$\phi_{y_{BOT}}$ = measured idealized yield curvature capacity at the bottom of the column

Δ_p = measured plastic displacement of the column = Δ_u - Δ_y

Equation 5-1 assumes that l_p is the same at top and bottom of the column. The curvature over a 254 mm (10 in) rather than 127 mm (5 in) gauge length was used for top and bottom of the column. The 254 mm (10 in) gauge length was used because most of plastic deformation was concentrated over that region according to the measured curvature and strain values. The elasto-plastic idealization for the average measured moment-curvature over the first and last 254 mm (10 in) of the column height was used to find the values of the yield and ultimate curvature capacities at top and bottom of the column. Table 5-90 summarizes the values used in Eq. 5-1 to determine the measured l_p for specimens with high shear. The values of l_p of 0.98, 0.96, 1.12 and 1.27 times the total depth of the column were found based on Eq. 5-1 for specimens ISH1.0, ISH1.25, ISH1.5 and ISH1.5T, respectively.

Chapter 6. Analysis of Specimens

6.1. Introduction

Detailed analyses of the specimens with low and high shear were performed to evaluate the adequacy of analytical models in estimating the lateral load carrying capacity and displacements. Strain rate effect on the material properties of the specimens was taken into account in the calculation of analytical lateral load and displacements. Cross sectional properties were determined using SPMC[34]. A comparison between SPMC[34] and xSECTION[28] was done since the program xSECTION[28] is used by Caltrans as a design tool. A theoretical plastic hinge length, calculated using different methods, was compared with the measured plastic hinge. Shear and bond slip deflections were added to the flexural deflection to obtain the total deformation. Push over analysis was performed with SAP 2000[10] using the section properties from SPMC[34] and including the effect of the bond slip and shear deformations in the section properties. A comparison of the push over analysis results was done between SAP 2000[10] and wFRAME[27]. wFRAME[27] is a 2-D push over analysis program used by Caltrans's engineers to perform seismic analysis in bridge frames and bridge bents.

Caltrans[7], Tanaka and Park[30] and Benzoni et al.[4] shear equations were used to calculate the shear capacity, and each was compared to the measured results. Shear stiffness was calculated based on the equation developed by Park and Paulay[22] and was compared with the measured shear stiffness. The effects of the interlocking spiral distance and the shear stress are discussed based on the performance of the specimens.

6.2. Strain Rate Effect on Material Properties

Stress-strain properties of the concrete and steel are determined by slow monotonic tests. High rate of loading such as earthquake ground motions can affect the properties of the materials. High strain rate increases the yield strength of steel and the compressive capacity of concrete. Kulkami and Shah[14] studied the effect of the high strain rate based on monotonic tests of reinforced beams conducted at high loading rates. According to Kulkami and Shah[14] the yield strength of the steel due to the effect of the strain rate is increasing by the following factors:

$$R_s = 0.0328Ln(x) + 0.9973 \qquad \text{[for 310 MPA (45 ksi) steel]} \qquad (6\text{-}1)$$

$$R_s = 0.0124Ln(x) + 0.9632 \qquad \text{[for 520 MPA (75.4 ksi) steel]} \qquad (6\text{-}2)$$

Where

x= relative strain rate, dynamic strain rate / quasi_static strain rate

Kulkami and Shah[14] also recommended the following factor for increase in concrete compression strength due to the effect of the strain rate

$$R_c = 0.022Ln(x) + 0.9973 \qquad (6\text{-}3)$$

There are no reported studies of strain rate effect under cyclic dynamic loading. Therefore, Equations 6-1, 6-2 and 6-3 were used to calculate the effect of the strain rate on the yield strength of steel and concrete compression strength. The measured strain rate in the specimens was determined as follows

$$\dot{\varepsilon} = \frac{\varepsilon_{i+1} - \varepsilon_i}{\Delta t} \tag{6-4}$$

Where

$\dot{\varepsilon}$ = measured strain rate
ε_i = measured strain at time i^{th}
Δt = time step

Since strain rate increases the yield strength of the steel, the motion at which the extreme longitudinal bars yielded was used to study the strain rate effect. A typical strain rate history is shown in Fig. 6-1. Strain rate versus strain is plotted in Fig. 6-2. According to Figs. 6-1 and 6-2 the measured strain rate varies with time and strain. Taking into account that the Eqs. 6-1 and 6-2 were developed for a constant strain rate, a procedure to find the strain rate at the yield strength of steel was developed. Hence, the strain rate used to calculate the strain rate effect (Eqs. 6-1 and 6-2) was taken as the strain rate corresponding to the strain immediately after the static yield strain was reached. Strain rate was calculated for strain gauges placed on three extreme longitudinal bars located at the base on the column and 127 mm (5 in) above of the base for specimens with low shear. Only two extreme longitudinal bars were instrumented with strain gauges in specimens with high shear. In order to have the same number of data points for specimens with low shear, strain gauges at 254 mm (10 in) were also used to calculate the strain rate in specimens with high shear. An approximate quasi-static strain rate of 100με was calculated for concrete by dividing the displacement rate by the length of the concrete cylinders. An average quasi-static strain rate for the steel of 612 με was measured in static testing of the sample longitudinal bars.

Tables 6-1 through 6-6 show the strain values with the corresponding strain rate and the relative increasing in yield strength of steel for all specimens. The measured yield strength of the longitudinal bars for each specimen was reported in Table 3-3. The relative increase in the yield strength was found using linear interpolation between the values obtained from Equations 6-1 and 6-2. An average increasing of 5% and 8 % was used for the yield stress of the longitudinal reinforcement for specimen ISL1.0 and ISL1.5, respectively. Based on the average increase of the yield stress of the longitudinal reinforcement (Tables 6-3 through 6-6), 5% increase for ISH1.0, 4% increase for ISH1.25, 5% increase for ISH1.5, and 6 % increase for ISH1.5T was used for the yield stress of the longitudinal reinforcement.

The extreme longitudinal bars yielded in compression were used to study the strain rate effect in the concrete. The motion at which the extreme longitudinal bars yield

in compression was used to study the strain rate effect since the yield strain of the steel corresponds to the similar level of strain of the peak concrete compression stress. The same procedure used to find the strain rate at the yield strength of steel was used. Tables 6-7 through 6-12 show the strain values with the corresponding strain rate and the relative increase in concrete compression strength for all specimens. A 14 % of the average increase of the concrete compression strength was used for ISL1.0 and ISL1.5. Based on the average increasing of the concrete compression strength (Tables 6-9 through 6-12), 8% increase for ISH1.0, 9% increase for ISH1.5 and 12 % increase for ISH1.25 and ISH1.5T was used for the concrete compression strength.

6.3. Moment Curvature Analysis

Program SPMC[34] was used to perform moment curvature analysis of the specimens. The measured yield stress of the longitudinal reinforcement and the measured concrete compression strength described in Section 3.3 were increased due to the strain rate effect described in the previous section. The yield stress and concrete compression strength used in SPMC[34] are shown in Table 6-13. The average value of the measured axial load described in Sections 4.5 and 5.5 were used in the M-ϕ analysis for specimens with low and high shear, respectively. SPMC[34] input and parameters were discussed in Section 2.13.1. Elasto-plastic idealizations of the M-ϕ curves were done by equalizing the areas under each curve. The effect on the idealized moment curvature properties with and without strain rate effect is shown in Tables 6-14 and 6-15 for specimens with low and high shear, respectively. The difference in the idealized moment due to strain rate effect ranges from 6% to 7% for all specimens. The difference in the idealized yield curvature ranges between 3% and 4% while the ultimate curvature varies from 3% to 6%.

A comparison between SPMC[34] and xSECTION[28] was done since the program xSECTION[28] is used by Caltrans as a design tool. Mander et al.[14] model was used to model the confined concrete stress-strain relationship. The simple model, described in user's manual for xSECTION[28], was used for unconfined concrete stress-strain relationship. Park's model[22] was used for steel stress-strain relationship in xSECTION[28]. Four sub-section, two polygonal and two arc strips, were used to establish the concrete geometry in xSECTION[28]. In addition, reinforcing bars were laid out using single schemes option. The same material properties used in SPMC[34] were also used in xSECTION[28]. Figures 6-3 through 6-8 present the calculated and idealized M-ϕ curves using SPMC[34] and xSECTION[28] for all specimens. Tables 6-16 and 6-17 show a comparison of the moment curvature properties for the specimens with low and high shear using SPMC[34] and xSECTION[28]. Differences between 5% and 7% were found between the idealized plastic moment using SPMC[34] and xSECTION[28]. The difference in the idealized yield curvature ranged between 2% and 7% while the ultimate curvature varied from 6% to 20%. The difference in the concrete and steel model, concrete geometry as well as the failure criteria used in SPMC[34] and xSECTION[28] can produce slight differences in the M-ϕ results. In general, these differences are acceptable considering the level of approximation in other steps of the structural analysis.

6.4. Plastic Hinge Length

The equivalent length of a structural member at which the plastic curvature is assumed constant for estimating plastic rotation is called plastic hinge length, l_p. Different empirical equations of plastic hinge length have been proposed. Four empirical formulas for plastic hinge length were compared to the measured plastic hinge length. The measured material properties modified by the strain rate effect were used to determine the plastic hinge length.

The expression developed by Paulay and Priestley[22] defined the plastic hinge length as follows

$$l_p = 0.08L + 0.022\, f_y\, d_{bl} \quad \text{(MPa)} \tag{6-5a}$$

$$l_p = 0.08L + 0.15\, f_y\, d_{bl} \quad \text{(ksi)} \tag{6-5b}$$

Where

L = distance from the point of maximum moment to the point of contra-flexure
d_b = diameter of longitudinal reinforcement
f_y = yield strength of the longitudinal reinforcement

Baker's[3] expression for member confined by transversal steel is defined as follows

$$l_p = 0.8 k_1 k_3 \left(\frac{z}{d}\right) c \tag{6-6}$$

Where

c = neutral axis depth at the ultimate moment
k_1 = 0.7 for mild steel and 0.9 for cold-work steel
k_3 = 0.6 for f'_c = 35.2 MPa (5100 psi) or 0.9 for f'_c = 11.7 MPa (1700 psi)
z = distance of critical section to the point of contra-flexure
d = effective depth of the member

According to Caltrans, SDC[7] Section 7.6.3, Paulay and Priestley[23] expression is used but is limited as follows

$$l_p = 0.08L + 0.022\, f_y\, d_{bl} \geq 0.044\, f_{ye}\, d_{bl} \quad \text{(MPa)} \tag{6-7a}$$

$$l_p = 0.08L + 0.15\, f_y\, d_{bl} \geq 0.3\, f_{ye}\, d_{bl} \quad \text{(ksi)} \tag{6-8b}$$

Dowell and Hines[11] derived an expression for the plastic hinge length that included the aspect ratio, axial load ratio and the longitudinal and transversal steel ratio. According to Dowell and Hines[11] the plastic hinge length is defined as follows:

$$l_p = \frac{\mu L}{2} + w \tan\theta \left(1 - \frac{\eta}{2}\right) + \frac{w^2 \tan^2\theta}{\mu L}\left(\frac{\eta^2}{8} - \frac{\eta}{6}\right) \tag{6-9}$$

Where

μ = over-strength ratio = $1 - \frac{M_n}{M_u}$

M_n = idealized yield moment capacity

M_u = ultimate moment capacity

L = cantilever length (distance from the point of maximum moment to the point of contra-flexure)

w = column depth

$\eta = \frac{V_s}{V_u}$

V_s = shear resisted by transversal steel

V_u = applied shear force

θ = shear crack angle

According to Dowell and Hines[11] the first term in Equation 6-9 is the over-strength ratio, the second term is associated with constant tension shift and the third term reduces the constant tension shift due to the flattening shear cracks near the critical section.

A 45° shear crack angle was selected based on the inclination of the shear cracks observed in the test specimens. Caltrans[7], Tanaka and Park[30] and Benzoni et al.[4] shear equations, described in Section 6.6.1, were used to calculate the shear resisted by transverse steel.

The measured plastic hinge length was reported in Sections 4.13 and 5.15. The calculated and measured plastic hinge lengths, as a fraction of column depth are given in Table 6-18. Larger values of l_p, especially for specimen with high shear, are obtained using Dowell and Hines's[11] equation compare to the other three equations. Differences of 25% to 36% were found between the Dowell and Hines's[11] equation using Caltrans[7] shear equation and the measured l_p for specimens with low shear. For specimens with high shear, differences of 8% to 37% were found between the Dowell and Hines's[11] equation using Benzoni's[4] shear equation and the measured l_p. All the empirical formulas for plastic hinge length underestimate the measured plastic hinge length. The Dowell and Hines's[11] l_p equation using Benzoni's[4] shear equation was used in the analysis because its average difference (27%) between the calculated and measured l_p was the smallest.

6.5. Load-Deflection Analysis of ISL1.0 and ISL1.5

The total deflection including flexural, bond slip, and shear deformations were determined using hand calculations. A comparison between the push over analysis performed in SAP 2000[10] and wFRAME[27] was done based on the section properties from SPMC[34] and including the effect of the bond slip and shear deformations. A comparison of the experimental and the analytical force-displacement curves are presented in this section.

6.5.1. Total Deflection

The total deflection is calculated as the summation of flexural, shear, and bond slip deformations. Hence, the deformation at yield is calculated as follows:

$$\Delta_y = \Delta_{fy} + \Delta_{bsy} + \Delta_{sy} \tag{6-10}$$

Where

Δ_{fy} = flexural deformation at yield
Δ_{bsy} = bond slip deformation at yield
Δ_{sy} = shear deformation at yield

The ultimate deformation is calculated as the summation of the deformation at yield and the plastic deformation as follows:

$$\Delta_u = \Delta_y + \Delta_p \tag{6-11}$$

The plastic deformation of the cantilever column, with the plastic rotation assumed to be concentrated at midheight of the plastic hinge, is calculated as follows:

$$\Delta_p = \theta_p \left(L - \frac{l_p}{2} \right) \tag{6-12}$$

Where

θ_p = plastic rotation = $(\phi_u - \phi_y) l_p$
l_p = equivalent plastic hinge length
ϕ_u = ultimate curvature capacity
ϕ_y = idealized yield curvature capacity

No additional bond slip and shear deformation are included in the ultimate deformation if the equivalent plastic hinge length includes the effect of these deformations.

6.5.1.1. Deflection due to Flexural

Deflection due to flexural for cantilever column was calculated by using the moment area moment theorem:

$$\Delta_f = \int_0^l \phi(x) x dx \tag{6-13}$$

Where

l = column length
ϕ = measured curvature
x = column height location at the point of curvature measurement

Assuming that the member is cracked and using the Equation 6-13, the flexural deformation at yield can be calculated by the following equation:

$$\Delta_{fy} = \frac{1}{3}\phi_{fy} l^2 \tag{6-14}$$

Where

ϕ_{fy} = idealized yield curvature due to flexure

The idealized moment curvature properties from SPMC[34] including the strain rate effect were used to calculate the flexural deformation at yield and the plastic deformation. Flexural deformations at yield of 10 mm (0.40 in) for ISL1.0 and 13 mm (0.52 in) for ISL1.5 were found using Equation 6-14. Plastic deformation of 36 mm (1.43 in) and 42 mm (1.66 in) were found for specimens ISL1.0 and ISL1.5, respectively.

6.5.1.2.Deflection due to Bond Slip

The Wehbe's Method[35] was used to calculated bond slip deformation. Wehbe's Method[35] established that the bond slip deflection is equal to the product of the bond slip rotation at the base of the column and the length of the element as follows:

$$\Delta_{bs} = \theta_{bs} L \tag{6-15}$$

Where

θ_{bs} = rotation due to bond slip

L = length of the element

The rotation due to bond slip is associated with the elongation of the tensile bar within the support that is revealed at the base or top of the column as a concentrated rotation and is assumed to occur about the neutral axis of the column cross section. The rotation due to bond slip can be calculated as follows

$$\theta_{bs} = \frac{\delta l}{d - c} \tag{6-16}$$

Where

d = effective section depth

c = distance form the extreme compression fiber to the neutral axis

δl = additional elongation of the longitudinal outermost bar, defined as follows

When the calculated steel strain, ε_s, is less or equal to yield strain, ε_y, δl is calculated as:

$$\delta l = \frac{d_b f_s^{\,2}}{315 E_s u} \quad \text{(MPa)} \tag{6-17a}$$

$$\delta l = \frac{d_b f_s^{\,2}}{8 E_s u} \quad \text{(psi)} \tag{6-17b}$$

The yield and hardening strains are assumed to be the same. When the calculated steel strain, $\varepsilon_{s,}$ is greater than yield strain, ε_y, δl is calculated as

$$\delta l = \frac{d_b}{315u}\left(\varepsilon_s f_s - \varepsilon_s f_y + \varepsilon_y f_s\right) \text{ (MPa)} \tag{6-18a}$$

$$\delta l = \frac{d_b}{8u}\left(\varepsilon_s f_s - \varepsilon_s f_y + \varepsilon_y f_s\right) \text{ (psi)} \tag{6-18b}$$

Where

d_b = bar diameter
f_s = stress in longitudinal reinforcement
E_s = elastic modulus of steel
ε_s = calculated steel strain
ε_y = yield steel strain
f_y = yield steel stress

$$u = \frac{9.5\sqrt{f_c'}}{d_b} \le 5.5 \text{ (MPa)} \tag{6-19a}$$

$$u = \frac{5.5\sqrt{f_c'}}{d_b} \le 800 \text{ (psi)} \tag{6-19b}$$

The strain at the outermost bar as well as the distance of the neutral axis was obtained from the output of SPMC[34] including the strain rate effect included. Since the idealized M-ϕ equivalent yield point is not on the calculated M-ϕ curve, the bond slip deformations at the equivalent yield point is calculated as follows

$$\Delta_{ybs} = \frac{\Delta_{y1bs}}{M_{y1}} M_y \tag{6-20}$$

Where

Δ_{ybd} = bond slip deformation at the equivalent yield point
Δ_{y1bd} = bond slip deformation at the first reinforcement bar yield
M_{y1} = moment at the first reinforcement bar yield

Bond slip deformations at yield of 2.2 mm (0.086 in) and 2.3 mm (0.091 in) were found for specimens ISL1.0 and ISL1.5, respectively.

6.5.1.3.Deflection due to Shear

Park and Paulay[22] developed expressions for the shear stiffness of uncracked and cracked reinforced concrete members. The shear stiffness for uncracked members was developed for normal weight concrete and μ, Poisson's ratio of approximately 0.16 to 0.30. Based on the principles of elasticity, the shear stiffness for uncracked member is defined as follows:

$$K'_v = \frac{0.4E_c b_w d}{f} \tag{6-21}$$

Where

K'_v = shear stiffness for uncracked members of a unit length

E_c = elastic modulus of concrete = $4733\sqrt{f'_c}\,(MPa)$ $57000\sqrt{f'_c}\,(psi)$

b_w = section width perpendicular to the applied shear

d = effective section depth parallel to applied shear

f = non-uniform shear stress factor = 1.2 for rectangular section or 1.0 for T and I sections.

The cracked shear stiffness of reinforced concrete member with 45° diagonal cracks, based on the truss action principles, is given by

$$K_{v,45} = \frac{\rho_v}{1+4n\rho_v} E_s b_w d \tag{6-22}$$

Where

$K_{v,45}$ = shear stiffness for cracked member of a unit length

n = modular ratio = $\frac{E_s}{E_c}$

E_s = elastic modulus of the steel reinforcement

ρ_v = shear reinforcement ratio = $\frac{A_v}{sb_w}$

A_v = area of shear reinforcement

s = spacing of shear reinforcement

The expressions of uncracked and cracked shear stiffness were developed for a rectangular, I or T section. Since the specimens have an oval shape, an equivalent rectangular section was assumed. Hence, an equivalent section width, b_{ew}, equal to the cross sectional area divide by total depth was calculated. Uncracked shear stiffness of 1.12×10^6 kN/m x m (2.51×10^5 Kip/in x in) and 1.34×10^6 kN/m x m (3.0×10^5 Kip/in x in) were found for specimens ISL1.0 and ISL1.5, respectively. Cracked shear stiffness of 1.08×10^5 kN/m x m (2.42×10^4Kip/in x in) for ISL1.0 and 1.26×10^5 kN/m x m (2.84×10^4Kip/in x in) for ISL1.5 were found using Equation 6-22. Park and Paulay[21] indicated that the shear stiffness of a diagonal cracked member is approximately 0.1 to

0.3 times the shear stiffness of the uncracked member. Ratio of the cracked and the uncracked shear stiffness was 0.097 and 0.95 for the ISL1.0 and ISL1.5 respectively.

Once the shear stiffness per unit length is calculated, the deflection due to shear on the cracked section is determined as follows

$$\Delta_s = \frac{VL}{K_{v,45}} \tag{6-23}$$

Where

V = applied shear force
L = length of the member

Deflection due to shear at yield of 2.2 mm (0.098 in) and 2.7 mm (0.11 in) were calculated for specimens ISL1.0 and ISL1.5, respectively.

6.5.1.4.Comparison of Analytical and Experimental Results

Figures 6-9 and 6-10 show a comparison between analytical and idealized measured flexural (including bond slip deformation) for specimens ISL1.0 and ISL1.5, respectively. The analytical results underestimated by 13% and overestimated by 15% the combined flexural and bond slip deformation at yield for ISL1.0 and ISL1.5, respectively. According to Wehbe's Method[35], the bond slip contributes 18% and 15% of the summation of flexural and bond slip deformations for specimen ISL1.0 and ISL1.5, respectively.

A comparison of the analytical force-displacement curve with flexural deformation only and the experimental results are shown in Figures 6-11 and 6-12 for ISL1.0 and ISL1.5, respectively. A difference of 39% and 27% was found between the analytical and the experimental yield deformations for ISL1.0 and ISL1.5, respectively. The analytical force-displacement curve including the bond slip and shear deformations are also shown in the figures. A better agreement was found between the experimental results and the analytical results for the yield deformations with a difference of 13% and 1% for ISL1.0 and ISL1.5, respectively. No significant improvement was achieved in the ultimate displacement when the bond slip and shear were included at yield. A difference between experimental and analytical ultimate displacement of 70% for ISL1.0 and 66% for ISL1.5 was obtained when bond slip and shear deformation were included. The analytical lateral load capacity overestimated the experimental load by 0.4 % and 10 % when the strain rate effect is included.

6.5.2. Push Over Analysis

A push over analysis was performed using SAP 2000[10] based on the sectional properties from SPMC[34] and including the effect of the bond slip and shear deformations. A beam element with a plastic hinge (lump plasticity) at the bottom of the column was

selected to model the specimens. The column bases were modeled as a fixed support. The average value of the measured axial load described in Sections 4.5 was applied as an initial load before the lateral loading.

The moment of inertia about the bending axes for the beam element was modified in order to take into account the effect of cracking, bond slip deformation and shear deformation at yield as follows:

$$I_e = \frac{M_y L^2}{3E_c \Delta_y} \tag{6-24}$$

Where

M_y = idealized yield moment capacity from M-ϕ analysis

L = length of the member

E_c = elastic modulus of concrete = $4733\sqrt{f'_c}\,(MPa)$ $57000\sqrt{f'_c}\,(psi)$

Δ_y = yield displacement including bond slip and shear deformations

A moment of the inertia about the bending axes of 38641 cm^4 (928 in^4) and 67863 cm^4 (1630 in^4) was used in the section properties for ISL1.0 and ISL1.5, respectively.

The hinge properties used in SAP 2000[10] are presented in Table 6-19. The idealized yield and ultimate moment were found using SPMC[34] program and include the strain rate effect. The yield rotation was calculated as follows

$$\theta_y = \frac{M_y L}{2E_c I_e} \tag{6-25}$$

The ultimate rotation was calculated as the yield rotation plus the plastic rotation, described in Equation 6-12.

Program wFRAME[27] was also used to perform push over analysis. Two spans, one column and one pile need to be defined to perform an analysis. The two spans are used to apply the axial load and the pile is used to provide the boundary conditions at the base. The same material properties used in SAP 2000[10] were also used in wFRAME[27]. Equation 6-24 was used to calculate the moment of inertia about the bending axis. The idealized yield moment capacity from SPMC[34] analysis was used as the plastic moment capacity in wFRAME[27]. The base was modeled as a fixed support. The average values of the measured axial load described in Sections 4.5 were applied as an initial load before the lateral loading.

Figures 6-13 and 6-14 show the experimental, SAP 2000[10] and wFRAME[27] force-displacement curves for specimen ISL1.0 and ISL1.5, respectively. The experimental lateral load capacity differs in 0.4% using SAP 2000[10] and in 1.2% using wFRAME[27] for ISL1.0. A difference of 10% was found between the experimental and analytical lateral load capacity using SAP 2000[10] and wFRAME[27] for ISL1.5. The

experimental yield displacement differs by 2% using SAP 2000[10] and by 2.5% using wFRAME[27] for ISL1.0 and by 1% using SAP 2000[10] and by 1.5% using wFRAME[27] for ISL1.5. The measured ultimate displacement was 320% and 280% more than the ultimate displacement from SAP 2000[10], for specimens ISL1.0 and ISL1.5, respectively. The wFRAME[27] stops once the potential failure mechanism is formed. Therefore, no plastic deformation is reported.

6.6. Load-Deflection Analysis of ISH1.0, ISH1.25, ISH1.5 and ISH1.5T

The experimental force-displacement curves and the analytical results, including flexural, bond slip and shear deformations were compared in this section. The push over analysis performed in SAP 2000[10] and wFRAME[27] was compared based on the sectional properties from SPMC[34] and including the effect of the bond slip, shear deformations, and head rotation. The shear capacity was calculated according to three different methods and they were compared to the experimental results. Park and Paulay[22] and Priestley et. al.[24] expressions for the shear stiffness were used to compare with the experimental results.

6.6.1. Total Deformation

The total deflection is calculated as the summation of flexural, shear and bond slip deformations. The column is assumed to bend in double curvature with rotationally rigid ends for analytical calculations. Therefore, an equivalent cantilever column with a length equal to half of the clear height of the column was used to calculate the deformations. The deformation obtained from the cantilever column was multiplied by two to find the deformation for the double curvature column.

6.6.1.1. Deflection due to Flexural

Equation 6-13 was used to calculate the deflection due to flexure. The idealized moment curvature properties, from SPMC[34] including the strain rate effect, were used to calculate the flexural deformation at yield and the plastic deformation. Flexural deformations at yield of 5.8 mm (0.23 in), 6.1 mm (0.24 in), 7.2 mm (0.28 in), and 6.9 mm (0.27 in) were calculated for ISH1.0, ISH1.25, ISH1.5 and ISH1.5T, respectively. Equation 6-12 was used to calculate plastic deformations of 32 mm (1.24 in), 38 mm (1.49 in), 45 mm (1.78 in) and 41 mm (1.62 in) in ISH1.0, ISH1.25, ISH1.5 and ISH1.5T, respectively.

6.6.1.2. Deflection due to Bond Slip

The Wehbe's Method[35] was used to calculated bond slip deformation. Equations 6-15 through 6-20 and the output of SPMC[34] with the strain rate effect were used to calculate bond slip deformation at the idealized equivalent yielding. Bond slip deformations at yield of 2.36 mm (0.093 in), 2.23 mm (0.088 in), 2.49 mm (0.098 in),

and 2.30 mm (0.090 in) were found for specimens ISH1.0, ISH1.25, ISH1.5 and ISH1.5T, respectively.

6.6.1.3. Deflection due to Shear

Equations 6-22 and 6-23 were used to calculate the cracked shear stiffness of reinforced concrete member and the shear deformation. Deflection due to shear at yield of 7.6 mm (0.30 in), 5.9 mm (0.23 in), 6.2 mm (0.24 in), and 6.6 mm (0.26 in) were calculated for specimens ISH1.0, ISH1.25, ISH1.5 and ISH1.5T, respectively.

6.6.1.4.Comparison of Analytical and Experimental Results

Figures 6-15 through 6-18 show a comparison between analytical and idealized measured flexural and bond slip deformations for specimens with high shear. The analytical results underestimated by 25%, 43%, 51% and 48% the flexural and bond slip deformation at yield for ISH1.0, ISH1.25, ISH1.5 and ISH1.5T, respectively. According to Wehbe's Method[35], the bond slip contributes by 29%, 27%, 26%, and 25% of the summation of flexural and bond slip deformations for specimen ISH1.0, ISH1.25, ISH1.5 and ISH1.5T, respectively. The head rotation reported in Section 5.7 affected the correlation between the analytical and experimental results. The effect of the head rotation was included in the push over analysis described in the following section.

A comparison between the analytical force-displacement curve with flexural deformation only and the experimental results is shown in Figures 6-19 through 6-22 for specimens with high shear. A difference of 73%, 71%, 77% and 74% was found between the analytical and the experimental yield deformations for ISH1.0, ISH1.25, ISH1.5 and ISH1.5T, respectively. The analytical force-displacement curve including the bond slip and shear deformations are also show in the figures. An improvement at the yield deformation was found between the experimental and analytical results with a difference of 25%, 32%, 50% and 41% for ISH1.0, ISH1.25, ISH1.5 and ISH1.5T, respectively. No significant improvement was achieved in the ultimate displacement when the bond slip and shear were included at yield. A difference between the experimental and analytical ultimate displacement of 52%, 51%, 52% and 44% was obtained for ISH1.0, ISH1.25, ISH1.5 and ISH1.5T, respectively. The analytical lateral load capacity underestimated the experimental load by 4 % for ISH1.0 and overestimated the experimental load by 8%, 13% and 15% for ISH1.25, ISH1.5 and ISH1.5T, respectively.

6.6.2. Push Over Analysis

A push over analysis was performed using SAP 2000[10] based on the sectional properties from SPMC[34] and including the effect of the bond slip and shear deformations. A beam element with a plastic hinge (lumped plasticity) at the top and bottom of the column was selected to model the specimens. The boundary condition of the base was modeled as a fixed connection. Since some rotation was recorded at the top of the loading head, half of the length of the head was modeled as a beam element with

rotational spring at the end (Fig. 6-27). The rotational stiffness used in the spring element was obtained from a linear regression of the measured moment and rotation recorded at the mid height of loading head. Figure 6-23 through 6-26 show the moment at the mid height of the head versus head rotation with the corresponding linear regression. The rotational stiffness used in the spring element of each specimen is listed in Table 6-20. The average values of the measured axial load described in Section 5.5 was applied as an initial load before the lateral load was applied.

The column moment of inertia about the bending axis for the beam element was modified to take into account the effect of cracking, bond slip deformation and shear deformation at yield as follows:

$$I_e = \frac{M_y L^2}{6 E_c \Delta_y} \tag{6-26}$$

Where

M_y = idealized yield moment capacity from M-ϕ analysis

L = clear length of the column

E_c = elastic modulus of concrete = $4733\sqrt{f'_c}\,(MPa)$ $57000\sqrt{f'_c}\,(psi)$

Δ_y = yield displacement including bond slip and shear deformations

The moment of inertia about the bending axis used in the model of each specimen is listed in Table 6-20.

The hinge properties used in SAP 2000[10] are presented in Table 6-20. The idealized yield and ultimate moment were found using SPMC[34] program and include the strain rate effect. The yield rotation was calculated as follows

$$\theta_y = \frac{\phi_y L}{6} + \theta_{bsy} + \theta_{sy} \tag{6-27}$$

Where

ϕ_y = effective yield curvature

θ_{bsy} = rotation due bond slip at yield

θ_{sy} = rotation due shear at yield (yield shear displacement divided by column height)

The ultimate rotation was calculated as the yield rotation plus the plastic rotation, described in Equation 6-12.

Program wFRAME[27] was also used to perform a push over analysis. Two spans, one column and one pile need to be defined to perform the analysis. The two spans are used to apply the axial load and the ends of the spans are used to define the boundary condition of the superstructure. The pile is used to provide the boundary conditions at the base. The column was divided in two segments. The first segment represents the column

itself and the second segment represents half length of the loading head. The same material properties used in SAP 2000[10] were also used in wFRAME[27]. Equation 6-26 was used to calculate the moment of inertia about the bending axis. The idealized yield moment capacity from SPMC[34] analysis was used as the plastic moment capacity in wFRAME[27]. The boundary condition at the base was modeled as a fixed connection. A rotational spring was connected to the end of one of the spans to model the head rotation effect (Fig. 6-28) but both ends are free to move in the plane. The average values of the measured axial load described in Sections 5.5 was applied as an initial load before lateral loading.

Figures 6-29 through 6-32 show a comparison of the experimental force-displacement curve and the results of the program SAP 2000[10] and wFRAME[27] for specimens with high shear. The force-displacement from SAP 2000[10] shows a trilinear curve that corresponds to the yielding at the bottom of the column followed by the yielding of the top of the column and the plastic deformation until failure of the bottom plastic hinge. The force-displacement curves from wFRAME[27] show a bilinear curve because the program stops once the failure mechanism is formed. Therefore, no plastic deformation is reported. The bilinear curve corresponds to the yielding of the bottom followed by the yielding of the top of the column. A good agreement was found between the results from the programs SAP 2000[10] and wFRAME[27]. A maximum difference between the programs of 3% and 5% was found for the corresponding force and displacement at the yielding of the bottom of the column, respectively. For the yielding of the top of the column maximum differences between the programs of 1% and 5% was found for the corresponding force and displacement, respectively.

The elasto-plastic idealization of the experimental and SAP 2000[10] results are shown in the figures. The equivalent lateral load from SAP 2000[10] overestimated the experimental load. Differences between equivalent lateral loads of the experimental and SAP 2000[10] results were 6%, 7%, 7% and 11% for ISH1.0, ISH1.25, ISH1.5 and ISH1.5T, respectively. Differences between the equivalent yield displacement of the experimental and SAP 2000[10] results were 1%, 11%, 6% and 13% for ISH1.0, ISH1.25, ISH1.5 and ISH1.5T, respectively. The SAP 2000[10] ultimate displacement underestimated by 51%, 37%, 40% and 28% the experimental ultimate displacement for ISH1.0, ISH1.25, ISH1.5 and ISH1.5T, respectively.

6.6.3. Shear Capacity Analysis

Caltrans[7], Tanaka and Park[30] and Benzoni et al.[4] shear equations were used to calculate the shear capacity and the results were compared to experimental results. Caltrans shear capacity for ductile concrete members is defined in Section 3.6.1 in SDC[7] as follows:

$$V_n = V_c + V_s \tag{6-28}$$

Where

V_n = Nominal shear strength

V_c = Nominal shear capacity provided by concrete
V_s = Nominal shear capacity provided by shear reinforcement

According to SDC[7], Section 3.6.2, the concrete shear capacity (V_c) of members designed for ductility shall consider the effects of flexure and axial load as specified in the following equation

$$V_c = \nu_c x A_e \tag{6-29}$$

Where

ν_c = Permissible shear stress carried by concrete defined in the Equations 6-30 and 6-31, for regions inside the plastic hinge zone and outside the plastic hinge zone, respectively. For members whose net axial load is in tension, $\nu_c = 0$.
A_e = Effective shear area = $0.8 x A_g$
A_g = Gross cross section area

ν_c for inside of the plastic hinge can be found according to the following equation

$$\nu_c = F1 x F2 x \sqrt{f'_c} \le 0.33\sqrt{f'_c}\,(MPa) = 4\sqrt{f'_c}\,(psi) \tag{6-30}$$

ν_c for outside of the plastic hinge can be found according to the following equation

$$\nu_c = 0.25 x F2 x \sqrt{f'_c} \le 0.33\sqrt{f'_c}\,(MPa) \tag{6-31a}$$

$$\nu_c = 3 x F2 x \sqrt{f'_c} \le 4\sqrt{f'_c}\,(psi) \tag{6-31b}$$

Where

f'_c = Compressive strength of unconfined concrete

F1 is given by

$$F1 = 0.025 \le \frac{\rho_s f_{yh}}{12.5} + 0.305 - 0.083\mu_d < 0.25(MPa) \tag{6-32a}$$

$$F1 = 0.3 \le \frac{\rho_s f_{yh}}{150} + 3.67 - \mu_d < 3(psi) \tag{6-32b}$$

Where

ρ_s = Ratio of volume of spiral or hoop reinforcement to the core volume confined by the spiral or hoop reinforcement (measured out-to-out), for columns with circular or interlocking core sections, defined by Equation 6-33.
f_{yh} = Nominal yield stress of transverse column reinforcement (MPa, ksi)
μ_d = is defined as the local displacement ductility demand. However, SDC[7] specifies that the global displacement ductility demand μ_D shall be used in the determination of

the F1 provided a significant portion of the global displacement is attributed to the deformation of the column or pier. In all other cases a local displacement ductility demand μ_d shall be used in F1.

ρ_s can be found according to the following equation

$$\rho_s = \frac{4A_b}{D's} \tag{6-33}$$

Where

A_b = Area of individual reinforcing steel bar (mm², in²)

D' = cross-sectional dimension of confined concrete core measured between the centerline of the peripheral hoop or spiral

s = Spacing of transverse reinforcement measured along the longitudinal axis of the structural member (mm, in)

F2 is given by

$$1 + \frac{P_c}{13.8xA_g} < 1.5(MPa) \tag{6-34a}$$

$$1 + \frac{P_c}{2000xA_g} < 1.5(psi) \tag{6-34b}$$

Where

P_c = The column axial force including the effects of the overturning

A_g = Gross cross section area (mm², in²)

According to SDC[7], Section 3.6.3, the shear reinforcement capacity (V_s) for confined circular or interlocking core sections is defined as follows

$$V_s = \frac{A_v f_{yh} D'}{s} \tag{6-35}$$

Where

A_v = Total area of shear reinforcement = $n\left(\frac{\pi}{2}\right)A_b$

n = number of individual interlocking spirals or hoop core sections

A_b = Area of individual reinforcing steel bar (mm², in²)

Tanaka and Park[31] report that the shear capacity of the concrete in columns with interlocking spirals can be determine as follows

$$V_C = \nu_c\, b_w\, d \tag{6-36}$$

Where

ν_c = nominal shear capacity of the concrete
b_w = width of the column
$d = 0.5b_w + d_{il} + 0.318\ D'$
d_{il} = distance between the centers of adjacent spirals and
D' = cross-sectional dimension of confined concrete core measured between the centerline of the peripheral hoop or spiral ≈ 2 times the radius of the circular core section surrounded by spirals (measured to outside of the spiral), r_1

The nominal shear capacity of the concrete, ν_c, defined by Eq. 6-30 was used for comparison purpose.

Tanaka and Park[30] developed three expressions for the shear capacity of the spirals based on the assumption of a 45° diagonal tension crack. In the first expression assumed that the effectiveness of the interlocking spirals is equivalent to the transverse section shown in Fig. 6-33 and it was recommended in practical design, when d_{il} of approximately r_1 is used

$$V_s = \frac{\pi}{4}\left(2A_{sp}f_{yh}\right)\frac{D'}{s} + 2A_{sp}f_{yh}\frac{d_{il}}{s} \tag{6-37}$$

Where

A_{sp} = area of the spiral bar section
f_{yh} = specified yield strength of the spiral
s = center to center spacing of the spirals along the column

In the second expression it is assumed that the inner longitudinal bars provide a perfect interlock of the spirals, and therefore all the part of the spirals are effective against shear. This expression is the same as Eq. 6-35 used by Caltrans. In Eq. 6-35, the shear capacity of the interlocking spirals is assumed to be n times that of the single spiral, where n is the number of individual interlocking spirals.

The third expression was developed based on the exclusion of the part of spirals in the interlocking region from the calculation of the shear capacity (Fig. 6-34). It is assumed that the interlocking parts of the spirals are not effective against shear when large cracks are formed in the interlocking region (Fig. 6.34) and those parts are used to anchor the spirals. Therefore, the average cosine of θ (Avg.cos(θ)) between angles 0 and θ in Fig. 6-35 needs to be calculated and the Eq. 6-37 is modified as:

$$V_s = \frac{\pi}{4}\left(2A_{sp}f_{yh}\right)\frac{D'}{s} + Avg.\cos(\theta)2A_{sp}f_{yh}\frac{d_{il}}{s} \tag{6-38}$$

Where

$$Avg.\cos(\theta) = \frac{1}{\sin(\theta)}\left(\frac{\sin(2\theta)}{4} + \frac{\theta}{2}\right)$$, average cosine of θ in Fig. 6-35

$$\theta = a\sin\left(\frac{\frac{d_{il}}{2}}{r_1}\right)$$, defined according to Fig 6-32

Notice that when θ is assumed to be 30° ($d_{il} = r_1$), Avg.cos (θ) becomes 0.96, and Eq. 6-37 and Eq. 6-38 lead to nearly the same results.

Benzoni et al.[4] method is based on the shear strength model developed by Priestly et al[25] that proposed a shear equation that takes into account the effect of three components as follows:

$$V_n = V_C + V_S + V_P \tag{6-39}$$

Where

V_C = shear force carried by concrete

V_S = shear force carried by transverse steel

V_P = lateral component of the compression strut of the column due to the applied axial load

The concrete contribution depends of the displacement ductility, μ_d, and can be obtained as follows:

$$V_C = 0.8 A_g K \sqrt{f'_c} \tag{6-40}$$

Where

A_g = gross section area

K = 0.29 MPa (3.5 psi) when $\mu_d \leq 2$, and 0.1 MPa (1.2 psi) when $\mu_d \geq 4$. Linear interpolation is used for displacement ductilities between 2 and 4.

The shear force carried by transverse steel proposed by Benzoni et al.[4] is a modified version of the Equation 6-37 developed by Tanaka and Park[30] that included the effect of neutral axis depth, c, and shear crack angle, φ, as follows:

$$V_s = \frac{\pi}{2} A_{sp} f_{yh} \frac{\frac{D'}{2} - c}{s} \cot(\varphi) + 2 A_{sp} f_{yh} \frac{d_{il}}{s} \cot(\varphi) + \frac{\pi}{2} A_{sp} f_{yh} \frac{D'}{2s} \cot(\varphi) \quad \text{for } c \leq \frac{D'}{2} \tag{6-41a}$$

$$V_s = \frac{\pi}{2} A_{sp} f_{yh} \frac{D'}{2s} \cot(\varphi) + 2 A_{sp} f_{yh} \frac{d_{il} + \frac{D'}{2} - c}{s} \cot(\varphi) \quad \text{for } \frac{D'}{2} < c \leq \frac{D'}{2} + d_{il} \tag{6-41b}$$

$$V_s = \frac{\pi}{2} A_{sp} f_{yh} \frac{D' + d_{il} - c}{s} \cot(\varphi) \qquad \text{for } c \geq \frac{D'}{2} + d_{il} \tag{6-41c}$$

The lateral component of the compression strut of the column due to the applied axial load, V_p, is found as follows

$$V_P = \frac{D-c}{2a} P \tag{6-42}$$

Where

P = applied axial load
D = section depth or diameter
c = depth of the compression zone at the bottom of the column
a = total column length for a cantilever column (fixed-pinned) and half of the length for a column in reversed bending (fixed-fixed)

The contribution of the cross ties in ISH1.5T of 33 kN (7.4 Kips) was included in the shear reinforcement capacity. A 45° diagonal crack and the measured material properties with strain rate effect were used in all the methods. Figures 6-36 through 6-39 compare the experimental results and the shear capacity calculated using the three methods based on the displacement ductility capacities that accounted for flexure only. Based on the shear methods, a shear failure would occur when the shear capacity curve intercepts the experimental results. According to Caltrans[7], Tanaka and Park[30] and Benzoni et al.[4] methods a shear failure would be expected at displacement of 21.6 mm (0.85 in), 19.8 mm (0.78 in) and 17 mm (0.67 in) for ISH1.0, respectively. For specimen ISH1.25 shear failure would be expected at displacement of 36 mm (1.42 in), 34 mm (1.34 in) and 25 mm (0.98 in) based on Caltrans[7], Tanaka and Park[30] and Benzoni et al.[4] methods, respectively. All the methods underestimated the shear capacity of specimens ISH1.0 and ISH1.25 since both failed in shear/flexural mode at displacement of 98.5 mm (3.88 in) and 105.4 mm (4.15 in), respectively. Specimens ISH1.5 and ISH1.5T failed in flexural mode at displacement of 127.5 mm (5.02 in) and 101.6 mm (4.0 in), respectively. Based on Caltrans[7] and Tanaka and Park[30] methods a shear failure would be expected at displacement of 43.7 mm (1.72 in) and 42.7 mm (1.68 in) for specimen ISH1.5 and at displacement of 44.4 mm (1.75 in) and 43.2 mm (1.70 in) for specimen ISH1.5T. According to Benzoni et al.[4] method a shear failure would be expected at displacement of 36.8 mm (1.45 in) in specimen ISH1.5. Based on Benzoni et al.[4] method specimen ISH1.5T would not fail in shear which is in agreement with the actual failure mode.

A most realistic estimate of the shear capacity was made when the bond slip and shear deformations were included in the calculation of the displacement ductility capacity. Table 6-21 shows the shear capacity of the specimens and their components (V_s, V_c and V_p) calculated according to Caltrans[7], Tanaka and Park[30] and Benzoni et al.[4] methods and based on the displacement ductility capacities that accounted for flexure, bond slip and shear deformation. The shear capacity for ISH1.5T using Caltrans[7] and Benzoni et al.[4] was not reported since the shear capacity did not intercept the experimental results (Fig 6-43). The shear reinforcement capacity used by Caltrans[7] method was 24%, 15%, and 8% higher than the capacity estimated by Tanaka and Park[30] method for ISH1.0, ISH1.25, and ISH1.5, respectively. A difference of 87%, 57%, and

52% was found between the shear reinforcement capacities estimated by Caltrans[7] and Benzoni et al.[4] equations for ISH1.0, ISH1.25, and ISH1.5, respectively. The concrete shear capacity from Caltrans[5] method was 24%, 35% and 24% less than the combined concrete and axial capacity estimated by Benzoni et al.[2] method for ISH1.0, ISH1.25, and ISH1.5, respectively.

A comparison between experimental results and the shear capacity calculated using the three methods, including bond slip and shear deformation in the calculation of the displacement ductility capacity, is shown in Figs. 6-40 through 6-43 for specimens with high shear. Based on the Caltrans[7], Tanaka and Park[30] and Benzoni et al.[4] methods a shear failure would be expected at displacement of 28.4 mm (1.12 in), 22.8 mm (0.90 in) and 25.4 mm (1.0 in) for ISH1.0, respectively. For specimen ISH1.25 shear failure would be expected at displacement of 78.7 mm (3.1 in), 69.8 mm (2.75 in) and 48.3 mm (1.9 in) based on Caltrans[7], Tanaka and Park[30] and Benzoni et al.[4] methods, respectively. All the methods underestimated the shear capacity of specimens ISH1.0 and ISH1.25 since both failed in shear/flexural mode at displacement of 98.5 mm (3.88 in) and 105.4 mm (4.15 in), respectively. Nonetheless, a better agreement between the measured and calculated shear capacities was found when the bond slip and shear deformation were included. Specimens ISH1.5 and ISH1.5T failed in flexural mode at displacement of 127.5 mm (5.02 in) and 101.6 mm (4.0 in), respectively. Based on the Caltrans[7], Tanaka and Park[30] and Benzoni et al.[4] methods a shear failure in ISH1.5 would be expected at displacement of 84.3 mm (3.32 in), 81.3 mm (3.20 in), and 53.3 mm (2.1 in), respectively. Taking into account that specimen ISH1.5 did not fail in shear, a conservative value of shear capacity was achieved using Caltrans[7], Tanaka and Park[30] and Benzoni et al.[4] methods. According to the Tanaka and Park[30] method ISH1.5, would fail in shear at displacement of 100.3 mm (3.95 in). Based on the Caltrans[7] and Benzoni et al.[4] methods specimen ISH1.5T would not fail in shear which is in agreement with the experimental results. In general, Caltrans[7] method presented the closest correlation compared with the experimental results.

6.6.4. Shear Stiffness

According to Park and Paulay[22], before the formation of flexural or diagonal cracks, the shear stiffness of the reinforced concrete member can be calculated using Eq. 6-21. Park and Paulay[22] also state that after the formation of diagonal shear cracks, the shear stiffness of reinforced concrete member is calculated using Eq. 6-22. There is no an expression for the post yield shear stiffness. Priestley et. al.[24] suggested that the shear stiffness drops in proportion to the ratio of the flexural stiffness. Hence, the plastic shear stiffness can be calculated as the product of the uncracked shear stiffness and the ratio of the post yield flexural stiffness and the uncracked flexural stiffness.

The uncracked flexural stiffness was calculated as the ratio of cracking lateral force and the corresponding displacement. The cracking lateral force was defined as the cracking moment divided by one half of the clear length of the column, assuming bending in double curvature. The cracking moment was calculated as follows

$$M_{cr} = \frac{\left(\frac{P}{A_g} + f_t\right)(I)}{\frac{D}{2}} \quad (6\text{-}43)$$

Where

P = axial load

A_g = gross area

f_t = tensile strength in flexure = $0.623\sqrt{f'_c}\,(MPa) = 7.5\sqrt{f'_c}\,(psi)$

I = moment of inertia around the bending axes

D = depth of the column

The cracking displacement was calculated by the following equation

$$\Delta_{cr} = \frac{1}{3}\phi_{cr} l^2 \quad (6\text{-}44)$$

Where

l = one half of the column length, assuming double curvature

ϕ_{cr} = cracking curvature

The post yield flexural stiffness was based on a tri-linear idealization model assumed for the flexural deformation of the column (Fig. 6-44). The post yield flexural stiffness, K_{pf}, was defined as follows

$$K_{pf} = \frac{(F_u - F_y)}{(\Delta_u - \Delta_y)} \quad (6\text{-}45)$$

Where

F_u = ultimate lateral force = $\frac{M_u}{l}$

F_y = idealized yield force = $\frac{M_y}{l}$

Δ_u = ultimate displacement = $\Delta_y + \Delta_p$

Δ_y = yield displacement based on Eq. 6-13

Table 6-22 shows the ratio of the uncracked flexural stiffness and the post yield flexural stiffness as well as the uncracked shear stiffness and the post yield shear stiffness based on the assumption of Priestley et. al.[24].

The measured shear deformation was reported in Section 5.12 for specimens with high shear. Figures 5-155 through 5-158 show a bilinear behavior, in all the specimens. The measured lateral force and shear deformations were idealized by a bi-linear curve to quantify the cracked and post yield stiffness. The elastic slope was defined by the force

corresponding to the first reinforcement yield and the corresponding shear displacement on the measured curve. Once the elastic slope was defined the post yield slope was established by equalizing the area between the measured and the idealized curve. The descending part of the measured curve was ignored. Therefore, the ultimate point was assumed at the maximum lateral force with the corresponding shear deformation. Figures 6-45, 6-46, 6-47 and 6-48 show the measured lateral force and shear deformation with the corresponding idealized curve for specimens ISH1.0, ISH1.25, ISH1.5 and ISH1.5T, respectively. Table 6-23 shows a comparison between uncracked and cracked shear stiffness using Park and Paulay[22] equations and the elastic slope from the measured results. The measured post yield shear stiffness is about 8%, 12%, 12% and 9% of the uncracked shear stiffness for ISH1.0, ISH1.25, ISH1.5 and ISH1.5T, respectively. The cracked shear stiffness underestimated the measured post yield shear stiffness by approximate 24%, 37%, 28% and 16% for ISH1.0, ISH1.25, ISH1.5 and ISH1.5T, respectively. Table 6-24 shows a comparison between post yield shear stiffness using Priestley et. al.[24] method and the post yield stiffness from the measured results. The post yield shear stiffness using Priestley et. al.[24] method underestimated the measured results by about 73%, 46%, 36% and 68% for ISH1.0, ISH1.25, ISH1.5 and ISH1.5T, respectively. A modified shear stiffness model is proposed in Chapter 7 to improve the correlation between the analytical and measured results.

6.7. Effect of Interlocking Distance and Shear Stress

The effect of the horizontal spacing of the spirals measured center-to-center of the spirals, d_i, or interlocking distance was studied by Tanaka and Park[30]. In order to ensure the adequate shear transfer between spirals and prevent wide opening of diagonal tension cracks within the interlocking region during the inelastic range of cyclic loading, Tanaka and Park[30] suggested that the in-plane component of the spiral bar force (the component parallel to the column shear force) at the middepth of the column section should be a considerable portion the spiral bar force. The in-plane component of the spiral bar force is related to d_i through the angle θ as shown in Fig. 6-49. Satisfactory behavior was reported by Tanaka and Park[30] in two columns tested with $\theta = 35°$ or a in-plane component of the spirals bar force ($F \cos(\theta)$) equal to 0.82 times the spiral force, F, and a d_i of approximately 1.15 times R. As a result, Tanaka and Park[30] suggest d_i should not be greater than 1.2 times the radius of the spirals, R. Tanaka and Park[30] did not test columns with di greater than 1.2 times R.

Buckingham[5] tested and compared the behavior of columns with interlocking spirals with d_i of 1.2 and 1.46 times R. According to Buckingham[5], wider shear cracks were observed in the column with d_i of 1.46R compare to the column with d_i of 1.2R under a displacement ductility of 2. Twenty percent more degradation of the peak load was measured in the column with d_i of 1.46R for a displacement ductility of 2 to 4. The failure of the column with d_i of 1.46R was caused by rupture of the spirals reinforcement whereas the column with d_i of 1.2R failed due to concrete core deterioration. No vertical cracks were reported.

Section 4.3 presented the observed and measured performance of the specimens with low shear and d_i of 1.0R and 1.5R. The performance for both specimens was very similar and satisfactory with a displacement ductility of 9.6 and 10.4 for specimens with d_i of 1.0R and 1.5R, respectively. The failure in both columns was due to rupture of the spirals and buckling of the longitudinal bars at the bottom of the column in the plastic hinge zone. Higher average strains in the spirals were measured in specimen with d_i of 1.5R compared with specimen with d_i of 1.0R (Fig. 6-50). As a result slight degradation of the load capacity (Fig. 6-51) was observed in the specimen with d_i of 1.5R compared with specimen with d_i of 1.0R. Nevertheless, this degradation was seen from displacement ductility of 7.4 to 10.4 which exceeded the target design displacement ductility of 5. Since the column with d_i of 1.5 did not lead to excessive shear cracking and based on the satisfactory displacement ductility capacity achieved in that column, the Caltrans provision for the maximum value of d_i is believed to be adequate for columns with low shear.

The observed and measured performance of the specimens with high shear was reported in Section 5-3. Similar performance was observed in specimens with d_i of 1.0R and 1.25R. Specimens with d_i of 1.0R and 1.25R failed in shear after a ductile behavior with a displacement ductility of 4.7 and 5.0, respectively. Vertical cracks located in the interlocking region were observed in the specimen with high shear and d_i of 1.5R at about 58 % of the maximum force. Large interlocking distance can make the column vulnerable to large vertical shear stress at middepth of the column (Fig. 6-52). This vertical stress is in direct proportion with the shear force in the column, at least in the linear range. Since relatively large amount of plain concrete is present in the interlocking region in columns with d_i of 1.5R compared with column with d_i of 1.0R (Fig. 6-53), and taking into account the reduction of the horizontal component of the spirals bar force at the middepth of the section column (Tanaka and Park[30]), vertical cracks were formed due to a vertical stress at the interlocking region. Based on the observed performance of ISH1.5T, horizontal cross ties connecting the hoops reduced and delayed vertical cracks in the interlocking region in columns subjected to high average shear stress with d_i of 1.5R. Specimens with high shear and d_i of 1.5R did not achieve the target displacement ductility capacities of 5 but exceeded the minimum specified displacement ductility of 3, according to SDC[7].

The normalized lateral force and displacement is shown in Fig. 6-54. Similar degradation of the load capacity is observed in specimens with di of 1.0R and 1.25R from displacement ductility of 3.61 to 4.7 and from displacement ductility of 3.7 to 5, respectively. Specimen with di of 1.5R without and with cross ties showed load degradation from displacement ductility of 3 to 4 and from displacement ductility of 2.8 to 3.8, respectively. However, less degradation is observed in specimens with di of 1.5R and cross ties compared to the others specimens. The displacement ductility capacity versus the average shear stress index defined in Section 2.2 is shown in Fig. 6-55. In general, the displacement ductility capacity decreased when the average shear stress index increase. This is expected since columns subjected high shear fail in shear/flexural

mode. The average shear stress index, defined in section 2.2, should be used as a control design parameter to choose d_i and the addition of cross ties in columns with high shear.

Chapter 7. Description of the Existing and Modified Shear Stiffness Model

7.1. Introduction

The uncracked and cracked shear stiffness for reinforced concrete members was developed by Park and Paulay[22] in early 70's. The uncracked shear stiffness was developed based on the principles of elasticity whereas the cracked shear stiffness was developed based on the 45° truss action principles. Park and Paulay[22] equations have been used because of their simplicity. The difference of the cracked shear stiffness using Park and Paulay[22]'s equation and the experimental results obtained in the current study ranged between 19% and 58%. Section 5.12 showed a bilinear behavior of the measured lateral force versus shear deformation. Currently, there are no expressions for the post yield shear stiffness. Even thought, in Priestley et al.[23] suggested that the shear stiffness drops in proportion to the ratio of the flexural stiffness, differences of 40% to 73% were found between the experimental results and Priestley et al.[24]'s method to estimate the post yield shear stiffness.

A detailed review of the uncracked and cracked shear stiffness is presented this chapter. A modified shear stiffness model was proposed based on the 45° truss action principles and the experimental results of scale columns. The application of the modified was illustrated through examples of typical columns with different aspect ratios.

7.2. Shear Stiffness using Park and Paulay Method

According to Park and Paulay[22], before the formation of flexural or diagonal cracks, the shear stiffness of the reinforced concrete member can be calculated using the principles of elasticity. The modulus of rigidity, G in concrete can be taken as follows

$$G = \frac{E_c}{2(1+\nu)} \tag{7-1}$$

Where

E_c = Modulus of elasticity of the concrete = $4733\sqrt{f'_c}\,(MPa)$ $57000\sqrt{f'_c}\,(psi)$

ν = Poisson's ratio

Value of ν for concrete varies from 0.16 to 0.30. Assuming ν=0.25, G can be taken as $0.4E_c$. The shear area of a rectangular cross section area can be expressed as 5/6 of the product of the width, b_w, and the effective depth, d. Substituting $G = 0.4E_c$ and the shear area into Eq. 7-1, the shear force for a rectangular cross section can be expressed as

$$F = \frac{E_c b_w d}{3}\Delta_s \tag{7-2}$$

According to Park and Paulay[22] the shear stiffness K_v' is defined as the magnitude of the shear force that when applied to concrete member of unit length, will caused unit shear displacement at one end of the concrete member relative to the other. Applying the previous definition to Eq. 7-2, the uncracked shear stiffness for a rectangular cross section of a concrete member of unit length is calculated as follows

$$K_v' = \frac{E_c b_w d}{3} \tag{7-3}$$

Diagonal cracks are expected in concrete member subjected to large shear forces. According to Park and Paulay[22] these cracks increase the shear deformation of the concrete member and the load is likely to be carried by a truss action. The shear distortion of a reinforced concrete member of the analogous truss model was used by Park and Paulay[22]. The truss model postulated by Mörsch[20] consisted of an equivalent truss with compression concrete struts parallel to the diagonal cracks generally at 45° and stirrups acting as tension members. The bottom chord of the truss model is represented by the longitudinal tension and top chord is represented by flexural compression zone (Figure 7-1). In order to determine the shear distortion of the reinforced concrete element Park and Paulay[22] assumed that the chord members are infinity rigid. Figure 7-2 shows the shear distortion of a reinforced concrete element using the analogous truss. The elongation of the stirrups, Δ_s, and the shortening of the compression strut, Δ_c, are shown in Fig. 7-2. The Williot's principal was applied by Park and Paulay[22] to find the shear distortion, Δ_v, as follows

$$\Delta_v = \Delta_s + \Delta_R = \Delta_s + \sqrt{2}\Delta_c \tag{7-4}$$

The elongation of the stirrups, Δ_s, can be calculated as follows

$$\Delta_s = \frac{V_s s}{E_s A_v} \tag{7-5}$$

Where

V_s = shear force
s = spacing of the stirrups
E_s = elastic modulus of steel
A_v = area of the stirrups

The shortening of the diagonal strut is found from

$$\Delta_c = \frac{2\sqrt{2}V_s}{E_c b_w} \tag{7-6}$$

Where

b_w = width of the concrete member

Substituting Eq. 7-5 and 7-6 into Eq. 7-4, the shear distortion per unit length, θ_v, can be expressed as follows

$$\theta_v = \frac{\Delta_v}{d} = \left(\frac{V_s s}{E_s A_v} + \sqrt{2} \frac{2\sqrt{2} V_s}{E_c b_w} \right) = \frac{V_s}{E_s b_w d} \left(\frac{s b_w}{A_v} + \frac{4 E_s}{E_c} \right) \tag{7-7}$$

Substituting $\rho_v = \frac{A_v}{s b_w}$ and the modular ratio, n = $\frac{E_s}{E_c}$, into Eq. 7-7, the shear distortion per unit length, θ_v, becomes

$$\theta_v = \frac{V_s s}{E_s b_w d} \left(\frac{1}{\rho_v} + 4n \right) \tag{7-8}$$

According to Park and Paulay[22] the cracked shear stiffness of reinforced concrete member of unit length, based on the truss model with 45° diagonal cracks, is the value of the V_s when $\theta_v = 1$ as follows

$$K_{v,45} = \frac{\rho_v}{1 + 4n\rho_v} E_s b_w d \tag{7-9}$$

Similar expression was developed by Park and Paulay[22] for different inclination of compression struts α and stirrups β as follows

$$K_v = \frac{\rho_v \sin^4 \alpha \sin^4 \beta (\cot \alpha + \cot \beta)^2}{\sin^4 \alpha + 4n\rho_v \sin^4 \beta} E_s b_w d \tag{7-10}$$

7.3. Proposed Shear Stiffness Model

A comparison between the calculated shear stiffness and experimental results was done in Section 6.6.4. The difference of the cracked shear stiffness using Park and Paulay[22]'s equation and the experimental results varied between 19% and 58%. There is no expression available for the post yield shear stiffness. Priestley et al.[24] suggested that the shear stiffness drops in proportion to the ratio of the flexural stiffness. Hence, the plastic shear stiffness can be calculated as the product of the uncracked shear stiffness and the ratio of the post yield flexural stiffness and the uncracked flexural stiffness. Differences of 40% to 73% were found between the experimental results and Priestley et al.'s[23] method to estimate the plastic shear capacity. A modified shear stiffness model was developed in this study to improve correlation between analytical and the experimental results.

7.3.1. Formulation of the Column Shear Stiffness

Diagonal cracks increase the shear deformation of the reinforced concrete member. The first diagonal cracks were observed in the test specimens at the plastic hinge zone as an extension of previous developed flexural cracks. In Section 5.12 it was reported that on average, 60% to 70% of the total shear deformation comes from the panel 1 and 4 located at the plastic hinge zones of the column. As results, it is reasonable to calculate the shear stiffness of the member as the contribution of two different values of shear stiffness relative to the amount of cracking expected along the length of the member (Figure 7-3) as follows

$$K_v = \frac{1}{\frac{n_{pr} d}{K_d} + \frac{L - n_{pr} d}{K_{d-L}}} \tag{7-11}$$

Where

K_v = shear stiffness of the member

n_{pr} = number of potential plastic regions = 1 for a bending in single curvature and 2 for a bending in double curvature

K_d = stiffness at potential plastic region over a length equal to effective column depth, d.

K_{d-L} = stiffness of the remaining member length between plastic region(s)

d = effective column depth

L= clear length of the column

Section 5.12, showed a bilinear behavior of the measured lateral force versus shear deformation. Hence, two shear stiffness that represents the bilinear behavior need to be defined. The first shear stiffness corresponds to the elastic behavior and it is defined as the contribution of the cracked stiffness and the uncracked stiffness as follows

$$K_{vE} = \frac{1}{\frac{n_{pr} d}{K_{v,45}} + \frac{L - n_{pr} d}{K_v'}} \tag{7-12}$$

Where

K_{vE} = elastic shear stiffness

$K_{v,45}$ = cracked shear stiffness defined by Eq. 7-9

K_v'= uncracked shear stiffness defined by Eq. 7-3

Based on Section 6.5.1.3, a lower bound of the elastic shear stiffness, $K_{vE,}$ equal to the 10% of the K_v' can be used.

The post yield shear stiffness that represents the second slope can be defined as the contribution of the plastic shear stiffness and the cracked stiffness as follows

$$K_{vPY} = \frac{1}{\frac{n_{pr}d}{K_P} + \frac{L - n_{pr}d}{K_{v,45}}} \quad (7\text{-}13)$$

Where

K_{vPY} = post yield shear stiffness
K_P = plastic shear stiffness

7.3.2. Plastic Shear Stiffness Models

Different models of plastic shear stiffness, K_P, were studied. The common consideration in evaluating these models was that they needed to be simple. One approach was to assume the contribution of the axial stiffness of the spirals (K_s) cut by a 45° diagonal crack and the concrete shear friction through 45° diagonal crack interface (K_c) (Fig. 7-4). The development length of the spirals is needed to calculate the axial stiffness of the spirals. Since no specific simple method to calculate the development length of a spiral is available, the axial stiffness of the spirals could not determined without resorting to complex finite element models. As a result, this approach was not used to calculate plastic shear stiffness.

Another model based on modifications of the Park and Paulay[22] cracked shear stiffness and calibrated using experimental results was developed to calculate plastic shear stiffness, K_P. The cracked shear stiffness was calculated based on the shear distortion of a reinforced concrete element using the analogous truss. The shear distortion was defined by Eq. 7-8 and depends of the elongation of the stirrups, Δ_s, and the shortening of the compression strut, Δ_c. Equations 7-5 and 7-6 define the elongation of the stirrups, Δ_s, and the shortening of the compression strut, Δ_c and they are expressed in terms of the modulus of elasticity of the steel and concrete, respectively. Considerable shear distortion occurs at the post yield stage. Therefore, the modulus of steel and concrete are the only variables that contribute to the increasing of the shear distortion in a reinforced concrete element. The modulus of the steel and concrete were verified based on the experimental results.

As discussed in Sections 4.11 and 5-13, maximum spirals strains in most of the locations for all the specimens were below yield. The displacement measured in the horizontal transducers (H1, H2, H3) of the panel instrumentation (Figure 7-5) was divided by the original length in order to calculate the measured horizontal strain. Tables 7-1 through 7-4 show the lateral load for the predominant direction of motion with the corresponding horizontal strain from the horizontal transducers (H1, H2, H3) for specimens with high shear. The maximum horizontal strains of 0.003, 0.0034, 0.0028 and 0.0012 were recorded in specimens ISH1.0, ISH1.25, ISH1.5 and ISH1.5T, respectively. These strains are close or below to the yield strain of 0.0031. These results as well as the strain gauges in the spirals confirm that the spirals barely yield. Therefore,

the steel in the spirals was in the elastic range and the elastic modulus was used for the steel.

Higher strains in the concrete struts are expected at the post yield state in relation with the strain recorded in the strain gauges located at the spirals and in the horizontal transducers (H1, H2, H3) of the panel instrumentation. The diagonal displacement transducers (D1, D2, D3, D4) of the panel instrumentation for specimen ISH1.0 coincided with the concrete struts in the predominant direction of motion (Figure 7-6). Table 7-5 shows the strain measured in the diagonal transducers (D1, D2, D3, D4) for ISH1.0. Strain higher than 0.002 was measured in the diagonal transducer located in the plastic hinge zones (D1, D4), starting from the motion that corresponded to a displacement ductility of 1 (run 6) to the last motion. The strain increased during each run with a maximum of -0.014 and -0.007 for the diagonal transducer at the plastic hinge zone D1 and D4, respectively. These levels of strain did not correspond to the elastic range for the concrete; therefore the elastic modulus for the concrete used in Eq. 7-6 is not applicable after the columns yields.

Based on the strain in the diagonal transducers and taking into account that the steel is in the elastic range; the modulus of the concrete is the only variable that needs to be modified in order to produce a large shear distortion at the post yield stage. A bilinear idealization of the Hognestad model[25] for the concrete stress-strain relationship was developed. The slope of the elastic portion of the idealized curve was based on a compression stress of $0.45f'_c$ with the corresponding strain from the Hognestad model[25], according to the definition of the E_c in the commentary of the Section 8.5, ACI[1]. Once the elastic portion was defined the second slope was established by equalizing the area between the Hognestad model[26] and the idealized curve (Fig. 7-7). In order to produce a positive second slope, the ultimate stress was defined as the average between the peak and ultimate stress of the Hognestad model[26]. The bilinear representation of the Hognestad model[26] was determined for concrete compressive strength, f'_c, of 20.68 MPa (3000 psi) to 55.15 MPa (8000 psi). The value of the second slope from the idealized model, E_{cp}, versus the concrete compression strength, f'_c, is plotted in Fig. 7-8. A linear regression of Fig. 7-8 indicated that the second slope of the idealized curve of the Hognestad model[26], E_{cp}, is 12.16 times the concrete compression strength, f'_c. As a result, the value of E_{cp} is defined as follows

$$E_{cp} = 12 f_{c'} \tag{7-14}$$

Vecchio and Collins[33] determined the stress-strain relationship for the cracked concrete by testing 30 reinforced concrete panels under different uniform biaxial stress and pure shear. They found that the principal compressive stress in the concrete, f_{c2}, are not only a function of the principal compressive strain ε_2 but also of principal tensile strains ε_1. As a results the cracked concrete subjected to high tensile strains perpendicular to the direction of the compression is softer and weaker than concrete in a standard cylinder test (Fig. 7-9). In order to account for the effect of the principal tensile

strains ε_1, Vecchio and Collins[33] developed the following expression for the stress-strain relationship for the cracked concrete

$$f_{c2} = f_{c2\max}\left[2\left(\frac{\varepsilon_2}{\varepsilon_c'}\right)-\left(\frac{\varepsilon_2}{\varepsilon_c'}\right)^2\right] \tag{7-15}$$

Where

f_{c2max} = maximum principal compressive stress in the concrete, where

$$\frac{f_{c2\max}}{f_c'} = \frac{1}{0.8-0.34\frac{\varepsilon_1}{\varepsilon_c'}} \le 1.0$$

ε_c' = strain at peak stress f'$_c$ measured in concrete cylinders tests

The previous expression was developed for shear cracks in one direction and not for an "x" pattern shear cracks expected under earthquake loads, which eventually will produced additional softening of the cracked concrete material. If the effect of the principal tensile strains ε_1 is implemented into the Hognestad model[26], a significant reduction of the second slope from the idealized model, E_{cp}, (Eq. 7-14) can be obtained. Due to the difficulty to calculate the principal tensile strain at the post yield stage, a factor β_p that represent the softening of the cracked concrete due to the principal tensile strains and shear cracks patterns was introduced into the Equation 7-14 as follows

$$\beta_p E_{cp} = 12\beta_P f_{c'} \tag{7-16}$$

Experimental post yield stiffness from the present and other studies were used to estimate B_p. As a result, the modulus of elasticity of the concrete, E_c, in Equation 7-6 was replaced by Eq. 7-16. The expression for shortening of the diagonal strut, Δ_{cp}, at the post yield stage becomes:

$$\Delta_c = \frac{2\sqrt{2}V_s}{\beta_p E_{cp} b_w} \tag{7-17}$$

Since the steel in the spirals was in the elastic range for the post yield stage of the columns, Equations 7-5 and 7-17 were substituted into Eq. 7-4 and the shear distortion per unit length at the post yield stage, θ_{vp} was found as follows:

$$\theta_{vp} = \frac{\Delta_v}{d} = \left(\frac{V_s s}{E_s A_v} + \sqrt{2}\,\frac{2\sqrt{2}V_s}{\beta_p E_{cp} b_w}\right) = \frac{V_s}{E_s b_w d}\left(\frac{s b_w}{A_v} + \frac{4E_s}{\beta_p E_{cp}}\right) \tag{7-18}$$

Substituting $\rho_v = \frac{A_v}{sb_w}$ and the modular ratio $n_p = \frac{E_s}{E_{cp}}$ into Eq. 7-18, the shear distortion per unit length, θ_{vp}, becomes

$$\theta_{vp} = \frac{V_s}{E_s b_w d}\left(\frac{1}{\rho_v} + \frac{4n_n}{\beta_p}\right) \tag{7-19}$$

The plastic shear stiffness of reinforced concrete member of unit length, based on the truss model with 45° diagonal cracks, is the value of the V_s when $\theta_{vp} = 1$ as follows

$$K_p = \frac{\beta_p \rho_v}{\beta_p + 4n_p\rho_v} E_s b_w d \tag{7-20}$$

Substituting Eq. 7-9 and 7-20 into 7-13 and replacing the post yield shear stiffness, K_{vPY}, by the experimental post yield stiffness, K_{vPYE} and solving for β_p, the following equation is found

$$\beta_p = 4nK_{vPYE}n_p d\,\frac{\rho_v}{\left(-K_{vPYE}L - 4K_{vPYE}Ln\rho_v + 4nK_{vPYE}n_p d\rho_v + \rho_v E_s b_w d\right)} \tag{7-21}$$

The experimental values of the post yield stiffness of two columns with a two-way hinge (THD1, THD2), tested at the University of Nevada, Reno[8], one column (COL1) from the study by Priestley et al.[24] and the four column from the present study were used to calculate the factor β_p. All the columns were tested in double curvature. Table 7-6 present the most relevant details of the columns that are not part of this study. Table 7-7 list the experimental post yield stiffness, K_{vPYE} used with the corresponding values of β_p. An average value of 0.293 for the factor β_p was obtained from values reported in Table 7-7. Based on the average value of the factor β_p, a reduction of 30% is expected in the second slope of the idealized curve of the Hognestad model[26], E_{cp}.

To verify the β_p value, the principal tensile strains ε_1 (Eq. 7-15) was implemented into the Hognestad model[26]. An iterative solution was done in order to obtain the tensile strains ε_1 that reduced by 30% the idealized second slope of a cracked concrete with $\varepsilon_1 = 0$. A tensile transverse strain of 0.0149 was found. Figure 7-10 shows the comparison between the stress-strain relationship for the cracked concrete with tensile strain of 0 and 0.015.

The diagonal displacement transducers (D1, D2, D3, D4) of the panel instrumentation for ISH1.25, ISH1.5 and ISH1.5T were used to verify the magnitude of the tensile transverse strain at each motion. These transducers coincided with the direction of the principal tensile strain in the predominant direction of motion (Fig. 7-6). The diagonal displacement transducers in ISH1.0 were not used since they did not

coincided with the direction of the principal tensile strain in the predominant direction of motion. Tables 7-8, 7-9 and 7-10 show the strain measured in the diagonal transducers (D1, D2, D3, D4) for ISH1.25, ISH1.5, ISH1.5T, respectively. As expected, higher strains were measured in the diagonal transducer located in the plastic hinge zones (D1, D4). The strain at the plastic hinge zone increased each run with an average strain for the post yield range of 0.0110, 0.0122 and 0.0119 for ISH1.25, ISH1.5 and ISH1.5T respectively. These strains were slightly smaller than the calculated tensile strain of 0.015. Taking into account that Eq. 7-15 used to calculated the tensile strain considered only shear cracks in one direction, the difference between experimental and calculate are believe to be acceptable.

Taking into account the previous considerations, Eq. 7-15 with β_p of 0.3 can be substituted into Eq. 7-20, and the plastic shear stiffness of reinforced concrete member of unit length, based on the truss model with 45° diagonal cracks can be calculated as

$$K_p = \frac{9\rho_v f_c^{'}}{9f_c^{'} + 10E_s\rho_v} E_s b_w d \tag{7-22}$$

7.4. Comparison of the Proposed and Existing Shear Stiffness Model

The measured shear stiffness was compared with the proposed and existing shear stiffness models. The effect of the strain rate on the material properties was taken into account.

Table 7-11 compares the elastic measured shear stiffness with the cracked shear stiffness and proposed elastic shear stiffness (Eq. 7-12). The lower bound of the elastic shear stiffness, $K_{vE,}$ of $0.1K_v$' was used. The cracked shear stiffness by Park and Paulay[22] underestimated the experimental stiffness by 24%, 37%, 28% and 16% for ISH1.0, ISH1.25, ISH1.5 and ISH1.5T, respectively. A better agreement was obtained between the proposed stiffness and the experimental stiffness with a difference of 24%, 14%, 17% and 16% for ISH1.0, ISH1.25, ISH1.5 and ISH1.5T, respectively. The proposed stiffness overestimated the experimental stiffness for ISH1.0 and ISH1.5T and underestimated the experimental stiffness for ISH1.25 and ISH1.5.

Table 7-12 compares the post yield measured shear stiffness with the post yield shear stiffness defined by Eq. 7-13 with Eq. 7-22 and post yield shear stiffness proposed by Priestley et al[24]. The post yield stiffness proposed by Priestley et al[24] underestimated the experimental stiffness by 73%, 46%, 36% and 68% for ISH1.0, ISH1.25, ISH1.5 and ISH1.5T, respectively. Significant improvement was achieved using the proposed post yield shear stiffness and the experimental stiffness with difference of 13%, 2%, 19% and 15% for ISH1.0, ISH1.25, ISH1.5 and ISH1.5T, respectively. Except for ISH1.5T, the proposed post yield shear stiffness underestimated the experimental stiffness.

7.5. Ultimate Shear Deformation

The ultimate shear deformation can be calculated as follows

$$\Delta_u = \Delta_{vE} + \Delta_{vPY} \tag{7-23}$$

Where

$\Delta_{vE} = \dfrac{F_y}{K_{vE}}$, elastic shear deformation

$\Delta_{vPY} = \dfrac{\Delta F}{K_{vPY}}$, post yield shear deformation

F_y = equivalent lateral yield force capacity from a bilinear idealization

$\Delta F = F_u - F_y$

F_u = ultimate lateral force capacity

K_{vE} = elastic shear stiffness defined by Eq. 7-12

K_{vPY} = post yield shear stiffness defined by Eq. 7-13

Table 7-13 shows the effect of the ultimate shear deformation on the displacement ductility capacity of ISH1.0, ISH1.25, ISH1.5 and ISH1.5T. An increase in the displacement ductility capacity of 19%, 15%, 24% and 23% was obtained when the ultimate shear deformation was included in the calculation of the ultimate deformation.

7.6. Application to a Typical Column

A 1219 mm (48 in) diameter bridge column with longitudinal and transversal steel ratios of 2% and 0.75% was selected to illustrate the application of the proposed shear stiffness model. The axial load index was 10%. Table 7-14 summaries the material properties as well as the relevant details of the column used to calculate the shear stiffness. Different column heights were selected to obtain aspect ratios from 2 to 7.5.

Equations 7-20 and 7-21 were used to calculate the elastic and post yield shear stiffness. Table 7-15 shows a summary of the values used in Eq. 7-12 and 7-13. Table 7-16 shows the elastic and post yield shear stiffness for different aspect ratios. Both elastic and post yield stiffness reduced when the aspect ratio increased. Moment-curvature analysis was performed using RCMC[35] program. A bilinear idealization was used to calculate the equivalent yield moment. The shear deformation at yield was calculated as the ratio of the equivalent lateral yield force capacity from the bilinear idealization and the elastic shear stiffness from Eq. 7-20. The equivalent lateral force was calculated as the equivalent yield moment divided by the height of the column. Equation 7-30 was used to calculate the ultimate shear deformation. The ultimate lateral force capacity was obtained from the ratio of the ultimate moment from M–ϕ analysis and the height of the column. Table 7-16 shows the corresponding lateral force used to calculate the yield and ultimate shear deformation for different aspect ratios. In order to quantify the effect of the shear deformation, yield deformation due to flexure and ultimate deformation were

calculated using Eq. 6-14 and 6.11, respectively. Paulay and Priestley's[22] plastic hinge length was used in the calculation of the plastic deformation. Figure 7-11 shows the contribution of the yield deformation due to shear to the total yield deformation for different aspects ratios. The contribution of the shear deformation at yield decreased when the aspect ratio increased. No significant contribution of shear deformation at yield was found for aspects ratio larger than 5. Figure 7-12 shows the effect of the ultimate shear deformation on the displacement ductility capacity for different aspects ratios. Ultimate shear deformation increased by 18%, 13% and 9% the displacement ductility capacity for column with aspect ratio of 2.0, 2.5 and 3.0, respectively. No significant increasing of the ductilities was obtained for columns with aspect ratio larger than 5.

Chapter 8. Design Procedure for Cross Ties

8.1. Introduction

No design procedures are currently available for cross ties connecting interlocking hoops. Based on the observed performance of specimens with high shear (Section 5.3), vertical cracks located in the interlocking region were observed in the specimen with di of 1.5R at about 58 % of the maximum force. Significant vertical shear stress is produced at the middepth of the column section in columns with d_i of 1.5R (Section 6.7). Due to the lack of confinement and the reduction of the horizontal component of the spirals bar force at middepth of the column, vertical cracks were formed due to the vertical shear stress at the interlocking region. Based on the observed and measured performance, horizontal cross ties connecting the interlocking hoops not only reduced and delayed vertical cracks in the interlocking region but also reduced the strength degradation compared with specimens without cross ties.

Three methods were studied to provide background for to the design of horizontal cross ties. A comparison among the three methods was made and reported in this chapter. Final simple recommendations for the design of horizontal cross ties connecting interlocking hoops are also presented in this chapter.

8.2. Shear Capacity Method

The shear capacity method was used to design the horizontal cross ties for specimen ISH1.5T and it is based on the shear reinforcement capacity (V_s) for confined circular or interlocking core sections defined in SDC[7] Section 3.6.3. The spiral shear capacity (V_s) is defined as follows

$$V_s = \frac{A_v f_{yh} D'}{s} \tag{8-1}$$

Where

A_v = Total area of shear reinforcement = $n\left(\frac{\pi}{2}\right)A_b$ (8-2)

n = number of individual interlocking spirals or hoop core sections

A_b = Area of individual reinforcing steel bar

f_{yh} = nominal yield stress of spirals or hoops

D' = cross-sectional dimension of confined concrete core measured between the centerline of the peripheral hoops or spiral (D'≈2xR)

s = spacing of spirals measured along the longitudinal axis of the structural member

The horizontal spacing of the spirals measured center-to-center of the spirals, d_i, or interlocking distance can be expressed in terms of the spiral radius, R (measured to outside of the spiral) as

$$d_i = \alpha R \tag{8-3}$$

Where

α = 1.0 to 1.5 based on BDS[6] Section 8.18.1.4.

Tanaka and Park[30] stated that when a shear force is applied to a column with interlocking spirals, the component of the spiral tension force at the middepth of the column section in the direction of the shear force is equal to the spiral tension force times cosine of the angle θ as shown in Fig. 8-1. The angle θ is related with d_i by the following equation:

$$\theta = \sin^{-1}\left(\frac{\frac{d_i}{2}}{R}\right) \tag{8-4}$$

Substitute Eq. 8-3 into Eq. 8-4, the angle θ becomes

$$\theta = \sin^{-1}\left(\frac{\alpha}{2}\right) \tag{8-5}$$

Based on Tanaka and Park[30] recommendation, the shear reinforcement capacity (V_s) at middepth of the column section can be found as follows

$$V_s = \frac{A_v f_{yh} D'}{s}\cos(\theta) \tag{8-6}$$

Since satisfactory seismic performance for columns with α=1.0 (d_i =1.0R) was found on previous and present experimental studies, the shear reinforcement capacity at middepth of the column section with α=1.0 was taken as a reference point for the design of horizontal cross ties for column with α>1.0. Therefore, the shear force that the cross ties need to resist should be equal to

$$V_t = V_{s1} - V_s \tag{8-7}$$

Where

$V_{s1} = \frac{A_v f_{yh} D'}{s} \cos(30)$ (Reference point column with α=1.0) and

V_t = shear capacity of the ties expressed as

$$V_t = A_t f_{yt} \left(\frac{\alpha R}{s_t} \right) \tag{8-8}$$

Where

A_t = area of two legs of bars = 2 A_{tie}

f_{yt} = nominal yield stress of ties

s_t = spacing of the ties

Assuming that D'= 2 x R (Fig. 8-1) and $f_{yh} = f_{yt}$, Eq. 8-8 can be substituted into Eq. 8-7 and the ratio A_t/s_t can be found as follows

$$\frac{A_t}{s_t} = \frac{1}{2} n\pi \left(\frac{\sqrt{3} - \sqrt{4 - \alpha^2}}{\alpha.} \right) \frac{A_b}{s} \tag{8-9}$$

If the cross ties and the spirals have the same bar size ($A_{tie} = A_b$), Eq. 8-9 can be rewritten in order to find the spacing of the ties as follows

$$s_t = \frac{1}{\beta} s \tag{8-10}$$

Where

$$\beta = n\pi \left(\frac{\sqrt{3} - \sqrt{4 - \alpha^2}}{4\alpha} \right)$$

Figure 8-2 shows the inverse of β versus α for n = 2 and 3 where n = the number of the interlocking spirals. The value of $1/\beta$ can be interpreted as the required spacing of the cross ties as a function of the spacing of the spirals. Based on Fig. 8-2 closer spacing of cross ties is required as α increases. In addition a closer spacing of cross ties is needed in column with two interlocking spirals compared with three interlocking spirals. Based on Eq. 8-10 the required spacing of the cross ties for columns with α of 1.5 needs to be at least 2.33 times the spacing of the spirals. Since the spacing of the spirals in ISH1.5T was 25.4 mm (1 in), a spacing of cross ties of 57.15 mm (2.25 in) was selected.

Two additional methods to design the cross ties were studied in order to compare and evaluate the design of the cross ties by the shear capacity method. The equilibrium of spirals force at the middepth method and the shear friction method are presented in Section 8.3 and Section 8.4, respectively.

8.3. Equilibrium of Spiral Forces at Middepth Method

This method is based on the equilibrium of the horizontal spiral force at the middepth of the column section. The component of the spiral tension force at the middepth of the column section in the direction of the shear force (Fig. 8-1) can be expressed as

$$T_v = T\cos(\theta) \tag{8-11}$$

Where

T = spiral tension force = $A_b f_y$

Previous experimental studies have shown satisfactory seismic performance for columns with α=1.0 (d_i =1.0R). Therefore, a column with α=1.0 was taken as the reference point for design the cross ties for columns with α>1.0. Thus, the difference of tension forces at the middepth of the column section between columns with α=1.0 and α>1.0 has to be taken by the cross ties as follows

$$T_{tie} = T_{1.0} - T_v \tag{8-12}$$

Where

T_{tie} = tension force carry by the ties = $A_t f_y$

$T_{1.0}$ = tension force in a column with α of 1.0 = $4A_b f_y \cos(30)$

Substituting Eq. 8-11 into Eq. 8-12 and taking into account the difference between the spacing of the spirals and cross ties, the ratio of A_t/s_t can be found as follows

$$\frac{A_t}{s_t} = \frac{4A_b}{s}\left(\cos(30) - \cos(\theta)\right) \tag{8-13}$$

Assuming that A_{tie} is equal to the area used in the spiral reinforcement A_b, and replacing cos(θ) by $\frac{\sqrt{4-\alpha^2}}{2}$ Eq. 8-13 can be rearranged in order to find the spacing of the ties as follows

$$s_t = \frac{1}{\gamma}s \tag{8-14}$$

Where

$\gamma = 2\cos(30^o) - \sqrt{4-\alpha^2}$

8.4. Shear-Friction Method

The shear–friction concept was used to find the area of cross ties needed in the interlocking region to resist the vertical shear at middepth of the section (Fig.8-3). The derivation of the vertical shear was based on uncracked beam theory. According to the ACI[1] code, the shear strength, $V_{n,}$ can be found as follows

$$V_n = \mu f_y A_{vf} \tag{8-15}$$

Where

A_{vf} = area of reinforcement extending across the potential crack at 90° (Fig 8-3)

μ = coefficient of friction between materials along the potential crack (μ = 1.4 for concrete cast monolithically- ACI[1] 11.7.4.3)

f_y = nominal yield stress of steel reinforcement

To account for the contribution of the spirals at the middepth and to allow for different spacing for the cross ties and spirals, Eq. 8-15 can be modified as follows:

$$V_n = \mu f_y \left(A_t + 4A_b \cos(\theta) \frac{s_t}{s} \right) \tag{8-16}$$

From Eq. 8-16, the area of the ties A_t required can be found as follows

$$A_t = \frac{V_n}{\mu f_y} - 4A_b \cos(\theta) \frac{s_t}{s} \tag{8-17}$$

In order to provided adequate reinforcement in the interlocking region, the shear strength V_n needs to be equal to the applied shear demand, V_u, calculated over the tie spacing as follows:

$$V_u = qt \tag{8-18}$$

Where

q = the shear flow = τ t

t = width of the member cross-sectional area, measured at the point where shear stress is to be determined

τ = shear stress $= \frac{VQ}{It}$

V = plastic shear demand

I = moment of inertia of the entire cross-sectional area computed about the neutral axis

Then the applied shear demand, V_u becomes

$$V_u = \frac{VQ}{I} s_t \tag{8-19}$$

Recalling that $V_n = V_u$ and substituting Eq. 8-19 into Eq. 8-17 and replacing $\cos(\theta)$ by $\frac{\sqrt{4-\alpha^2}}{2}$, the area of the required ties A_t can be found as follow:

$$A_t = \left(\lambda \frac{V}{\mu f_y} - \frac{2A_b\sqrt{4-\alpha^2}}{s} \right) s_t \tag{8-20}$$

Where

$$\lambda = \frac{Q}{I}$$

The maximum shear stress occurs at neutral axis. At neutral axis, λ can be found as follows:

$$\lambda = \frac{3\alpha R\pi R + 8R_c^{\,2} + 3\alpha^2 R^2}{2\alpha^3 R^3 + 3R_c^{\,3}\pi + 3R_c\alpha^2 R^2\pi + 16\alpha R R_c^{\,2}} \tag{8-21}$$

Where

R_c = the radius of the column (Fig. 8-1)

To simplify Eq. 8-20 the shear formula for an equivalent rectangular section was used and the ratio of A_t/s_t was found as shown in Eq. 8-22. The equivalent rectangular column was defined as the equivalent section width, b_{ew}, times the total depth. b_{ew} was found as the cross sectional area divide by total depth.

$$\frac{A_t}{s_t} = \left(\frac{3Vt}{2\mu f_y A_g} - \frac{2A_b\sqrt{4-\alpha^2}}{s} \right) \tag{8-22}$$

Where

A_g = gross area of section

8.5. Comparison of Different Methods and Design Recommendations

Figure 8-4 shows the required spacing of the cross ties using the shear capacity method with n=2, the equilibrium of spiral forces at middepth method, and the shear friction method. Since the shear friction method depends on parameters other than α, the

shear force (V), the nominal yield stress, (f_y), gross area, (A_g), the area of the spirals, and the spacing of the spirals, (s), of the specimens ISH1.0, ISH1.25 and ISH1.5 were used. Similar cross ties spacing was obtained for the three methods for α between 1.35 and 1.5. Larger spacing was obtained with equilibrium of force at the middepth method compared to the two others methods for α of less than 1.3. Cross ties spacing of 4 times the spacing of the spirals is needed for column with α of 1.25 based on the shear capacity method and shear friction method.

8.6. Recommended Simple Method for Design

Since vertical cracks were formed due to a vertical stress at the interlocking spirals region, it is reasonable to include the shear force in the expression to design the horizontal cross ties. Even though the shear friction account for the shear force, a negative ratio of A_t/s_t (Eq. 8-22) can be obtained for columns subjected to a shear index lowers than 7.

It should be noted that no column with a moderate shear index of 5 and d_i of 1.5 was tested to provide the evidence of the absence or the need for cross ties in the interlocking region. As a results and taking into account the comparison of the previous methods, the experimental results for the columns tested in the present study and the relatively low cost of cross ties, the following design recommendation for cross ties are proposed:

- The shear index should be used as a control design parameter to choose the cross ties in columns reinforced with interlocking spirals.

- The shear index is calculated by dividing the average shear stress by $0.083\sqrt{f'c}$ [MPa] or $\sqrt{f'c}$ [psi]. The average shear stress is found as the ratio between the lateral force capacity and the effective shear area which is defined as the gross area multiplied by 0.8.

- For columns with shear index between 3 and 7, and with horizontal distance between the centers of the spirals, d_i, between 1.25R and 1.5R, additional ties connecting the spirals need to be provided.

- For columns with shear index equal or greater than 7, additional horizontal ties connecting the spirals need to be provide regardless of the horizontal distance between the centers of the spirals, d_i.

- The individual cross tie bar should be of the same size as the spiral reinforcement and need be spaced at 2 times the spacing of the spirals. Cross ties should be detailed with 135 deg hook in one end and 90 deg hook in the other.

Chapter 9. Summary and Conclusions

9.1. Summary

The seismic performance of bridge columns with double interlocking spirals was studied though the experimental test of six specimens. The primary test variables were the level of average shear stress and the horizontal distance between the centers of the spirals, d_i, as a function of the radius of the spirals, R. Two 1/4-scale specimens with d_i of 1.0R and 1.5R subjected to low average shear stress and two 1/5-scale specimens with d_i of 1.0R and 1.5R subjected to high average shear stress were built, instrumented and tested at James E. Rogers and Louis Wiener Large-Scale Structures Laboratory at the University of Nevada, Reno. Based on the test results of the first two high shear columns, two additional variables, one an intermediate level of d_i (specimen ISH1.25) and the other with supplementary cross ties and d_i of 1.5R (specimen ISH1.5T) were studied after observed vertical cracks in one of the high shear columns with d_i of 1.5R.

All the columns were designed based on the BDS[6] and SDC[7] Caltrans design provisions. Typical steel ratios of 2.0% and 2.8% were chosen for the longitudinal reinforcement. The transverse steel ratios of 0.6%, 0.9% and 1.1% were selected based on target displacement ductility of 5 as well as the limitations of Caltrans provisions. Additional cross ties with the same bar size as the spirals and spacing of 2.0 times the spacing of the spirals were established based on a design recommendation from the present study. An axial load index of 10% was used based on recommendations by Caltrans. The scaling values used for the specimens were based on the capacity of the shake table system. The specimens with low average shear stress (ISL1.0, ISL1.5) were tested in single curvature whereas the specimens with high average shear stress (ISH1.0, ISH1.25, ISH1.5 and ISH1.5T) were tested in double curvature. All the columns had an oval shape and were tested under increasing amplitudes of the Sylmar record from the 1994 Northridge Earthquake using a shake table system. The loading was in the strong direction of the columns until failure. The columns were instrumented to measure acceleration, axial force, lateral force, lateral displacement, and curvature.

The seismic performance of two columns with d_i of 1.0R and 1.5R subjected to low shear stress was similar and satisfactory. Displacement ductility of 9.6 and 10.4 was achieved in specimens with d_i of 1.0R and 1.5R, respectively. The failure in both columns was due to rupture of the spirals and buckling of the longitudinal bars at the bottom of the column in the plastic hinge zone. Higher average strains in the spirals were measured in the specimen with d_i of 1.5R compared with the specimen with d_i of 1.0R. As a result slight degradation of the load capacity was observed in the specimen with d_i of 1.5R compared with the specimen with d_i of 1.0R. Nevertheless, this degradation occurred after displacement ductilities of 7.4 had been reached 10.4 which exceeded the target design displacement ductility of 5. In addition the column with d_i of 1.5R did not experience excessive shear cracking compared to the column with d_i of 1.0R.

Specimens with di of 1.0R and 1.25R subjected to high average shear stress showed similar seismic performance. Both columns failed in shear after a ductile

behavior with a displacement ductility of 4.7 and 5.0 for columns with d_i of 1.0R and 1.25R, respectively.

Vertical cracks located in the interlocking region were observed in the specimen with high shear and d_i of 1.5R at displacement ductility of 0.7. Vertical shear stress is believed to have led to the crack. This vertical stress is in direct proportion with the shear force in the column. Since relatively large area of plain concrete is present in the interlocking region in columns with d_i of 1.5R compared with columns with d_i of 1.0R, and taking into account the reduction of the horizontal component of the spirals bar force at the middepth of the section column (Tanaka and Park[29]), the column with d_i of 1.5R was more susceptible to vertical cracking. Based on the observed performance of ISH1.5T, horizontal cross ties connecting the hoops reduced and delayed vertical cracks in the interlocking region in columns subjected to high shear stress with d_i of 1.5R. Specimens with high shear and d_i of 1.5R did not achieve the target displacement ductility capacities of 5 but exceeded the minimum specified displacement ductility of 3. Similar degradation of the load capacity was observed in specimens with d_i of 1.0R and 1.25R from displacement ductilities of 3.61 to 4.7 and from displacement ductilities of 3.7 to 5, respectively. Specimens with d_i of 1.5R without and with cross ties experienced strength degradation after displacement ductilities of 3 and 2.8, respectively. However, less degradation was observed in specimens with d_i of 1.5R and cross ties compared to the others specimens. In general, the displacement ductility capacity decreased when the average shear stress index increased.

Detailed analyses of the specimens with low and high shear were performed to predict the lateral load carrying capacity and displacements. Strain rate effect on the material properties of the specimens was taken into account in the calculation of the lateral load and displacements. Program SPMC[34] was used to perform the moment curvature analyze. Elasto-plastic idealization of the M-ϕ curves was used to calculate the moment capacity, the flexural deformation at yield and the plastic deformation. A better agreement was found between experimental and analytical results for the yield deformations when bond slip and shear deformations were included. A difference between experimental and analytical ultimate displacement of 66% to 70% and 30% to 51% for specimens with low and high shear were found. These differences can be reduced if the appropriate plastic hinge length and ultimate shear deformation are used. The best correlation between experimental and analytical plastic hinge length was found using Dowell's[11] l_p equation and Benzoni's[4] shear equation with a difference of 27% between the calculated and measured l_p.

A modified shear stiffness model was proposed based on the 45° truss action principles and the experimental results of columns from this and two other studies. Significant improvement was achieved using the proposed post yield shear stiffness and the measured stiffness with difference between 3% and 24 %. Based on the proposed shear model, the displacement ductility capacity was increased by 15% to 24% when the ultimate shear deformation was included in the calculation of the ultimate deformation in specimens with high shear. The application of the proposed modified shear model was

illustrated through examples of typical columns with different aspect ratio. Based on the this application, ultimate shear deformation increased by 18%, 13% and 9% for the displacement ductility capacity for column with aspect ratios of 2.0, 2.5 and 3.0, respectively. No significant increase of the ductility was obtained for columns with aspect ratio larger than 5.

A comparison between three different methods to design the horizontal cross ties connecting the interlocking hoops was done. Design recommendation for additional horizontal cross ties were proposed based on the comparison of the three methods and experimental results of the column tested in the present study.

9.2. Conclusions

Based on the experimental and analytical studies performed in this research, the following observations and conclusions were made for bridge columns reinforced with double interlocking spirals:

1. The seismic performances of columns with d_i of 1.0R and 1.5R subjected to low average shear stress were similar and satisfactory with displacement ductility capacities of 9.6 and 10.4, respectively.

2. Slight degradation of the load capacity was observed in the specimen with d_i of 1.5R compared with specimen with d_i of 1.0R. However, this degradation was after the displacement ductility reached 7.4, which exceeded the target design displacement ductility of 5.

3. Since column with d_i of 1.5R did not lead to excessive shear cracking and based on the satisfactory displacement ductility capacity achieved in that column, Caltrans provision of maximum d_i value of 1.5R is adequate for column with low shear.

4. The seismic performance of the specimens with di of 1.0R and 1.25R subjected to high average shear stress was similar with a good agreement with the target ductility of 5. Both columns failed in shear after ductile behavior with a displacement ductility of 4.7 and 5.0 for column with d_i of 1.0R and 1.25R, respectively.

5. Vertical cracks located in the interlocking region were observed in the specimen with high shear and d_i of 1.5R under relatively small earthquakes.

6. Since a relatively larger area of plain concrete exists in the interlocking region in columns with d_i of 1.5R compared with column with d_i of 1.0R, and taking into account the reduction of the horizontal component of the spirals bar force at the middepth of the section column, vertical cracks were formed due to a vertical shear stress in the interlocking region.

7. Based on the observed and measured performances, horizontal cross ties connecting the interlocking hoops not only reduced and delayed vertical cracks in the interlocking region in the column with d_i of 1.5 but also reduced the strength degradation compared with specimens without cross ties.

8. The displacement ductility capacity decreased when the average shear stress index increased.

9. A better agreement was found between experimental and analytical results for the yield deformations when bond slip and shear deformations were included.

10. Dowell's[11] plastic hinge length, l_p, using Benzoni's[4] shear capacity showed the closest correlation with the measured l_p.

11. Based on the proposed shear stiffness model, an increase in the displacement ductility capacity of 15% to 24% was obtained when the ultimate shear deformation was included in the calculation of the ultimate deformation in specimens with high shear.

9.3. Recommendations

The following recommendations are for columns reinforced with interlocking spirals and they are based on the experimental and analytical studies presented in this study.

1. The average shear stress index should be used as a control design parameter to choose the horizontal distance between the centers of the spirals, d_i, and the addition of cross ties in columns reinforced with interlocking spirals.

2. The shear index is calculated by dividing the average shear stress by $0.083\sqrt{f'c}$ [MPa] or $\sqrt{f'c}$ [psi]. The average shear stress is found as the ratio between the lateral force capacity and the effective shear area which is defined as the gross area multiplied by 0.8.

3. For columns with shear index equal to or less than 3, the horizontal distance between the centers of the spirals, d_i, can be taken as any value between d_i = 1.0R and d_i = 1.5R, where R is the radius of the spirals measured to outside or the spiral.

4. For columns with shear index between 3 and 7, the horizontal distance between the centers of the spirals, d_i, can be taken as any value between d_i = 1.0R and d_i = 1.25, where R is the radius of the spirals. When d_i is selected between 1.25R and 1.5R, cross ties connecting the spirals need to be provided.

5. For columns with shear index equal or greater than 7, cross ties connecting the spirals need to be provided regardless of the horizontal distance between the centers of the spirals, d_i.

6. The individual cross tie bars should be of the same size as the spiral reinforcement. A maximum spacing of 2 times the spacing of the spirals should be used for the additional horizontal ties. Horizontal ties should be detailed with 135° hook in one end and 90° hook in the other.

7. Bond slip and shear deformation should be included in the calculation of the idealized yield displacement.

8. Ultimate shear deformation needs to be included in the calculation of ultimate displacement for column with aspect ratio of less than 3.0.

REFERENCE

1. **American Concrete Institute Committee 318**, "Building Code Requirements for Structural Concrete (ACI 318-02)", American Concrete Institute, Farmington Hills, Michigan, 2002, 443 pp.
2. **Ashraf EI-Bahy, Sashi K. Kunnath, Andrew Taylor, and Williams C. S.,** "Cumulative Seismic Damage of Reinforced Bridge Piers", Technical Report NCEER-96-00XX, 1996.
3. **Baker, A. L. L and Amarkone, A. M. N.,** "Inelastic Hyperstatic Frames Analysis", Proceeding of the International Symposium on the Flexural Mechanic of Reinforced Concrete, ASCE-ACI, Miami, November 1964, pp. 85-142.
4. **Benzoni, G., Priestley, M.J.N., and Seible, F.,** "Seismic Shear Strength of Columns with Interlocking Spiral Reinforcement", 12th World Conference on Earthquake Engineering, Auckland, New Zealand, 2000, 8 pp.
5. **Buckingham, G.C.,** "Seismic Performance of Bridge Columns with Interlocking Spirals Reinforcement", M.S. Thesis, Washington State University, Pullman, Washington, 1992, 146 pp.
6. **California Department of Transportation**, "Bridge Design Specifications", Engineering Service Center, Earthquake Engineering Branch, California, July 2000.
7. **California Department of Transportation**, "Seismic Design Criteria Version 1.2", Engineering Service Center, Earthquake Engineering Branch, California, December 2001.
8. **Cheng Z., Saiidi, S., and Sanders D.,** "Seismic Design of Two-Way Hinges", (In Preparation), CCEER, University of Nevada, Reno.
9. **Chopra, A.,** "Dynamic of Structures", Prentice Hall, USA 1995, 729 pp.
10. **Computer and Structures INC.,** "Structural Analysis Program SAP-2000", Version 8, Berkeley, California, USA, June 2002, 419 pp.
11. **Dowell R., and Hines E.,** "Plastic Hinge Length of Reinforced Concrete Bridge Columns", Third National Seismic Conference & Workshop On Bridges & Highways, April- May, pp. 323-334.
12. **JSCE Concrete Committee,** "Standard Specification for Design and Construction of Concrete Structures" (in Japanese), Japan Society of Civil Engineers, Japan 1996, 230 pp.
13. **Kim, Jin-Keun and Park, Chan-Kyu,** "The Behavior of Concrete Columns with Interlocking Spirals", Engineering Structures, Vol. 21, No 11, October 1999, pp. 945-953.
14. **Kulkarni, S.M., and S. P. Shah,** "Response of Reinforced Concrete Beams at High Strain Rates", ACI Structural Journal, Vol. 95, No. 6, November-December 1998, pp. 705-715.
15. **Laplace, P., Sanders, D., and Saiidi, M.,** "Experimental Study and Analysis of Retrofit Flexure and Shear Dominated Circular Reinforced Concrete Bridge Columns Subjected to Shake Table Excitation", Report No. CCEER-01-6, University of Nevada, Reno 2001, 439 pp.

16. **Laplace, P., Sanders, D., Douglas, B., and Saiidi, M.,** "Shake Table Testing of Flexure Dominated Reinforced Concrete Bridge Columns", Report No. CCEER-99-13, University of Nevada, Reno 1999, 148 pp.
17. **Mander, J. Priestley, M.J.N and Park, R.,** "Theoretical Stress-Strain Model for Confined Concrete Columns", ASCE Journal of Structural Engineering, Vol. 114, No 8, August 1988, pp 1804-1846.
18. **Mc Guire W., Gallagher R., Ziemian D.,** "Matrix Structural Analysis", First Edition, John Wiley & Sons, New York 1979, 460 pp.
19. **Mizugami, Y.,** "Efficiency of Lateral Reinforcement in Interlocking Spirals Re-bar", presented at the 16th US-Japan Bridge Engineering Workshop, October 2-4, 2000, pp. 265-276.
20. **Mösrh, E.,** Concrete-Steel Construction, McGraw-Hill Book Company, New York, 1909, 368 pp. (English translation by E.P. Goodrich of 3rd ed. of Der Eisenbetonbau, 1st ed., 1902.)
21. **Ordaz, M., Montoya C., "**DEGTRA 2000 " Version 2.0.2, Instituto de Ingeniería, Universidad Nacional Autónoma de México, 2000.
22. **Park, R. and Paulay, T.,** "Reinforced Concrete Structures", John Wiley & Sons, USA 1975, 769 pp.
23. **Paulay, T. and Priestley, M.J.N.,** "Seismic Design of Reinforced Concrete and Masonry Buildings", John Wiley & Sons, USA 1992, 744 pp.
24. **Priestley, M. J. N., Seible, F., and Benzoni, G.,** "Seismic Performance of Circular Columns with Low Longitudinal Steel Ratios", Rep. No. SSRP-97/15, University of California, San Diego, La Jolla, California, 75 pp.
25. **Priestley, M. J. N., Verma, R. and Xias, Y.,** "Seismic Shear Strength of Reinforced Concrete Columns," ASCE Journal of Structural Engineering, Vol. 120, No. 8, August 1994, pp 2310-2329.
26. **Priestley, N., Seible, F., Calvi, G.,** "Seismic Design and Retrofit of Bridges", John Wiley & Sons, New York 1996, 686 pp.
27. **Seyed Mahan, M.,** "User's Manual for wFPREP and wFRAME", Version 1.13, California Department of Transportation, USA 1995, 16 pp.
28. **Seyed Mahan, M.,** "User's Manual for xSECTION", Version 2.40, California Department of Transportation, USA March 1999, 21 pp.
29. **Standard New Zealand**, " Concrete Structures Standards (NZS 3101:1995), Standards Association of New Zealand, Wellington, New Zealand, 1995, 520 pp.
30. **Tanaka, H., and Park, R.,** "Seismic Design and Behavior of Reinforced Concrete Columns with Interlocking Spirals", ACI Structural Journal, Vol. 90, No 2, March-April 1993, pp. 192-203.
31. **Tanaka, H., and Park, R.,** "Use of Interlocking Spirals for Transverse Reinforcement in Bridges Columns", Department of Civil Engineering, University of Canterbury, New Zealand, 1999, 458 pp.
32. **Tsitotas M.A., and Tegos I.A.,** "Seismic Behaviour of R/C Columns and Beams with Interlocking Spirals", Advance in Earthquake Engineering, Vol 2, Oct 30-Nov 1, 1996, pp. 449-461.

33. **Vecchio, Frank J., Collins, Michael P.,** "The Modified Compression-Field Theory for Reinforced Concrete Elements Subjected Shear", ACI Journal, Vol. 83, No 2, March-April 1986, pp. 219-231
34. **Wehbe, N., and Saiidi, S.,** "Moment-Curvature Analysis for Interlocking Spirals SPMC V 1.0", Report No. CCEER-03-1, University of Nevada, Reno, May 2003, 114 pp.
35. **Wehbe, N., Saiidi, S., and Sanders, D.,** "Effects of Confinement and Flare on the Seismic Performance of Reinforced Concrete Bridges Columns", Report No. CCEER-97-2, University of Nevada, Reno 1997, 407 pp.

Table 1-1 Relevant Details of the Previous Studies Specimens with Interlocking Spirals

Author	Specimen No	Dimensions						Aspect Ratio	di	f'c		Axial Load Factor	Shear Index	Steel reinforcement		μ_c
		Width		Depth		Height								ρl	ρs	
		[mm]	[in]	[mm]	[in]	[mm]	[in]		(xR)	[MPa]	[psi]	[P/f'c Ag]		[%]	[%]	
Tanaka and Park	1	600	23.6	400	15.7	1784	70	3.0	1.20	21.2	3075	0.1	4.93	2.14	1.08	10
	2	600	23.6	400	15.7	1784	70	3.0	1.20	29.7	4308	0.3	5.55	2.14	0.92	10
	3	600	23.6	400	15.7	1784	70	3.0	1.20	24.6	3568	0.5	6.11	2.14	1.15	12
Buckingham et al	1	391	15.4	254	10.0	1219	48	3.1	1.20	31.7	4600	0.09	7.72	2.11	0.44	4
	2	391	15.4	254	10.0	1219	48	3.1	1.20	31.7	4600	0.09	7.18	3.02	1.78	7
	3	422	16.6	254	10.0	1219	48	2.9	1.47	31.7	4600	0.09	7.89	1.94	0.44	4
	4	391	15.4	254	10.0	1219	48	3.1	1.20	31.7	4600	0.09	7.38	1.66	0.44	4
	5	391	15.4	254	10.0	1219	48	3.1	1.20	31.7	4600	0.09	4.99	2.11	0.89	8
	6	391	15.4	254	10.0	1219	48	3.1	1.20	31.7	4600	0	T*	2.11	0.44	8
Tsitotas and Tegos	1	300	11.8	205	8.1	650	26	2.2	1.00	22.5	3263	0.1	9.07	2.09	1.43	N.A
Benzoni et al	1	600	23.6	400	15.7	2440	96	2.0	1.11	35.2	5101	0.022	6.63	2.90	0.40	3
	2	600	23.6	400	15.7	2440	96	2.0	1.11	35.2	5101	-0.1	5.08	2.90	0.40	4
	3	600	23.6	400	15.7	2440	96	2.0	1.11	35.2	5101	0.35	8.98	2.90	0.40	2
	4	600	23.6	400	15.7	2440	96	2.0	1.11	35.2	5101	-0.1 to 0.35	8.30	2.90	0.40	6
Mizugami	1	600	23.6	900	35.4	3000	118	3.3	1.09	28.1	4076	0.03	1.74	1.63	0.19	7
	2	600	23.6	900	35.4	3000	118	3.3	1.09	39.7	5758	0.02	1.53	1.63	0.29	8
	3	600	23.6	900	35.4	3000	118	3.3	1.09	29.2	4235	0.03	1.81	1.63	0.52	7
	4	850	33.5	600	23.6	1620	64	1.9	1.09	30.9	4482	0.05	3.33	1.05	0.46	12
	5	850	33.5	600	23.6	1620	64	1.9	1.09	29.3	4250	0.05	3.17	1.05	0.23	10
	6	850	33.5	600	23.6	1620	64	1.9	1.09	31.4	4554	0.05	3.28	1.05	0.12	8

Note: d_i = the spacing between center to center of the spirals
xR = times the spiral radius
ρl = ratio of longitudinal reinforcement
ρs = ratio of transversal reinforcement to concrete core
μ_c = Local displacement ductility capacity

Table 2-1 Test Variables for Column Specimens

Specimen	Shear Index	d_i (x R)
ISL1.0	3.0	1.0
ISL1.5	3.0	1.5
ISH1.0	7.0	1.0
ISH1.25	7.0	1.25
ISH1.5	7.0	1.5
ISH1.5T	7.0	1.5

Table 2-2 Longitudinal Bars Size in the Interlocking Portion

Size Of The Rebars Used Outside The Interlocking Portion	Size Of The Rebars Required Inside The Interlocking Portion
32.3 mm ϕ (#10)	19.1 mm ϕ (#6)
35.8 mm ϕ (#11)	25.4 mm ϕ (#8)
43 mm ϕ (#14)	28.7 mm ϕ (#9)
57.3 mm ϕ (#18)	35.8 mm ϕ (#11)

Table 2-3 Model Scale Factors for Different Parameters

Dimension	Factor
Model Scale	Model Scale = l_r
Time (axial to lateral mass ratio = 1)	$\sqrt{l_r}$
Time (axial to lateral mass ratio ≠ 1)	$\sqrt{\frac{w_i}{P} l_r}$ where w_i = weight of the inertia system P = applied axial force on the column
Length	l_r
Force	l_r^2
Area	l_r^2
Stress	1.0
Strain	1.0
Strain Rate	$1/\sqrt{l_r}$
Mass	l_r^2
Period	$\sqrt{l_r}$
Moment	l_r^2

Table 2-4 Shake Table Specifications

Dimension	Capacity
Table Size	4.3m x 4.3m (14ft x 14ft)
Table Weight	146.8 kN (33 kip)
Maximum Payload	444.8 kN (100 kip)
Maximum Acceleration	1g at 444.8 kN (100 kip) Payload 2.4g at 0 kN (0 kip) Payload
Maximum Velocity	101.6 cm/sec (40 in/sec)
Maximum Static Displacement	+/- 35.6cm (14 in)
Maximum Dynamic Displacement	+/- 30.5cm (12 in)
Roll Capacity (max payload)	542 kN-m (400 kip-ft) moment
Pitch Capacity (max payload)	1356 kN-m (1000 kip-ft) moment
Yaw Capacity (max payload)	542 kN-m (400 kip-ft) moment
Maximum Actuator Force	734 kN (165 kip)
Operating Frequency	1-30hz

Table 2-5 Summary of Values Last Iteration

		Specimens					
		ISL1.0	**ISL1.5**	**ISH1.0**	**ISH1.25**	**ISH1.5**	**ISH1.5T**
ϕ_y	[Rad/m]	0.01444	0.01130	0.01608	0.01534	0.01442	0.01442
	[Rad/in]	0.00037	0.00029	0.00041	0.00039	0.00037	0.00037
ϕ_u	[Rad/m]	0.14591	0.14591	0.11260	0.13028	0.11969	0.11972
	[Rad/in]	0.00371	0.00371	0.00286	0.00331	0.00304	0.00304
ϕ_p	[Rad/m]	0.13147	0.13461	0.09652	0.11493	0.10527	0.10530
	[Rad/in]	0.00334	0.00342	0.00245	0.00292	0.00267	0.00267
L_p	[cm]	21.5	24.3	19.4	19.4	19.4	19.4
	[in]	8.5	9.59	7.65	7.65	7.65	7.65
θ_p	[Rad]	0.028	0.033	0.019	0.022	0.020	0.020
Δ_p	[cm]	3.86	5.59	2.40	3.13	3.18	3.18
	[in]	1.52	2.20	0.94	1.23	1.25	1.25
Δ_y^{col}	[cm]	1.04	1.26	0.58	0.65	0.74	0.74
	[in]	0.41	0.50	0.23	0.26	0.29	0.29
Δ_c	[cm]	4.90	6.85	2.98	3.79	3.92	3.92
	[in]	1.93	2.70	1.17	1.49	1.54	1.54
μ		4.7	5.4	5.1	5.8	5.3	5.3

Table 2-6 Design Parameters of the Specimens

Specimen	Scale Factor	Shear Index	Aspect Ratio	d_i	Steel reinforcement	
					ρ_l	ρ_s
				(x R)	[%]	[%]
ISL1.0	0.25	3.0	3.3	1.0	2.0	1.1
ISL1.5		3.0	3.6	1.5	2.0	1.1
ISH1.0	0.2	7.0	2.0	1.0	2.9	0.6
ISH1.25		7.0	2.0	1.25	2.8	0.9
ISH1.5		7.0	2.1	1.5	2.9	0.9
ISH1.5T*		7.0	2.1	1.5	2.9	0.9**
Note: ρ_l = ratio of longitudinal reinforcement						
ρ_s = ratio of transversal reinforcement to concrete core						
* = column with additional cross ties						
** = steel ratio from additional cross ties is not included						

Table 2-7 Footing Height

Specimen	Footing Height cm [in]
ISL1.0	66.0 [26]
ISL1.5	68.6 [27]
ISH1.0	71.2 [28]
ISH1.25	66.0 [26]
ISH1.5	78.7 [31]
ISH1.5T	78.7 [31]

Table 2-8 Material Properties Program SPMC

Material Properties			Specimens		
			Low Shear	High Shear	
Unconfined Concrete	f'_c	MPa	34.5	34.5	
		psi	5000	5000	
	ε_o		0.002	0.002	
	ε_c		0.005	0.005	
Confined Concrete	f'_{cc}	MPa	49.3	ISH1.0	ISH1.25,ISH1.5 and ISH1.5T
				43.2	47.1
		psi	7146	6273	6832
	ε'_{cc}		0.006	0.005	0.006
	ε_{cu}		0.017	0.012	0.015
Steel	f_y	MPa	475	475	
		psi	68000	68000	
	E	MPa	200000	200000	
		psi	29000000	29000000	
	ε_{sh}		0.015	0.015	
	ε_{su}		0.09	0.09	

Table 2-9 Plastic Moment, Idealized Yield Curvature and Ultimate Curvature

Idealized Values		Specimen					
		ISL1.0	ISL1.5	ISH1.0	ISH1.25	ISH1.5	ISH1.5T
M_p	kN-m	230	316	160	190	225	225
	Kips-in	2038	2796	1418	1678	1992	1992
ϕ_y	Rad/m	0.01444	0.01130	0.01608	0.01534	0.01442	0.01442
	Rad/in	0.00037	0.00029	0.00041	0.00039	0.00037	0.00037
ϕ_u	Rad/m	0.14591	0.14591	0.11260	0.13028	0.11969	0.11972
	Rad/in	0.00371	0.00371	0.00286	0.00331	0.00304	0.00304

Table 2-10 Elastic Shear, Idealized Yield Displacement and Elastic Stiffness

		Specimens					
		ISL1.0	**ISL1.5**	**ISH1.0**	**ISH1.25**	**ISH1.5**	**ISH1.5T**
V_p	[kN]	156	173	218	237	257	257
	[Kips]	35	39	49	53	58	58
Δ_y^{col}	[cm]	1.04	1.26	0.58	0.65	0.74	0.74
	[in]	0.41	0.50	0.23	0.26	0.29	0.29
Ke	[kN/cm]	150	137	375	363	350	349
	[Kips/in]	85	78	214	207	200	199

Table 2-11 Comparison of Results Dynamic Analysis Program RCShake

		Specimen ISL1.0			Specimen ISL1.5		
		EQ Motion			EQ Motion		
EQ Parameter	**Units**	**El Centro**	**Sylmar**	**ATC-32D**	**El Centro**	**Sylmar**	**ATC-32D**
Unscaled EQ Acceleration	[g]	0.32	0.606	0.44	0.32	0.606	0.44
Scaled EQ Acceleration Factor		2.48	1.30	1.79	3.17	1.66	2.286
Scaled EQ Acceleration	[g]	0.79	0.79	0.79	1.01	1.01	1.01
Unscaled Duration	[s]	54	30	20	54	30	20
Scale Time Factor		0.522	0.522	0.522	0.522	0.522	0.522
Scaled Duration	[s]	28	16	10	28	16	10
Column Response							
Maximum Top Deflection	cm	4.11	5.31	4.11	4.67	6.30	4.75
	in	1.62	2.09	1.62	1.84	2.48	1.87
Maximum Lateral Force	kN	156	156	156	173	173	173
	Kips	35	35	35	39	39	39
Maximum Ductility Demand		4.0	5.1	3.9	3.7	5.0	3.8

Table 3-1 Footing Concrete Compressive Strength

		Specimens					
Day	**Units**	**ISL1.0**	**ISL1.5**	**ISH1.0**	**ISH1.5**	**ISH1.25**	**ISH1.5T**
7	**MPa**	26.4		26.6		31.6	
	psi	3829		3853		4590	
14	**MPa**	31.3		37.2		38.6	
	psi	4544		5395		5603	
28	**MPa**	31.9		41.0		39.6	
	psi	4624		5944		5751	
Test	**MPa**	48.8	44.6	41.7	42.1	39.5	40.8
	psi	7083	6462	6051	6105	5727	5922
Test Average	**MPa**	**46.7**		**41.9**		**40.1**	
	psi	**6772**		**6078**		**5824**	

Table 3-2 Column Concrete Compressive Strength

		Specimens					
Day	**Units**	**ISL1.0**	**ISL1.5**	**ISH1.0**	**ISH1.5**	**ISH1.25**	**ISH1.5T**
7	**MPa**	21.1		25.3		29.9	
	psi	3064		3668		4337	
14	**MPa**	23.4		28.9		34.6	
	psi	3401		4195		5023	
28	**MPa**	28.1		29.1		40.4	
	psi	4075		4215		5866	
Test	**MPa**	36.9	36.7	30.9	31.3	42.7	47.5
	psi	5350	5328	4481	4546	6197	6886
Test Average	**MPa**	**36.8**		**31.1**		**45.1**	
	psi	**5339**		**4514**		**6542**	

Table 3-3 Longitudinal Steel Bars 9.5 mm ϕ (# 3) Properties

		Specimens		
Properties	**Units**	**ISL1.0-ISL1.5**	**ISH1.0-ISH1.5**	**ISH1.25-ISH1.5T**
f_y	**MPa**	462	443	431
	ksi	67	64	63
ε_{sh}		Not Measured	Not Measured	0.008
f_u	**MPa**	709	664	685
	ksi	103	96	99
ε_{su}		Not Measured	Not Measured	0.16

Table 3-4 Plain Wires (W2.8 and W2.0) Properties

		Specimens	
Properties	**Units**	**ISL1.0-ISL1.5 (W2.8)**	**ISH1.0-ISH1.5-ISH1.25-ISH1.5T (W2.0)**
f_y	**MPa**	445	432
	ksi	65	63
f_u	**MPa**	529	511
	ksi	77	74
ε_{su}		Not Measured	0.08

Table 4-1 Loading Protocol

	ISL1.0		ISL1.5	
	FREE VIBRATION			
	FINE TUNNING			
	FREE VIBRATION			
Run No	**(g)**	**(x Sylmar)**	**(g)**	**(x Sylmar)**
1	0.06	0.1	0.06	0.1
2	0.12	0.2	0.12	0.2
3	0.18	0.3	0.24	0.4
	FREE VIBRATION			
4	0.30	0.5	0.36	0.6
5	0.45	0.75	0.48	0.8
6	0.61	1	0.61	1
	FREE VIBRATION			
7	0.76	1.25	0.76	1.25
8	0.91	1.5	0.91	1.5
9	1.06	1.75	1.06	1.75
10	1.21	2	1.21	2
11			1.29	2.125

Table 4-2 Performance Specimen ISL1.0

Run	(X Sylmar)	PGA(g)	μ_d	PERFORMANCE
1 to 3	0.1 - 0.3	0.06 - 0.18	0.2-0.8	Flexural Cracks
4	0.5	0.30	1.5	First Spalling and Shear Cracks
5 to 7	0.75 - 1.25	0.45 - 0.76	1.7-2.8	Extension of Cracks and Spalling
8 to 9	1.5 – 1.75	0.91 – 1.06	4.1-5.6	Spirals and Long. Bars Visible
10	2	1.21	9.6	Flexural Failure

Table 4-3 Performance Specimen ISL1.5

Run	(X Sylmar)	PGA(g)	μ_d	PERFORMANCE
1 to 6	0.1 - 1	0.06 - 0.24	0.1-1.5	Flexural Cracks
7	1.25	0.76	2.4	First Spalling And Shear Cracks
8	1.5	0.91	3.1	Extension of Cracks and Spalling
9 to 10	1.75 – 2.0	1.06 – 1.21	4.5-7.5	Spirals Visible
11	2.125	1.29	10.4	Flexural Failure

Table 4-4 Target and Achieved Peak Table Accelerations for Specimen ISL1.0

Run No	Input Motion [x Sylmar]		Target [g]	Achieved [g]	Achieved PGA / Target PGA Target PGA
1	0.1	Max	0.06	0.07	1.10
		Min	-0.03	-0.04	1.47
2	0.2	Max	0.12	0.14	1.17
		Min	-0.06	-0.08	1.33
3	0.3	Max	0.18	0.22	1.19
		Min	-0.09	-0.12	1.38
4	0.5	Max	0.30	0.32	1.06
		Min	-0.15	-0.22	1.49
5	0.75	Max	0.45	0.54	1.18
		Min	-0.22	-0.34	1.52
6	1	Max	0.61	0.73	1.21
		Min	-0.30	-0.45	1.52
7	1.25	Max	0.76	0.94	1.25
		Min	-0.37	-0.60	1.62
8	1.5	Max	0.91	1.13	1.25
		Min	-0.45	-0.81	1.81
9	1.75	Max	1.06	1.33	1.26
		Min	-0.52	-0.97	1.87
10	2	Max	1.21	1.53	1.26
		Min	-0.60	-1.13	1.90

Table 4-5 Target and Achieved Peak Table Accelerations for Specimen ISL1.5

Run No	Input Motion		Target	Achieved	Achieved PGA / Target PGA
	[x Sylmar]		[g]	[g]	Target PGA
1	0.1	Max	0.06	0.07	1.18
		Min	-0.03	-0.05	1.74
2	0.2	Max	0.12	0.14	1.19
		Min	-0.06	-0.09	1.50
3	0.3	Max	0.18	0.27	1.50
		Min	-0.09	-0.18	1.97
4	0.5	Max	0.30	0.42	1.39
		Min	-0.15	-0.28	1.89
5	0.75	Max	0.45	0.59	1.31
		Min	-0.22	-0.38	1.69
6	1	Max	0.61	0.77	1.26
		Min	-0.30	-0.45	1.52
7	1.25	Max	0.76	0.94	1.25
		Min	-0.37	-0.59	1.59
8	1.5	Max	0.91	1.16	1.28
		Min	-0.45	-0.79	1.76
9	1.75	Max	1.06	1.36	1.28
		Min	-0.52	-0.96	1.83
10	2	Max	1.21	1.58	1.30
		Min	-0.60	-1.13	1.89
11	2.125	Max	1.29	1.69	1.31
		Min	-0.63	-1.22	1.93

Table 4-6 Target and Achieved Spectral Response Acceleration for Specimen ISL1.0

Run No	Input Motion [x Sylmar]	Period [s]	Target [g]	Achieved [g]	Achieved / Target
1	0.1	0.319	0.10	0.11	1.12
2	0.2	0.328	0.18	0.21	1.14
3	0.3	0.328	0.27	0.34	1.22
4	0.5	0.427	0.58	0.51	0.89
5	0.75	0.441	0.74	0.74	0.99
6	1.0	0.493	0.54	0.62	1.15
7	1.25	0.581	0.59	0.46	0.77
8	1.5	0.676	0.78	0.69	0.88
9	1.75	0.676	0.91	0.77	0.85
10	2.0	0.676	1.04	0.84	0.81

Table 4-7 Target and Achieved Spectral Response Acceleration for Specimen ISL1.5

Run No	Input Motion [x Sylmar]	Period [s]	Target [g]	Achieved [g]	Achieved / Target
1	0.1	0.319	0.11	0.09	0.81
2	0.2	0.319	0.22	0.17	0.78
3	0.4	0.388	0.41	0.47	1.15
4	0.6	0.413	0.57	0.63	1.09
5	0.8	0.441	0.72	0.63	0.87
6	1.0	0.441	0.92	0.78	0.85
7	1.25	0.532	0.46	0.54	1.16
8	1.5	0.676	0.71	0.71	1.00
9	1.75	0.676	0.79	0.83	1.05
10	2.0	0.676	0.88	0.94	1.08
11	2.125	0.676	0.91	1.00	1.10

Table 4-8 Measured Peak Forces and Displacement for Specimen ISL1.0

Peak Force								
	Maximum				Minimum			
Motion	Force		Displacement		Force		Displacement	
xSylmar	[kN]	[Kips]	[mm]	[in]	[kN]	[Kips]	[mm]	[in]
0.1	45.9	10.3	2.8	0.11	-50.6	-11.4	-2.7	-0.11
0.2	55.2	12.4	3.7	0.15	-70.6	-15.9	-5.7	-0.23
0.3	111.7	25.1	12.1	0.47	-132.9	-29.9	-13.8	-0.54
0.5	134.1	30.1	20.5	0.81	-155.9	-35.0	-25.5	-1.00
0.75	135.9	30.5	21.2	0.83	-138.8	-31.2	-24.3	-0.96
1	141.3	31.8	25.5	1.00	-154.5	-34.7	-33.3	-1.31
1.25	142.8	32.1	31.8	1.25	-165.0	-37.1	-46.6	-1.84
1.5	134.4	30.2	34.4	1.35	-169.3	-38.0	-69.9	-2.75
1.75	120.3	27.0	30.3	1.19	-173.0	-38.9	-94.8	-3.73
2	135.2	30.4	38.4	1.51	-171.6	-38.6	-137.7	-5.42
Peak Displacement								
	Maximum				Minimum			
Motion	Force		Displacement		Force		Displacement	
xSylmar	[kN]	[Kips]	[mm]	[in]	[kN]	[Kips]	[mm]	[in]
0.1	45.9	10.33	2.8	0.11	-42.0	-9.4	-2.8	-0.11
0.2	50.8	11.43	4.1	0.16	-70.6	-15.9	-5.7	-0.23
0.3	111.7	25.12	12.1	0.47	-120.4	-27.1	-14.7	-0.58
0.5	134.1	30.14	20.5	0.81	-155.9	-35.0	-25.5	-1.00
0.75	127.2	28.59	22.7	0.89	-138.8	-31.2	-24.3	-0.96
1	138.0	31.01	27.4	1.08	-154.5	-34.7	-33.3	-1.31
1.25	134.3	30.19	36.2	1.43	-160.4	-36.1	-52.8	-2.08
1.5	125.7	28.25	35.8	1.41	-168.1	-37.8	-77.4	-3.05
1.75	120.3	27.04	30.3	1.19	-161.7	-36.4	-104.8	-4.13
2	131.8	29.64	43.8	1.72	-163.9	-36.8	-162.5	-6.40

Table 4-9 Measured Peak Forces and Displacement for Specimen ISL1.5

Peak Force								
	Maximum				Minimum			
Motion	Force		Displacement		Force		Displacement	
xSylmar	[kN]	[Kips]	[mm]	[in]	[kN]	[Kips]	[mm]	[in]
0.1	40.6	9.12	1.9	0.07	-43.7	-9.83	-2.4	-0.09
0.2	62.9	14.13	3.7	0.14	-69.9	-15.72	-6.0	-0.23
0.4	144.9	32.56	15.7	0.62	-152.2	-34.21	-24.3	-0.96
0.6	147.8	33.22	17.2	0.68	-142.6	-32.06	-22.6	-0.89
0.8	159.7	35.89	24.1	0.95	-155.1	-34.88	-28.1	-1.11
1	152.3	34.23	20.4	0.80	-142.1	-31.95	-24.1	-0.95
1.25	166.9	37.52	29.8	1.17	-167.5	-37.66	-43.0	-1.69
1.5	161.0	36.20	37.9	1.49	-167.2	-37.59	-57.2	-2.25
1.75	139.3	31.32	30.1	1.18	-175.1	-39.35	-82.7	-3.25
2	150.9	33.93	36.0	1.42	-177.6	-39.93	-115.3	-4.54
2.125	144.0	32.36	33.4	1.31	-164.9	-37.08	-137.9	-5.43
Peak Displacement								
	Maximum				Minimum			
Motion	Force		Displacement		Force		Displacement	
xSylmar	[kN]	[Kips]	[mm]	[in]	[kN]	[Kips]	[mm]	[in]
0.1	40.6	9.12	1.9	0.07	-35.0	-7.87	-2.8	-0.11
0.2	62.9	14.13	3.7	0.14	-69.9	-15.72	-6.0	-0.23
0.4	128.3	28.85	16.3	0.64	-152.2	-34.21	-24.3	-0.96
0.6	144.9	32.58	19.4	0.76	-142.6	-32.06	-22.6	-0.89
0.8	149.7	33.65	24.9	0.98	-135.1	-30.37	-28.3	-1.11
1	145.9	32.79	21.7	0.85	-142.1	-31.95	-24.1	-0.95
1.25	158.0	35.51	33.0	1.30	-167.5	-37.66	-43.0	-1.69
1.5	161.0	36.20	37.9	1.49	-152.9	-34.38	-69.5	-2.74
1.75	127.5	28.66	30.4	1.20	-169.4	-38.09	-98.1	-3.86
2	150.9	33.93	36.0	1.42	-176.0	-39.57	-138.3	-5.45
2.125	135.4	30.45	36.1	1.42	-123.3	-27.72	-216.5	-8.52

Table 4-10 Dynamic Properties from Low Level Elastic Response for Specimen ISL1.0

Motion	Frequency	Period	Stiffness	
[xSylmar]	[Hz]	[s]	[Kip/in]	[kN/mm]
0.1	3.13	0.32	104	18
0.2	3.05	0.33	98	17
0.3	3.05	0.33	98	17
0.5	2.34	0.43	58	10
0.75	2.27	0.44	55	10
1	2.03	0.49	44	8
1.25	1.72	0.58	31	5
1.5	1.48	0.68	23	4
1.75	1.48	0.68	23	4
2	1.48	0.68	23	4

Table 4-11 Dynamic Properties from Snap Ramp for Specimen ISL1.0

Motion	Frequency	Period	Stiffness		Damping
[xSylmar]	[Hz]	[s]	[Kip/in]	[kN/mm]	[%]
0.1	3.05	0.33	98	17	2.56
0.2	N/A				
0.3					
0.5	2.77	0.36	81	14	3.93
0.75	2.34	0.43	58	10	5.72
1	N/A				
1.25	1.80	0.56	34	6	6.56
1.5	N/A				
1.75					
2					

Table 4-12 Calculated Dynamic Properties from Peak Force with the Corresponding Displacement for Specimen ISL1.0

Motion	Force		Displacement		Stiffness		Freq.	Period
[xSylmar]	[Kips]	[kN]	[in]	[mm]	[Kip/in]	[kN/mm]	[Hz]	[s]
0.1	11.4	50.6	0.11	2.7	108	19	3.20	0.31
0.2	15.9	70.6	0.23	5.7	70	12	2.58	0.39
0.3	29.9	132.9	0.54	13.8	55	10	2.28	0.44
0.5	35.0	155.9	1.00	25.5	35	6	1.81	0.55
0.75	31.2	138.8	0.96	24.3	33	6	1.75	0.57
1	34.7	154.5	1.31	33.3	27	5	1.58	0.63
1.25	37.1	165.0	1.84	46.6	20	4	1.38	0.72
1.5	38.0	169.3	2.75	69.9	14	2	1.14	0.87
1.75	38.9	173.0	3.73	94.8	10	2	0.99	1.01
2	38.6	171.6	5.42	137.7	7	1	0.82	1.22

Table 4-13 Dynamic Properties from Low Level Elastic Response for Specimen ISL1.5

Motion	Frequency	Period	Stiffness	
[xSylmar]	[Hz]	[s]	[Kip/in]	[kN/mm]
0.1	3.13	0.32	104	18
0.2	3.13	0.32	104	18
0.4	2.58	0.39	71	12
0.6	2.42	0.41	62	11
0.8	2.27	0.44	55	10
1	2.27	0.44	55	10
1.25	1.88	0.53	37	7
1.5	N/A	N/A	N/A	N/A
1.75	1.48	0.68	23	4
2	1.48	0.68	23	4
2.125	1.48	0.68	23	4

Table 4-14 Dynamic Properties from Snap Ramp for Specimen ISL1.5

Motion	Frequency	Period	Stiffness		Damping
[xSylmar]	[Hz]	[s]	[Kip/in]	[kN/mm]	[%]
0.1	3.05	0.33	99	17	2.15
0.2	N/A				
0.4					
0.6	2.42	0.41	62	11	3.93
0.8	N/A				
1					
1.25	2.27	0.44	55	10	5.08
1.5	N/A				
1.75					
2					
2.125					

Table 4-15 Calculated Dynamic Properties from Peak Force with the Corresponding Displacement for Specimen ISL1.5

Motion	Force		Displacement		Stiffness		Freq.	Period
[xSylmar]	[Kips]	[kN]	[in]	[mm]	[Kip/in]	[kN/mm]	[Hz]	[s]
0.1	9.8	43.7	0.09	2.4	106	19	3.16	0.32
0.2	15.7	69.9	0.23	6.0	67	12	2.51	0.40
0.4	34.2	152.2	0.96	24.3	36	6	1.84	0.54
0.6	32.1	142.6	0.89	22.6	36	6	1.84	0.54
0.8	34.9	155.1	1.11	28.1	32	6	1.72	0.58
1	32.0	142.1	0.95	24.1	34	6	1.78	0.56
1.25	37.7	167.5	1.69	43.0	22	4	1.45	0.69
1.5	37.6	167.2	2.25	57.2	17	3	1.25	0.80
1.75	39.4	175.1	3.25	82.7	12	2	1.07	0.94
2	39.9	177.6	4.54	115.3	9	2	0.91	1.10
2.125	37.1	164.9	5.43	137.9	7	1	0.80	1.25

Table 4-16 Flexural and Shear Deformation Percentages for Specimen ISL1.0

Motion [xSylmar]	δ_f/δ_T [%]	δ_s/δ_T [%]
0.10	89%	11%
0.20	86%	14%
0.30	87%	13%
1.25	96%	4%
1.50	87%	13%
1.75	86%	14%
2.00	87%	13%

Table 4-17 Flexural and Shear Deformation Percentages for Specimen ISL1.5

Motion [xSylmar]	δ_f/δ_T [%]	δ_s/δ_T [%]
0.10	93%	7%
0.20	66%	34%
0.40	61%	39%
0.80	61%	39%
1.25	68%	32%
2.00	84%	16%
2.125	88%	12%

Table 4-18 Measured Strain in Longitudinal Bars at –152 mm (-6 in) and 0 mm (0 in) from the Top of the Footing for Specimen ISL1.0

Height		Strain Gages Number		Run No									
[mm]	[in]			1	2	3	4	5	6	7	8	9	10
-152.4	-6	1	Max	12	40	756	1276	1327	1443	1602	1732	1710	1928
			Min	-244	-356	-815	-1045	-1074	-1164	-1264	-1281	-1341	-1344
		2	Max	32	49	699	1253	1324	1450	1623	1706	1666	1887
			Min	-203	-300	-614	-808	-802	-876	-944	-1009	-1069	-1083
		3	Max	12	27	435	1060	1149	1266	1384	1415	1319	1546
			Min	-177	-243	-417	-530	-563	-611	-659	-720	-768	-816
		4	Max	-10	28	165	472	660	1000	1120	1075	880	1129
			Min	-149	-153	-155	-157	-119	-132	-339	-412	-431	-503
0	0	1	Max	427	718	2340	14655	14824	14944	21407	23040	19409	27960
			Min	-551	-849	-1508	-3292	-129	-1215	-3699	-7708	-14679	-17580
		2	Max	406	716	2406	13911	14296	15326	20745	23337	23021	31349
			Min	-578	-841	-1469	-2017	668	366	-825	-2308	-2732	-1601
		3	Max	212	466	1869	3576	7376	13475	15414	17156	14733	21919
			Min	-462	-629	-908	-1055	-1296	-805	618	-540	-1064	-1010
		4	Max	10	55	946	1925	2132	2771	4095	12437	14571	18265
			Min	-207	-191	-325	-404	-363	-351	-633	-551	4559	6417
		6	Max	-19	310	1495	12338	11289	14115	15460	19521	23881	33348
			Min	-201	-188	-299	-318	7504	7465	5327	4631	4116	3945
		7	Max	-80	87	983	2599	2275	12733	16204	15328	15607	15772
			Min	-152	-155	-148	-144	17	20	8374	6264	5454	3706
		8	Max	238	790	2682	16450	13374	15140	21201	31588	41015	41015
			Min	-573	-685	-1071	-1470	907	837	269	1267	2286	7053
		9	Max	84	702	10486	15517	12597	15059	23302	34460	40064	40064
			Min	-849	-973	-1203	-489	-583	-963	-1414	408	6601	23559
		10	Max	262	869	3407	15005	11746	14286	21661	32660	40117	40117
			Min	-615	-693	-1174	-2074	-600	-921	-953	910	6071	15073

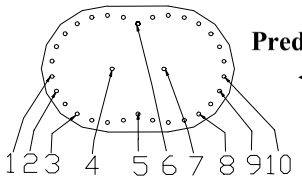

Predominant direction of motion

(All values in microstrain)

Table 4-19 Measured Strain in Longitudinal Bars at 127 mm (5 in) from the Top of the Footing for Specimen ISL1.0

Height		Strain Gages Number		Run No									
[mm]	[in]			1	2	3	4	5	6	7	8	9	10
127	5	1	**Max**	**582**	**1132**	**3378**	**15866**	**14199**	**15552**	**20295**	**18110**	**14364**	**40209**
			Min	-659	-1075	-2101	-6206	-3518	-5050	-8738	-12651	-11052	942
		2	**Max**	**500**	**1097**	**3172**	**17234**	**15112**	**16764**	**19593**	**13231**	**7809**	**5401**
			Min	-747	-1172	-2301	-9238	-5780	-7925	-15069	-28118	-40118	-40118
		3	**Max**	**240**	**718**	**2215**	**13086**	**12109**	**13325**	**15803**	**13604**	**9401**	**11681**
			Min	-625	-852	-1366	-3282	-1058	-2752	-6244	-11486	-20557	-40250
		5	**Max**	**-218**	**121**	**961**	**2132**	**1665**	**2996**	**17167**	**18735**	**22153**	**32281**
			Min	-305	-279	-346	-351	-362	-353	-250	5760	5688	6013
		6	**Max**	**-19**	**494**	**1353**	**6213**	**5451**	**16698**	**20019**	**28321**	**39337**	**40277**
			Min	-310	-316	-415	-390	1808	1967	6267	6240	7559	7993
		7	**Max**	**-37**	**255**	**1175**	**2938**	**2444**	**15707**	**17663**	**21455**	**29120**	**40734**
			Min	-155	-147	-141	-132	-154	-78	8693	8583	8520	11531
		8	**Max**	**272**	**1113**	**4383**	**14673**	**11972**	**16786**	**26029**	**35940**	**40390**	**40390**
			Min	-737	-912	-2070	-4108	-2853	-3048	-3935	-4011	-5387	-7471
		9	**Max**	**312**	**1197**	**9115**	**13810**	**11784**	**16096**	**25626**	**36121**	**40210**	**40210**
			Min	-768	-942	-2201	-5716	-3576	-3672	-4478	-4482	-12038	-33679
		10	**Max**	**424**	**1273**	**11149**	**13205**	**12087**	**16763**	**26871**	**37455**	**40197**	**40197**
			Min	-699	-906	-1773	-5443	-3176	-3118	-3203	-2999	-7431	-17139

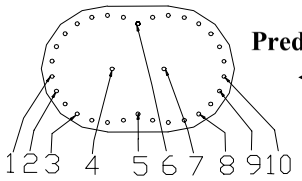

Predominant direction of motion

(All values in microstrain)

Table 4-20 Measured Strain in Longitudinal Bars at 254 mm (10 in) from the Top of the Footing for Specimen ISL1.0

Height		Strain Gages Number		Run No									
[mm]	[in]			1	2	3	4	5	6	7	8	9	10
254	10	1	**Max**	**602**	**1025**	**2744**	**8255**	**10654**	**11547**	**15564**	**17680**	**17388**	**23667**
			Min	-617	-991	-1844	-2641	-3105	-2505	-3210	-3139	-2565	-1200
		2	**Max**	**527**	**947**	**2716**	**9407**	**10979**	**12073**	**16397**	**11183**	**17332**	**23702**
			Min	-659	-1025	-1836	-2626	-3174	-2885	-3899	-5510	-6808	-4892
		3	**Max**	**336**	**680**	**2108**	**3423**	**5371**	**12120**	**12490**	**12959**	**10980**	**17049**
			Min	-591	-834	-1295	-1734	-1817	-2706	-3776	-3908	-5394	-8091
		5	**Max**	**-267**	**25**	**710**	**1863**	**1532**	**2520**	**13671**	**19474**	**20922**	**25418**
			Min	-376	-366	-367	-346	-365	-370	-339	6594	5752	5583
		6	**Max**	**4**	**29**	**94**	**139**	**161**	**364**	**600**	**517**	**550**	**1092**
			Min	-18	-13	-35	-295	-189	-169	-176	-134	-145	-208
		8	**Max**	**263**	**1109**	**3032**	**16902**	**12574**	**15311**	**23998**	**35031**	**40427**	**40427**
			Min	-822	-999	-1881	-2393	-2228	-2077	-1491	-1245	-1754	-3176
		9	**Max**	**279**	**1154**	**3479**	**17564**	**13384**	**15573**	**23775**	**35402**	**40290**	**40290**
			Min	-805	-971	-1887	-2742	-2650	-2405	-315	-1255	-9189	-17525
		10	**Max**	**310**	**1139**	**3338**	**15675**	**12474**	**15994**	**25032**	**36275**	**40171**	**40171**
			Min	-740	-928	-1836	-3546	-2262	-1674	-459	-476	-1024	-3425

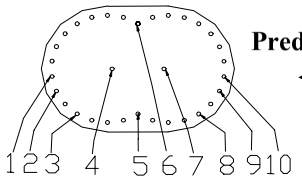

Predominant direction of motion

(All values in microstrain)

Table 4-21 Measured Strain in Longitudinal Bars at 381 mm (15 in) and 508 mm (20 in) from the Top of the Footing for Specimen ISL1.0

Height [mm]	Height [in]	Strain Gages Number		Run No 1	2	3	4	5	6	7	8	9	10
381	15	1	Max	352	836	2651	7018	9381	12164	14215	13700	12693	17283
			Min	-607	-943	-1719	-2643	-2814	-3215	-3368	-3077	-2278	-855
		2	Max	206	662	2279	6702	9139	10147	11656	11480	11126	15532
			Min	-723	-1020	-1737	-2171	-3366	-3554	-3896	-3724	-3291	-2071
		3	Max	96	537	2101	3084	3372	6064	12301	12462	9934	14032
			Min	-730	-995	-1541	-1787	-1727	-2424	-4102	-5037	-5295	-4365
		5	Max	-298	-120	633	1632	1378	2073	2726	3813	13156	14623
			Min	-354	-339	-338	-304	-292	-295	-598	-818	-837	2339
		10	Max	177	948	2737	14035	11518	13773	15330	21142	28364	37710
			Min	-719	-878	-1536	-1851	-1382	-961	637	883	1076	1235
508	20	1	Max	278	663	2308	3080	3391	6203	9142	8830	7471	12134
			Min	-619	-915	-1621	-2034	-2097	-3186	-5115	-6076	-6614	-6740
		2	Max	272	635	2294	2985	3181	4148	7768	7721	6553	10656
			Min	-641	-928	-1638	-2014	-1984	-2576	-4561	-6534	-7217	-6990
		3	Max	95	304	1179	1646	1740	1815	1894	1812	1577	2003
			Min	-437	-558	-821	-889	-820	-889	-970	-1059	-1154	-1217
		4	Max	-64	145	901	1701	1853	2132	2479	2451	1949	2638
			Min	-304	-334	-279	-224	-239	-294	-542	-622	-645	-715
		5	Max	-298	-184	576	1405	1179	1751	2289	2570	2748	2862
			Min	-331	-328	-316	-278	-307	-307	-575	-919	-1134	-1186
		6	Max	5	783	2388	2815	2818	5476	14313	13910	16761	20487
			Min	-724	-830	-1416	-1807	-1832	-2929	-3016	-1245	-73	-334

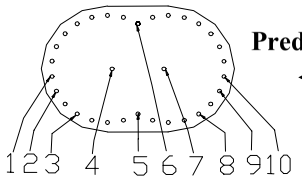

Predominant direction of motion

(All values in microstrain)

Table 4-22 Measured Strain in Longitudinal Bars at –152 mm (-6 in) from the Top of the Footing for Specimen ISL1.5

Height		Strain Gages Number		Run No										
[mm]	[in]			1	2	3	4	5	6	7	8	9	10	11
-152.4	-6	1	Max	27	128	1790	1935	2031	1969	2166	2299	2306	2434	2684
			Min	-296	-485	-1369	-1338	-1575	-1433	-1712	-1816	-1913	-1993	-1978
		2	Max	45	148	2150	2269	2381	2291	2558	3105	3836	6615	9045
			Min	-312	-504	-2313	-2067	-2403	-2204	-2610	-2728	-3002	-4213	-2908
		3	Max	35	124	1790	1916	2084	1978	2265	2491	2527	2806	6302
			Min	-325	-518	-1427	-1415	-1648	-1508	-1820	-1902	-1990	-2151	-2198
		4	Max	-74	-25	662	782	1198	933	1678	1989	2217	2475	2268
			Min	-112	-108	-108	-58	-102	-101	-183	-539	-813	-899	-900
		5	Max	-48	5	792	680	998	680	1574	2042	2339	2638	2589
			Min	-84	-83	-83	-46	-91	-85	-101	-428	-634	-846	-866
		10	Max	66	256	1904	1917	2187	1990	2507	9176	15544	24141	33915
			Min	-333	-483	-1597	-1713	-1922	-1814	-2057	-2771	-2410	-2430	-1968

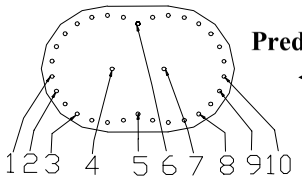

Predominant direction of motion

(All values in microstrain)

Table 4-23 Measured Strain in Longitudinal Bars at 0 mm (0 in) from the Top of the Footing for Specimen ISL1.5

Height [mm]	Height [in]	Strain Gages Number		Run No 1	2	3	4	5	6	7	8	9	10	11
0	0	1	**Max**	**232**	**660**	**8437**	**12933**	**13607**	**12741**	**15546**	**31312**	**36395**	**38136**	**39686**
			Min	-709	-1046	-2802	-3536	-3487	-2404	-6132	647	5903	7897	7741
		2	**Max**	**261**	**721**	**6392**	**3585**	**4180**	**4403**	**2862**	**1597**	**1713**	**4393**	**11777**
			Min	-751	-1107	-6397	817	1114	1365	-2157	-9368	-5617	-3177	-2709
		3	**Max**	**194**	**623**	**11111**	**12966**	**13774**	**12594**	**17541**	**19211**	**15060**	**17442**	**40102**
			Min	-500	-677	-1850	-322	-719	426	-4740	-7539	-10271	-11226	-8757
		5	**Max**	**-156**	**41**	**1658**	**1514**	**1904**	**1622**	**4764**	**14773**	**17422**	**18186**	**10866**
			Min	-257	-266	-320	-358	-434	-413	-373	1231	7688	6315	3764
		6	**Max**	**144**	**465**	**1995**	**1903**	**2481**	**2040**	**5162**	**4446**	**6608**	**11235**	**13580**
			Min	-149	-149	-139	62	303	175	439	1221	912	748	-244
		7	**Max**	**-131**	**116**	**1562**	**1254**	**1662**	**1231**	**3267**	**16319**	**17563**	**22225**	**25302**
			Min	-276	-288	-304	-304	-333	-333	-294	115	6880	6783	7881
		8	**Max**	**531**	**1177**	**17126**	**13891**	**17554**	**14465**	**23275**	**33244**	**35678**	**19314**	**40156**
			Min	-632	-882	-1704	-832	-1719	-1419	-3134	-4781	-1632	6831	10112
		9	**Max**	**442**	**1004**	**15461**	**12803**	**15991**	**13129**	**22886**	**33963**	**32951**	**10418**	**39144**
			Min	-460	-637	-1396	52	-678	-431	-1887	-3320	-24	8323	8557
		10	**Max**	**480**	**1075**	**18896**	**15039**	**18958**	**15777**	**26547**	**37897**	**40103**	**40103**	**40103**
			Min	-513	-646	-1262	1597	688	1012	417	-603	1230	-675	-7151

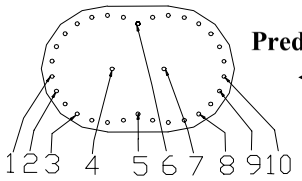

Predominant direction of motion

(All values in microstrain)

Table 4-24 Measured Strain in Longitudinal Bars at 127 mm (5 in) from the Top of the Footing for Specimen ISL1.5

Height		Strain Gages Number		Run No										
[mm]	[in]			1	2	3	4	5	6	7	8	9	10	11
127	5	1	**Max**	**139**	**633**	**10488**	**11235**	**12710**	**11885**	**15170**	**16964**	**12294**	**14444**	**9174**
			Min	-598	-928	-7035	-4367	-2520	-2445	-4477	-7296	-13089	-21120	-15988
		2	**Max**	**121**	**665**	**8853**	**10108**	**10831**	**10697**	**12914**	**15191**	**10965**	**12550**	**18309**
			Min	-594	-893	-7659	-4182	-1987	-2309	-3102	-5888	-12275	-25715	-15856
		3	**Max**	**131**	**604**	**2733**	**5157**	**8999**	**8544**	**10007**	**12057**	**9499**	**10763**	**13890**
			Min	-494	-755	-1971	-2069	-2276	-2499	-4199	-5262	-8129	-12082	-9155
		4	**Max**	**-111**	**2**	**958**	**1114**	**1372**	**1181**	**1992**	**2718**	**3027**	**16256**	**18140**
			Min	-183	-176	-198	-176	-200	-200	-182	-190	-811	-825	5576
		5	**Max**	**-124**	**30**	**1245**	**1062**	**1402**	**1118**	**2549**	**15205**	**16783**	**17830**	**20760**
			Min	-167	-158	-160	-180	-219	-222	-194	-106	6706	6141	5881
		6	**Max**	**-108**	**58**	**1197**	**338**	**728**	**403**	**1866**	**3928**	**3205**	**2380**	**2253**
			Min	-179	-177	-371	-650	-871	-908	-886	-1091	-1666	-1674	466
		7	**Max**	**0**	**156**	**541**	**617**	**1044**	**852**	**1084**	**1276**	**1116**	**1121**	**4404**
			Min	-79	-79	-1545	-1043	-386	-740	-349	-386	-581	-624	-1199
		8	**Max**	**426**	**1317**	**7137**	**3221**	**4334**	**3732**	**6738**	**8369**	**8721**	**7829**	**6202**
			Min	-573	-870	-2368	-2553	-4175	-2828	-13319	-11122	-2274	1425	1825
		9	**Max**	**362**	**1178**	**13825**	**11043**	**13119**	**11411**	**18038**	**28453**	**39509**	**40150**	**40150**
			Min	-448	-711	-1521	-767	-575	-949	608	1939	3795	8361	21059
		10	**Max**	**352**	**1211**	**15948**	**12908**	**14996**	**13231**	**16428**	**4765**	**4244**	**4488**	**5110**
			Min	-485	-759	-1563	-940	-1075	-1312	133	660	1670	2244	746

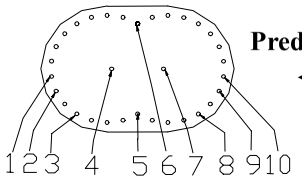

Predominant direction of motion

(All values in microstrain)

Table 4-25 Measured Strain in Longitudinal Bars at 254 mm (10 in) from the Top of the Footing for Specimen ISL1.5

Height		Strain Gages Number		Run No										
[mm]	[in]			1	2	3	4	5	6	7	8	9	10	11
254	10	1	Max	145	584	2895	4665	11263	8542	12586	14050	13856	16118	14651
			Min	-598	-922	-2321	-2504	-3801	-3409	-4339	-4452	-4798	-4988	-2856
		2	Max	144	556	2791	3177	10680	4184	11622	13506	13027	15115	19310
			Min	-567	-846	-1987	-1884	-3669	-2218	-4832	-5146	-5097	-6646	-5586
		3	Max	-131	-8	900	1047	1286	1117	1840	2158	2729	12981	12018
			Min	-195	-186	-179	-163	-200	-201	-173	-204	-519	-520	5562
		5	Max	-141	3	1165	1021	1332	1008	2329	3270	15287	16172	16258
			Min	-168	-166	-175	-176	-199	-216	-189	-257	-276	5169	4946
		6	Max	-137	-1	1357	1165	1626	1195	2877	12639	14093	16377	18855
			Min	-175	-179	-182	-190	-209	-223	-207	-99	4092	4046	3863
		7	Max	-103	113	1525	1301	1792	1321	3070	14416	16566	19853	24623
			Min	-179	-180	-205	-207	-231	-232	-197	-71	4496	4485	4954
		8	Max	462	1051	16387	12685	15006	13056	17553	23955	31832	40142	40142
			Min	-511	-771	-1525	196	-91	-208	1684	2401	3529	4617	9241
		9	Max	459	984	13782	10339	12342	10547	15476	22523	29714	40142	40142
			Min	-571	-811	-1557	-610	-591	-932	654	1849	3267	5549	7170
		10	Max	361	849	13688	10752	9392	9944	7318	5364	8296	6341	5156
			Min	-547	-785	-1547	-578	408	-742	2324	893	3027	3580	3661

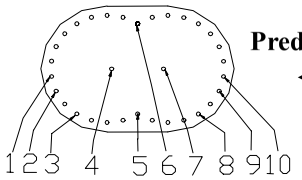

Predominant direction of motion

(All values in microstrain)

Table 4-26 Measured Strain in Longitudinal Bars at 381 mm (15 in) and 508 mm (20 in) from the Top of the Footing for Specimen ISL1.5

Height		Strain Gages Number		Run No										
[mm]	[in]			1	2	3	4	5	6	7	8	9	10	11
381	15	1	Max	127	540	2641	2896	4295	3102	8620	10128	9141	10761	11956
			Min	-543	-847	-2014	-1891	-2348	-1974	-3904	-4456	-4288	-4168	-2735
		2	Max	102	489	2532	2739	3804	2982	8934	10839	9594	10648	12469
			Min	-571	-866	-2038	-1904	-2287	-2003	-3759	-4960	-4407	-3592	-2345
		3	Max	92	452	2510	2741	3118	2830	9544	11341	9431	10419	11913
			Min	-583	-853	-1912	-1787	-2020	-1825	-2554	-5953	-5593	-4349	-2972
		4	Max	-94	12	915	1042	1287	1110	1817	2064	2327	2511	2224
			Min	-166	-156	-141	-108	-145	-153	-116	-129	-434	-683	-708
		5	Max	-151	-52	1059	927	1222	963	2103	2912	3089	12740	11500
			Min	-177	-176	-173	-167	-202	-216	-191	-323	-733	-768	3500
		10	Max	152	759	3084	3304	7980	4249	14543	8304	4376	4691	4412
			Min	-403	-597	-1713	-1937	-2485	-2298	-1297	1808	3055	3366	3192
508	20	1	Max	69	452	2704	2951	4369	3202	7873	9481	8391	10222	11169
			Min	-570	-837	-1858	-1757	-2258	-1830	-3014	-4080	-4104	-4232	-2868
		2	Max	25	390	2355	2545	3348	2737	5748	9419	7802	9228	9300
			Min	-539	-785	-1802	-1700	-2053	-1754	-2646	-4093	-4665	-4197	-2941
		3	Max	69	385	2291	2463	2646	2504	3004	3690	4295	5966	7361
			Min	-495	-746	-1676	-1602	-1823	-1655	-2114	-2395	-3303	-4708	-3838
		4	Max	-115	-30	885	1020	1255	1102	1679	1976	1930	2051	1795
			Min	-180	-162	-133	-71	-121	-128	-80	-72	-349	-518	-544
		5	Max	-147	-65	1058	949	1181	967	1981	2624	2815	2941	2625
			Min	-165	-163	-162	-121	-147	-155	-125	-328	-736	-968	-997
		10	Max	199	822	5159	5295	8614	5816	12734	13881	17220	25814	11362
			Min	-391	-590	-1374	-1480	-1720	-1613	-493	431	867	1104	3900

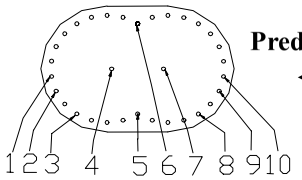

Predominant direction of motion

(All values in microstrain)

Table 4-27 Measured Strain in Spirals at -152 mm (-6 in) from the Top of the Footing for Specimen ISL1.0

Height		Strain Gages Number		Run No									
[mm]	[in]			1	2	3	4	5	6	7	8	9	10
-152	-6	1	**Max**	**-33**	**-30**	**-25**	**18**	**3**	**-2**	**13**	**535**	**1774**	**2050**
			Min	-59	-63	-80	-53	-63	-75	-82	-3	-49	-270
		3	**Max**	**-29**	**-24**	**-22**	**-22**	**-42**	**-42**	**-45**	**-41**	**-40**	**-40**
			Min	-46	-41	-43	-46	-73	-87	-85	-86	-80	-89
		4	**Max**	**-27**	**-24**	**-27**	**-22**	**-24**	**-19**	**-14**	**-1**	**-1**	**-1**
			Min	-39	-35	-40	-44	-48	-47	-45	-29	-27	-32
		7	**Max**	**-20**	**-25**	**-29**	**-20**	**-17**	**-12**	**-13**	**-23**	**-19**	**-24**
			Min	-36	-40	-46	-42	-40	-36	-33	-46	-41	-51
		8	**Max**	**98**	**102**	**102**	**109**	**98**	**101**	**98**	**103**	**103**	**104**
			Min	86	87	80	75	79	74	63	55	42	37
		10	**Max**	**27**	**24**	**28**	**31**	**9**	**16**	**12**	**29**	**22**	**30**
			Min	11	9	0	-6	-24	-22	-32	-20	-28	-28

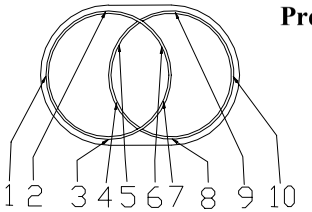

Predominant direction of motion

(All values in microstrain)

Table 4-28 Measured Strain in Spirals at 0 mm (0 in) from the Top of the Footing for Specimen ISL1.0

Height		Strain Gages Number		Run No									
[mm]	[in]			1	2	3	4	5	6	7	8	9	10
0	0	1	**Max**	**29**	**24**	**20**	**2**	**17**	**48**	**148**	**187**	**107**	**234**
			Min	-19	-37	-70	-102	-126	-183	-221	-257	-297	-309
		3	**Max**	**0**	**0**	**-1**	**-10**	**-40**	**-40**	**-14**	**41**	**79**	**700**
			Min	-37	-44	-95	-106	-107	-110	-135	-245	-325	-297
		4	**Max**	**0**	**2**	**12**	**17**	**11**	**13**	**44**	**135**	**177**	**389**
			Min	-21	-18	-25	-125	-102	-174	-209	-96	-82	-123
		5	**Max**	**-66**	**-70**	**-61**	**5**	**-12**	**-10**	**17**	**-26**	**-75**	**-25**
			Min	-77	-81	-83	-97	-119	-196	-329	-550	-774	-1169
		6	**Max**	**-27**	**-19**	**2**	**30**	**-22**	**-54**	**-71**	**-83**	**-112**	**-198**
			Min	-41	-42	-41	-23	-48	-104	-203	-330	-486	-849
		7	**Max**	**-5**	**2**	**3**	**76**	**52**	**142**	**480**	**804**	**1174**	**2270**
			Min	-18	-9	-16	-46	-64	-64	-90	-138	-165	-169
		8	**Max**	**-3**	**36**	**69**	**120**	**158**	**172**	**157**	**258**	**328**	**290**
			Min	-30	-135	-224	-125	-15	-13	7	27	91	129
		9	**Max**	**-18**	**-18**	**-8**	**-3**	**-21**	**-8**	**-13**	**36**	**22**	**-18**
			Min	-31	-36	-47	-44	-55	-56	-86	-107	-199	-214
		10	**Max**	**83**	**77**	**84**	**215**	**11**	**12**	**16**	**50**	**98**	**181**
			Min	38	15	-23	71	-107	-124	-126	-88	-91	-58

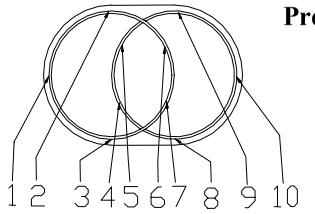

Predominant direction of motion

(All values in microstrain)

Table 4-29 Measured Strain in Spirals at 127 mm (5 in) from the Top of the Footing for Specimen ISL1.0

Height		Strain Gages Number		Run No									
[mm]	11			1	2	3	4	5	6	7	8	9	10
127	5	2	**Max**	**-15**	**-20**	**32**	**43**	**63**	**117**	**65**	**-32**	**148**	**722**
			Min	-32	-43	-178	-376	-391	-382	-384	-392	-398	-295
		3	**Max**	**-27**	**5**	**-3**	**-34**	**-132**	**-160**	**-135**	**-28**	**53**	**366**
			Min	-45	-17	-53	-225	-295	-387	-475	-572	-670	-1193
		4	**Max**	**-5**	**4**	**-7**	**-25**	**-63**	**-83**	**-96**	**-83**	**-72**	**724**
			Min	-16	-30	-147	-357	-333	-319	-322	-310	-297	-322
		5	**Max**	**-31**	**-35**	**-40**	**-60**	**-73**	**-78**	**-76**	**-79**	**-89**	**-29**
			Min	-44	-70	-164	-305	-224	-161	-169	-197	-239	-654
		6	**Max**	**-9**	**1**	**14**	**59**	**11**	**-2**	**1**	**-808**	**-2556**	**-2579**
			Min	-25	-20	-24	-653	-941	-1930	-6360	-6612	-5518	-4338
		7	**Max**	**-44**	**5**	**37**	**49**	**-19**	**14**	**-20**	**-89**	**-52**	**278**
			Min	-63	-44	-51	-100	-142	-178	-247	-358	-509	-548
		9	**Max**	**1**	**11**	**20**	**3**	**-16**	**-16**	**-16**	**-95**	**-109**	**579**
			Min	-15	-16	-67	-115	-116	-227	-350	-408	-348	-393
		10	**Max**	**-13**	**3**	**98**	**120**	**108**	**136**	**228**	**74**	**4**	**171**
			Min	-41	-37	-39	-99	-138	-195	-278	-356	-401	-464

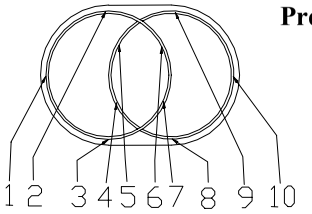

Predominant direction of motion

(All values in microstrain)

Table 4-30 Measured Strain in Spirals at 254 mm (10 in) from the Top of the Footing for Specimen ISL1.0

Height		Strain Gages Number		Run No									
[mm]	[in]			1	2	3	4	5	6	7	8	9	10
254	10	1	**Max**	**3**	**0**	**-9**	**-74**	**-123**	**-132**	**-134**	**183**	**422**	**511**
			Min	-25	-47	-162	-303	-336	-415	-553	-665	-769	-989
		2	**Max**	**-37**	**206**	**1085**	**2656**	**2347**	**6047**	**14511**	**15711**	**18821**	**27214**
			Min	-159	-149	-128	-57	-26	1	2221	4674	4439	4347
		3	**Max**	**-53**	**-33**	**-42**	**-53**	**-166**	**-199**	**-237**	**-241**	**-205**	**-102**
			Min	-75	-57	-83	-256	-286	-326	-378	-453	-577	-750
		4	**Max**	**-17**	**-6**	**3**	**-2**	**-44**	**-52**	**-58**	**-18**	**176**	**560**
			Min	-28	-18	-18	-73	-132	-172	-229	-227	-230	-247
		5	**Max**	**-8**	**-17**	**-28**	**-52**	**-155**	**-103**	**251**	**136**	**135**	**4534**
			Min	-59	-70	-137	-359	-360	-397	-375	-364	-428	-418
		6	**Max**	**20**	**128**	**186**	**270**	**235**	**348**	**662**	**741**	**657**	**617**
			Min	-6	19	10	-7	-46	-117	-249	-298	-383	-663
		7	**Max**	**30**	**28**	**37**	**29**	**-8**	**13**	**36**	**9**	**96**	**443**
			Min	15	3	-9	-32	-62	-74	-84	-95	-96	-140
		8	**Max**	**-8**	**11**	**23**	**146**	**102**	**145**	**158**	**390**	**635**	**693**
			Min	-39	-37	-44	-53	-66	-67	-132	-184	-202	-218
		9	**Max**	**13**	**12**	**-22**	**-10**	**-77**	**-23**	**26**	**254**	**393**	**986**
			Min	-54	-59	-232	-348	-358	-445	-571	-289	-367	-2434
		10	**Max**	**-52**	**-3**	**8**	**-12**	**-44**	**-73**	**-120**	**-216**	**-233**	**-180**
			Min	-77	-43	-79	-122	-131	-205	-252	-473	-563	-565

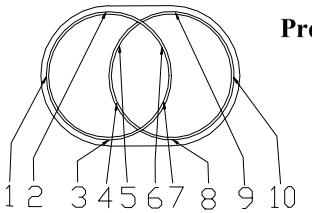

Predominant direction of motion

(All values in microstrain)

Table 4-31 Measured Strain in Spirals at 381 mm (15 in) and 508 mm (20 in) from the Top of the Footing for Specimen ISL1.0

Height		Strain Gages Number		Run No									
[mm]	[in]			1	2	3	4	5	6	7	8	9	10
381	15	1	**Max**	**-5**	**0**	**-9**	**-42**	**-118**	**-160**	**-213**	**-240**	**-142**	**-43**
			Min	-41	-49	-217	-405	-460	-532	-576	-609	-630	-641
		3	**Max**	**-20**	**-15**	**-18**	**-94**	**-223**	**-260**	**-292**	**-336**	**-381**	**-452**
			Min	-41	-42	-164	-428	-513	-566	-616	-652	-745	-763
		4	**Max**	**-21**	**-21**	**-11**	**-10**	**-75**	**-104**	**-153**	**18**	**322**	**900**
			Min	-31	-47	-56	-71	-138	-261	-274	-324	-363	-394
		7	**Max**	**-56**	**-45**	**-43**	**-67**	**-84**	**-107**	**-127**	**-148**	**-174**	**-226**
			Min	-72	-63	-83	-122	-132	-163	-228	-309	-375	-433
		8	**Max**	**-17**	**-12**	**-19**	**-72**	**-125**	**-110**	**-113**	**24**	**111**	**610**
			Min	-34	-35	-132	-293	-314	-306	-293	-394	-537	-523
		10	**Max**	**6**	**9**	**-9**	**-59**	**-164**	**-221**	**-285**	**-289**	**-311**	**-167**
			Min	-68	-85	-178	-288	-428	-524	-686	-828	-810	-768
508	20	1	**Max**	**-15**	**-15**	**-37**	**-9**	**7**	**38**	**15**	**-12**	**-29**	**-13**
			Min	-56	-76	-144	-172	-155	-151	-184	-234	-262	-301
		3	**Max**	**34**	**36**	**189**	**265**	**238**	**274**	**313**	**390**	**570**	**764**
			Min	-28	-41	-58	33	42	57	58	45	18	21
		4	**Max**	**-26**	**-1**	**-2**	**-68**	**-186**	**-226**	**-264**	**-274**	**-302**	**-305**
			Min	-34	-34	-174	-393	-463	-495	-502	-540	-656	-706
		7	**Max**	**-6**	**-4**	**-5**	**-19**	**-96**	**-126**	**-164**	**-175**	**-165**	**-6**
			Min	-20	-20	-86	-296	-360	-414	-481	-531	-611	-648
		8	**Max**	**0**	**27**	**0**	**-89**	**-199**	**-210**	**-239**	**-239**	**-195**	**-79**
			Min	-13	-10	-278	-438	-452	-506	-532	-624	-729	-808
		10	**Max**	**-26**	**-31**	**-31**	**-21**	**-10**	**-23**	**-30**	**-19**	**-31**	**-52**
			Min	-56	-64	-93	-103	-92	-117	-129	-102	-92	-1045

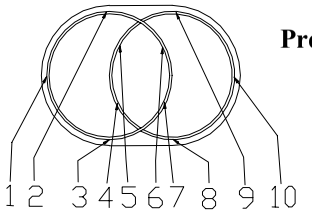

Predominant direction of motion

(All values in microstrain)

Table 4-32 Measured Strain in Spirals at -152 mm (-6 in) and 0 mm (0 in) from the Top of the Footing for Specimen ISL1.5

Height		Strain Gages Number		Run No										
[in]	[mm]			1	2	3	4	5	6	7	8	9	10	11
-6	-152	1	**Max**	**25**	**29**	**27**	**43**	**43**	**35**	**51**	**58**	**61**	**67**	**61**
			Min	13	14	-30	-11	4	-11	-1	-6	-11	-8	-1
		2	**Max**	**3**	**4**	**3**	**3**	**6**	**3**	**10**	**11**	**3**	**11**	**11**
			Min	-5	-5	-34	-39	-39	-39	-39	-44	-57	-63	-93
		3	**Max**	**39**	**45**	**71**	**70**	**86**	**50**	**143**	**170**	**182**	**193**	**183**
			Min	23	26	26	24	6	-4	20	16	12	8	15
		8	**Max**	**6**	**14**	**14**	**11**	**2**	**-6**	**21**	**14**	**24**	**47**	**47**
			Min	-2	4	-33	-23	-27	-38	-18	-31	-44	-34	-19
0	0	1	**Max**	**0**	**2**	**29**	**3**	**280**	**28**	**2335**	**7012**	**9235**	**41280**	**41280**
			Min	-11	-14	-55	-79	-55	-85	-15	697	2796	4166	3291
		2	**Max**	**19**	**36**	**44**	**41**	**56**	**25**	**55**	**113**	**136**	**78**	**1969**
			Min	-11	-24	-58	-111	-53	-82	-149	-201	-243	-384	-414
		3	**Max**	**-106**	**-95**	**-69**	**-72**	**-101**	**-115**	**-91**	**-101**	**-16**	**-23**	**314**
			Min	-113	-115	-160	-174	-241	-244	-246	-318	-343	-339	-1430
		4	**Max**	**18**	**29**	**129**	**124**	**297**	**16**	**344**	**233**	**209**	**266**	**333**
			Min	-74	-79	-54	-66	-470	-510	-551	-562	-508	-477	-461
		5	**Max**	**55**	**74**	**181**	**141**	**186**	**165**	**265**	**341**	**381**	**470**	**592**
			Min	44	59	53	54	47	41	59	95	109	128	-118
		7	**Max**	**26**	**35**	**136**	**126**	**149**	**126**	**188**	**441**	**554**	**736**	**1197**
			Min	5	-3	-17	-26	-51	-70	-62	-38	-31	-78	-135
		8	**Max**	**114**	**127**	**128**	**95**	**86**	**66**	**169**	**219**	**190**	**157**	**150**
			Min	102	100	-44	-13	-71	-51	-30	-44	-140	-217	-704
		9	**Max**	**-3**	**0**	**1**	**14**	**60**	**31**	**119**	**133**	**200**	**305**	**414**
			Min	-39	-49	-114	-83	-93	-67	-142	-112	-111	-141	-241
		10	**Max**	**4**	**6**	**78**	**156**	**301**	**194**	**465**	**581**	**504**	**735**	**697**
			Min	-11	-12	-167	-191	-226	-220	-167	-273	-205	-167	-256

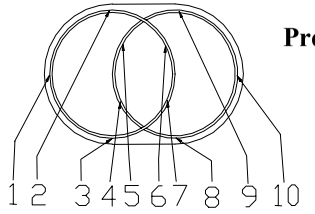

Predominant direction of motion

(All values in microstrain)

Table 4-33 Measured Strain in Spirals at 127 mm (5 in) from the Top of the Footing for Specimen ISL1.5

Height		Strain Gages Number		Run No										
[in]	[mm]			1	2	3	4	5	6	7	8	9	10	11
5	127	1	**Max**	**26**	**68**	**84**	**-89**	**-123**	**-103**	**90**	**1692**	**1171**	**774**	**40200**
			Min	-69	-88	-310	-296	-390	-356	-372	-259	593	252	64
		2	**Max**	**27**	**30**	**37**	**43**	**52**	**42**	**25**	**-82**	**-309**	**-348**	**1401**
			Min	11	13	-1	-11	-84	-38	-236	-374	-593	-1102	-4149
		3	**Max**	**14**	**15**	**10**	**10**	**2**	**11**	**-4**	**49**	**130**	**508**	**2539**
			Min	-2	-7	-135	-108	-155	-115	-211	-255	-293	-403	-389
		4	**Max**	**25**	**26**	**125**	**91**	**145**	**96**	**166**	**288**	**206**	**277**	**174**
			Min	-1	-8	-21	-14	-35	-25	-76	-514	-921	-304	-193
		5	**Max**	**-26**	**-26**	**53**	**13**	**51**	**13**	**200**	**253**	**562**	**641**	**212**
			Min	-39	-52	-63	-68	-69	-79	-68	-768	-196	-328	-250
		6	**Max**	**-4**	**-1**	**11**	**1**	**89**	**12**	**220**	**641**	**489**	**423**	**401**
			Min	-14	-14	-21	-38	-49	-48	-15	-15	-55	-232	-2958
		7	**Max**	**21**	**26**	**34**	**30**	**35**	**24**	**118**	**138**	**-8**	**-50**	**2622**
			Min	10	15	15	15	1	1	14	-30	-133	-229	-260
		8	**Max**	**14**	**22**	**11**	**-24**	**-56**	**-40**	**-38**	**108**	**63**	**93**	**143**
			Min	2	-5	-149	-142	-217	-165	-307	-288	-347	-350	-322

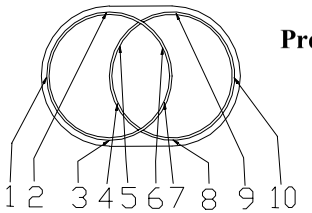

Predominant direction of motion

(All values in microstrain)

Table 4-34 Measured Strain in Spirals at 254 mm (10 in) from the Top of the Footing for Specimen ISL1.5

Height		Strain Gages Number		Run No										
[in]	[mm]			1	2	3	4	5	6	7	8	9	10	11
10	254	1	Max	27	40	39	-73	-111	-83	-112	-150	306	1369	383
			Min	-36	-49	-215	-230	-266	-252	-404	-490	-648	-125	-352
		2	Max	11	14	12	-15	-16	-16	-18	-96	-181	-216	1654
			Min	-20	-20	-255	-285	-365	-331	-493	-604	-653	-749	-825
		3	Max	28	34	41	48	64	55	70	34	64	75	521
			Min	3	-3	2	20	25	20	-29	-135	-212	-243	-243
		4	Max	-41	-42	70	113	141	133	62	102	40	239	617
			Min	-50	-55	-101	-152	-444	-278	-1013	-691	-645	-1219	-370
		5	Max	603	601	603	511	641	594	-195	55	52	52	632
			Min	575	562	511	447	551	526	-457	-666	-470	-589	-639
		6	Max	16	19	293	306	426	266	960	1635	1927	2004	2966
			Min	4	-2	-7	7	-66	-80	-52	-50	-30	-8	-642
		7	Max	23	26	128	141	212	143	347	548	907	1353	1812
			Min	14	15	7	2	-7	-19	-4	-19	17	247	178
		8	Max	19	21	32	-16	-25	-32	-54	5	126	569	560
			Min	9	8	-55	-81	-123	-106	-187	-253	-292	-230	-642
		9	Max	-41	-65	-77	-102	-118	-113	-46	-18	-15	41	164
			Min	-57	-83	-128	-130	-173	-154	-190	-208	-277	-261	-321

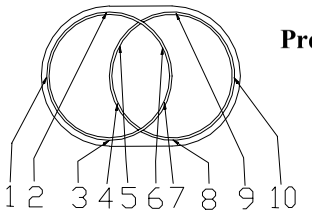

Predominant direction of motion

(All values in microstrain)

Table 4-35 Measured Strain in Spirals at 381 mm (15 in) and 508 mm (20 in) from the Top of the Footing for Specimen ISL1.5

Height		Strain Gages Number		Run No										
[in]	[mm]			1	2	3	4	5	6	7	8	9	10	11
15	381	3	**Max**	**-18**	**-18**	**11**	**0**	**1**	**1**	**-11**	**-22**	**-64**	**-67**	**-13**
			Min	-34	-42	-65	-100	-176	-139	-163	-236	-236	-261	-227
		4	**Max**	**-18**	**-16**	**229**	**230**	**255**	**259**	**288**	**259**	**64**	**-294**	**-48**
			Min	-39	-38	-50	102	11	12	-71	-250	-794	-994	-1167
		7	**Max**	**31**	**38**	**55**	**49**	**96**	**38**	**193**	**341**	**414**	**532**	**711**
			Min	19	17	1	14	-8	-10	-53	-64	172	221	267
		8	**Max**	**24**	**32**	**51**	**-7**	**-47**	**-34**	**-60**	**-87**	**102**	**420**	**2562**
			Min	14	15	-86	-126	-216	-175	-256	-387	-397	-682	-664
		9	**Max**	**13**	**19**	**61**	**69**	**96**	**86**	**111**	**192**	**184**	**221**	**282**
			Min	-5	-5	-119	-141	-175	-162	-196	-225	-258	-323	-397
		10	**Max**	**17**	**16**	**16**	**9**	**4**	**9**	**9**	**-10**	**-4**	**49**	**420**
			Min	-2	-12	-99	-120	-150	-139	-198	-229	-292	-327	-280
20	508	1	**Max**	**-9**	**15**	**-6**	**-102**	**-185**	**-150**	**-206**	**-224**	**-260**	**-306**	**-342**
			Min	-77	-99	-260	-275	-358	-321	-414	-466	-504	-550	-613
		3	**Max**	**33**	**39**	**36**	**11**	**14**	**7**	**18**	**55**	**26**	**55**	**146**
			Min	17	15	-114	-161	-226	-201	-248	-252	-265	-271	-296
		4	**Max**	**24**	**27**	**91**	**145**	**193**	**177**	**213**	**247**	**235**	**230**	**198**
			Min	11	6	-3	3	-1	-13	8	10	20	30	35
		7	**Max**	**12**	**12**	**18**	**15**	**31**	**14**	**25**	**39**	**47**	**44**	**11**
			Min	2	2	-8	-21	-26	-38	-36	-3	-19	-58	-212
		8	**Max**	**17**	**24**	**30**	**-1**	**-2**	**8**	**29**	**68**	**94**	**230**	**224**
			Min	5	8	-53	-77	-103	-137	-108	-151	-248	-391	-479
		10	**Max**	**13**	**28**	**36**	**17**	**10**	**6**	**23**	**24**	**-32**	**-80**	**-64**
			Min	-8	-12	-57	-47	-57	-69	-43	-63	-246	-331	-246

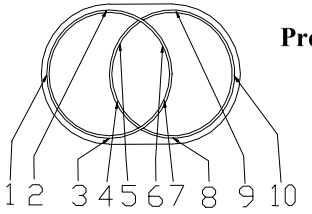

Predominant direction of motion

(All values in microstrain)

Table 4-36 Comparison of Methods to Calculate Idealized Force-Displacement Curve Specimen ISL1.0

Method	F_{y1*}		D_{y1*}		F_{y*}		D_{y*}		μ_{D**}
	[kN]	[Kips]	[mm]	[in]	[kN]	[Kips]	[mm]	[in]	
Method 1+	113.1	25.4	9.7	0.38	161.4	36.3	13.8	0.54	**11.7**
Method 2++	113.1	25.4	11.7	0.46	163.0	36.7	16.9	0.67	**9.5**
Method 3+++	83.9	18.9	7.8	0.31	162.1	36.4	15.1	0.60	**10.6**

* See Figure 4-71 for Definition
** Displacement ductility capacity
+1st bar Yield Point
++ Force of 1st bar yield
+++ One-half of the peak force

Table 4-37 Comparison of Methods to Calculate Idealized Force-Displacement Curve Specimen ISL1.5

Method	F_{y1*}		D_{y1*}		F_{y*}		D_{y*}		μ_{D**}
	[kN]	[Kips]	[mm]	[in]	[kN]	[Kips]	[mm]	[in]	
Method 1+	99.5	22.4	9.8	0.39	166.8	37.5	16.4	0.65	**11.5**
Method 2++	99.5	22.4	10.8	0.42	167.7	37.7	18.2	0.72	**10.4**
Method 3+++	89.0	20.0	9.1	0.36	167.1	37.6	17.0	0.67	**11.1**

* See Figure 4-71 for Definition
** Displacement ductility capacity
+1st bar Yield Point
++ Force of 1st bar yield
+++ One-half of the peak force

Table 4-38 Summary of the Values Used to Calculated Experimental Plastic Hinge Length l_p

Variables		Specimen	
		ISL1.0	**ISL1.5**
ϕ_y	**[Rad/mm]**	1.37E-02	7.92E-03
	[Rad/in]	5.41E-04	3.12E-04
ϕ_u	**[Rad/mm]**	2.18E-01	1.67E-01
	[Rad/in]	8.58E-03	6.57E-03
Δ_y	**[mm]**	16.9	18.2
	[in]	0.67	0.72
Δ_u	**[mm]**	161.0	188.5
	[in]	6.34	7.42
L	**[mm]**	1473	1829
	[in]	58	72
l_p	**[mm]**	351	428
	[in]	13.8	16.8

Table 5-1 Loading Protocol

	ISH1.0		ISH1.25		ISH1.5		ISH1.5T	
	FREE VIBRATION							
	FINE TUNNING							
	FREE VIBRATION							
Run No	**(g)**	**(x Sylmar)**	**(g)**	**(x Sylmar)**	**(g)**	**(x Sylmar)**	**(g)**	**(x Sylmar)**
1	0.06	0.1	0.06	0.1	0.06	0.1	0.06	0.1
2	0.12	0.2	0.12	0.2	0.12	0.2	0.12	0.2
3	0.24	0.4	0.30	0.5	0.24	0.4	0.24	0.4
4	0.30	0.5	0.45	0.75	0.36	0.6	0.36	0.6
	FREE VIBRATION				0.45	0.75	0.45	0.75
5	0.45	0.75	0.61	1	FREE VIBRATION			
6	0.61	1	0.76	1.25	0.61	1	0.61	1
7	0.76	1.25	FREE VIBRATION		0.76	1.25	0.76	1.25
	FREE VIBRATION		0.91	1.5	FREE VIBRATION			
8	0.91	1.5	1.06	1.75	0.91	1.5	0.91	1.5
9	1.06	1.75	1.21	2	1.06	1.75	1.06	1.75
10	1.21	2	1.29	2.125	1.21	2	1.21	2
11			1.36	2.25	1.29	2.125	1.29	2.125
12			1.44	2.375	1.36	2.25	1.36	2.25
13					1.44	2.375	1.44	2.375
14							1.52	2.5
15							1.59	2.625

Table 5-2 Performance Specimen ISH1.0

Run	(X Sylmar)	PGA(g)	μ_d	PERFORMANCE
1 to 3	0.1 - 0.4	0.06 - 0.24	0.06 - 0.4	FLEXURAL CRACKS
4 to 5	0.5 - 0.75	0.36 - 0.45	0.6 - 0.9	SHEAR CRACKS
6 to 8	1.0 - 1.5	0.61 - 0.91	1.4 - 2.5	INCREASE CRACKS AND FIRST SPALLING
9	1.75	1.06	3.6	LONG. BARS VISIBLE
10	2	1.21	4.7	SHEAR FAILURE

Table 5-3 Performance Specimen ISH1.25

Run	(X Sylmar)	PGA(g)	μ_d	PERFORMANCE
1 to 3	0.1 - 0.5	0.06 - 0.30	0.1 - 0.6	FLEXURAL CRACKS
4 to 5	0.75 - 1.0	0.45 - 0.61	1 - 1.4	SHEAR CRACKS
6 to 8	1.25 - 1.75	0.76 - 1.06	1.6 - 2.2	INCREASE CRACKS AND FIRST SPALLING
9 to 10	2.0 - 2.125	1.21 - 1.29	2.7 - 2.9	SPIRALS VISIBLE INCREASING SPALLING
11	2.25	1.36	3.7	LONG. BARS VISIBLE
12	2.375	1.44	5.0	SHEAR FAILURE

Table 5-4 Performance Specimen ISH1.5

Run	(X Sylmar)	PGA(g)	μ_d	PERFORMANCE
1 to 3	0.1 - 0.4	0.06 - 0.24	0.2 - 0.7	FLEXURAL AND VERTICAL CRACKS
4 to 5	0.6 - 0.75	0.36 - 0.45	0.9 - 1.0	SHEAR CRACKS
6 to 7	1.0 - 1.25	0.61 - 0.76	1.4 - 1.7	INCREASE CRACKS AND FIRST SPALLING
8 to 10	1.5 - 2.0	0.91 - 1.21	2.2 - 3.1	SPIRALS AND LONG. BARS VISIBLE
11	2.125	1.29	3.2	DAMAGE IN THE CORE
12	2.25	1.36	3.4	BUCKLING OF LONG. BARS
13	2.375	1.44	4.0	FLEXURAL FAILURE

Table 5-5 Performance Specimen ISH1.5T

Run	(X Sylmar)	PGA(g)	μ_d	PERFORMANCE
1 to 4	0.1 - 0.6	0.06 - 0.36	0.1 - 0.7	FLEXURAL CRACKS
5 to 6	0.75 - 1.0	0.45 - 0.61	0.8 - 1.2	SHEAR CRACKS
7 to 9	1.25 - 1.75	0.76 - 1.06	1.7 - 2.5	INCREASE CRACKS AND FIRST SPALLING
10	2	1.21	2.80	SPIRALS AND LONG. BARS VISIBLE
11 to 12	2.125 - 2.25	1.29 - 1.36	2.9 - 3.0	DAMAGE IN THE CORE
13 to 14	2.375 - 2.5	1.44 - 1.51	3.1 - 3.4	BUCKLING OF LONG. BAR
15	2.625	1.59	3.8	FLEXURAL FAILURE

Table 5-6 Target and Achieved Peak Table Accelerations for Specimen ISH1.0

Run No	Input Motion [x Sylmar]		Target [g]	Achieved [g]	Achieved PGA / Target PGA
1	**0.1**	**Max**	**0.06**	**0.06**	**0.93**
		Min	-0.03	-0.04	1.45
2	**0.2**	**Max**	**0.12**	**0.11**	**0.91**
		Min	-0.06	-0.08	1.28
3	**0.4**	**Max**	**0.24**	**0.22**	**0.92**
		Min	-0.12	-0.14	1.20
4	**0.5**	**Max**	**0.30**	**0.30**	**1.00**
		Min	-0.15	-0.16	1.07
5	**0.75**	**Max**	**0.45**	**0.47**	**1.03**
		Min	-0.22	-0.25	1.10
6	**1**	**Max**	**0.61**	**0.71**	**1.17**
		Min	-0.30	-0.40	1.34
7	**1.25**	**Max**	**0.76**	**0.87**	**1.15**
		Min	-0.37	-0.52	1.41
8	**1.5**	**Max**	**0.91**	**1.04**	**1.15**
		Min	-0.45	-0.59	1.31
9	**1.75**	**Max**	**1.06**	**1.25**	**1.18**
		Min	-0.52	-0.67	1.29
10	**2**	**Max**	**1.21**	**1.38**	**1.14**
		Min	-0.60	-0.58	0.98

Table 5-7 Target and Achieved Peak Table Accelerations for Specimen ISH1.25

Run No	Input Motion [x Sylmar]		Target [g]	Achieved [g]	Achieved PGA / Target PGA
1	**0.1**	**Max**	**0.06**	**0.06**	**1.01**
		Min	-0.03	-0.05	1.54
2	**0.2**	**Max**	**0.12**	**0.15**	**1.24**
		Min	-0.06	-0.11	1.85
3	**0.5**	**Max**	**0.30**	**0.29**	**0.95**
		Min	-0.15	-0.19	1.27
4	**0.75**	**Max**	**0.45**	**0.50**	**1.10**
		Min	-0.22	-0.29	1.30
5	**1.0**	**Max**	**0.61**	**0.66**	**1.09**
		Min	-0.30	-0.36	1.20
6	**1.25**	**Max**	**0.76**	**0.87**	**1.15**
		Min	-0.37	-0.49	1.31
7	**1.5**	**Max**	**0.91**	**1.03**	**1.14**
		Min	-0.45	-0.56	1.25
8	**1.75**	**Max**	**1.06**	**1.24**	**1.17**
		Min	-0.52	-0.65	1.25
9	**2.0**	**Max**	**1.21**	**1.45**	**1.20**
		Min	-0.60	-0.76	1.28
10	**2.125**	**Max**	**1.29**	**1.45**	**1.12**
		Min	-0.63	-0.72	1.14
11	**2.25**	**Max**	**1.36**	**1.46**	**1.07**
		Min	-0.67	-0.78	1.17
12	**2.375**	**Max**	**1.44**	**1.52**	**1.06**
		Min	-0.71	-0.75	1.06

Table 5-8 Target and Achieved Peak Table Accelerations for Specimen ISH1.5

Run No	Input Motion [x Sylmar]		Target [g]	Achieved [g]	Achieved PGA / Target PGA
1	**0.1**	**Max**	**0.06**	**0.07**	**1.09**
		Min	-0.03	-0.05	1.59
2	**0.2**	**Max**	**0.12**	**0.12**	**1.00**
		Min	-0.06	-0.07	1.23
3	**0.4**	**Max**	**0.24**	**0.24**	**0.97**
		Min	-0.12	-0.14	1.15
4	**0.6**	**Max**	**0.36**	**0.38**	**1.06**
		Min	-0.18	-0.21	1.18
5	**0.75**	**Max**	**0.45**	**0.48**	**1.05**
		Min	-0.22	-0.27	1.20
6	**1.0**	**Max**	**0.61**	**0.66**	**1.08**
		Min	-0.30	-0.36	1.22
7	**1.25**	**Max**	**0.76**	**0.81**	**1.07**
		Min	-0.37	-0.47	1.26
8	**1.5**	**Max**	**0.91**	**0.99**	**1.09**
		Min	-0.45	-0.53	1.19
9	**1.75**	**Max**	**1.06**	**1.11**	**1.05**
		Min	-0.52	-0.59	1.14
10	**2.0**	**Max**	**1.21**	**1.29**	**1.07**
		Min	-0.60	-0.66	1.11
11	**2.125**	**Max**	**1.29**	**1.35**	**1.05**
		Min	-0.63	-0.69	1.09
12	**2.25**	**Max**	**1.36**	**1.43**	**1.05**
		Min	-0.67	-0.73	1.08
13	**2.375**	**Max**	**1.44**	**1.45**	**1.01**
		Min	-0.71	-0.75	1.06

Table 5-9 Target and Achieved Peak Table Accelerations for Specimen ISH1.5T

Run No	Input Motion [x Sylmar]		Target [g]	Achieved [g]	Achieved PGA / Target PGA
1	**0.1**	**Max**	**0.06**	**0.06**	**1.06**
		Min	-0.03	-0.06	1.86
2	**0.2**	**Max**	**0.12**	**0.11**	**0.91**
		Min	-0.06	-0.10	1.71
3	**0.4**	**Max**	**0.24**	**0.18**	**0.75**
		Min	-0.12	-0.15	1.25
4	**0.6**	**Max**	**0.36**	**0.31**	**0.86**
		Min	-0.18	-0.23	1.29
5	**0.75**	**Max**	**0.45**	**0.42**	**0.93**
		Min	-0.22	-0.30	1.32
6	**1.0**	**Max**	**0.61**	**0.60**	**0.99**
		Min	-0.30	-0.43	1.43
7	**1.25**	**Max**	**0.76**	**0.78**	**1.03**
		Min	-0.37	-0.46	1.24
8	**1.5**	**Max**	**0.91**	**0.93**	**1.02**
		Min	-0.45	-0.60	1.35
9	**1.75**	**Max**	**1.06**	**1.05**	**0.99**
		Min	-0.52	-0.67	1.28
10	**2.0**	**Max**	**1.21**	**1.19**	**0.98**
		Min	-0.60	-0.74	1.24
11	**2.125**	**Max**	**1.29**	**1.26**	**0.98**
		Min	-0.63	-0.73	1.15
12	**2.25**	**Max**	**1.36**	**1.31**	**0.96**
		Min	-0.67	-0.68	1.02
13	**2.375**	**Max**	**1.44**	**1.36**	**0.95**
		Min	-0.71	-0.72	1.01
14	**2.5**	**Max**	**1.52**	**1.44**	**0.95**
		Min	-0.75	-0.81	1.09
15	**2.625**	**Max**	**1.59**	**1.54**	**0.97**
		Min	-0.78	-0.93	1.18

Table 5-10 Target and Achieved Spectral Response Acceleration for Specimen ISH1.0

Run No	Input Motion [x Sylmar]	Period [s]	Target [g]	Achieved [g]	Achieved / Target
1	0	0.321	0.09	0.09	1.00
2	0.2	0.321	0.18	0.18	1.02
3	0.4	0.321	0.36	0.36	1.01
4	0.5	0.351	0.42	0.37	0.89
5	0.75	0.356	0.69	0.62	0.91
6	1.0	0.356	0.91	0.76	0.83
7	1.25	0.376	1.42	1.07	0.76
8	1.5	0.532	0.62	0.73	1.17
9	1.75	0.581	0.77	0.89	1.15
10	2.0	0.641	1.19	1.15	0.96

Table 5-11 Target and Achieved Spectral Response Acceleration for Specimen ISH1.25

Run No	Input Motion [x Sylmar]	Period [s]	Target [g]	Achieved [g]	Achieved / Target
1	0	0.301	0.09	0.08	0.96
2	0.2	0.301	0.17	0.19	1.10
3	0.5	0.321	0.38	0.41	1.09
4	0.75	0.321	0.56	0.62	1.10
5	1.0	0.326	0.83	0.72	0.86
6	1.25	0.330	1.13	0.89	0.79
7	1.5	0.330	1.35	0.89	0.66
8	1.75	0.415	1.43	0.97	0.68
9	2.0	0.415	1.63	1.23	0.75
10	2.125	0.500	0.90	0.87	0.97
11	2.25	0.513	1.00	0.98	0.98
12	2.375	0.513	1.05	1.06	1.01

Table 5-12 Target and Achieved Spectral Response Acceleration for Specimen ISH1.5

Run No	Input Motion [x Sylmar]	Period [s]	Target [g]	Achieved [g]	Achieved / Target
1	0.1	0.356	0.08	0.08	1.01
2	0.2	0.376	0.22	0.21	0.98
3	0.4	0.398	0.47	0.45	0.95
4	0.6	0.398	0.71	0.69	0.98
5	0.75	0.427	0.79	0.74	0.94
6	1.00	0.427	1.05	1.04	0.99
7	1.25	0.556	0.55	0.68	1.25
8	1.5	0.641	0.80	0.91	1.14
9	1.75	0.641	0.93	0.95	1.02
10	2.0	0.641	1.09	0.96	0.88
11	2.125	0.709	0.97	0.87	0.90
12	2.25	0.709	0.91	0.82	0.90
13	2.375	0.855	0.96	0.84	0.87

Table 5-13 Target and Achieved Spectral Response Acceleration for Specimen ISH1.5T

Run No	Input Motion [x Sylmar]	Period [s]	Target [g]	Achieved [g]	Achieved / Target
1	0.1	0.284	0.10	0.11	1.12
2	0.2	0.284	0.19	0.22	1.16
3	0.4	0.341	0.46	0.41	0.90
4	0.5	0.341	0.69	0.60	0.88
5	0.75	0.353	0.89	0.81	0.92
6	1.00	0.353	1.18	1.18	1.00
7	1.25	0.415	0.87	1.16	1.33
8	1.5	0.415	1.04	1.69	1.62
9	1.75	0.526	0.88	1.05	1.20
10	2.0	0.568	1.06	1.14	1.07
11	2.125	0.602	1.08	1.10	1.01
12	2.25	0.602	1.15	1.19	1.04
13	2.375	0.602	1.21	1.25	1.03
14	2.50	0.602	1.27	1.29	1.01
15	2.625	0.602	0.99	0.99	1.00

Table 5-14 Axial Load Variation for Specimens with High Shear

		Specimen			
		ISH1.0	**ISH1.25**	**ISH1.5**	**ISH1.5T**
Target Axial Load	**[kN]**	-275	-300	-259	-346
	[kips]	-62	-67	-58	-78
Max. Axial Load Variation	**[kN]**	-283	-331	-276	-367
	[kips]	-64	-74	-62	-82
Min. Axial Load Variation	**[kN]**	-249	-288	-241	-331
	[kips]	-56	-65	-54	-74
Average Axial Load Variation	**[kN]**	-259	-304	-253	-341
	[kips]	-58	-68	-57	-77

Table 5-15 Measured Peak Forces and Displacement for Specimen ISH1.0

Peak Force								
	Maximum				**Minimum**			
Motion	**Force**		**Displacement**		**Force**		**Displacement**	
xSylmar	**[kN]**	**[Kips]**	**[mm]**	**[in]**	**[kN]**	**[Kips]**	**[mm]**	**[in]**
0.1	27.2	6.1	3.3	0.13	-31.2	-7.0	-1.2	-0.05
0.2	58.2	13.1	6.1	0.24	-59.6	-13.4	-3.9	-0.16
0.4	108.4	24.4	11.9	0.47	-117.8	-26.5	-9.2	-0.36
0.5	126.5	28.4	14.2	0.56	-145.8	-32.8	-13.4	-0.53
0.75	154.9	34.8	19.8	0.78	-191.5	-43.1	-19.9	-0.78
1	173.0	38.9	25.8	1.02	-220.3	-49.5	-28.8	-1.13
1.25	167.7	37.7	25.8	1.02	-229.1	-51.5	-40.1	-1.58
1.5	136.2	30.6	18.5	0.73	-236.6	-53.2	-53.2	-2.10
1.75	152.4	34.3	19.2	0.76	-241.3	-54.2	-76.1	-2.99
2	100.8	22.7	2.2	0.09	-218.3	-49.1	-87.5	-3.44
Peak Displacement								
	Maximum				**Minimum**			
Motion	**Force**		**Displacement**		**Force**		**Displacement**	
xSylmar	**[kN]**	**[Kips]**	**[mm]**	**[in]**	**[kN]**	**[Kips]**	**[mm]**	**[in]**
0.1	22.6	5.1	3.7	0.15	-27.8	-6.2	-1.7	-0.07
0.2	52.9	11.9	6.4	0.25	-59.6	-13.4	-3.9	-0.16
0.4	108.4	24.4	11.9	0.47	-116.6	-26.2	-9.4	-0.37
0.5	125.3	28.2	14.6	0.58	-140.8	-31.6	-13.5	-0.53
0.75	150.6	33.9	19.9	0.79	-189.7	-42.6	-20.9	-0.82
1	173.0	38.9	25.8	1.02	-217.3	-48.9	-30.3	-1.19
1.25	165.2	37.1	26.2	1.03	-223.5	-50.2	-43.5	-1.72
1.5	131.8	29.6	19.2	0.76	-228.3	-51.3	-60.8	-2.40
1.75	151.6	34.1	19.8	0.78	-230.2	-51.8	-86.9	-3.42
2	89.2	20.1	5.6	0.22	-130.1	-29.2	-212.2	-8.35

Table 5-16 Measured Peak Forces and Displacement for Specimen ISH1.25

Peak Force								
	Maximum				Minimum			
Motion	Force		Displacement		Force		Displacement	
xSylmar	[kN]	[Kips]	[mm]	[in]	[kN]	[Kips]	[mm]	[in]
0.1	26.6	6.0	1.7	0.07	-23.5	-5.3	-2.1	-0.08
0.2	51.1	11.5	4.4	0.17	-49.9	-11.2	-4.4	-0.17
0.5	114.4	25.7	13.2	0.52	-144.7	-32.5	-13.2	-0.52
0.75	135.0	30.3	16.8	0.66	-190.7	-42.9	-21.2	-0.84
1	169.3	38.1	17.1	0.67	-217.9	-49.0	-29.4	-1.16
1.25	164.3	36.9	17.5	0.69	-226.0	-50.8	-34.3	-1.35
1.5	155.9	35.0	17.5	0.69	-235.1	-52.9	-37.9	-1.49
1.75	150.7	33.9	16.7	0.66	-242.2	-54.5	-45.4	-1.79
2	144.5	32.5	14.8	0.58	-250.5	-56.3	-57.5	-2.26
2.125	145.8	32.8	15.2	0.60	-251.2	-56.5	-61.6	-2.43
2.25	148.6	33.4	15.7	0.62	-247.8	-55.7	-78.1	-3.07
2.375	147.3	33.1	12.5	0.49	-236.0	-53.1	-93.9	-3.70
Peak Displacement								
	Maximum				Minimum			
Motion	Force		Displacement		Force		Displacement	
xSylmar	[kN]	[Kips]	[mm]	[in]	[kN]	[Kips]	[mm]	[in]
0.1	24.1	5.4	1.9	0.08	-21.3	-4.8	-2.5	-0.10
0.2	49.6	11.1	4.5	0.18	-46.6	-10.5	-4.5	-0.18
0.5	114.4	25.7	13.2	0.52	-144.6	-32.5	-14.0	-0.55
0.75	128.2	28.8	16.9	0.67	-190.7	-42.9	-21.2	-0.84
1	163.4	36.7	17.9	0.71	-217.9	-49.0	-29.3	-1.16
1.25	159.4	35.8	18.1	0.71	-222.2	-50.0	-34.4	-1.36
1.5	155.3	34.9	17.7	0.70	-227.9	-51.2	-38.8	-1.53
1.75	150.7	33.9	16.7	0.66	-236.9	-53.3	-46.7	-1.84
2	143.1	32.2	15.0	0.59	-241.5	-54.3	-58.4	-2.30
2.125	145.8	32.8	15.2	0.60	-244.2	-54.9	-72.2	-2.84
2.25	147.3	33.1	15.8	0.62	-232.7	-52.3	-88.4	-3.48
2.375	139.8	31.4	12.7	0.50	-113.2	-25.5	-163.9	-6.45

Table 5-17 Measured Peak Forces and Displacement for Specimen ISH1.5

Peak Force								
	Maximum				Minimum			
Motion	Force		Displacement		Force		Displacement	
xSylmar	[kN]	[Kips]	[mm]	[in]	[kN]	[Kips]	[mm]	[in]
0.1	38.7	8.7	4.2	0.16	-45.0	-10.1	-6.1	-0.24
0.2	74.6	16.8	9.0	0.36	-85.5	-19.2	-11.6	-0.46
0.4	120.3	27.0	18.0	0.71	-144.3	-32.4	-22.3	-0.88
0.6	132.1	29.7	21.9	0.86	-168.5	-37.9	-30.1	-1.18
0.75	134.5	30.2	22.6	0.89	-176.6	-39.7	-31.9	-1.26
1	141.0	31.7	27.0	1.06	-207.1	-46.6	-43.2	-1.70
1.25	138.0	31.0	26.5	1.04	-217.5	-48.9	-52.9	-2.08
1.5	131.9	29.7	24.5	0.97	-237.5	-53.4	-71.0	-2.80
1.75	148.3	33.3	30.1	1.19	-243.4	-54.7	-87.5	-3.44
2	157.0	35.3	34.4	1.36	-247.1	-55.6	-98.5	-3.88
2.125	160.4	36.1	35.7	1.41	-252.6	-56.8	-112.7	-4.44
2.25	162.3	36.5	37.6	1.48	-238.9	-53.7	-107.4	-4.23
2.375	152.4	34.3	32.8	1.29	-220.1	-49.5	-114.2	-4.50
Peak Displacement								
	Maximum				Minimum			
Motion	Force		Displacement		Force		Displacement	
xSylmar	[kN]	[Kips]	[mm]	[in]	[kN]	[Kips]	[mm]	[in]
0.1	37.2	8.4	4.6	0.18	-43.5	-9.8	-6.7	-0.26
0.2	74.5	16.8	9.6	0.38	-83.2	-18.7	-12.4	-0.49
0.4	119.8	26.9	18.4	0.72	-144.1	-32.4	-22.9	-0.90
0.6	132.1	29.7	21.9	0.86	-168.5	-37.9	-30.1	-1.18
0.75	132.0	29.7	22.8	0.90	-175.1	-39.4	-32.8	-1.29
1	140.9	31.7	27.1	1.07	-200.2	-45.0	-44.6	-1.75
1.25	134.8	30.3	26.6	1.05	-215.7	-48.5	-53.3	-2.10
1.5	128.4	28.9	24.7	0.97	-232.8	-52.3	-73.8	-2.90
1.75	145.0	32.6	31.8	1.25	-235.6	-53.0	-92.3	-3.64
2	151.4	34.0	34.9	1.37	-245.2	-55.1	-109.8	-4.32
2.125	158.1	35.5	36.9	1.45	-236.7	-53.2	-113.1	-4.45
2.25	160.4	36.1	38.0	1.49	-232.4	-52.3	-117.0	-4.60
2.375	150.7	33.9	33.2	1.31	-196.5	-44.2	-128.2	-5.05

Table 5-18 Measured Peak Forces and Displacement for Specimen ISH1.5T

Peak Force								
	Maximum				Minimum			
Motion	Force		Displacement		Force		Displacement	
xSylmar	[kN]	[Kips	[mm	[in]	[kN]	[Kips]	[mm]	[in]
0.1	35.2	7.9	2.5	0.10	-31.6	-7.1	-2.8	-0.11
0.2	68.0	15.3	5.9	0.23	-69.7	-15.7	-6.5	-0.26
0.4	105.9	23.8	10.9	0.43	-120.0	-27.0	-13.1	-0.51
0.6	120.3	27.0	13.5	0.53	-153.3	-34.5	-18.3	-0.72
0.75	131.5	29.6	15.1	0.59	-167.8	-37.7	-20.9	-0.82
1	169.0	38.0	24.0	0.94	-210.0	-47.2	-31.7	-1.25
1.25	196.4	44.1	33.3	1.31	-236.4	-53.1	-45.1	-1.78
1.5	217.0	48.8	41.8	1.65	-246.7	-55.5	-55.3	-2.18
1.75	217.5	48.9	45.3	1.78	-250.4	-56.3	-66.9	-2.63
2	236.6	53.2	53.8	2.12	-251.2	-56.5	-75.7	-2.98
2.125	245.6	55.2	63.5	2.50	-247.0	-55.5	-78.8	-3.10
2.25	251.1	56.4	72.1	2.84	-242.8	-54.6	-81.2	-3.20
2.375	251.7	56.6	76.1	3.00	-238.5	-53.6	-83.8	-3.30
2.5	248.9	56.0	83.6	3.29	-239.1	-53.8	-90.3	-3.55
2.625	233.8	52.6	80.7	3.18	-232.0	-52.2	-99.4	-3.91
Peak Displacement								
	Maximum				Minimum			
Motion	Force		Displacement		Force		Displacement	
xSylmar	[kN]	[Kips	[mm	[in]	[kN]	[Kips]	[mm]	[in]
0.1	33.0	7.4	2.6	0.10	-30.8	-6.9	-3.0	-0.12
0.2	66.5	14.9	6.1	0.24	-69.7	-15.7	-6.5	-0.26
0.4	102.3	23.0	11.1	0.44	-120.0	-27.0	-13.1	-0.51
0.6	115.9	26.1	13.8	0.54	-153.3	-34.5	-18.3	-0.72
0.75	131.5	29.6	15.1	0.59	-164.3	-36.9	-20.9	-0.82
1	167.3	37.6	24.2	0.95	-210.0	-47.2	-31.7	-1.25
1.25	196.4	44.1	33.3	1.31	-236.4	-53.1	-45.1	-1.78
1.5	213.4	48.0	42.5	1.67	-245.1	-55.1	-56.3	-2.22
1.75	216.2	48.6	45.9	1.81	-248.0	-55.8	-67.6	-2.66
2	234.3	52.7	55.9	2.20	-248.3	-55.8	-76.2	-3.00
2.125	242.1	54.4	64.8	2.55	-239.6	-53.9	-79.2	-3.12
2.25	246.8	55.5	73.5	2.90	-242.8	-54.6	-81.2	-3.20
2.375	251.1	56.4	80.9	3.19	-232.9	-52.4	-84.1	-3.31
2.5	246.6	55.4	83.8	3.30	-232.7	-52.3	-90.3	-3.56
2.625	233.7	52.5	82.4	3.25	-229.3	-51.6	-101.6	-4.00

Table 5-19 Distance of the Inflection Point Relative to the Top of the Column

	Specimen										
Motion	**ISH1.0**		**Motion**	**ISH1.25**		**Motion**	**ISH1.5**		**Motion**	**ISH1.5T**	
[xSylmar]	**[mm]**	**[in]**	**[xSylmar]**	**[mm]**	**[in]**	**[xSylmar]**	**[mm]**	**[in]**	**[xSylmar]**	**[mm]**	**[in]**
0.1	762	30.0	0.1	1008	39.7	0.1	354	13.9	0.1	489.9	19.3
0.2	717	28.2	0.2	758	29.8	0.2	509	20.0	0.2	552.4	21.7
0.4	691	27.2	0.5	734	28.9	0.4	616	24.3	0.4	656	25.8
0.5	696	27.4	0.75	777	30.6	0.6	682	26.9	0.6	691.4	27.2
0.75	692	27.2	1	819	32.3	0.75	688	27.1	0.75	721.6	28.4
1	699	27.5	1.25	830	32.7	1	800	31.5	1	811.9	32.0
1.25	709	27.9	1.5	823	32.4	1.25	880	34.6	1.25	914.2	36.0
1.5	709	27.9	1.75	824	32.4	1.5	922	36.3	1.5	950.1	37.4
1.75	702	27.6	2	820	32.3	1.75	949	37.4	1.75	968	38.1
2	726	28.6	2.125	803	31.6	2	929	36.6	2	982.8	38.7
			2.25	781	30.8	2.125	883	34.8	2.125	978	38.5
			2.375	667	26.3	2.25	880	34.6	2.25	965.9	38.0
						2.375	974	38.3	2.375	965	38.0
									2.5	962.4	37.9
									2.625	1014	39.9
ht*/2=	737	29.0	**ht*/2=**	800	31.5	**ht*/2=**	876	34.5	**ht*/2=**	876	34.5

* Clear Height of the Column

Table 5-20 Head Rotation in ISH1.0

Motion	**Force**		**Displacement**		**Rotation**
[xSylmar]	**[kN]**	**[Kips]**	**[mm]**	**[in]**	**[Degree]**
0.1	-31.2	-7.0	-1.3	-0.05	0.072
0.2	-59.6	-13.4	-4.0	-0.16	0.056
0.4	-117.82	-26.5	-9.2	-0.36	0.159
0.5	-145.83	-32.8	-13.4	-0.53	0.213
0.75	-191.53	-43.1	-19.9	-0.78	0.320
1	-220.31	-49.5	-28.8	-1.13	0.379
1.25	-229.11	-51.5	-40.1	-1.58	0.407
1.5	-236.56	-53.2	-53.2	-2.10	0.548
1.75	-241.29	-54.2	-76.0	-2.99	0.499
2	-218.28	-49.1	-87.5	-3.44	0.540

Table 5-21 Head Rotation in ISH1.25

Motion	Force		Displacement		Rotation
[xSylmar]	[kN]	[Kips]	[mm]	[in]	[Degree]
0.1	-23.5	-5.3	-2.1	-0.08	0.077
0.2	-49.9	-11.2	-4.4	-0.17	0.133
0.5	-144.7	-32.5	-13.2	-0.52	0.307
0.75	-190.7	-42.9	-21.2	-0.84	0.361
1	-217.9	-49.0	-29.4	-1.16	0.415
1.25	-226.0	-50.8	-34.3	-1.35	0.466
1.5	-235.1	-52.9	-37.9	-1.49	0.402
1.75	-242.2	-54.5	-45.4	-1.79	0.520
2	-250.5	-56.3	-57.5	-2.26	0.533
2.125	-251.2	-56.5	-61.6	-2.43	0.471
2.25	-247.8	-55.7	-78.1	-3.07	0.520
2.375	-236.0	-53.1	-93.9	-3.70	0.407

Table 5-22 Head Rotation in ISH1.5

Motion	Force		Displacement		Rotation
[xSylmar]	[kN]	[Kips]	[mm]	[in]	[Degree]
0.1	-45.0	-10.1	-6.1	-0.24	0.087
0.2	-85.5	-19.2	-11.6	-0.46	0.172
0.4	-144.3	-32.4	-22.3	-0.88	0.410
0.6	-168.5	-37.9	-30.1	-1.18	0.530
0.75	-176.6	-39.7	-31.9	-1.26	0.638
1	-207.1	-46.6	-43.2	-1.70	0.709
1.25	-217.5	-48.9	-52.9	-2.08	0.929
1.5	-237.5	-53.4	-71.0	-2.80	0.983
1.75	-243.4	-54.7	-87.5	-3.44	1.101
2	-247.1	-55.6	-98.5	-3.88	1.129
2.125	-252.6	-56.8	-112.7	-4.44	1.078
2.25	-238.9	-53.7	-107.4	-4.23	0.991
2.375	-220.1	-49.5	-114.2	-4.50	1.091

Table 5-23 Head Rotation in ISH1.5T

Motion	Force		Displacement		Rotation
[xSylmar]	[kN]	[Kips]	[mm]	[in]	[Degree]
0.1	-31.6	-7.1	-2.8	-0.11	0.085
0.2	-69.7	-15.7	-6.5	-0.26	0.187
0.4	-120.0	-27.0	-13.1	-0.51	0.323
0.6	-153.3	-34.5	-18.3	-0.72	0.384
0.75	-167.8	-37.7	-20.9	-0.82	0.399
1	-210.0	-47.2	-31.7	-1.25	0.617
1.25	-236.4	-53.1	-45.1	-1.78	0.806
1.5	-246.7	-55.5	-55.3	-2.18	0.830
1.75	-250.4	-56.3	-66.9	-2.63	0.847
2	-251.2	-56.5	-75.7	-2.98	0.901
2.125	-247.0	-55.5	-78.8	-3.10	0.893
2.25	-242.8	-54.6	-81.2	-3.20	0.876
2.375	-238.5	-53.6	-83.8	-3.30	0.863
2.5	-239.1	-53.8	-90.3	-3.55	0.893
2.625	-232.0	-52.2	-99.4	-3.91	0.855

Table 5-24 Dynamic Properties from Low Level Elastic Response for Specimen ISH1.0

Input Motion	Frequency	Period	Stiffness	
[x Sylmar]	[Hz]	[s]	[Kip/in]	[kN/mm]
0.1	3.12	0.32	80	14
0.2	3.12	0.32	80	14
0.4	3.12	0.32	80	14
0.5	2.85	0.35	66	12
0.75	2.81	0.36	65	11
1	2.81	0.36	65	11
1.25	2.66	0.38	58	10
1.5	1.88	0.53	29	5
1.75	1.72	0.58	24	4
2	1.56	0.64	20	3

Table 5-25 Dynamic Properties from Snap Ramp for Specimen ISH1.0

	Snap Ramp				
Motion	**Frequency**	**Period**	**Stiffness**		**Damping**
[xSylmar]	**[Hz]**	**[s]**	**[Kip/in]**	**[kN/mm]**	**[%]**
0.1	2.95	0.34	71	12	3.5
0.2	N/A				
0.4					
0.5	2.55	0.39	53	9	4.42
0.75	N/A				
1					
1.25	2.15	0.47	38	7	5.96
1.5	N/A				
1.75					
2					

Table 5-26 Calculated Dynamic Properties from Peak Force with the Corresponding Displacement for Specimen ISH1.0

Motion	**Force**		**Displacement**		**Stiffness**		**Freq.**	**Period**
[xSylmar]	**[Kips]**	**[kN]**	**[in]**	**[mm]**	**[Kip/in]**	**[kN/mm]**	**[Hz]**	**[s]**
0.1	7.0	31.2	0.05	1.3	142	25	4.17	0.24
0.2	13.4	59.6	0.16	4.0	86	15	3.24	0.31
0.4	26.5	117.8	0.36	9.2	73	13	3.00	0.33
0.5	32.8	145.8	0.53	13.4	62	11	2.76	0.36
0.75	43.1	191.5	0.78	19.9	55	10	2.59	0.39
1	49.5	220.3	1.13	28.8	44	8	2.31	0.43
1.25	51.5	229.1	1.58	40.1	33	6	2.00	0.50
1.5	53.2	236.6	2.10	53.2	25	4	1.76	0.57
1.75	54.2	241.3	2.99	76.0	18	3	1.49	0.67
2	49.1	218.3	3.44	87.5	14	2	1.32	0.76

Table 5-27 Dynamic Properties from Low Level Elastic Response for Specimen ISH1.25

Input Motion	Frequency	Period	Stiffness	
[x Sylmar]	[Hz]	[s]	[Kip/in]	[kN/mm]
0.1	3.32	0.30	90	16
0.2	3.32	0.30	90	16
0.5	3.12	0.32	80	14
0.75	3.12	0.32	80	14
1	3.07	0.33	77	14
1.25	3.03	0.33	75	13
1.5	3.03	0.33	75	13
1.75	2.41	0.41	48	8
2	2.41	0.41	48	8
2.125	2	0.50	33	6
2.25	1.95	0.51	31	5
2.375	1.95	0.51	31	5

Table 5-28 Dynamic Properties from Snap Ramp for Specimen ISH1.25

	Snap Ramp				
Motion	Frequency	Period	Stiffness		Damping
[xSylmar]	[Hz]	[s]	[Kip/in]	[kN/mm]	[%]
0.1	3.13	0.32	80	14	3.9
0.2	N/A				
0.5					
0.75	3.05	0.33	76	13	6.30
1	N/A				
1.25					
1.5	2.73	0.37	61	11	7.35
1.75	N/A				
2					
2.125					
2.25					
2.375					

Table 5-29 Calculated Dynamic Properties from Peak Force with the Corresponding Displacement for Specimen ISH1.25

Motion	Force		Displacement		Stiffness		Freq.	Period
[xSylmar]	[Kips]	[kN]	[in]	[mm]	[Kip/in]	[kN/mm]	[Hz]	[s]
0.1	5.3	23.5	0.08	2.1	63	11	2.77	0.36
0.2	11.2	49.9	0.17	4.4	65	11	2.82	0.35
0.5	32.5	144.7	0.52	13.2	63	11	2.77	0.36
0.75	42.9	190.7	0.84	21.2	51	9	2.50	0.40
1	49.0	217.9	1.16	29.4	42	7	2.28	0.44
1.25	50.8	226.0	1.35	34.3	38	7	2.15	0.47
1.5	52.9	235.1	1.49	37.9	35	6	2.08	0.48
1.75	54.5	242.2	1.79	45.4	30	5	1.93	0.52
2	56.3	250.5	2.26	57.5	25	4	1.74	0.57
2.125	56.5	251.2	2.43	61.6	23	4	1.69	0.59
2.25	55.7	247.8	3.07	78.1	18	3	1.49	0.67
2.375	53.1	236.0	3.70	93.9	14	3	1.32	0.76

Table 5-30 Dynamic Properties from Low Level Elastic Response for Specimen ISH1.5

Input Motion	Frequency	Period	Stiffness	
[x Sylmar]	[Hz]	[s]	[Kip/in]	[kN/mm]
0.1	2.81	0.36	65	11
0.2	2.66	0.38	58	10
0.4	2.5	0.40	51	9
0.6	2.5	0.40	51	9
0.75	2.34	0.43	45	8
1	2.34	0.43	45	8
1.25	1.8	0.56	27	5
1.5	1.56	0.64	20	3
1.75	1.56	0.64	20	3
2	1.56	0.64	20	3
2.125	1.41	0.71	16	3
2.25	1.41	0.71	16	3
2.375	1.17	0.85	11	2

Table 5-31 Dynamic Properties from Snap Ramp for Specimen ISH1.5

	Snap Ramp				
Motion	**Frequency**	**Period**	**Stiffness**		**Damping**
[xSylmar]	**[Hz]**	**[s]**	**[Kip/in]**	**[kN/mm]**	**[%]**
0.1	2.60	0.38	55	10	4.24
0.2	N/A				
0.4					
0.6					
0.75	2.19	0.46	39	7	6.36
1	N/A				
1.25					
1.5	1.88	0.53	29	5	7.73
1.75	N/A				
2					
2.125					
2.25					
2.375					

Table 5-32 Calculated Dynamic Properties from Peak Force with the Corresponding Displacement for Specimen ISH1.5

Motion	**Force**		**Displacement**		**Stiffness**		**Freq.**	**Period**
[xSylmar]	**[Kips]**	**[kN]**	**[in]**	**[mm]**	**[Kip/in]**	**[kN/mm]**	**[Hz]**	**[s]**
0.1	10.1	45.0	0.24	6.1	42	7	2.26	0.44
0.2	19.2	85.5	0.46	11.6	42	7	2.27	0.44
0.4	32.4	144.3	0.88	22.3	37	6	2.12	0.47
0.6	37.9	168.5	1.18	30.1	32	6	1.98	0.51
0.75	39.7	176.6	1.26	31.9	32	6	1.97	0.51
1	46.6	207.1	1.70	43.2	27	5	1.83	0.55
1.25	48.9	217.5	2.08	52.9	23	4	1.69	0.59
1.5	53.4	237.5	2.80	71.0	19	3	1.53	0.65
1.75	54.7	243.4	3.44	87.5	16	3	1.39	0.72
2	55.6	247.1	3.88	98.5	14	3	1.32	0.76
2.125	56.8	252.6	4.44	112.7	13	2	1.25	0.80
2.25	53.7	238.9	4.23	107.4	13	2	1.25	0.80
2.375	49.5	220.1	4.50	114.2	11	2	1.16	0.86

Table 5-33 Dynamic Properties from Low Level Elastic Response for Specimen ISH1.5T

Input Motion	Frequency	Period	Stiffness	
[x Sylmar]	[Hz]	[s]	[Kip/in]	[kN/mm]
0.1	3.52	0.28	101	18
0.2	3.52	0.28	101	18
0.4	2.93	0.34	70	12
0.5	2.93	0.34	70	12
0.75	2.83	0.35	66	11
1	2.83	0.35	66	11
1.25	2.41	0.41	48	8
1.5	2.41	0.41	48	8
1.75	1.9	0.53	30	5
2	1.76	0.57	25	4
2.125	1.66	0.60	23	4
2.25	1.66	0.60	23	4
2.375	1.66	0.60	23	4
2.5	1.66	0.60	23	4
2.625	1.66	0.60	23	4

Table 5-34 Dynamic Properties from Snap Ramp for Specimen ISH1.5T

	Snap Ramp				
Motion	Frequency	Period	Stiffness		Damping
[xSylmar]	[Hz]	[s]	[Kip/in]	[kN/mm]	[%]
0.1	3.03	0.33	75	13	5.61
0.2	N/A				
0.4					
0.6					
0.75	2.73	0.37	61	11	6.14
1	N/A				
1.25					
1.5	2.44	0.41	49	9	7.21
1.75	N/A				
2					
2.125					
2.25					
2.375					
2.5					
2.625					

Table 5-35 Calculated Dynamic Properties from Peak Force with the Corresponding Displacement for Specimen ISH1.5T

Motion	Force		Displacement		Stiffness		Freq.	Period
[xSylmar]	[Kips]	[kN]	[in]	[mm]	[Kip/in]	[kN/mm]	[Hz]	[s]
0.1	7.1	31.6	0.11	2.8	65	11	2.82	0.35
0.2	15.7	69.7	0.26	6.5	61	11	2.74	0.37
0.4	27.0	120.0	0.51	13.1	52	9	2.53	0.39
0.5	34.5	153.3	0.72	18.3	48	8	2.42	0.41
0.75	37.7	167.8	0.82	20.9	46	8	2.37	0.42
1	47.2	210.0	1.25	31.7	38	7	2.15	0.47
1.25	53.1	236.4	1.78	45.1	30	5	1.91	0.52
1.5	55.5	246.7	2.18	55.3	25	4	1.77	0.57
1.75	56.3	250.4	2.63	66.9	21	4	1.62	0.62
2	56.5	251.2	2.98	75.7	19	3	1.52	0.66
2.125	55.5	247.0	3.10	78.8	18	3	1.48	0.68
2.25	54.6	242.8	3.20	81.2	17	3	1.44	0.69
2.375	53.6	238.5	3.30	83.8	16	3	1.41	0.71
2.5	53.8	239.1	3.55	90.3	15	3	1.36	0.74
2.625	52.2	232.0	3.91	99.4	13	2	1.28	0.78

Table 5-36 Comparison of Deflection at the Top Panel Nodes and Deflection at the Bottom of the Head Specimen ISH1.0

Run	Displacement at Nodes 7 and 8*		Bottom Head Displacement		Lateral Force	
	[mm]	[in]	[mm]	[in]	[kN]	[Kips]
1	-0.02	0.00	-1.79	-0.07	-31.2	-7.0
2	-3.45	-0.14	-4.60	-0.18	-59.6	-13.4
3	-7.02	-0.28	-9.16	-0.36	-117.8	-26.5
4	-10.35	-0.41	-13.03	-0.51	-145.8	-32.8
5	-16.64	-0.66	-18.89	-0.74	-191.5	-43.1
6	-25.00	-0.98	-27.39	-1.08	-220.3	-49.5
7	-36.00	-1.42	-38.57	-1.52	-229.1	-51.5
8	-49.13	-1.93	-50.81	-2.00	-236.6	-53.2
9	-70.88	-2.79	-73.93	-2.91	-241.3	-54.2
10	-93.04	-3.66	-85.13	-3.35	-195.1	-43.9

* Top nodes panel configuration (Figure 5-154)

Table 5-37 Comparison of Deflection at the Top Panel Nodes and Deflection at the Bottom of the Head Specimen ISH1.25

Run	Displacement at Nodes 7 and 8*		Bottom Head Displacement		Lateral Force	
	[mm]	[in]	[mm]	[in]	[kN]	[Kips]
1	-1.36	-0.05	-1.92	-0.08	-23.5	-5.3
2	-3.17	-0.12	-3.80	-0.15	-49.9	-11.2
3	-10.84	-0.43	-11.54	-0.45	-144.7	-32.5
4	-17.08	-0.67	-19.26	-0.76	-190.7	-42.9
5	-24.24	-0.95	-27.04	-1.06	-217.9	-49.0
6	-28.51	-1.12	-31.63	-1.25	-226.0	-50.8
7	-32.29	-1.27	-35.66	-1.40	-235.1	-52.9
8	-39.20	-1.54	-42.47	-1.67	-242.2	-54.5
9	-50.21	-1.98	-54.43	-2.14	-250.5	-56.3
10	-54.75	-2.16	-58.94	-2.32	-251.2	-56.5
11	-69.26	-2.73	-75.10	-2.96	-247.8	-55.7
12	-94.16	-3.71	-104.41	-4.11	-193.0	-43.4

* Top nodes panel configuration (Figure 5-154)

Table 5-38 Comparison of Deflection at the Top Panel Nodes and Deflection at the Bottom of the Head Specimen ISH1.5

Run	Displacement at Nodes 7 and 8*		Bottom Head Displacement		Lateral Force	
	[mm]	[in]	[mm]	[in]	[kN]	[Kips]
1	-3.42	-0.13	-5.66	-0.22	-45.0	-10.1
2	-7.77	-0.31	-10.55	-0.42	-85.5	-19.2
3	-16.28	-0.64	-19.83	-0.78	-144.3	-32.4
4	-22.39	-0.88	-26.84	-1.06	-168.5	-37.9
5	-24.74	-0.97	-28.01	-1.10	-176.6	-39.7
6	-34.58	-1.36	-38.84	-1.53	-207.1	-46.6
7	-43.01	-1.69	-47.15	-1.86	-217.5	-48.9
8	-60.44	-2.38	-64.97	-2.56	-237.5	-53.4
9	-75.24	-2.96	-80.68	-3.18	-243.4	-54.7
10	-85.30	-3.36	-91.50	-3.60	-247.1	-55.6
11	-97.77	-3.85	-106.11	-4.18	-252.6	-56.8
12	-93.51	-3.68	-101.31	-3.99	-238.9	-53.7
13	-113.22	-4.46	-107.46	-4.23	-220.1	-49.5

* Top nodes panel configuration (Figure 5-154)

Table 5-39 Comparison of Deflection at the Top Panel Nodes and Deflection at the Bottom of the Head Specimen ISH1.5T

Run	Displacement at Nodes 7 and 8*		Bottom Head Displacement		Lateral Force	
	[mm]	[in]	[mm]	[in]	[kN]	[Kips]
1	-2.95	-0.12	-2.22	-0.09	-31.6	-7.1
2	-5.57	-0.22	-5.31	-0.21	-69.7	-15.7
3	-10.74	-0.42	-11.03	-0.43	-120.0	-27.0
4	-14.74	-0.58	-15.90	-0.63	-153.3	-34.5
5	-17.16	-0.68	-18.37	-0.72	-167.8	-37.7
6	-25.52	-1.00	-27.88	-1.10	-210.0	-47.2
7	-37.41	-1.47	-40.09	-1.58	-236.4	-53.1
8	-46.77	-1.84	-50.08	-1.97	-246.7	-55.5
9	-57.08	-2.25	-61.61	-2.43	-250.4	-56.3
10	-64.97	-2.56	-70.12	-2.76	-251.2	-56.5
11	-68.46	-2.70	-73.19	-2.88	-247.0	-55.5
12	-70.56	-2.78	-75.76	-2.98	-242.8	-54.6
13	-73.28	-2.89	-78.43	-3.09	-238.5	-53.6
14	-79.11	-3.11	-84.71	-3.34	-239.1	-53.8
15	-89.61	-3.53	-101.65	-4.00	-229.3	-51.6

* Top nodes panel configuration (Figure 5-154)

Table 5-40 Shear Deformation for Individual Panel for the Predominant Direction of Motion Specimen ISH1.0

Run No	Shear Deformation [% Δ_ST*]			
	Panel 1	Panel 2	Panel 3	Panel 4
1	9%	13%	33%	44%
2	7%	18%	39%	36%
3	10%	14%	32%	44%
4	13%	17%	34%	37%
5	13%	17%	29%	41%
6	21%	16%	21%	42%
7	23%	17%	17%	43%
8	24%	15%	16%	45%
9	27%	13%	16%	44%
10	28%	10%	20%	43%
* Shear deformation at the top of the column				

Table 5-41 Shear Deformation for Individual Panel for the Predominant Direction of Motion Specimen ISH1.25

Run No	Shear Deformation [% Δ_sT*]			
	Panel 1	Panel 2	Panel 3	Panel 4
1	14%	11%	26%	49%
2	21%	8%	30%	41%
3	38%	8%	14%	41%
4	50%	15%	2%	32%
5	35%	17%	12%	37%
6	32%	16%	15%	37%
7	32%	16%	15%	36%
8	36%	16%	11%	38%
9	40%	14%	7%	40%
10	41%	14%	5%	40%
11	42%	12%	5%	40%
12	50%	5%	6%	39%

* Shear deformation at the top of the column

Table 5-42 Shear Deformation for Individual Panel for the Predominant Direction of Motion Specimen ISH1.5

Run No	Shear Deformation [% Δ_sT*]			
	Panel 1	Panel 2	Panel 3	Panel 4
1	25%	22%	22%	31%
2	29%	20%	20%	31%
3	35%	25%	6%	34%
4	26%	25%	13%	37%
5	26%	26%	11%	36%
6	35%	29%	5%	31%
7	36%	26%	7%	31%
8	45%	17%	3%	36%
9	42%	13%	8%	37%
10	42%	13%	7%	38%
11	49%	9%	9%	43%
12	58%	8%	12%	40%
13	45%	9%	11%	35%

* Shear deformation at the top of the column

Table 5-43 Shear Deformation for Individual Panel for the Predominant Direction of Motion Specimen ISH1.5T

Run No	Shear Deformation [% Δ_sT*]			
	Panel 1	Panel 2	Panel 3	Panel 4
1	16%	20%	27%	37%
2	27%	20%	25%	28%
3	47%	23%	16%	14%
4	46%	23%	18%	13%
5	39%	21%	21%	19%
6	31%	17%	28%	24%
7	25%	14%	34%	28%
8	29%	14%	32%	26%
9	35%	13%	28%	24%
10	38%	13%	25%	23%
11	40%	13%	24%	23%
12	40%	13%	23%	24%
13	41%	12%	23%	24%
14	41%	11%	23%	25%
15	40%	10%	25%	26%
* Shear deformation at the top of the column				

Table 5-44 Flexural and Shear Deformation Percentages for Specimen ISH1.0

Motion [xSylmar]	δ_f/δ_T [%]	δ_s/δ_T [%]
0.10	57%	43%
0.20	59%	41%
0.40	56%	44%
0.50	63%	37%
0.75	65%	35%
1.0	75%	25%
1.25	78%	22%
1.50	81%	19%
1.75	81%	19%
2.0	76%	24%

Table 5-45 Flexural and Shear Deformation Percentages for Specimen ISH1.25

Motion	δ_f/δ_T	δ_s/δ_T
[xSylmar]	[%]	[%]
0.10	82%	18%
0.20	76%	24%
0.50	80%	20%
0.75	84%	16%
1.0	78%	22%
1.25	76%	24%
1.50	76%	24%
1.75	77%	23%
2.0	78%	22%
2.125	80%	20%
2.250	82%	18%

Table 5-46 Flexural and Shear Deformation Percentages for Specimen ISH1.5

Motion	δ_f/δ_T	δ_s/δ_T
[xSylmar]	[%]	[%]
0.10	87%	13%
0.20	87%	13%
0.40	85%	15%
1.0	83%	17%
1.25	84%	16%
1.50	86%	14%
1.75	83%	17%
2.0	82%	18%
2.3125	83%	17%

Table 5-47 Flexural and Shear Deformation Percentages for Specimen ISH1.5T

Motion [xSylmar]	δ_f/δ_T [%]	δ_s/δ_T [%]
0.10	65%	35%
0.20	63%	37%
0.40	78%	22%
0.60	78%	22%
0.75	75%	25%
1.0	72%	28%
1.25	65%	35%
1.50	66%	34%
1.75	69%	31%
2.0	71%	29%
2.125	70%	30%
2.25	68%	32%
2.375	69%	31%
2.5	68%	32%
2.625	68%	32%

Table 5-48 Measured Strains in Longitudinal Bars at–229 mm (-9 in), –152 mm (-6 in), –76 mm (-3 in) and 0 mm (0 in) from the Top of the Footing for Specimen ISH1.0

Height		Strain Gages Number		Run No									
[mm]	[in]			1	2	3	4	5	6	7	8	9	10
-228.6	-9	1	**Max**	**112**	**208**	**467**	**646**	**942**	**1093**	**1131**	**1065**	**1165**	**939**
			Min	-139	-207	-374	-463	-668	-812	-889	-983	-1059	-1048
		6	**Max**	**-138**	**-12**	**69**	**136**	**294**	**419**	**540**	**642**	**760**	**785**
			Min	-319	-353	-460	-530	-615	-704	-738	-736	-768	-741
-152.4	-6	1	**Max**	**220**	**457**	**985**	**1240**	**1601**	**1714**	**1717**	**1610**	**1773**	**1417**
			Min	-261	-378	-638	-787	-1193	-1442	-1556	-1714	-1807	-1756
		6	**Max**	**-115**	**55**	**269**	**485**	**901**	**1182**	**1410**	**1547**	**1717**	**1710**
			Min	-459	-566	-789	-926	-1158	-1319	-1398	-1365	-1453	-1381
-76.2	-3	1	**Max**	**257**	**738**	**1525**	**1823**	**2418**	**2488**	**2404**	**2309**	**2866**	**2381**
			Min	-403	-527	-797	-968	-1488	-1883	-2072	-2389	-2613	-3140
		6	**Max**	**-105**	**116**	**610**	**1024**	**1751**	**2007**	**2239**	**2463**	**2952**	**4372**
			Min	-508	-673	-1015	-1215	-1546	-1821	-1884	-1842	-2084	-2068
0	0	1	**Max**	**221**	**686**	**1491**	**1811**	**2800**	**9801**	**10558**	**8041**	**9794**	**8870**
			Min	-394	-496	-730	-852	-1207	-1277	-1055	-3774	-5106	-2895
		2	**Max**	**289**	**769**	**1594**	**1929**	**2401**	**3013**	**5477**	**5445**	**7873**	**3462**
			Min	-388	-517	-795	-950	-1503	-2010	-2831	-4153	-5837	-3901
		3	**Max**	**70**	**380**	**934**	**1181**	**1998**	**2385**	**2359**	**2069**	**2486**	**1508**
			Min	-259	-281	-286	-284	-272	-492	-454	-419	-477	-642
		4	**Max**	**-142**	**-11**	**491**	**799**	**1488**	**2107**	**2366**	**2580**	**13044**	**12214**
			Min	-263	-264	-264	-226	-217	-779	-1198	-1545	-1507	851
		5	**Max**	**-159**	**77**	**805**	**1302**	**2156**	**2371**	**2631**	**6135**	**12222**	**12873**
			Min	-514	-661	-950	-1091	-1329	-1556	-1702	-2579	-2306	-266
		6	**Max**	**-111**	**142**	**1017**	**1592**	**2434**	**2755**	**12700**	**14679**	**23190**	**24126**
			Min	-558	-757	-1178	-1419	-1798	-2149	-3124	-3412	-1491	490

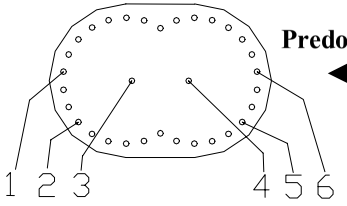

Predominant direction of motion

(All values in microstrain)

Table 5-49 Measured Strains in Longitudinal Bars at 127 mm (5 in) and 254 mm (10 in) from the Top of the Footing for Specimen ISH1.0

Height		Strain Gages Number		Run No									
[mm]	[in]			1	2	3	4	5	6	7	8	9	10
127	5	1	**Max**	**281**	**797**	**1707**	**2085**	**2863**	**11258**	**8626**	**4179**	**3104**	**71561**
			Min	-588	-887	-1500	-1843	-2876	-5599	-7349	-11532	-20265	-33803
		2	**Max**	**312**	**754**	**1608**	**1933**	**2351**	**7562**	**8201**	**3792**	**3810**	**32833**
			Min	-410	-684	-1244	-1557	-2119	-6338	-8062	-10770	-15797	-13131
		3	**Max**	**-181**	**81**	**593**	**815**	**1371**	**2014**	**1996**	**2618**	**6132**	**31175**
			Min	-619	-650	-649	-642	-622	-623	-546	-466	-384	1263
		4	**Max**	**-257**	**-67**	**503**	**971**	**1941**	**3644**	**12671**	**14838**	**20105**	**18590**
			Min	-365	-364	-363	-342	-339	-345	-227	3133	3703	5192
		5	**Max**	**-65**	**194**	**1104**	**1599**	**2736**	**10959**	**14753**	**20038**	**27389**	**26772**
			Min	-457	-627	-922	-1047	-1303	-1677	-282	965	2795	6086
		6	**Max**	**-212**	**125**	**1401**	**2111**	**9646**	**11878**	**18651**	**25088**	**34825**	**34160**
			Min	-831	-1157	-1713	-2010	-5675	-5424	-3166	-1368	1090	5069
254	10	1	**Max**	**260**	**715**	**1679**	**2108**	**2579**	**2747**	**2840**	**2880**	**6744**	**71774**
			Min	-547	-832	-1380	-1637	-2026	-2229	-2278	-2423	-3083	-4462
		2	**Max**	**342**	**774**	**1628**	**1956**	**2434**	**2705**	**3059**	**3243**	**7948**	**31912**
			Min	-438	-715	-1247	-1508	-1943	-2339	-2737	-3211	-5711	-4765
		3	**Max**	**-133**	**110**	**668**	**941**	**1524**	**2077**	**2040**	**1674**	**2294**	**789**
			Min	-583	-637	-653	-616	-569	-644	-630	-639	-679	-25892
		4	**Max**	**-401**	**-162**	**483**	**830**	**1768**	**2556**	**3590**	**14829**	**20391**	**71970**
			Min	-546	-564	-578	-520	-520	-713	-1078	-1067	3131	6771
		5	**Max**	**-95**	**254**	**1211**	**1753**	**2875**	**9458**	**12929**	**16647**	**16028**	**70033**
			Min	-617	-833	-1176	-1311	-1562	-1930	-896	98	1315	-4225
		6	**Max**	**-154**	**284**	**1485**	**2174**	**7271**	**10463**	**14417**	**20145**	**28070**	**71128**
			Min	-843	-1137	-1621	-1819	-2908	-4562	-2229	-1025	833	4137

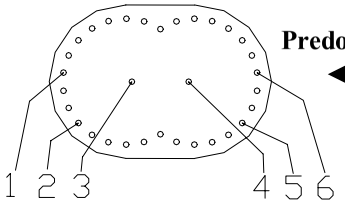

Predominant direction of motion

(All values in microstrain)

Table 5-50 Measured Strains in Longitudinal Bars at 381 mm (15 in) and 1092 mm (43 in) from the Top of the Footing for Specimen ISH1.0

Height		Strain Gages Number		Run No									
[mm]	[in]			1	2	3	4	5	6	7	8	9	10
381	15	1	**Max**	**239**	**609**	**1499**	**1939**	**2383**	**2522**	**2425**	**1939**	**1918**	**1105**
			Min	-417	-651	-1068	-1232	-1503	-1635	-1605	-1498	-1459	-1311
		2	**Max**	**344**	**769**	**1522**	**1757**	**2105**	**2172**	**2091**	**1907**	**2248**	**70515**
			Min	-382	-614	-1047	-1226	-1521	-1620	-1565	-1541	-1625	-1483
		5	**Max**	**-193**	**135**	**1051**	**1596**	**2389**	**2642**	**2987**	**12419**	**15994**	**72290**
			Min	-635	-821	-1098	-1196	-1312	-1340	-1252	-1045	1707	3196
		6	**Max**	**-350**	**56**	**1128**	**1831**	**2634**	**3148**	**6658**	**13799**	**19726**	**70269**
			Min	-927	-1165	-1548	-1679	-1857	-1901	-1917	-1074	1149	3321
1092	43	1	**Max**	**-105**	**49**	**540**	**1012**	**1613**	**2036**	**2189**	**2319**	**2426**	**11937**
			Min	-449	-559	-762	-813	-913	-1048	-1075	-1155	-1312	-1182
		2	**Max**	**-34**	**63**	**421**	**764**	**1204**	**1461**	**1588**	**1753**	**1867**	**2358**
			Min	-256	-326	-470	-499	-444	-301	-425	-503	-871	-1245
		5	**Max**	**-389**	**-310**	**-110**	**100**	**664**	**1087**	**1216**	**1225**	**1508**	**1153**
			Min	-521	-564	-647	-667	-708	-742	-597	-655	-688	-1413
		6	**Max**	**-559**	**-433**	**-202**	**22**	**711**	**1267**	**1335**	**1193**	**1466**	**1175**
			Min	-715	-783	-907	-953	-1099	-1154	-980	-1026	-1023	-1419

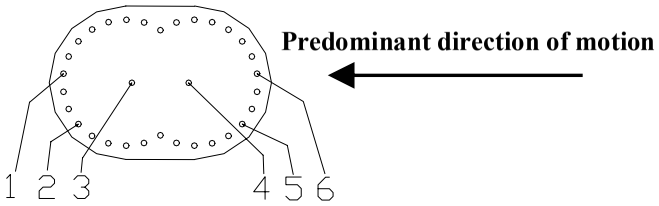

(All values in microstrain)

Table 5-51 Measured Strains in Longitudinal Bars at 1219 mm (48 in) and 1346 mm (53 in) from the Top of the Footing for Specimen ISH1.0

Height		Strain Gages Number		Run No									
[mm]	[in]			1	2	3	4	5	6	7	8	9	10
1219	48	1	Max	-59	178	787	1219	1909	2332	2869	14495	16830	22398
			Min	-563	-731	-993	-1072	-1214	-1332	-1328	-1063	2360	3252
		2	Max	93	273	825	1181	1752	2097	2199	2749	14638	17189
			Min	-307	-438	-650	-699	-694	-680	-824	-1053	-973	3967
		3	Max	-345	-224	204	787	1286	1880	2232	2339	2521	2784
			Min	-602	-660	-737	-763	-812	-788	-986	-1252	-1285	-1187
		4	Max	-387	-301	-79	45	468	914	1042	1302	1862	1376
			Min	-483	-502	-555	-581	-516	-417	-389	-296	-140	-509
		5	Max	-293	-148	194	539	1213	1590	1714	1973	2387	2124
			Min	-519	-596	-766	-848	-999	-1190	-1290	-1430	-1526	-1873
		6	Max	-463	-216	333	765	1609	2267	2446	2695	3927	3230
			Min	-844	-974	-1309	-1514	-1758	-1849	-1956	-2102	-2102	-2751
1346	53	1	Max	-747	-921	-1327	-1569	-1868	-2058	-2285	-4181	-5360	-6994
			Min	-1097	-1480	-2425	-3059	-3923	-4518	-5047	-9892	-13929	-17553
		2	Max	-797	-1001	-1484	-1781	-2162	-2409	-2679	-4997	-6584	-8502
			Min	-1147	-1560	-2582	-3272	-4217	-4869	-5441	-10708	-15153	-19061
		3	Max	-847	-1080	-1641	-1994	-2455	-2761	-3074	-5813	-7808	-10011
			Min	-1197	-1640	-2739	-3485	-4511	-5220	-5836	-11524	-16377	-20570
		4	Max	-897	-1160	-1798	-2207	-2749	-3112	-3469	-6629	-9032	-11519
			Min	-1247	-1719	-2896	-3698	-4804	-5572	-6231	-12340	-17601	-22078
		5	Max	-947	-1240	-1955	-2420	-3043	-3463	-3863	-7445	-10256	-13028
			Min	-1297	-1799	-3053	-3910	-5098	-5923	-6625	-13156	-18825	-23587
		6	Max	-997	-1320	-2112	-2633	-3336	-3815	-4258	-8260	-11480	-14536
			Min	-1347	-1879	-3210	-4123	-5391	-6275	-7020	-13971	-20049	-25095

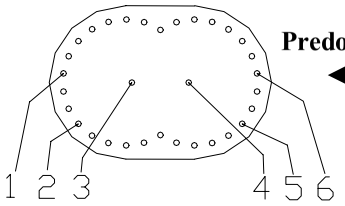

Predominant direction of motion

(All values in microstrain)

Table 5-52 Measured Strains in Longitudinal Bars at 1473 mm (58 in), 1549 mm (61 in), 1626 mm (64 in) and 1702 mm (67 in) from the Top of the Footing for Specimen ISH1.0

Height		Strain Gages Number		Run No									
[mm]	[in]			1	2	3	4	5	6	7	8	9	10
1473	58	1	Max	41	387	1219	1641	2531	15160	17819	24527	32922	38480
			Min	-556	-747	-1017	-1142	-1312	-916	2204	3649	6457	10745
		2	Max	188	461	1219	1632	2387	12833	14649	20181	27263	31919
			Min	-359	-560	-885	-1002	-1193	-1343	2168	3009	5349	9518
		3	Max	-22	92	614	943	1518	3042	15666	18098	22980	24795
			Min	-253	-262	-260	-236	-180	-171	-47	8907	9296	11665
		4	Max	-94	-9	310	610	961	1335	1834	2882	3604	3294
			Min	-247	-255	-270	-195	-195	-222	-192	-4	242	505
		5	Max	-144	121	674	926	1374	1728	1665	-3437	-4878	-9031
			Min	-611	-777	-1158	-1346	-1683	-2625	-11689	-14989	-27533	-60938
		6	Max	-167	142	742	1016	1484	540	-2959	-6589	-8859	-21125
			Min	-756	-979	-1512	-1830	-2815	-13539	-16251	-22468	-47736	-82466
1549	61	1	Max	61	322	967	1372	2149	2333	2563	13831	16486	21970
			Min	-476	-611	-816	-911	-1058	-1221	-1477	-1519	785	1837
		6	Max	-125	216	766	979	1396	1786	1955	2242	7783	2632
			Min	-602	-741	-1084	-1284	-1546	-1866	-2156	-2028	-5443	-5666
1626	64	1	Max	90	211	537	772	1378	1639	1776	1902	2081	2261
			Min	-288	-348	-455	-511	-588	-688	-763	-905	-1126	-1215
		6	Max	-151	181	666	860	1278	1813	2041	2258	2711	2448
			Min	-566	-685	-1012	-1229	-1523	-1757	-1939	-1922	-1929	-1831
1702	67	1	Max	40	113	335	505	919	1152	1288	1400	1645	1872
			Min	-153	-191	-266	-301	-364	-427	-469	-541	-684	-730
		6	Max	-60	43	334	462	711	1007	1144	1265	1603	1417
			Min	-195	-232	-369	-472	-656	-830	-947	-975	-996	-952

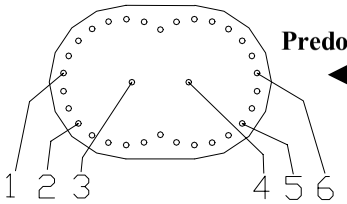

Predominant direction of motion

(All values in microstrain)

Table 5-53 Measured Strains in Longitudinal Bars at–229 mm (-9 in), –152 mm (-6 in), –76 mm (-3 in) and 0 mm (0 in) from the Top of the Footing for Specimen ISH1.25

Height		Strain Gages		Run No											
[mm]	[in]	Number		1	2	3	4	5	6	7	8	9	10	11	12
-229	-9	1	Max	-113	1	629	1350	1667	1804	1929	2099	2292	2509	2764	3034
			Min	-241	-320	-704	-867	-941	-962	-1004	-1025	-1102	-1192	-1246	-1304
		6	Max	67	155	1294	1822	2021	2072	2139	2167	2243	2389	2426	2523
			Min	-148	-280	-868	-1285	-1651	-1806	-1885	-1966	-2054	-2137	-2225	-2267
-152	-6	1	Max	-141	50	1353	2119	2403	2606	2890	3717	9625	13621	15486	17823
			Min	-397	-531	-1060	-1277	-1420	-1448	-1529	-1573	-1501	-377	274	519
		6	Max	157	326	1626	1999	2159	2187	2250	2298	2417	2639	2748	2906
			Min	-165	-346	-991	-1422	-1779	-1911	-1971	-2052	-2161	-2286	-2437	-2527
-76	-3	1	Max	-137	209	1904	5272	11818	12545	14659	18375	24012	30066	30595	9393
			Min	-593	-839	-1666	-3006	-4128	-2948	-2023	-1333	-525	-209	253	4348
		6	Max	245	574	2117	2650	3125	3827	4776	5203	6053	7482	7721	8483
			Min	-244	-478	-1268	-1905	-2793	-3944	-4961	-5911	-7088	-7996	-8103	-7530
0	0	1	Max	-128	238	2034	13386	13740	15377	17709	21648	27509	34251	41241	35520
			Min	-584	-832	-1622	-1924	-2975	-1359	-734	123	1329	1544	2170	4881
		2	Max	-166	204	1875	9703	12821	14378	16297	19554	24141	29305	34743	38748
			Min	-490	-637	-1079	-1214	912	753	1151	1745	2472	3342	4800	8157
		3	Max	-88	-70	957	1672	6849	9764	11292	12963	15090	17377	19682	21371
			Min	-150	-150	-143	-123	-150	3223	5111	5645	5920	6363	7091	8196
		4	Max	-13	131	1077	1532	1866	2216	2868	9139	12190	13612	15125	16668
			Min	-141	-148	-136	-111	-166	-192	-143	33	4587	6376	6752	7423
		5	Max	245	545	894	808	1492	2157	3159	3397	4376	3890	2680	2057
			Min	-210	-394	-778	-778	-657	-555	-555	-717	-1248	-1341	-2992	-4155
		6	Max	390	925	2734	10098	12801	11799	10433	9232	8667	9476	10068	8764
			Min	-251	-497	-1291	-2575	-4097	-4979	-6391	-8717	-11886	-14136	-15709	-14184

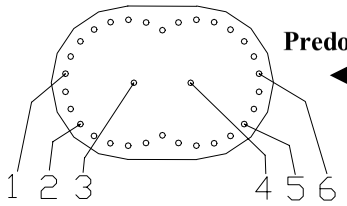

Predominant direction of motion

(All values in microstrain)

Table 5-54 Measured Strains in Longitudinal Bars at 127 mm (5 in) and 254 mm (10 in) from the Top of the Footing for Specimen ISH1.25

Height		Strain Gages		Run No											
[mm]	[in]	Number		1	2	3	4	5	6	7	8	9	10	11	12
127	5	1	Max	-160	175	2223	8116	10249	6804	5573	5226	4837	4076	3954	3470
			Min	-623	-887	-1711	-2798	-2990	-1243	-748	-438	-269	214	-320	-246
		2	Max	-192	39	1918	3571	12575	12734	14189	17183	21626	26609	31396	31354
			Min	-546	-718	-1211	-1379	-1489	132	367	614	998	1171	1713	3823
		3	Max	-167	-113	972	1788	2927	5725	11091	13301	15295	17612	20401	22997
			Min	-208	-211	-197	-187	-218	-18	2076	6171	6836	7089	7691	9587
		4	Max	17	186	903	1086	1176	1125	1359	1777	2159	2797	4668	6434
			Min	-168	-191	-189	-164	-147	-120	-99	-73	-129	-157	-92	794
		5	Max	337	739	2099	2878	3406	3683	4107	4263	4696	5792	6129	6383
			Min	-219	-408	-918	-1101	-1306	-1362	-1423	-1553	-1751	-2253	-4036	-7764
		6	Max	560	1113	3596	10645	13071	12785	12769	12347	12884	14642	15339	13502
			Min	-218	-563	-1804	-4781	-4950	-4923	-5356	-7211	-9980	-12776	-14947	-11555
254	10	1	Max	-198	124	2157	3605	9127	12056	13927	16903	21582	26251	31152	36204
			Min	-663	-911	-1566	-1851	-1927	-1005	176	782	1363	2504	3825	5802
		2	Max	-211	-15	1541	2401	2812	3905	9216	10986	12998	17068	20678	13157
			Min	-495	-640	-1008	-1109	-1221	-1246	-1207	197	386	414	995	3306
		3	Max	-145	-127	774	1490	1121	1212	2119	3206	4423	5018	4703	5118
			Min	-206	-208	-199	-152	-3415	-5374	-6489	-7893	-8986	-9108	-10880	-15505
		4	Max	0	101	902	1263	1414	1486	1518	1782	2014	2151	2225	2147
			Min	-190	-222	-204	-147	-151	-71	-32	-105	-326	-500	-620	-631
		5	Max	238	542	1744	2227	2415	2320	2183	2020	1941	1927	1906	1595
			Min	-185	-341	-745	-847	-924	-949	-968	-1028	-1100	-1193	-1328	-1514
		6	Max	537	990	2821	4775	6207	6818	7215	7138	7392	8339	8794	8637
			Min	-151	-462	-1462	-2305	-3377	-3411	-3355	-3377	-3591	-3744	-4015	-4929

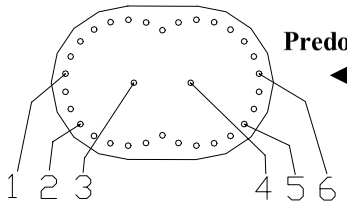

Predominant direction of motion

(All values in microstrain)

Table 5-55 Measured Strains in Longitudinal Bars at 381 mm (15 in) and 1219 mm (48 in) from the Top of the Footing for Specimen ISH1.25

Height		Strain Gages		Run No											
[mm]	[in]	Number		1	2	3	4	5	6	7	8	9	10	11	12
381	15	1	**Max**	**-216**	**5**	**1764**	**2948**	**5605**	**7359**	**8636**	**10303**	**13081**	**14778**	**19205**	**23977**
			Min	-605	-812	-1299	-1398	-1315	-584	322	1175	1398	1327	1254	2454
		2	**Max**	**-219**	**-54**	**1130**	**1850**	**2195**	**2343**	**2457**	**2646**	**3057**	**9158**	**10711**	**12404**
			Min	-458	-570	-849	-905	-903	-870	-861	-861	-1044	-1054	674	1058
		5	**Max**	**166**	**365**	**1302**	**1659**	**1733**	**1654**	**1561**	**1464**	**1339**	**1320**	**1316**	**1128**
			Min	-163	-298	-634	-747	-800	-812	-824	-863	-914	-951	-1016	-1109
		6	**Max**	**461**	**828**	**2221**	**2721**	**2740**	**2737**	**2648**	**2570**	**2443**	**2446**	**2795**	**2983**
			Min	-145	-391	-1031	-1369	-1497	-1527	-1571	-1600	-1669	-1747	-1839	-2158
1219	48	1	**Max**	**-334**	**-314**	**-162**	**-48**	**1403**	**1491**	**1561**	**1601**	**1643**	**1709**	**1778**	**32004**
			Min	-400	-403	-655	-753	-894	-1017	-1102	-1184	-1248	-1309	-1241	-914
		2	**Max**	**-186**	**-174**	**-98**	**-51**	**220**	**37**	**9**	**0**	**42**	**107**	**239**	**69316**
			Min	-221	-221	-327	-383	-494	-485	-466	-497	-559	-589	-536	-395
		5	**Max**	**-74**	**-62**	**414**	**1440**	**1963**	**2191**	**2358**	**2493**	**2584**	**2563**	**2391**	**69971**
			Min	-148	-162	-269	-306	-653	-901	-976	-1080	-1239	-1334	-1355	-1469
		6	**Max**	**81**	**96**	**769**	**1963**	**2504**	**2687**	**2873**	**3099**	**3436**	**3887**	**4441**	**31607**
			Min	-30	-57	-242	-351	-826	-970	-1022	-1032	-1096	-1276	-1518	-1769

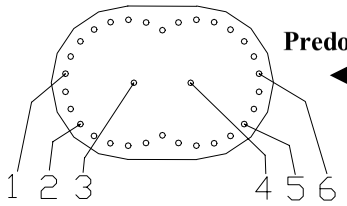

Predominant direction of motion

(All values in microstrain)

Table 5-56 Measured Strains in Longitudinal Bars at 1346 mm (53 in) and 1473 mm (58 in) from the Top of the Footing for Specimen ISH1.25

Height		Strain Gages		Run No											
[mm]	[in]	Number		1	2	3	4	5	6	7	8	9	10	11	12
1346	53	1	Max	-322	-267	22	424	1954	2053	2208	2318	2541	3060	3755	33552
			Min	-460	-493	-961	-1223	-1621	-1757	-1813	-1887	-2013	-2315	-2685	-2246
		2	Max	-295	-262	-89	54	1200	1300	1353	1331	1374	1756	2124	33674
			Min	-385	-401	-657	-799	-1035	-1092	-1153	-1262	-1413	-1489	-1436	-1373
		3	Max	-216	-207	-154	123	469	566	743	991	1304	1526	1137	33936
			Min	-231	-226	-216	-206	-221	-168	-124	-106	-49	-107	-369	-1674
		4	Max	-113	-90	359	1073	1648	1982	2381	2769	3095	3235	3263	33843
			Min	-164	-173	-199	-181	-215	-148	-88	-238	-447	-606	-631	-494
		5	Max	-5	23	659	1603	2274	2575	3158	10284	12560	14684	15570	69534
			Min	-109	-134	-269	-306	-687	-868	-868	-777	3058	3385	3287	2915
		6	Max	151	221	1451	4242	8284	10374	12248	15802	18800	23805	27588	34047
			Min	-50	-105	-322	-362	242	1821	2640	3333	4162	3914	5260	-13157
1473	58	1	Max	-273	-176	364	1024	2289	2482	2507	2605	4096	6805	8804	32008
			Min	-501	-583	-1337	-1899	-3148	-5239	-7555	-9782	-11813	-14208	-15881	-10354
		2	Max	-272	-214	47	478	1400	1465	1519	1486	1565	1957	2031	69746
			Min	-403	-442	-780	-966	-1194	-1290	-1406	-1672	-1923	-2615	-10545	-13862
		3	Max	-206	-188	-81	471	839	1019	1296	1751	2299	2359	2029	24814
			Min	-223	-221	-221	-212	-223	-191	-138	-109	-53	4	23	-51780
		4	Max	-121	-74	574	1158	1897	2379	3728	8564	12657	15228	16521	14436
			Min	-197	-209	-237	-223	-255	-202	-85	625	3988	6357	7758	-10887
		5	Max	45	152	1407	2365	12042	13613	15427	18436	21397	21327	8258	7824
			Min	-164	-224	-475	-560	-836	4630	5015	5198	5340	4302	2651	2783
		6	Max	196	362	1913	8076	15245	17102	20215	24891	30480	30811	10220	7316
			Min	-132	-225	-566	-664	1791	4230	4723	5653	6749	6516	2381	2566

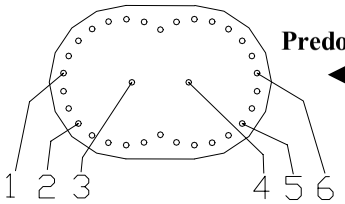

Predominant direction of motion

(All values in microstrain)

Table 5-57 Measured Strains in Longitudinal Bars at 1600 mm (63 in), 1676 mm (66 in), 1753 mm (69 in) and 1829 mm (72 in) from the Top of the Footing for Specimen ISH1.25

Height		Strain Gages		Run No											
[mm]	[in]	Number		1	2	3	4	5	6	7	8	9	10	11	12
1600	63	1	Max	-213	-83	788	1095	1642	-1467	-3092	-4279	-5744	-5613	-7860	32537
			Min	-510	-633	-1574	-5118	-12995	-15610	-17481	-20999	-27491	-36574	-44047	-30832
		2	Max	-278	-203	297	732	1495	1530	1575	1451	1001	-3268	-5156	52590
			Min	-444	-508	-922	-1109	-1280	-1366	-1623	-2454	-10062	-16100	-23110	-24291
		3	Max	-165	-146	312	1029	1463	1707	2098	2863	10187	12450	11255	9214
			Min	-181	-180	-169	-132	-185	-171	-132	-98	-7	5688	6970	6831
		4	Max	-62	-18	493	940	1627	2063	3056	8929	7016	2510	3009	3195
			Min	-120	-130	-138	-131	-159	-100	-1	518	1541	-2261	-1829	-10700
		5	Max	-17	144	1441	2408	13354	14072	15467	18729	23370	27610	30698	29238
			Min	-263	-326	-605	-682	-954	4854	5382	5459	5756	6463	7223	8830
		6	Max	76	225	1537	2737	10164	12430	13739	16553	20944	25249	28847	29726
			Min	-195	-312	-722	-882	-1560	-561	361	751	921	671	126	127
1676	66	1	Max	-167	-76	428	834	1777	1902	2103	2366	3424	6317	8650	9750
			Min	-353	-430	-1042	-1516	-1879	-2008	-2179	-2524	-3798	-5180	-4789	-2173
1753	69	1	Max	-92	-47	179	454	1235	1333	1464	1561	1742	1958	2077	2154
			Min	-183	-223	-633	-925	-1190	-1276	-1348	-1431	-1504	-1504	-1437	-1247
		6	Max	33	105	966	1757	2166	2320	2468	2688	3218	7089	10209	10648
			Min	-109	-154	-428	-584	-1048	-1139	-1216	-1285	-1496	-1915	-1835	-1556
1829	72	1	Max	-27	-5	69	133	548	616	693	748	837	991	1096	1165
			Min	-72	-89	-227	-314	-465	-505	-538	-581	-628	-640	-622	-535
		6	Max	1	22	533	1045	1311	1439	1553	1706	2086	2339	2498	2477
			Min	-51	-71	-189	-269	-496	-533	-565	-589	-660	-787	-874	-942

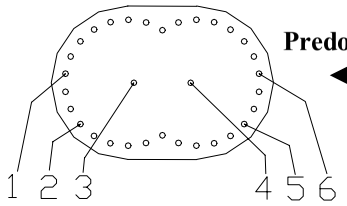

Predominant direction of motion

(All values in microstrain)

Table 5-58 Measured Strains in Longitudinal Bars at–229 mm (-9 in), –152 mm (-6 in), –76 mm (-3 in) and 0 mm (0 in) from the Top of the Footing for Specimen ISH1.5

Height		Strain Gages		Run No												
[mm]	[in]	Number		1	2	3	4	5	6	7	8	9	10	11	12	13
-229	-9	1	Max	226	593	1411	1780	1838	2086	2134	2164	2373	2452	2605	2895	2749
			Min	-318	-495	-819	-1030	-1113	-1338	-1526	-1783	-1932	-2018	-2022	-2020	-1654
		6	Max	150	441	1341	1830	1927	2006	2077	2292	2378	2519	2646	2751	2815
			Min	-297	-431	-688	-938	-1037	-1229	-1324	-1482	-1623	-1725	-1771	-1799	-1826
-152	-6	1	Max	322	828	1749	2078	2184	2405	2424	2502	2806	6547	8456	10033	8680
			Min	-366	-587	-1013	-1265	-1364	-1665	-1870	-2146	-2268	-2548	-3450	-2974	-187
		6	Max	215	696	1790	2222	2284	2358	2429	4064	15806	16017	17394	18728	18944
			Min	-442	-631	-945	-1275	-1399	-1584	-1709	-2255	-2052	-330	155	812	1783
-76	-3	1	Max	323	772	1582	1908	1967	2210	2208	2286	2664	11715	12263	12865	10975
			Min	-362	-561	-965	-1213	-1291	-1641	-1849	-2165	-2330	-2605	-3505	-1919	2012
		6	Max	314	978	2296	4095	6685	13189	15138	19928	24300	30551	32894	34378	13404
			Min	-506	-770	-1191	-1413	-1191	-1041	978	1379	1717	1999	4294	6593	8093
0	0	1	Max	353	934	1805	2191	2262	7188	10983	11853	12942	15846	17330	19024	16649
			Min	-374	-587	-955	-1168	-1225	-1461	-1827	-4728	-4930	-2360	-351	3283	10425
		2	Max	508	1374	3725	10103	10543	13863	13697	12074	14750	18037	19840	21501	21639
			Min	-578	-885	-1398	-1656	-666	-2451	-3636	-8163	-8668	-9246	-9118	-9176	-2551
		3	Max	6	408	981	1280	1439	2894	12673	20588	21449	22396	22169	21650	19122
			Min	-214	-226	-259	-334	-387	-387	-252	8014	14783	15125	15618	16149	10795
		4	Max	-1	353	1028	1690	1839	13140	15935	16964	19096	15594	10960	9119	7871
			Min	-196	-196	-224	-298	-316	-293	8972	9436	9466	8876	7405	5911	4041
		5	Max	474	1448	12061	17565	16344	17509	21219	27791	12513	9022	7903	7369	6696
			Min	-738	-1125	-1391	-752	655	390	879	1588	-9400	-14830	-14441	-15467	-13973
		6	Max	307	976	2174	14108	15087	16563	16488	20894	15950	7626	7300	7302	6850
			Min	-439	-651	-966	-985	4479	4255	4344	4763	5281	5034	5253	5358	5449

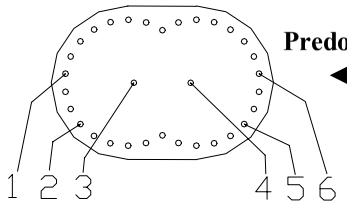

Predominant direction of motion

(All values in microstrain)

Table 5-59 Measured Strains in Longitudinal Bars at 127 mm (5 in), 254 mm (10 in) and 381 mm (15 in) from the Top of the Footing for Specimen ISH1.5

Height		Strain Gages		Run No												
[mm]	[in]	Number		1	2	3	4	5	6	7	8	9	10	11	12	13
127	5	1	**Max**	**448**	**1194**	**2181**	**7960**	**7617**	**8856**	**8081**	**7540**	**9050**	**9647**	**9486**	**13443**	**10771**
			Min	-899	-1414	-2242	-8882	-8140	-10058	-9139	-10775	-13493	-15632	-13782	-5730	2788
		2	**Max**	**407**	**1254**	**4745**	**7861**	**7650**	**9578**	**8499**	**7000**	**8836**	**9690**	**10829**	**12696**	**13807**
			Min	-1122	-1717	-7972	-11645	-10976	-12244	-11294	-15144	-19404	-22270	-21299	-28338	-32505
		3	**Max**	**-93**	**232**	**777**	**868**	**889**	**1804**	**2433**	**15273**	**18157**	**18688**	**17986**	**17495**	**16017**
			Min	-390	-385	-371	-360	-357	-362	-248	-198	10280	12490	12853	13236	7850
		4	**Max**	**-156**	**148**	**862**	**1197**	**1298**	**2890**	**15879**	**17797**	**20926**	**24497**	**24285**	**23162**	**19725**
			Min	-375	-375	-375	-375	-402	-402	72	10876	10845	12808	15723	16596	13873
		5	**Max**	**644**	**1704**	**8714**	**18749**	**17658**	**20242**	**24796**	**34607**	**43191**	**52668**	**56743**	**60234**	**63923**
			Min	-1001	-1562	-6146	-6656	-4034	-4515	-2646	-1609	-637	-777	2849	6092	12653
		6	**Max**	**451**	**1216**	**2385**	**14849**	**13440**	**14562**	**16993**	**23199**	**29482**	**35853**	**37709**	**39491**	**40205**
			Min	-812	-1240	-1835	-2480	-1954	-2264	-736	-140	121	237	2927	4729	8039
254	10	1	**Max**	**458**	**1193**	**2218**	**3962**	**5083**	**7350**	**7850**	**8508**	**12908**	**16372**	**18515**	**21050**	**18586**
			Min	-957	-1449	-2277	-3375	-5266	-7556	-8071	-8857	-9066	-7844	-7771	-1683	8230
		2	**Max**	**318**	**1109**	**2262**	**4303**	**5942**	**8158**	**8877**	**9847**	**13283**	**16084**	**12863**	**8058**	**6791**
			Min	-1048	-1557	-2317	-4223	-7528	-9173	-9478	-11491	-12868	-13341	-11944	-8296	204
		3	**Max**	**-209**	**84**	**826**	**1012**	**1019**	**1404**	**1867**	**2399**	**2459**	**2406**	**2089**	**2422**	**1366**
			Min	-447	-445	-426	-351	-351	-363	-225	-452	-671	-755	-752	-699	-2661
		4	**Max**	**-191**	**85**	**545**	**758**	**902**	**1815**	**2346**	**12386**	**15639**	**16936**	**16636**	**16372**	**15502**
			Min	-402	-397	-392	-367	-365	-353	-367	-371	6535	8589	9960	10609	10978
		5	**Max**	**546**	**1508**	**2964**	**14345**	**14944**	**17756**	**19344**	**26689**	**34068**	**41532**	**44655**	**47735**	**50281**
			Min	-1033	-1515	-2247	-5277	-4453	-4718	-1296	-383	-27	984	7273	15529	26379
		6	**Max**	**458**	**1227**	**2472**	**8301**	**11838**	**12934**	**13399**	**17233**	**21998**	**26135**	**27435**	**28817**	**28631**
			Min	-854	-1261	-1779	-3808	-3321	-3302	-1068	-1751	-3102	-4533	-5615	-7928	-16528
381	15	1	**Max**	**432**	**1148**	**2241**	**2572**	**2666**	**3306**	**3751**	**4302**	**7548**	**12313**	**15567**	**16434**	**13602**
			Min	-932	-1392	-2120	-2428	-2529	-2935	-3290	-3659	-3895	-3815	-1931	579	4450
		2	**Max**	**314**	**1009**	**2078**	**2351**	**2355**	**2628**	**2834**	**3263**	**5449**	**9943**	**11982**	**13275**	**10636**
			Min	-988	-1418	-2045	-2281	-2327	-2507	-2682	-2978	-3457	-4644	-3790	-2824	-858
		5	**Max**	**476**	**1302**	**2896**	**7362**	**9354**	**14311**	**16640**	**20248**	**25999**	**30764**	**32513**	**34553**	**33558**
			Min	-873	-1290	-1829	-3981	-4158	-4626	-1478	120	902	713	2398	4671	6662
		6	**Max**	**440**	**1103**	**2428**	**2800**	**2752**	**8837**	**11188**	**14027**	**16589**	**18952**	**19345**	**20024**	**18885**
			Min	-639	-973	-1392	-1494	-1517	-1519	-676	551	1399	1578	2724	4139	5967

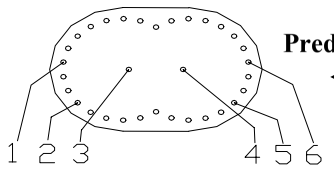

Predominant direction of motion

(All values in microstrain)

Table 5-60 Measured Strains in Longitudinal Bars at 1372 mm (54 in), 1499 mm (59 in) and 1626 mm (64 in) from the Top of the Footing for Specimen ISH1.5

Height		Strain Gages		Run No												
[mm]	[in]	Number		1	2	3	4	5	6	7	8	9	10	11	12	13
1372	54	1	Max	**-346**	**-266**	**356**	**958**	**1271**	**2210**	**2715**	**4406**	**7076**	**9378**	**10314**	**10994**	**12958**
			Min	-546	-588	-640	-543	-363	-327	-297	-267	419	1540	2437	3002	3716
		2	Max	**-433**	**-346**	**220**	**750**	**1019**	**1858**	**2280**	**2624**	**2769**	**3294**	**4219**	**5787**	**8886**
			Min	-611	-649	-689	-712	-651	-508	-501	-731	-977	-1059	-869	-525	239
		5	Max	**-144**	**-74**	**183**	**421**	**503**	**774**	**865**	**1127**	**1652**	**1904**	**1984**	**2056**	**1970**
			Min	-350	-408	-511	-565	-579	-861	-922	-1090	-1160	-1219	-1247	-1305	-1634
		6	Max	**-181**	**-122**	**118**	**344**	**421**	**673**	**755**	**1028**	**1648**	**1950**	**2024**	**2072**	**1915**
			Min	-340	-378	-440	-467	-479	-696	-782	-965	-1005	-1029	-997	-1008	-1283
1499	59	1	Max	**-49**	**-44**	**11**	**-100**	**-33**	**180**	**230**	**251**	**186**	**179**	**153**	**140**	**101**
			Min	-58	-56	-154	-420	-568	-694	-735	-754	-756	-780	-803	-813	-820
		2	Max	**-308**	**-143**	**562**	**1025**	**1228**	**2063**	**2454**	**10190**	**16279**	**17475**	**18292**	**19218**	**21156**
			Min	-631	-720	-829	-876	-803	-676	-683	-589	4264	6477	7038	8099	9181
		3	Max	**-520**	**-482**	**-149**	**163**	**420**	**962**	**1349**	**2335**	**2552**	**2701**	**2624**	**2631**	**2901**
			Min	-557	-557	-557	-524	-520	-550	-536	-594	-865	-962	-965	-909	-851
		4	Max	**-473**	**-433**	**-389**	**-321**	**-23**	**274**	**473**	**956**	**1221**	**1438**	**1441**	**1485**	**1595**
			Min	-562	-566	-573	-565	-474	-428	-488	-489	-508	-599	-599	-573	-528
		5	Max	**-64**	**71**	**448**	**706**	**793**	**1076**	**1183**	**1509**	**2084**	**2360**	**2484**	**2591**	**2602**
			Min	-403	-526	-729	-868	-920	-1329	-1371	-1496	-1585	-1617	-1622	-1683	-2025
		6	Max	**-94**	**39**	**397**	**636**	**706**	**944**	**1000**	**1346**	**1985**	**2368**	**2483**	**2576**	**2531**
			Min	-410	-519	-696	-794	-818	-1147	-1298	-1516	-1614	-1706	-1665	-1686	-1950
1626	64	1	Max	**-139**	**128**	**861**	**1247**	**1401**	**2216**	**2764**	**15152**	**17859**	**22285**	**23329**	**24575**	**27351**
			Min	-678	-842	-1093	-1060	-881	-863	-854	-653	4069	4357	6181	7434	9184
		2	Max	**-223**	**7**	**705**	**1142**	**1333**	**2191**	**2571**	**17890**	**18858**	**22166**	**23241**	**24474**	**27266**
			Min	-684	-821	-1010	-1075	-1003	-956	-1038	-882	5109	5353	6551	7994	9627
		4	Max	**-192**	**-172**	**-104**	**99**	**248**	**611**	**865**	**1705**	**2073**	**2361**	**2403**	**2517**	**2740**
			Min	-214	-211	-217	-209	-174	-172	-142	-138	-130	-212	-199	-142	-103
		5	Max	**62**	**307**	**943**	**1207**	**1277**	**1602**	**1752**	**2060**	**3803**	**6330**	**7650**	**9085**	**7729**
			Min	-518	-733	-1139	-1415	-1478	-1929	-1990	-2315	-6168	-10199	-10891	-11188	-13074
		6	Max	**-19**	**189**	**674**	**846**	**876**	**1029**	**1042**	**1363**	**1947**	**2932**	**3340**	**4057**	**3117**
			Min	-511	-680	-975	-1137	-1171	-1566	-1774	-2136	-2256	-7430	-8631	-9044	-10626

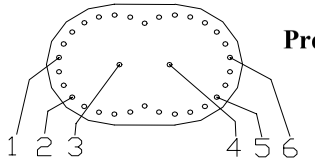

Predominant direction of motion ←

(All values in microstrain)

Table 5-61 Measured Strains in Longitudinal Bars at 1753 mm (69 in), 1829 mm (72 in), 1905 mm (75 in) and 1981 mm (78 in) from the Top of the Footing for Specimen ISH1.5

Height		Strain Gages		Run No												
[mm]	[in]	Number		1	2	3	4	5	6	7	8	9	10	11	12	13
1753	69	1	Max	-87	226	959	1349	1497	2404	14144	17055	19584	23907	24622	25858	28722
			Min	-661	-859	-1160	-1213	-1154	-1159	-986	3381	3610	3955	6204	7755	9356
		2	Max	-135	187	1028	1505	1682	2680	17748	20008	23004	28154	29167	30677	34025
			Min	-738	-936	-1263	-1398	-1421	-1461	-1253	3854	4038	3989	6855	8710	10641
		3	Max	-201	-17	364	595	670	1357	1927	19244	22167	23513	24000	24869	26776
			Min	-502	-539	-558	-490	-409	-362	-344	-306	14077	15050	15467	16622	17712
		4	Max	-367	-301	295	715	732	1174	1552	3089	17312	19525	19222	19430	20170
			Min	-436	-436	-437	-395	-405	-410	-380	-364	-173	11180	13042	13518	13903
		5	Max	118	437	1032	1261	1313	1392	-2154	-5865	-4607	-4996	-1864	1095	1399
			Min	-613	-894	-1487	-1822	-1899	-8306	-15263	-18515	-23720	-28686	-22270	-2524	-1929
		6	Max	95	338	776	944	984	1160	876	-4116	-3642	-1331	-1085	-575	-1985
			Min	-454	-669	-1059	-1253	-1287	-1690	-8172	-16644	-16970	-18047	-17367	-17449	-18120
1829	72	1	Max	-77	281	1072	1513	1686	2949	14492	21853	24800	30556	32141	32571	32571
			Min	-644	-797	-1042	-1109	-1088	-1094	-880	4216	4948	4948	7802	10371	12994
		6	Max	58	261	622	778	803	943	974	1322	1952	4286	5684	6646	6217
			Min	-364	-507	-787	-928	-971	-1333	-1622	-1921	-2288	-5621	-7704	-8194	-8340
1905	75	1	Max	-69	210	897	1303	1462	2409	2675	12544	16298	18811	20117	21293	23702
			Min	-603	-746	-992	-1075	-1065	-1106	-1409	-1195	685	914	2042	3116	4605
		6	Max	89	302	654	785	809	946	998	1397	1928	2248	2344	2425	2429
			Min	-348	-465	-680	-799	-844	-1153	-1409	-1660	-1757	-1801	-1783	-1777	-1783
1981	78	1	Max	-39	138	590	880	999	1679	2013	2373	2579	2999	6309	7776	9068
			Min	-380	-457	-603	-654	-658	-693	-853	-1104	-1306	-1617	-1891	-1522	-1039
		6	Max	61	217	473	578	606	713	755	1072	1573	1888	1995	2077	2086
			Min	-256	-335	-522	-641	-690	-960	-1198	-1438	-1543	-1610	-1615	-1622	-1638

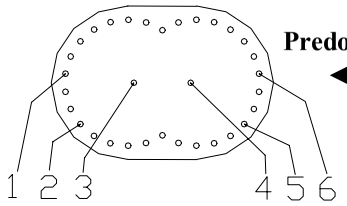

Predominant direction of motion

(All values in microstrain)

Table 5-62 Measured Strains in Longitudinal Bars at–229 mm (-9 in), –152 mm (-6 in), –76 mm (-3 in), 0 mm (0 in) and 127 mm (5 in) from the Top of the Footing for Specimen ISH1.5T

Height		Strain Gages		Run No														
[mm]	[in]	Number		1	2	3	4	5	6	7	8	9	10	11	12	13	14	15
-228.6	-9	1	Max	21	113	393	657	821	1464	1719	1906	2020	2223	2380	2559	2760	3005	2894
			Min	-146	-238	-507	-696	-807	-1036	-1152	-1224	-1328	-1409	-1455	-1499	-1564	-1619	-1441
		6	Max	-21	76	492	954	1179	1630	1929	2096	2261	2410	2512	2602	2712	2883	3090
			Min	-207	-356	-606	-732	-797	-1038	-1168	-1284	-1366	-1493	-1605	-1711	-1816	-1916	-1978
-152.4	-6	1	Max	99	413	1098	1442	1584	2118	2386	2764	3362	9197	10742	12381	14802	16429	16238
			Min	-264	-463	-831	-1075	-1214	-1570	-1709	-1867	-2160	-2632	-3540	-3294	-3394	-3220	1867
		6	Max	1	253	1172	1797	2058	2490	3190	8305	12122	14093	15334	16463	17881	19892	22019
			Min	-375	-613	-937	-1110	-1191	-1593	-1996	-2752	-2094	-2036	-2031	-2110	-2101	-1872	-748
-76.2	-3	1	Max	182	731	1526	1924	2135	8078	11858	15250	19275	25908	31443	36886	41943	43798	37846
			Min	-485	-776	-1269	-1634	-1868	-3926	-5272	-4926	-5281	-5856	-5721	-4923	-3198	2100	24706
		6	Max	29	528	1553	2370	2972	11394	13869	16594	18264	19124	18707	17650	16338	14909	10282
			Min	-569	-882	-1283	-1529	-1742	-3440	-4012	-3956	-3480	-3554	-3271	-2967	-2154	327	-2386
0	0	1	Max	357	1023	1842	2307	2666	13052	14812	16920	14625	11100	11558	16320	35024	71439	71439
			Min	-457	-784	-1372	-1816	-2206	-5773	-9494	-14961	-21012	-17032	-138	3880	7081	932	35360
		2	Max	359	1072	1895	2355	2632	13143	16090	19978	21477	22155	18288	12102	7012	5655	22903
			Min	-443	-675	-1066	-1317	-1456	-1516	-1540	-3294	-4821	-6390	-5806	-6150	-10175	-12202	-2962
		3	Max	-97	153	693	923	1025	2149	10386	12898	14040	15329	17361	19727	21583	22635	23003
			Min	-187	-185	-176	-169	-166	-157	-71	6618	7946	8609	9100	10182	11445	12849	13489
		4	Max	-145	44	766	1178	1483	5752	10539	3863	3621	3952	4294	4632	4655	4660	4264
			Min	-201	-196	-182	-189	-194	-178	2112	1900	2547	2892	2953	2971	2808	2832	2813
		5	Max	132	864	2005	3055	8905	7599	3910	2654	2596	2734	2956	2767	2558	2638	2474
			Min	-597	-951	-1408	-1715	-1628	-2415	1018	1098	1058	960	1028	1185	1231	1302	1079
		6	Max	56	685	1826	2851	9216	13614	18150	23438	28632	32666	32666	32666	32666	32666	32666
			Min	-640	-988	-1445	-1778	-1726	-3724	-5115	-7492	-9128	-14326	-21205	-31957	-43929	-43929	-712
127	5	1	Max	334	1044	1850	2272	2564	10829	12972	17430	19712	24560	28607	32039	28852	17075	11116
			Min	-528	-887	-1506	-1943	-2361	-7416	-5523	-4831	-5231	-5315	-4915	-4348	-3367	4026	6527
		2	Max	126	480	943	1171	1276	6670	7382	9870	10718	10970	7781	5729	4047	2846	9028
			Min	-271	-447	-761	-954	-1068	-2918	-2911	-2089	-2187	-1687	221	971	-270	-1435	280
		3	Max	-74	169	530	681	805	1520	2676	7685	10017	11750	14604	16852	18255	18511	17826
			Min	-167	-174	-195	-192	-202	-199	-248	-74	4111	5844	6534	8106	9339	10010	8041
		4	Max	-120	48	659	990	1213	2358	9990	11944	13695	14907	15091	15191	15356	15787	15273
			Min	-190	-192	-183	-178	-178	-171	-155	4286	4754	5205	5924	6466	6963	7291	7245
		5	Max	153	788	1916	2727	3417	10474	8081	11417	13352	14096	14126	13846	13806	16918	20029
			Min	-552	-869	-1244	-1423	-1527	-2514	-651	1260	2300	2917	3223	3079	3007	3035	4532
		6	Max	123	713	1778	2512	3076	10305	12855	16825	20676	23704	25280	26693	28588	31544	35194
			Min	-544	-873	-1274	-1479	-1581	-2225	-2262	-2558	-2465	-2880	-3565	-4211	-4514	-4346	132

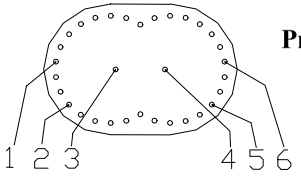

Predominant direction of motion

(All values in microstrain)

Table 5-63 Measured Strains in Longitudinal Bars at 254 mm (10 in), 381 mm (15 in) and 1372 mm (54 in) from the Top of the Footing for Specimen ISH1.5T

Height		Strain Gages		Run No														
[mm]	[in]	Number		1	2	3	4	5	6	7	8	9	10	11	12	13	14	15
254	10	1	Max	168	738	1697	2151	2381	4253	9920	13083	14639	18685	22036	25309	28139	29811	27716
			Min	-476	-789	-1292	-1634	-1807	-2431	-4278	-2991	-2116	-1711	-1415	-1067	-578	69	5971
		2	Max	183	736	1629	2008	2162	3225	5885	11144	12072	14495	17065	19704	22016	23472	22205
			Min	-366	-624	-1024	-1301	-1445	-1885	-2615	-3206	-2327	-1496	-1266	-1020	-608	-201	1976
		3	Max	-141	-29	338	602	729	1319	1919	2296	2282	2705	3198	4432	6003	6348	5733
			Min	-217	-214	-212	-174	-158	-158	-206	-263	-406	-555	-560	-550	-140	656	844
		4	Max	-153	20	514	908	1134	2199	3099	4122	8018	8867	8906	8905	8979	9158	9109
			Min	-227	-224	-221	-212	-203	-185	-195	-119	131	2294	2869	3226	3501	3743	3885
		5	Max	118	590	1493	2119	2447	7110	6917	4823	2165	1512	1521	1523	1514	1523	1528
			Min	-466	-724	-990	-1111	-1164	-1343	-36	1023	856	881	988	1004	937	825	930
		6	Max	92	609	1662	2352	2731	9324	11562	14658	17415	19597	20614	21471	22549	24173	25570
			Min	-539	-853	-1234	-1410	-1492	-1847	-1895	-1081	-635	-382	13	394	839	1454	2515
381	15	1	Max	98	392	820	1055	1176	1448	1081	1317	1038	907	706	576	513	486	538
			Min	-351	-519	-719	-799	-806	-799	-748	-605	-421	-153	-154	-207	-289	-312	-230
		2	Max	153	589	1187	1495	1660	2394	2758	4005	5821	8169	9353	9962	10287	10430	8933
			Min	-428	-672	-1024	-1214	-1288	-1522	-1668	-1707	-2078	-2155	-1464	-875	-481	-122	411
		5	Max	24	444	1521	2184	2480	3257	5320	6645	7613	8059	7835	7555	7461	7408	6811
			Min	-494	-730	-956	-1050	-1106	-1388	-1451	-1376	-875	-658	-578	-548	-480	-399	-182
		6	Max	8	395	1465	2114	2452	3205	5240	8369	10677	11885	12125	12285	12496	12829	12878
			Min	-525	-790	-1096	-1233	-1290	-1631	-1874	-1652	-1157	-949	-741	-599	-432	-166	483
1372	54	1	Max	-70	-15	85	731	1121	1982	3047	4168	5562	7269	8460	9349	10274	11712	13145
			Min	-175	-227	-319	-336	-355	-476	-538	-378	-18	71	192	424	759	1394	1864
		2	Max	141	194	331	604	1038	1959	2873	5391	7300	7356	7414	6595	3973	2385	2329
			Min	48	1	-89	-236	-224	-340	-561	34	1255	820	943	541	-45	-352	-287
		5	Max	-291	-249	-151	-97	-67	460	1232	1689	1871	2207	2396	2540	2699	2825	2843
			Min	-389	-440	-552	-636	-661	-848	-1112	-1235	-1331	-1375	-1363	-1349	-1410	-1548	-1713
		6	Max	-276	-203	-51	32	89	795	1487	2050	2237	2567	2807	3162	4170	6194	7266
			Min	-396	-456	-584	-686	-716	-923	-1310	-1454	-1583	-1687	-1737	-1800	-1939	-2317	-3064

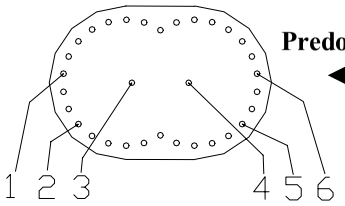

Predominant direction of motion ←

(All values in microstrain)

Table 5-64 Measured Strains in Longitudinal Bars at 1499 mm (59 in) and 1626 mm (64 in) from the Top of the Footing for Specimen ISH1.5T

Height		Strain Gages		Run No														
[mm]	[in]	Number		1	2	3	4	5	6	7	8	9	10	11	12	13	14	15
1499	59	1	Max	-23	58	328	904	1234	2128	4872	11214	12417	13761	14675	15465	16554	18439	21011
			Min	-174	-246	-363	-405	-432	-633	-738	86	1693	1439	1547	1746	2057	2591	3337
		2	Max	-67	4	290	908	1216	2286	6552	9789	12005	13493	14408	15358	16851	19204	22589
			Min	-217	-299	-398	-476	-500	-734	-857	453	769	125	-114	-72	196	769	1459
		3	Max	-206	-197	-166	-67	172	833	1440	2021	2383	2424	2351	2306	2318	2442	2742
			Min	-215	-214	-213	-213	-209	-218	-284	-250	-425	-501	-520	-522	-548	-626	-691
		4	Max	-197	-174	-135	-107	-57	287	711	1120	1487	1761	2261	2589	2685	2725	2706
			Min	-228	-235	-232	-228	-210	-194	-255	-234	-208	-161	-137	-227	-339	-369	-338
		5	Max	-241	-124	58	184	278	1162	1823	2483	2777	5798	10605	11250	12709	13707	13745
			Min	-421	-512	-688	-819	-875	-1153	-1555	-1765	-1948	-2109	-3598	-2621	-1625	-1464	-1464
		6	Max	-217	-88	113	263	386	1224	1797	2415	2799	6709	10630	12452	14472	15572	15867
			Min	-417	-515	-723	-883	-956	-1275	-1784	-1948	-2140	-2445	-3635	-2248	-1471	-1238	-1311
1626	64	1	Max	23	159	984	1418	1648	2503	12320	12951	15525	18404	19499	20507	21903	24458	28199
			Min	-209	-325	-479	-582	-629	-910	-1044	431	293	125	-90	-434	-668	-57	1155
		2	Max	15	156	983	1454	1674	2531	7387	11917	13244	16200	17056	17769	18983	21321	24854
			Min	-224	-345	-536	-633	-670	-953	-1060	-113	-241	-577	-912	-1292	-1297	-786	354
		3	Max	-210	-189	-83	251	420	975	1761	2728	5376	8794	9551	10042	10356	10958	11991
			Min	-231	-232	-229	-223	-192	-188	-217	-197	-97	1282	3667	4583	5215	5524	5564
		4	Max	-244	-204	-121	-63	-1	472	1062	1660	2231	2539	2536	3317	7256	8535	8641
			Min	-277	-279	-279	-271	-265	-263	-301	-264	-237	-173	-151	-93	214	3207	4456
		5	Max	-283	-69	276	504	652	1409	2005	3321	6765	10545	12775	15975	19112	20771	21071
			Min	-540	-666	-912	-1102	-1190	-1557	-2067	-2842	-6548	-7593	-4829	-3655	-3209	-3137	-3388
		6	Max	-248	-4	368	607	751	1428	2158	5060	6732	10241	13466	16679	19613	21324	21680
			Min	-576	-724	-1053	-1297	-1446	-1945	-3316	-7979	-9109	-9084	-7261	-6000	-5617	-5784	-6677

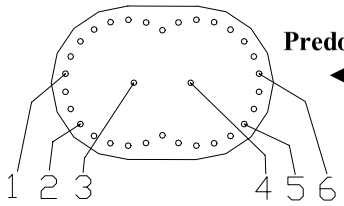

Predominant direction of motion

(All values in microstrain)

Table 5-65 Measured Strains in Longitudinal Bars at 1753 mm (69 in) and 1829 mm (72 in), 1905 mm (75 in) and 1981 mm (78 in) from the Top of the Footing for Specimen ISH1.5T

Height		Strain Gages		Run No														
[mm]	[in]	Number		1	2	3	4	5	6	7	8	9	10	11	12	13	14	15
1753	69	1	Max	35	266	813	1179	1377	2194	11199	12530	14933	17468	18473	19439	20871	23329	27027
			Min	-306	-461	-672	-790	-851	-1193	-1337	-801	-956	-1536	-2369	-3288	-4127	-4180	-3386
		2	Max	30	312	977	1471	1714	2722	11802	12659	16781	19698	20854	21746	23025	25282	28891
			Min	-348	-517	-758	-888	-955	-1379	-1569	-1490	-1741	-2396	-3522	-5003	-6208	-6428	-6004
		3	Max	-216	-188	88	322	440	883	1676	3026	9044	10500	10963	11425	12004	12914	14886
			Min	-236	-235	-234	-243	-242	-234	-252	-217	150	4576	5808	6478	7049	7526	7884
		4	Max	-195	-146	-39	239	357	731	1298	2012	2968	5695	8689	9668	10240	10929	11135
			Min	-230	-231	-238	-234	-237	-228	-281	-236	-270	-43	1878	5382	5931	6220	6887
		5	Max	-258	-21	345	563	665	1352	1737	5877	6863	10840	14433	17898	20883	22270	21386
			Min	-615	-789	-1130	-1369	-1496	-1953	-6490	-11175	-11669	-11762	-10347	-9839	-9340	-9312	-9941
		6	Max	-151	43	371	597	722	1353	1523	4143	5179	8804	11514	14104	16472	17543	16913
			Min	-506	-683	-1083	-1375	-1546	-2238	-9643	-10582	-10829	-11629	-11355	-11027	-10674	-10602	-10618
1829	72	1	Max	8	238	720	1068	1264	2035	2935	7921	11980	13144	14297	15391	16770	18822	21638
			Min	-291	-409	-572	-661	-710	-959	-1252	-1150	-471	-479	-810	-997	-1027	-811	-340
		6	Max	-138	65	353	523	625	1232	1811	2563	3515	9143	10879	13716	16563	18417	19220
			Min	-440	-573	-881	-1110	-1234	-1606	-2128	-2451	-3082	-3884	-3801	-3012	-2762	-2545	-2301
1905	75	1	Max	-11	72	327	567	714	1322	1840	2050	2236	2432	2567	2713	2893	3140	6436
			Min	-140	-201	-303	-368	-404	-560	-773	-935	-1041	-1214	-1409	-1540	-1650	-1762	-1968
		6	Max	-118	27	190	307	363	767	1200	1654	1864	2127	2323	2593	2976	3542	4439
			Min	-267	-339	-524	-649	-722	-935	-1182	-1285	-1339	-1337	-1307	-1331	-1432	-1579	-1735
1981	78	1	Max	-6	29	89	206	319	646	1176	1616	1866	2046	2129	2194	2268	2371	2490
			Min	-71	-98	-141	-159	-170	-248	-362	-430	-469	-556	-649	-722	-785	-827	-847
		6	Max	-4	34	81	118	152	414	639	980	1182	1521	1748	1922	2070	2162	2201
			Min	-61	-89	-162	-221	-257	-375	-535	-610	-668	-693	-702	-714	-752	-804	-847

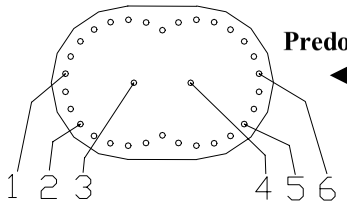

Predominant direction of motion ←

(All values in microstrain)

Table 5-66 Measured Strains in Spirals at 0 mm (0 in) and 152 mm (6 in) from the Top of the Footing for Specimen ISH1.0

Height		Strain Gages Number		Run No									
[mm]	[in]			1	2	3	4	5	6	7	8	9	10
0	0	4	Max	**-7**	**-1**	**-3**	**-15**	**-12**	**-29**	**-184**	**-316**	**-493**	**-606**
			Min	-22	-24	-46	-71	-125	-306	-421	-600	-812	-998
		5	Max	**32**	**39**	**43**	**50**	**69**	**81**	**157**	**204**	**251**	**269**
			Min	11	4	-24	-45	-98	-157	-208	-203	-166	-354
		6	Max	**5**	**25**	**53**	**65**	**75**	**120**	**136**	**117**	**177**	**1291**
			Min	-35	-34	-45	-44	-45	-97	-59	-52	-58	-90
152	6	1	Max	**-34**	**-6**	**31**	**1**	**47**	**159**	**371**	**743**	**1870**	**70034**
			Min	-88	-106	-162	-204	-290	-414	-518	-595	-597	-30904
		2	Max	**-16**	**-9**	**0**	**-77**	**-200**	**-286**	**-209**	**558**	**2098**	**16609**
			Min	-35	-35	-144	-344	-550	-688	-773	-708	-609	16
		3	Max	**-41**	**-29**	**-17**	**-68**	**-133**	**-266**	**-387**	**-496**	**-57**	**70914**
			Min	-75	-80	-101	-159	-333	-517	-688	-823	-874	-874
		4	Max	**-14**	**7**	**30**	**30**	**-7**	**-286**	**-547**	**-721**	**-1347**	**71219**
			Min	-33	-30	-33	-86	-351	-968	-1463	-2361	-2936	-2912
		5	Max	**-50**	**-39**	**-32**	**-76**	**-76**	**26**	**17**	**219**	**963**	**70462**
			Min	-69	-67	-92	-188	-332	-422	-497	-504	-536	-501
		6	Max	**-6**	**20**	**8**	**-61**	**-112**	**-99**	**-143**	**190**	**339**	**1415**
			Min	-50	-68	-150	-271	-468	-610	-654	-689	-754	-2481

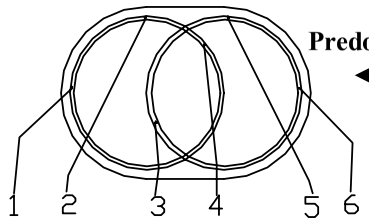

(All values in microstrain)

Table 5-67 Measured Strains in Spirals at 305 mm (12 in) and 457 mm (18 in) from the Top of the Footing for Specimen ISH1.0

Height		Strain Gages Number		Run No									
[mm]	[in]			1	2	3	4	5	6	7	8	9	10
305	12	1	Max	**-38**	**-35**	**-32**	**-56**	**-93**	**-241**	**-305**	**-317**	**-239**	**32402**
			Min	-48	-53	-103	-154	-274	-506	-678	-736	-822	-850
		2	Max	**-21**	**-18**	**37**	**-35**	**170**	**342**	**558**	**820**	**1004**	**2997**
			Min	-39	-42	-202	-504	-739	-815	-808	-781	-736	-711
		4	Max	**-25**	**-21**	**-19**	**-90**	**-337**	**-317**	**-188**	**-80**	**61**	**29792**
			Min	-35	-32	-133	-487	-762	-844	-891	-922	-971	-932
		5	Max	**-13**	**-8**	**36**	**68**	**94**	**108**	**196**	**298**	**729**	**4056**
			Min	-31	-41	-66	-185	-403	-512	-544	-577	-572	-1108
		6	Max	**-21**	**-14**	**-10**	**-20**	**-45**	**-170**	**-290**	**-139**	**683**	**31148**
			Min	-40	-48	-72	-104	-208	-427	-583	-676	-756	-592
457	18	1	Max	**-7**	**-7**	**-6**	**-45**	**-97**	**-230**	**-215**	**-269**	**-193**	**30624**
			Min	-19	-22	-93	-195	-368	-504	-590	-634	-685	-703
		2	Max	**7**	**10**	**10**	**-116**	**-123**	**0**	**96**	**103**	**128**	**69858**
			Min	-7	-13	-206	-454	-654	-740	-779	-823	-872	-814
		3	Max	**30**	**37**	**39**	**-2**	**-128**	**-142**	**-116**	**-123**	**-53**	**70158**
			Min	9	7	-72	-225	-320	-399	-429	-460	-469	-455
		4	Max	**-21**	**-19**	**-7**	**56**	**-160**	**-257**	**-247**	**-254**	**-262**	**30944**
			Min	-29	-29	-29	-293	-546	-655	-730	-794	-822	-789
		5	Max	**-58**	**-56**	**-44**	**-60**	**-133**	**-189**	**-198**	**-259**	**-320**	**70316**
			Min	-74	-74	-91	-170	-496	-746	-868	-952	-1006	-1032
		6	Max	**-33**	**-25**	**-14**	**-12**	**-65**	**-335**	**-367**	**-259**	**-216**	**31319**
			Min	-60	-70	-96	-131	-458	-728	-801	-819	-896	-899

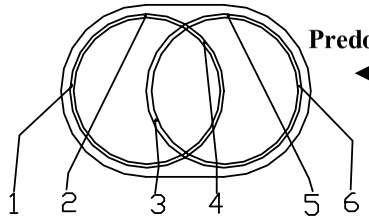

(All values in microstrain)

Table 5-68 Measured Strains in Spirals at 648 mm (26 in) and 826 mm (33 in) from the Top of the Footing for Specimen ISH1.0

Height		Strain Gages Number		Run No									
[mm]	[in]			1	2	3	4	5	6	7	8	9	10
648	26	1	Max	**-10**	**0**	**8**	**-8**	**-98**	**-315**	**-364**	**-239**	**-150**	**-139**
			Min	-34	-42	-100	-293	-496	-599	-652	-669	-701	-723
		2	Max	**-49**	**-46**	**-45**	**-57**	**-100**	**-187**	**-323**	**-392**	**-392**	**31340**
			Min	-58	-56	-64	-264	-862	-1067	-1139	-1207	-1244	-1363
		3	Max	**7**	**8**	**10**	**8**	**-35**	**-313**	**-579**	**-631**	**-639**	**34240**
			Min	-1	-2	-7	-105	-698	-961	-1050	-1099	-1162	-1094
		4	Max	**-16**	**-12**	**-13**	**-15**	**-24**	**-330**	**-539**	**-522**	**-525**	**-539**
			Min	-24	-22	-24	-58	-487	-839	-944	-988	-1033	-1033
		5	Max	**-52**	**-51**	**-49**	**-55**	**-64**	**74**	**196**	**227**	**289**	**31359**
			Min	-61	-59	-65	-80	-212	-411	-409	-461	-486	-482
826	33	1	Max	**-6**	**1**	**5**	**4**	**-2**	**-139**	**-106**	**-59**	**-7**	**-18**
			Min	-16	-16	-27	-66	-313	-478	-526	-559	-575	-593
		2	Max	**70**	**75**	**75**	**70**	**16**	**-201**	**-57**	**-3**	**70**	**72**
			Min	18	21	16	-8	-366	-587	-668	-712	-741	-741
		3	Max	**23**	**28**	**32**	**32**	**32**	**-82**	**-157**	**-202**	**-232**	**-291**
			Min	11	13	13	11	-129	-260	-328	-370	-410	-434
		4	Max	**-41**	**-38**	**-38**	**-38**	**-41**	**-191**	**-427**	**-559**	**-621**	**-663**
			Min	-50	-48	-49	-55	-212	-680	-854	-898	-877	-842
		5	Max	**-8**	**-8**	**-8**	**-8**	**-8**	**-34**	**-103**	**-34**	**43**	**43**
			Min	-34	-29	-34	-34	-75	-340	-751	-873	-949	-897
		6	Max	**5**	**8**	**8**	**10**	**15**	**-18**	**-173**	**-298**	**-300**	**-311**
			Min	-13	-6	-6	-4	-22	-182	-413	-547	-700	-697

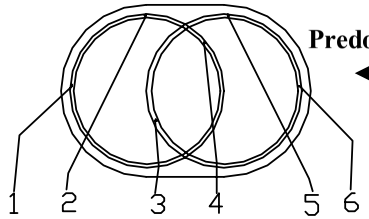

(All values in microstrain)

Table 5-69 Measured Strains in Spirals at 1016 mm (40 in) and 1168 mm (46 in) from the Top of the Footing for Specimen ISH1.0

Height		Strain Gages		Run No									
[mm]	[in]	Number		1	2	3	4	5	6	7	8	9	10
1016	40	1	Max	**-5**	**-1**	**2**	**2**	**-36**	**-352**	**-313**	**-332**	**-333**	**-345**
			Min	-13	-11	-13	-62	-578	-868	-931	-967	-1001	-1042
		2	Max	**56**	**58**	**58**	**53**	**147**	**296**	**365**	**348**	**362**	**378**
			Min	7	10	3	-139	-631	-782	-826	-855	-883	-874
		3	Max	**31**	**46**	**48**	**46**	**29**	**-343**	**-272**	**-257**	**-188**	**-178**
			Min	-6	-6	-6	-35	-447	-740	-821	-841	-865	-843
		4	Max	**-24**	**-19**	**-14**	**-15**	**-30**	**-466**	**-556**	**-692**	**-816**	**-777**
			Min	-36	-35	-47	-65	-852	-1228	-1414	-1471	-1433	-1408
		5	Max	**23**	**23**	**23**	**23**	**4**	**-129**	**-127**	**-127**	**-51**	**2**
			Min	-3	-3	-23	-44	-292	-591	-738	-782	-837	-793
		6	Max	**-24**	**-19**	**-15**	**-11**	**-9**	**-33**	**-155**	**-334**	**-373**	**-367**
			Min	-35	-31	-36	-36	-39	-209	-413	-573	-665	-714
1168	46	1	Max	**45**	**52**	**52**	**50**	**40**	**-278**	**-527**	**-541**	**-494**	**-106**
			Min	31	33	24	15	-297	-683	-801	-841	-917	-1027
		2	Max	**-45**	**-45**	**-45**	**-45**	**-36**	**146**	**238**	**220**	**361**	**815**
			Min	-68	-68	-124	-478	-853	-930	-1046	-1073	-1096	-1172
		3	Max	**31**	**38**	**38**	**15**	**-22**	**-180**	**-270**	**-298**	**-296**	**-217**
			Min	19	22	-25	-185	-307	-421	-556	-607	-648	-611
		4	Max	**-63**	**-65**	**-70**	**-79**	**-208**	**-102**	**9**	**97**	**255**	**222**
			Min	-76	-81	-93	-234	-630	-743	-783	-804	-1014	-1052
		5	Max	**-32**	**8**	**6**	**-41**	**-112**	**-329**	**-257**	**-262**	**-184**	**-208**
			Min	-48	-45	-61	-161	-494	-690	-817	-902	-946	-971
		6	Max	**23**	**30**	**32**	**39**	**44**	**-16**	**-155**	**-271**	**-192**	**-197**
			Min	5	9	-2	-5	-42	-171	-347	-506	-641	-684

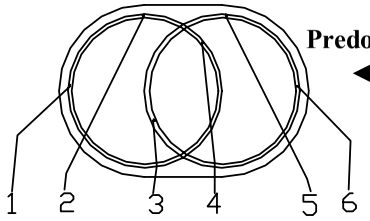

(All values in microstrain)

Table 5-70 Measured Strains in Spirals at 1321 mm (52 in) and 1473 mm (58 in) from the Top of the Footing for Specimen ISH1.0

Height		Strain Gages		Run No									
[mm]	[in]	Number		1	2	3	4	5	6	7	8	9	10
1321	52	1	Max	**-112**	**-108**	**-103**	**-133**	**-156**	**-246**	**-422**	**-385**	**-135**	**114**
			Min	-133	-138	-191	-267	-401	-530	-694	-807	-773	-770
		2	Max	**-11**	**-6**	**-6**	**-43**	**-126**	**-376**	**-505**	**-656**	**-1062**	**-1210**
			Min	-27	-29	-115	-346	-938	-1663	-1994	-2369	-2826	-2833
		3	Max	**43**	**45**	**45**	**24**	**-71**	**29**	**314**	**522**	**1006**	**1284**
			Min	27	27	-4	-126	-481	-687	-740	-759	-756	-629
		4	Max	**4**	**13**	**34**	**74**	**102**	**-270**	**290**	**401**	**1320**	**717**
			Min	-19	-26	-68	-291	-562	-836	-908	-1089	-1103	-827
		5	Max	**-26**	**-18**	**-18**	**-38**	**-252**	**-40**	**218**	**383**	**1381**	**2998**
			Min	-45	-45	-87	-341	-703	-806	-907	-991	-986	-570
		6	Max	**-1**	**4**	**6**	**-1**	**-43**	**-320**	**-105**	**87**	**253**	**334**
			Min	-24	-26	-61	-110	-322	-590	-673	-763	-749	-712
1473	58	4	Max	**6**	**11**	**13**	**4**	**-1**	**-10**	**-70**	**-142**	**-246**	**-427**
			Min	-8	-5	-8	-15	-29	-121	-290	-529	-612	-714
		5	Max	**11**	**23**	**23**	**6**	**-10**	**-207**	**774**	**981**	**1355**	**29452**
			Min	-33	-47	-89	-133	-314	-504	-546	-414	-442	-432
		6	Max	**18**	**29**	**50**	**52**	**41**	**-22**	**-100**	**-242**	**-214**	**-457**
			Min	-1	4	-3	-24	-59	-174	-362	-536	-698	-1110

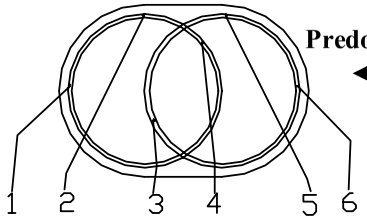

(All values in microstrain)

Table 5-71 Measured Strains in Spirals at 0 mm (0 in) and 178 mm (7 in) from the Top of the Footing for Specimen ISH1.25

Height		Strain Gages Number		Run No											
[mm]	[in]			1	2	3	4	5	6	7	8	9	10	11	12
0	0	8	Max	12	8	29	38	61	77	103	117	131	143	159	133
			Min	-2	-9	-2	1	1	5	22	15	-13	-115	-278	-418
		10	Max	24	27	87	99	68	8	3	-15	-22	-55	-87	-143
			Min	-27	-46	-92	-132	-281	-325	-353	-364	-374	-343	-302	-369
178	7	1	Max	0	-5	7	18	23	18	23	9	-47	-142	-218	-118
			Min	-14	-26	-44	-56	-79	-109	-125	-183	-276	-394	-601	-559
		2	Max	13	8	18	4	278	485	788	1137	1668	6610	18933	22007
			Min	-1	-8	-71	-173	-276	-310	-331	-327	-273	-38	4667	16710
		3	Max	-3	-12	-1	-26	-31	-15	22	22	138	570	2688	10177
			Min	-19	-29	-56	-205	-302	-298	-258	-254	-307	-288	-314	1099
		4	Max	-5	-5	2	-17	-81	-169	-204	-252	-321	-388	-321	-280
			Min	-19	-24	-47	-224	-483	-598	-672	-709	-769	-820	-848	-808
		5	Max	3	5	8	1	-73	-147	-150	-150	-150	-166	-150	221
			Min	-6	-6	-25	-273	-423	-395	-421	-449	-469	-520	-618	-520
		6	Max	1	-1	12	31	-1	1	10	-11	3	137	249	325
			Min	-13	-18	-15	-62	-182	-224	-240	-298	-358	-423	-490	-451
		7	Max	-8	-15	-6	1	-50	-99	-108	-83	89	474	864	957
			Min	-25	-27	-27	-113	-291	-403	-445	-524	-558	-500	-454	-384
		8	Max	8	3	13	6	-13	124	240	398	653	957	1449	1556
			Min	-6	-13	-29	-141	-264	-291	-319	-375	-400	-400	-361	-329
		9	Max	-8	-10	27	29	4	-80	-22	-22	18	175	214	170
			Min	-24	-31	-10	-63	-156	-188	-227	-301	-345	-364	-424	-410
		10	Max	17	22	22	17	3	-72	-129	-132	-132	-77	20	22
			Min	-61	-80	-155	-231	-304	-328	-349	-361	-382	-439	-458	-481

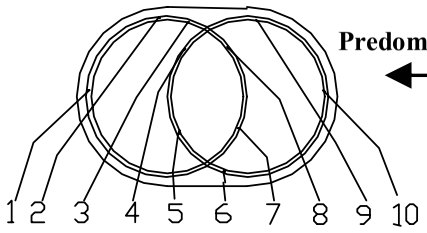

(All values in microstrain)

Table 5-72 Measured Strains in Spirals at 356 mm (14 in) and 533 mm (21 in) from the Top of the Footing for Specimen ISH1.25

Height		Strain Gages Number		Run No											
[mm]	[in]			1	2	3	4	5	6	7	8	9	10	11	12
356	14	1	Max	27	37	57	13	-26	-68	-114	-109	-63	2	113	264
			Min	-14	-24	-42	-51	-116	-181	-190	-188	-190	-190	-167	-91
		2	Max	23	23	23	40	42	18	40	37	40	40	97	-32
			Min	-29	-39	-61	-108	-266	-360	-380	-459	-562	-641	-691	-673
		3	Max	5	5	58	7	149	207	296	377	449	508	598	445
			Min	-2	-19	-21	-77	-142	-145	-138	-145	-168	-221	-242	-170
		4	Max	49	7	56	9	-73	-7	74	224	350	504	595	651
			Min	-3	-7	-26	-154	-250	-292	-297	-290	-301	-346	-395	-392
		5	Max	5	3	3	7	-72	-65	10	130	193	244	288	295
			Min	-9	-11	-37	-116	-225	-266	-276	-280	-310	-336	-350	-371
		6	Max	9	11	37	18	-68	-139	-130	-121	-61	13	97	231
			Min	-7	-12	-21	-156	-315	-369	-401	-431	-468	-501	-554	-573
		7	Max	-8	-10	6	4	-75	-221	-274	-325	-342	-358	-344	-318
			Min	-21	-28	-28	-89	-330	-418	-458	-506	-567	-634	-694	-666
		8	Max	-13	-13	9	9	143	216	361	497	624	717	867	998
			Min	-47	-60	-47	-47	-118	-158	-200	-214	-232	-274	-287	-354
		9	Max	1	-1	50	68	121	144	144	200	223	290	713	882
			Min	-8	-8	-54	-202	-364	-378	-394	-394	-470	-538	-586	-600
		10	Max	-12	16	81	-5	-77	-177	-225	-279	-274	-200	5	-21
			Min	-51	-70	-149	-265	-367	-404	-420	-437	-455	-474	-486	-525
533	21	1	Max	14	9	18	21	14	7	4	-14	-35	-61	-119	-174
			Min	2	-5	-33	-70	-107	-116	-123	-128	-137	-181	-225	-262
		2	Max	2	4	-4	-1	-92	-216	-263	-205	-181	-92	-138	31860
			Min	-8	-12	-30	-133	-322	-402	-452	-511	-574	-662	-733	-690
		5	Max	1	4	15	25	-153	-171	-160	-129	-136	-43	20	-45
			Min	-15	-15	-15	-195	-437	-512	-540	-584	-607	-612	-624	-684
		8	Max	13	13	15	61	328	587	770	929	1076	1223	1241	32432
			Min	4	4	1	-220	-342	-331	-343	-360	-371	-375	-431	-387
		9	Max	26	32	36	221	217	241	267	291	318	351	373	32603
			Min	15	11	-4	16	-94	-144	-169	-184	-204	-217	-224	-200
		10	Max	3	3	5	3	-9	-34	-76	-143	-164	-181	-188	-194
			Min	-11	-18	-48	-120	-178	-199	-215	-245	-276	-301	-322	-329

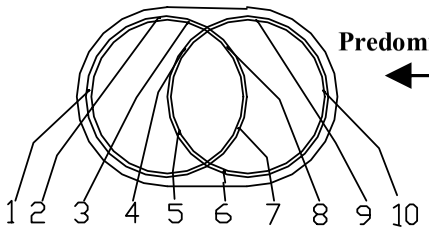

Predominant direction of motion

(All values in microstrain)

Table 5-73 Measured Strains in Spirals at 711mm (28 in) and 889 mm (35 in) from the Top of the Footing for Specimen ISH1.25

Height		Strain Gages Number		Run No											
[mm]	[in]			1	2	3	4	5	6	7	8	9	10	11	12
711	28	1	Max	-45	-52	-62	-57	-62	-69	-89	-124	-175	-231	-279	-323
			Min	-59	-69	-85	-85	-80	-94	-133	-189	-251	-293	-333	-370
		2	Max	12	14	15	16	-4	-15	-172	-187	-172	-157	-181	29855
			Min	2	2	-20	-62	-112	-310	-465	-528	-574	-617	-630	-578
		5	Max	4	-1	4	46	30	32	34	18	-3	178	398	519
			Min	-12	-15	-10	30	11	-1	-21	-89	-246	-355	-404	-381
		8	Max	-4	-4	2	11	-4	-39	-60	-92	-133	-183	-186	31902
			Min	-13	-13	-9	-6	-97	-183	-256	-345	-423	-467	-502	-457
		9	Max	5	6	13	28	8	-2	-5	-39	-76	-20	-60	32298
			Min	-4	-4	0	4	-25	-37	-61	-136	-218	-331	-392	-512
		10	Max	-20	-20	-4	-2	-48	-92	-113	-145	-193	-224	-247	-242
			Min	-39	-45	-50	-103	-242	-307	-369	-432	-483	-501	-527	-547
889	35	1	Max	22	29	25	32	22	32	57	83	125	169	181	69854
			Min	11	11	8	13	1	8	25	36	53	78	102	120
		2	Max	16	20	30	36	-12	81	135	202	249	265	243	31387
			Min	7	6	7	-5	-182	-294	-341	-366	-385	-385	-392	-356
		5	Max	2	4	4	9	-12	185	347	491	654	798	830	69592
			Min	-12	-10	-10	-5	-94	-293	-321	-330	-342	-360	-365	-339
		8	Max	-11	-9	-7	-1	-13	-62	-131	-132	-155	-188	-235	31979
			Min	-19	-18	-15	-15	-173	-462	-609	-684	-733	-760	-774	-725
		9	Max	-7	-6	-1	8	0	72	-23	18	60	173	255	31715
			Min	-16	-15	-9	-2	-11	-171	-340	-416	-468	-583	-604	-621
		10	Max	-13	-7	-4	4	2	9	25	27	28	92	-5	30944
			Min	-21	-20	-25	-18	-8	-2	11	11	14	-229	-352	-429

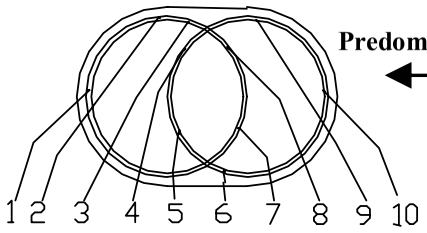

(All values in microstrain)

Table 5-74 Measured Strains in Spirals at 1067 mm (42 in) and 1245 mm (49 in) from the Top of the Footing for Specimen ISH1.25

Height		Strain Gages		Run No											
[in]	[mm]	Number		1	2	3	4	5	6	7	8	9	10	11	12
1067	42	1	Max	6	8	6	13	24	-71	-78	-92	-103	-108	-101	68521
			Min	-8	-6	-6	-1	-108	-194	-203	-217	-228	-221	-205	-214
		2	Max	25	28	39	49	134	56	120	168	195	225	285	31423
			Min	15	15	12	8	-340	-390	-403	-412	-431	-451	-447	-395
		5	Max	-10	-12	-12	-5	-19	-26	-198	-238	-257	-273	-270	70909
			Min	-24	-29	-26	-26	-66	-294	-403	-445	-477	-519	-578	-643
		8	Max	-7	-5	1	22	-8	-121	-168	-168	-180	-204	-235	31367
			Min	-14	-15	-8	-5	-244	-370	-410	-457	-508	-568	-637	-542
		9	Max	5	8	12	53	30	34	5	33	63	93	120	32035
			Min	-5	-2	4	1	-104	-267	-325	-361	-382	-409	-529	-530
		10	Max	-1	1	1	8	13	22	32	32	25	4	-45	69816
			Min	-13	-10	-13	-6	-8	4	11	4	-8	-66	-201	-245
1245	49	1	Max	-1	4	6	4	-89	-153	-169	-151	-139	-100	131	69667
			Min	-12	-12	-28	-149	-289	-343	-354	-356	-361	-359	-352	-391
		2	Max	4	6	14	83	92	193	249	301	334	542	1760	31220
			Min	-7	-5	-7	-102	-183	-188	-187	-199	-224	-241	-206	-9
		3	Max	-1	2	8	144	181	283	347	419	499	683	1791	31343
			Min	-11	-8	-5	-53	-83	-74	-42	-19	-11	-16	-43	71
		4	Max	-1	2	15	18	-74	-208	-284	-362	-424	1061	1690	33758
			Min	-11	-7	-7	-160	-383	-564	-644	-699	-755	-778	85	-1468
		5	Max	-8	-8	-8	1	-31	-86	-47	-5	57	150	402	69113
			Min	-24	-22	-22	-26	-142	-214	-242	-272	-334	-350	-427	-443
		6	Max	-22	-18	-18	-11	-13	31	89	130	151	341	705	69184
			Min	-36	-34	-34	-25	-270	-314	-337	-365	-428	-493	-601	-740
		7	Max	-11	-11	-11	-6	-27	-76	-36	-8	22	164	775	68316
			Min	-27	-25	-25	-27	-280	-343	-348	-364	-355	-376	-438	-471
		8	Max	-13	-9	-6	-1	-97	-168	-192	-213	-243	-241	-328	31243
			Min	-22	-19	-15	-164	-455	-540	-578	-623	-628	-744	-1263	-1356
		9	Max	-4	1	8	23	153	175	183	206	207	353	964	32123
			Min	-12	-8	-2	5	-166	-250	-273	-328	-486	-711	-870	-501
		10	Max	21	23	34	46	69	106	181	239	315	535	798	69078
			Min	4	7	-5	-5	-24	-24	-40	-42	-7	41	137	85

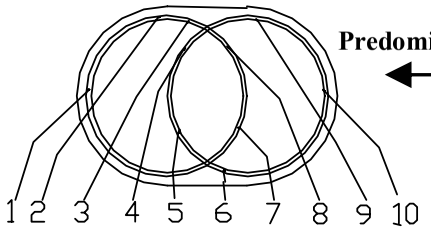

Predominant direction of motion

(All values in microstrain)

Table 5-75 Measured Strains in Spirals at 1422 mm (56 in) and 1600 mm (63 in) from the Top of the Footing for Specimen ISH1.25

Height		Strain Gages		Run No											
[in]	[mm]	Number		1	2	3	4	5	6	7	8	9	10	11	12
1422	56	1	Max	-4	-4	1	10	-4	-23	-64	-97	35	246	589	67619
			Min	-18	-18	-32	-41	-87	-124	-182	-275	-275	-229	-196	-175
		2	Max	0	4	13	6	-61	-104	-88	-65	130	508	1226	31884
			Min	-9	-6	-25	-114	-196	-201	-207	-254	-357	-454	-490	-4761
		3	Max	-9	-8	0	35	152	174	207	297	519	979	25454	32385
			Min	-18	-16	-15	-39	-103	-99	-77	-91	-95	-105	-164	23405
		4	Max	-4	0	18	27	-23	-120	-114	-29	96	216	291	34377
			Min	-12	-9	-5	-20	-270	-349	-381	-430	-460	-495	-517	-461
		5	Max	-12	-12	-5	13	-54	-215	-294	-356	-210	469	1112	69453
			Min	-26	-26	-24	-122	-512	-638	-689	-726	-742	-714	-591	-2659
		6	Max	-11	-11	-4	12	-59	-173	-201	-208	-159	839	9888	70218
			Min	-25	-25	-20	-229	-463	-505	-524	-533	-614	-614	-547	7972
		7	Max	2	2	4	82	-42	-45	-28	0	132	711	3961	31825
			Min	-7	-7	-13	-51	-216	-226	-206	-201	-207	-202	-143	1711
		8	Max	-11	-6	-4	39	346	377	313	468	1256	5819	31176	31176
			Min	-19	-15	-48	-113	-246	-269	-246	-241	-298	-390	1426	21024
		9	Max	-12	-8	2	95	339	598	921	1342	1873	6722	7839	29983
			Min	-20	-16	-22	-153	-229	-224	-159	-148	-161	-97	531	-1526
		10	Max	-4	1	19	40	66	105	151	265	450	624	659	69296
			Min	-20	-18	-18	-9	-9	-32	-55	-74	-118	-139	-71	-39
1600	63	8	Max	18	25	30	46	25	32	39	32	16	9	-10	-72
			Min	4	9	11	16	-17	-24	-44	-123	-172	-167	-142	-260
		9	Max	6	7	33	56	44	53	67	72	70	95	210	206
			Min	-5	-14	-26	-9	-51	-37	-20	-15	-22	-21	-35	-30
		10	Max	24	24	36	48	48	61	68	99	147	285	1126	71933
			Min	10	3	-45	-55	-131	-118	-80	-66	-57	-59	-148	-215

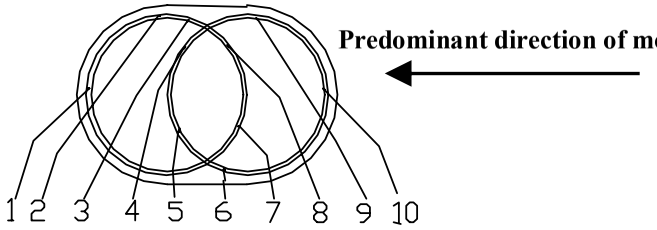

(All values in microstrain)

Table 5-76 Measured Strains in Spirals at 0 mm (0 in), 178 mm (7 in) and 356 mm (14 in) from the Top of the Footing for Specimen ISH1.5

Height		Strain Gages		Run No												
[in]	[mm]	Number		1	2	3	4	5	6	7	8	9	10	11	12	13
0	0	4	Max	-26	-12	0	-5	-26	-40	-26	-10	-26	-100	-204	-258	-304
			Min	-40	-40	-56	-95	-123	-225	-274	-297	-288	-431	-471	-468	-556
		5	Max	147	218	348	442	435	584	659	733	586	515	440	421	442
			Min	-48	-66	-50	-21	-23	-23	0	23	-5	-5	48	50	66
		6	Max	-15	39	188	134	132	281	342	456	426	424	445	654	902
			Min	-83	-87	-101	-104	-97	-120	-106	-122	-139	-139	-125	-134	-148
178	7	1	Max	41	115	190	238	183	263	463	627	991	1559	1213	1410	1799
			Min	-37	-55	-94	-156	-229	-348	-419	-469	-494	-568	-563	-520	-1268
		2	Max	20	20	17	-56	17	382	599	816	1046	1967	2652	3591	4175
			Min	-8	-35	-133	-298	-355	-498	-519	-514	-423	-300	314	889	1778
		3	Max	-10	-10	-13	-76	-99	-80	-59	-10	87	301	436	653	2364
			Min	-24	-24	-101	-176	-206	-239	-225	-190	-222	-246	-192	-236	-199
		4	Max	1	8	19	-106	-263	-312	-328	-171	-38	-1	47	91	891
			Min	-22	-25	-129	-389	-500	-686	-811	-985	-1084	-1149	-1177	-1196	-1128
		5	Max	7	14	7	-144	-261	-327	-399	-387	-287	-182	-261	-334	-334
			Min	-25	-49	-161	-301	-383	-455	-555	-786	-812	-868	-894	-926	-978
		6	Max	-42	-44	-79	-234	-369	-350	-148	-79	-118	-95	142	559	8133
			Min	-93	-172	-424	-545	-557	-670	-703	-691	-698	-700	-691	-684	-668
356	14	1	Max	-1	-6	-13	-71	-136	-171	-247	-275	-219	-159	-150	-52	90
			Min	-34	-59	-124	-196	-247	-329	-415	-505	-519	-549	-554	-552	-559
		2	Max	8	8	1	-78	-176	-71	94	247	370	486	512	491	514
			Min	-15	-32	-162	-280	-343	-412	-471	-515	-540	-573	-614	-649	-659
		3	Max	-16	-7	11	21	67	223	307	372	539	818	1059	1097	1185
			Min	-30	-28	-88	-158	-200	-233	-263	-272	-240	-172	-177	-188	-244
		4	Max	17	20	17	-78	-122	-57	-15	50	127	217	250	308	352
			Min	4	-3	-85	-273	-359	-431	-456	-482	-519	-591	-656	-686	-719
		5	Max	8	8	-6	-252	-321	-338	-352	-335	291	1185	1394	1654	11173
			Min	-11	-20	-247	-516	-595	-674	-739	-811	-811	-767	-347	-117	45
		6	Max	14	17	-11	-79	-76	-34	-32	266	375	610	589	615	2645
			Min	-34	-65	-183	-267	-311	-351	-381	-397	-432	-504	-576	-616	-581

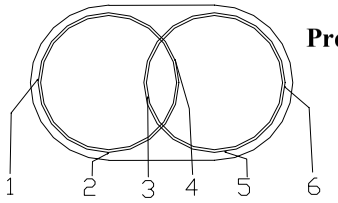

Predominant direction of motion

(All values in microstrain)

Table 5-77 Measured Strains in Spirals at 559 mm (22 in) and 762 mm (30 in) from the Top of the Footing for Specimen ISH1.5

Height		Strain Gages		Run No												
[in]	[mm]	Number		1	2	3	4	5	6	7	8	9	10	11	12	13
559	22	1	Max	-49	-49	-66	-142	-219	-275	-386	-472	-586	-574	-574	-588	-635
			Min	-84	-108	-173	-261	-326	-433	-535	-658	-774	-870	-937	-983	-1002
		2	Max	11	11	5	-93	-240	-182	-91	28	95	146	146	160	95
			Min	-5	-16	-309	-509	-551	-586	-598	-665	-719	-798	-840	-870	-886
		3	Max	1	1	-3	-170	-323	-337	-335	-307	-286	-275	-268	-247	-198
			Min	-12	-15	-286	-523	-607	-683	-676	-669	-695	-725	-753	-781	-783
		4	Max	4	4	-3	-145	-259	-229	-220	-166	-99	-57	-71	-68	-75
			Min	-10	-15	-278	-348	-399	-474	-518	-527	-537	-539	-585	-620	-632
		5	Max	23	34	99	113	132	171	171	192	204	222	234	250	290
			Min	2	4	-77	-196	-207	-256	-279	-317	-349	-372	-372	-375	-358
		6	Max	3	24	110	114	87	96	119	131	145	149	135	128	196
			Min	-32	-32	-46	-71	-87	-115	-122	-143	-171	-201	-224	-236	-241
762	30	1	Max	-23	-18	-41	-207	-320	-262	-260	-290	-269	-255	-262	-260	-285
			Min	-36	-53	-221	-396	-477	-548	-548	-608	-636	-647	-656	-663	-668
		2	Max	-9	-7	-8	-51	-145	-229	-97	90	189	240	234	222	150
			Min	-17	-19	-79	-219	-321	-545	-679	-739	-757	-784	-784	-797	-785
		3	Max	17	17	17	-39	-148	-97	-85	-39	-6	26	54	159	224
			Min	3	3	-62	-397	-494	-562	-585	-594	-601	-625	-611	-585	-574
		4	Max	18	18	16	-92	-155	81	46	-3	200	376	430	483	465
			Min	2	2	-125	-335	-370	-394	-448	-478	-501	-520	-527	-530	-516
		5	Max	-8	-1	46	190	329	513	613	759	913	1101	1157	1164	1071
			Min	-26	-26	-59	-173	-240	-300	-326	-342	-347	-331	-289	-282	-286
		6	Max	14	16	0	-155	-426	-335	-296	-245	-190	-160	-178	-199	-252
			Min	0	-9	-176	-453	-615	-703	-736	-775	-782	-810	-833	-842	-863

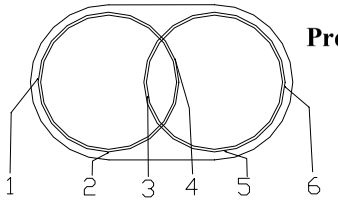

Predominant direction of motion

(All values in microstrain)

Table 5-78 Measured Strains in Spirals at 991 mm (39 in) and 1194 mm (47 in) from the Top of the Footing for Specimen ISH1.5

Height		Strain Gages		Run No												
[in]	[mm]	Number		1	2	3	4	5	6	7	8	9	10	11	12	13
991	39	1	**Max**	**-61**	**-59**	**-61**	**-130**	**-279**	**-343**	**-446**	**-512**	**-492**	**-443**	**-446**	**-446**	**-470**
			Min	-71	-73	-139	-339	-452	-603	-729	-821	-849	-857	-864	-882	-896
		2	**Max**	**-34**	**-31**	**-28**	**-33**	**-72**	**-112**	**-240**	**-194**	**-105**	**-53**	**-51**	**-52**	**-87**
			Min	-43	-45	-45	-74	-122	-262	-439	-581	-632	-673	-689	-697	-695
		3	**Max**	**-36**	**-34**	**-32**	**-92**	**-268**	**-349**	**-416**	**-446**	**-453**	**-453**	**-490**	**-501**	**-522**
			Min	-55	-55	-101	-300	-423	-601	-707	-797	-853	-922	-934	-934	-929
		4	**Max**	**-19**	**-16**	**-20**	**-162**	**-357**	**-388**	**-400**	**-385**	**-334**	**-252**	**-169**	**-116**	**-125**
			Min	-27	-27	-161	-414	-530	-672	-744	-793	-796	-800	-761	-751	-744
		5	**Max**	**-18**	**-14**	**-18**	**-70**	**-180**	**-188**	**-165**	**-127**	**-90**	**-88**	**-115**	**-130**	**-160**
			Min	-27	-28	-92	-191	-296	-407	-478	-535	-577	-623	-616	-610	-601
		6	**Max**	**12**	**22**	**22**	**1**	**-157**	**-287**	**-276**	**-243**	**-213**	**-176**	**-178**	**-199**	**-257**
			Min	-4	5	-9	-159	-350	-526	-610	-656	-703	-722	-733	-745	-724
1194	47	1	**Max**	**2**	**5**	**6**	**1**	**-96**	**-221**	**-273**	**-247**	**-264**	**-287**	**-314**	**-332**	**-315**
			Min	-6	-5	-8	-95	-284	-523	-579	-607	-614	-637	-656	-663	-652
		2	**Max**	**-27**	**-25**	**-21**	**-23**	**-41**	**498**	**764**	**944**	**897**	**915**	**930**	**951**	**903**
			Min	-34	-33	-36	-49	-216	-433	-397	-409	-419	-439	-460	-474	-482
		3	**Max**	**-15**	**-10**	**1**	**-22**	**-78**	**-106**	**-211**	**-106**	**-45**	**-17**	**-27**	**-20**	**-50**
			Min	-34	-41	-48	-110	-171	-329	-441	-506	-555	-606	-632	-648	-646
		4	**Max**	**-17**	**-12**	**-17**	**-177**	**-122**	**58**	**172**	**210**	**475**	**557**	**323**	**275**	**200**
			Min	-28	-33	-225	-380	-433	-534	-566	-631	-650	-675	-694	-698	-691
		5	**Max**	**27**	**50**	**227**	**382**	**460**	**539**	**739**	**1078**	**1269**	**1544**	**1629**	**1657**	**1537**
			Min	-8	-8	13	143	135	88	86	93	100	135	222	264	279
		6	**Max**	**12**	**12**	**16**	**7**	**-34**	**-97**	**-278**	**-431**	**-609**	**-537**	**-537**	**-544**	**-547**
			Min	-2	-2	-4	-44	-113	-301	-491	-732	-903	-973	-1001	-1015	-1029

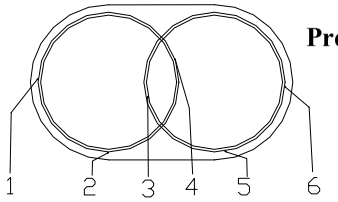

Predominant direction of motion

(All values in microstrain)

Table 5-79 Measured Strains in Spirals at 559 mm (22 in) and 762 mm (30 in) from the Top of the Footing for Specimen ISH1.5

Height		Strain Gages		Run No												
[in]	[mm]	Number		1	2	3	4	5	6	7	8	9	10	11	12	13
1397	55	1	Max	-298	-121	707	1175	1368	2224	4359	11553	16852	19365	20250	21247	23753
			Min	-673	-777	-855	-764	-617	-604	-520	729	5324	6549	7184	8470	9713
		2	Max	-2	2	12	-42	-133	-91	-35	-5	-35	-46	-42	-28	-39
			Min	-19	-16	-53	-170	-300	-460	-495	-509	-530	-572	-607	-628	-630
		3	Max	-67	-67	-78	-176	-254	-340	-421	-338	-268	-201	-143	-83	-14
			Min	-83	-88	-215	-340	-426	-558	-623	-651	-662	-704	-743	-762	-732
		4	Max	-97	-92	-110	-207	-268	-222	-95	102	201	278	299	316	308
			Min	-109	-114	-214	-343	-398	-421	-414	-416	-404	-407	-409	-402	-416
		5	Max	-72	-70	-79	-128	-197	-266	-300	-300	-315	-284	-200	-126	-57
			Min	-83	-87	-135	-240	-398	-564	-604	-647	-612	-638	-626	-642	-639
		6	Max	29	34	36	27	10	1	-64	-148	-176	-29	20	45	36
			Min	8	3	-15	-41	-59	-141	-227	-352	-499	-531	-552	-562	-552
1575	62	1	Max	90	65	60	4	-114	-175	-305	-393	-514	-461	-624	-668	-682
			Min	67	35	-5	-142	-272	-407	-517	-665	-817	-968	-1035	-1084	-1100
		2	Max	-50	-46	-16	-73	-177	-213	-255	-258	-105	234	268	332	328
			Min	-58	-55	-85	-195	-282	-383	-413	-434	-504	-574	-582	-578	-592
		3	Max	-22	-20	-25	-266	-373	-278	-171	5	154	428	604	551	377
			Min	-36	-36	-264	-482	-542	-554	-551	-554	-540	-577	-635	-651	-674
		4	Max	-27	-25	-32	-215	-332	-344	-369	-383	-498	-595	-608	-629	-640
			Min	-37	-37	-215	-500	-576	-645	-687	-742	-764	-880	-933	-979	-1008
		5	Max	-62	-51	-59	-116	-170	-253	-252	-276	-440	-208	-209	-240	-351
			Min	-81	-86	-177	-311	-495	-645	-691	-938	-1313	-1420	-1471	-1511	-1543
		6	Max	11	16	16	14	2	-42	-261	-132	39	224	162	125	206
			Min	-7	-12	-23	-37	-81	-289	-486	-578	-601	-599	-625	-655	-664
1753	69	4	Max	-87	-47	-51	38	116	254	173	234	256	115	254	250	33
			Min	-97	-62	-100	-62	-57	-33	-44	-78	-303	-480	-518	-525	-541
		5	Max	-51	-41	17	69	87	91	61	51	179	253	301	308	309
			Min	-86	-100	-115	-126	-126	-138	-127	-105	-118	-56	10	18	32
		6	Max	26	28	23	91	81	155	-14	450	1539	2161	2075	2073	2084
			Min	-2	-18	-86	-178	-232	-440	-626	-788	-767	-431	70	111	142

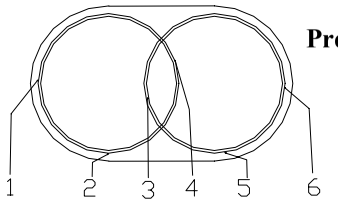

Predominant direction of motion

(All values in microstrain)

Table 5-80 Measured Strains in Spirals at 0 mm (0 in) and 178 mm (7 in) from the Top of the Footing for Specimen ISH1.5T

Height		Strain Gages		Run No														
[in]	[mm]	Number		1	2	3	4	5	6	7	8	9	10	11	12	13	14	15
0	0	8	Max	-12	0	2	0	-14	-14	-84	-143	-159	-91	-45	-19	-10	-42	-182
			Min	-26	-26	-35	-68	-103	-236	-296	-308	-326	-310	-294	-259	-266	-361	-497
		9	Max	15	33	78	115	140	173	138	133	156	163	85	13	-69	-157	-185
			Min	-57	-115	-217	-236	-229	-254	-243	-226	-217	-203	-226	-254	-287	-322	-366
		10	Max	32	44	76	65	75	88	117	126	137	157	359	704	866	1089	3000
			Min	-9	-39	-81	-83	-82	-120	-154	-169	-175	-214	-269	-152	-153	-144	237
178	7	1	Max	-9	-9	-18	-32	-51	-69	-101	99	257	314	384	568	688	707	1081
			Min	-41	-69	-129	-189	-231	-402	-496	-508	-540	-547	-554	-547	-545	-577	-524
		2	Max	4	6	42	71	63	239	870	1395	2002	2747	4116	5506	6389	10109	17990
			Min	-16	-26	-22	-19	-9	-75	-187	-187	-61	238	817	2217	3576	4457	8093
		3	Max	75	77	79	59	35	119	219	289	303	182	-179	-374	-395	-184	543
			Min	61	61	42	10	-14	-14	-118	-340	-658	-1047	-1320	-1485	-1594	-1622	-1578
		4	Max	-2	1	1	3	-4	-11	-104	-25	109	244	329	441	631	1031	1698
			Min	-16	-16	-16	-25	-36	-175	-268	-349	-435	-497	-537	-569	-571	-539	-451
		5	Max	-18	-13	-8	-2	-7	-6	-72	-183	-335	-388	-343	-314	-287	-215	-155
			Min	-27	-27	-26	-27	-28	-112	-368	-535	-659	-774	-860	-928	-1001	-1084	-1258
		6	Max	-13	-9	3	-16	-39	-46	-76	-183	-218	-239	-267	-338	-459	-663	-886
			Min	-30	-34	-44	-62	-69	-204	-299	-403	-513	-578	-668	-817	-1047	-1320	-1580
		7	Max	1	6	11	11	6	1	-15	152	479	650	784	896	1007	1234	2107
			Min	-15	-20	-33	-26	-17	-47	-163	-260	-316	-365	-406	-397	-420	-372	-309
		8	Max	-2	0	2	9	5	-2	-12	197	341	420	434	513	473	577	884
			Min	-16	-14	-16	-16	-35	-253	-392	-489	-591	-689	-765	-800	-865	-851	-833
		9	Max	-23	-6	3	-46	-62	-60	-144	-169	-209	-218	-148	-2	106	327	2153
			Min	-46	-58	-134	-237	-283	-386	-568	-728	-891	-1026	-1150	-1194	-1336	-1341	-1332
		10	Max	5	5	10	7	3	-7	-83	-113	-104	-2	35	37	5	54	341
			Min	-16	-39	-83	-125	-157	-262	-380	-487	-582	-684	-805	-932	-1011	-1009	-925

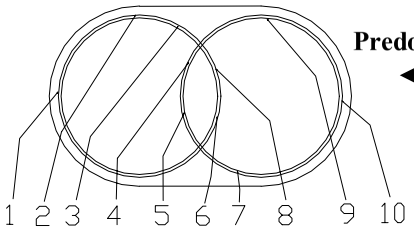

Predominant direction of motion

(All values in microstrain)

Table 5-81 Measured Strains in Spirals at 356 mm (14 in) and 559 mm (22 in) from the Top of the Footing for Specimen ISH1.5T

Height		Strain Gages		Run No														
[in]	[mm]	Number		1	2	3	4	5	6	7	8	9	10	11	12	13	14	15
356	14	1	Max	13	54	54	54	6	-12	-69	75	276	516	525	585	674	811	884
			Min	-1	-46	-142	-193	-236	-367	-426	-456	-481	-458	-412	-410	-406	-406	-385
		2	Max	16	19	42	104	163	295	492	699	822	1001	1129	1250	1331	1438	1561
			Min	-2	-7	-2	7	21	35	-49	-58	-53	-28	-21	2	56	100	165
		3	Max	5	8	8	3	-6	8	119	105	114	212	249	249	217	238	317
			Min	-9	-6	-25	-55	-37	-227	-364	-422	-452	-513	-596	-657	-719	-736	-805
		4	Max	-85	-85	-87	-41	-71	-85	-66	179	471	640	742	844	955	1106	1409
			Min	-101	-98	-133	-221	-504	-786	-337	-328	-256	-272	-295	-323	-344	-351	-291
		5	Max	39	41	44	39	6	-24	-70	-93	-54	69	213	311	373	415	568
			Min	25	25	25	-49	-168	-340	-484	-546	-576	-574	-600	-653	-683	-683	-646
		6	Max	-14	-14	5	5	5	0	-72	-2	74	153	294	447	598	742	1036
			Min	-21	-21	-21	-49	-90	-241	-390	-519	-612	-614	-640	-584	-522	-464	-369
		7	Max	-16	-19	-14	-14	-21	-68	-213	-423	-502	-499	-436	-377	-357	-357	-350
			Min	-66	-66	-66	-75	-165	-364	-599	-786	-908	-1011	-1104	-1203	-1241	-1318	-1320
		8	Max	-46	-46	-46	-67	-106	-25	218	185	-115	-22	31	71	20	62	-29
			Min	-60	-60	-97	-218	-248	-304	-390	-467	-537	-623	-721	-793	-894	-977	-1050
		9	Max	-11	-2	-6	-29	-72	-105	-181	-145	-56	-61	0	84	161	431	3123
			Min	-26	-29	-53	-151	-252	-355	-461	-564	-652	-688	-715	-752	-829	-858	-855
		10	Max	-7	5	3	-53	-99	-134	-196	-307	-259	-259	-263	-256	-243	-206	-132
			Min	-37	-53	-122	-261	-344	-432	-449	-479	-567	-631	-685	-710	-740	-812	-1034
559	22	1	Max	13	22	32	13	-1	-1	-117	-240	-236	-222	-233	-236	-247	-263	-291
			Min	-10	-24	-43	-126	-168	-394	-459	-479	-486	-500	-505	-514	-528	-531	-531
		2	Max	9	13	14	58	70	213	304	347	418	466	534	584	609	615	605
			Min	-5	-9	-15	1	0	-68	-167	-195	-182	-168	-166	-157	-161	-174	-175
		5	Max	-7	-7	-5	-1	-5	-17	-84	-186	-237	-177	-123	-91	-70	-35	16
			Min	-24	-21	-21	-24	-47	-244	-385	-455	-473	-469	-485	-501	-508	-504	-483
		8	Max	-9	-9	-8	-7	5	12	-141	-40	44	112	119	128	138	166	197
			Min	-19	-19	-21	-27	-32	-397	-522	-587	-635	-647	-659	-669	-674	-666	-642
		9	Max	-16	-5	-1	-46	-168	-159	-83	-53	-21	7	22	41	55	82	123
			Min	-36	-44	-86	-450	-583	-672	-675	-706	-750	-776	-789	-795	-813	-818	-824
		10	Max	-56	-54	-9	-14	-58	-63	-82	-82	-68	-65	-65	-68	-82	-82	-82
			Min	-70	-70	-70	-84	-89	-135	-163	-191	-219	-219	-238	-238	-238	-238	-238

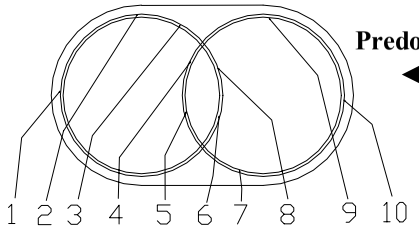

Predominant direction of motion

(All values in microstrain)

Table 5-82 Measured Strains in Spirals at 762 mm (30 in) and 991 mm (39 in) from the Top of the Footing for Specimen ISH1.5T

Height		Strain Gages		Run No														
[mm]	[in]	Number		1	2	3	4	5	6	7	8	9	10	11	12	13	14	15
762	30	1	Max	1	1	1	1	1	3	-18	-143	-166	-166	-219	-224	-224	-224	-286
			Min	-18	-25	-25	-25	-48	-201	-289	-372	-420	-469	-518	-536	-543	-571	-596
		2	Max	-9	-7	-5	-1	5	6	238	424	442	528	567	593	593	595	523
			Min	-18	-18	-18	-16	-15	-209	-256	-299	-333	-350	-387	-415	-430	-432	-429
		5	Max	-15	-15	-15	-3	-3	4	4	-74	-148	-212	-235	-283	-292	-285	-281
			Min	-22	-22	-22	-22	-22	-22	-123	-242	-370	-460	-512	-563	-606	-634	-650
		8	Max	-14	-14	-15	-15	-18	-20	-190	-259	-236	-157	-110	-86	-84	-92	-119
			Min	-22	-22	-23	-26	-30	-213	-627	-722	-763	-787	-805	-816	-826	-833	-841
		9	Max	-14	-9	-6	-19	-92	-121	-14	-40	-64	-105	-152	-177	-195	-200	-215
			Min	-27	-29	-40	-258	-417	-679	-744	-778	-836	-880	-897	-907	-920	-932	-929
		10	Max	19	23	23	23	16	73	168	212	227	232	212	216	214	210	163
			Min	-28	-28	-28	-52	-98	-142	-168	-168	-181	-179	-188	-186	-184	-168	-166
991	39	1	Max	-2	0	5	9	16	16	-21	-33	-146	-310	-313	-304	-297	-280	-262
			Min	-19	-19	-23	-21	-19	-12	-58	-320	-540	-591	-602	-616	-625	-625	-632
		2	Max	-9	-7	-6	-1	2	7	-50	64	157	238	284	328	364	405	432
			Min	-19	-18	-15	-14	-14	-82	-246	-285	-289	-277	-267	-258	-259	-256	-249
		5	Max	-13	-13	-13	-13	-13	-13	-18	-117	-173	-194	-217	-245	-259	-263	-263
			Min	-32	-29	-29	-27	-27	-57	-238	-273	-354	-395	-435	-448	-444	-435	-432
		8	Max	-5	-2	-1	1	4	25	-27	-164	-120	-101	-106	-98	-88	-64	-43
			Min	-14	-12	-9	-8	-7	-13	-360	-414	-432	-425	-460	-472	-477	-469	-457
		9	Max	-22	-20	-18	-14	-14	-11	-67	-112	-273	-426	-504	-509	-506	-486	-455
			Min	-30	-30	-27	-25	-27	-117	-276	-372	-532	-685	-766	-805	-829	-824	-800
		10	Max	3	10	12	12	15	19	-15	-22	-41	-78	-115	-132	-139	-141	-148
			Min	-11	-11	-8	-8	-4	-4	-43	-53	-102	-162	-202	-239	-257	-276	-283

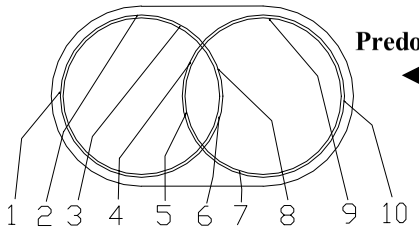

Predominant direction of motion

(All values in microstrain)

Table 5-83 Measured Strains in Spirals at 1194 mm (47 in) and 1397 mm (55 in) from the Top of the Footing for Specimen ISH1.5T

Height		Strain Gages		Run No													
[mm]	[in]	Number		1	2	3	4	5	6	7	8	9	10	11	12	13	14	15
1194	47	1	Max	-10	-6	-3	-1	1	4	-52	-232	-286	-323	-297	-281	-286	-276	-272
			Min	-22	-20	-17	-17	-13	-55	-421	-524	-561	-591	-619	-661	-694	-703	-710
		2	Max	-8	-7	-2	0	0	1	-39	-58	-16	22	29	47	57	76	83
			Min	-18	-14	-14	-14	-18	-34	-271	-353	-392	-416	-447	-450	-466	-478	-492
		5	Max	0	0	5	7	10	14	-14	-132	-239	-299	-350	-361	-357	-366	-373
			Min	-14	-11	-9	-11	-4	-7	-345	-556	-663	-744	-781	-793	-786	-779	-779
		8	Max	-11	-12	-11	-11	-12	-13	-68	-194	-230	-265	-296	-301	-326	-341	-362
			Min	-20	-19	-20	-20	-25	-128	-400	-558	-668	-696	-710	-722	-738	-749	-756
		9	Max	0	4	6	13	15	20	-19	-250	-228	-151	-96	-58	-60	-67	-88
			Min	-9	-6	-5	-2	1	-6	-410	-564	-685	-737	-777	-798	-812	-809	-791
		10	Max	4	6	6	8	11	15	20	43	-101	-22	6	29	45	55	41
			Min	-10	-8	-8	-6	-3	1	-15	-169	-267	-325	-355	-372	-381	-383	-379
1397	55	1	Max	-1	1	6	13	-8	-47	-163	-204	-227	-267	-260	-237	-207	-154	-96
			Min	-15	-12	-12	-112	-260	-473	-581	-597	-607	-623	-630	-644	-657	-671	-685
		2	Max	2	5	6	12	26	161	208	280	371	431	475	538	637	700	718
			Min	-6	-4	-4	-4	-2	-41	-145	-169	-203	-220	-239	-252	-276	-283	-260
		3	Max	2	5	9	12	13	222	411	546	662	744	797	862	924	993	1042
			Min	-6	-4	-4	-2	-2	-34	-97	-99	-106	-98	-109	-103	-99	-89	-78
		4	Max	-6	-5	-1	-2	-5	-9	-67	-131	-102	-36	43	136	218	284	333
			Min	-14	-14	-13	-16	-25	-86	-278	-359	-397	-410	-425	-432	-449	-426	-390
		5	Max	-9	-6	-6	-6	-6	-2	-53	-67	-67	-30	3	36	57	70	68
			Min	-20	-20	-18	-20	-23	-37	-104	-165	-214	-242	-277	-295	-326	-344	-335
		6	Max	-13	-13	-6	1	6	24	1	-61	4	29	34	41	66	103	131
			Min	-27	-27	-27	-24	-24	-29	-214	-349	-391	-444	-469	-502	-523	-539	-546
		7	Max	-9	-9	-6	1	1	24	-92	-237	-290	-272	-214	-170	-131	-89	-55
			Min	-20	-20	-18	-20	-20	-142	-438	-521	-585	-617	-641	-654	-671	-680	-696
		8	Max	8	12	15	15	16	20	-65	-63	-50	-23	-8	14	32	65	91
			Min	0	4	5	5	5	-78	-186	-227	-263	-269	-304	-330	-347	-348	-340
		9	Max	-25	-21	-14	-9	-2	4	-56	-264	-332	-323	-333	-333	-333	-314	-305
			Min	-34	-33	-34	-33	-32	-85	-514	-666	-733	-790	-818	-830	-843	-848	-843
		10	Max	10	10	15	19	19	29	63	29	-39	-50	-66	-71	-66	-59	-62
			Min	-2	-2	-2	-2	1	3	-20	-80	-145	-173	-194	-203	-217	-215	-222

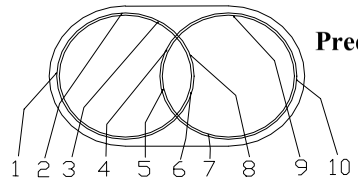

Predominant direction of motion

(All values in microstrain)

Table 5-84 Measured Strains in Spirals at 1575 mm (62 in) and 1753 mm (69 in) from the Top of the Footing for Specimen ISH1.5T

Height		Strain Gages		Run No														
[in]	[mm]	Number		1	2	3	4	5	6	7	8	9	10	11	12	13	14	15
1575	62	1	Max	-1	11	37	13	9	9	-33	-175	-284	-298	-298	-265	-240	-163	-80
			Min	-19	-22	-29	-52	-80	-207	-372	-497	-646	-709	-739	-764	-790	-804	-809
		2	Max	-1	1	4	35	55	95	207	401	529	631	671	717	767	828	971
			Min	-9	-7	-5	-9	-21	-74	-143	-140	-147	-157	-169	-174	-189	-195	-168
		3	Max	-2	0	4	6	0	15	-2	88	91	179	282	369	435	466	519
			Min	-12	-9	-11	-14	-36	-67	-215	-298	-301	-273	-252	-244	-244	-235	-268
		4	Max	-25	-22	-20	-19	-28	-57	-99	20	92	109	114	134	137	145	118
			Min	-33	-32	-30	-42	-112	-265	-423	-494	-524	-569	-608	-639	-672	-690	-693
		5	Max	14	14	17	19	21	21	-130	-75	21	88	145	166	166	175	221
			Min	-4	-4	-4	-4	-2	-105	-298	-372	-370	-413	-422	-445	-484	-501	-517
		6	Max	-15	-13	-8	-6	-6	-17	-131	-245	-252	-261	-259	-177	-103	-36	-8
			Min	-29	-29	-29	-31	-38	-203	-440	-567	-662	-741	-785	-813	-820	-836	-873
		7	Max	12	15	17	19	19	0	-157	-305	-357	-359	-378	-458	-507	-507	-526
			Min	-35	-35	-32	-30	-47	-289	-603	-737	-813	-890	-902	-982	-1057	-1116	-1235
		8	Max	-16	-13	-11	-9	-25	-58	-61	90	190	229	215	178	137	62	-8
			Min	-25	-22	-22	-37	-90	-178	-213	-244	-296	-344	-391	-446	-504	-535	-560
		9	Max	-18	-8	1	7	13	14	-50	-213	-26	97	70	40	65	127	137
			Min	-30	-32	-35	-40	-40	-75	-348	-508	-583	-616	-631	-671	-688	-701	-707
		10	Max	-9	-2	9	16	23	32	-42	-280	-354	-322	-252	-132	-79	-67	-109
			Min	-26	-30	-42	-53	-53	-90	-458	-558	-583	-597	-618	-636	-669	-692	-701
1753	69	8	Max	-8	-5	1	7	6	4	-34	-42	-61	-51	-61	-23	191	342	312
			Min	-16	-14	-12	-9	-15	-55	-109	-145	-180	-237	-250	-284	-352	-434	-493
		9	Max	5	14	21	28	28	28	-47	-211	-55	64	60	54	21	18	20
			Min	-7	-9	-20	-22	-22	-127	-352	-516	-547	-570	-572	-578	-602	-640	-723
		10	Max	1	5	17	19	24	24	-55	577	1447	2600	3089	2156	2200	2186	3144
			Min	-20	-25	-41	-55	-67	-134	-406	-432	-416	-281	568	993	991	803	800

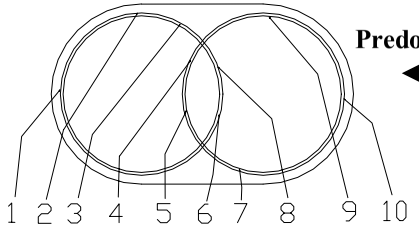

Predominant direction of motion

(All values in microstrain)

Table 5-85 Measured Strains in Cross Ties in Specimen ISH1.5T

Height		Strain Gages		Run No														
[mm]	[in]	Number		1	2	3	4	5	6	7	8	9	10	11	12	13	14	15
19	0.75	1	Max	4	15	124	169	185	362	361	299	227	213	211	231	255	304	362
			Min	-8	-9	1	-7	-2	19	64	46	29	32	26	25	26	36	67
		2	Max	-19	7	44	65	100	253	300	281	509	574	580	557	560	590	632
			Min	-44	-42	-40	-21	-9	9	65	74	102	95	121	149	163	169	188
191	7.5	1	Max	29	32	146	385	518	787	822	742	784	836	887	925	882	838	1345
			Min	13	1	3	71	116	46	18	64	67	50	32	22	15	-32	-71
362	14.25	1	Max	-8	-7	88	203	249	362	388	411	426	515	554	572	542	500	449
			Min	-18	-25	-23	16	32	-6	-79	-161	-232	-283	-319	-331	-320	-269	-311
		2	Max	4	4	76	218	297	488	607	720	729	774	789	798	868	920	1008
			Min	-41	-47	-47	31	124	146	128	124	97	81	72	54	52	52	54
533	21	1	Max	34	36	99	583	759	1079	1346	1505	1446	1391	1332	1316	1322	1390	1541
			Min	21	12	8	57	160	182	211	232	199	169	158	154	146	135	144
		2	Max	77	77	80	663	955	1178	1304	1327	1322	1378	1352	1336	1325	1256	1302
			Min	25	11	6	54	218	273	346	369	369	367	351	346	296	275	277
705	27.75	2	Max	53	53	55	225	521	869	1259	1487	1540	1558	1637	1709	1712	1686	1487
			Min	-3	-21	-49	-47	6	99	294	350	350	350	329	350	299	299	301
876	34.5	2	Max	56	56	59	59	61	68	524	662	704	748	842	944	1007	1033	989
			Min	42	42	31	26	19	21	47	246	295	344	353	358	362	362	362
1048	41.25	2	Max	78	78	80	43	43	131	691	712	758	798	784	772	758	738	707
			Min	64	64	64	22	29	32	-38	-12	-5	-8	-54	-79	-79	-66	-54
1219	48	2	Max	33	35	38	42	47	126	803	1027	1125	1220	1216	1204	1260	1264	1202
			Min	19	17	10	10	17	28	35	278	266	285	294	299	294	292	290
1391	54.75	1	Max	36	55	90	137	217	1046	1783	2063	2207	2222	2127	2053	2046	2087	2109
			Min	-6	-29	-48	-39	-21	-4	155	202	245	256	234	238	237	244	243
		2	Max	61	80	91	100	112	270	517	942	1182	1461	1615	1650	1652	1601	1498
			Min	19	3	-44	-76	-69	-76	142	282	342	361	359	356	342	331	328
1562	61.5	1	Max	64	70	76	255	523	1131	1677	2091	2235	2247	2195	2151	2127	2125	2083
			Min	50	41	28	39	82	105	162	194	318	401	418	423	419	409	383
		2	Max	49	49	53	67	280	559	612	798	934	1146	1336	1438	1477	1470	1384
			Min	35	30	28	32	46	120	206	271	278	297	287	287	278	264	260
1734	68.25	1	Max	18	21	39	139	232	373	465	528	501	535	482	426	388	403	425
			Min	4	-8	-22	-16	0	28	95	114	119	134	128	125	109	93	79
		2	Max	41	41	46	149	269	431	463	591	569	571	507	414	434	441	434
			Min	-16	-35	-38	33	90	112	146	242	220	173	124	114	95	92	95

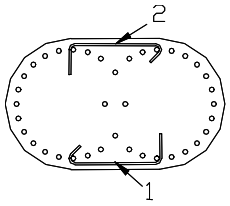

Predominant direction of motion

(All values in microstrain)

Table 5-86 Comparison of Methods to Calculate Idealized Force-Displacement Curve Specimen ISH1.0

Method	F_{y1*}		D_{y1*}		F_{y*}		D_{y*}		μ_{D**}
	[kN]	[Kips]	[mm]	[in]	[kN]	[Kips]	[mm]	[in]	
Method 1+	148.3	33.3	14.0	0.55	228.2	51.3	21.6	0.85	**4.6**
Method 2++	148.3	33.3	13.7	0.54	227.5	51.1	21.1	0.83	**4.7**
Method 3+++	120.6	27.1	9.6	0.38	223.3	50.2	17.7	0.70	**5.6**

* See Figure 4-71 for Definition
** Displacement ductility capacity
+1st bar Yield Point
++ Force of 1st bar yield
+++ One-half of the peak force

Table 5-87 Comparison of Methods to Calculate Idealized Force-Displacement Curve Specimen ISH1.25

Method	F_{y1*}		D_{y1*}		F_{y*}		D_{y*}		μ_{D**}
	[kN]	[Kips]	[mm]	[in]	[kN]	[Kips]	[mm]	[in]	
Method 1+	144.6	32.5	14.0	0.55	233.1	52.4	22.6	0.89	**4.7**
Method 2++	144.6	32.5	13.2	0.52	231.3	52.0	21.1	0.83	**5.0**
Method 3+++	125.6	28.2	11.4	0.45	231.2	52.0	21.0	0.83	**5.0**

* See Figure 4-71 for Definition
** Displacement ductility capacity
+1st bar Yield Point
++ Force of 1st bar yield
+++ One-half of the peak force

Table 5-88 Comparison of Methods to Calculate Idealized Force-Displacement Curve Specimen ISH1.5

Method	F_{y1*}		D_{y1*}		F_{y*}		D_{y*}		μ_{D**}
	[kN]	[Kips]	[mm]	[in]	[kN]	[Kips]	[mm]	[in]	
Method 1+	104.5	23.5	29.9	1.18	287.0	64.5	82.0	3.23	**1.6**
Method 2++	104.5	23.5	15.0	0.59	222.7	50.1	32.1	1.26	**4.0**
Method 3+++	123.6	27.8	18.5	0.73	224.3	50.4	33.6	1.32	**3.8**

* See Figure 4-71 for Definition
** Displacement ductility capacity
+1st bar Yield Point
++ Force of 1st bar yield
+++ One-half of the peak force

Table 5-89 Comparison of Methods to Calculate Idealized Force-Displacement Curve Specimen ISH1.5T

Method	F_{y1*}		D_{y1*}		F_{y*}		D_{y*}		μ_{D**}
	[kN]	[Kips]	[mm]	[in]	[kN]	[Kips]	[mm]	[in]	
Method 1+	132.7	29.8	14.3	0.56	233.2	52.4	25.2	0.99	**4.0**
Method 2++	132.7	29.8	15.1	0.59	235.2	52.9	26.7	1.05	**3.8**
Method 3+++	125.6	28.2	13.9	0.55	234.3	52.7	26.0	1.02	**3.9**

* See Figure 4-71 for Definition

** Displacement ductility capacity

+1st bar Yield Point

++ Force of 1st bar yield

+++ One-half of the peak force

Table 5-90 Summary of the Values Used to Calculated Experimental Plastic Hinge Length l_p

Variables		Specimen			
		ISH1.0	ISH1.25	ISH1.5	ISH1.5T
ϕ_p	[Rad/mm]	1.24E-01	1.16E-01	1.01E-01	7.39E-02
	[Rad/in]	4.88E-03	4.58E-03	3.97E-03	2.91E-03
Δ_y	[mm]	21.1	21.1	32.1	26.7
	[in]	0.83	0.83	1.26	1.05
Δ_u	[mm]	98.6	105.5	127.6	101.6
	[in]	3.88	4.15	5.02	4.00
L	[mm]	1473	1600	1753	1753
	[in]	58	63	69	69
l_p	[mm]	363	384	480	541
	[in]	14.3	15.1	18.9	21.3

Table 6-1 Relative Increase in Tensile Yield Strength of Steel due Strain Rate Effect Specimen ISL1.0

Strain	Location		Motion	Strain	Strain Rate	Relative Increase in Fy		
Gauge*	[mm]	[in]	[xSlymar]	[με]	[με/sec]	Fy=310 Mpa [45 ksi]	Fy=520 Mpa [75 ksi]	Fy=462 Mpa [67 ksi]
8	0	0	0.3	2389	16022	1.09	1.02	1.04
9	0	0	0.3	2333	27145	1.11	1.03	1.05
10	0	0	0.3	2329	17626	1.10	1.02	1.04
8	127	5	0.3	2349	26395	1.11	1.03	1.05
9	127	5	0.3	2448	26264	1.11	1.03	1.05
10	127	5	0.3	2408	28699	1.11	1.03	1.05
							Average=	**1.05**

* For detail location see Figure 3-13

Table 6-2 Relative Increase in Tensile Yield Strength of Steel due Strain Rate Effect Specimen ISL1.5

Strain	Location		Motion	Strain	Strain Rate	Relative Increase in Fy		
Gauge*	[mm]	[in]	[xSlymar]	[με]	[με/sec]	Fy=310 Mpa [45 ksi]	Fy=520 Mpa [75 ksi]	Fy=462 Mpa [67 ksi]
8	0	0	0.4	2478	49277	1.13	1.04	1.06
9	0	0	0.4	2706	378111	1.20	1.06	1.10
10	0	0	0.4	2487	11495	1.08	1.02	1.04
8	127	5	0.4	4298	561228	1.21	1.07	1.11
9	127	5	0.4	5468	396979	1.20	1.06	1.10
10	127	5	0.4	2324	52675	1.13	1.04	1.06
							Average=	**1.08**

* For detail location see Figure 3-13

Table 6-3 Relative Increase in Tensile Yield Strength of Steel due Strain Rate Effect Specimen ISH1.0

Strain	Location		Motion	Strain	Strain Rate	Relative Increase in Fy		
Gauge*	[mm]	[in]	[xSlymar]	[με]	[με/sec]	Fy=310 Mpa [45 ksi]	Fy=520 Mpa [75 ksi]	Fy=462 Mpa [67 ksi]
5	0	0	0.75	N/A	N/A	N/A	N/A	N/A
6	0	0	0.75	2217	13101	1.09	1.02	1.05
5	127	5	0.75	2291	20375	1.10	1.03	1.05
6	127	5	0.75	2257	21210	1.10	1.03	1.06
5	254	10	0.75	2288	21231	1.10	1.03	1.06
6	254	10	0.75	2333	19744	1.10	1.03	1.05
							Average=	**1.05**

* For detail location see Figure 3-14

Table 6-4 Relative Increase in Tensile Yield Strength of Steel due Strain Rate Effect Specimen ISH1.25

Strain	Location		Motion	Strain	Strain Rate	Relative Increase in Fy		
Gauge*	[mm]	[in]	[xSlymar]	[με]	[με/sec]	Fy=310 Mpa [45 ksi]	Fy=520 Mpa [75 ksi]	Fy=462 Mpa [67 ksi]
5	0	0	0.75	2420	66122	1.14	1.04	1.08
6	0	0	0.75	2174	1639	1.02	1.00	1.01
5	127	5	0.75	2405	30735	1.12	1.03	1.07
6	127	5	0.75	2264	12263	1.09	1.02	1.05
5	254	10	0.75	2282	8629	1.07	1.02	1.04
6	254	10	0.75	2207	13113	1.09	1.02	1.05
							Average=	**1.04**

* For detail location see Figure 3-14

Table 6-5 Relative Increase in Tensile Yield Strength of Steel due Strain Rate Effect Specimen ISH1.5

Strain Gauge*	Location [mm]	Location [in]	Motion [xSlymar]	Strain [με]	Strain Rate [με/sec]	Relative Increase in Fy Fy=310 Mpa [45 ksi]	Fy=520 Mpa [75 ksi]	Fy=462 Mpa [67 ksi]
5	0	0	0.4	N/A	N/A	N/A	N/A	N/A
6	0	0	0.4	N/A	N/A	N/A	N/A	N/A
5	127	5	0.4	2302	39253	1.12	1.03	1.07
6	127	5	0.4	2215	11064	1.08	1.02	1.04
5	254	10	0.4	2223	29444	1.11	1.03	1.06
6	254	10	0.4	2300	10776	1.08	1.02	1.04
							Average=	**1.05**

* For detail location see Figure 3-14

Table 6-6 Relative Increase in Tensile Yield Strength of Steel due Strain Rate Effect Specimen ISH1.5T

Strain Gauge*	Location [mm]	Location [in]	Motion [xSlymar]	Strain [με]	Strain Rate [με/sec]	Relative Increase in Fy Fy=310 Mpa [45 ksi]	Fy=520 Mpa [75 ksi]	Fy=462 Mpa [67 ksi]
5	0	0	0.6	2291	27188	1.11	1.03	1.06
6	0	0	0.6	2231	24427	1.11	1.03	1.06
5	127	5	0.6	2175	23864	1.11	1.03	1.06
6	127	5	0.6	2263	15152	1.09	1.02	1.05
5	254	10	0.6	N/A	N/A	N/A	N/A	N/A
6	254	10	0.6	2181	11921	1.08	1.02	1.05
							Average=	**1.06**

* For detail location see Figure 3-14

Table 6-7 Relative Increase in Concrete Compression Strength due Strain Rate Effect Specimen ISL1.0

Strain Gauge*	Location [mm]	Location [in]	Motion [xSlymar]	Strain [με]	Strain Rate [με/sec]	Relative Increase in f'_c
1	0	0	0.5	-2532	-47019	1.13
2	0	0	0.5	N/A	N/A	N/A
3	0	0	0.5	N/A	N/A	N/A
1	127	5	0.5	-2318	-105770	1.15
2	127	5	0.5	-2460	-130029	1.16
3	127	5	0.5	-2505	-42278	1.13
					Average=	**1.14**

* For detail location see Figure 3-13

Table 6-8 Relative Increase in Concrete Compression Strength due Strain Rate Effect Specimen ISL1.5

Strain Gauge*	Location [mm]	Location [in]	Motion [xSlymar]	Strain [με]	Strain Rate [με/sec]	Relative Increase in f'_c
1	0	0	0.6	-2520	-43356	1.13
2	0	0	0.6	N/A	N/A	N/A
3	0	0	0.6	N/A	N/A	N/A
1	127	5	0.6	-2548	-66918	1.14
2	127	5	0.6	-2527	-60352	1.14
3	127	5	0.6	N/A	N/A	N/A
					Average=	**1.14**

* For detail location see Figure 3-13

Table 6-9 Relative Increase in Concrete Compression Strength due Strain Rate Effect Specimen ISH1.0

Strain Gauge*	Location [mm]	Location [in]	Motion [xSlymar]	Strain [με]	Strain Rate [με/sec]	Relative Increase in f'c
1	0	0	1.0	N/A	N/A	N/A
2	0	0	1.0	N/A	N/A	N/A
1	127	5	1.0	-2390	-40382	1.13
2	127	5	1.0	-2219	-2616	1.07
1	254	10	1.0	-2229	747	1.04
2	254	10	1.0	-2262	-5230	1.08
					Average=	**1.08**

* For detail location see Figure 3-14

Table 6-10 Relative Increase in Concrete Compression Strength due Strain Rate Effect Specimen ISH1.25

Strain Gauge*	Location [mm]	Location [in]	Motion [xSlymar]	Strain [με]	Strain Rate [με/sec]	Relative Increase in f'c
1	0	0	1.0 X Slym	-2644	-65901	1.14
2	0	0	1.0 X Slym	N/A	N/A	N/A
1	127	5	1.0 X Slym	-2813	-43327	1.13
2	127	5	1.0 X Slym	N/A	N/A	N/A
1	254	10	1.0 X Slym	-2164	-14047	1.11
2	254	10	1.0 X Slym	N/A	N/A	N/A
					Average=	**1.12**

* For detail location see Figure 3-14

Table 6-11 Relative Increase in Concrete Compression Strength due Strain Rate Effect Specimen ISH1.5

Strain Gauge*	Location [mm]	Location [in]	Motion [xSlymar]	Strain [με]	Strain Rate [με/sec]	Relative Increase in f'c
1	0	0	0.4	N/A	N/A	N/A
2	0	0	0.4	N/A	N/A	N/A
1	127	5	0.4	-2224	-2986	1.07
2	127	5	0.4	-2290	-17966	1.11
1	254	10	0.4	-2245	-4768	1.08
2	254	10	0.4	-2233	-7837	1.09
					Average=	**1.09**

* For detail location see Figure 3-14

Table 6-12 Relative Increase in Concrete Compression Strength due Strain Rate Effect Specimen ISH1.5T

Strain Gauge*	Location [mm]	Location [in]	Motion [xSlymar]	Strain [με]	Strain Rate [με/sec]	elative Increase in f'c
1	0	0	1.0	-2196	-32449	1.12
2	0	0	1.0	N/A	N/A	N/A
1	127	5	1.0	-2214	-28723	1.12
2	127	5	1.0	-2167	-34581	1.13
1	254	10	1.0	-2248	-10160	1.10
2	254	10	1.0	N/A	N/A	N/A
					Average=	**1.12**

* For detail location see Figure 3-14

Table 6-13 Yield Stress and Concrete Compression Strength used in SPMC

Material Properties	Units	Specimens					
		ISL1.0	ISL1.5	ISH1.0	ISH1.5	ISH1.25	ISH1.5T
f'_c	MPa	42044	41836	33643	33913	50448	50417
	psi	6098	6068	4879	4919	7317	7312
fy	MPa	485	498	466	467	449	456
	Ksi	70	72	68	68	65	66

Table 6-14 Effect of the Strain Rate on the Idealized Moment Curvature Properties for Specimens with Low Shear

		Specimen			
		ISL1.0		ISL1.5	
		Strain Rate Effect			
		with	without	with	without
Mp	kN-m	241	228	339	317
	Kips-in	2133	2021	2999	2807
ϕ_y	[Rad/m]	0.0142	0.0142	0.0118	0.0114
	[Rad/in]	0.000361	0.000359	0.000300	0.000289
ϕ_u	[Rad/m]	0.124	0.124	0.109	0.110
	[Rad/in]	0.00314	0.00316	0.00278	0.00280

Table 6-15 Effect of the Strain Rate on the Idealized Moment Curvature Properties for Specimens with High Shear

		Specimen							
		ISH1.0		ISH1.25		ISH1.5		ISH1.5T	
		Strain Rate Effect							
		with	without	with	without	with	without	with	without
Mp	kN-m	160	152	200	188	221	208	238	223
	Kips-in	1419	1343	1771	1662	1957	1845	2107	1978
ϕ_y	[Rad/m]	0.0159	0.0154	0.0144	0.0138	0.0141	0.0136	0.0134	0.0129
	[Rad/in]	0.000405	0.000392	0.000365	0.000350	0.000359	0.000345	0.000341	0.000328
ϕ_u	[Rad/m]	0.099	0.102	0.107	0.114	0.108	0.115	0.099	0.102
	[Rad/in]	0.00251	0.0026	0.00272	0.00288	0.00275	0.00291	0.00251	0.00259

Table 6-16 Comparison of the Moment Curvature Properties for the Specimens with Low Shear Using SPMC and xSECTION

		Specimen			
		ISL1.0		ISL1.5	
		SPMC	***xSECTION***	***SPMC***	***xSECTION***
Mp	[kN-m]	241	258	339	358
	[Kips-in]	2133	2288	2999	3168
ϕ_y	[Rad/m]	0.0142	0.0133	0.0118	0.0116
	[Rad/in]	0.000361	0.000338	0.000300	0.000295
ϕ_u	[Rad/m]	0.124	0.116	0.109	0.103
	[Rad/in]	0.00314	0.002957	0.00278	0.002618

Table 6-17 Comparison of the Moment Curvature Properties for the Specimens with High Shear Using SPMC and xSECTION

		Specimen							
		ISH1.0		ISH1.25		ISH1.5		ISH1.5T	
		SPMC	*xSECTION*	*SPMC*	*xSECTION*	*SPMC*	*xSECTION*	*SPMC*	*xSECTION*
Mp	[kN-m]	160	169	200	210	221	233	238	252
	[Kips-in]	1419	1496	1771	1855	1957	2066	2107	2227
ϕ_y	[Rad/m]	0.0159	0.0156	0.0144	0.0139	0.0141	0.0139	0.0134	0.0131
	[Rad/in]	0.000405	0.000397	0.000365	0.000352	0.000359	0.000353	0.000341	0.000333
ϕ_u	[Rad/m]	0.099	0.085	0.107	0.088	0.108	0.094	0.099	0.082
	[Rad/in]	0.00251	0.00216	0.00272	0.00224	0.00275	0.002388	0.00251	0.002073

Table 6-18 Calculated and Measured Plastic Hinge Length expressed as a Fraction of Column Depth

Specimen	Paulay & Priestley	Baker & Amarkone	Caltrans	Dowell & Hines			Measured	Depth of Column	
				Vs based on					
				Caltrans	Tanaka & Park	Benzoni et al		[mm]	[in]
ISL1.0	0.49	0.55	0.49	0.59	0.50	0.50	**0.79**	445	17.50
ISL1.5	0.49	0.58	0.49	0.53	0.53	0.54	**0.83**	514	20.25
ISH1.0	0.42	0.41	0.52	0.83	0.86	0.91	**0.99**	368	14.50
ISH1.25	0.40	0.35	0.47	0.69	0.72	0.80	**0.97**	397	15.625
ISH1.5	0.39	0.40	0.45	0.69	0.70	0.80	**1.13**	425	16.75
ISH1.5T	0.39	0.36	0.44	0.66	0.66	0.80	**1.27**	425	16.75

Table 6-19 Hinge Properties used in SAP 2000

		Specimen	
	Units	**ISL1.0**	**ISL1.5**
M_y	[kN-m]	241	339
	[Kips-in]	2133	2999
θ_y	[Rad]	0.01347	0.0135
M_u	[kN-m]	241	339
	[Kips-in]	2133	2999
θ_u	[Rad]	0.03786	0.0406

Table 6-20 Rotational Stiffness, Moment of Inertia and Hinge Properties used in SAP 2000

Properties	Units	Specimen			
		ISH1.0	ISH1.25	ISH1.5	ISH1.5T
$K_{m\theta}$	[kNxm/Rad]	31613	34344	17425	22153
	[Kipsxin/Rad]	279799	303970	154224	196071
I	[cm^4]	13424	17772	25767	23059
	[in^4]	323	427	619	554
M_y	[kNxm]	160	200	221	238
	[Kipsxin]	1419	1771	1957	2107
θ_y	[Rad]	0.0103	0.00854	0.0087	0.00859
M_u	[kNxm]	160	200	221	238
	[Kipsxin]	1419	1771	1957	2107
θ_u	[Rad]	0.0316	0.0381	0.0406	0.0378

$K_{m\theta}$ = rotational stiffness for spring element

Table 6-21 Calculated Shear Capacity using Caltrans, Tanaka and Benzoni Methods

Method		Units	Specimen			
			ISH1.0	ISH1.25	ISH1.5	ISH1.5T
Caltrans	V_c	[kN]	117	94	88	N/A
		[Kips]	26	21	20	N/A
	V_s	[kN]	103	155	155	N/A
		[Kips]	23	35	35	N/A
	V_n	**[kN]**	**220**	**249**	**242**	N/A
		[Kips]	**49**	**56**	**54**	N/A
Tanaka	V_c	[kN]	117	94	88	53
		[Kips]	26	21	20	12
	V_s	[kN]	83	135	143	176
		[Kips]	19	30	32	40
	V_n	**[kN]**	**200**	**229**	**231**	**230**
		[Kips]	**45**	**51**	**52**	**52**
Benzoni	V_c	[kN]	107	87	69	N/A
		[Kips]	24	20	16	N/A
	V_s	[kN]	55	99	102	N/A
		[Kips]	12	22	23	N/A
	V_p	[kN]	47	57	46	N/A
		[Kips]	10	13	10	N/A
	V_n	**[kN]**	**209**	**243**	**217**	N/A
		[Kips]	**47**	**55**	**49**	N/A

N/A = Not Applicable

Table 6-22 Uncracked and Post Yield Shear Stiffness Using Priestley's Method

		Specimen			
	[Units]	**ISH1.0**	**ISH1.25**	**ISH1.5**	**ISH1.5T**
K_{pf} / K_{ucf}		0.00182	0.00395	0.00494	0.00212
K'_v	[kN/m]	464666	575833	468867	571648
	[Kips/in]	2653	3288	2677	3264
K_{ps}	[kN/m]	847	2274	2315	1209
	[Kips/in]	4.8	13.0	13.2	6.9

K_{ucf} = uncracked flexural stiffness

K_{pf} = post yield flexural stiffness

K'_v = uncracked shear stiffness

K_{ps} = post yield shear stiffness

Table 6-23 Uncracked, Cracked and Measured Cracked Shear Stiffness

	[Units]	**ISH1.0**	**ISH1.25**	**ISH1.5**	**ISH1.5T**
K'_v	[kN/m]	464666	575833	468867	571648
	[Kips/in]	2653	3288	2677	3264
$K_{v,45}$	[kN/m]	28598	42148	40594	41454
	[Kips/in]	163	241	232	237
K_{VM}	[kN/m]	37398	66653	56325	49162
	[Kips/in]	214	381	322	281

K'_v = uncracked shear stiffness

$K_{v,45}$ = cracked shear stiffness

K_{VM} = elastic measured shear stiffness

Table 6-24 Post Yield Measured and Calculated Shear Stiffness Using Priestley's Method

		Specimen			
	[Units]	**ISH1.0**	**ISH1.25**	**ISH1.5**	**ISH1.5T**
K_{ps}	[kN/m]	847	2274	2315	1209
	[Kips/in]	4.8	13.0	13.2	6.9
K_{psM}	[kN/m]	3146	4225	3590	3771
	[Kips/in]	18.0	24.1	20.5	21.5

K'_v = uncracked shear stiffness

K_{ps} = post yield shear stiffness

K_{psM} = Measured post yield shear stiffness

Table 7-1 Horizontal Strain from Transducers (H1, H2, H3) Specimen ISH1.0

Run No	Lateral Force		Horizontal Strain		
	[kN]	[Kips]	H1	H2	H3
1	-31.2	-7.0	0.00004	0.0001	0.0002
2	-59.6	-13.4	0.0001	0.0001	0.0002
3	-117.8	-26.5	0.0002	0.0001	0.0003
4	-145.8	-32.8	0.0007	0.0001	0.0006
5	-191.5	-43.1	0.0015	0.0006	0.0013
6	-220.3	-49.5	0.0020	0.0015	0.0020
7	-229.1	-51.5	0.0024	0.0019	0.0024
8	-236.6	-53.2	0.0026	0.0021	0.0026
9	-241.3	-54.2	0.0028	0.0025	0.0030
10	-195.1	-43.9	0.0030	0.0025	0.0032

Table 7-2 Horizontal Strain from Transducers (H1, H2, H3) Specimen ISH1.25

Run No	Lateral Force		Horizontal Strain		
	[kN]	[Kips]	H1	H2	H3
1	-23.5	-5.3	0.000004	0.000004	0.000004
2	-49.9	-11.2	0.000004	0.000004	0.000023
3	-144.7	-32.5	0.0001	0.0001	0.0001
4	-190.7	-42.9	0.0002	0.0001	0.0002
5	-217.9	-49.0	0.0006	0.0002	0.0000
6	-226.0	-50.8	0.0007	0.0000	0.0003
7	-235.1	-52.9	0.0009	0.0000	0.0004
8	-242.2	-54.5	0.0011	0.0002	0.0006
9	-250.5	-56.3	0.0013	0.0003	0.0008
10	-251.2	-56.5	0.0015	0.0004	0.0011
11	-247.8	-55.7	0.0019	0.0006	0.0021
12	-193.0	-43.4	0.0021	0.0009	0.0034

Table 7-3 Horizontal Strain from Transducers (H1, H2, H3) Specimen ISH1.5

Run No	Lateral Force		Horizontal Strain		
	[kN]	[Kips]	H1	H2	H3
1	-45.0	-10.1	0.00001	0.00001	0.00001
2	-85.5	-19.2	0.0001	0.00004	0.000003
3	-144.3	-32.4	0.0004	0.0001	0.0001
4	-168.5	-37.9	0.0008	0.0004	0.0002
5	-176.6	-39.7	0.0010	0.0005	0.0003
6	-207.1	-46.6	0.0013	0.0005	0.0006
7	-217.5	-48.9	0.0014	0.0004	0.0010
8	-237.5	-53.4	0.0015	0.0002	0.0015
9	-243.4	-54.7	0.0016	0.0000	0.0018
10	-247.1	-55.6	0.0018	0.0003	0.0020
11	-252.6	-56.8	0.0021	0.0006	0.0024
12	-238.9	-53.7	0.0024	0.0008	0.0024
13	-196.5	-44.2	0.0027	0.0012	0.0028

Table 7-4 Horizontal Strain from Transducers (H1, H2, H3) Specimen ISH1.5T

Run No	Lateral Force		Horizontal Strain		
	[kN]	[Kips]	H1	H2	H3
1	-31.6	-7.1	0.00005	0.00005	0.000003
2	-69.7	-15.7	0.0001	0.00001	0.000055
3	-120.0	-27.0	0.0000	0.0000	0.0002
4	-153.3	-34.5	0.0001	0.0001	0.0002
5	-167.8	-37.7	0.0001	0.0001	0.0002
6	-210.0	-47.2	0.0004	0.0001	0.0008
7	-236.4	-53.1	0.0006	0.0000	0.0003
8	-246.7	-55.5	0.0007	0.0002	0.0001
9	-250.4	-56.3	0.0007	0.0003	0.0001
10	-251.2	-56.5	0.0009	0.0004	0.0003
11	-247.0	-55.5	0.0009	0.0004	0.0004
12	-242.8	-54.6	0.0010	0.0006	0.0005
13	-238.5	-53.6	0.0012	0.0006	0.0005
14	-239.1	-53.8	0.0012	0.0006	0.0006
15	-229.3	-51.6	0.0012	0.0007	0.0007

Table 7-5 Diagonal Strain from Transducers (D1, D2, D3, D4) Specimen ISH1.0

Run No	Lateral Force		Diagonal Strain			
	[kN]	[Kips]	D1	D2	D3	D4
1	-31.2	-7.0	-0.0003	-0.00001	-0.0001	-0.0002
2	-59.6	-13.4	-0.0004	-0.0005	-0.0001	-0.0001
3	-117.8	-26.5	-0.0008	-0.0007	-0.0003	-0.0002
4	-145.8	-32.8	-0.0010	-0.0006	-0.0002	-0.0004
5	-191.5	-43.1	-0.0016	-0.0006	-0.0001	-0.0008
6	-220.3	-49.5	-0.0025	-0.0005	-0.0003	-0.0017
7	-229.1	-51.5	-0.0036	-0.0004	-0.0004	-0.0029
8	-236.6	-53.2	-0.0052	-0.0005	-0.0003	-0.0042
9	-241.3	-54.2	-0.0078	-0.0005	-0.0003	-0.0061
10	-195.1	-43.9	-0.0145	-0.0007	-0.0003	-0.0073

Table 7-6 Relevant Details of Two Columns with a Two-Way Hinge and Circular Column Priestley Study

	THD1	THD2	COL1
Diameter	406 mm (16 in)	406 mm (16 in)	696 mm (24 in)
Height	1219 mm (48 in)	1625 mm (64 in)	1829 mm (72 in)
Cover to Main Rebar	33.34 mm (1.312 in)	33.34 mm (1.312 in)	20 mm (0.8 in)
Longitudinal Steel	Grade 60 14- 22.2 mm ϕ (#7)	Grade 60 13-22.2 mm ϕ (#7)	Grade 60 12-12.7 mm ϕ (#4)
Transversal Steel	Grade 60 Spiral 9.5 mm ϕ (#3) @ 38.1 mm (1.5 in)	Grade 60 Spiral 9.5 mm ϕ (#3) @ 38.1 mm (1.5 in)	Grade 40 Spiral 6.35 mm ϕ (#2) @ 76.4 mm (3 in)
f'_c	53.2 MPa (7720 psi)	40.7 MPa (5910 psi)	30 MPa (4350 psi)
f_{yh} (spirals)	551.6 MPa (80 ksi)	551.6 MPa (80 ksi)	361 MPa (52.3 ksi)
f_{yl} (rebars)	427.5 MPa (62 ksi)	427.5 MPa (62 ksi)	462 MPa (67 ksi)

Table 7-7 Experimental Post Yield Stiffness, K_{vpye} with the Corresponding β_P.

	Units	THD1	THD2	COL1	ISH1.0	ISH1.25	ISH1.5	ISH1.5T
K_{vpye}	[kN/m]	9649	11716	4396	3146	4225	3842	3771
	[Kips/in]	55.1	66.9	25.1	18	24.1	21.9	21.5
β_P		0.187	0.307	0.242	0.350	0.304	0.375	0.254

Table 7-8 Diagonal Strain from Transducers (D1, D2, D3, D4) Specimen ISH1.25

Run No	Lateral Force		Diagonal Strain			
	[kN]	[Kips]	D1	D2	D3	D4
1	-23.5	-5.3	0.0001	0.000003	0.000005	0.000005
2	-49.9	-11.2	0.0002	0.00002	0.00001	0.00001
3	-144.7	-32.5	0.0015	0.00001	0.00004	0.0008
4	-190.7	-42.9	0.0028	0.0004	0.00004	0.0016
5	-217.9	-49.0	0.0046	0.00060	0.0001	0.0027
6	-226.0	-50.8	0.0055	0.00065	0.0004	0.0035
7	-235.1	-52.9	0.0065	0.00072	0.0005	0.0042
8	-242.2	-54.5	0.0082	0.00083	0.0006	0.0054
9	-250.5	-56.3	0.0110	0.00094	0.0008	0.0076
10	-251.2	-56.5	0.0120	0.00104	0.0010	0.0087
11	-247.8	-55.7	0.0151	0.00121	0.0014	0.0110
12	-193.0	-43.4	0.0189	0.00128	0.0019	0.0157

Table 7-9 Diagonal Strain from Transducers (D1, D2, D3, D4) Specimen ISH1.5

Run No	Lateral Force		Diagonal Strain			
	[kN]	[Kips]	D1	D2	D3	D4
1	-45.0	-10.1	0.0004	0.000005	0.00012	0.00016
2	-85.5	-19.2	0.0008	0.00005	0.00022	0.00040
3	-144.3	-32.4	0.0024	0.00051	0.00023	0.00093
4	-168.5	-37.9	0.0037	0.00105	0.00003	0.00141
5	-176.6	-39.7	0.0042	0.00132	0.00006	0.00171
6	-207.1	-46.6	0.0066	0.00180	0.00036	0.00250
7	-217.5	-48.9	0.0086	0.00213	0.00089	0.00333
8	-237.5	-53.4	0.0125	0.00252	0.00138	0.00568
9	-243.4	-54.7	0.0157	0.00271	0.00175	0.00798
10	-247.1	-55.6	0.0179	0.00287	0.00215	0.00968
11	-252.6	-56.8	0.0208	0.00320	0.00243	0.01209
12	-238.9	-53.7	0.0200	0.00323	0.00242	0.01139
13	-196.5	-44.2	0.0235	0.00330	0.00266	0.01329

Table 7-10 Diagonal Strain from Transducers (D1, D2, D3, D4) Specimen ISH1.5T

Run No	Lateral Force		Diagonal Strain			
	[kN]	[Kips]	D1	D2	D3	D4
1	-31.6	-7.1	0.0001	0.000010	0.00005	0.00005
2	-69.7	-15.7	0.0004	0.00001	0.00006	0.00011
3	-120.0	-27.0	0.0012	0.00008	0.00002	0.00025
4	-153.3	-34.5	0.0019	0.00037	0.00000	0.00055
5	-167.8	-37.7	0.0024	0.00053	0.00006	0.00075
6	-210.0	-47.2	0.0042	0.00085	0.00000	0.00123
7	-236.4	-53.1	0.0071	0.00110	0.00040	0.00286
8	-246.7	-55.5	0.0096	0.00127	0.00060	0.00440
9	-250.4	-56.3	0.0125	0.00122	0.00071	0.00630
10	-251.2	-56.5	0.0147	0.00123	0.00083	0.00795
11	-247.0	-55.5	0.0159	0.00123	0.00097	0.00870
12	-242.8	-54.6	0.0169	0.00127	0.00099	0.00928
13	-238.5	-53.6	0.0180	0.00130	0.00100	0.00996
14	-239.1	-53.8	0.0195	0.00136	0.00100	0.01110
15	-229.3	-51.6	0.0219	0.00137	0.00110	0.01287

Table 7-11 Comparison between Measured Shear Stiffness, Proposed and Existing Shear Stiffness Model

		ISH1.0	ISH1.25	ISH1.5	ISH1.5T
K_{VM}	[kN/m]	37398	66653	56325	49162
	[Kips/in]	214	381	322	281
$K_{v,45}$	[kN/m]	28598	42148	40594	41454
	[Kips/in]	163	241	232	237
	Diff.[%]	-24	-37	-28	-16
K_{VE}	[kN/m]	46467	57583	46887	57165
	[Kips/in]	265	329	268	326
	Diff.[%]	24	-14	-17	16

K_{VM} = measured cracked shear stiffness

$K_{v,45}$ = calculated fully cracked shear stiffness (Park and Paulay)

K_{vE} = calculated shear stiffness (proposed)

Diff. = difference between experimental and analytical results

Table 7-12 Comparison between Measured Post Yield Shear Stiffness, Priestley Post Yield Shear Stiffness and Proposed Post Yield Shear Stiffness

	[Units]	ISH1.0	ISH1.25	ISH1.5	ISH1.5T
K_{psM}	[kN/m]	3146	4225	3590	3771
	[Kips/in]	18.0	24.1	20.5	21.5
K_{ps}	[kN/m]	847	2274	2315	1209
	[Kips/in]	4.8	13.0	13.2	6.9
	Diff.[%]	-73	-46	-36	-68
K_{vpy}	[kN/m]	2745	4121	2905	4336
	[Kips/in]	15.7	23.5	16.6	24.8
	Diff.[%]	-13	-2	-19	15

K_{psM} = Measured post yield shear stiffness

K_{ps} = post yield shear stiffness by Priestley

K_{vpy} = post yield shear stiffness proposed

Diff. = difference between experimental and analytical results

Table 7-13 Effect of the Ultimate Shear Deformation in the Displacement Ductility Capacity

		Specimen			
	[Units]	**ISH1.0**	**ISH1.25**	**ISH1.5**	**ISH1.5T**
Δ_{vPY}	[mm]	61	55	105	90
	[in]	0.35	0.32	0.60	0.5
Δ_u	[mm]	326	359	421	393
	[in]	1.86	2.05	2.41	2.2
Δ_{u+vPY}	[mm]	387	415	526	483
	[in]	2.21	2.37	3.00	2.76
μ_u		3.00	3.65	3.83	3.6
μ_{u+vPY}		3.57	4.21	4.79	4.45

Δ_{vPY} = ultimate shear deformation

Δ_u = ultimate deformation

Δ_{u+vPY} = ultimate deformation including shear deformation

μ_u = displacement ductility capacity without shear deformation

μ_{u+vPY} = displacement ductility capacity with shear deformation

Table 7-14 Material Properties and Relevant Details of the Column Used in the Application Example of the Proposed Shear Stiffness

Diameter	1219 mm (48 in)
Height	2438mm (96 in) to 9144 mm (360 in)
Clear Cover	50.8 mm (2 in)
Longitudinal Steel	Grade 60 28- 31.75 mm ϕ (#10)
Transversal Steel	Grade 60 Spiral 12.7 mm ϕ (#4) @ 63.5 mm (2.5 in)
f'_c	34.5 MPa (5000 psi)
Axial Load	4025.6 kN (905 Kips)

Table 7-15 Material Properties and Relevant Details of the Column Used in the Application Example of the Proposed Shear Stiffness

E_s	199948	Mpa
	29000	ksi
f_c'	34.5	Mpa
	5	ksi
E_c	27789.4	Mpa
	4031	ksi
d	1140	mm
	45	in
b_w	1024	mm
	40.33	in
K'_v	10814274	(kN/mm)/mm
	2431146	(kips/in)xin
A_v	258	mm^2
	0.4	in^2
ρ_v	0.00397	
n	7.20	
$K_{v,45}$	831114	(kN/mm)/mm
	186842	(kips/in)xin
K_p	34858	(kN/mm)/mm
	7836	(kips/in)xin

Table 7-16 Yield and Ultimate Shear Deformation with the Corresponding Force and Stiffness for Different Aspect Ratios

		Aspect Ratio						
	[Units]	**2**	**2.5**	**3**	**3.75**	**5**	**6.25**	**7.5**
Ke	**[kN/mm]**	671	646	623	592	547	508	474
	[kips/in]	3829	3690	3560	3382	3121	2898	2705
F_y	**[kN]**	2254	1803	1502	1202	901	721	601
	[kips]	507	405	338	270	203	162	135
Δ_{vy}	**[mm]**	3.36	2.79	2.41	2.03	1.65	1.42	1.27
	[in]	0.132	0.110	0.095	0.080	0.065	0.056	0.050
Kpy	**[kN/mm]**	29	29	28	27	26	25	24
	[kips/in]	167	163	160	155	148	141	135
ΔF	**[kN]**	179	143	119	95	72	57	48
	[kips]	40	32	27	21	16	13	11
Δ_{vPY}	**[mm]**	8.85	8.27	7.89	7.51	7.13	6.91	6.75
	[in]	0.348	0.326	0.311	0.296	0.281	0.272	0.266

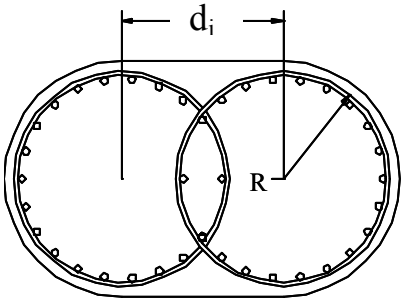

Figure 2-1 Interlocking Spirals Cross Section

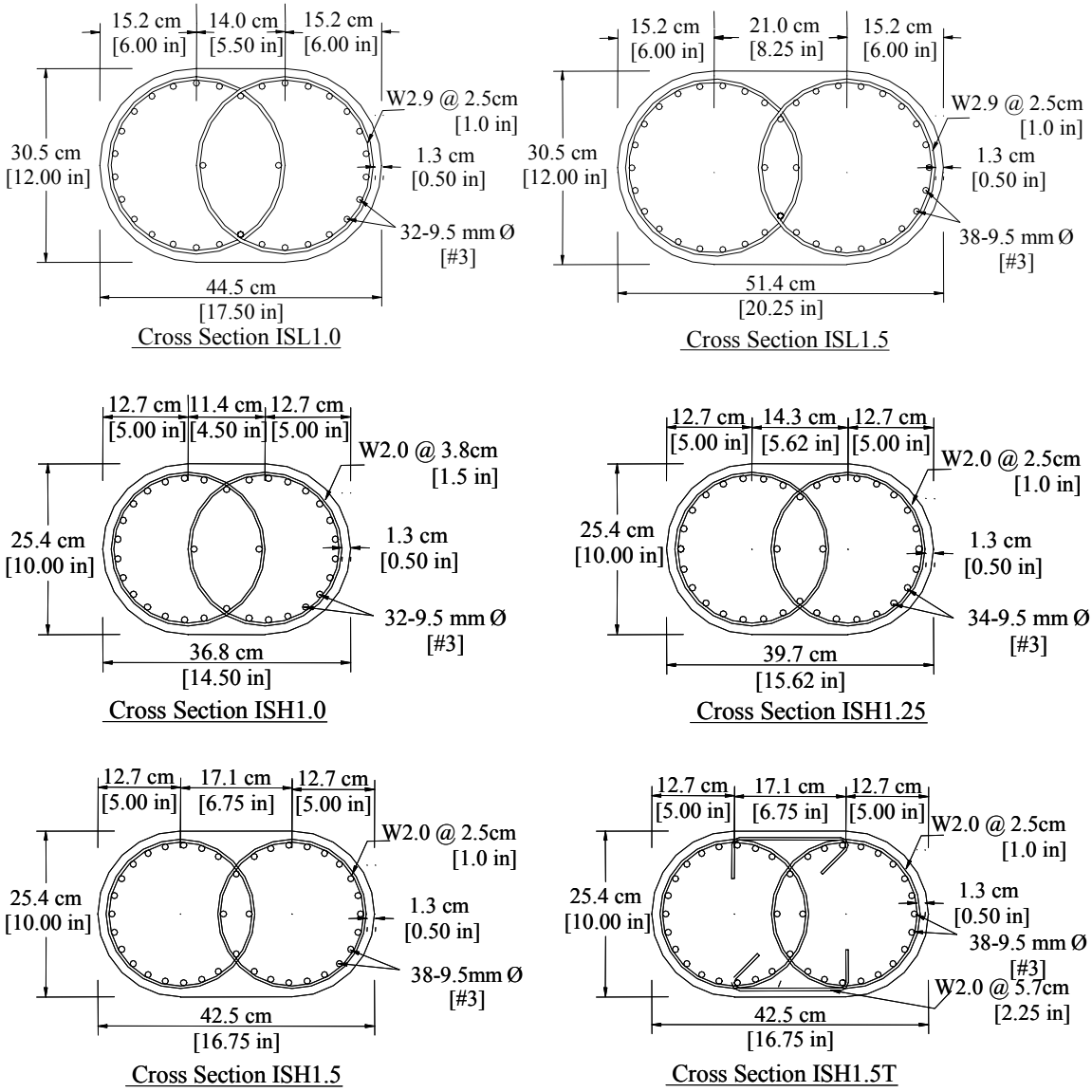

Figure 2-2 Specimens Cross Sections

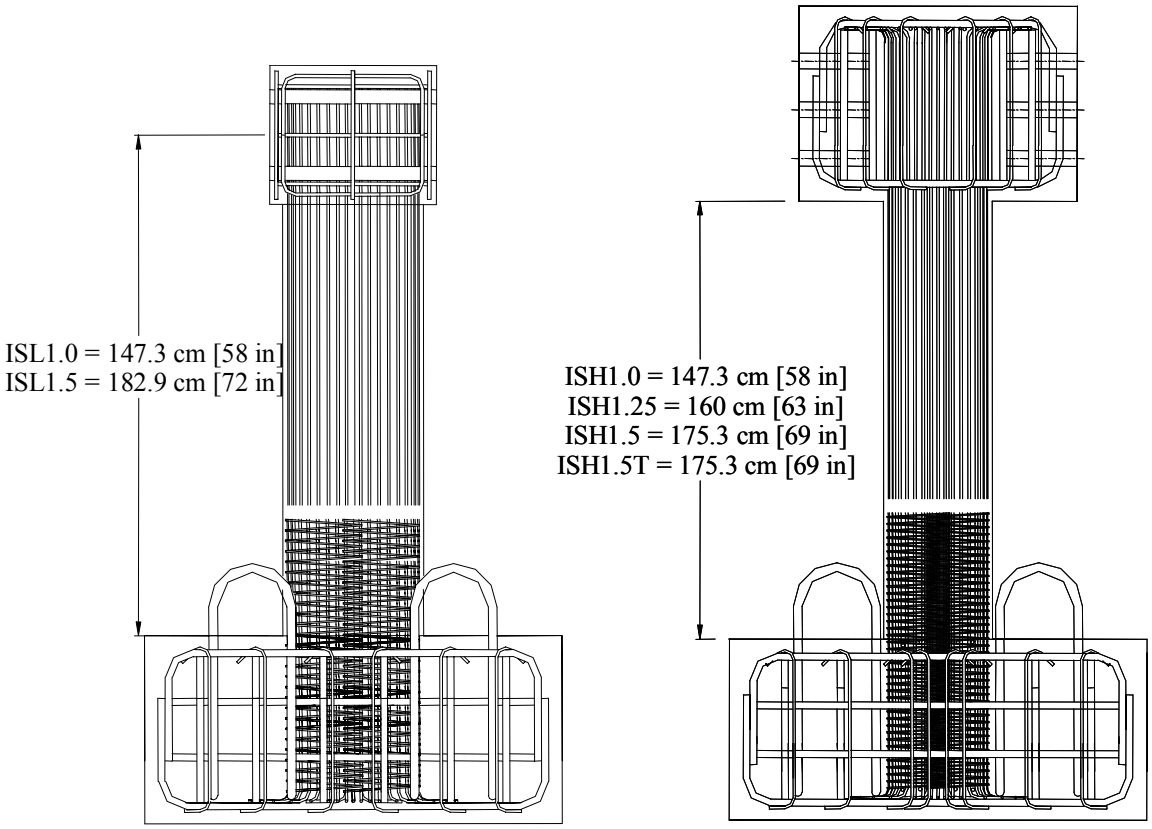

Longitudinal section
ISL1.0 and ISL1.5

Longitudinal section ISH1.0,
ISH1.25, ISH1.5 and ISH1.5T

Figure 2-3 Specimens Elevation

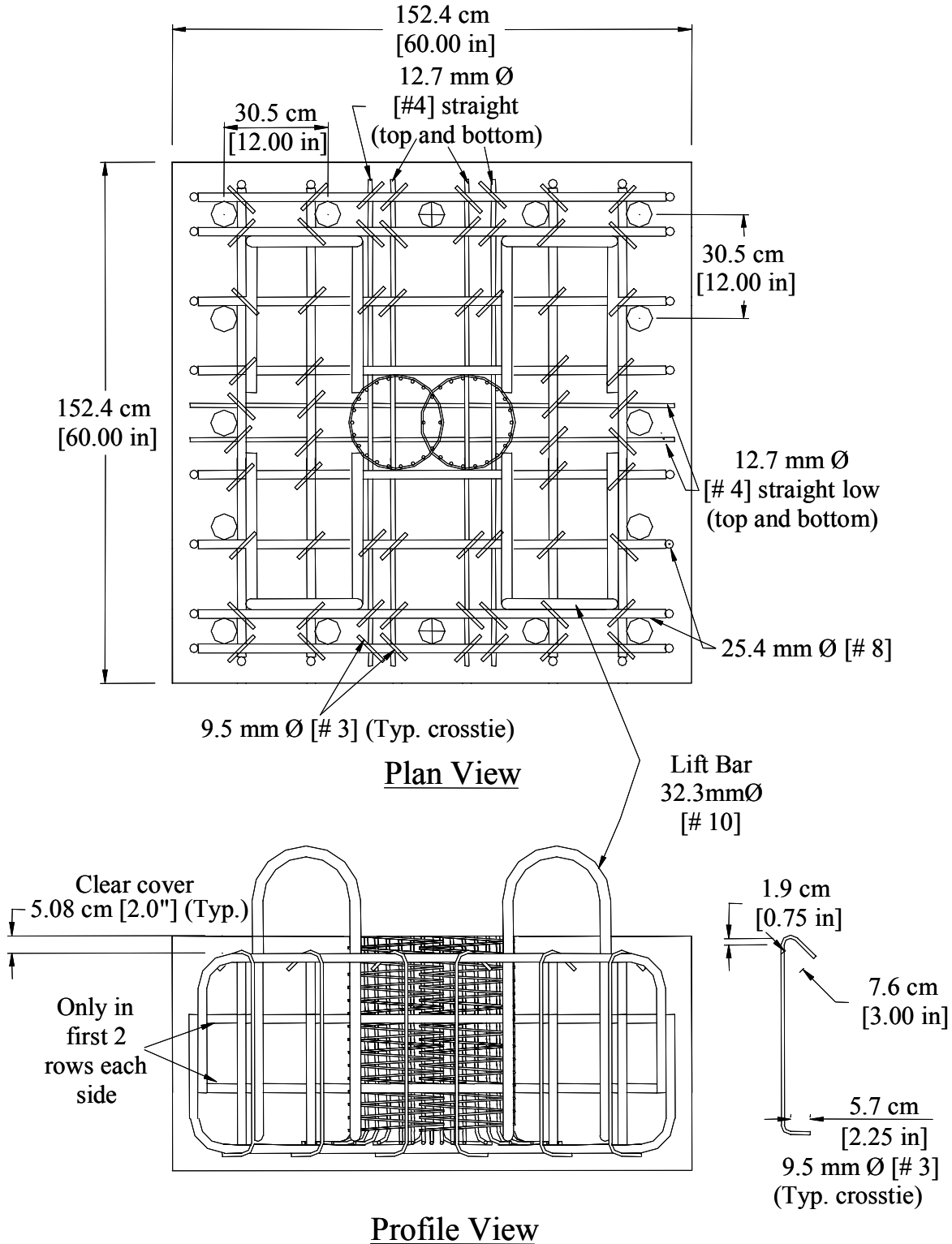

Figure 2-4 Typical Plan and Profile View of the Footing

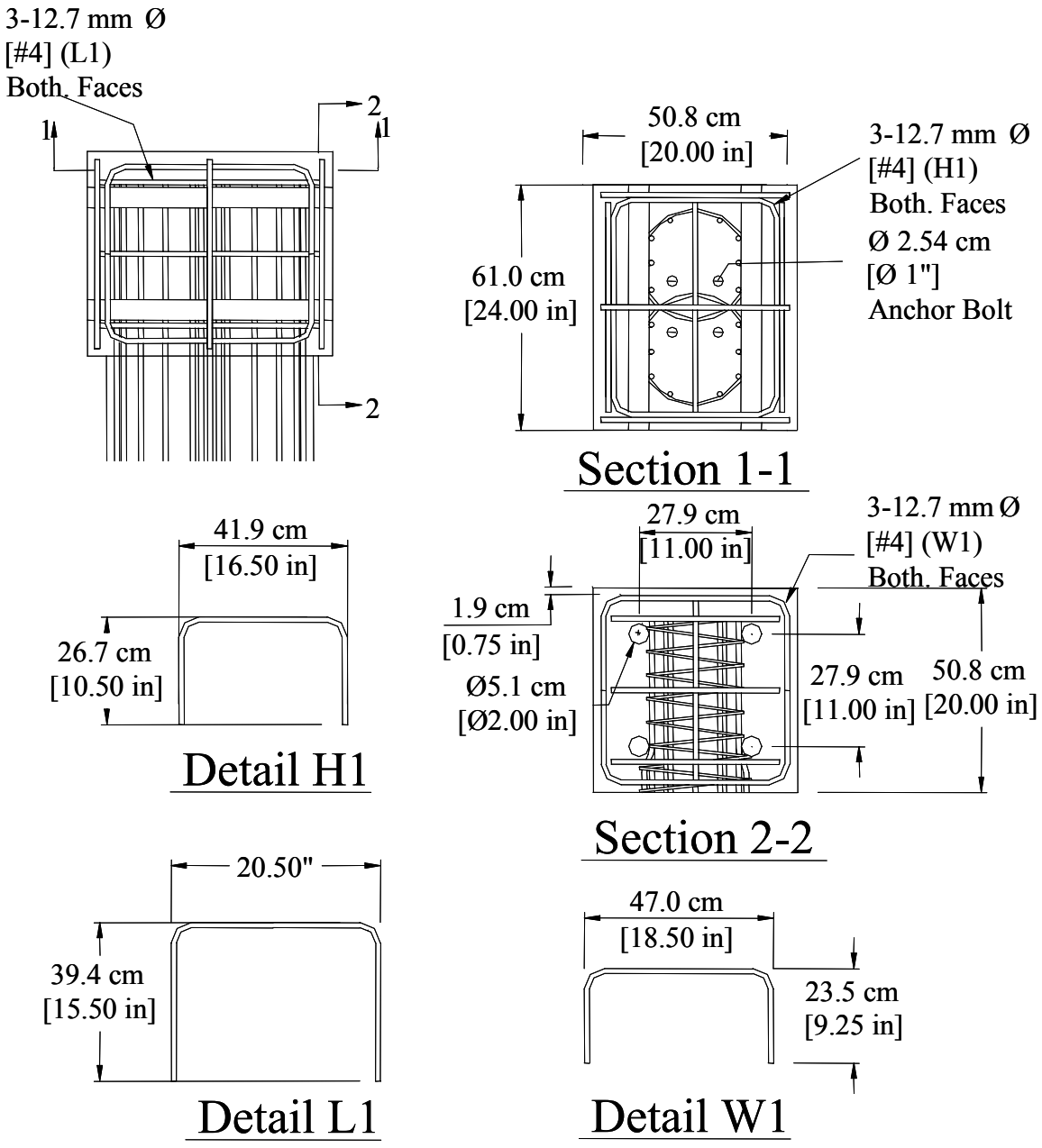

Figure 2-5 Plan and Section View of the Top Specimen Head with Low Shear

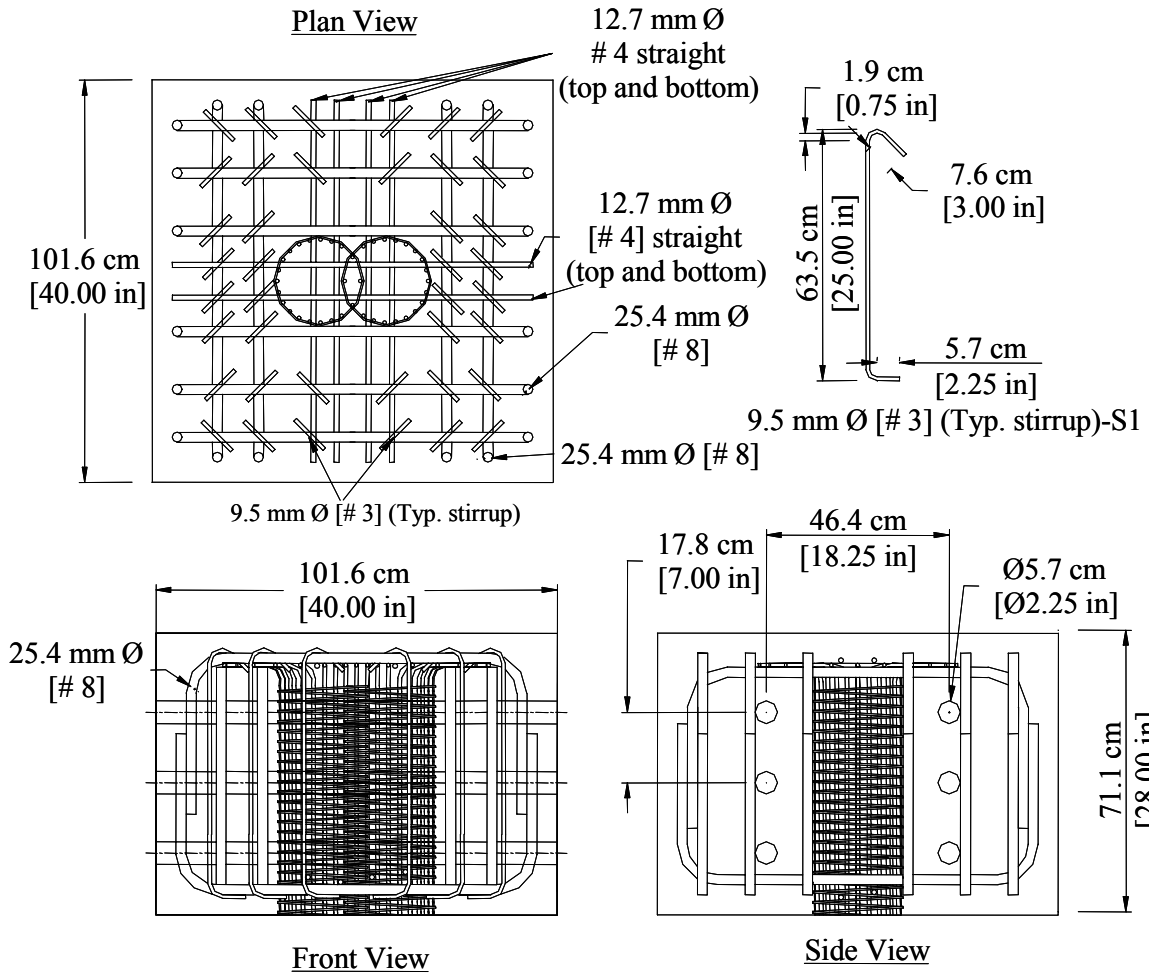

Figure 2-6 Plan and Section View of the Top Specimen Head with High Shear

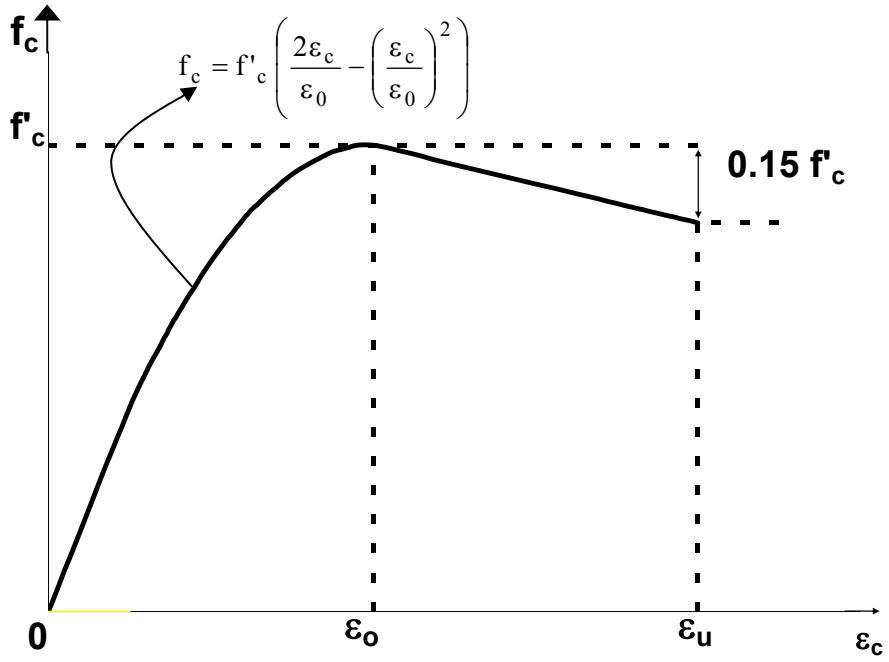

Figure 2-7 The Hognestad Model for Unconfined Concrete

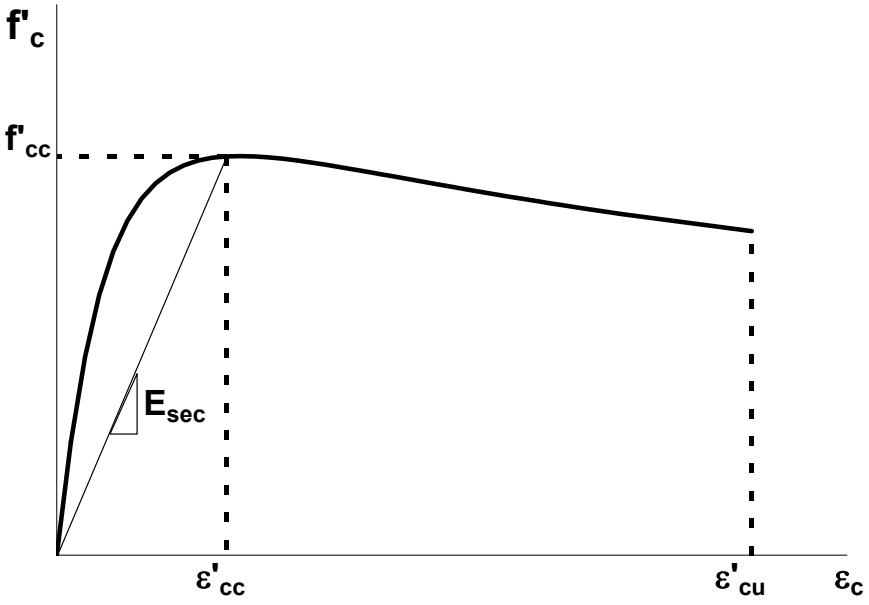

Figure 2-8 The Modified Mander et al Model for Confined Concrete

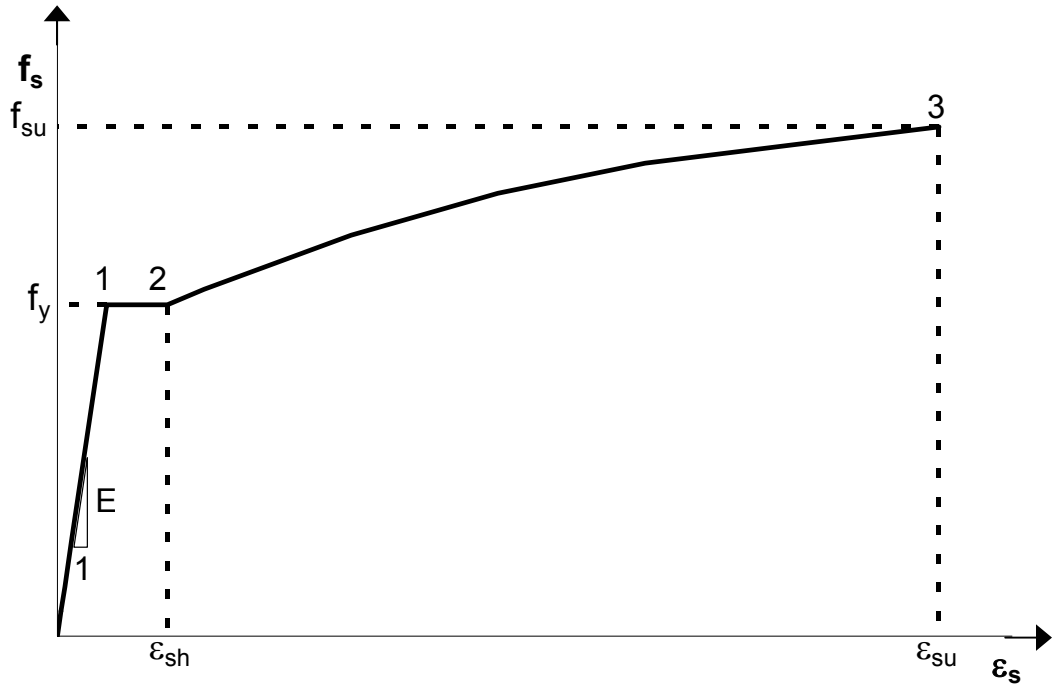

Figure 2-9 The Parabolic Strain Hardening Steel Model

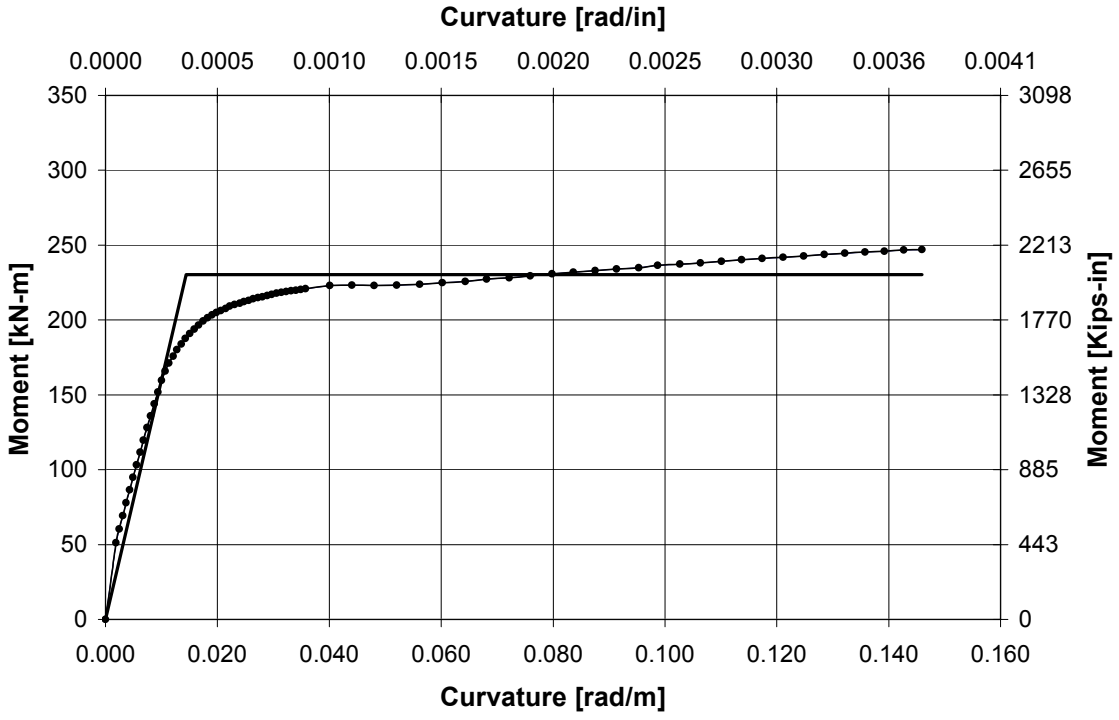

Figure 2-10 M-ϕ Curve Specimen ISL1.0

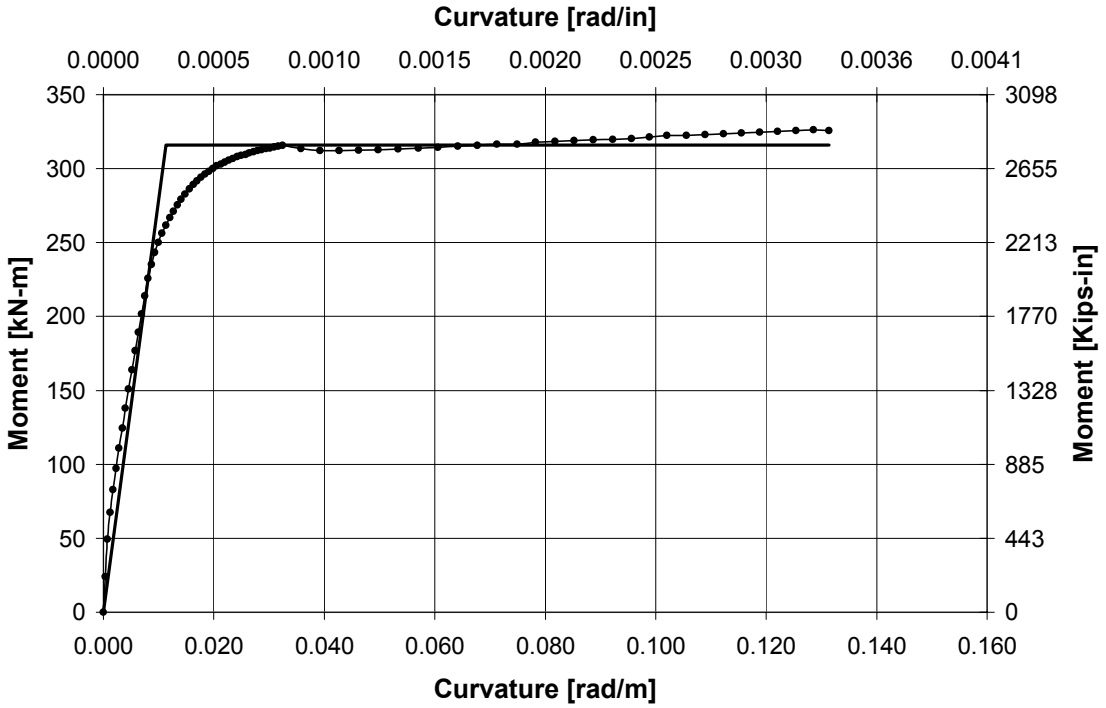

Figure 2-11 M-ϕ Curve Specimen ISL1.5

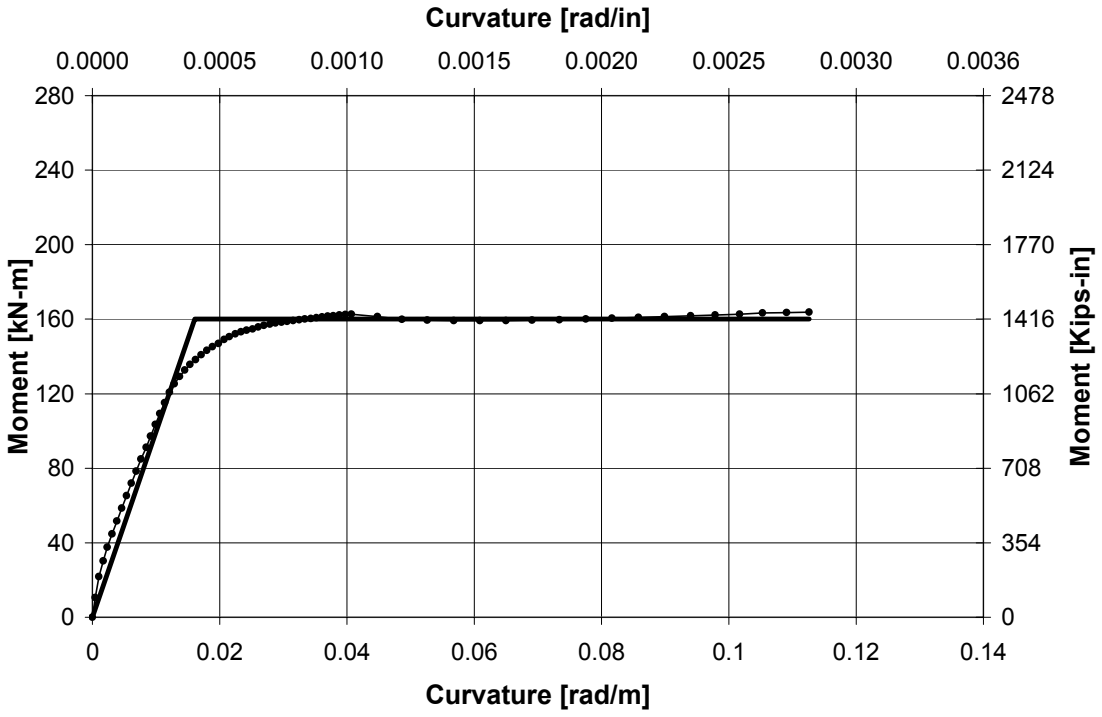

Figure 2-12 M-ϕ Curve Specimen ISH1.0

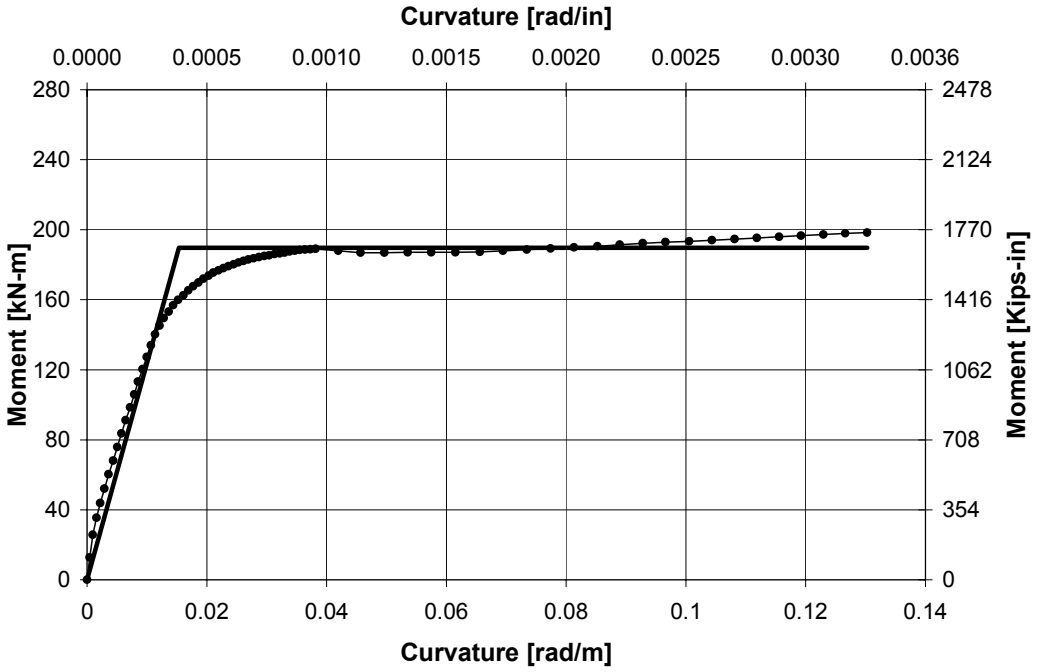

Figure 2-13 M-ϕ Curve Specimen ISH1.25

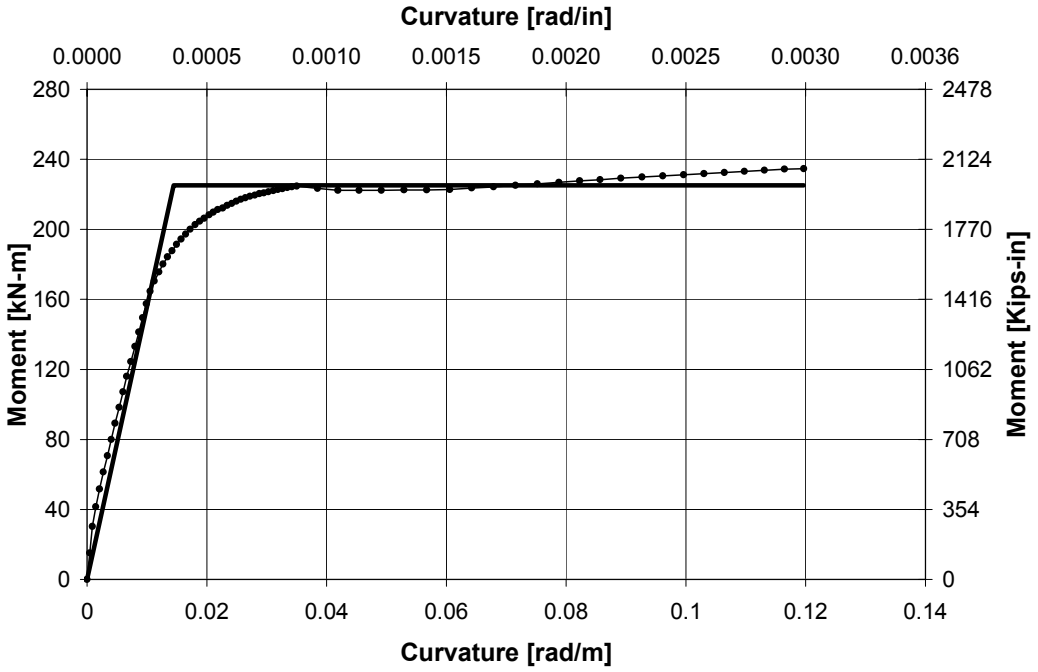

Figure 2-14 M-ϕ Curve Specimen ISH1.5

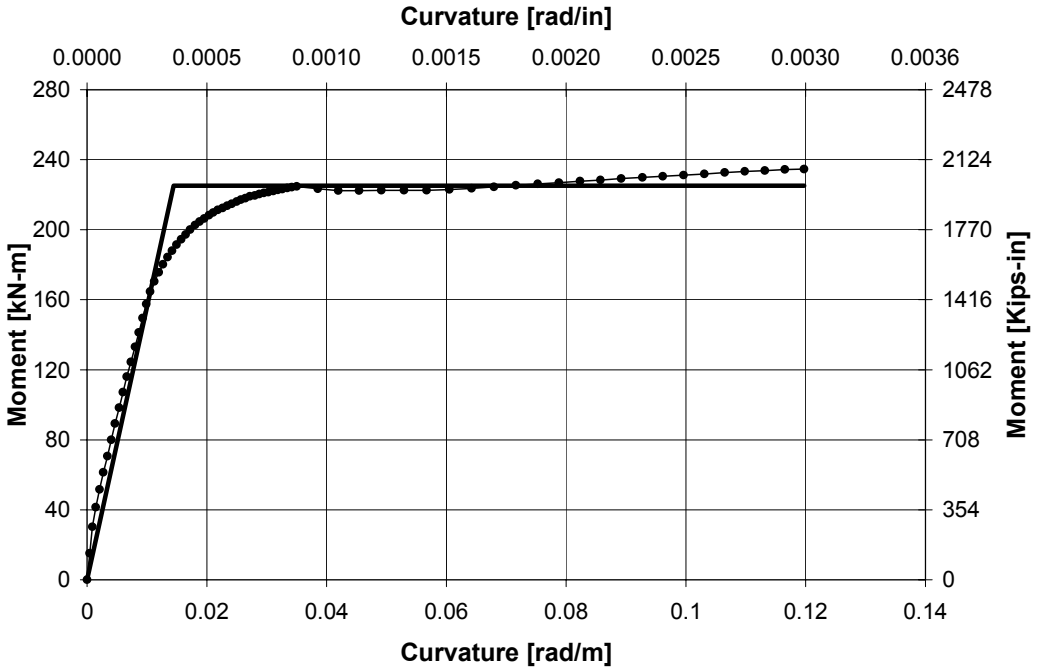

Figure 2-15 M-ϕ Curve Specimen ISH1.5T

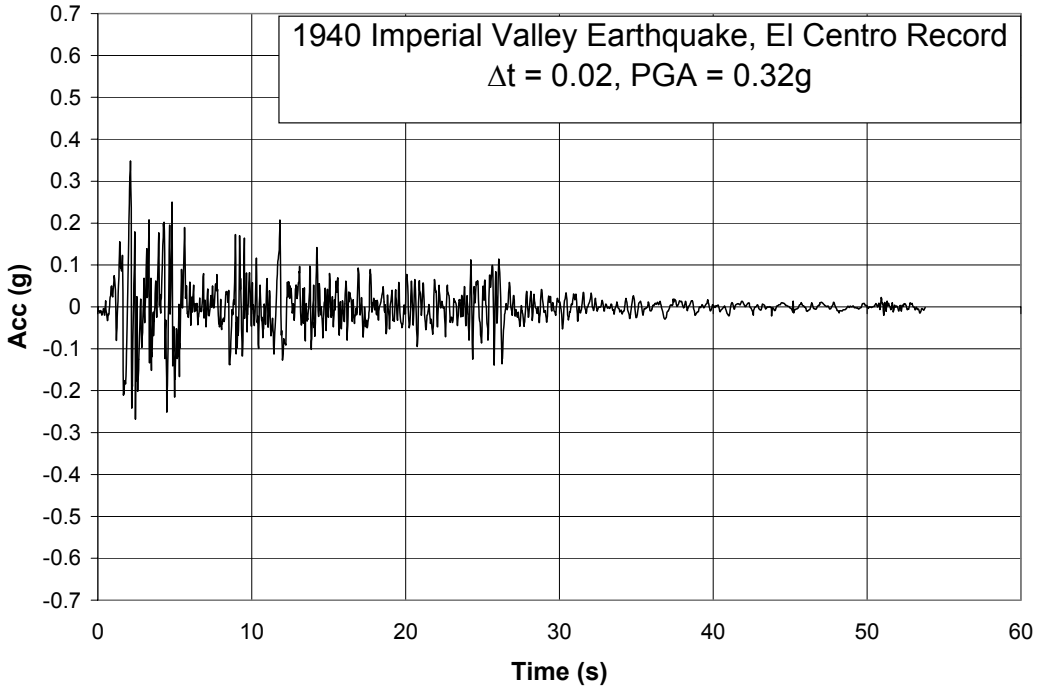

Figure 2-16 El Centro Record

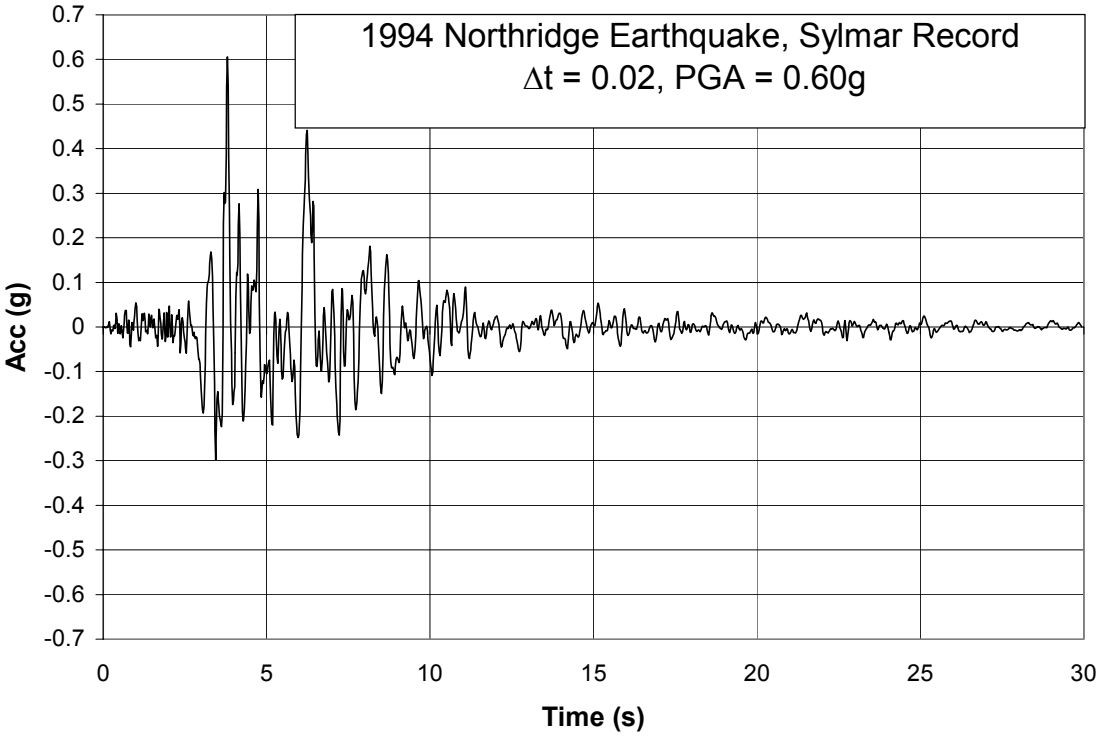

Figure 2-17 Sylmar Record

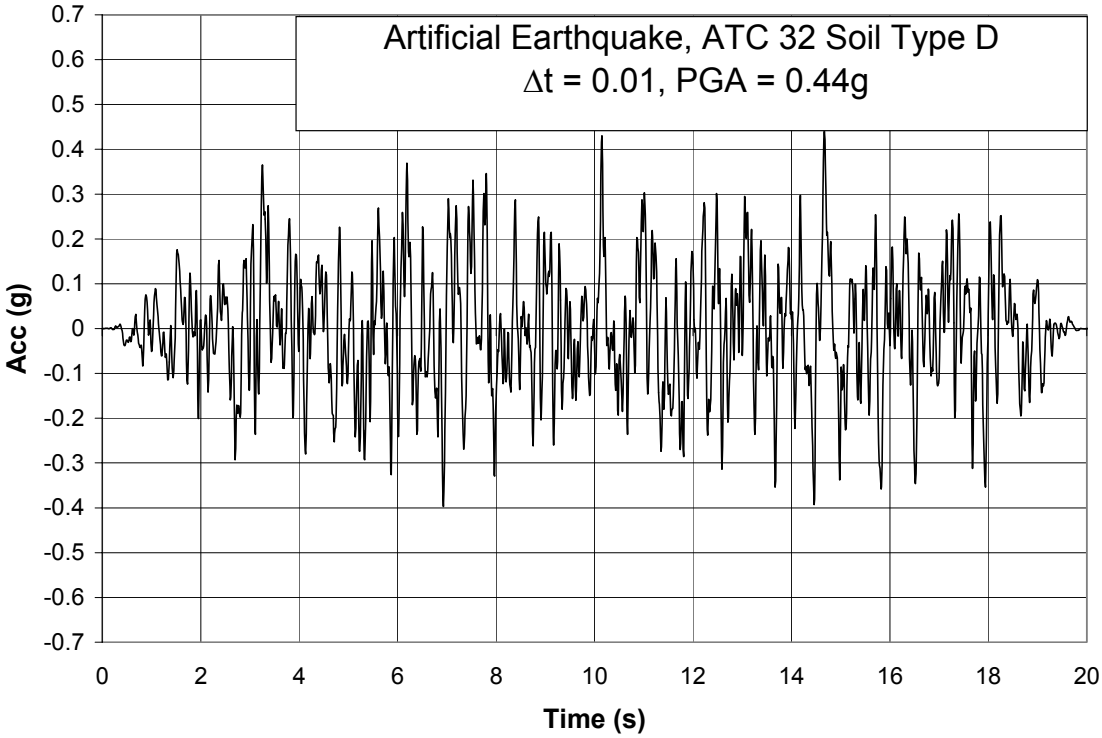

Figure 2-18 ATC 32-D Artificial Earthquake

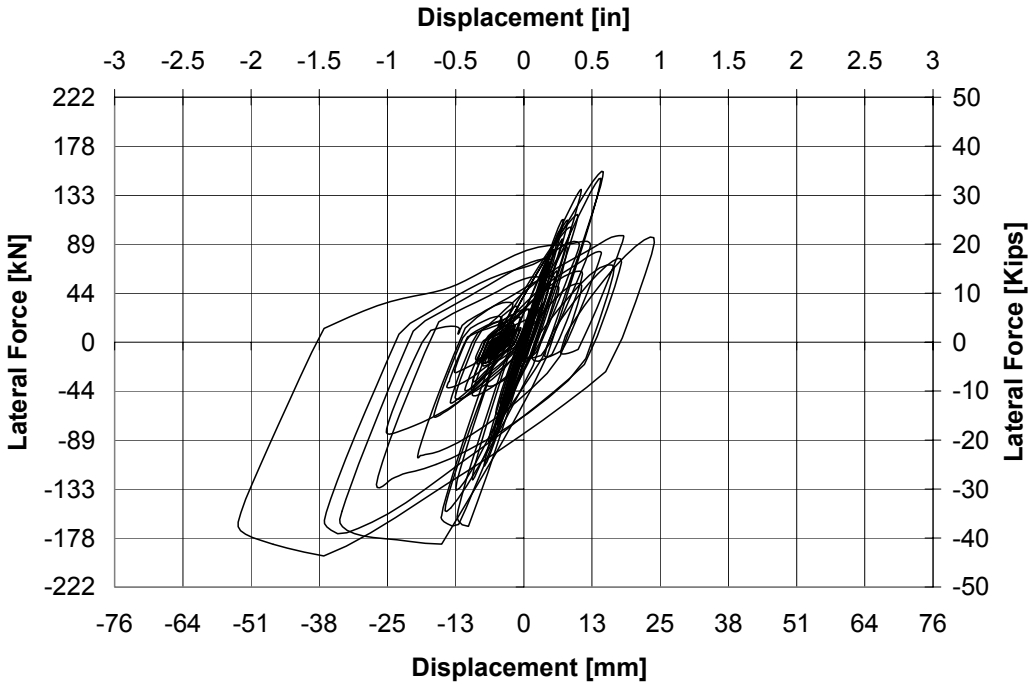

Figure 2-19 RCShake Force Displacement Hysteresis Curve for Sylmar Record Specimen ISL1.0

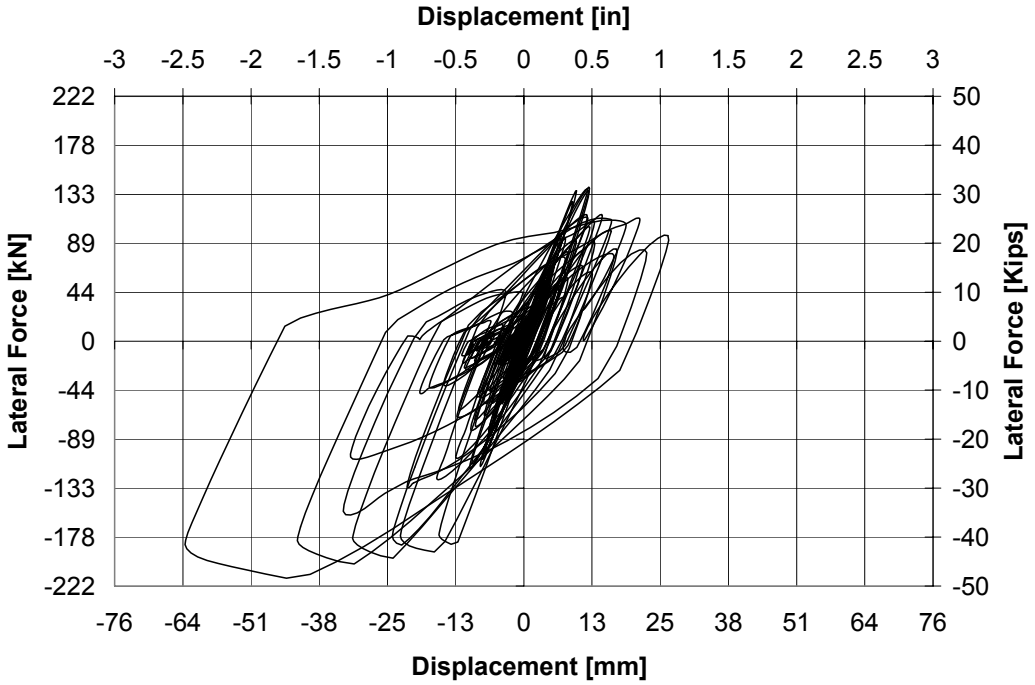

Figure 2-20 RCShake Force Displacement Hysteresis Curve for Sylmar Record Specimen ISL1.5

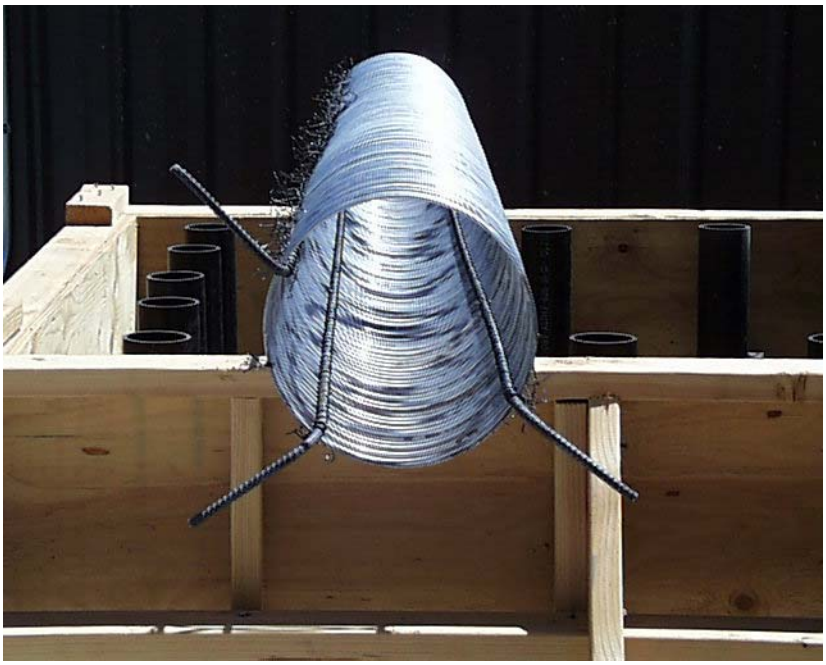

Figure 3-1 Individual Spiral Cage

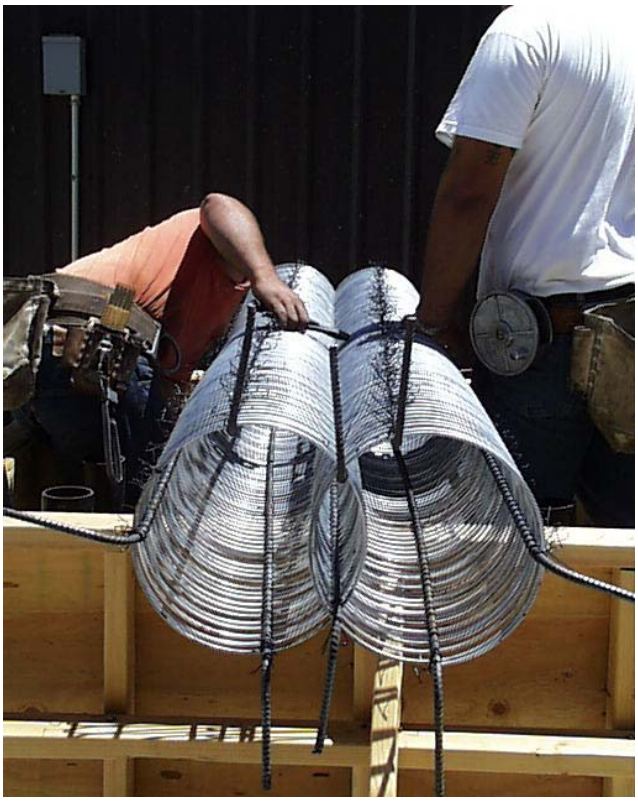

Figure 3-2 Steel Cage of the Column

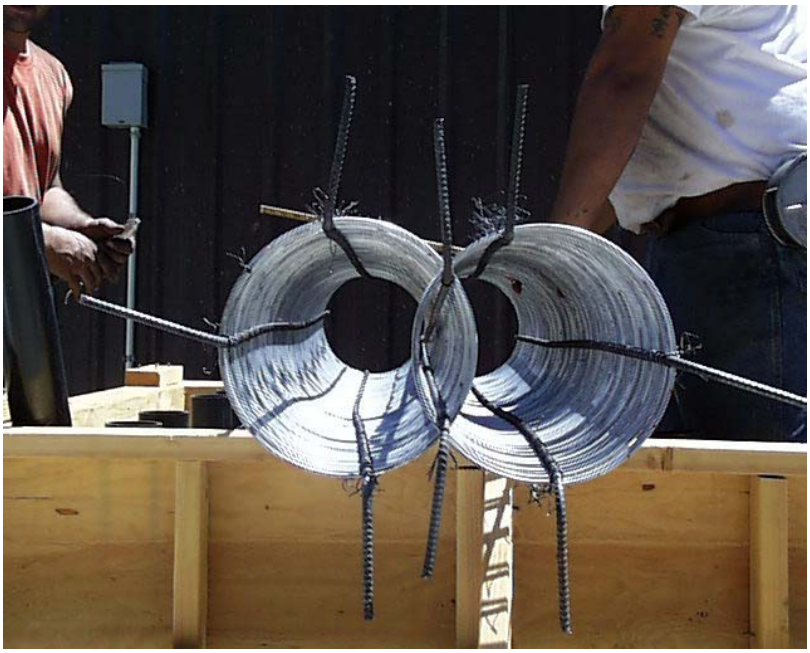

Figure 3-3 Steel Cage of the Column Ready to Strain Gages Installation

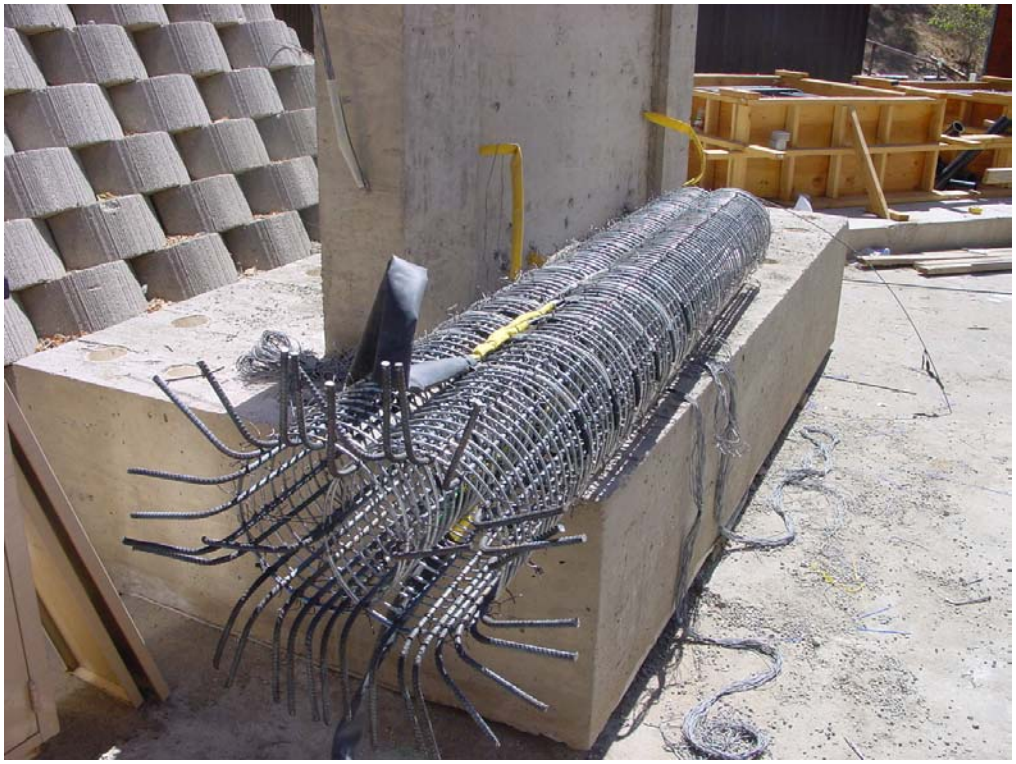

Figure 3-4 Steel Cage of the Column Completed

Figure 3-5 Steel Bottom Mats of the Footing and the PVC Pipes

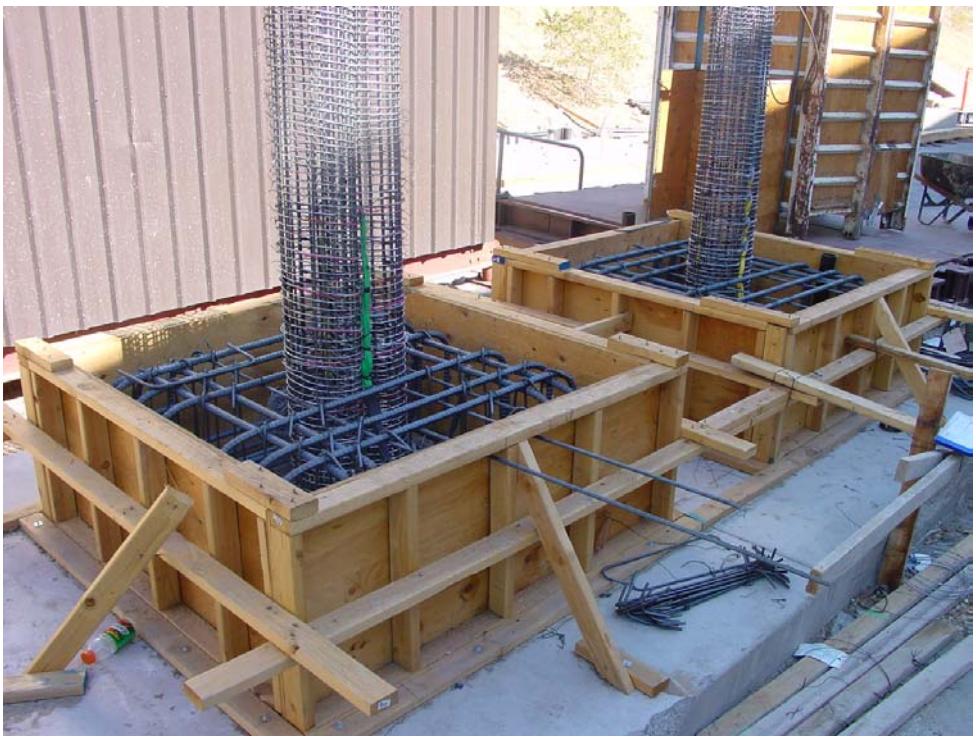

Figure 3-6 Footing Ready for Pouring of Concrete

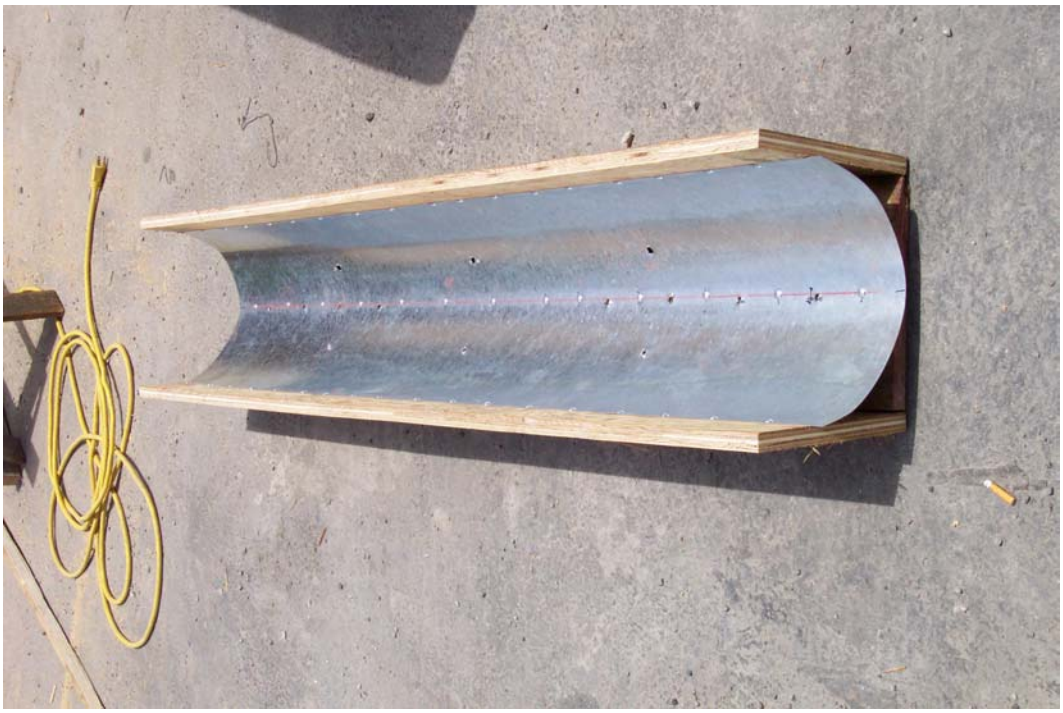

Figure 3-7 Wood and Steel Laminates Used for Column Form

Figure 3-8 Column Form with Lateral Straps

Figure 3-9 Top Specimen Head for Specimens with High Shear

Figure 3-10 Column Form for Specimens with High Shear

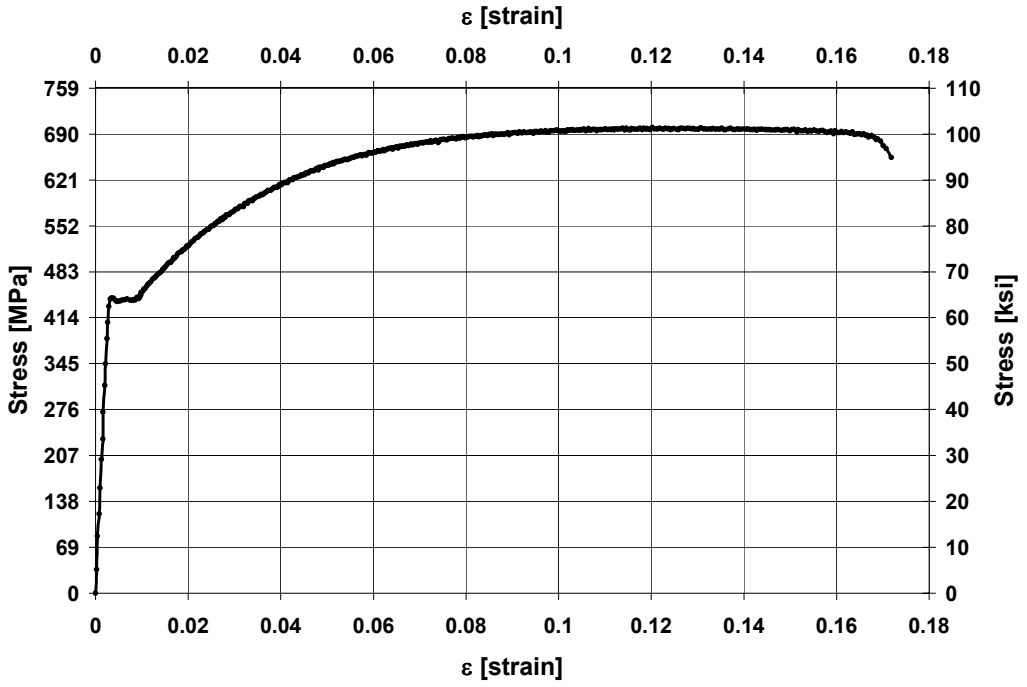

Figure 3-11 Stress-Strains for Typical Sample Test Bar No 3

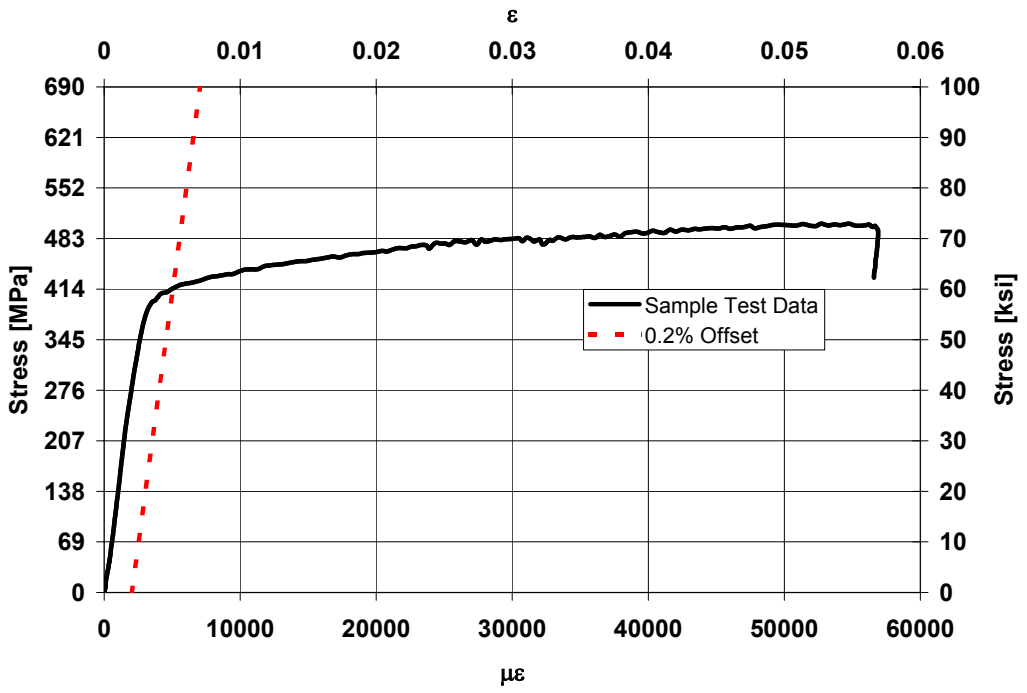

Figure 3-12 Stress-Strains for Typical Sample Test Plain Wire

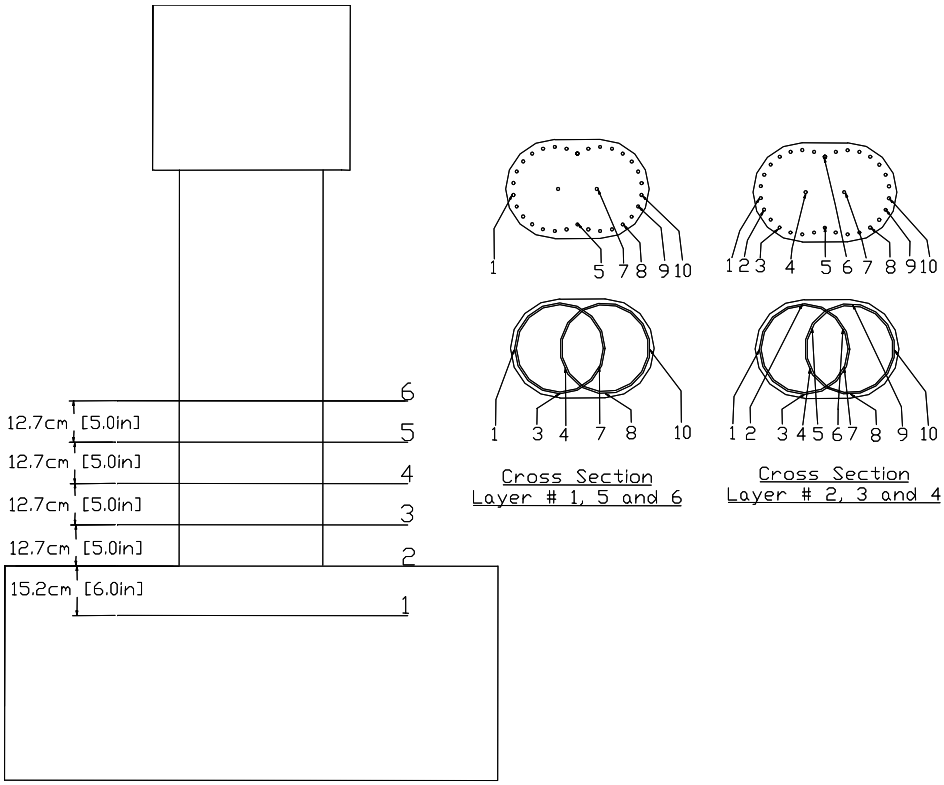

Figure 3-13 Strain Gauge Location Specimens ISL1.0 and ISL1.5

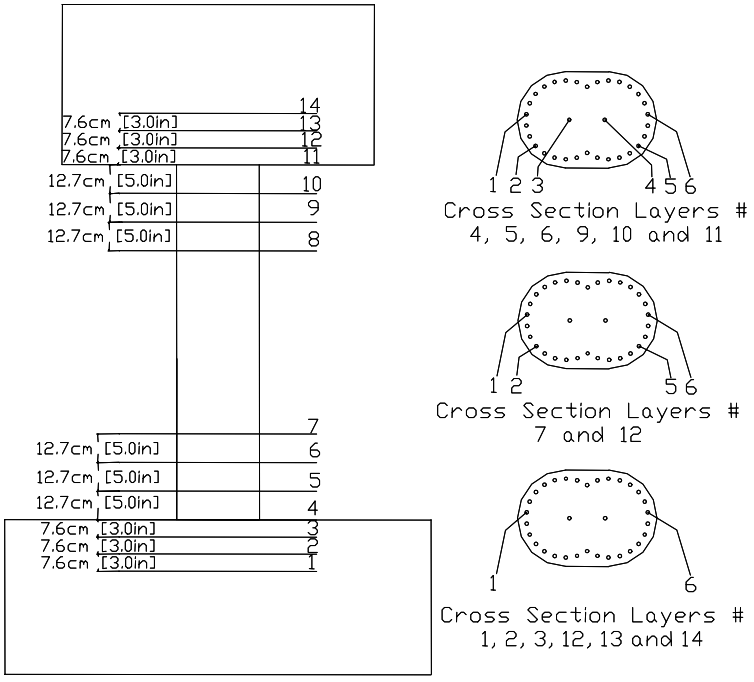

Figure 3-14 Strain Gauge Location in Longitudinal Steel Specimens with High Shear

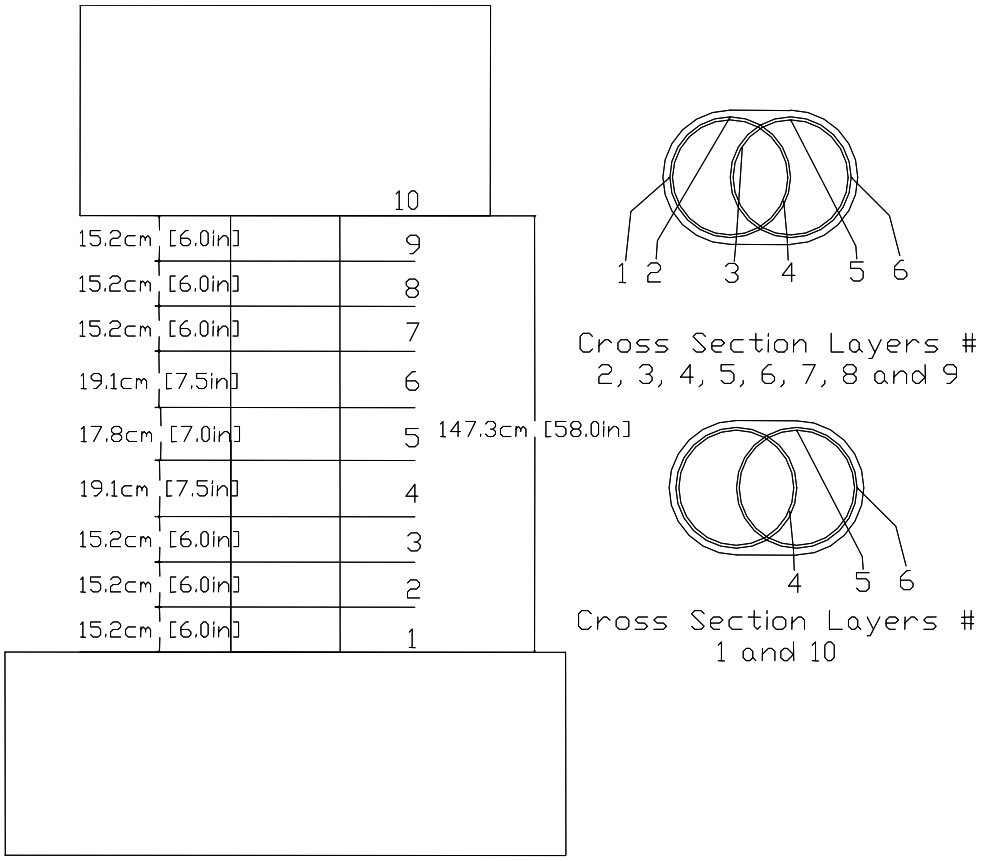

Figure 3-15 Strain Gauge Location in Transverse Steel Specimens ISH1.0

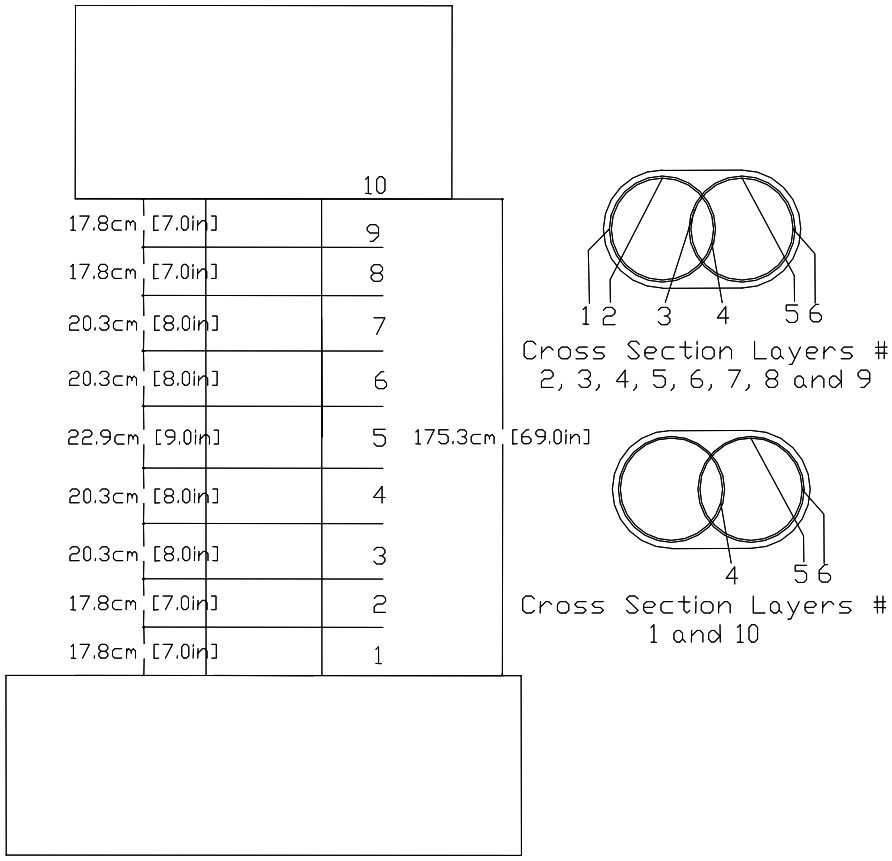

Figure 3-16 Strain Gauge Location in Transverse Steel Specimens ISH1.5

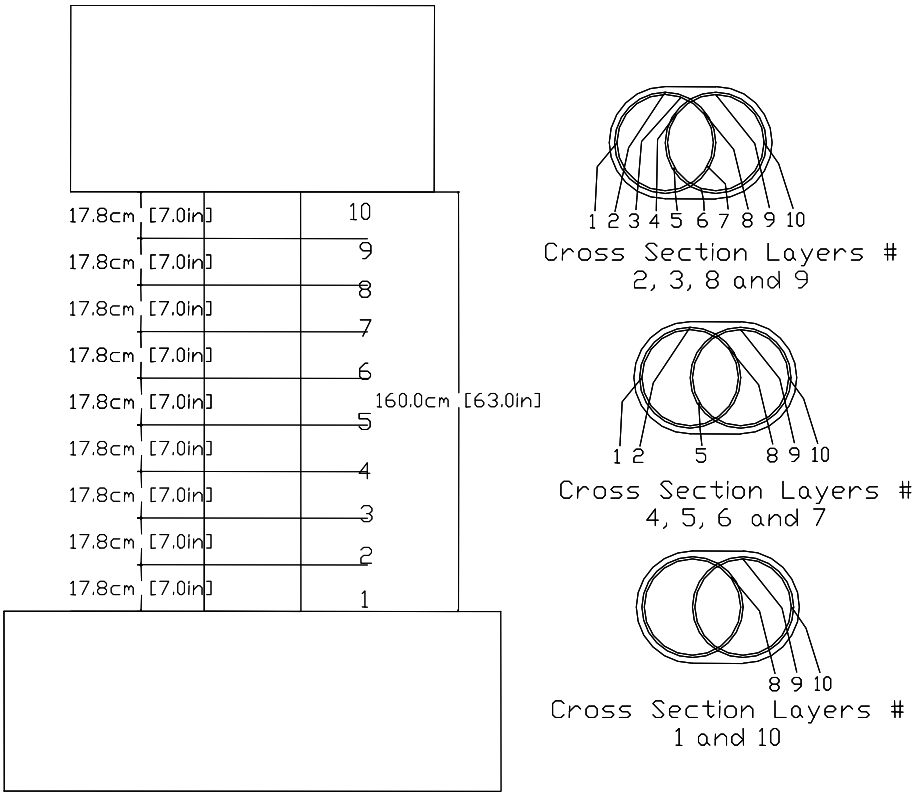

Figure 3-17 Strain Gauge Location in Transverse Steel Specimens ISH1.25

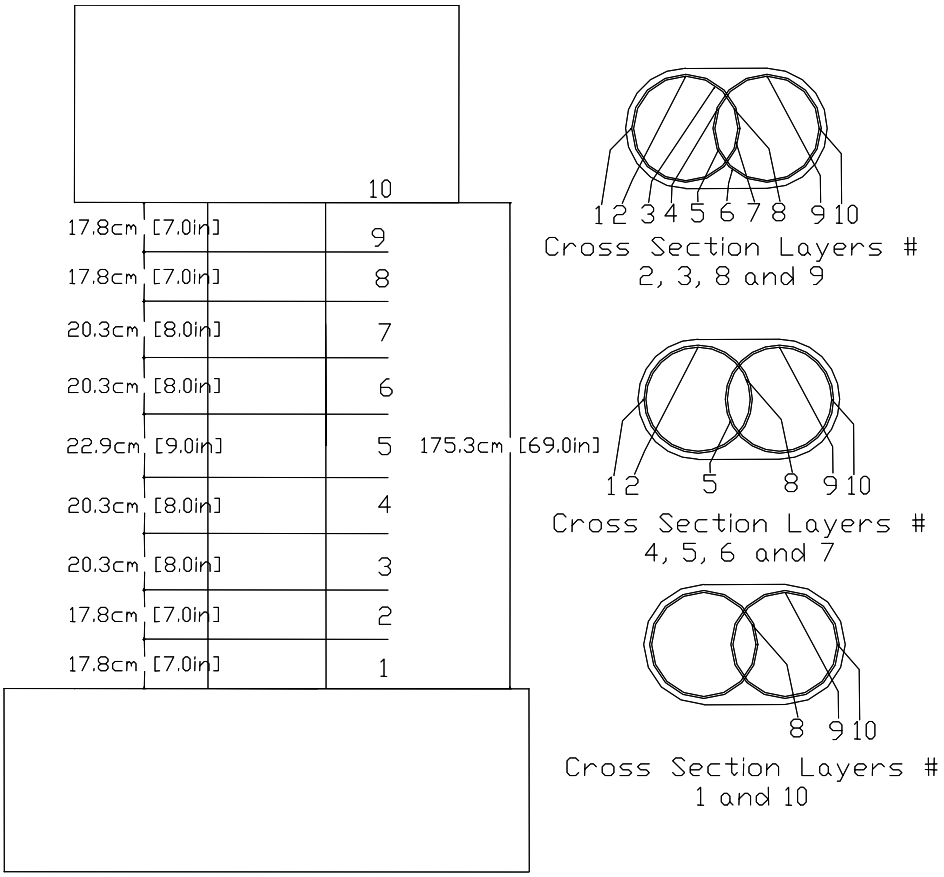

Figure 3-18 Strain Gauge Location in Transverse Steel Specimens ISH1.5T

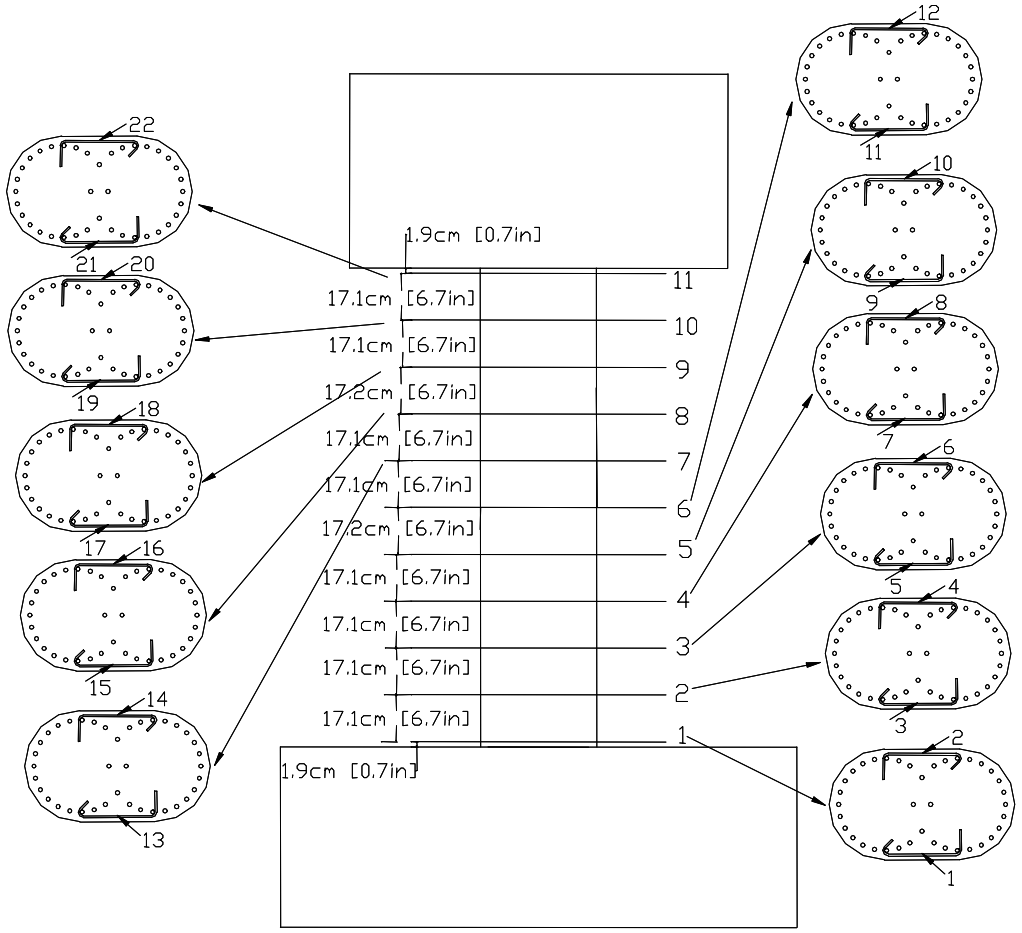

Figure 3-19 Strain Gauge Location in Cross Ties Specimens ISH1.5T

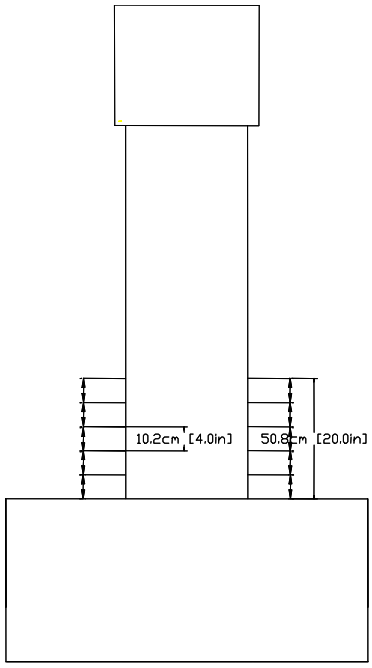

a) Details of Location Curvature Instrumentation

b) Photo of Curvature Instrumentation

Figure 3-20 Curvature Instrumentation Specimens with Low Shear

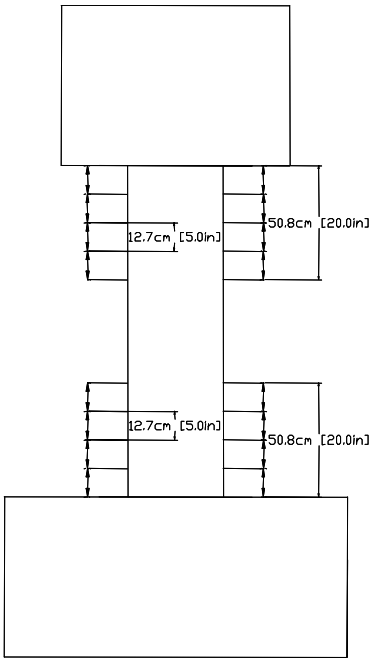

a) Details of Location Curvature Instrumentation

b) Photo of Curvature Instrumentation

Figure 3-21 Curvature Instrumentation Specimens with High Shear

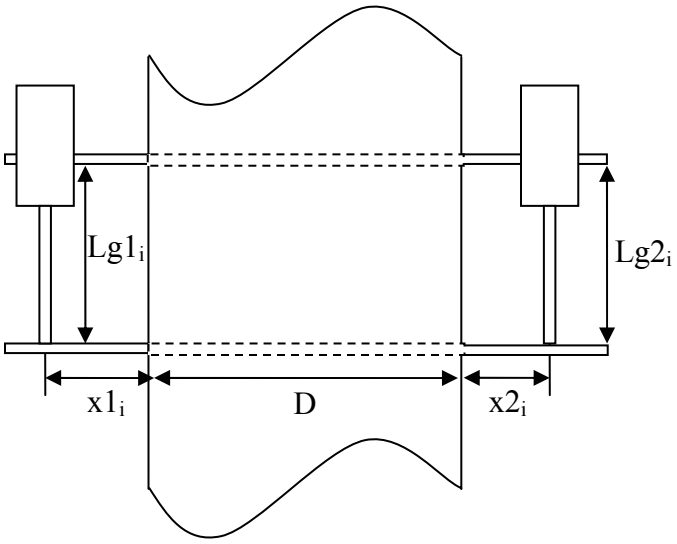

Figure 3-22 Curvature Instrumentation

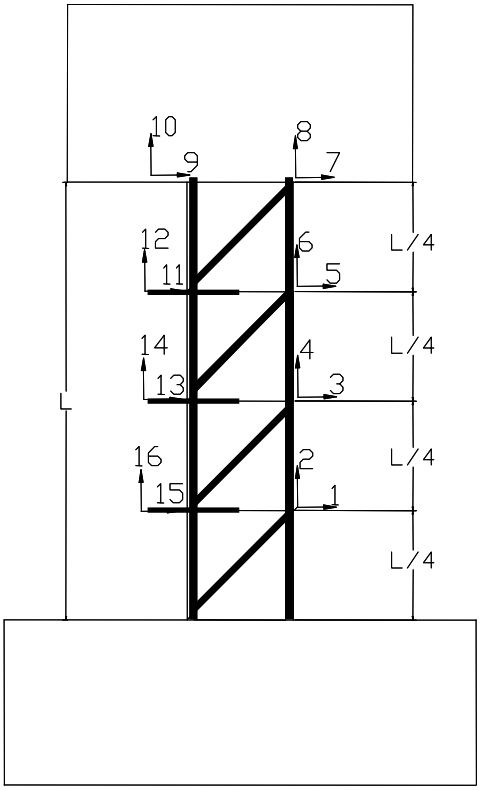

Figure 3-23 Total Displacements Panel Configuration

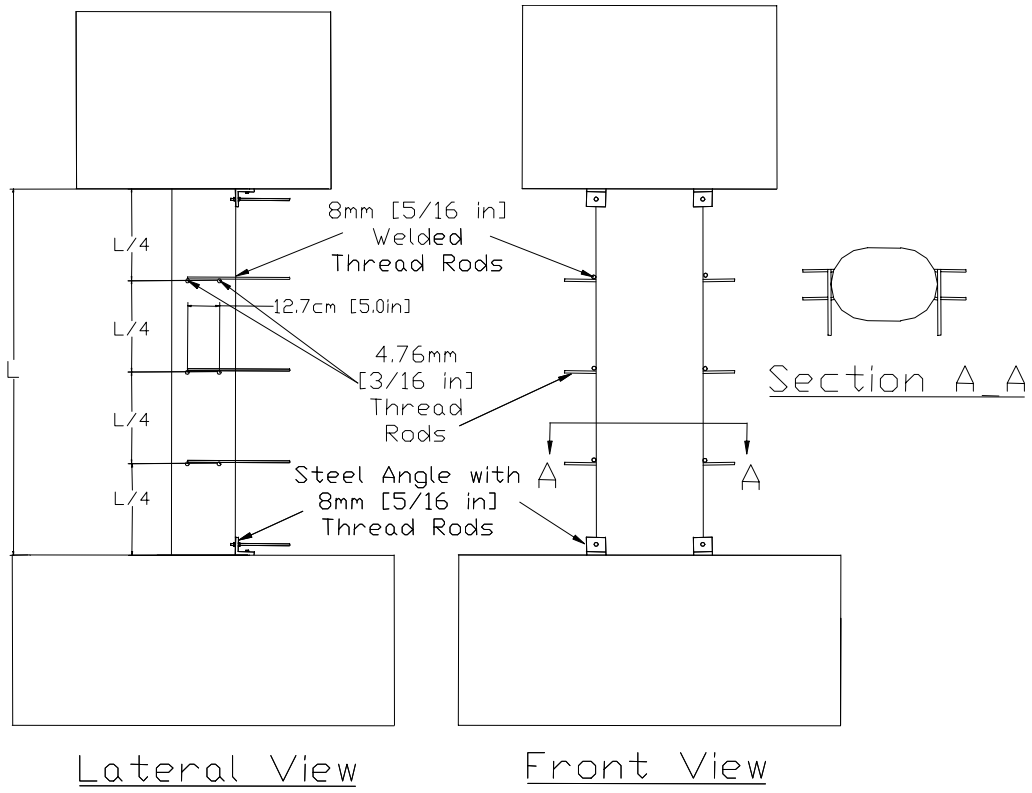

Figure 3-24 Panel Instrumentation

Figure 3-25 Novotecknik Transducers with Aluminum Channel and Rods Ends

Figure 3-26 Panel Configuration Specimens with High Shear

Figure 3-27 Axial Load System

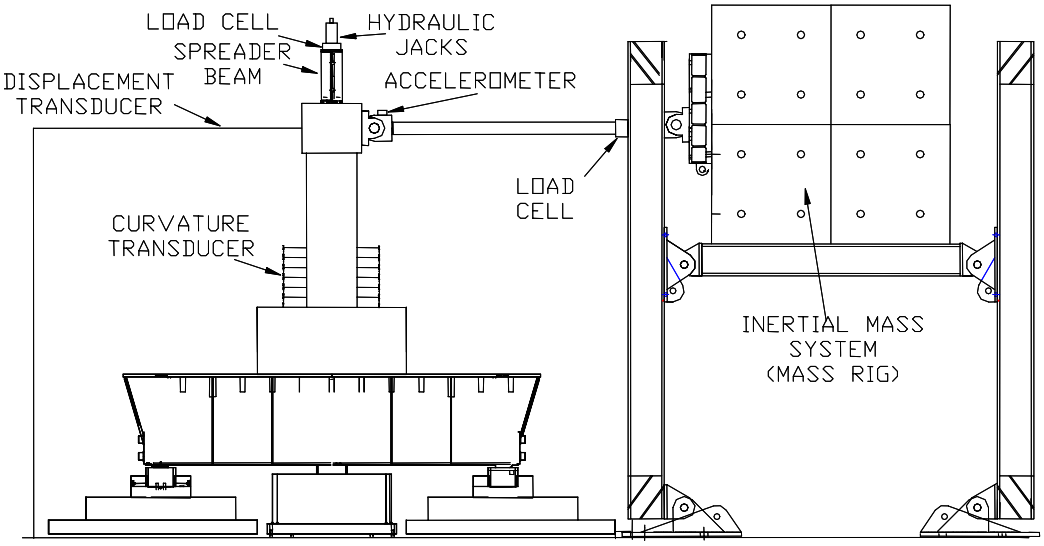

Figure 3-28 Schematic of the Test Setup for Specimens with Low Shear

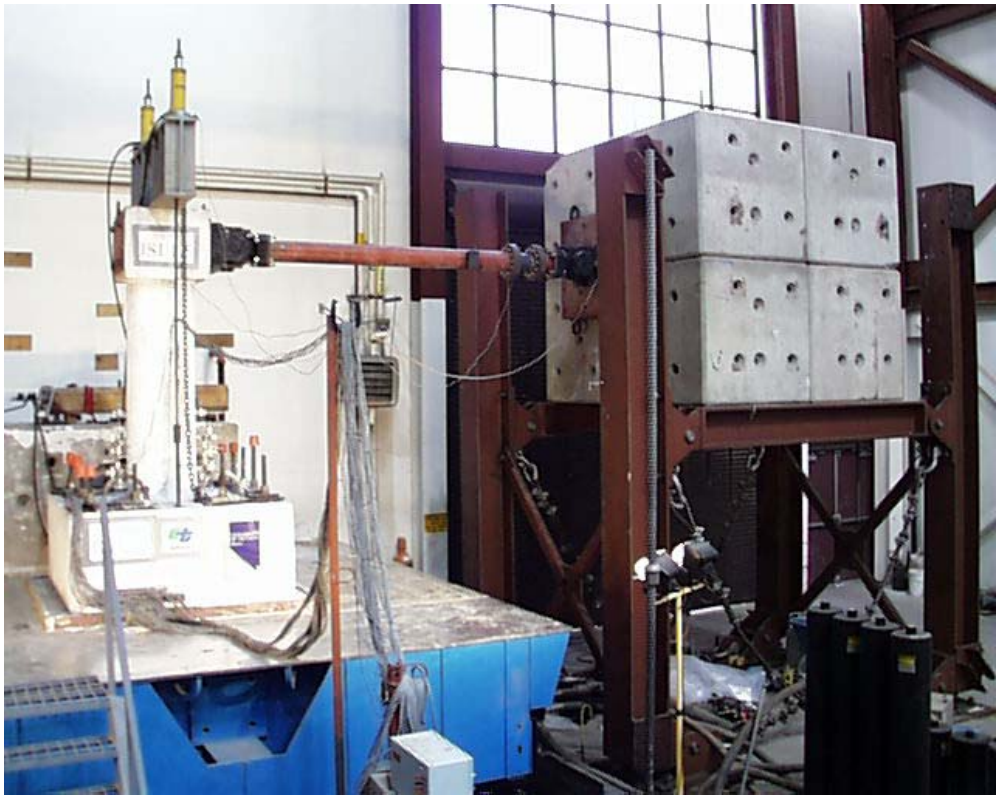

Figure 3-29 Test Setup for Specimens with Low Shear

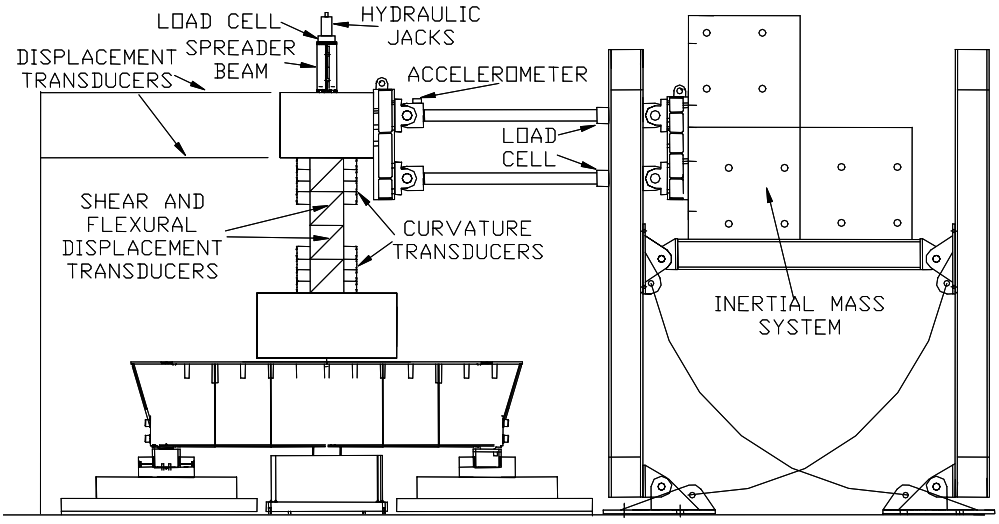

Figure 3-30 Schematic of the Test Setup for Specimens with High Shear

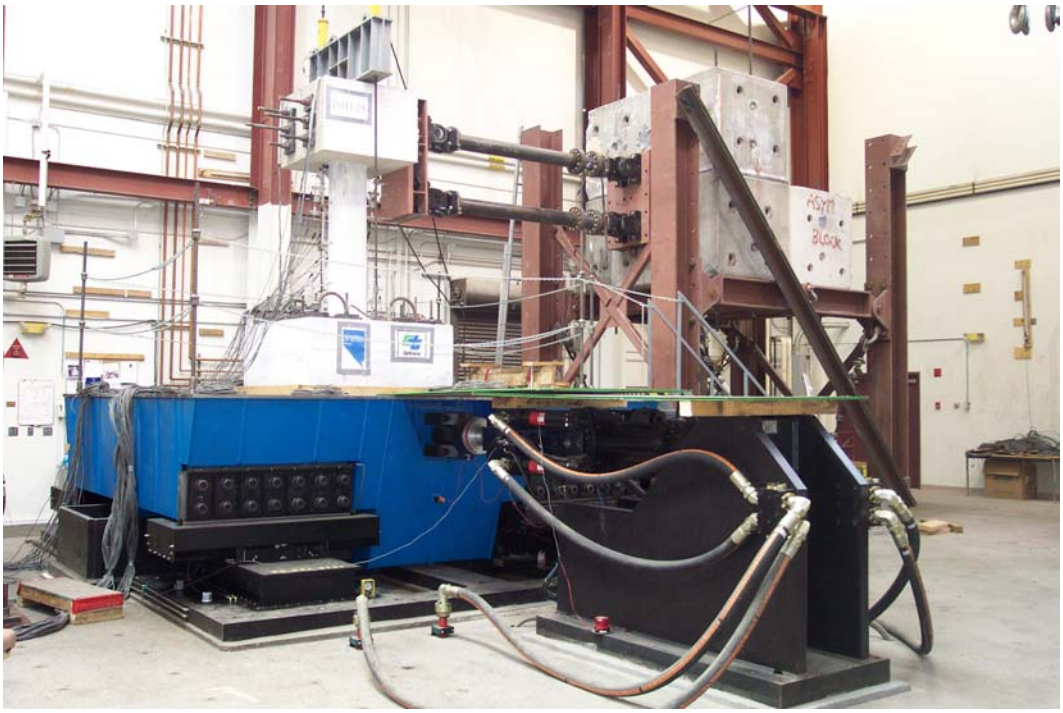

Figure 3-31 Test Setup for Specimens with High Shear

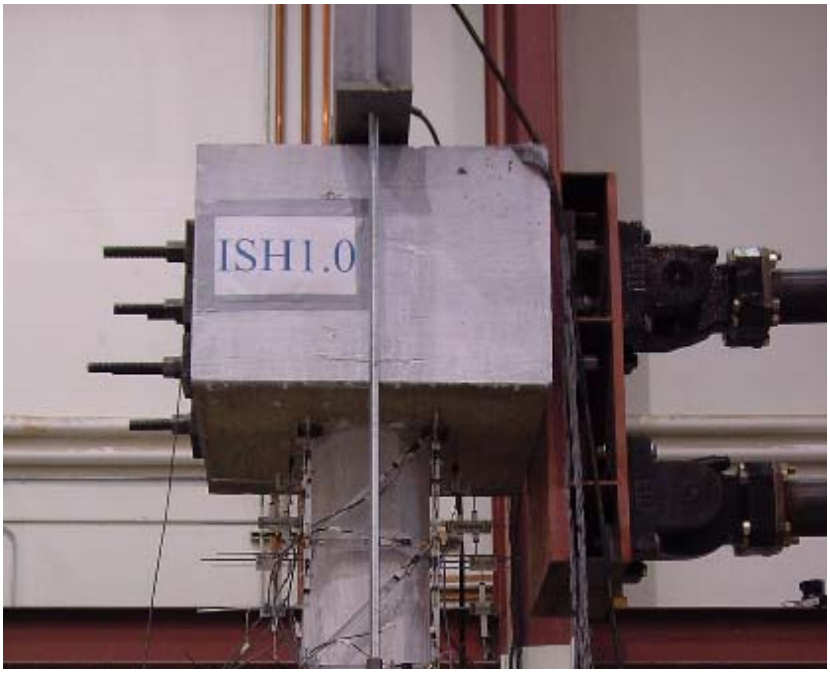

Figure 3-32 Link Connector Plate

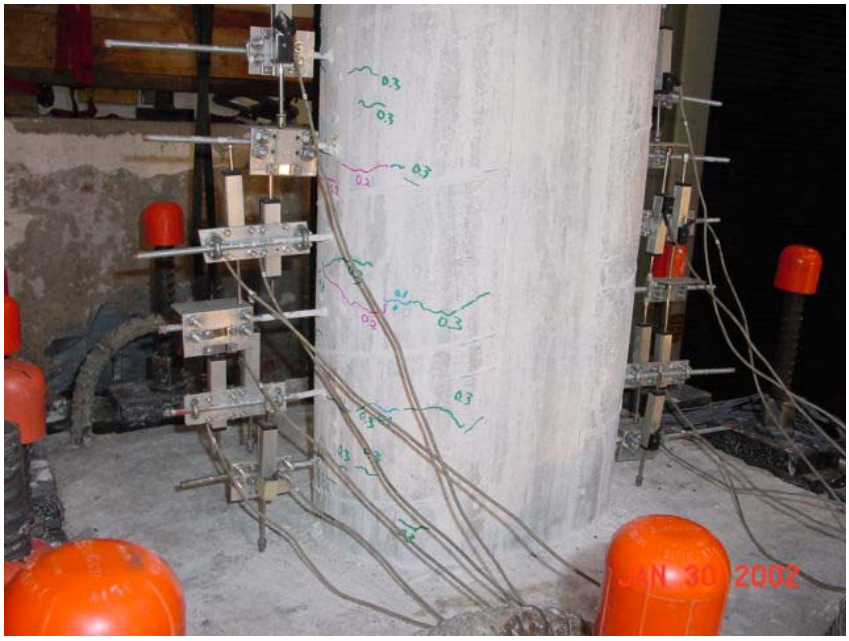

Figure 4-1 Flexural Cracks (μ_d = 0.2-0.8) Specimen ISL1.0

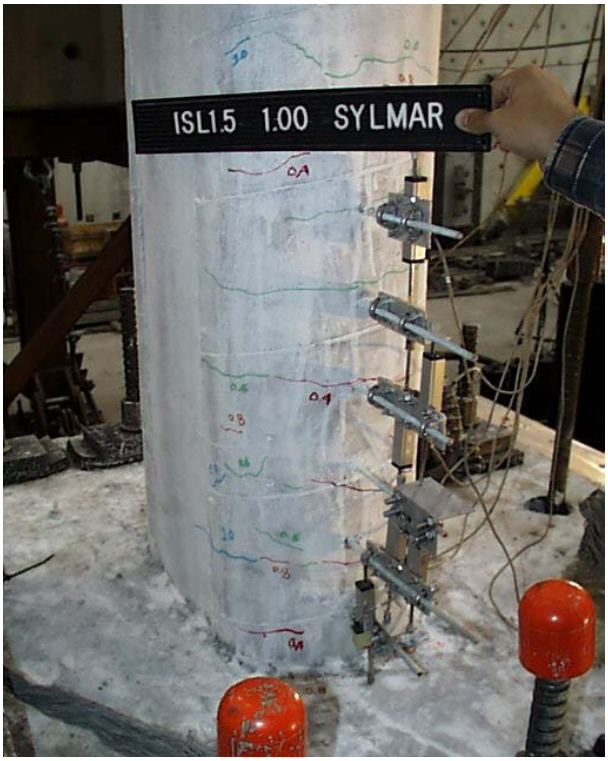

Figure 4-2 Flexural Cracks (μ_d = 0.1-1.5) Specimen ISL1.5

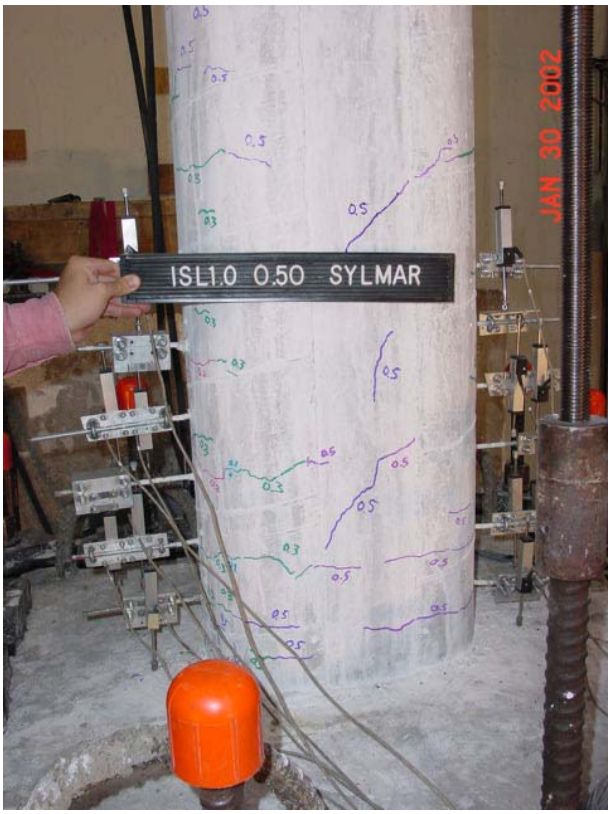

Figure 4-3 Shear Cracks (μ_d = 1.5) Specimen ISL1.0

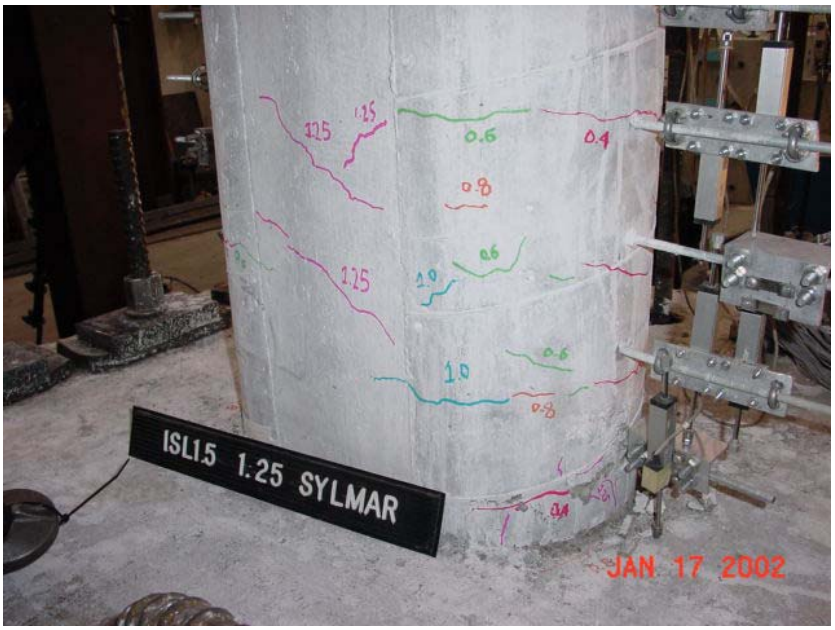

Figure 4-4 Shear Cracks (μ_d = 2.4) Specimen ISL1.5

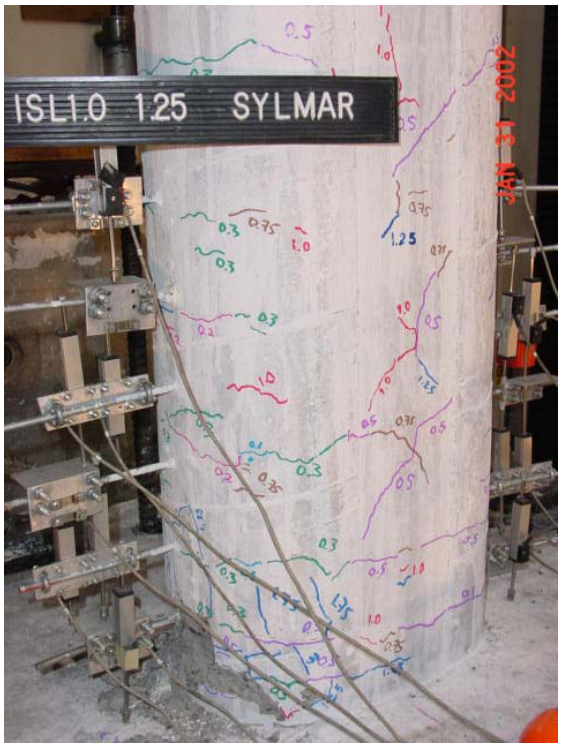

Figure 4-5 Increasing of Cracks and Spalling (μ_d = 2.8) Specimen ISL1.0

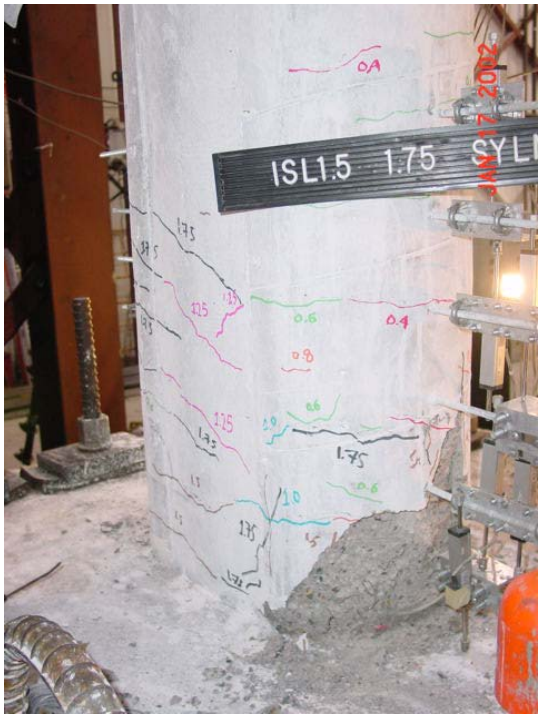

Figure 4-6 Increasing of Cracks and Spalling (μ_d = 3.1) Specimen ISL1.5

Figure 4-7 Spirals and Long. Bars Visible (μ_d = 5.6) Specimen ISL1.0

Figure 4-8 Spirals Visible (μ_d = 7.5) Specimen ISL1.5

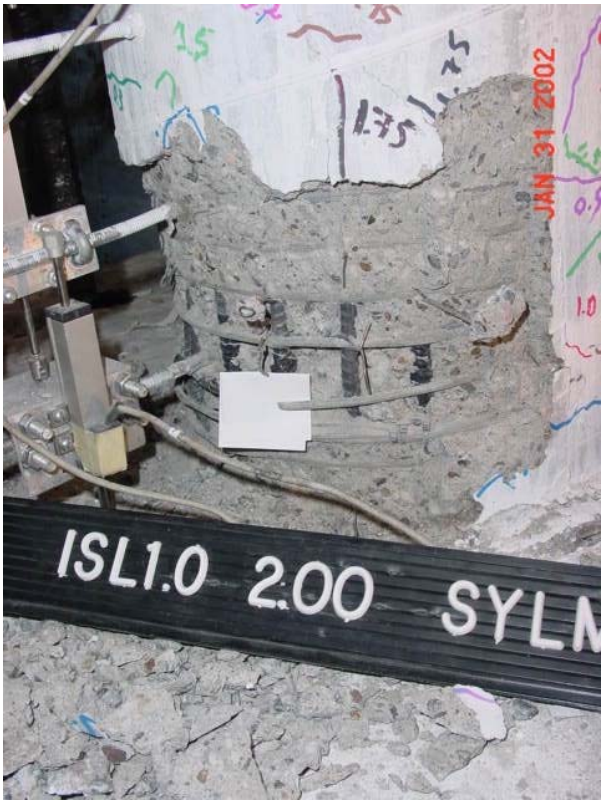

Figure 4-9 Failure (μ_d = 9.6) Specimen ISL1.0

Figure 4-10 Failure (μ_d = 9.6) Specimen ISL1.5

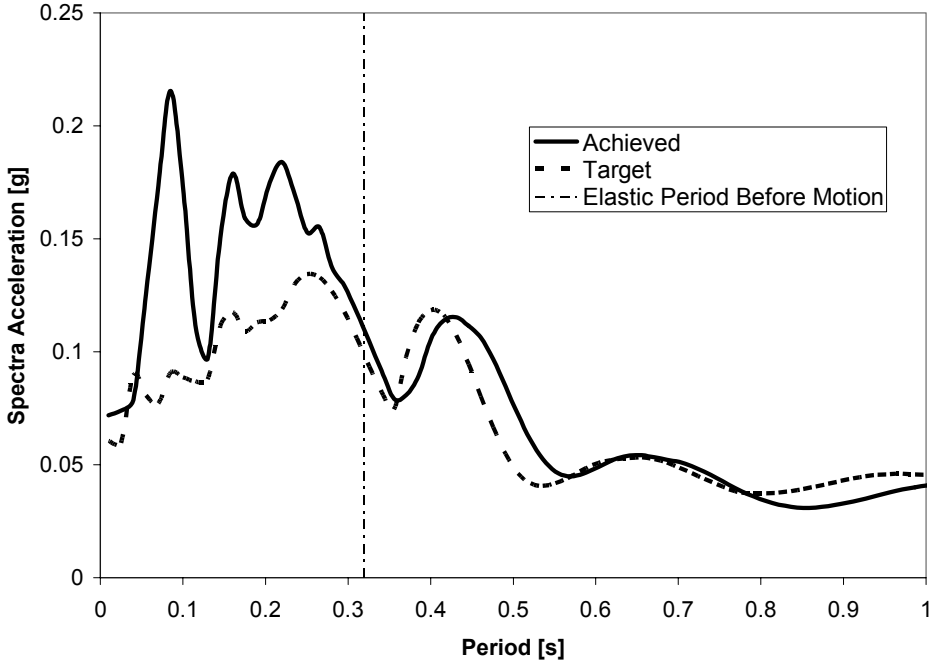

Figure 4-11 Comparison of Achieved and Target Response Spectra for 0.1 x Sylmar Specimen ISL1.0

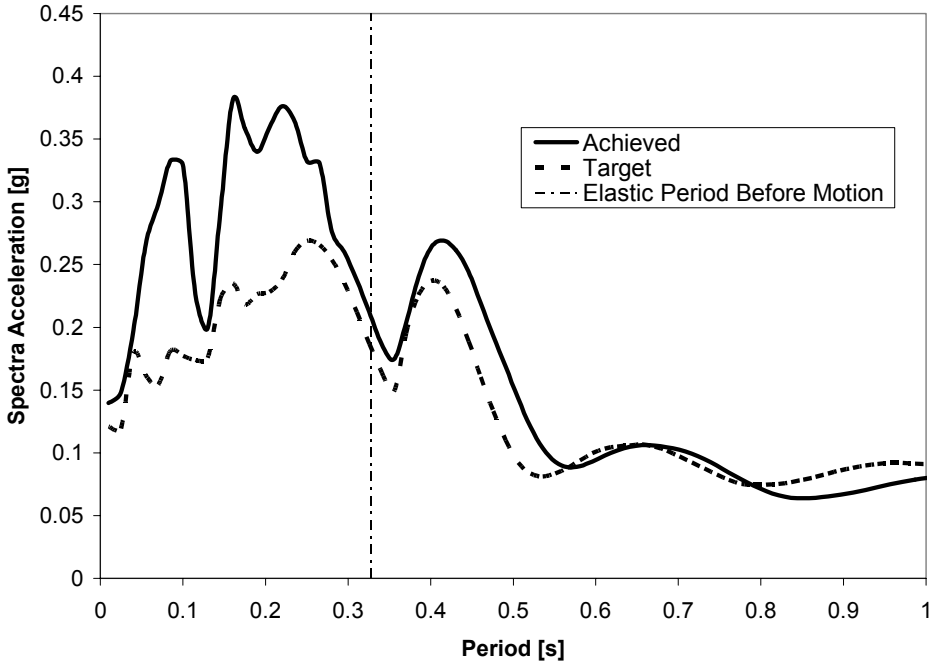

Figure 4-12 Comparison of Achieved and Target Response Spectra for 0.2 x Sylmar Specimen ISL1.0

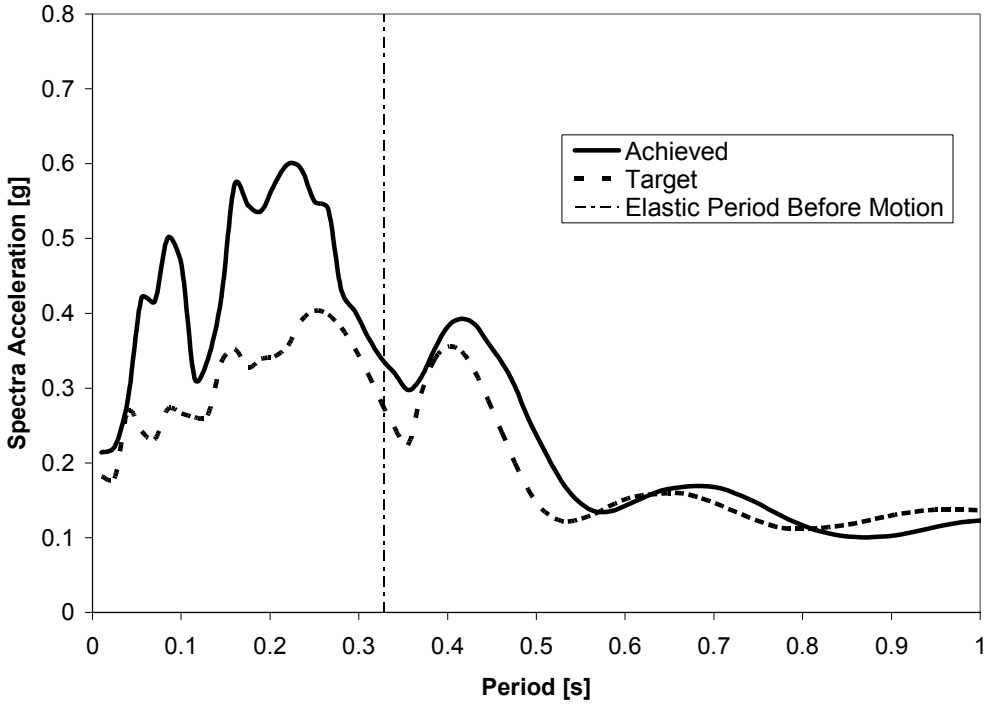

Figure 4-13 Comparison of Achieved and Target Response Spectra for 0.3 x Sylmar Specimen ISL1.0

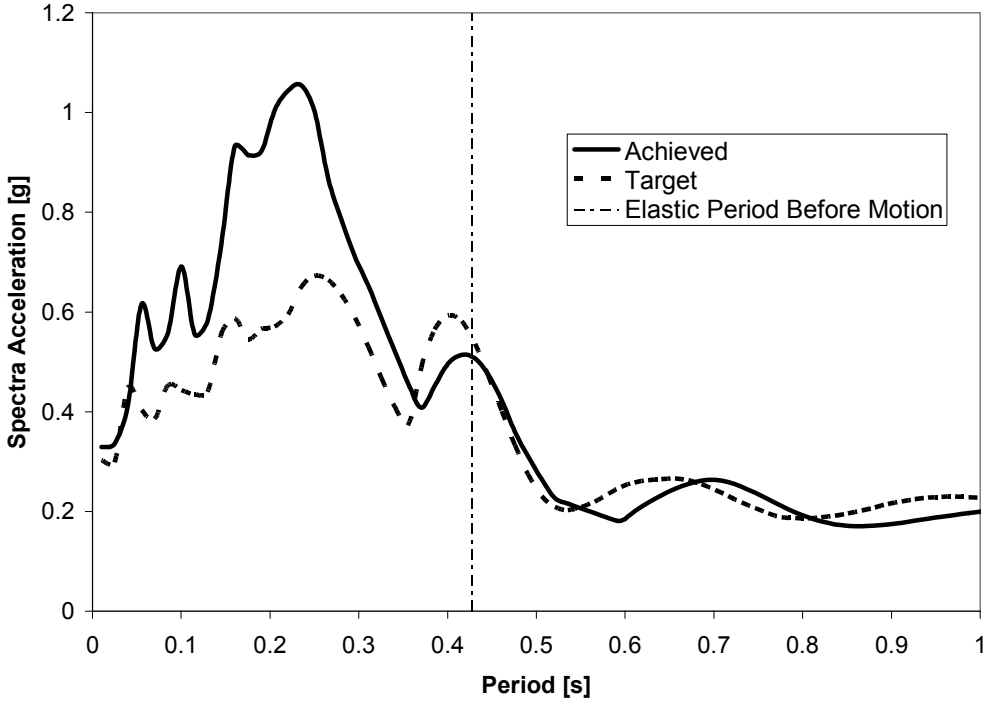

Figure 4-14 Comparison of Achieved and Target Response Spectra for 0.5 x Sylmar Specimen ISL1.0

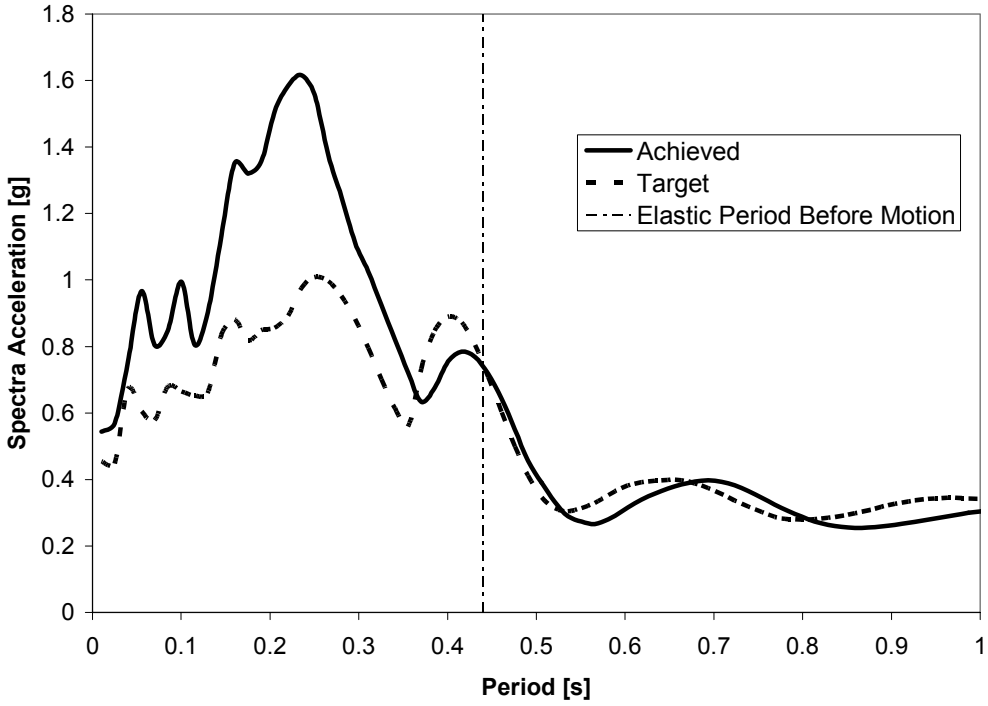

Figure 4-15 Comparison of Achieved and Target Response Spectra for 0.75 x Sylmar Specimen ISL1.0

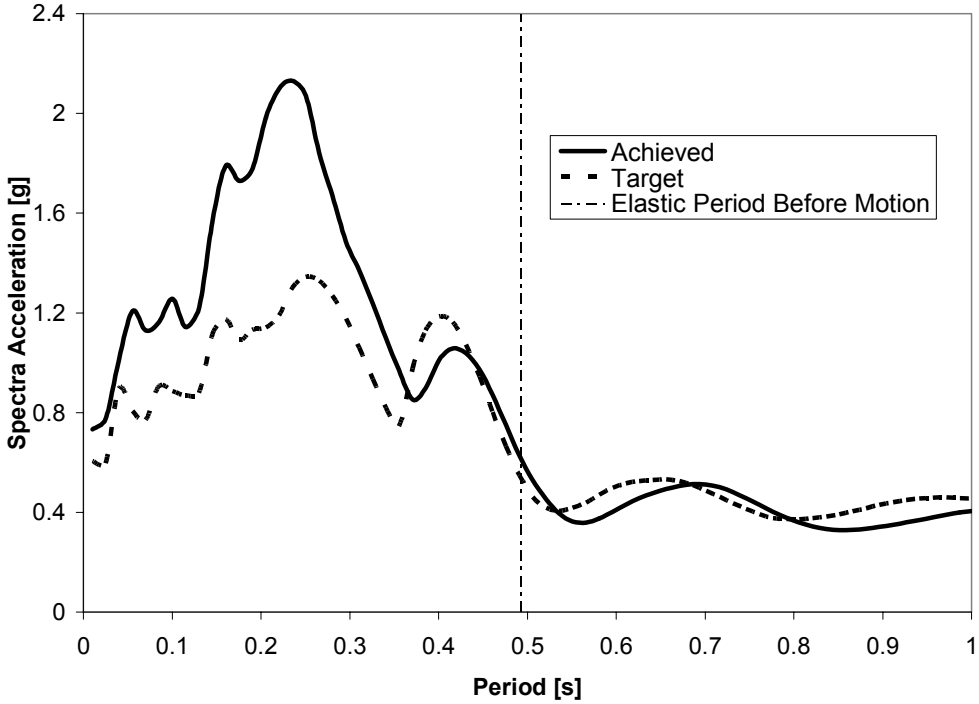

Figure 4-16 Comparison of Achieved and Target Response Spectra for 1.0 x Sylmar Specimen ISL1.0

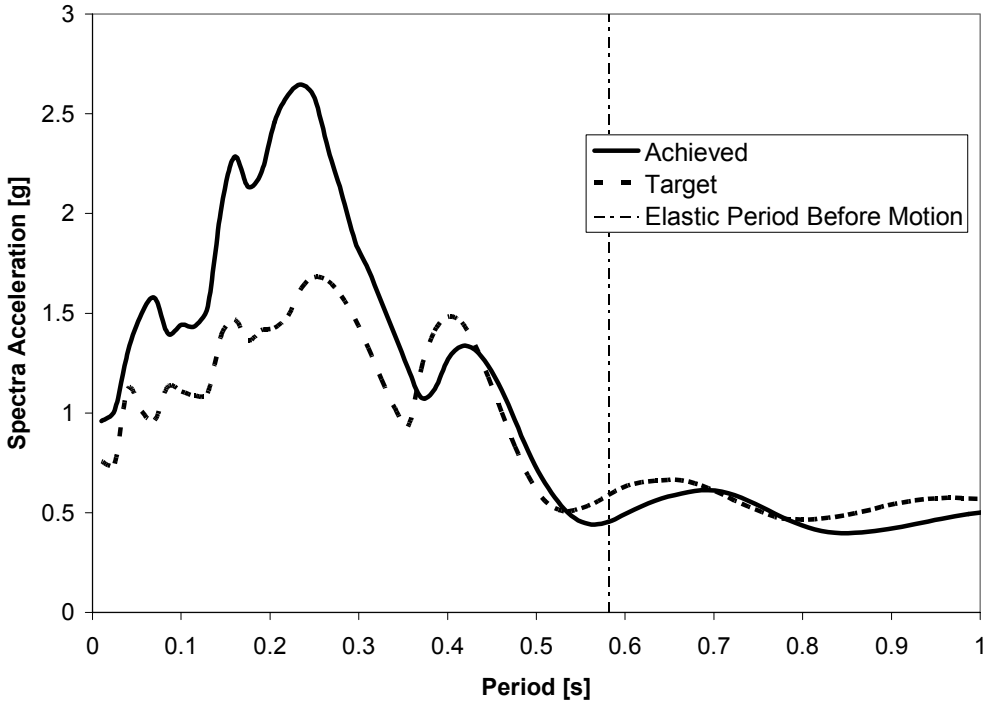

Figure 4-17 Comparison of Achieved and Target Response Spectra for 1.25 x Sylmar Specimen ISL1.0

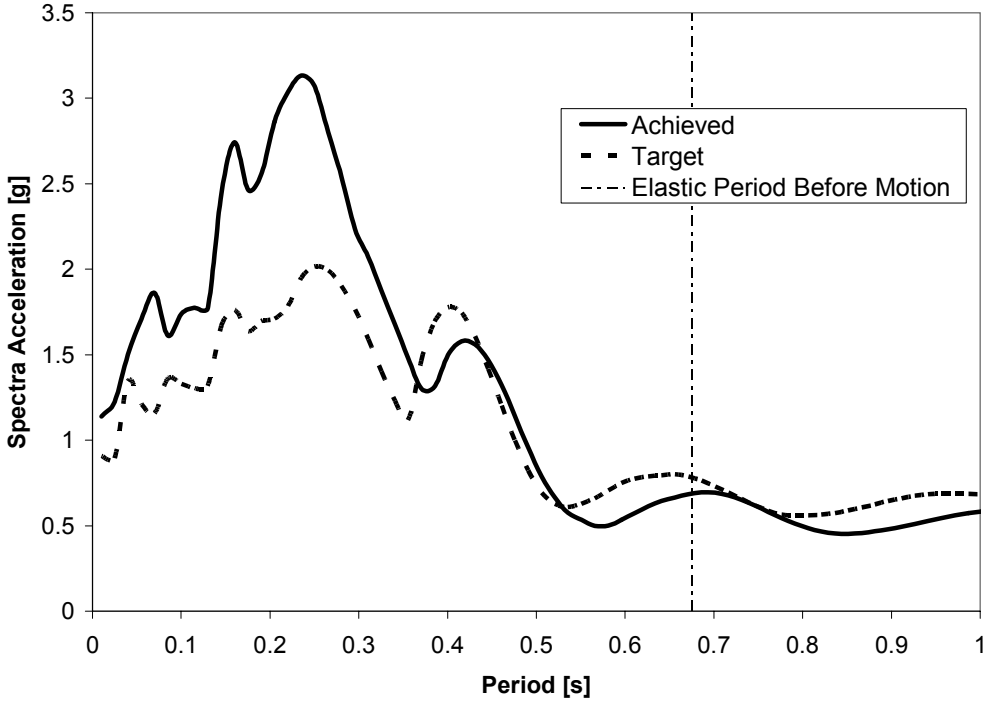

Figure 4-18 Comparison of Achieved and Target Response Spectra for 1.5 x Sylmar Specimen ISL1.0

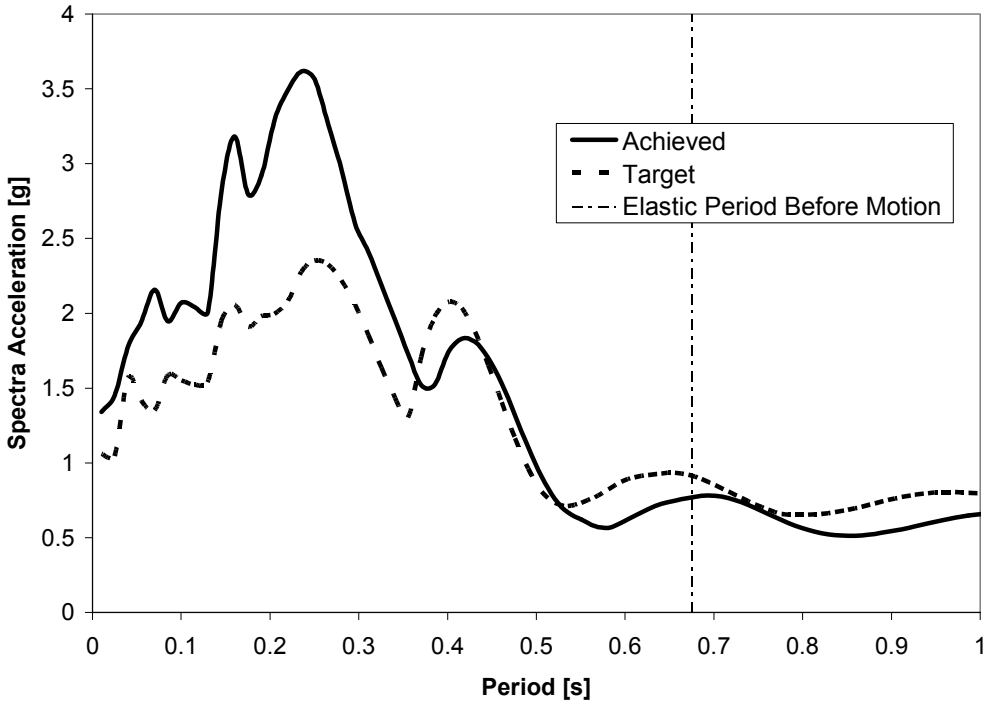

Figure 4-19 Comparison of Achieved and Target Response Spectra for 1.75 x Sylmar Specimen ISL1.0

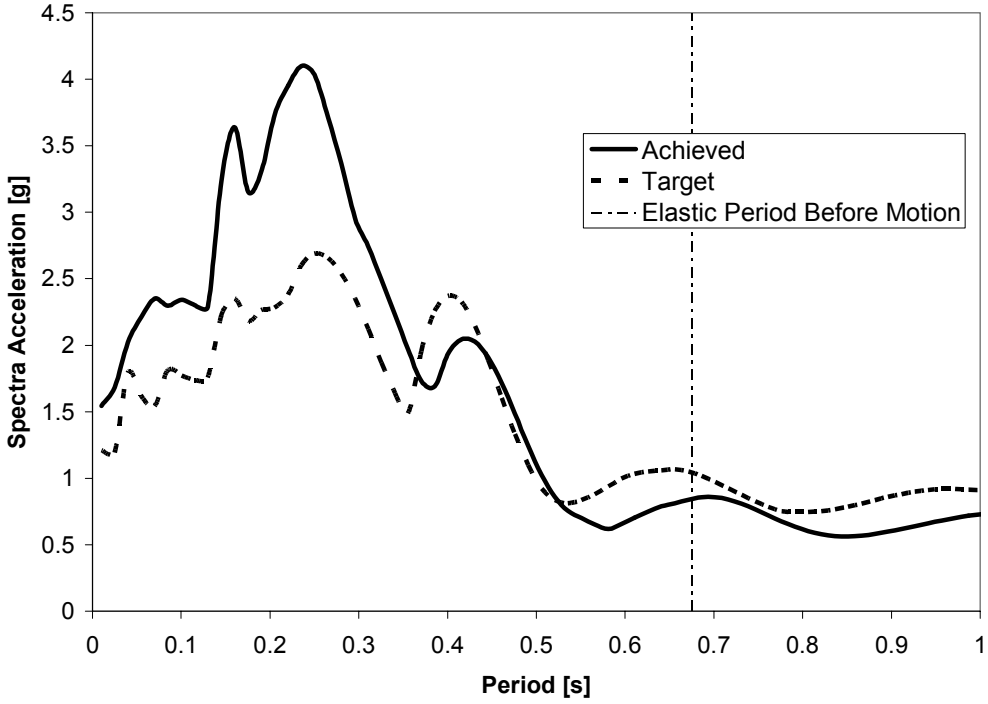

Figure 4-20 Comparison of Achieved and Target Response Spectra for 2.0 x Sylmar Specimen ISL1.0

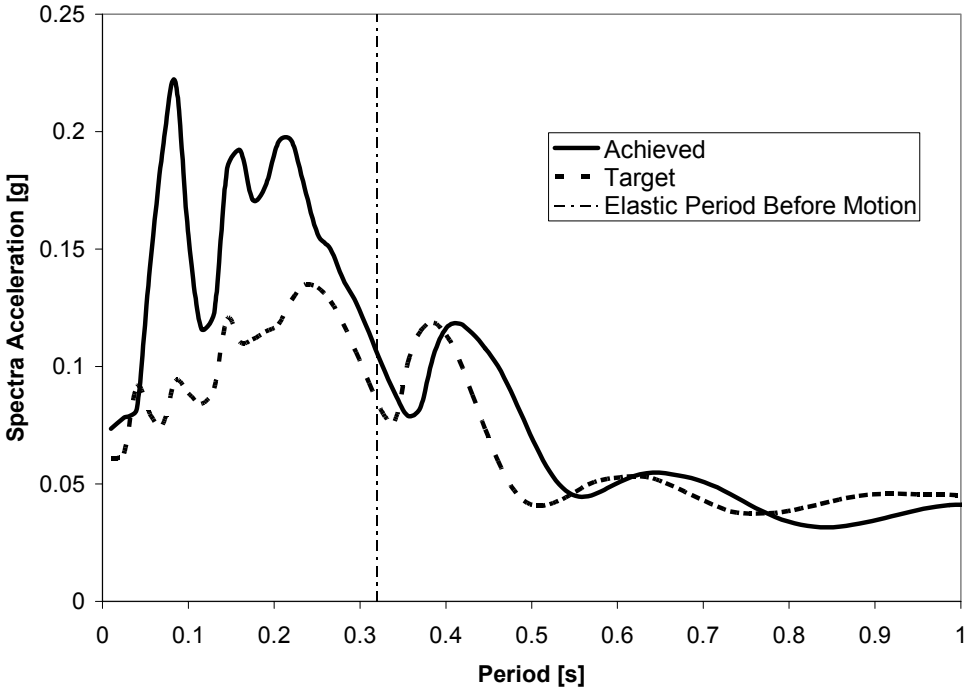

Figure 4-21 Comparison of Achieved and Target Response Spectra for 0.1 x Sylmar Specimen ISL1.5

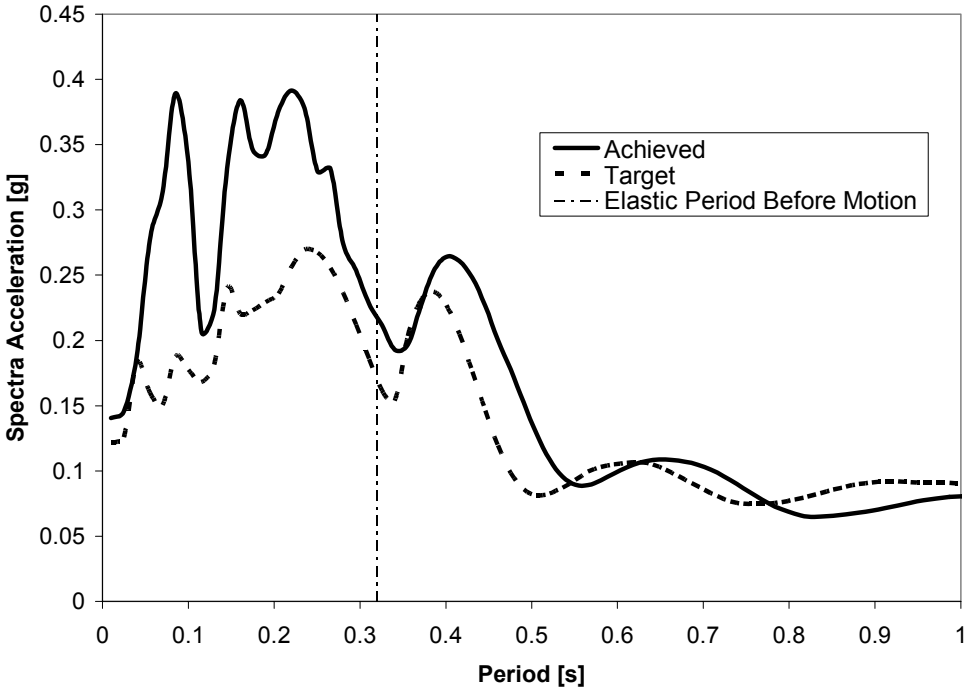

Figure 4-22 Comparison of Achieved and Target Response Spectra for 0.2 x Sylmar Specimen ISL1.5

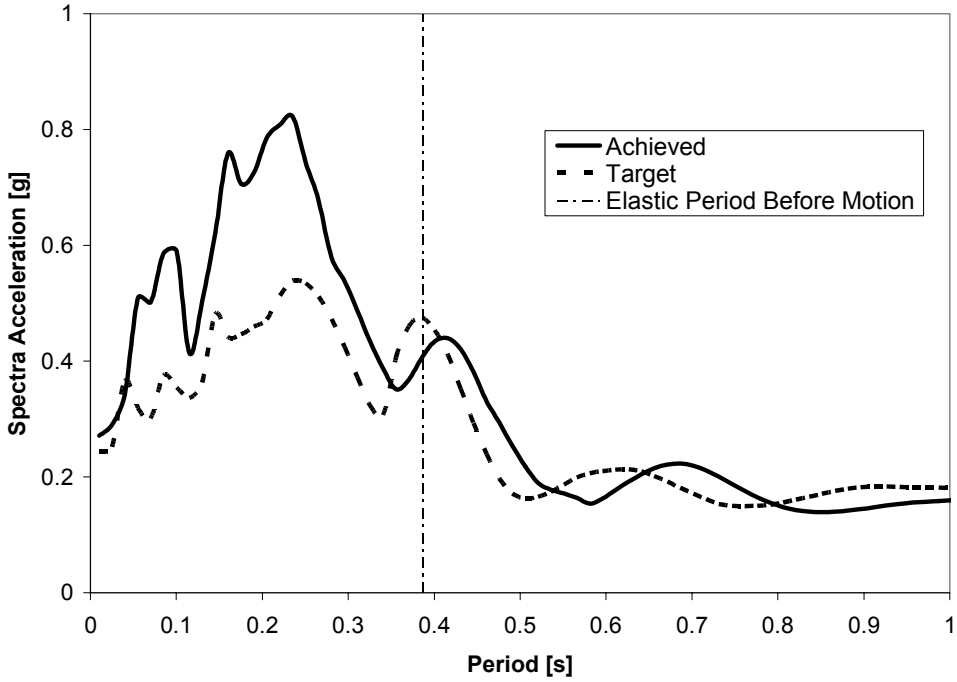

Figure 4-23 Comparison of Achieved and Target Response Spectra for 0.4 x Sylmar Specimen ISL1.5

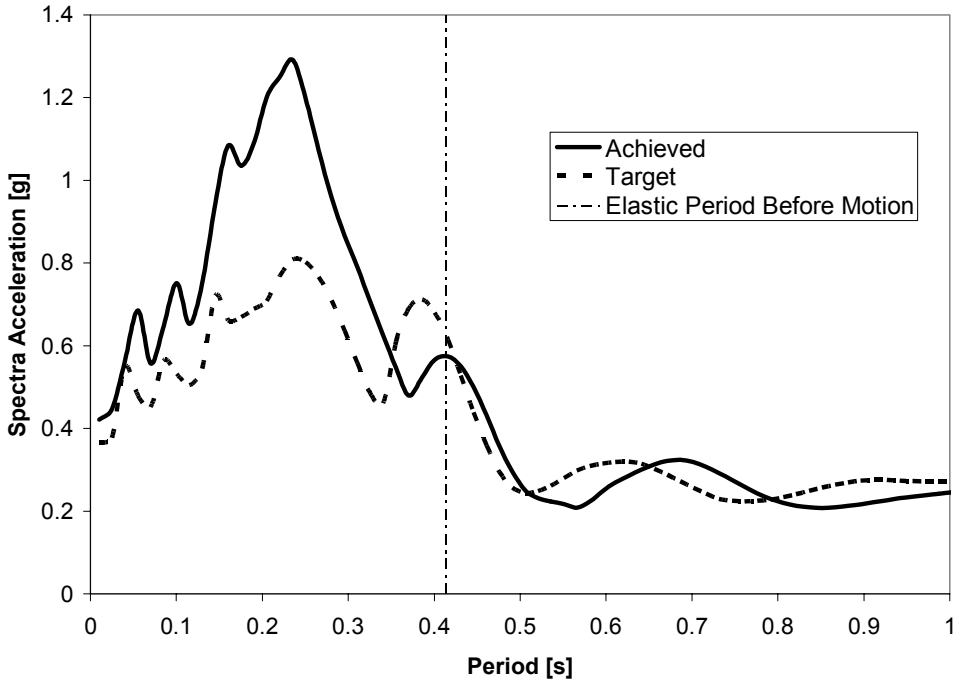

Figure 4-24 Comparison of Achieved and Target Response Spectra for 0.6 x Sylmar Specimen ISL1.5

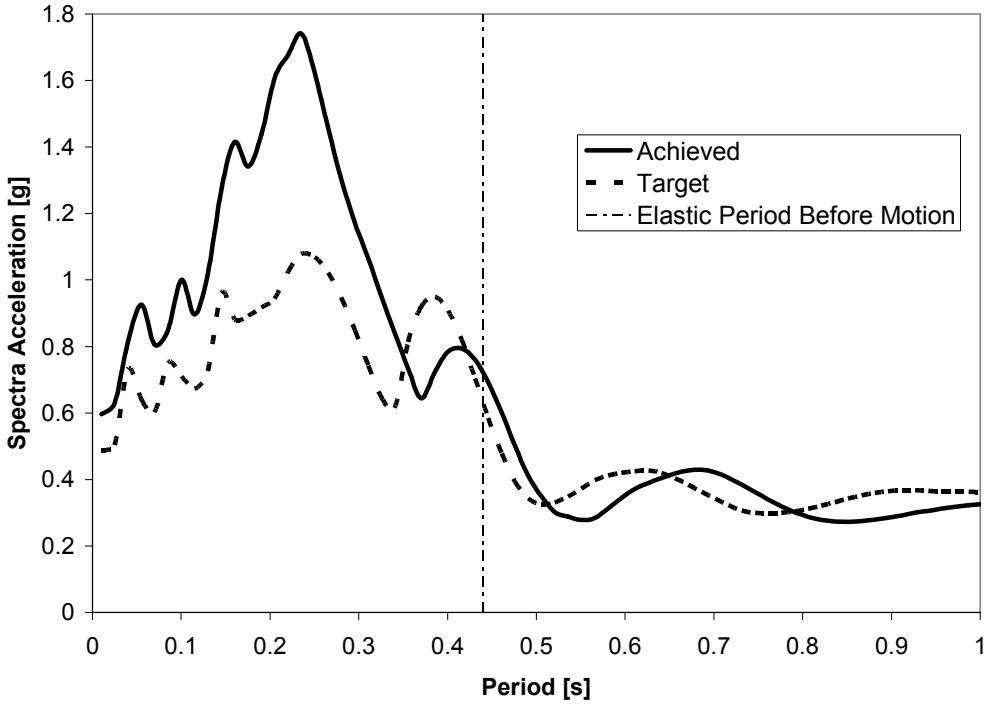

Figure 4-25 Comparison of Achieved and Target Response Spectra for 0.8 x Sylmar Specimen ISL1.5

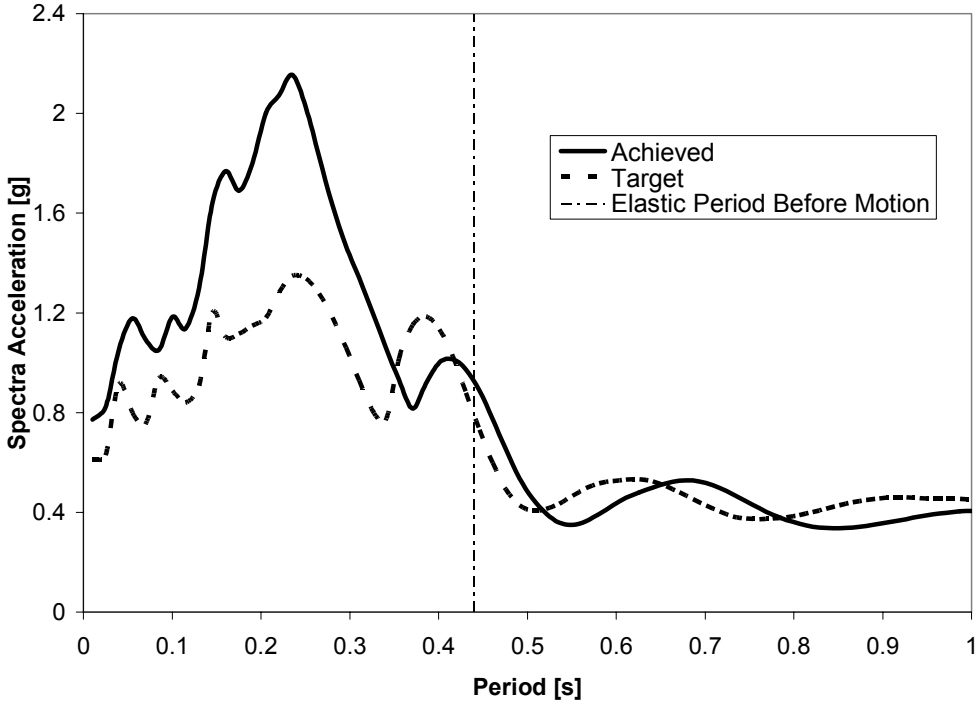

Figure 4-26 Comparison of Achieved and Target Response Spectra for 1.0 x Sylmar Specimen ISL1.5

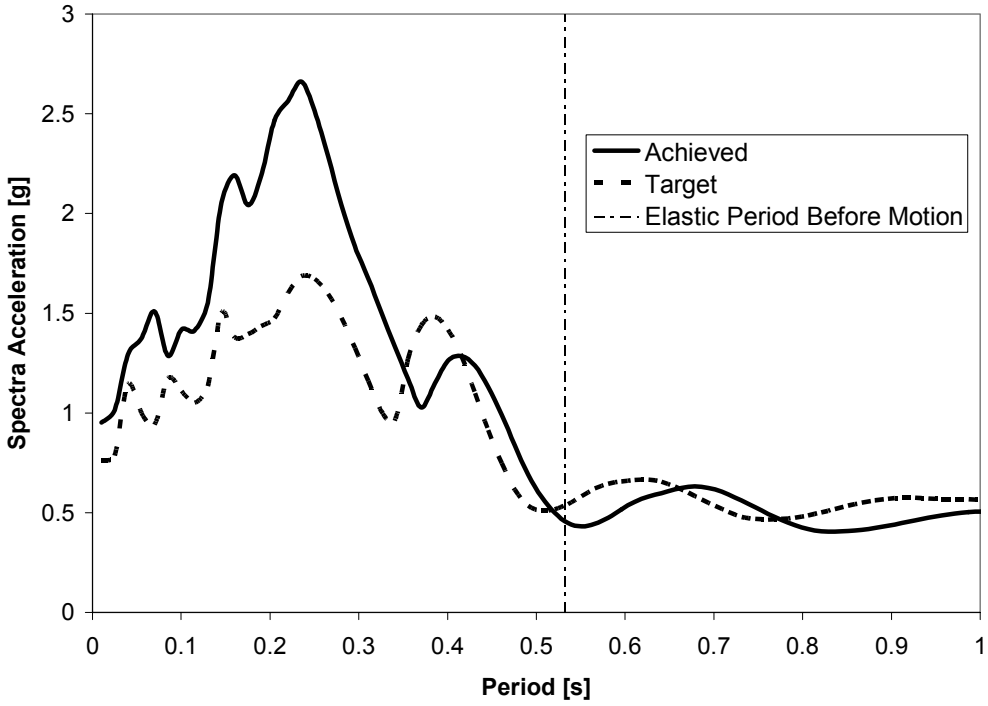

Figure 4-27 Comparison of Achieved and Target Response Spectra for 1.25 x Sylmar Specimen ISL1.5

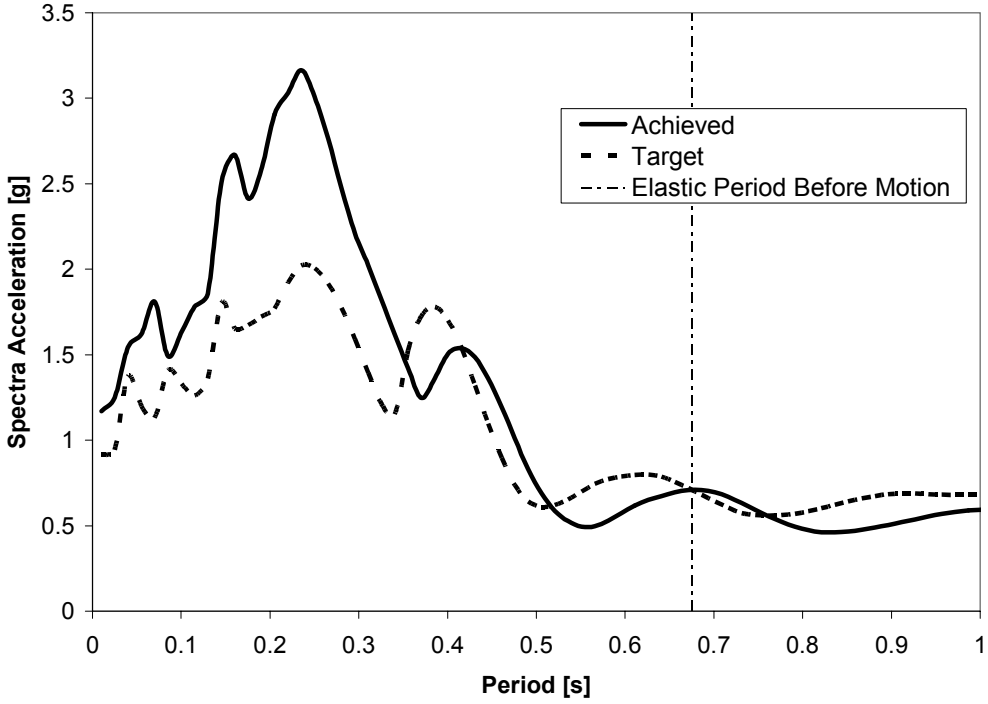

Figure 4-28 Comparison of Achieved and Target Response Spectra for 1.5 x Sylmar Specimen ISL1.5

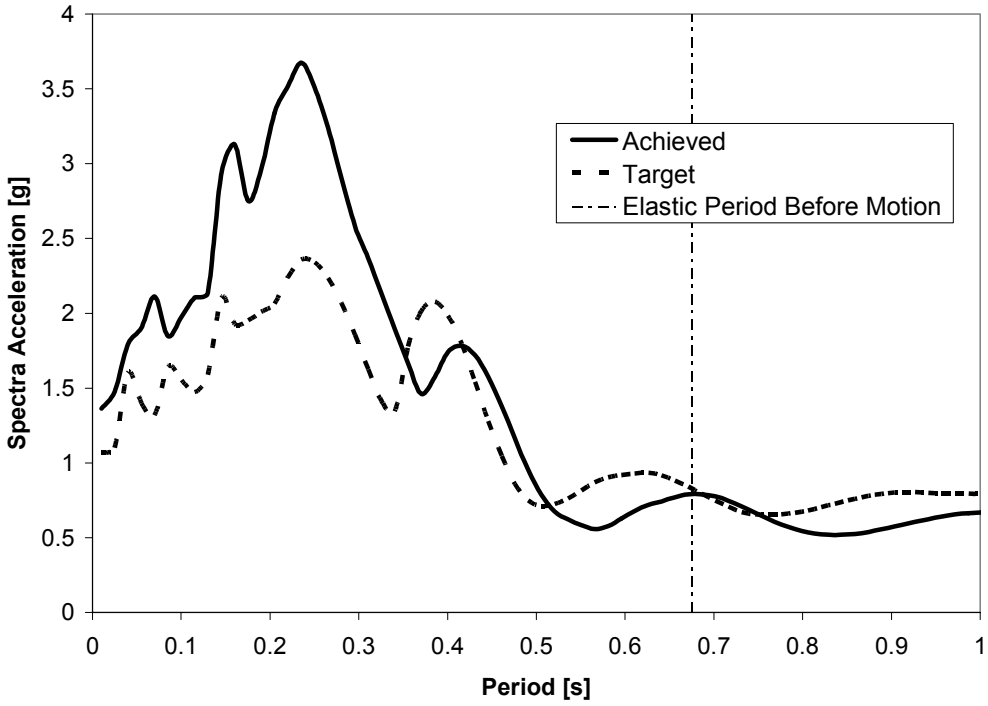

Figure 4-29 Comparison of Achieved and Target Response Spectra for 1.75 x Sylmar Specimen ISL1.5

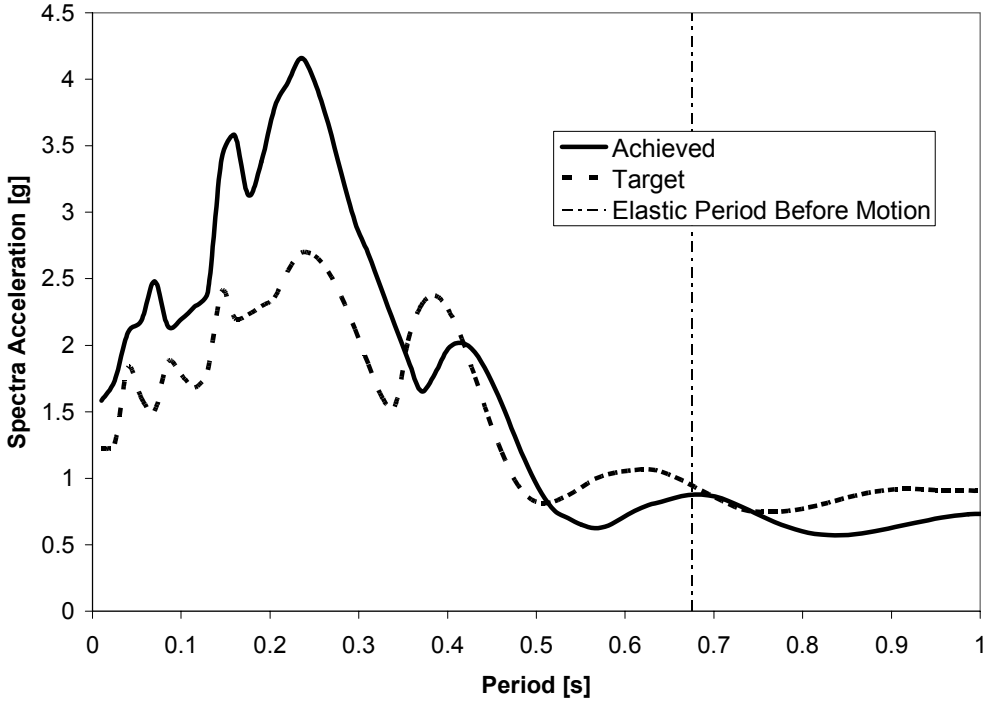

Figure 4-30 Comparison of Achieved and Target Response Spectra for 2.0 x Sylmar Specimen ISL1.5

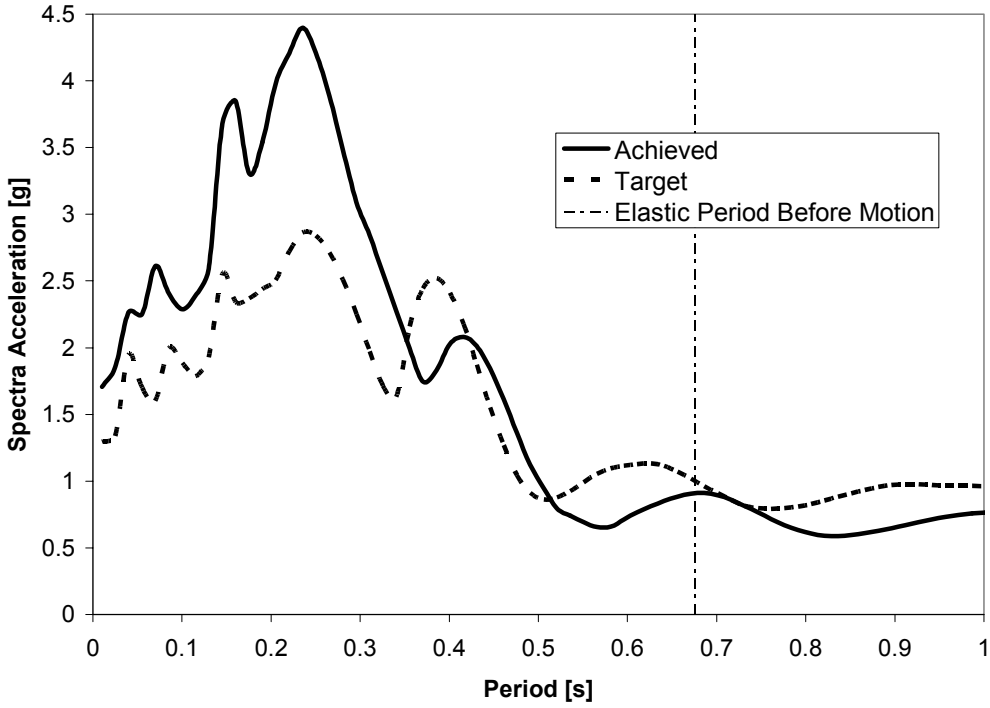

Figure 4-31 Comparison of Achieved and Target Response Spectra for 2.125 x Sylmar Specimen ISL1.5

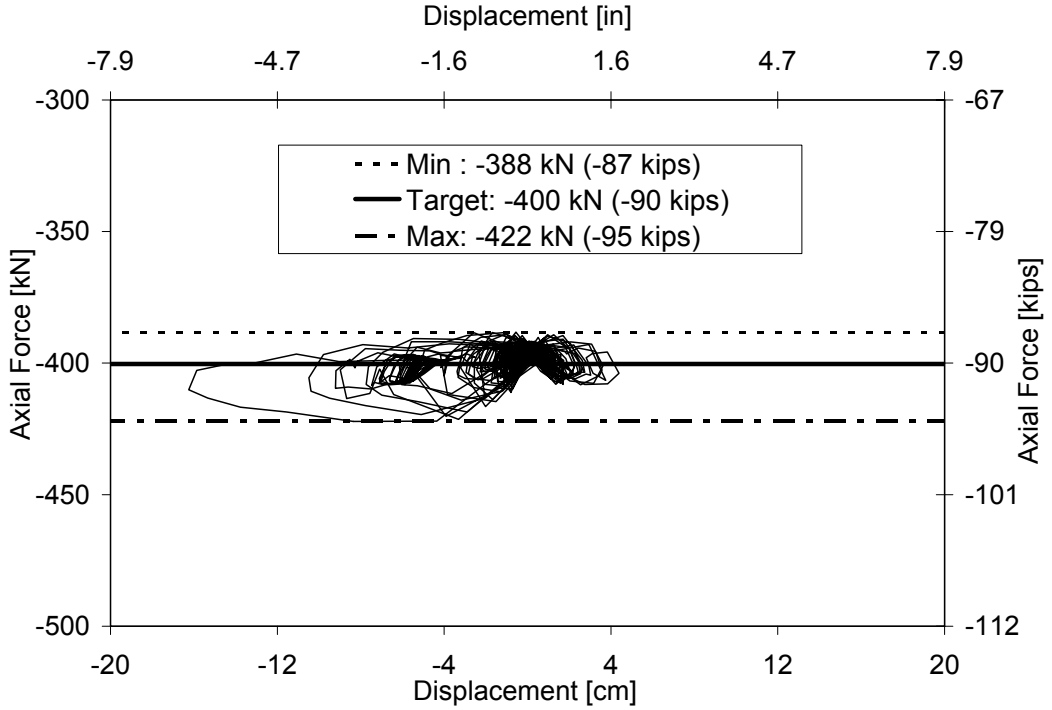

Figure 4-32 Axial Load Variation Specimen ISL1.0

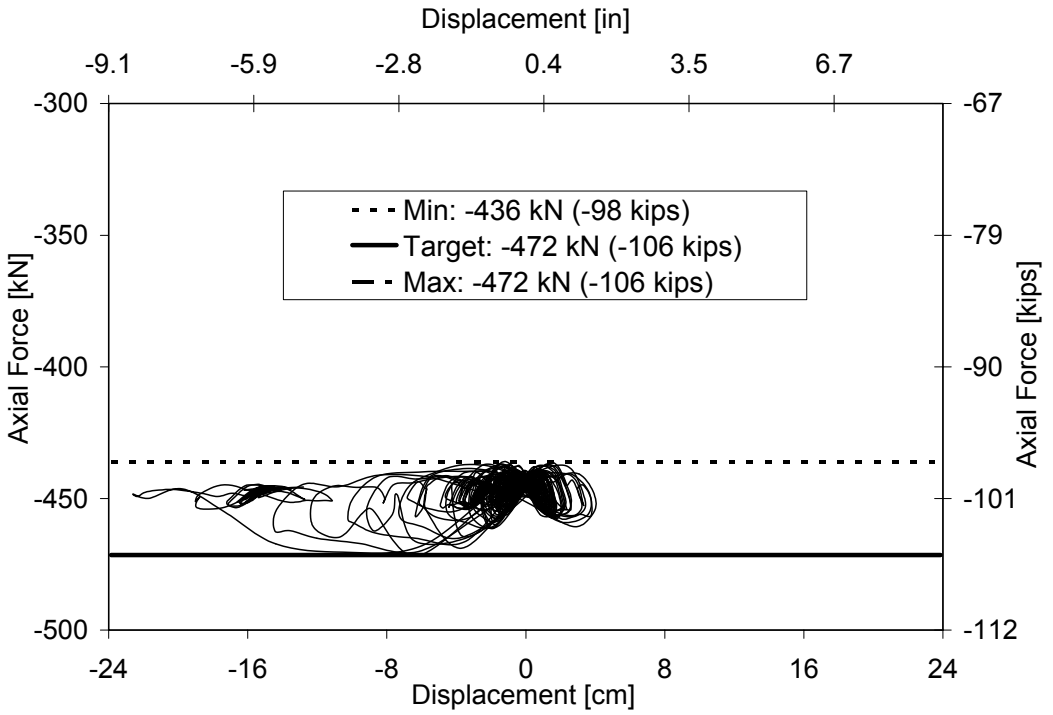

Figure 4-33 Axial Load Variation Specimen ISL1.5

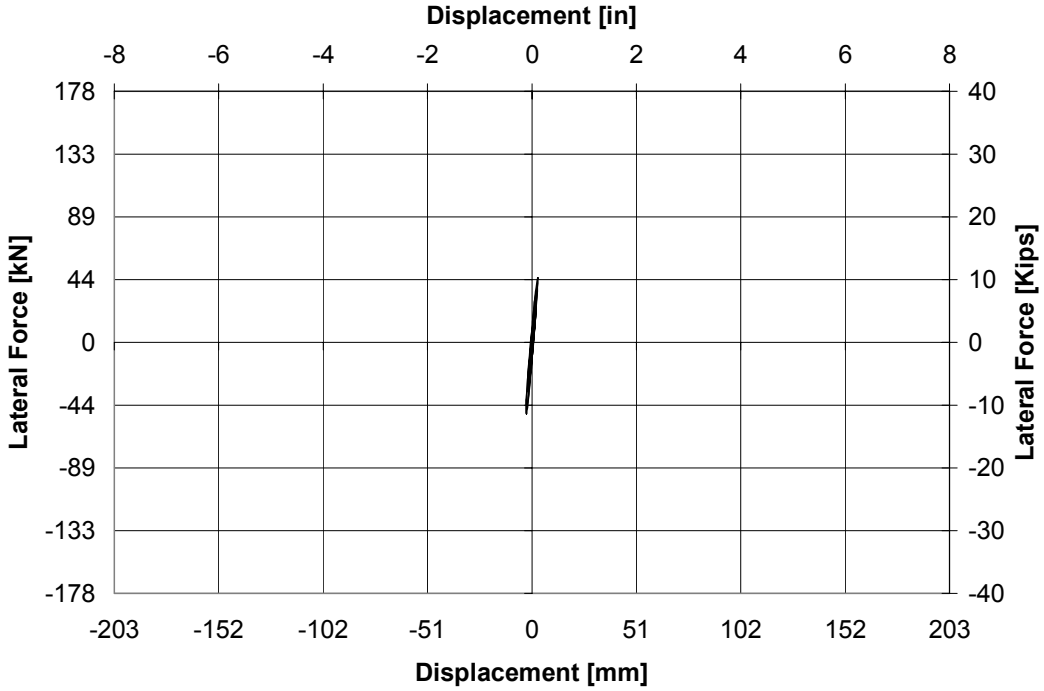

Figure 4-34 Force Displacement Hysteresis Curve for ISL1.0 at 0.1xSlymar

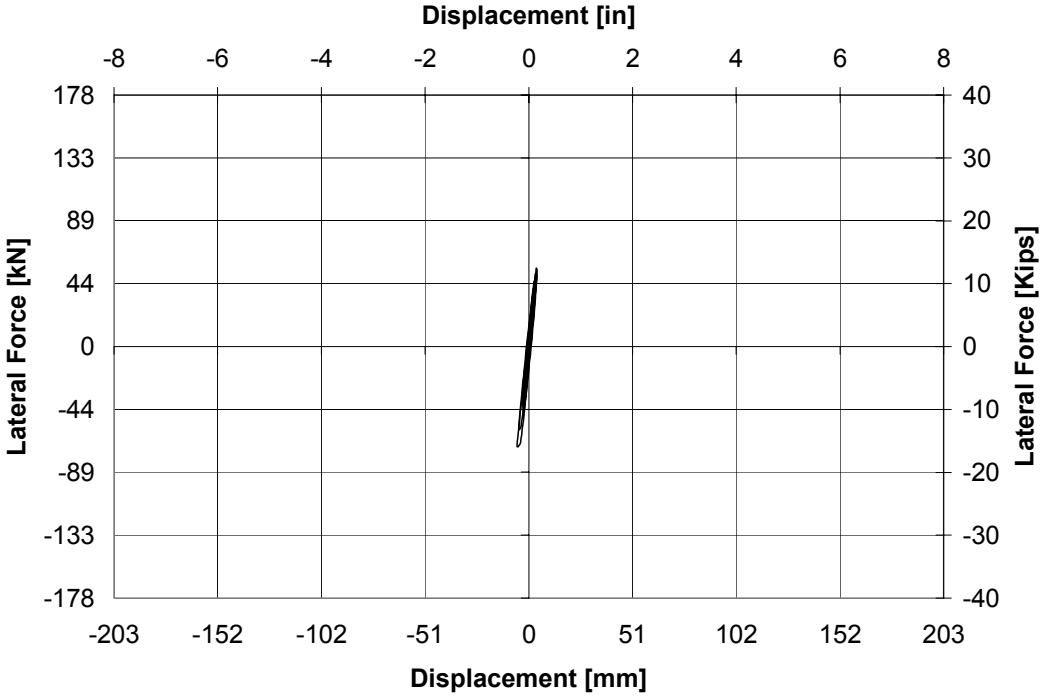

Figure 4-35 Force Displacement Hysteresis Curve for ISL1.0 at 0.2xSlymar

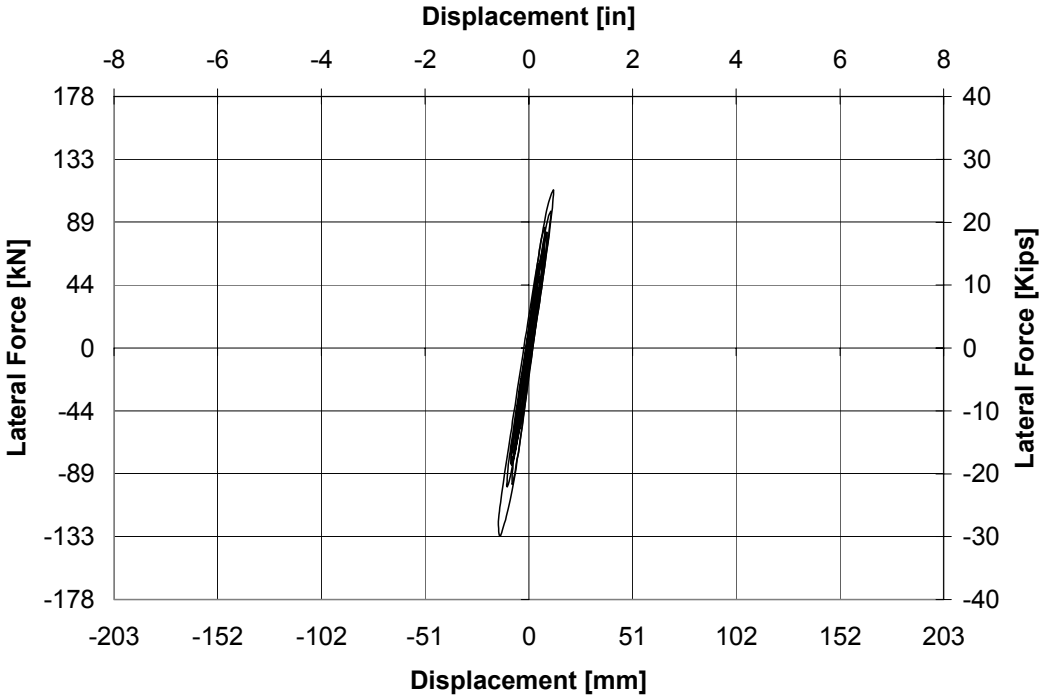

Figure 4-36 Force Displacement Hysteresis Curve for ISL1.0 at 0.3xSlymar

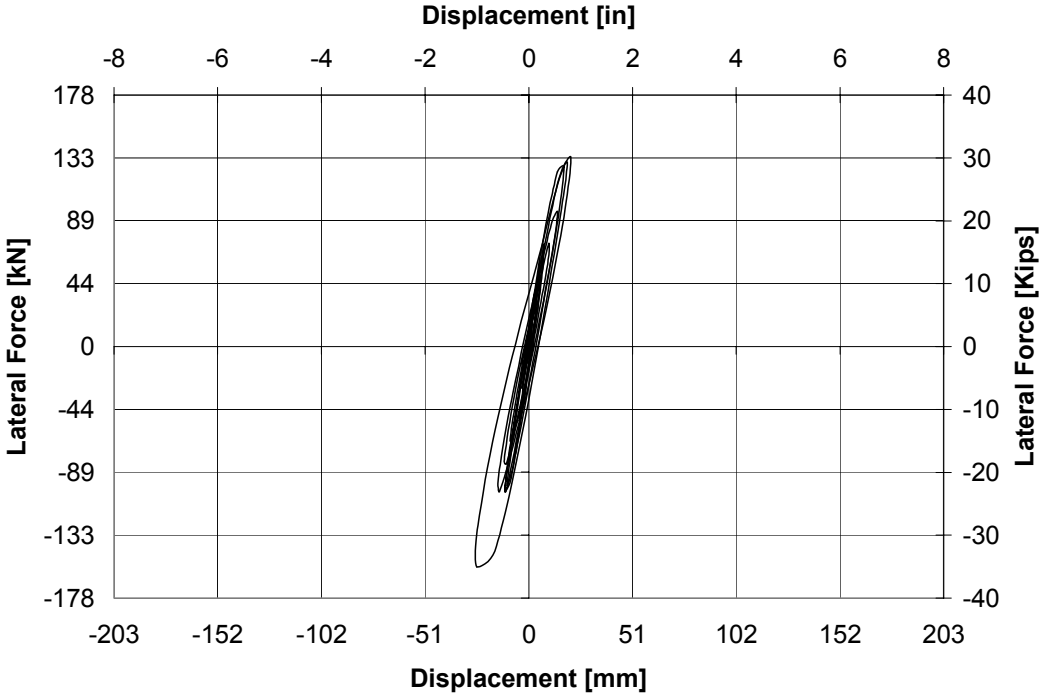

Figure 4-37 Force Displacement Hysteresis Curve for ISL1.0 at 0.5xSlymar

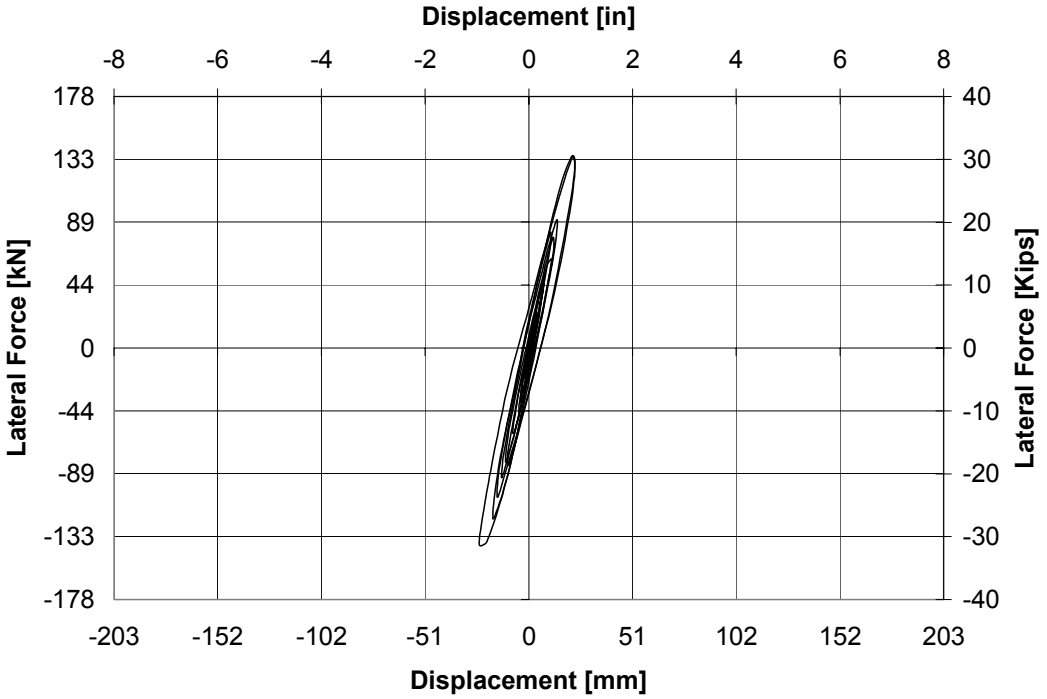

Figure 4-38 Force Displacement Hysteresis Curve for ISL1.0 at 0.75xSlymar

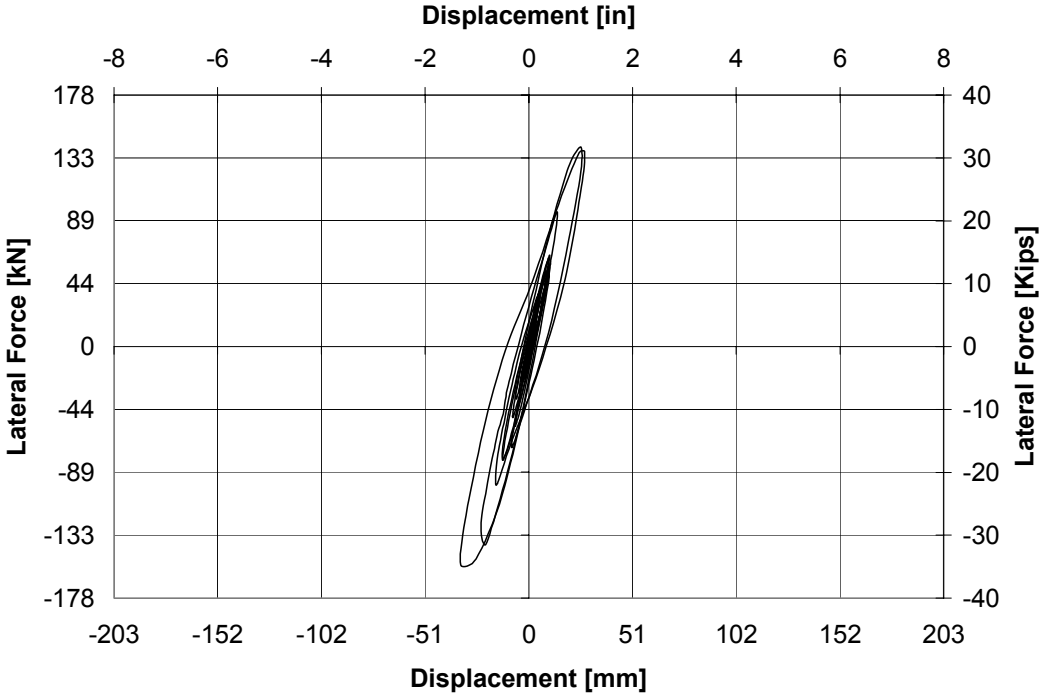

Figure 4-39 Force Displacement Hysteresis Curve for ISL1.0 at 1.0xSlymar

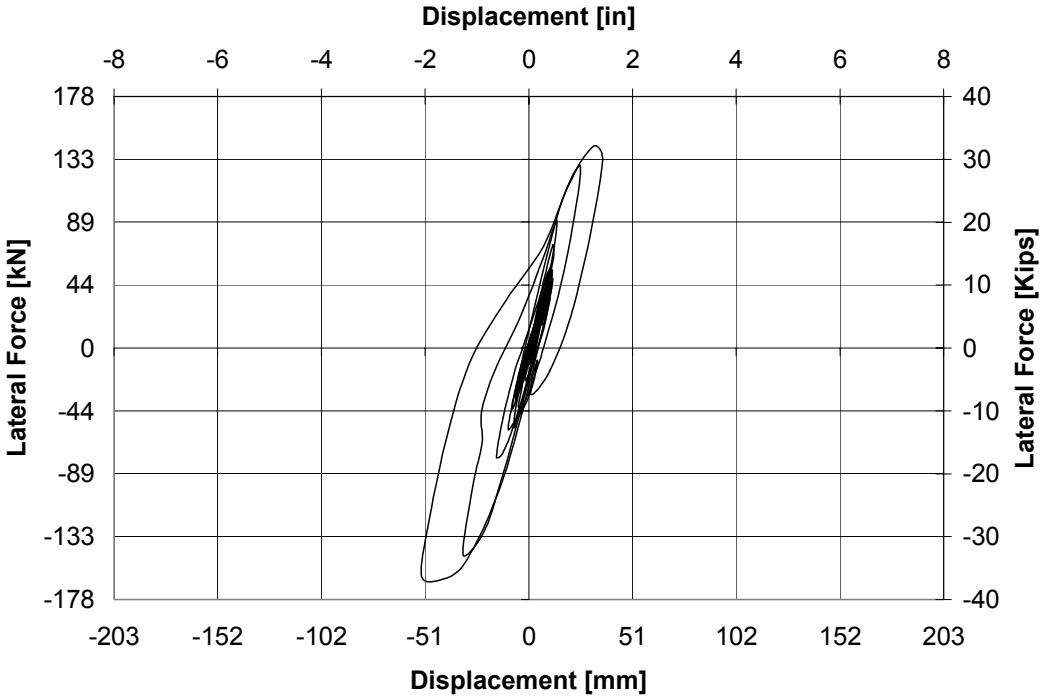

Figure 4-40 Force Displacement Hysteresis Curve for ISL1.0 at 1.25xSlymar

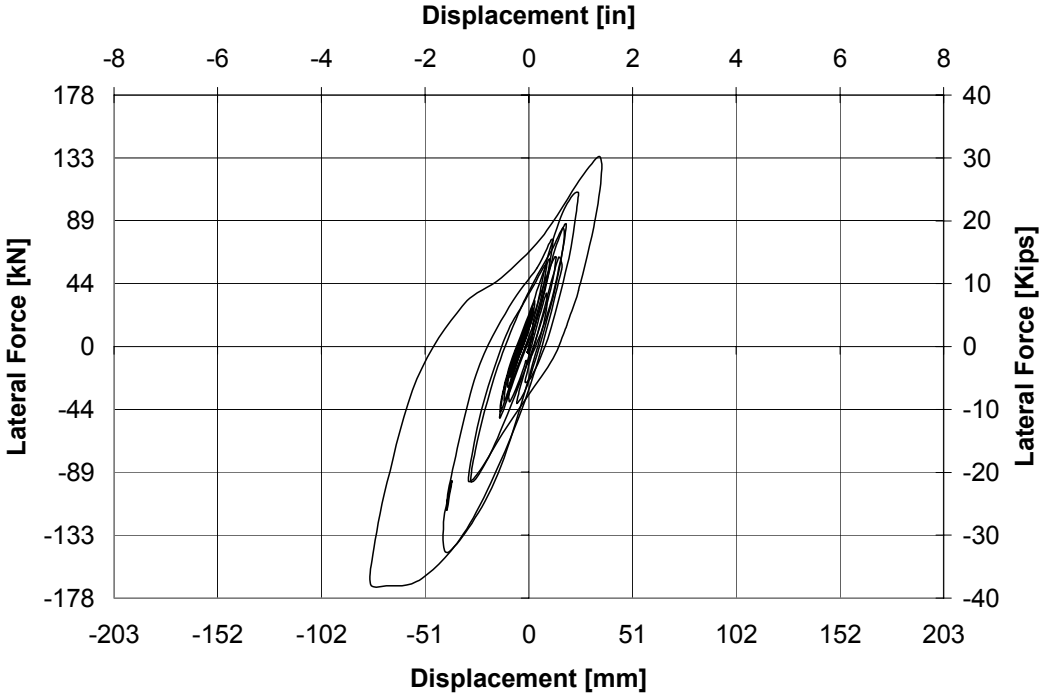

Figure 4-41 Force Displacement Hysteresis Curve for ISL1.0 at 1.5xSlymar

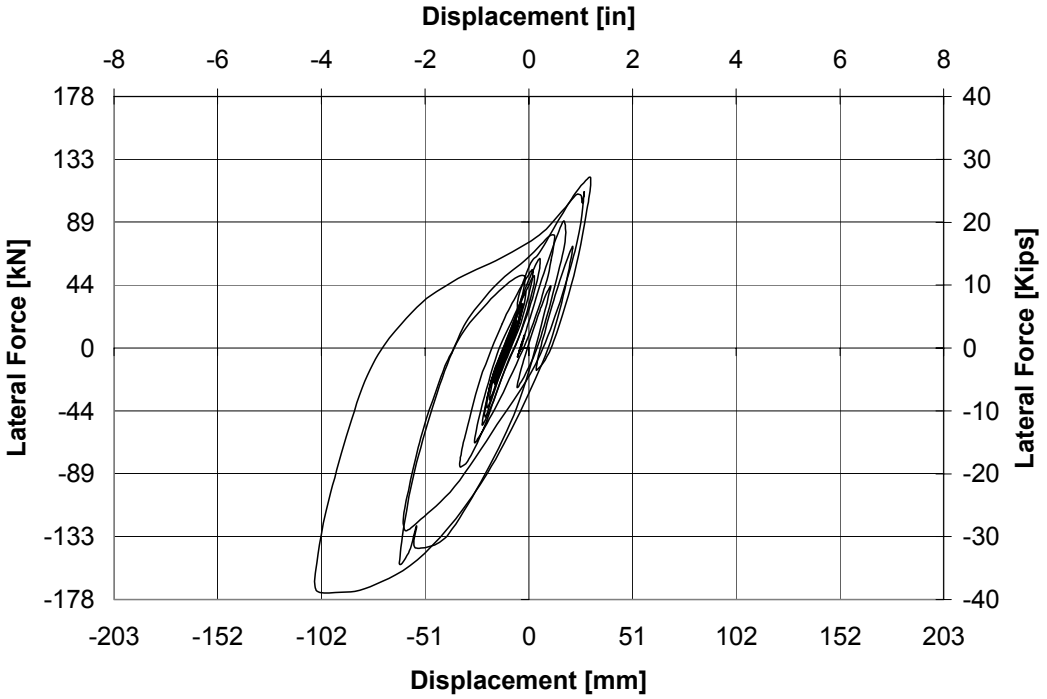

Figure 4-42 Force Displacement Hysteresis Curve for ISL1.0 at 1.75xSlymar

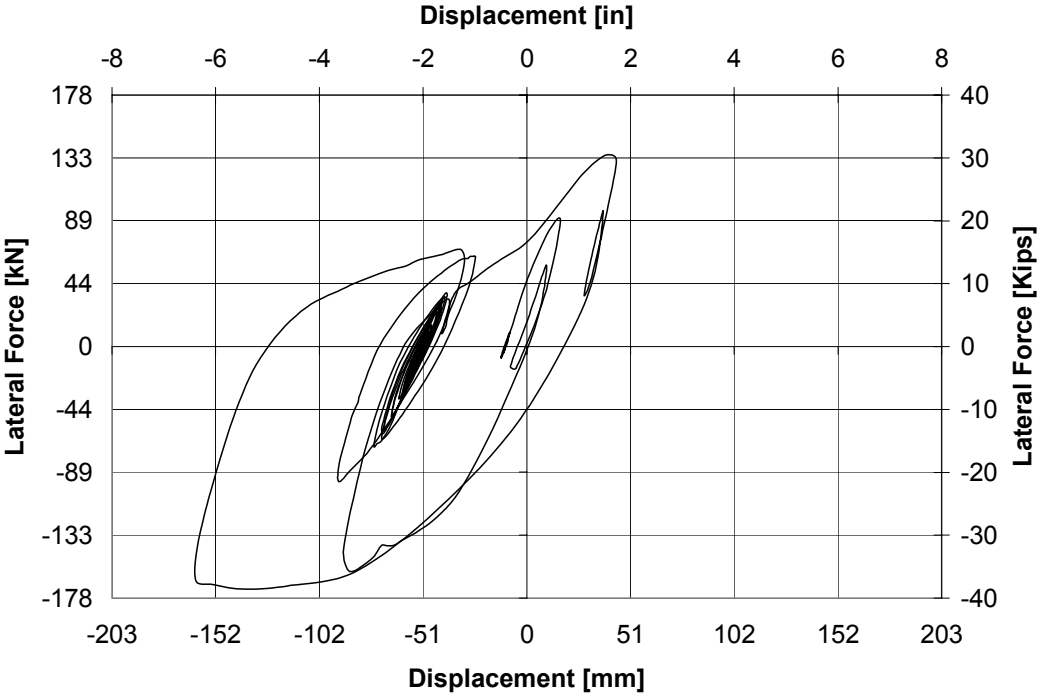

Figure 4-43 Force Displacement Hysteresis Curve for ISL1.0 at 2.0xSlymar

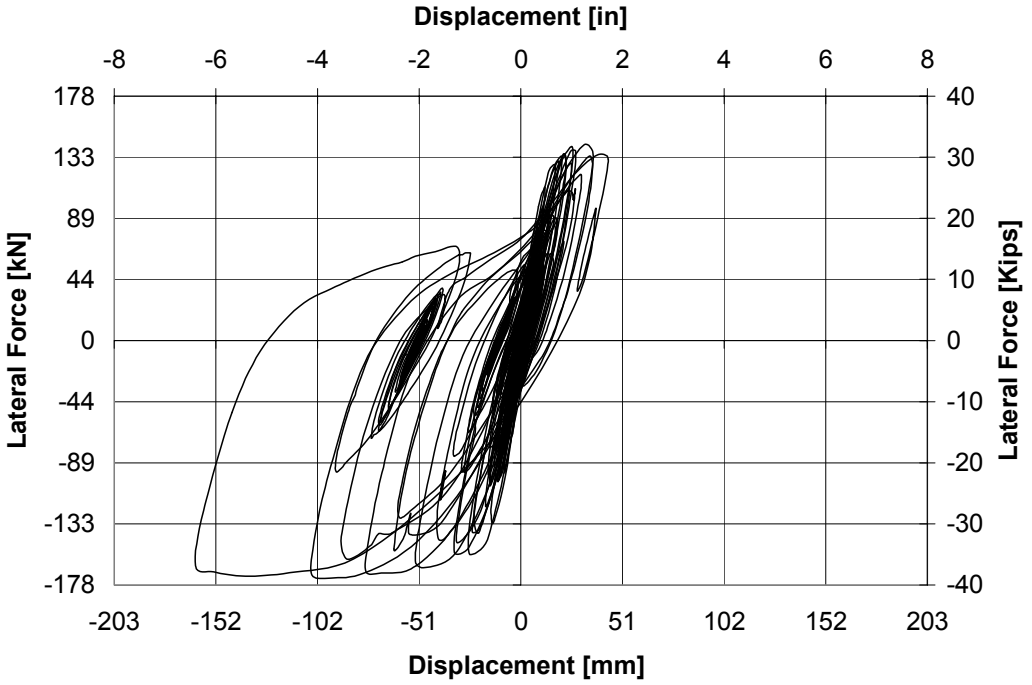

Figure 4-44 Accumulated Force Displacement Hysteresis Curve for ISL1.0

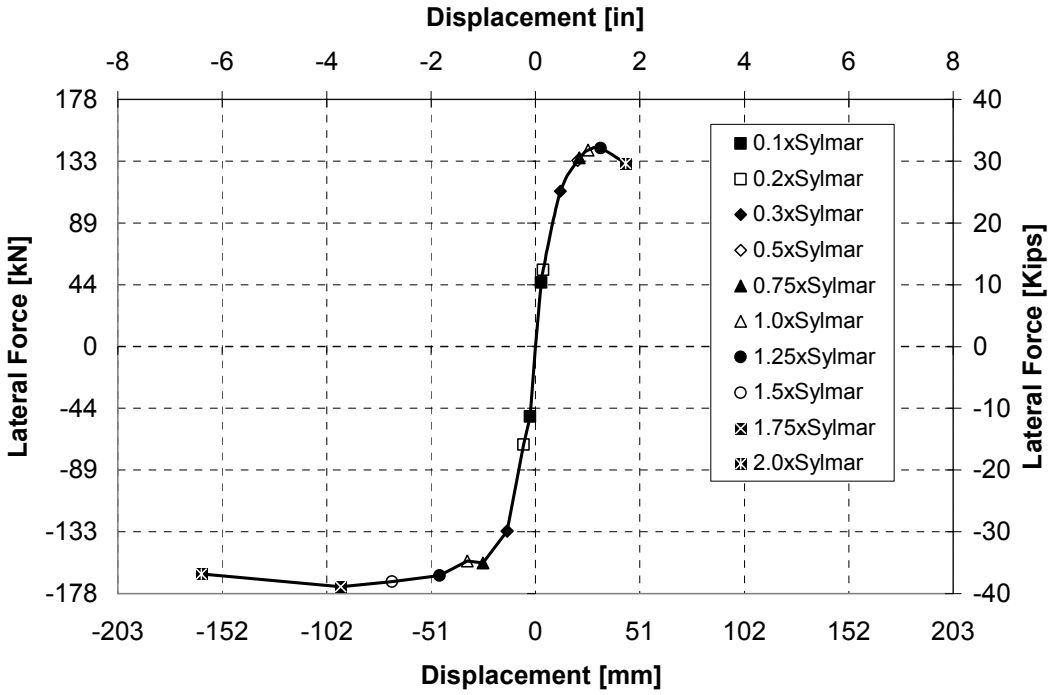

Figure 4-45 Envelope of Accumulated Force Displacement Hysteresis Curve for ISL1.0

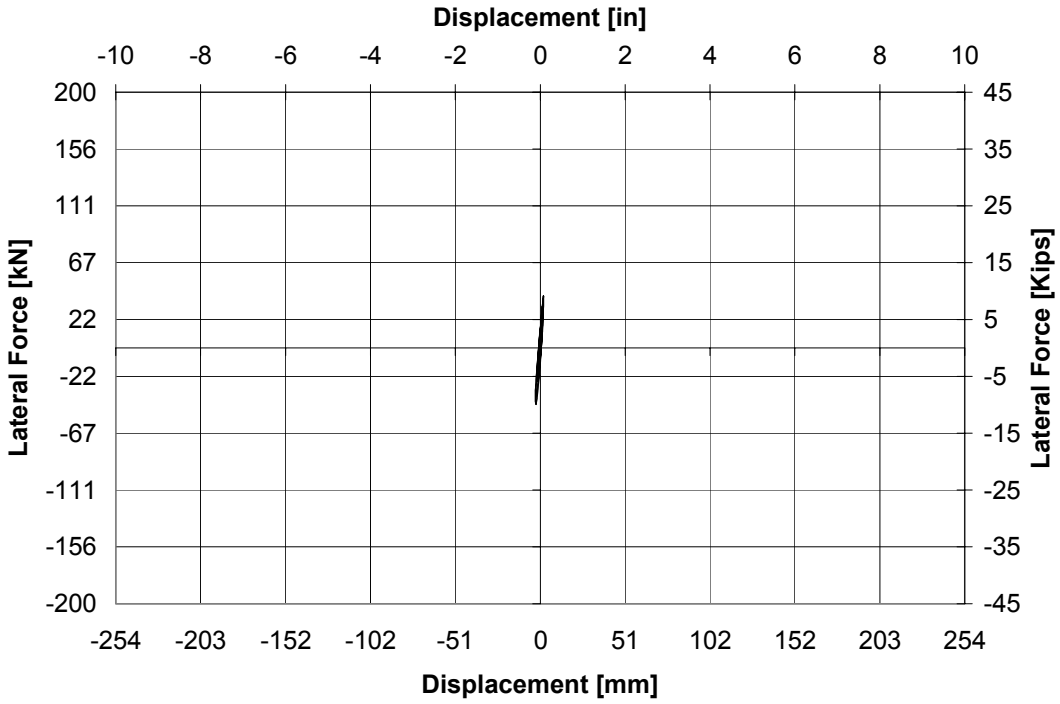

Figure 4-46 Force Displacement Hysteresis Curve for ISL1.5 at 0.1xSlymar

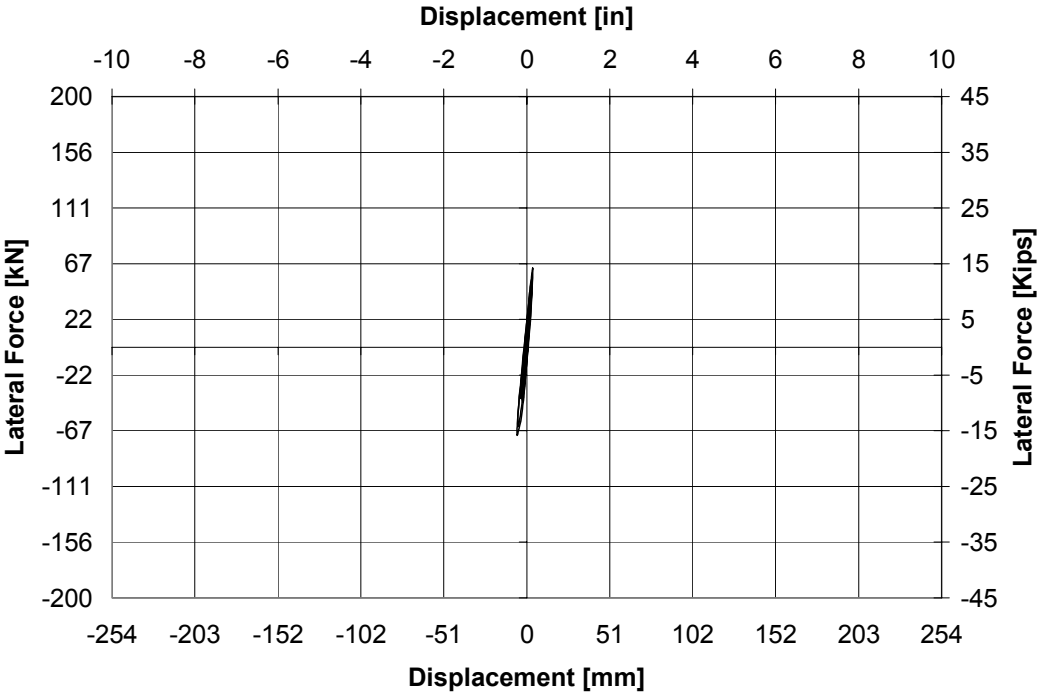

Figure 4-47 Force Displacement Hysteresis Curve for ISL1.5 at 0.2xSlymar

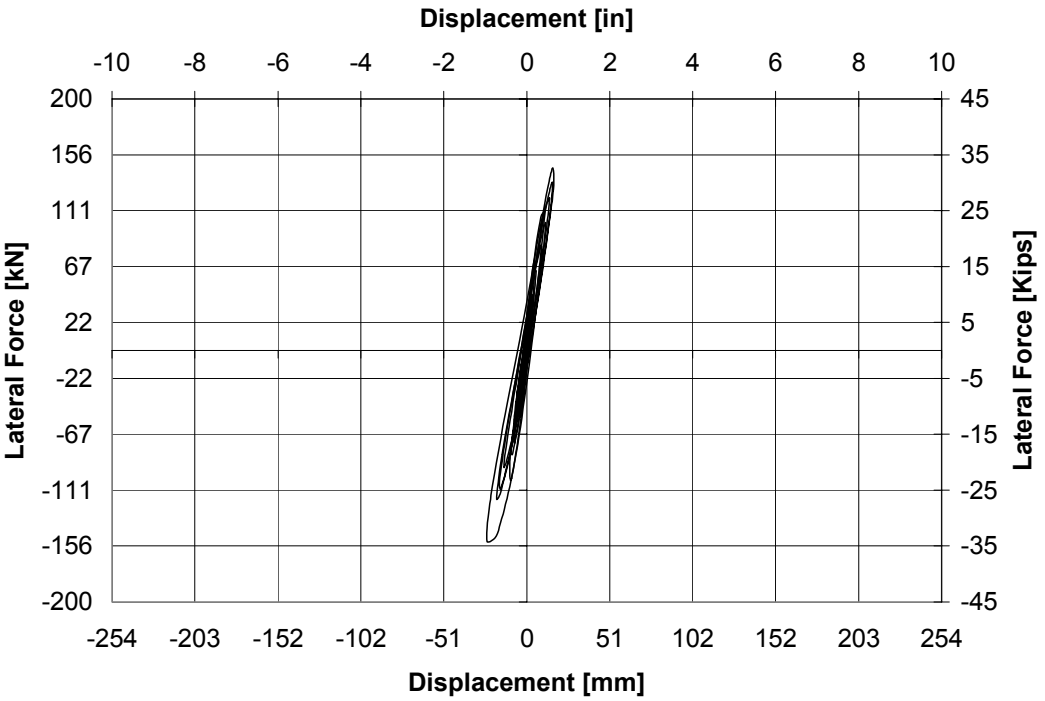

Figure 4-48 Force Displacement Hysteresis Curve for ISL1.5 at 0.4xSlymar

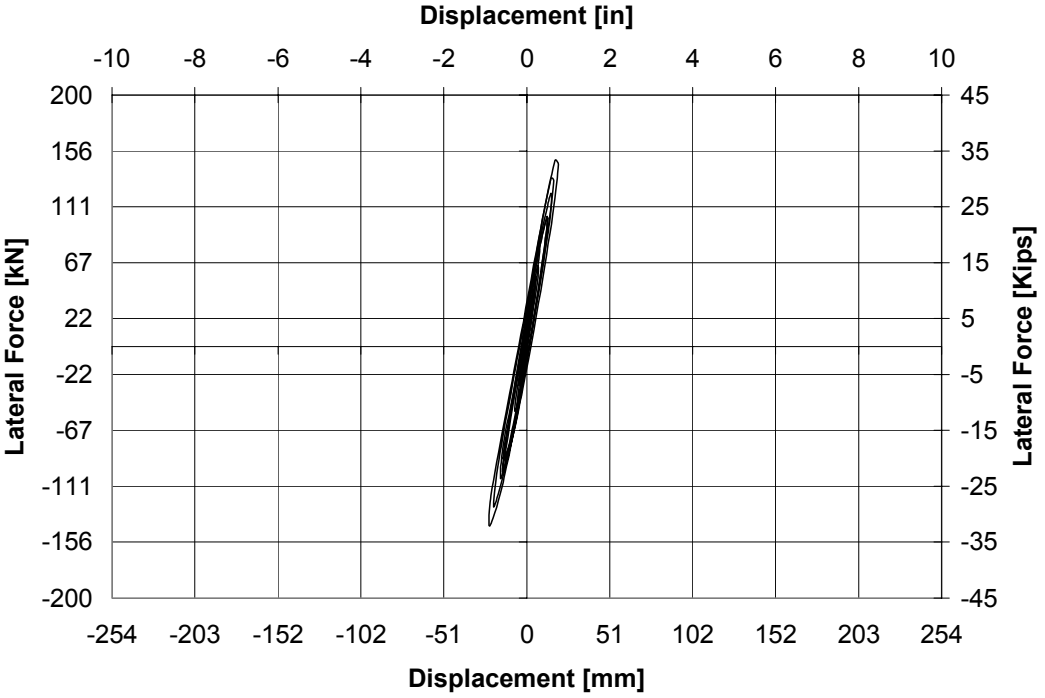

Figure 4-49 Force Displacement Hysteresis Curve for ISL1.5 at 0.6xSlymar

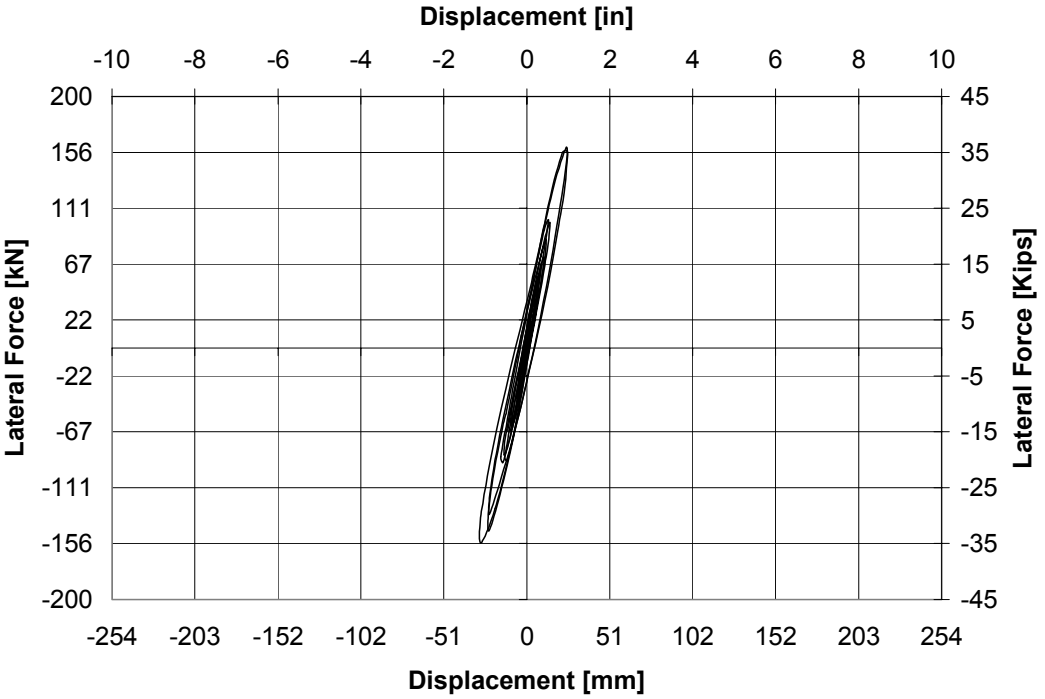

Figure 4-50 Force Displacement Hysteresis Curve for ISL1.5 at 0.8xSlymar

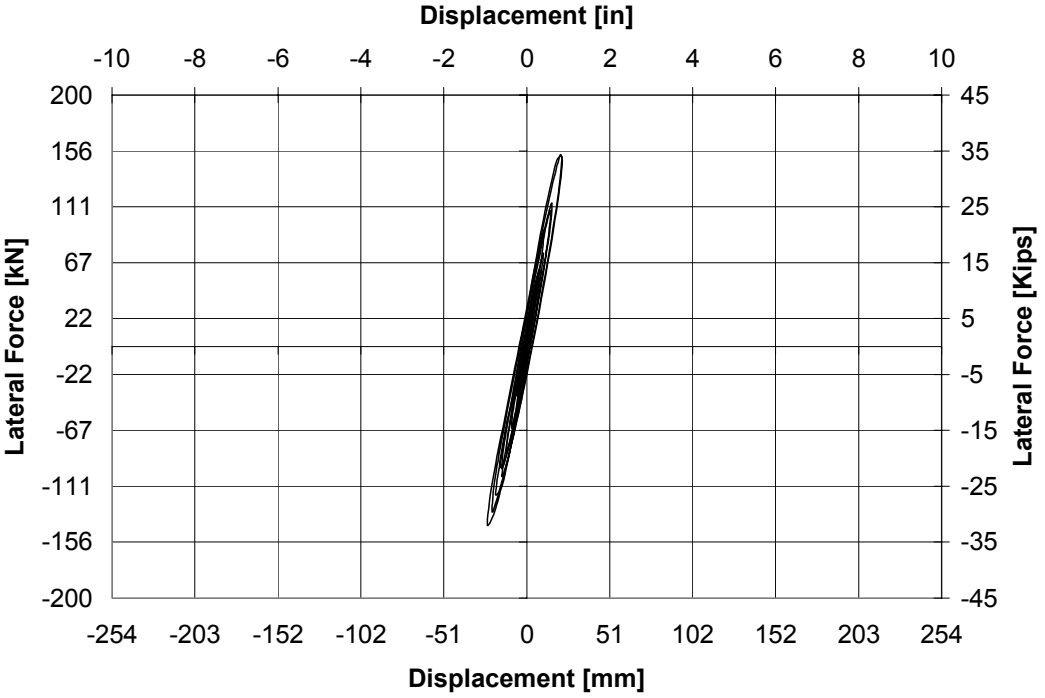

Figure 4-51 Force Displacement Hysteresis Curve for ISL1.5 at 1.0xSlymar

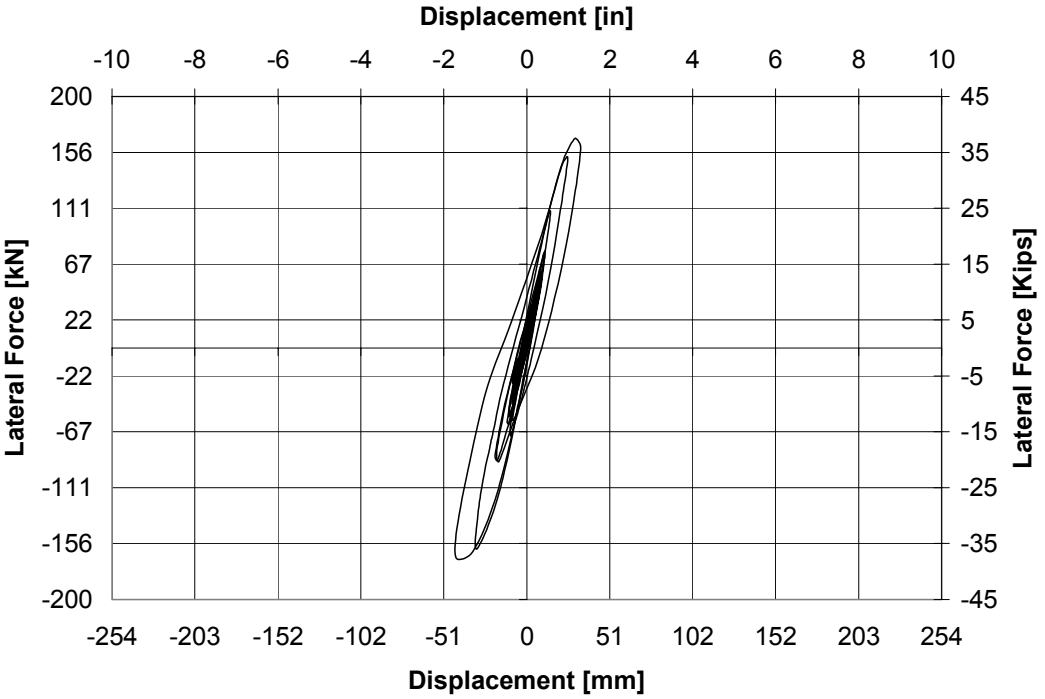

Figure 4-52 Force Displacement Hysteresis Curve for ISL1.5 at 1.25xSlymar

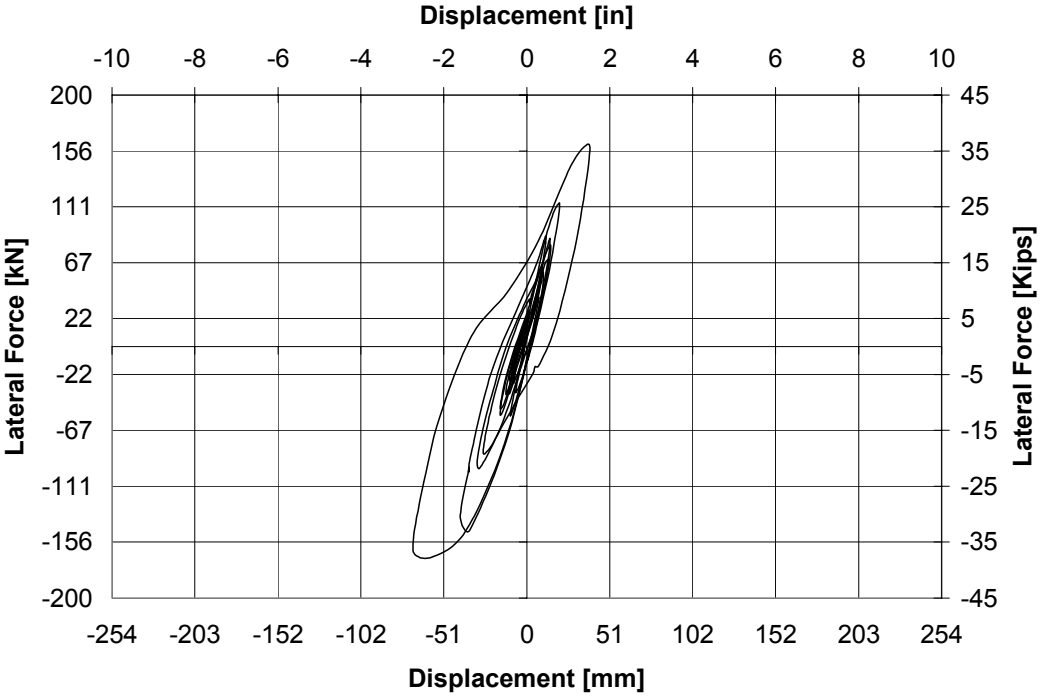

Figure 4-53 Force Displacement Hysteresis Curve for ISL1.5 at 1.5xSlymar

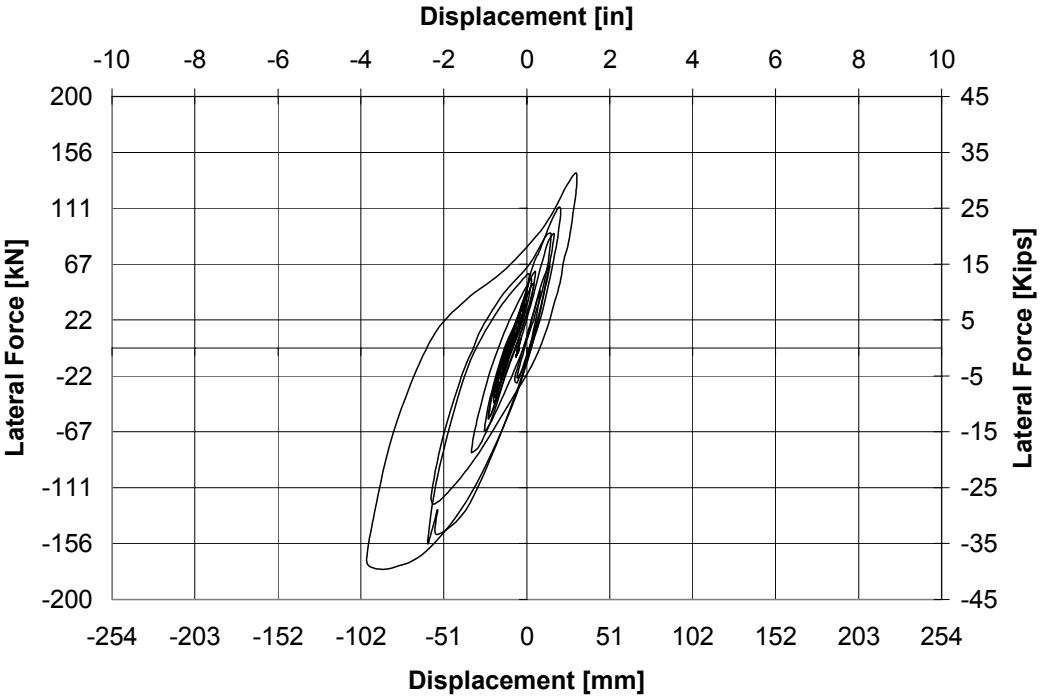

Figure 4-54 Force Displacement Hysteresis Curve for ISL1.5 at 1.75xSlymar

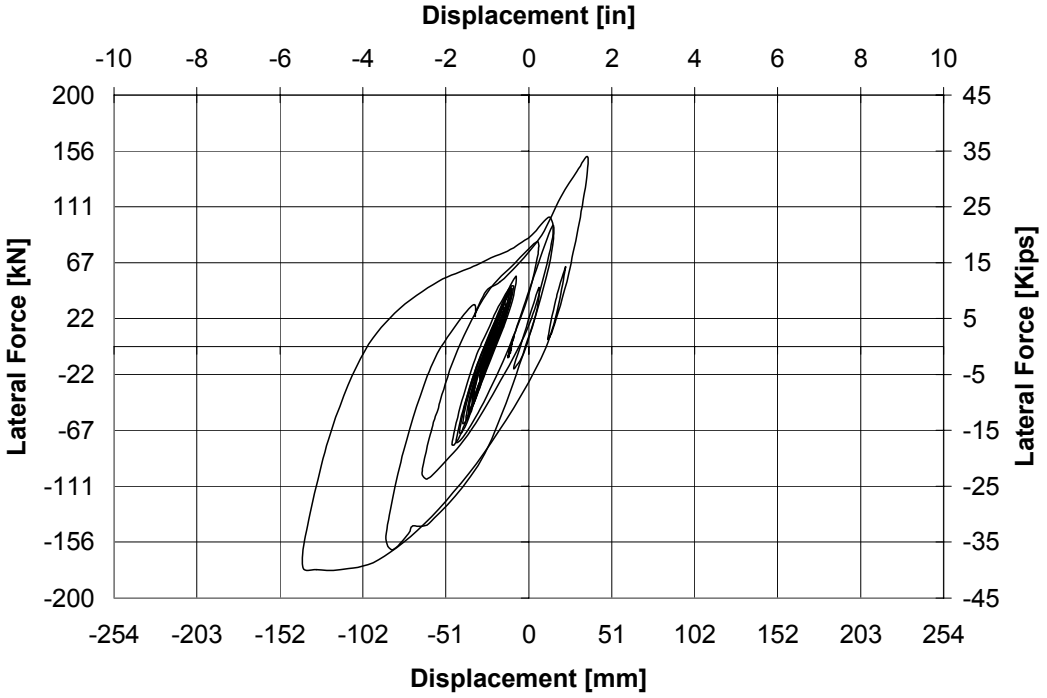

Figure 4-55 Force Displacement Hysteresis Curve for ISL1.5 at 2.0xSlymar

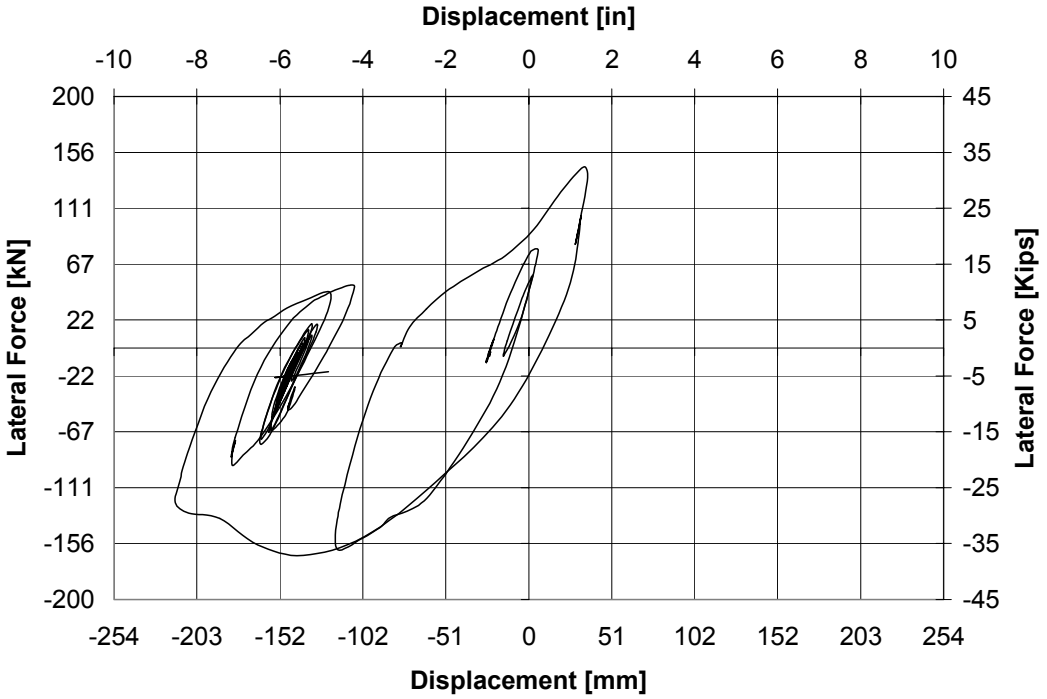

Figure 4-56 Force Displacement Hysteresis Curve for ISL1.5 at 2.125xSlymar

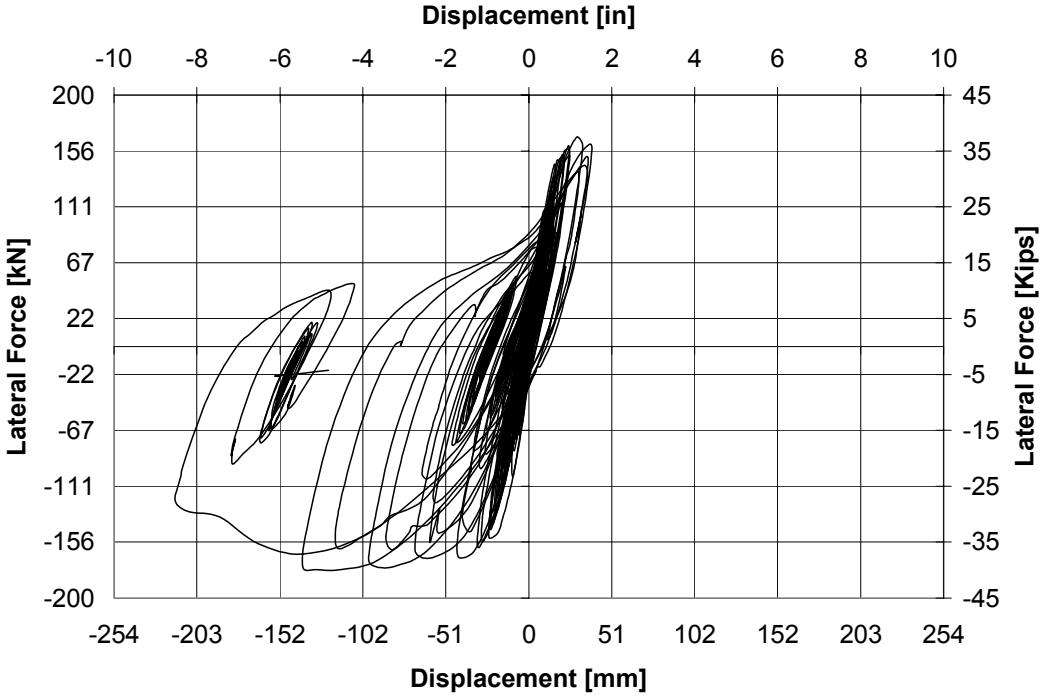

Figure 4-57 Accumulated Force Displacement Hysteresis Curve for ISL1.5

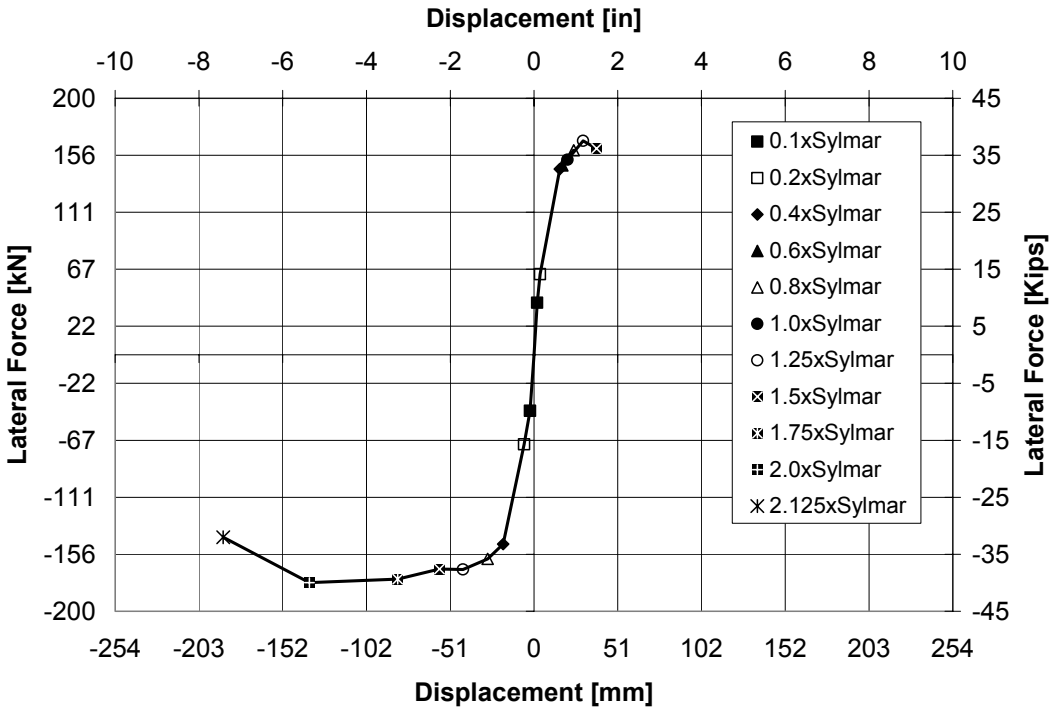

Figure 4-58 Envelope of Accumulated Force Displacement Hysteresis Curve for ISL1.5

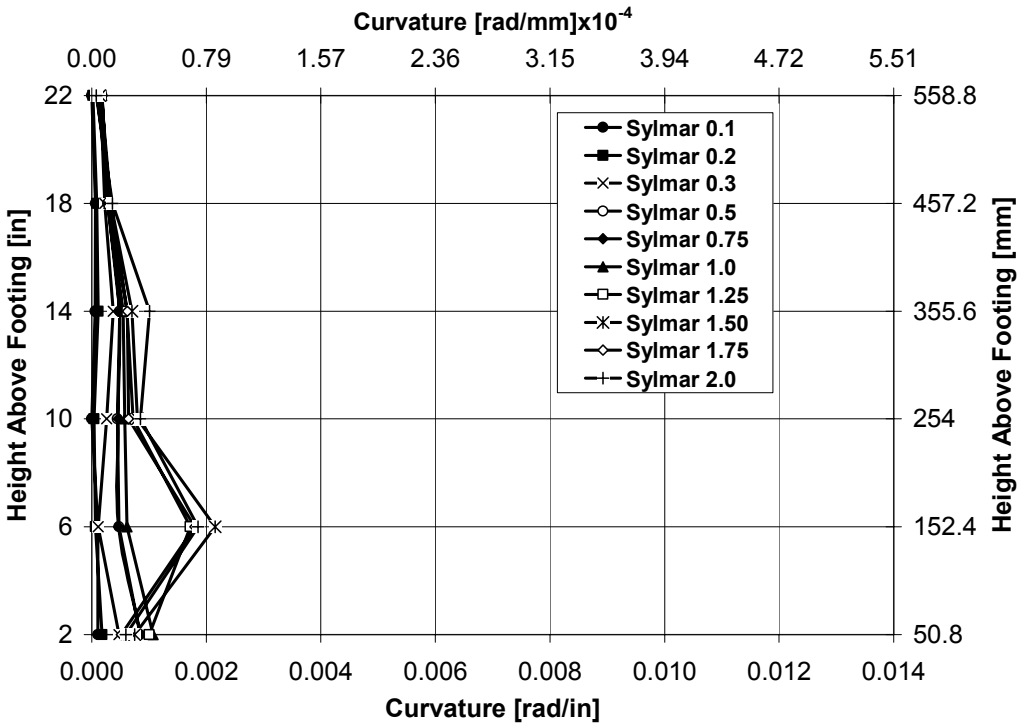

Figure 4-59 Curvature Profile at the Maximum Peak Lateral Force for Specimen ISL1.0

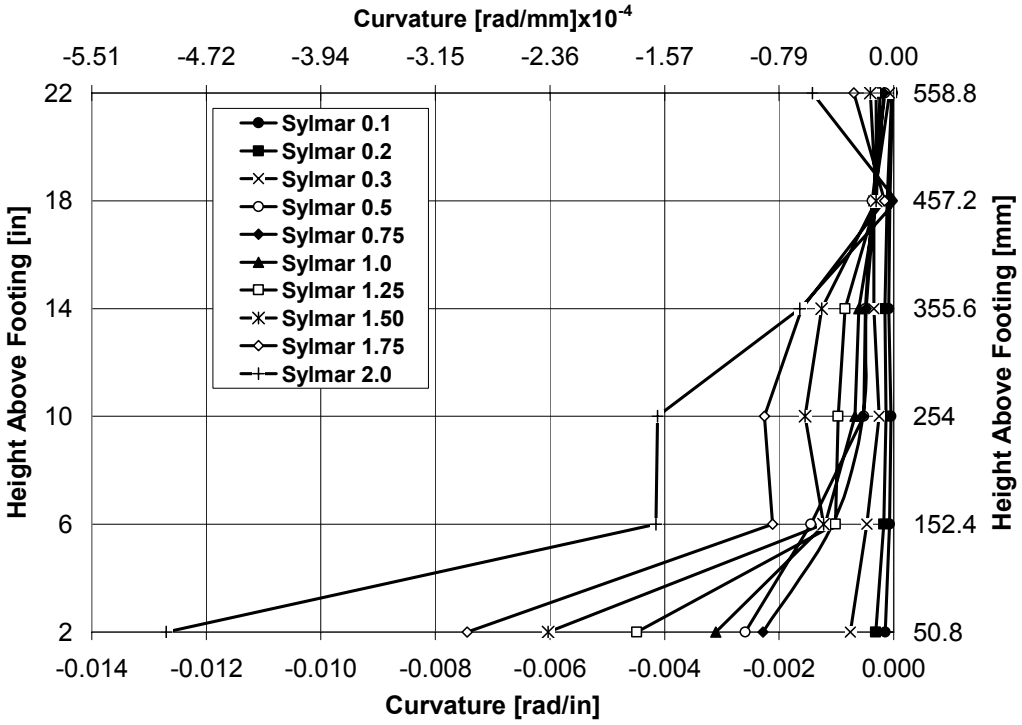

Figure 4-60 Curvature Profile at the Minimum Peak Lateral Force for Specimen ISL1.0

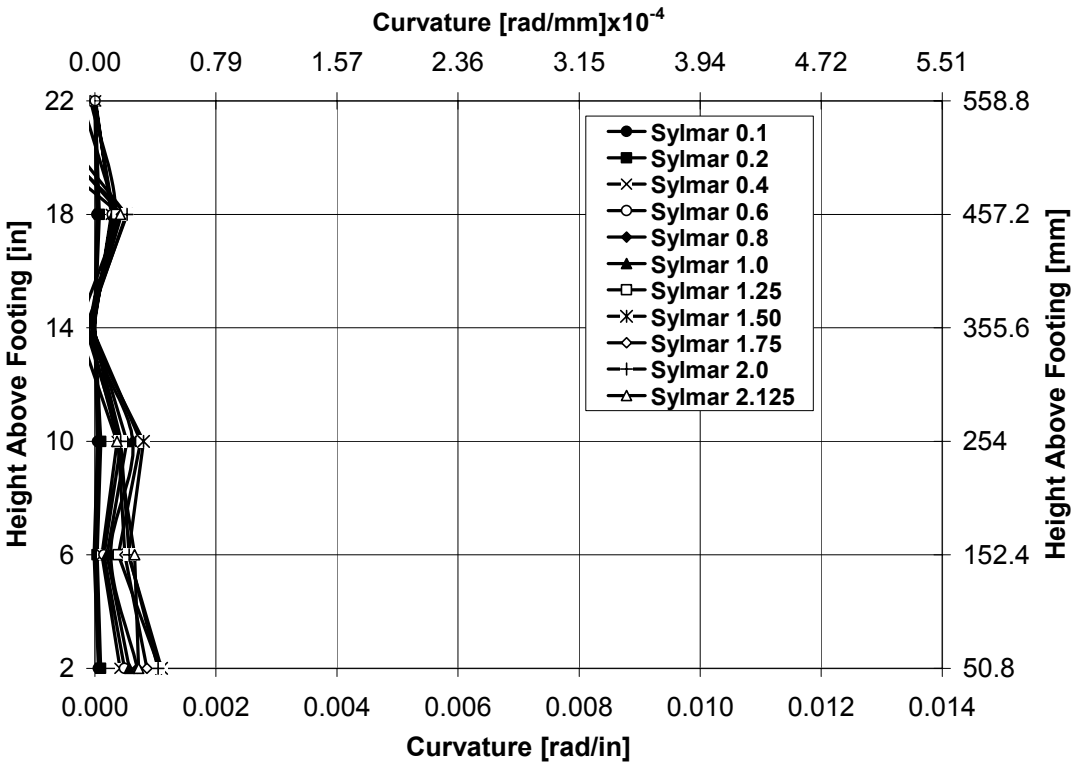

Figure 4-61 Curvature Profile at the Maximum Peak Lateral Force for Specimen ISL1.5

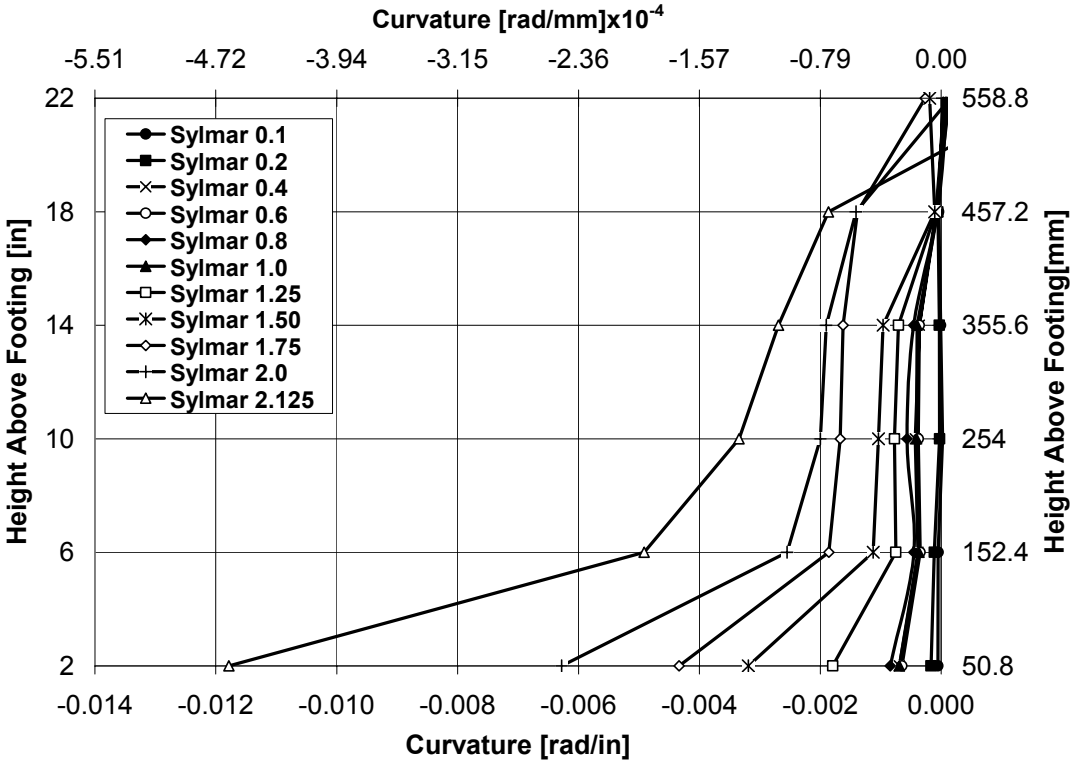

Figure 4-62 Curvature Profile at the Minimum Peak Lateral Force for Specimen ISL1.5

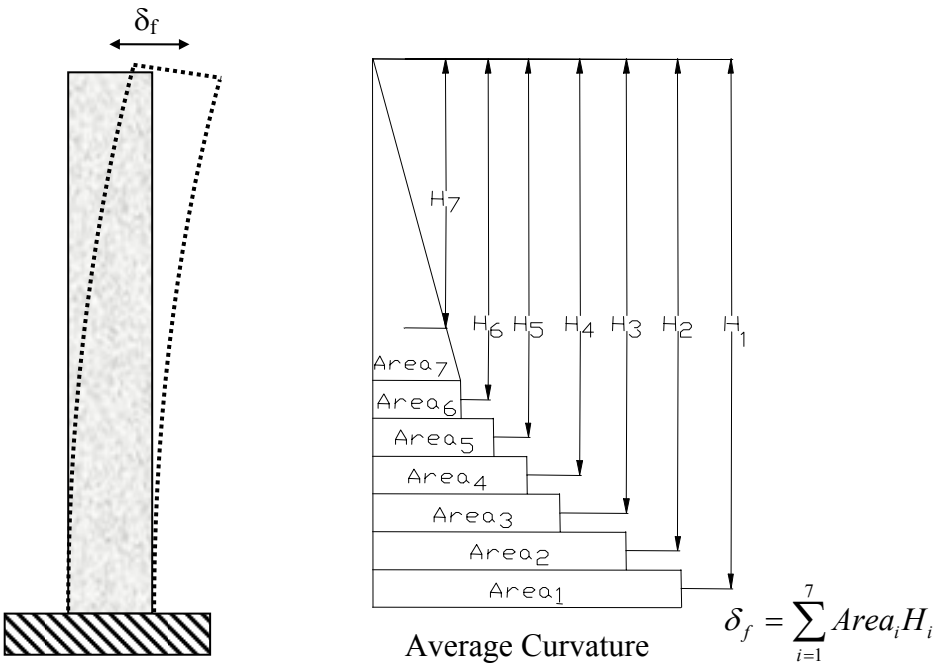

Figure 4-63 Moment Area Method to Calculate Flexural Deformation

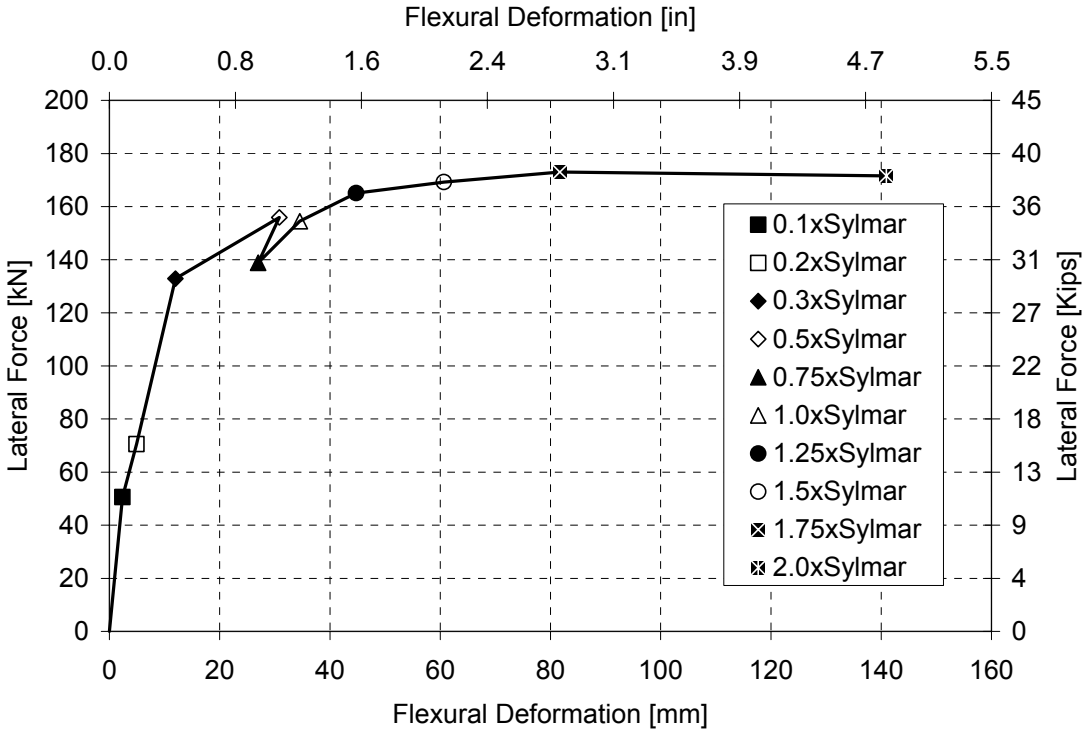

Figure 4-64 Lateral Force versus Flexural Deformation for Specimen ISL1.0

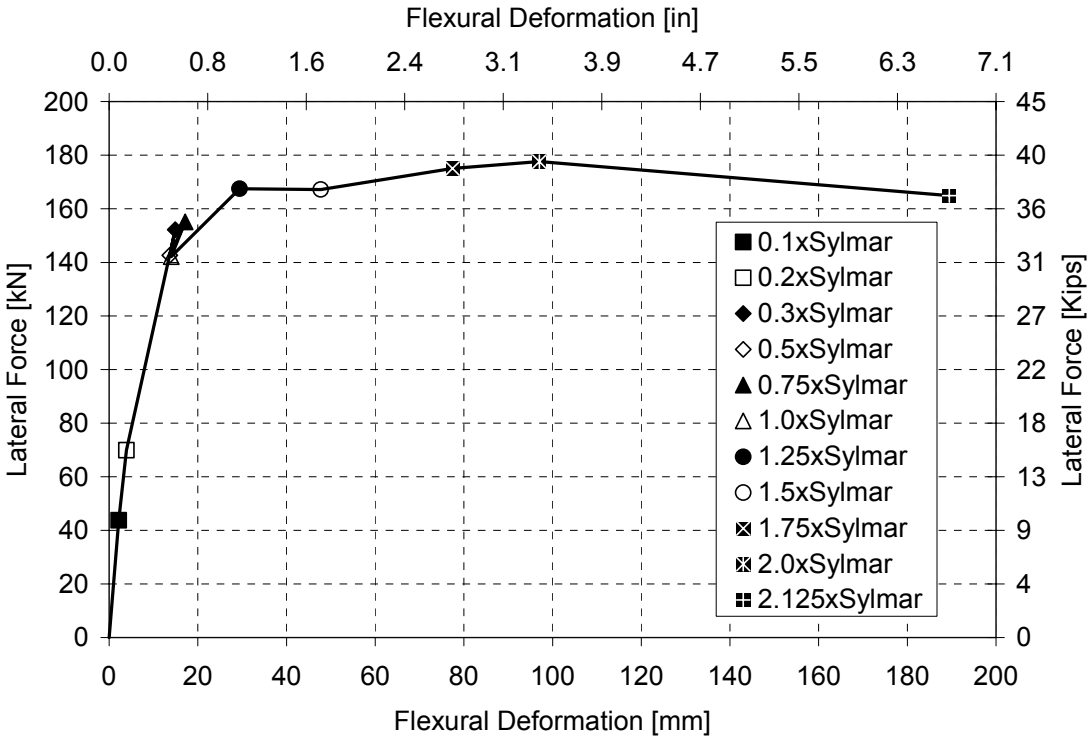

Figure 4-65 Lateral Force versus Flexural Deformation for Specimen ISL1.5

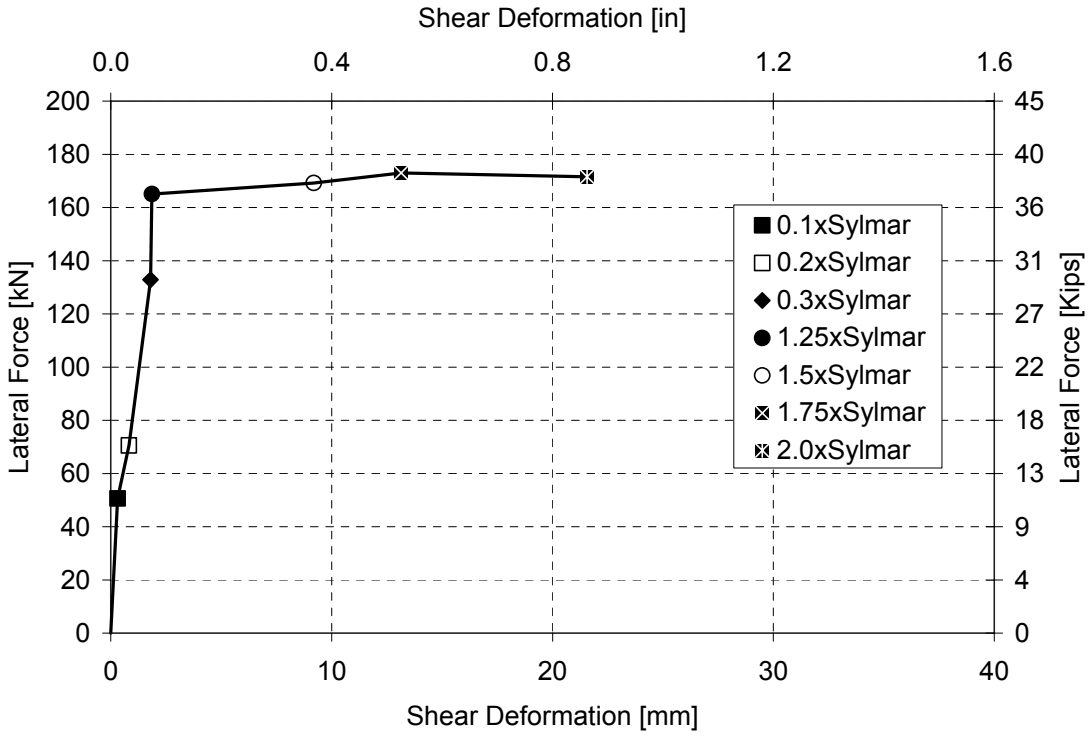

Figure 4-66 Lateral Force versus Shear Deformation for Specimen ISL1.0

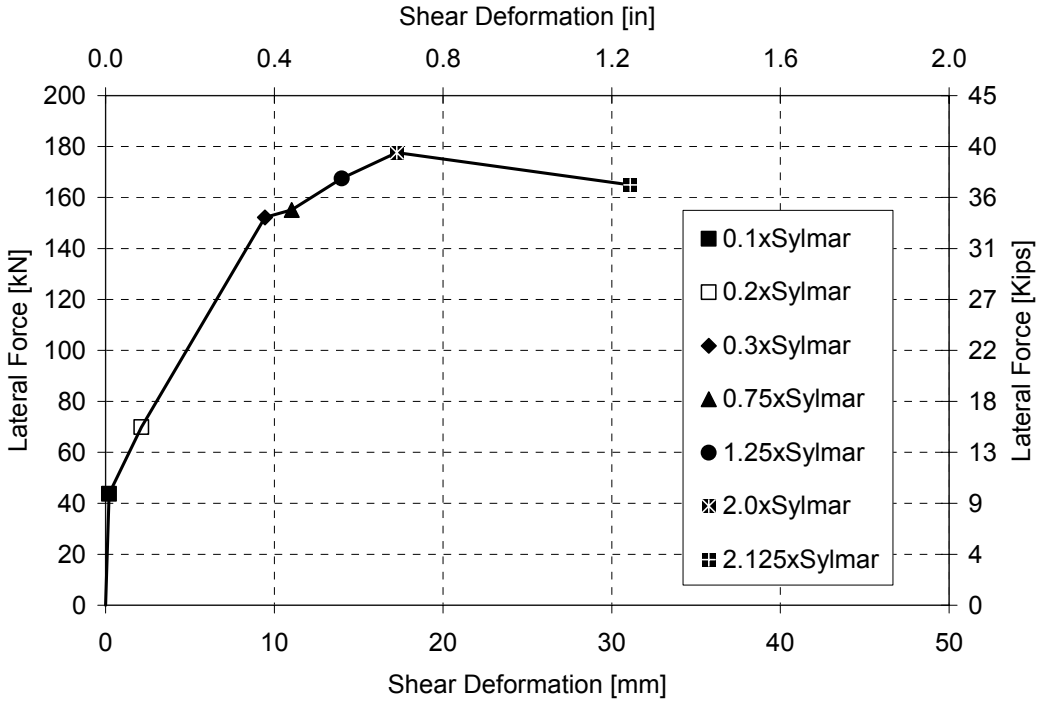

Figure 4-67 Lateral Force versus Shear Deformation for Specimen ISL1.5

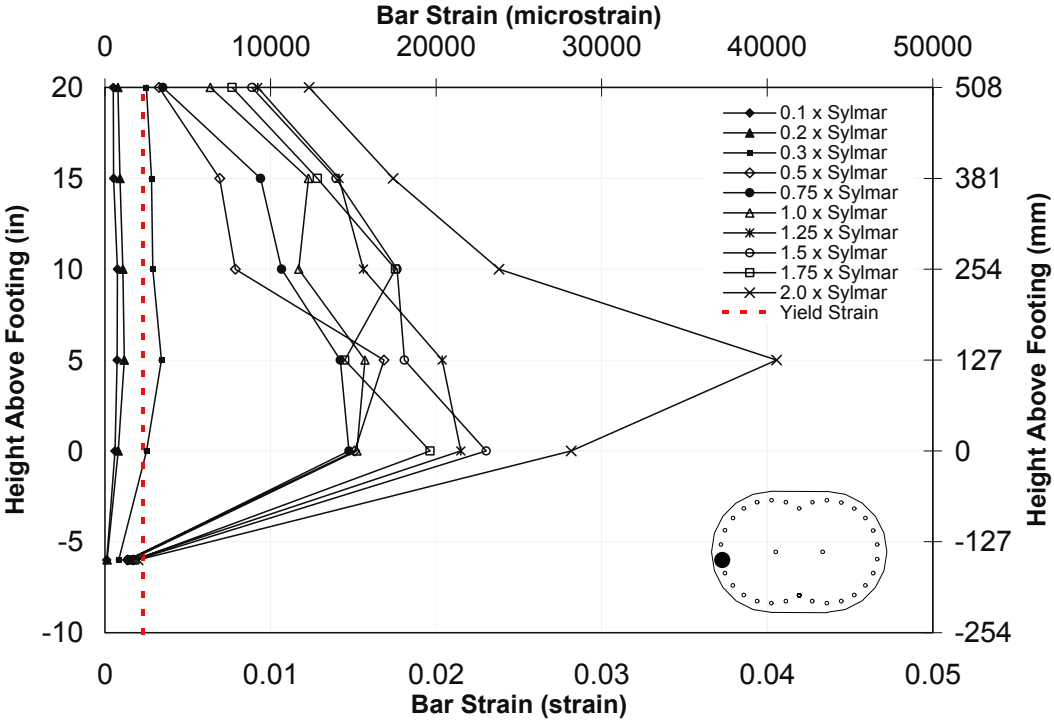

Figure 4-68 Strain Profile Strain Gauge # 1 Specimen ISL1.0

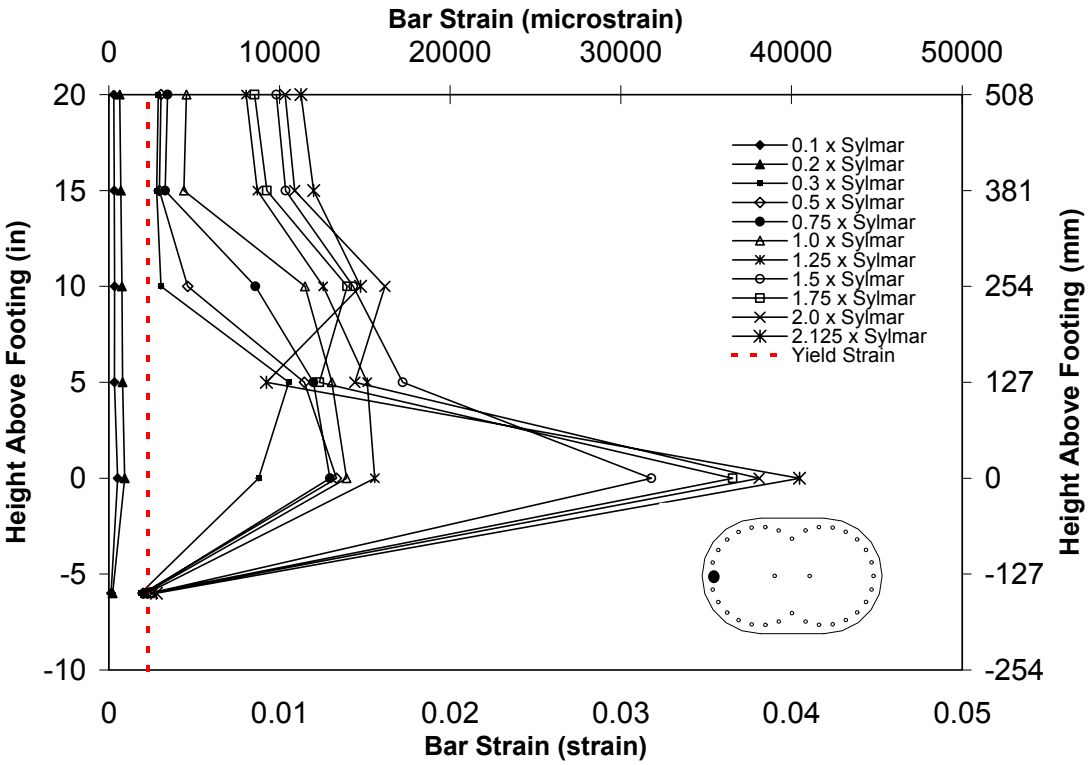

Figure 4-69 Strain Profile Strain Gauge # 1 Specimen ISL1.5

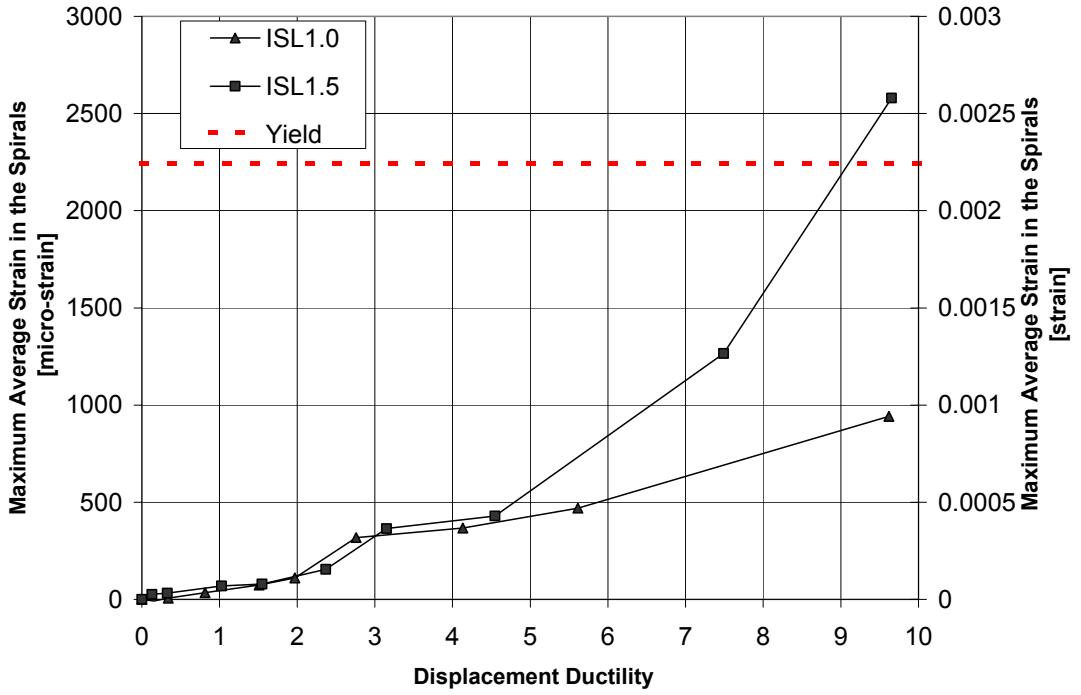

Figure 4-70 Maximum Average Strain in the Spirals Specimens ISL1.0 and ISL1.5

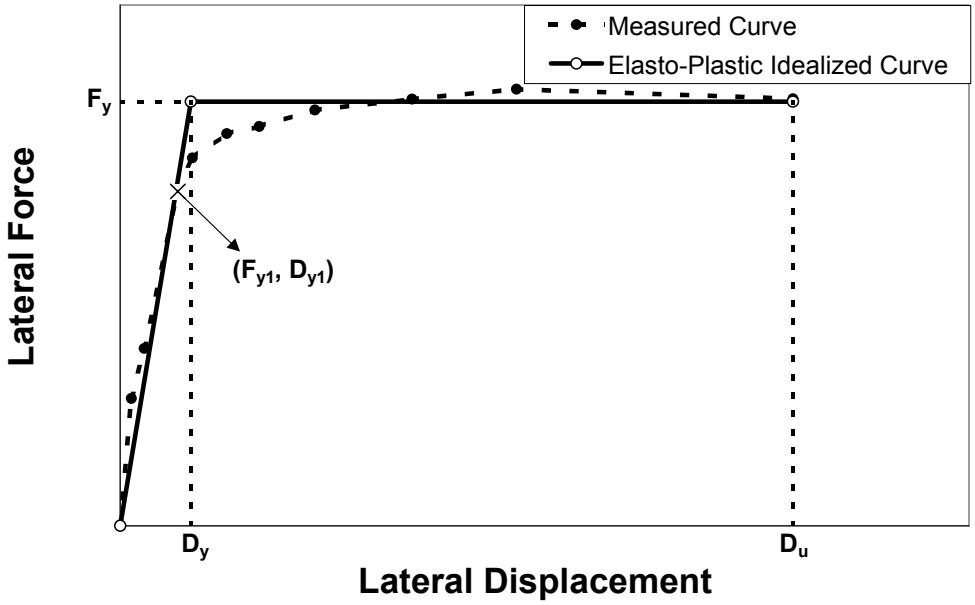

Figure 4-71 Elasto-Plastic Idealized Curve

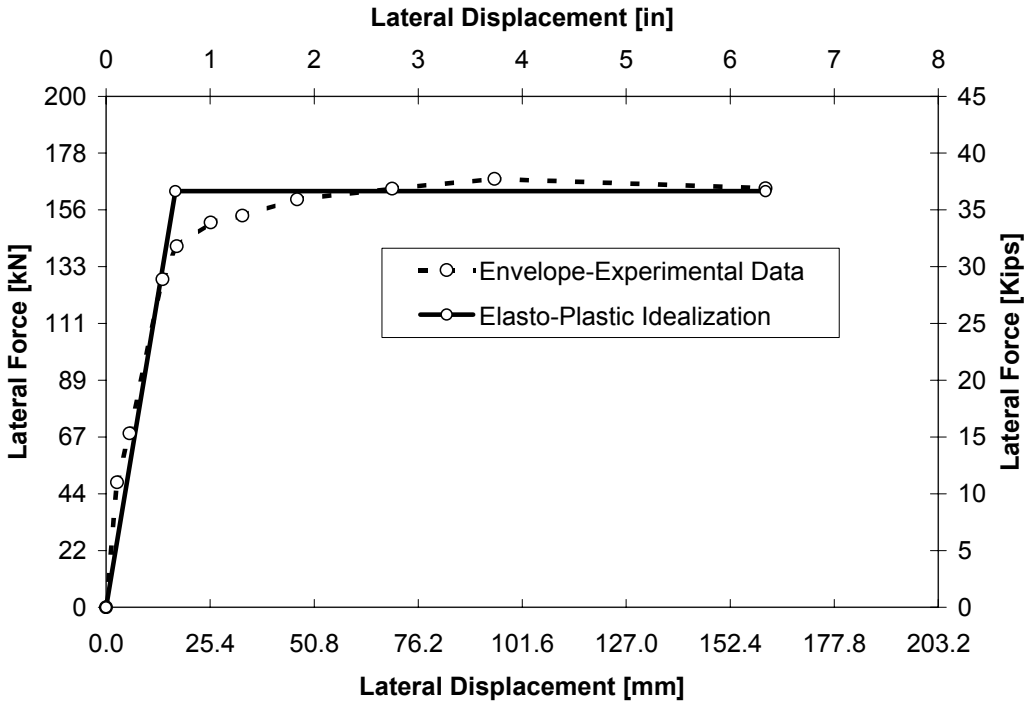

Figure 4-72 Elasto-Plastic Idealized Curve Specimen ISL1.0

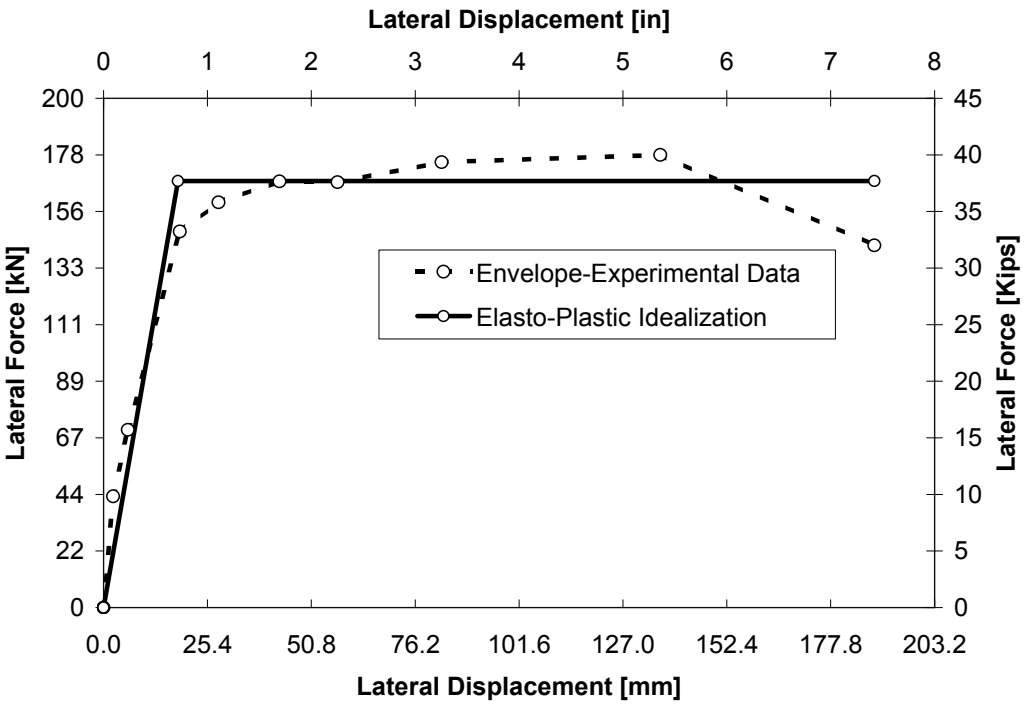

Figure 4-73 Elasto-Plastic Idealized Curve Specimen ISL1.5

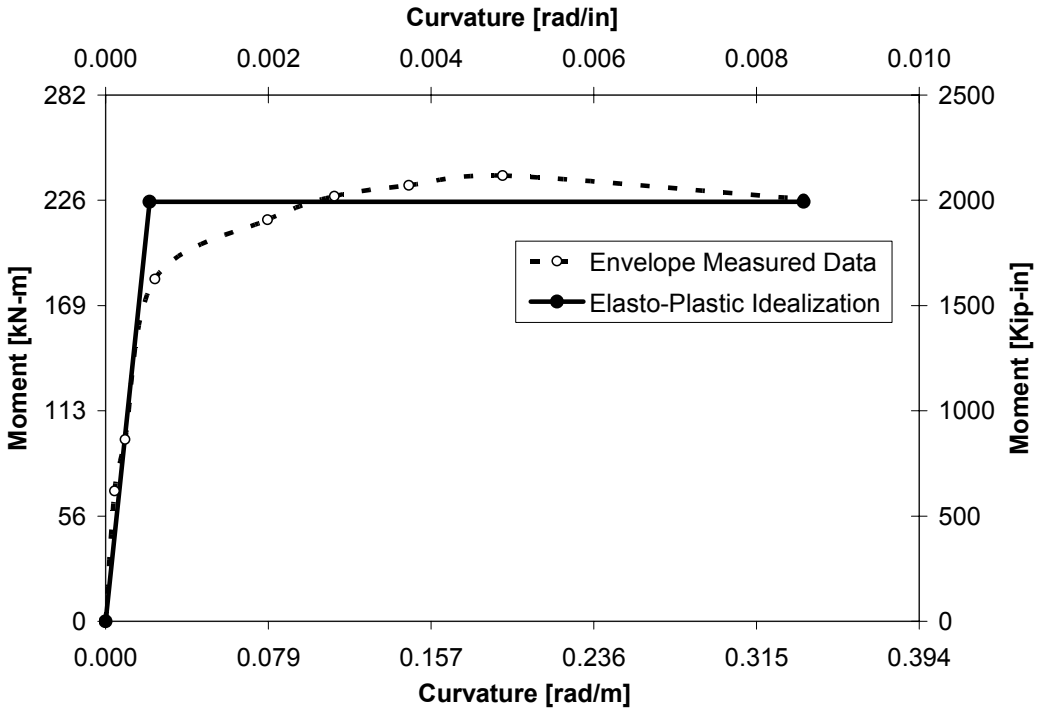

Figure 4-74 The Elasto-Plastic Idealization for the Average Measured Moment-Curvature at 50.8 mm (2 in) and 152.4 mm (6 in) Specimen ISL1.0

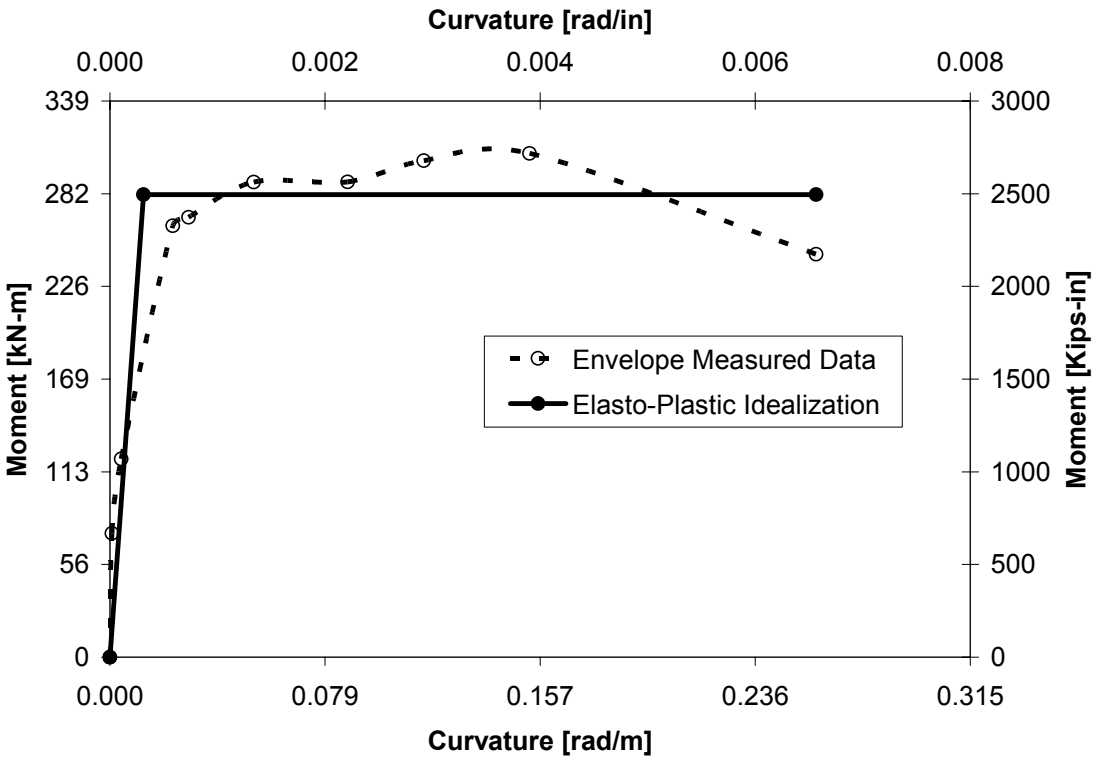

Figure 4-75 The Elasto-Plastic Idealization for the Average Measured Moment-Curvature at 50.8 mm (2 in) and 152.4 mm (6 in) Specimen ISL1.5

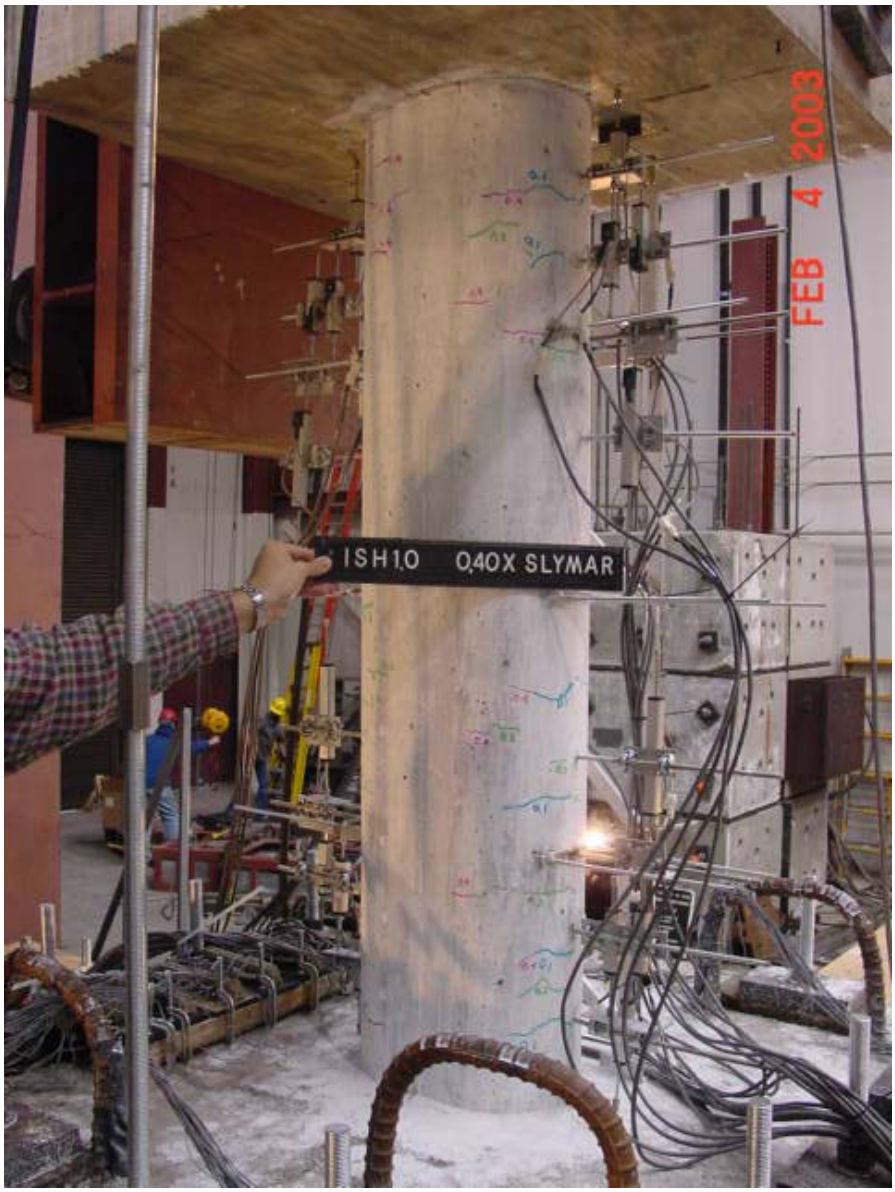

Figure 5-1 Flexural Cracks (μ_d = 0.06-0.4) Specimen ISH1.0

Figure 5-2 Flexural Cracks (μ_d = 0.1-0.6) Specimen ISH1.25

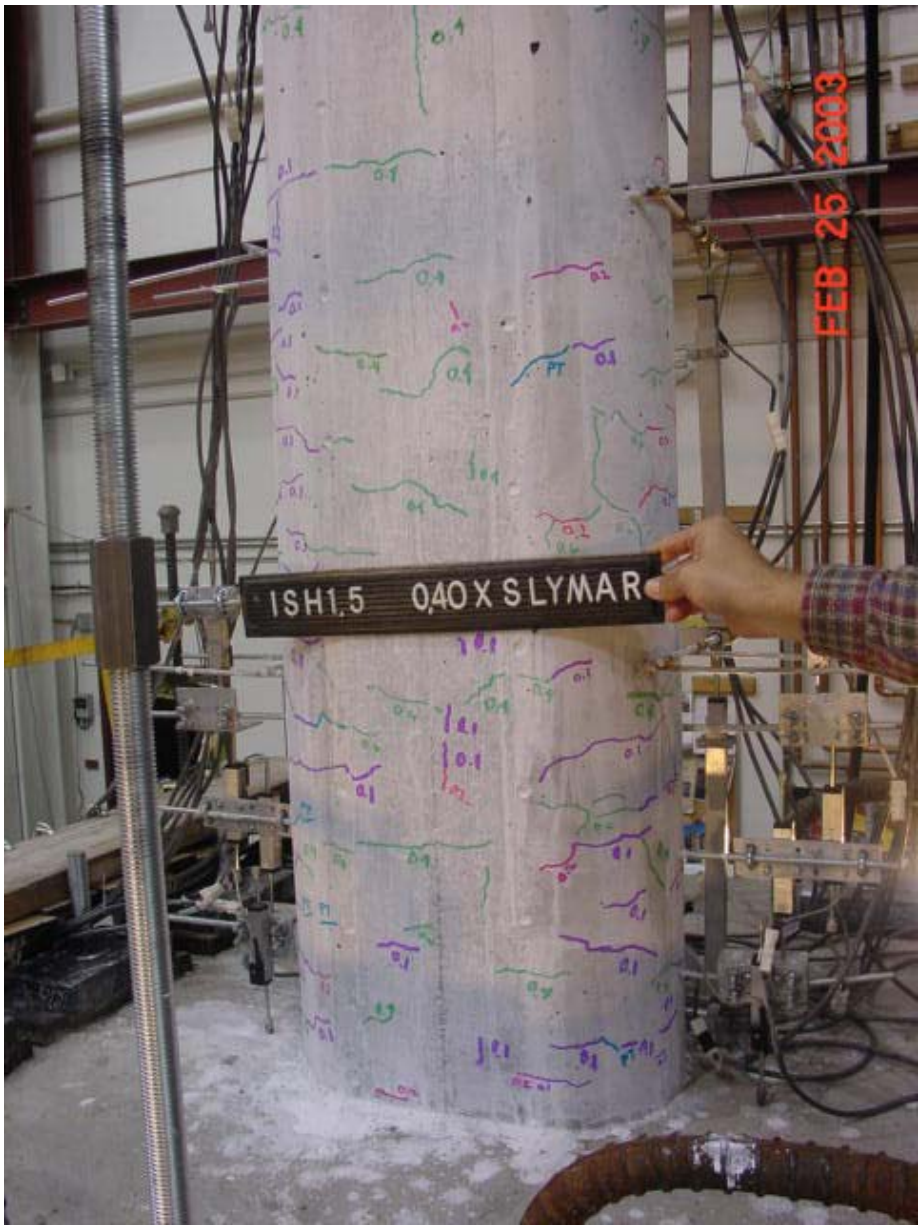

Figure 5-3 Flexural Cracks (μ_d = 0.2-0.7) Specimen ISH1.5

Figure 5-4 Flexural Cracks (μ_d = 0.1-0.6) Specimen ISH1.5T

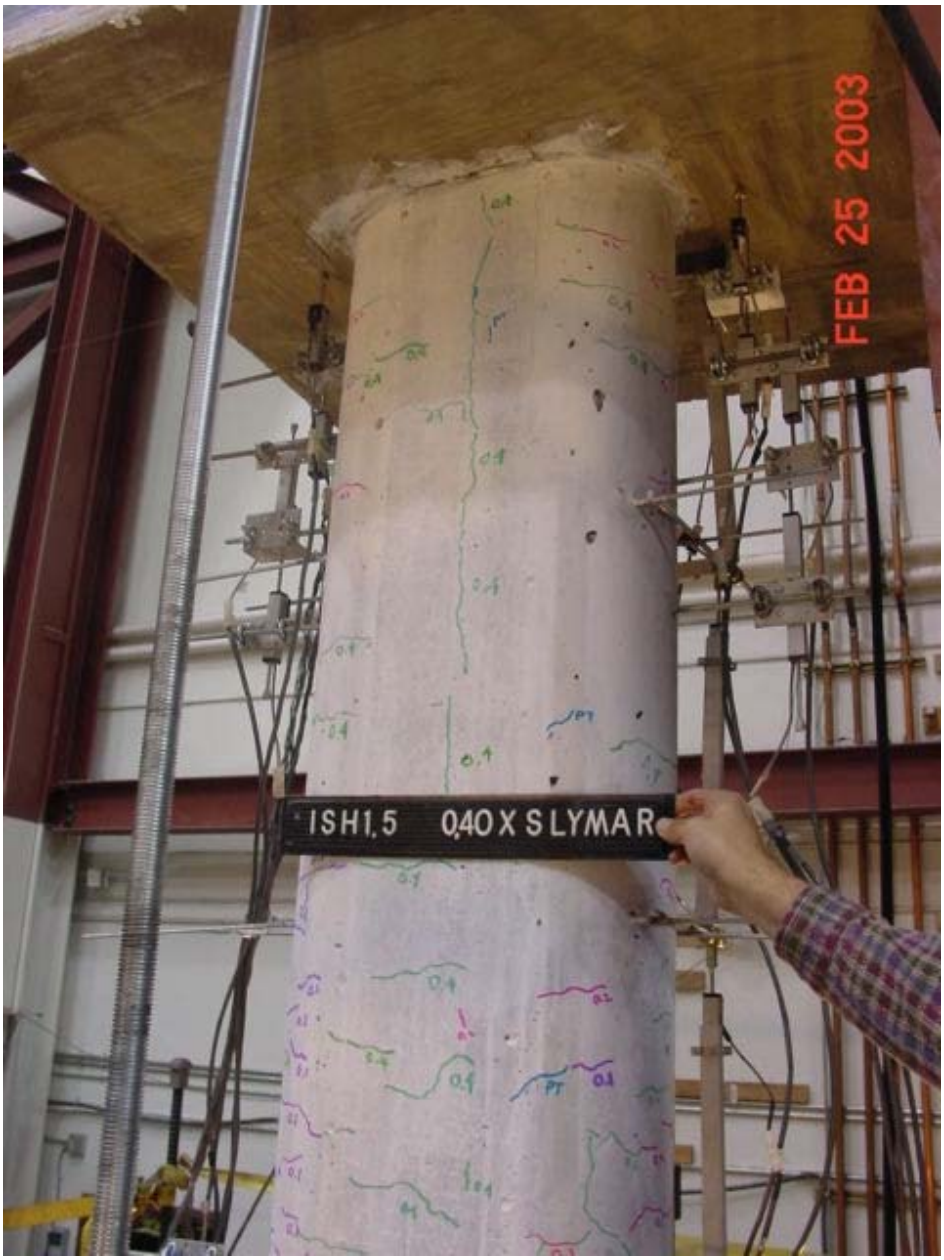

Figure 5-5 Vertical Crack ($\mu_d = 0.7$) Specimen ISH1.5

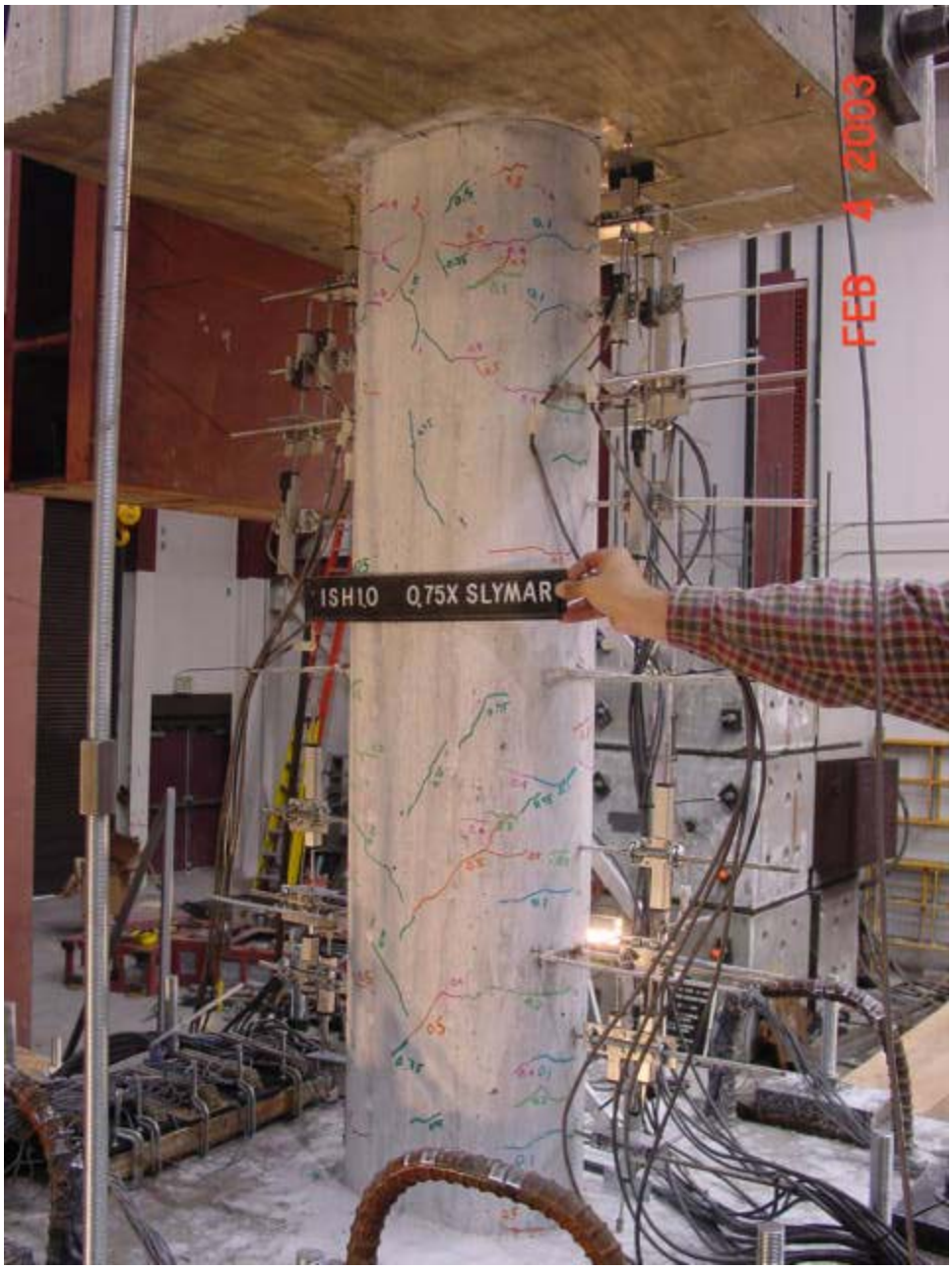

Figure 5-6 Shear Cracks Top and Bottom (μ_d = 0.9) Specimen ISH1.0

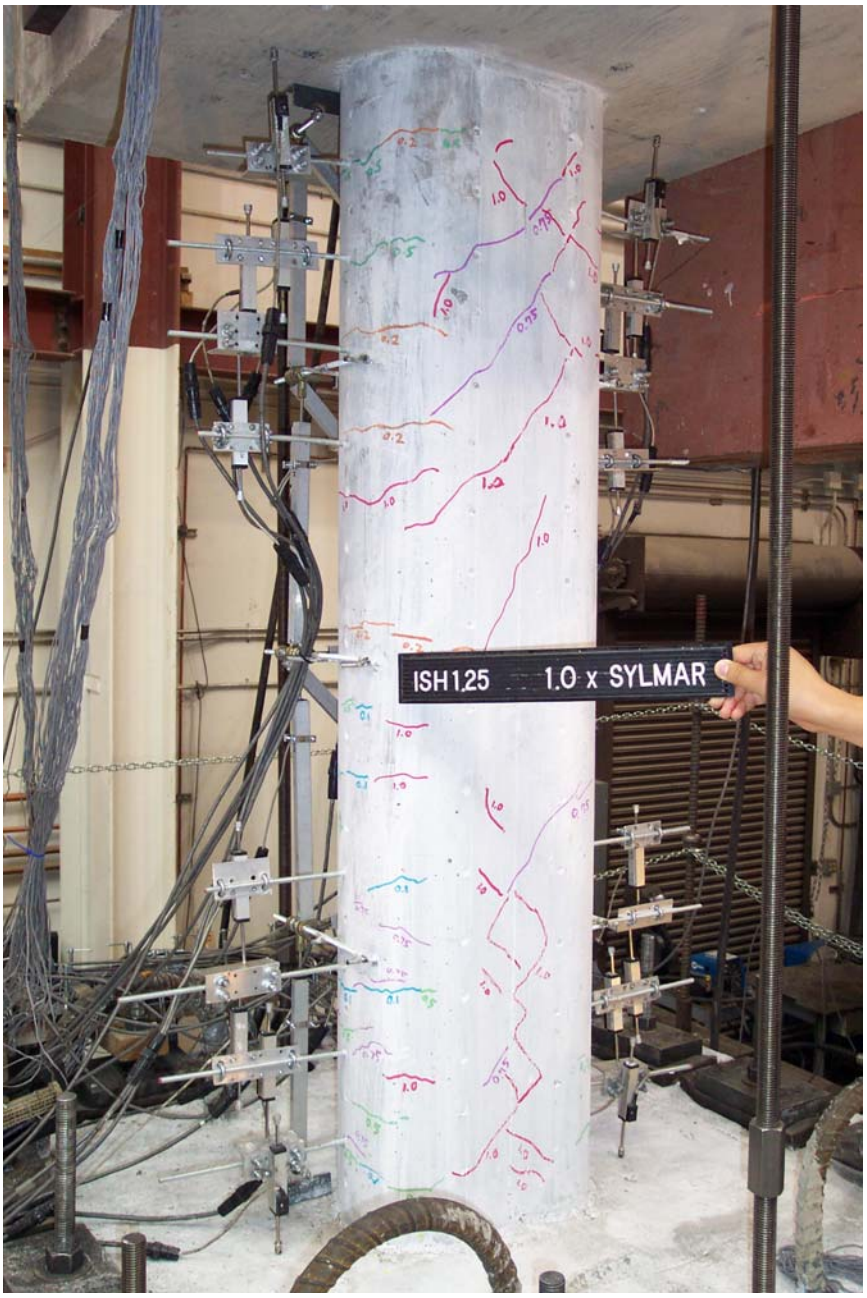

Figure 5-7 Shear Cracks Top and Bottom (μ_d = 1.4) Specimen ISH1.25

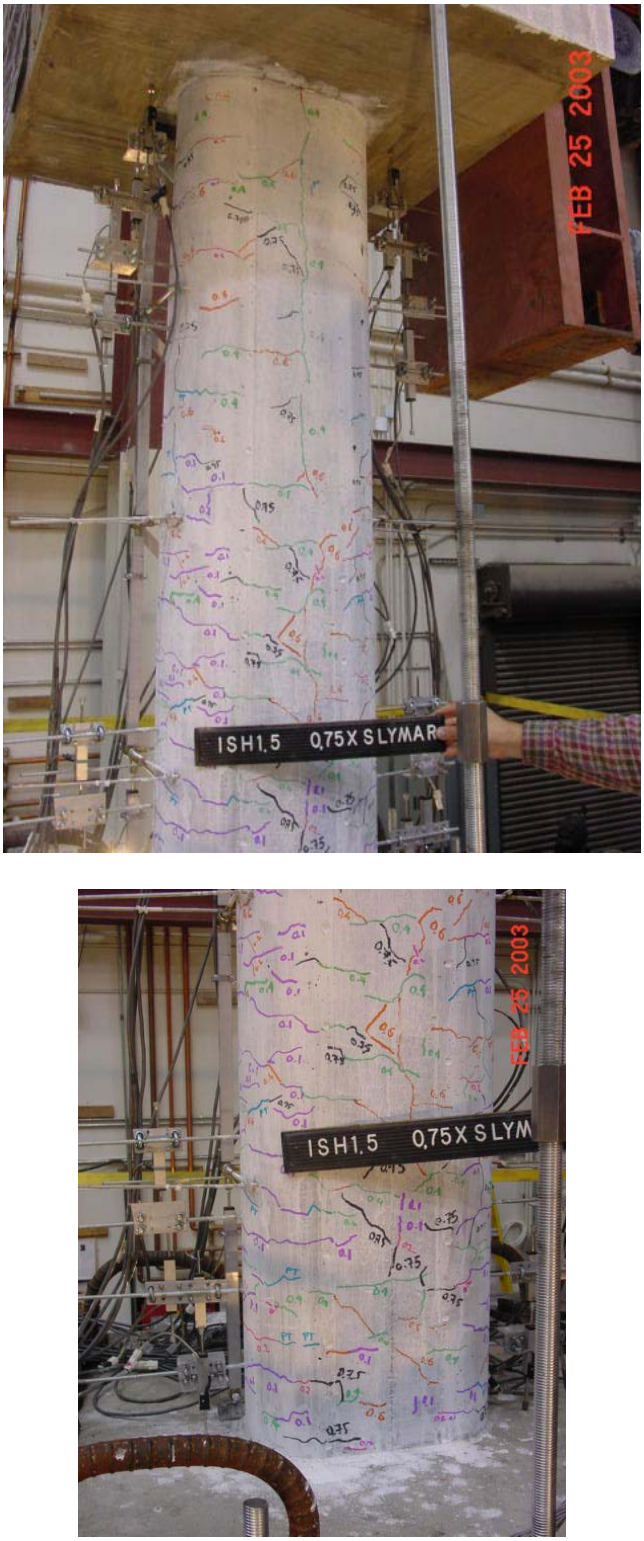

Figure 5-8 Shear Cracks Top and Bottom (μ_d = 1.0) Specimen ISH1.5

Figure 5-9 Shear Cracks Top and Bottom and Localized Vertical Cracks (μ_d = 1.2) Specimen ISH1.5T

Figure 5-10 Increasing of Flexural, Shear Crack and Spalling (μ_d = 2.5) Specimen ISH1.0

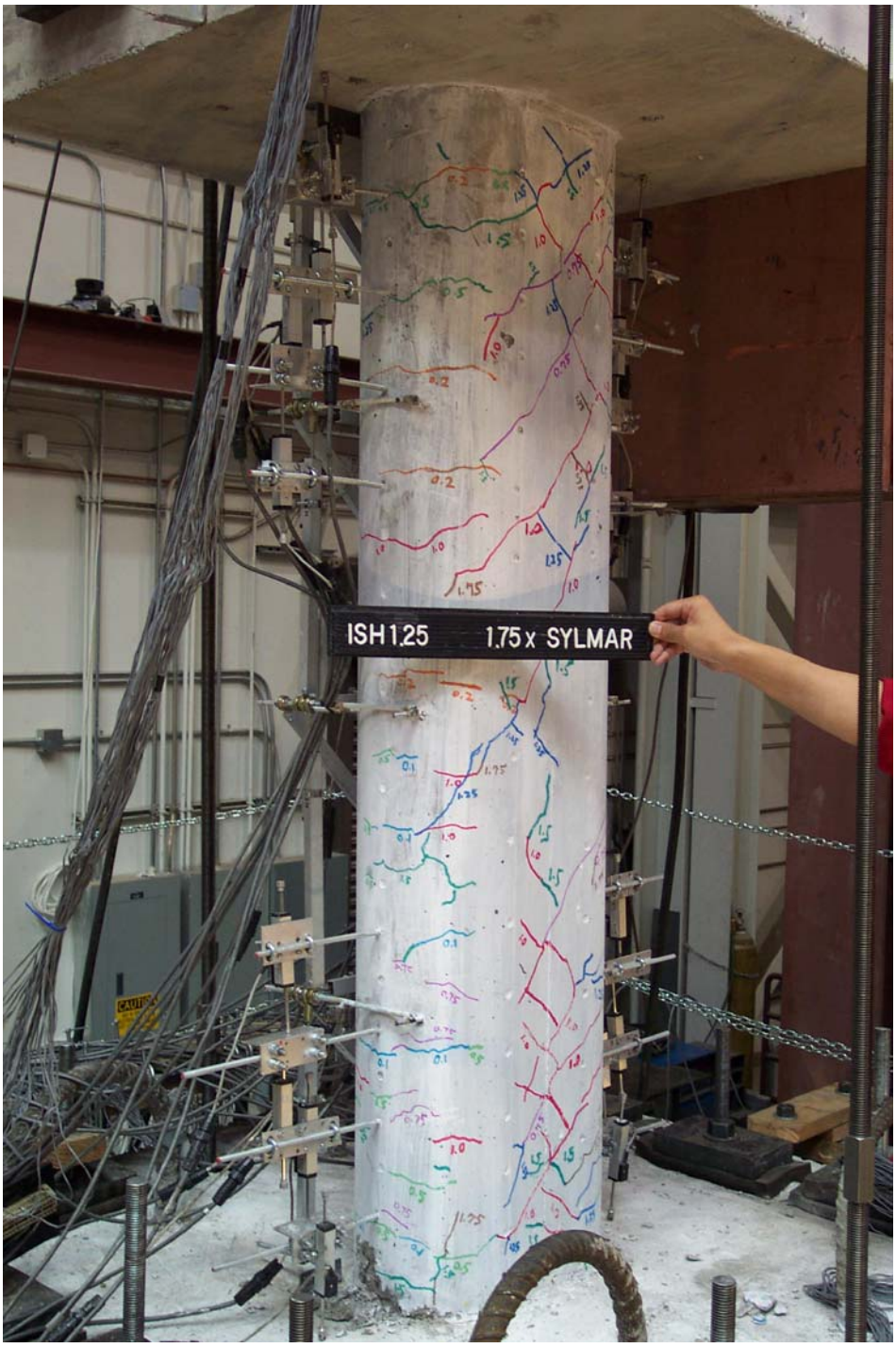

Figure 5-11 Increasing of Flexural, Shear Crack and Spalling (μ_d = 2.2) Specimen ISH1.25

Figure 5-12 Increasing of Flexural, Shear Crack and Spalling (μ_d = 1.7) Specimen ISH1.5

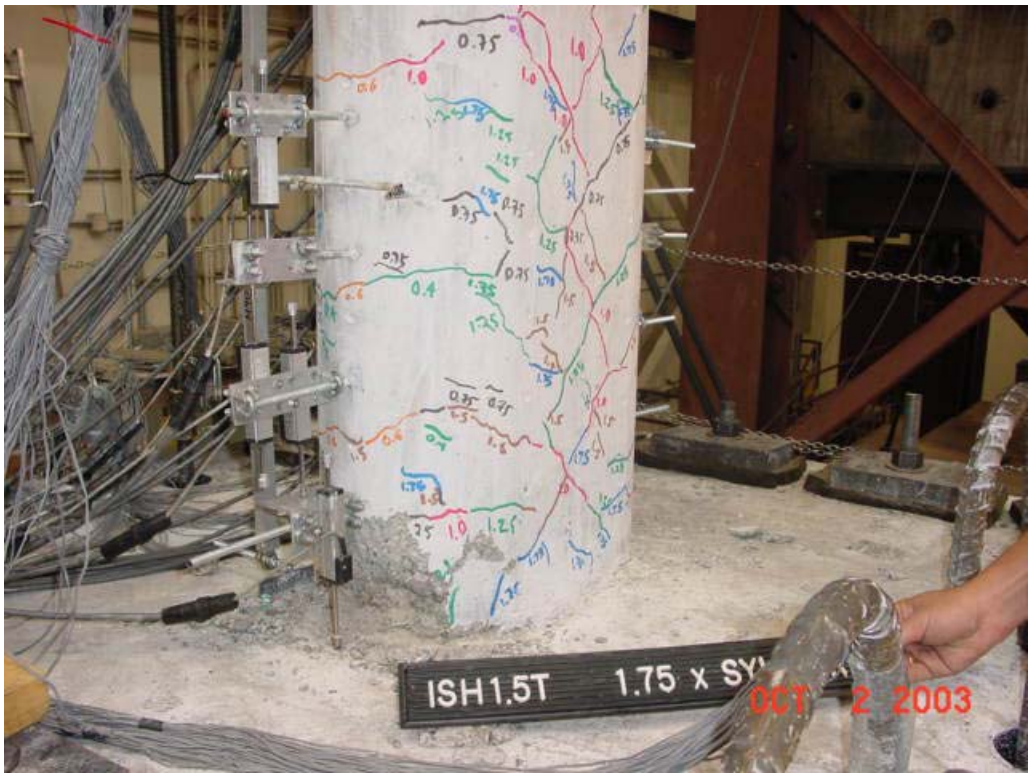

Figure 5-13 Increasing of Flexural, Shear Crack and Spalling (μ_d = 2.5) Specimen ISH1.5T

Figure 5-14 Spirals Visible Top and Bottom of the Column (μ_d = 2.9) Specimen ISH1.25

Figure 5-15 Longitudinal Bars Visible at Top and Bottom of the Column ($\mu_d = 3.6$) Specimen ISH1.0

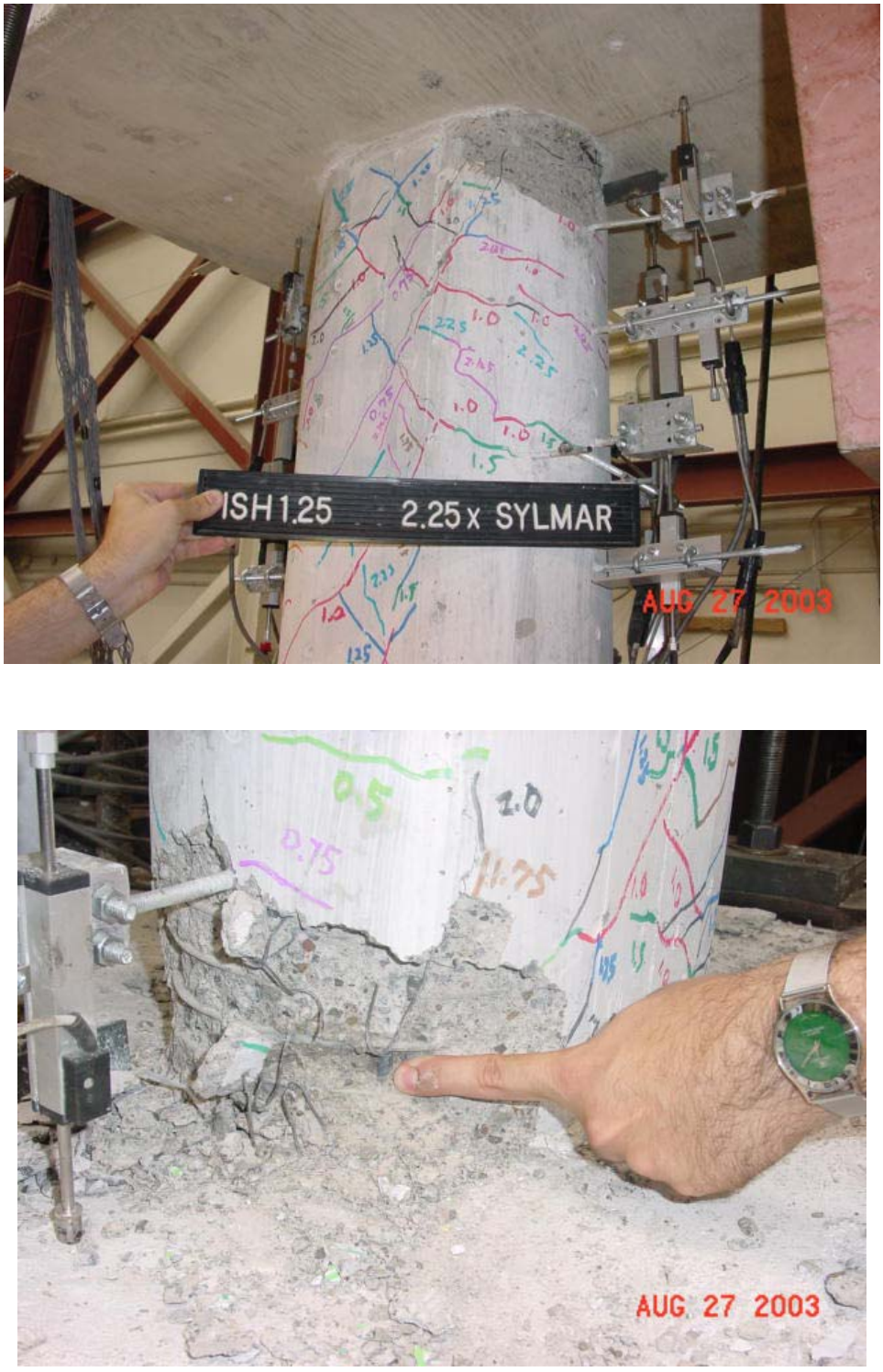

Figure 5-16 Longitudinal Bars Visible at Top and Bottom of the Column (μ_d = 3.7) Specimen ISH1.25

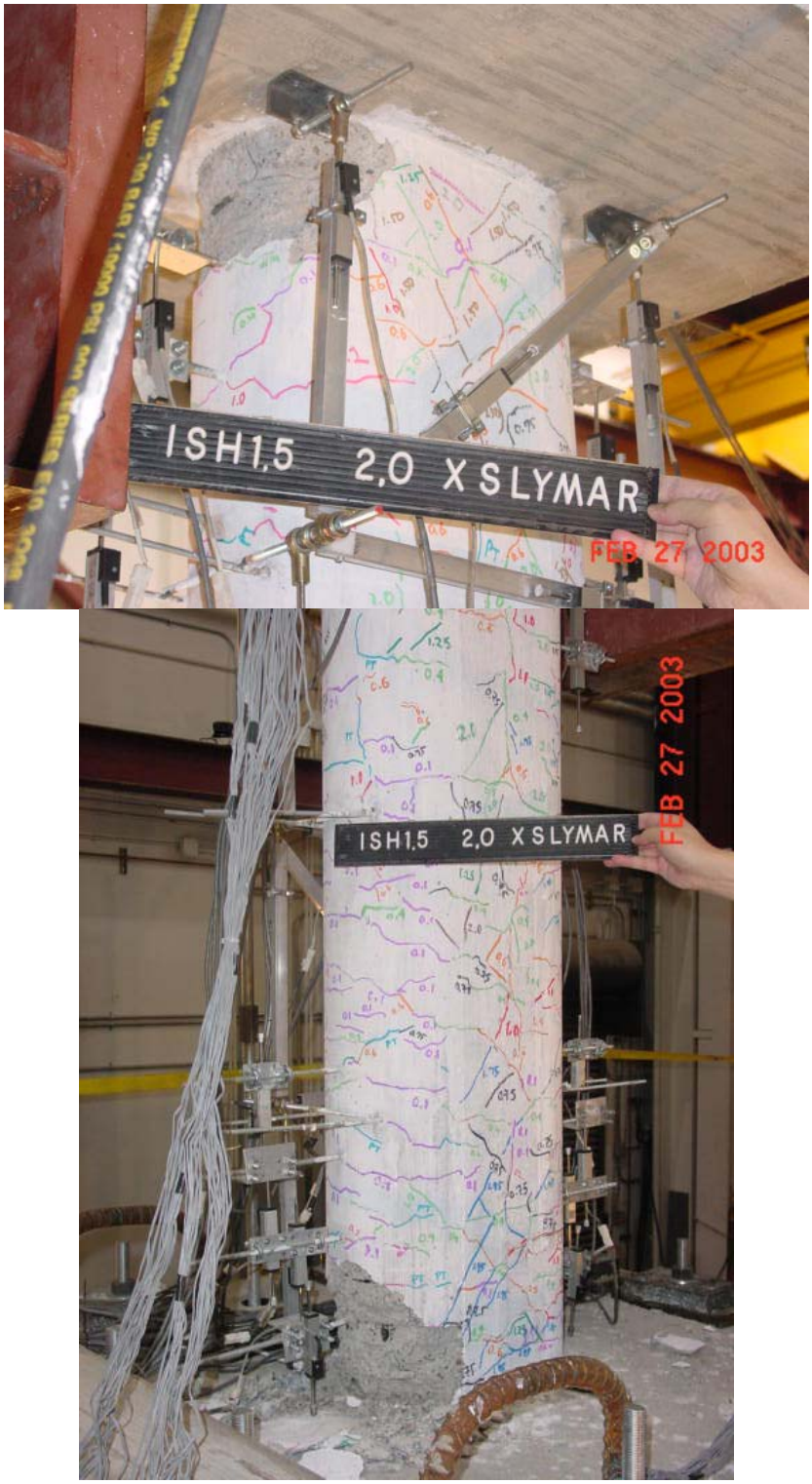

Figure 5-17 Longitudinal Bars Visible at Top and Bottom of the Column ($\mu_d = 2.2$) Specimen ISH1.5

Figure 5-18 Longitudinal Bars Visible at Top and Bottom of the Column (μ_d = 2.8) Specimen ISH1.5T

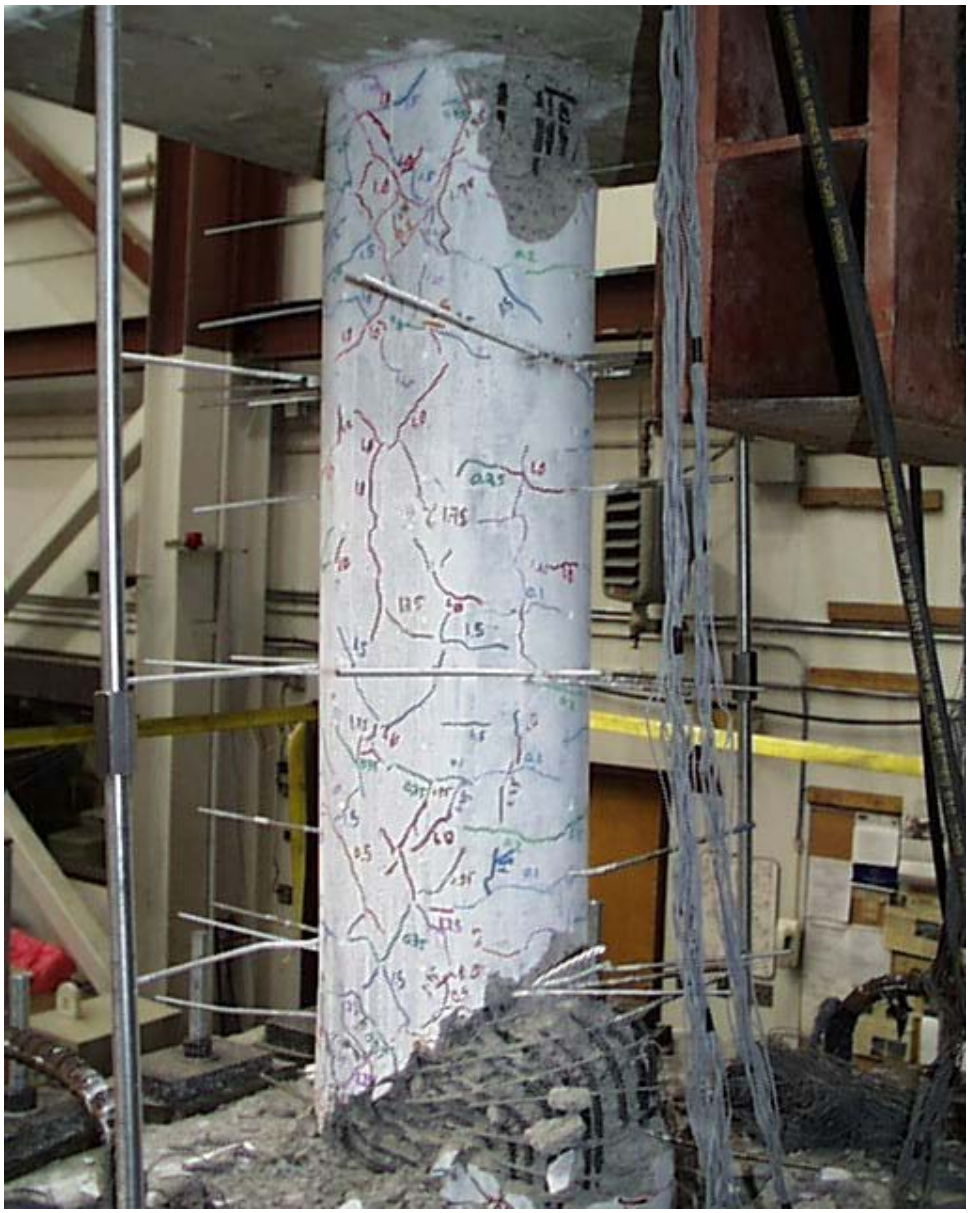

Figure 5-19 Shear Failure at the Bottom of the Column (μ_d = 4.7) Specimen ISH1.0

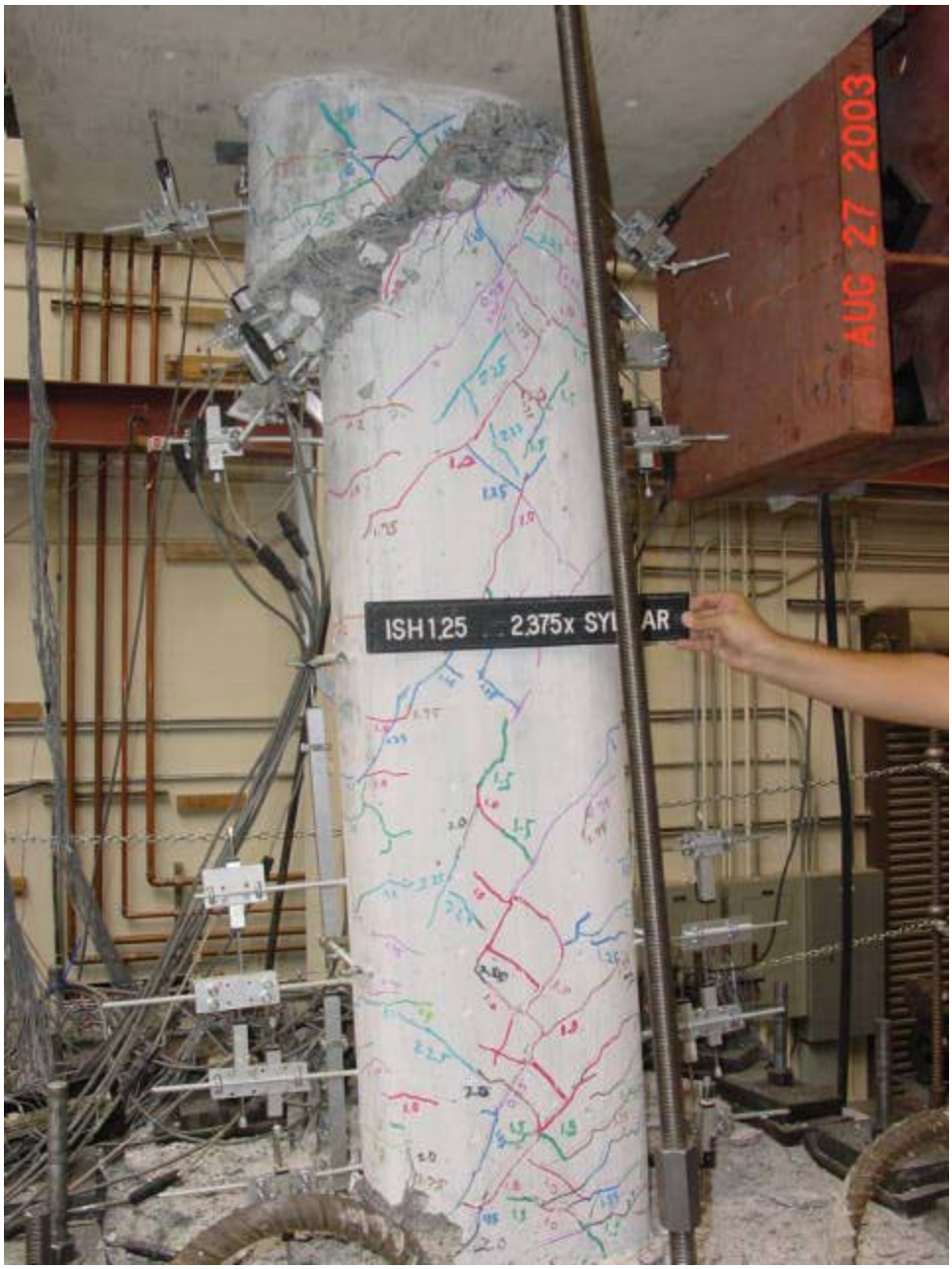

Figure 5-20 Shear Failure at the Top of the Column (μ_d = 5.0) Specimen ISH1.25

Figure 5-21 Damage of the Core Bottom of the Column (μd = 2.9) Specimen ISH1.5

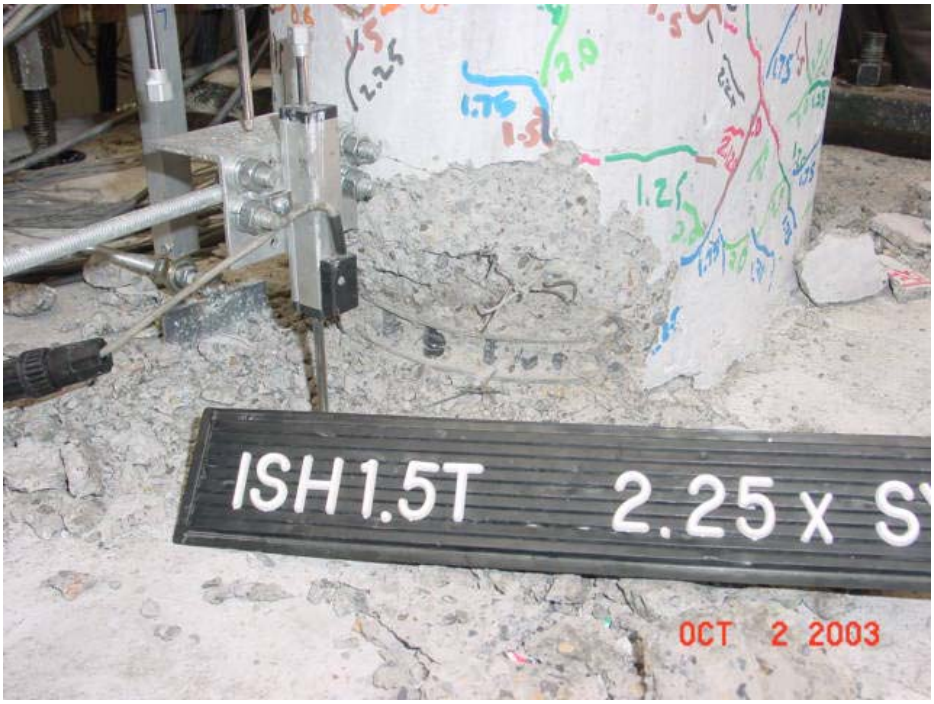

Figure 5-22 Damage of the Core Bottom of the Column (μd = 3.0) Specimen ISH1.5T

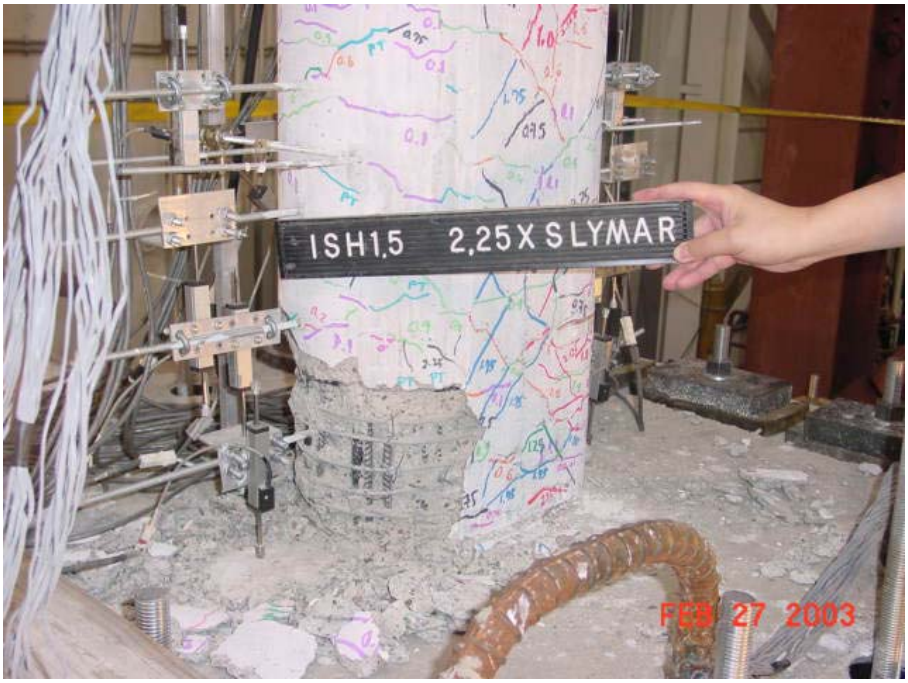

Figure 5-23 Buckling of the Longitudinal Bars at the Bottom of the Column (μ_d = 3.4) Specimen ISH1.5

Figure 5-24 Buckling of the Longitudinal Bars at the Bottom of the Column (μ_d = 3.4) Specimen ISH1.5T

Figure 5-25 Failure (μ_d = 4.0) Specimen ISH1.5

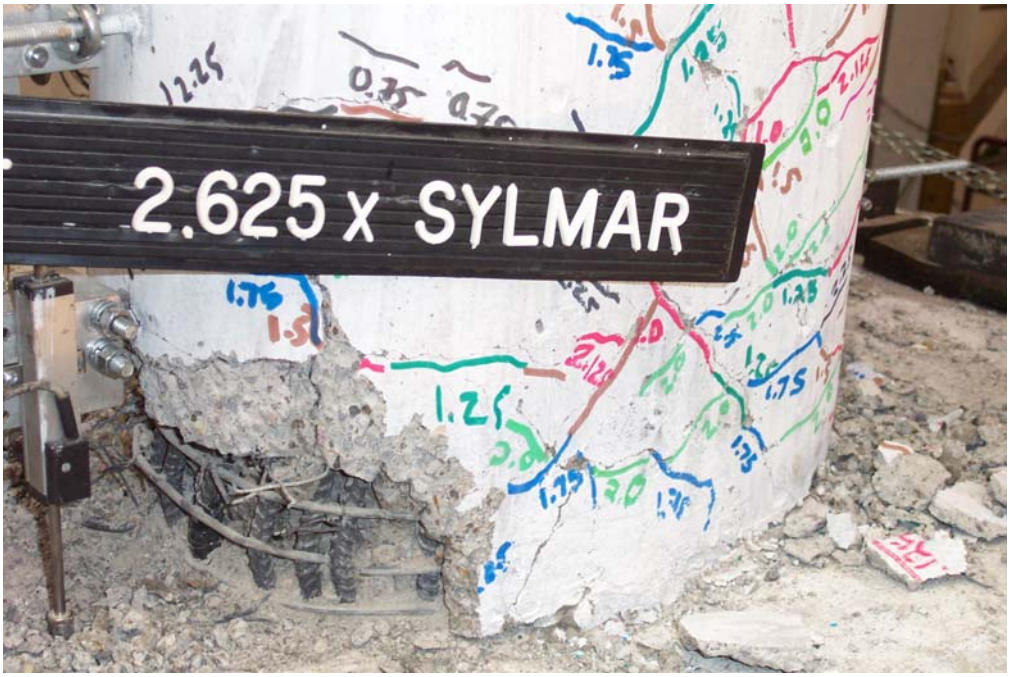

Figure 5-26 Failure (μ_d = 3.8) Specimen ISH1.5T

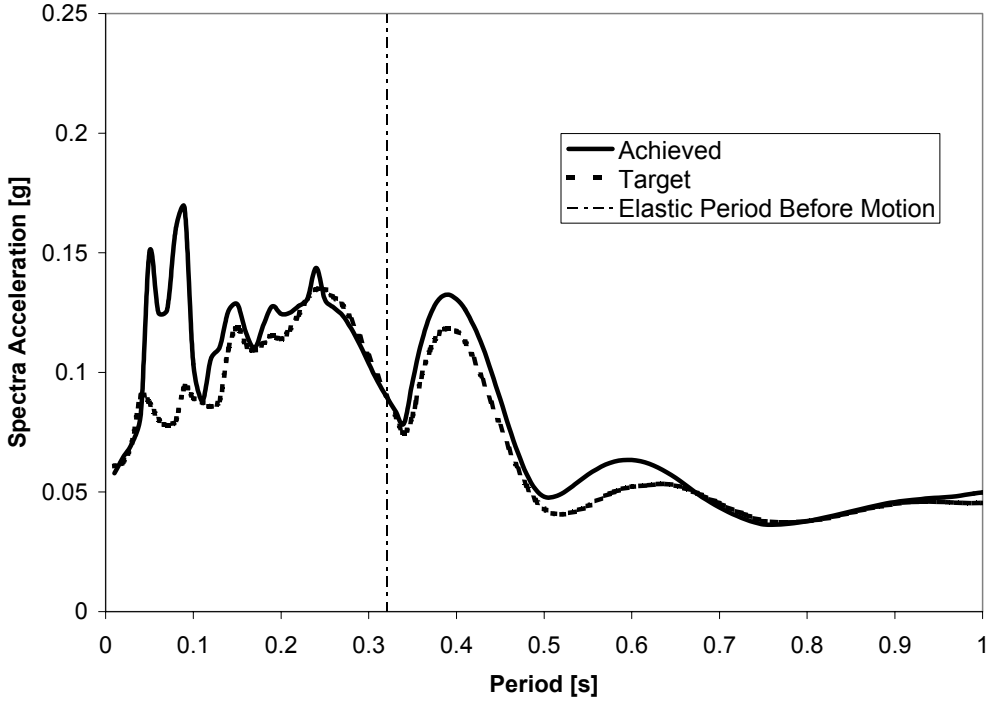

Figure 5-27 Comparison of Achieved and Target Response Spectra for 0.1 x Sylmar Specimen ISH1.0

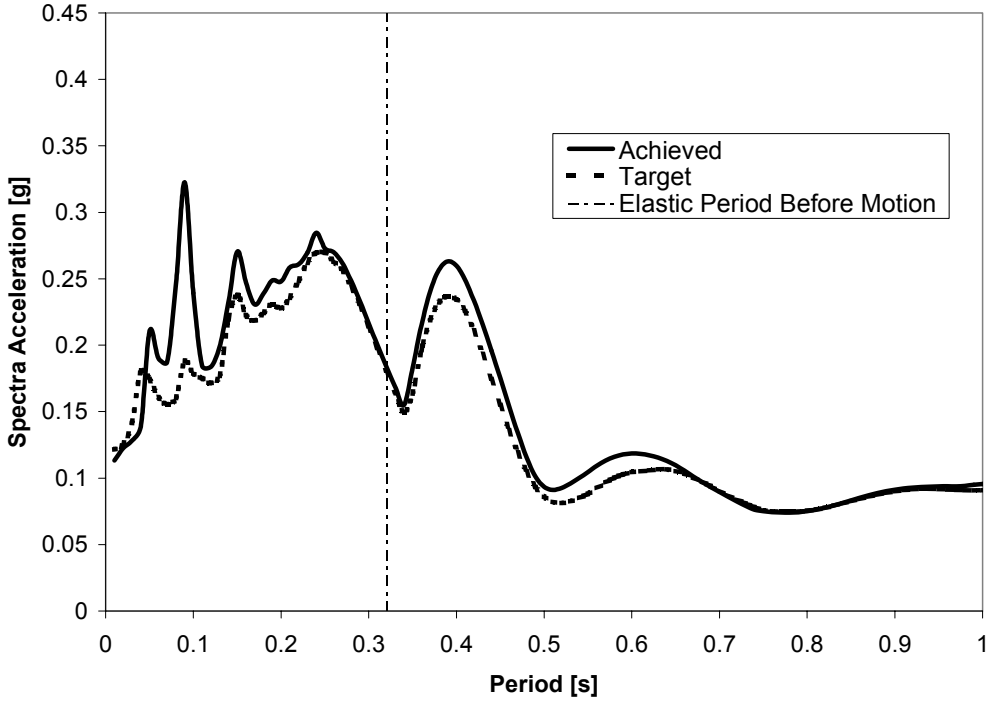

Figure 5-28 Comparison of Achieved and Target Response Spectra for 0.2 x Sylmar Specimen ISH1.0

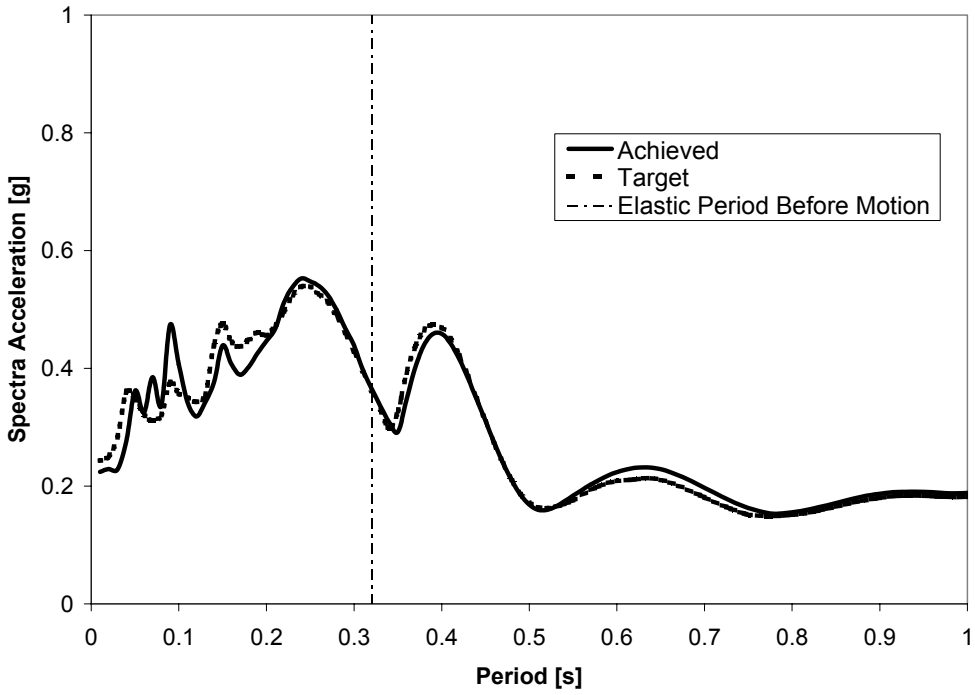

Figure 5-29 Comparison of Achieved and Target Response Spectra for 0.4 x Sylmar Specimen ISH1.0

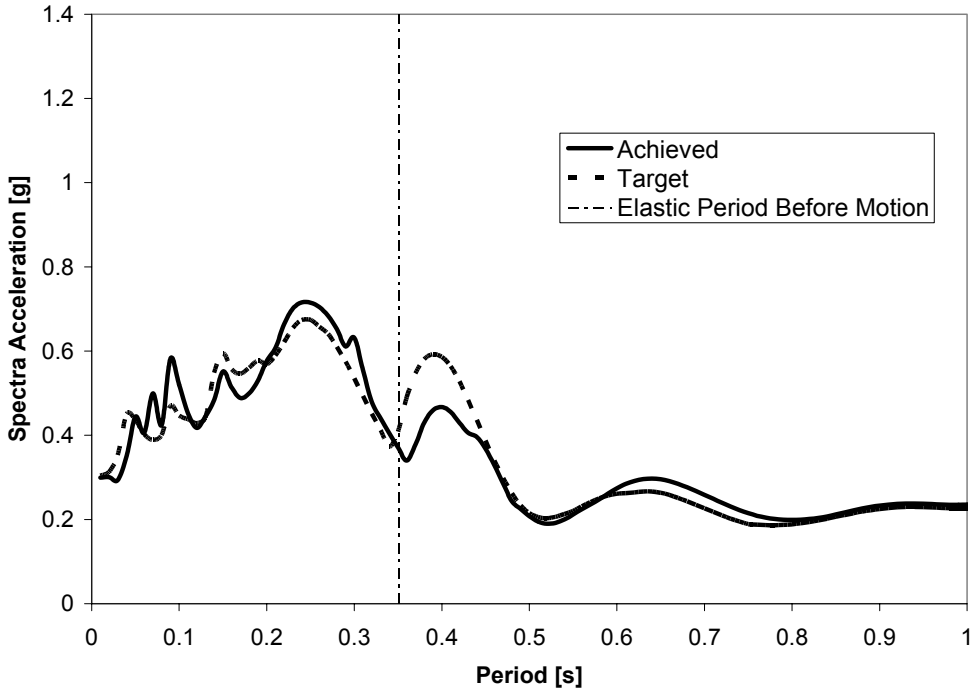

Figure 5-30 Comparison of Achieved and Target Response Spectra for 0.5 x Sylmar Specimen ISH1.0

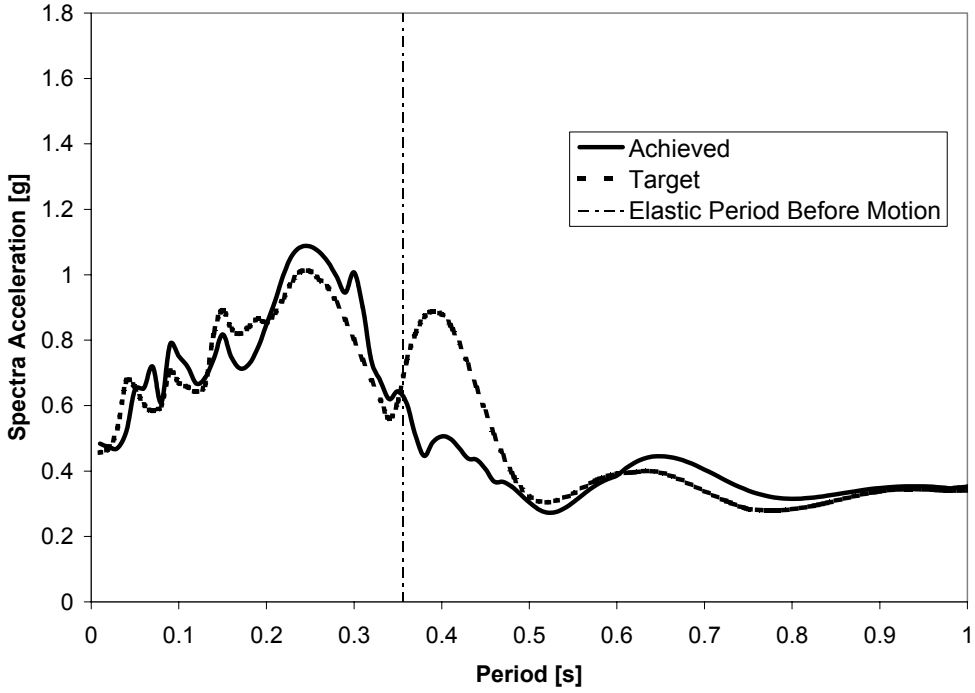

Figure 5-31 Comparison of Achieved and Target Response Spectra for 0.75 x Sylmar Specimen ISH1.0

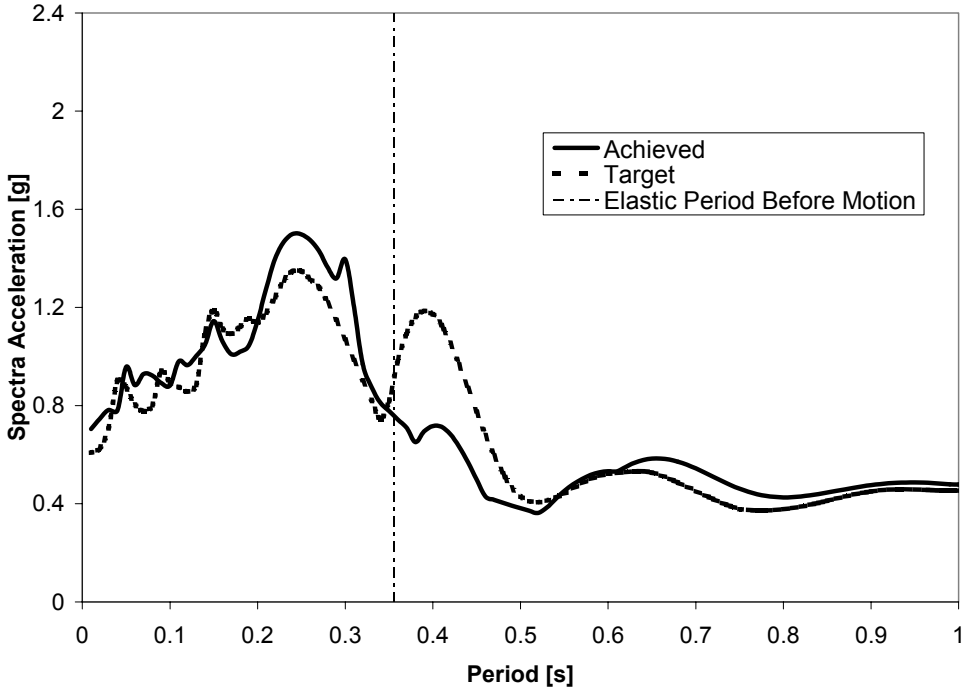

Figure 5-32 Comparison of Achieved and Target Response Spectra for 1.0 x Sylmar Specimen ISH1.0

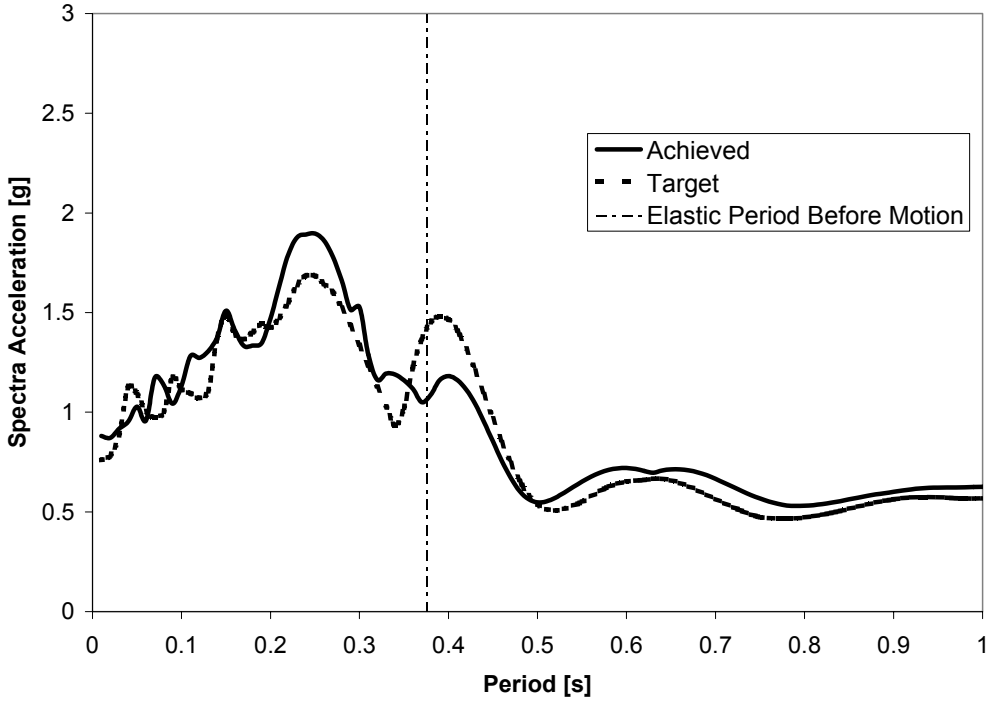

Figure 5-33 Comparison of Achieved and Target Response Spectra for 1.25 x Sylmar Specimen ISH1.0

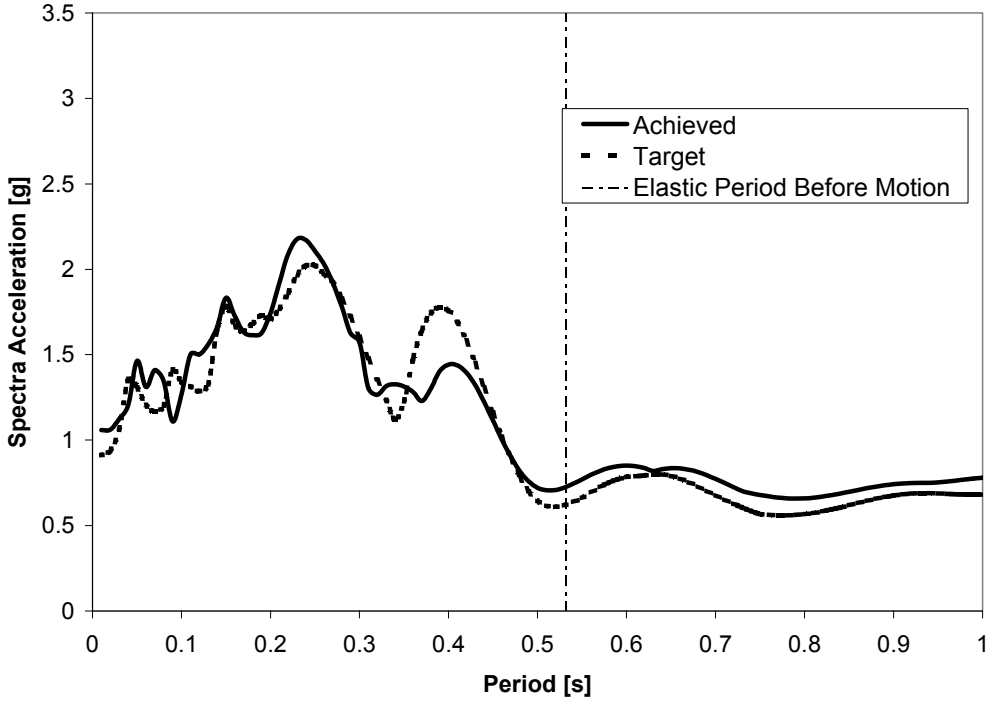

Figure 5-34 Comparison of Achieved and Target Response Spectra for 1.5 x Sylmar Specimen ISH1.0

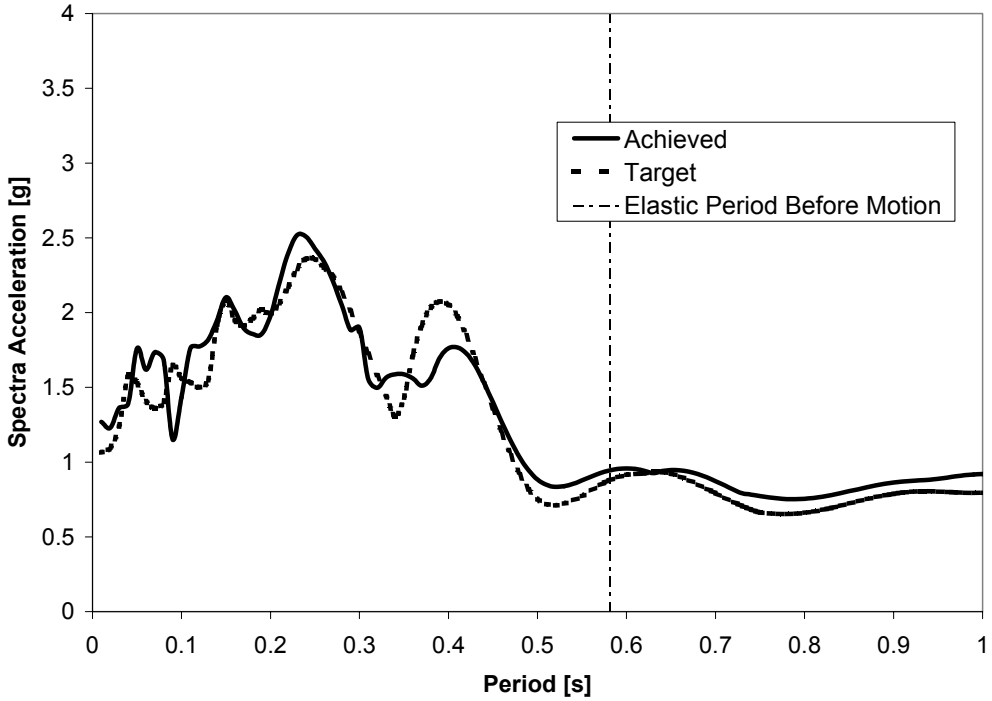

Figure 5-35 Comparison of Achieved and Target Response Spectra for 1.75 x Sylmar Specimen ISH1.0

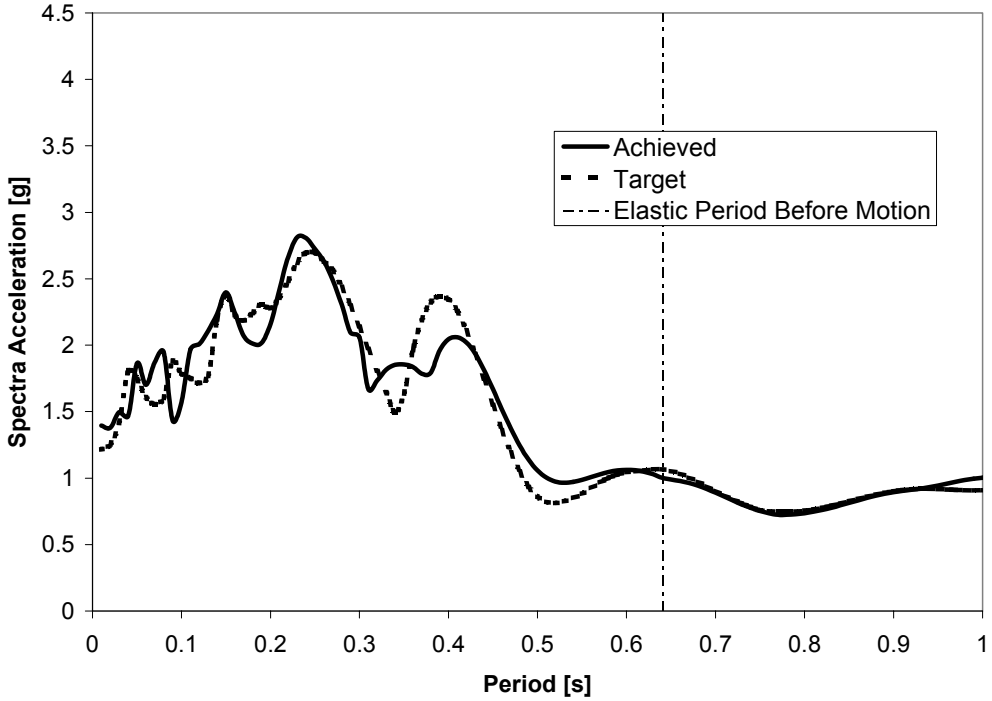

Figure 5-36 Comparison of Achieved and Target Response Spectra for 2.0 x Sylmar Specimen ISH1.0

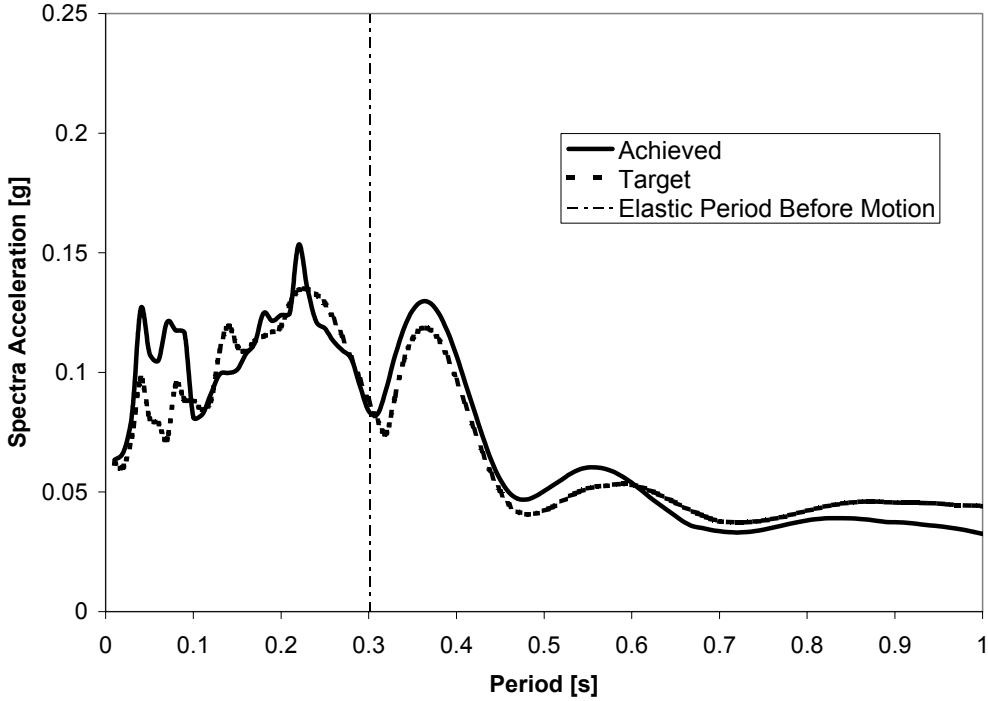

Figure 5-37 Comparison of Achieved and Target Response Spectra for 0.1 x Sylmar Specimen ISH1.25

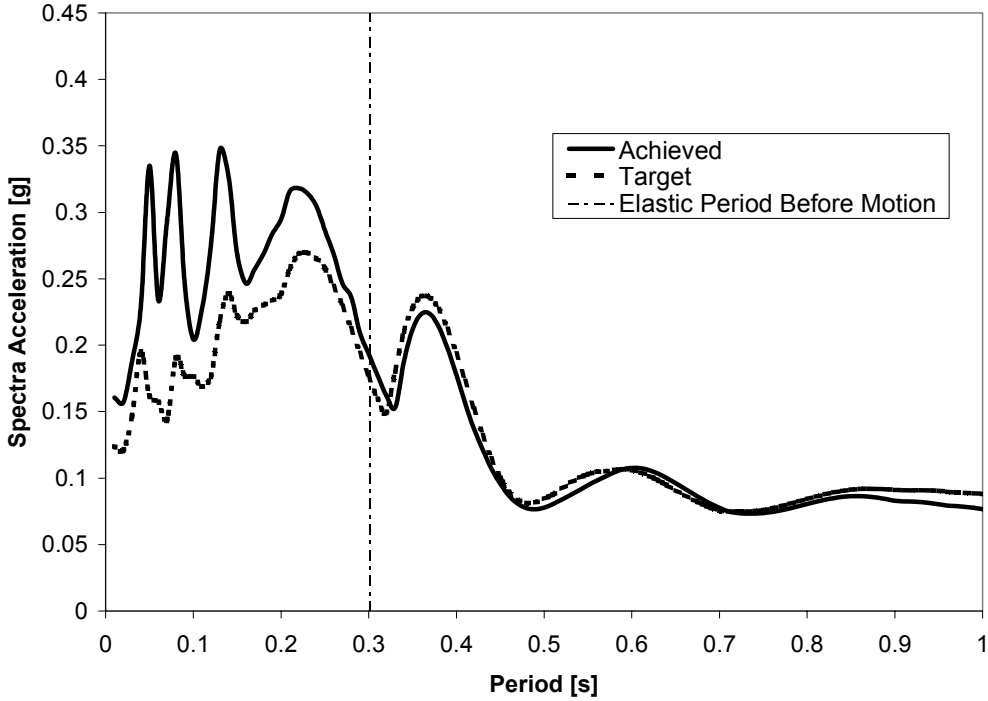

Figure 5-38 Comparison of Achieved and Target Response Spectra for 0.2 x Sylmar Specimen ISH1.25

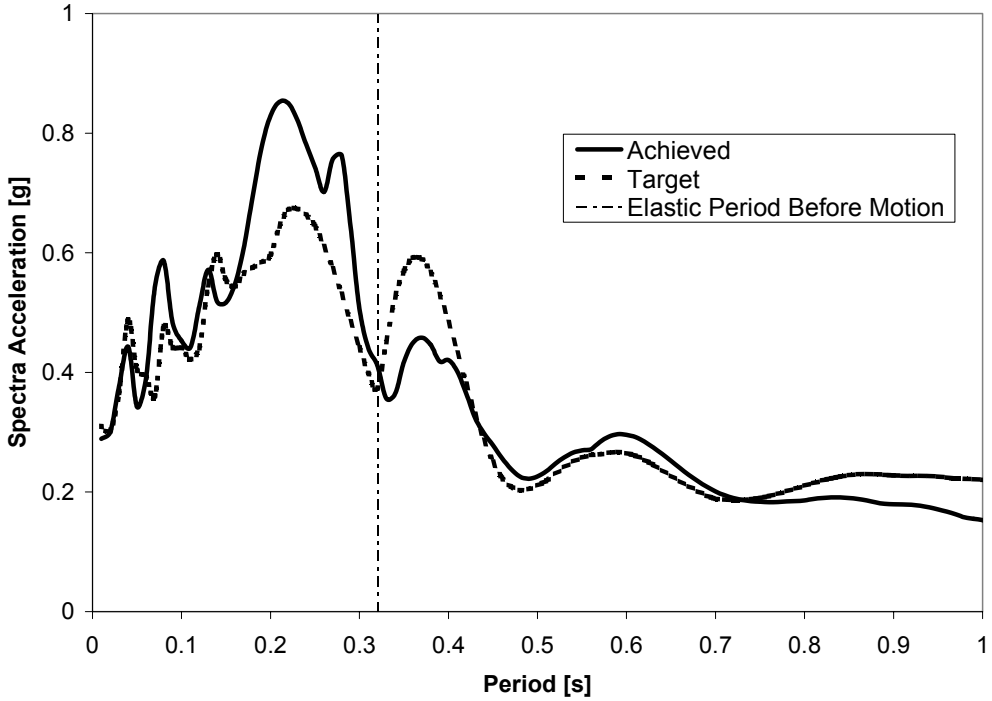

Figure 5-39 Comparison of Achieved and Target Response Spectra for 0.5 x Sylmar Specimen ISH1.25

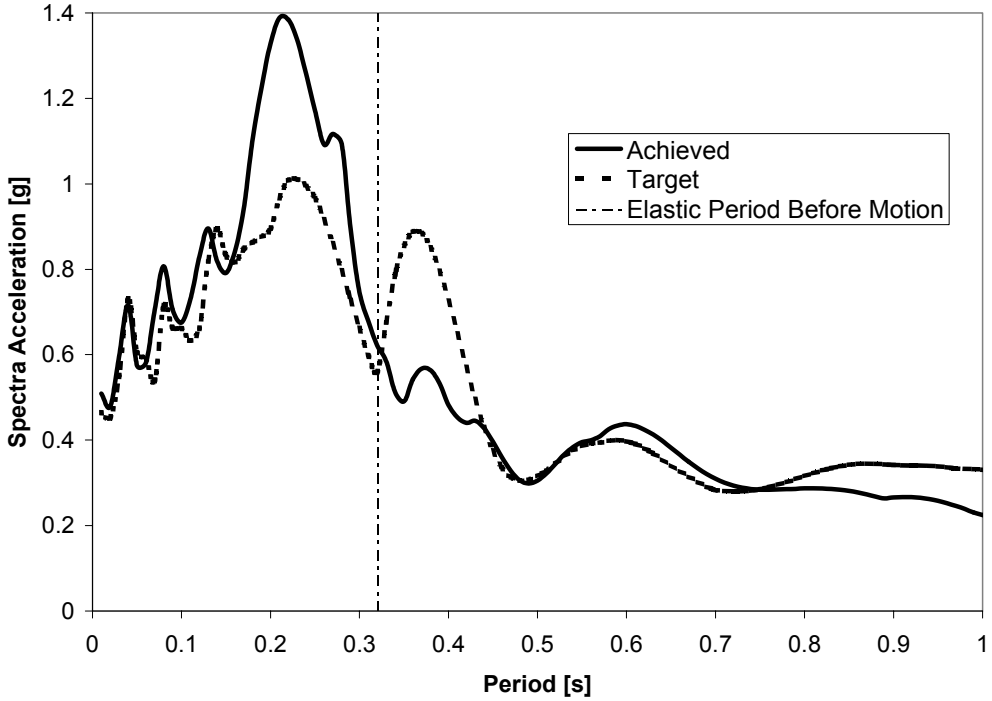

Figure 5-40 Comparison of Achieved and Target Response Spectra for 0.75 x Sylmar Specimen ISH1.25

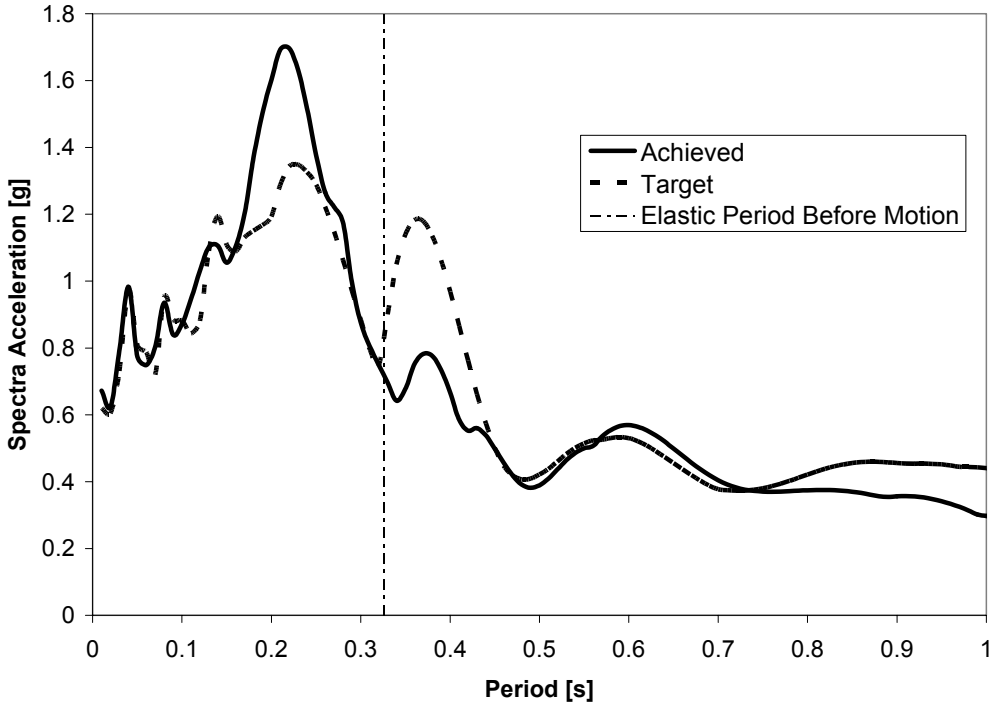

Figure 5-41 Comparison of Achieved and Target Response Spectra for 1.0 x Sylmar Specimen ISH1.25

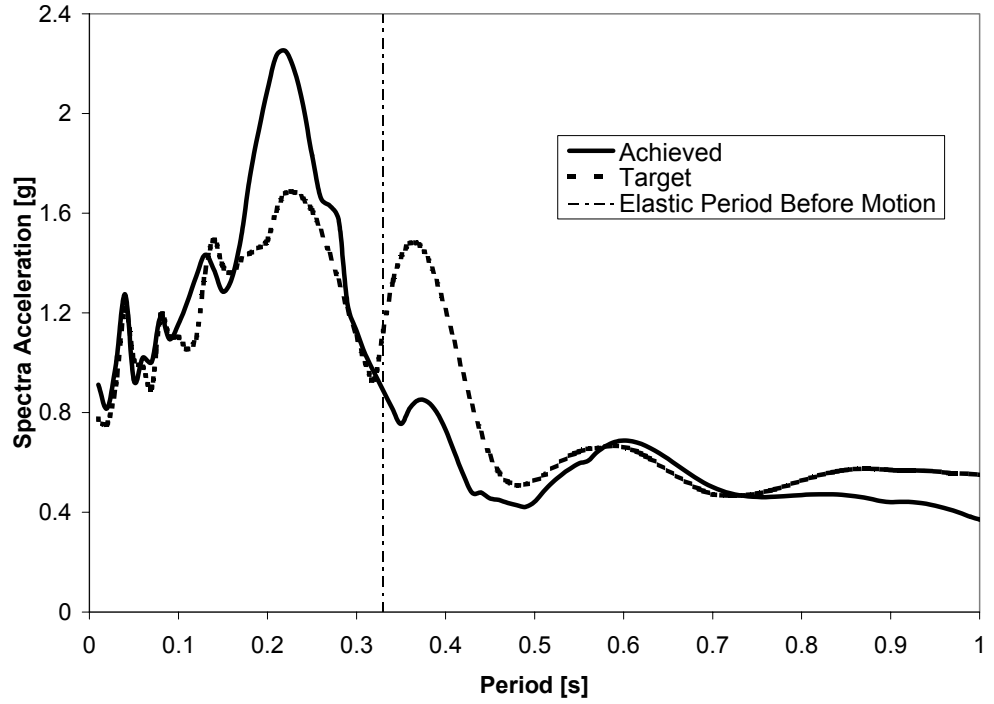

Figure 5-42 Comparison of Achieved and Target Response Spectra for 1.25 x Sylmar Specimen ISH1.25

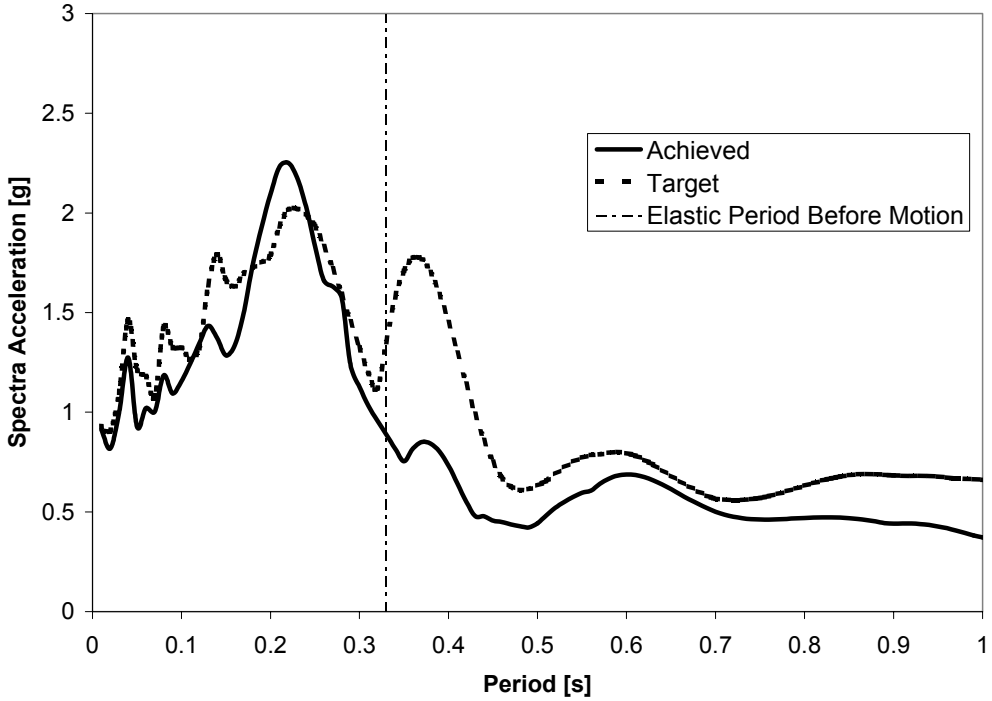

Figure 5-43 Comparison of Achieved and Target Response Spectra for 1.5 x Sylmar Specimen ISH1.25

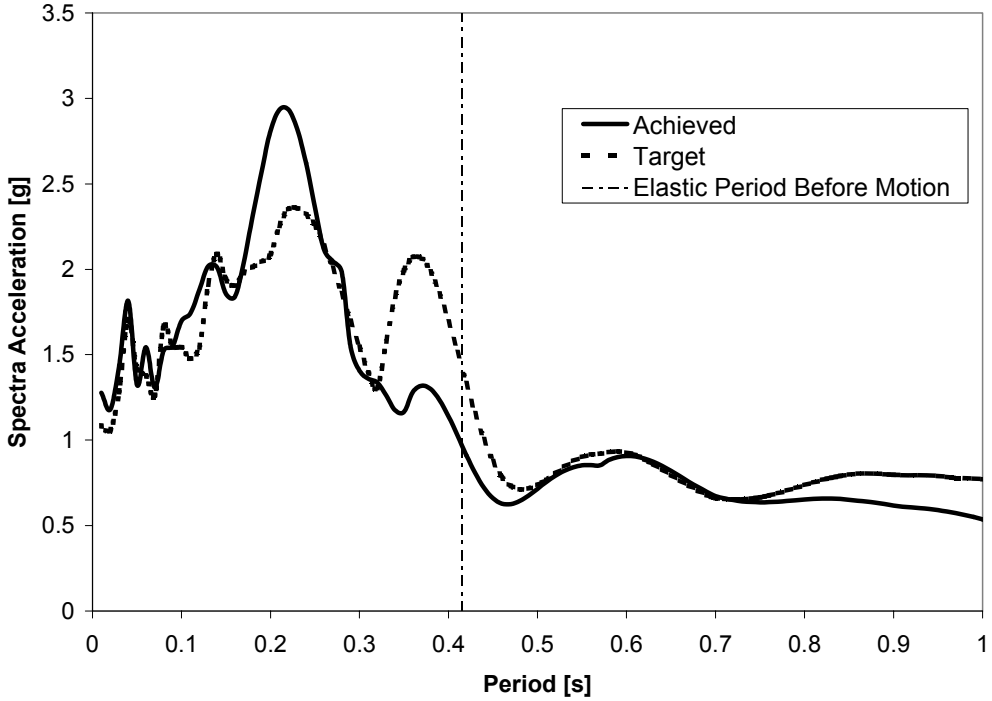

Figure 5-44 Comparison of Achieved and Target Response Spectra for 1.75 x Sylmar Specimen ISH1.25

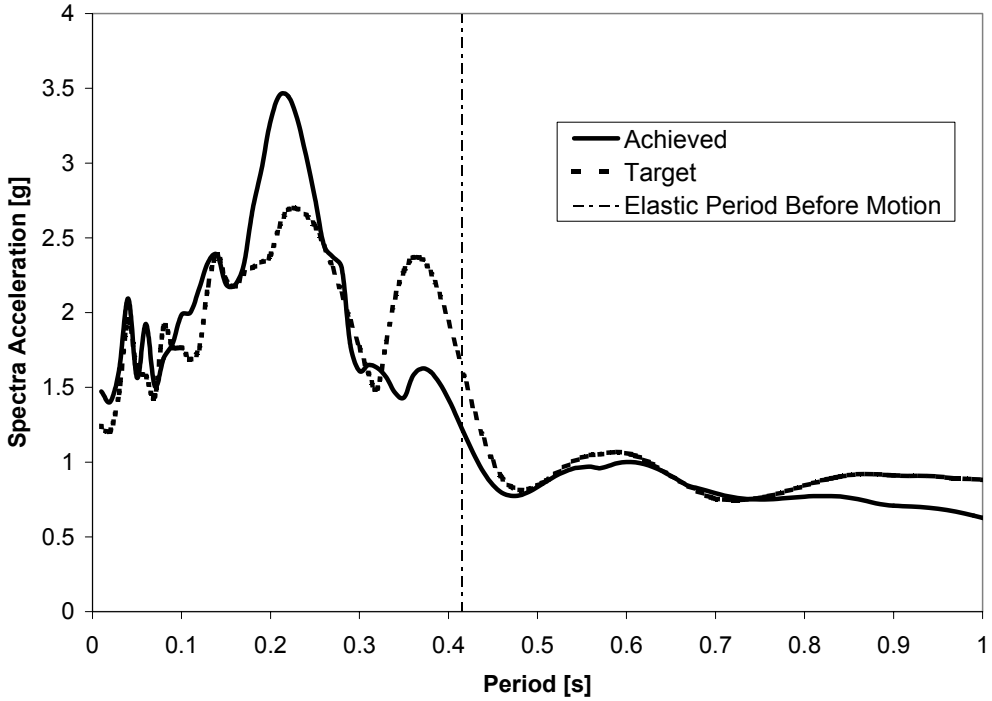

Figure 5-45 Comparison of Achieved and Target Response Spectra for 2.0 x Sylmar Specimen ISH1.25

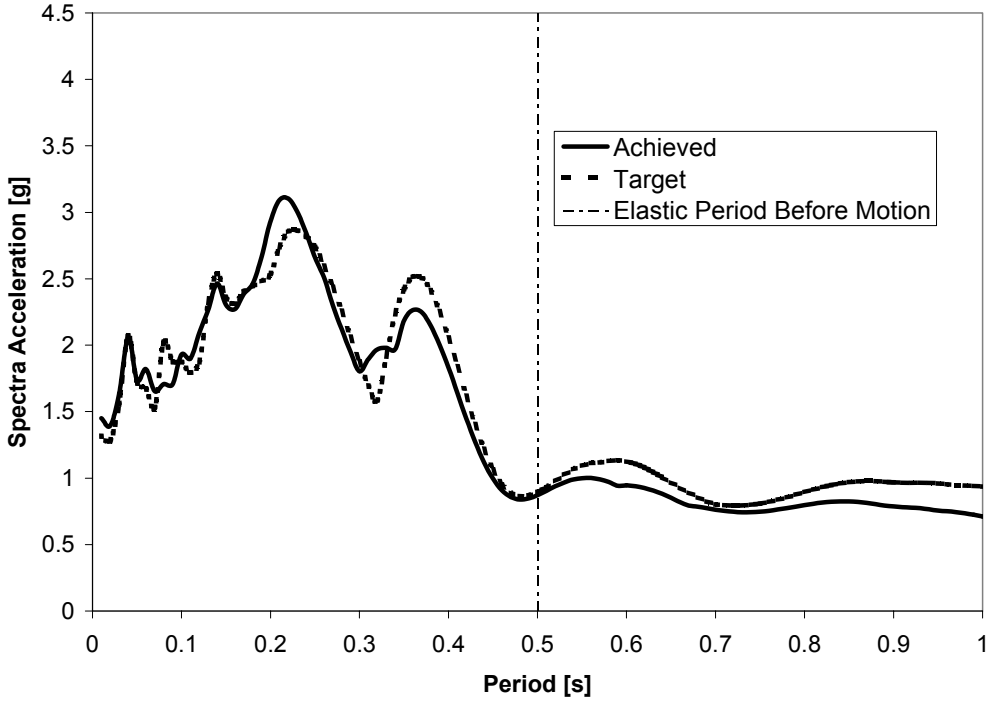

Figure 5-46 Comparison of Achieved and Target Response Spectra for 2.125 x Sylmar Specimen ISH1.25

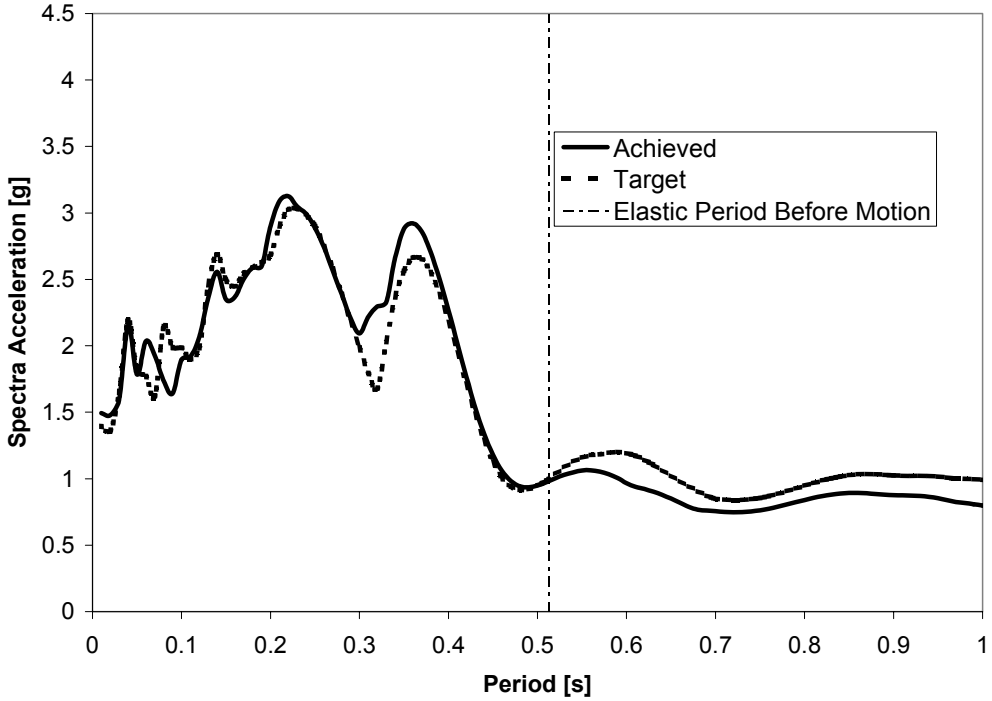

Figure 5-47 Comparison of Achieved and Target Response Spectra for 2.25 x Sylmar Specimen ISH1.25

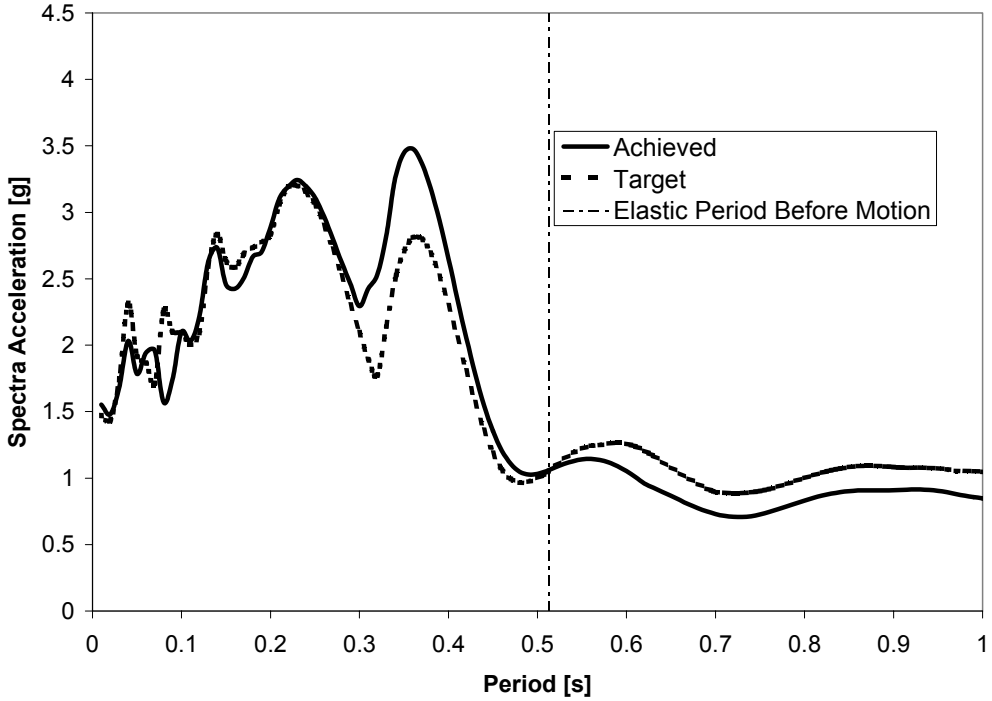

Figure 5-48 Comparison of Achieved and Target Response Spectra for 2.375 x Sylmar Specimen ISH1.25

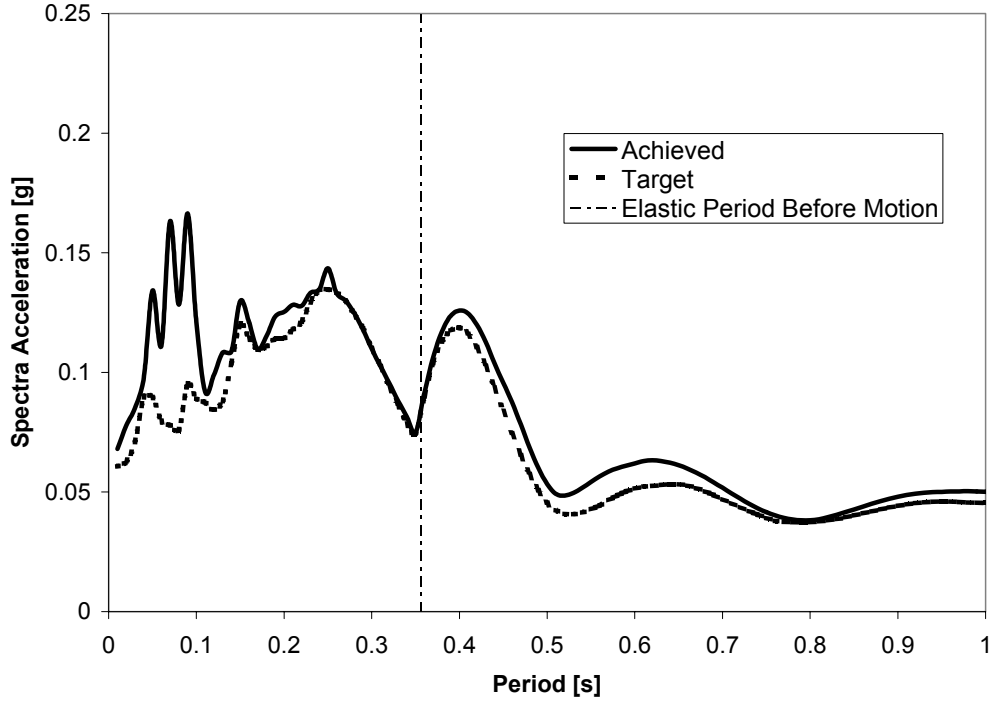

Figure 5-49 Comparison of Achieved and Target Response Spectra for 0.1 x Sylmar Specimen ISH1.5

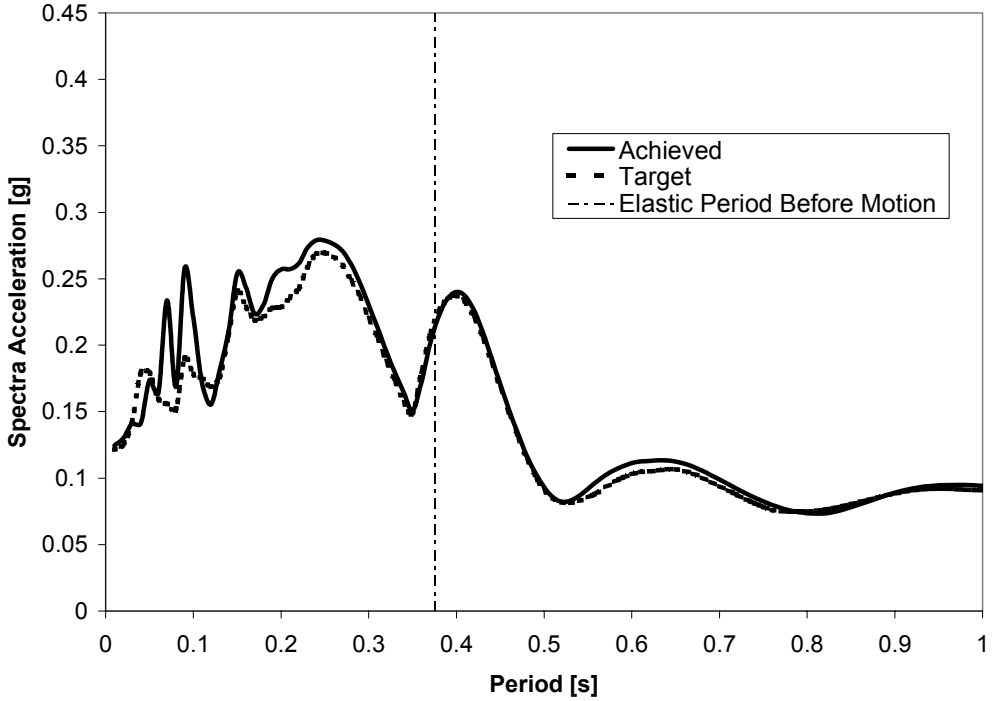

Figure 5-50 Comparison of Achieved and Target Response Spectra for 0.2 x Sylmar Specimen ISH1.5

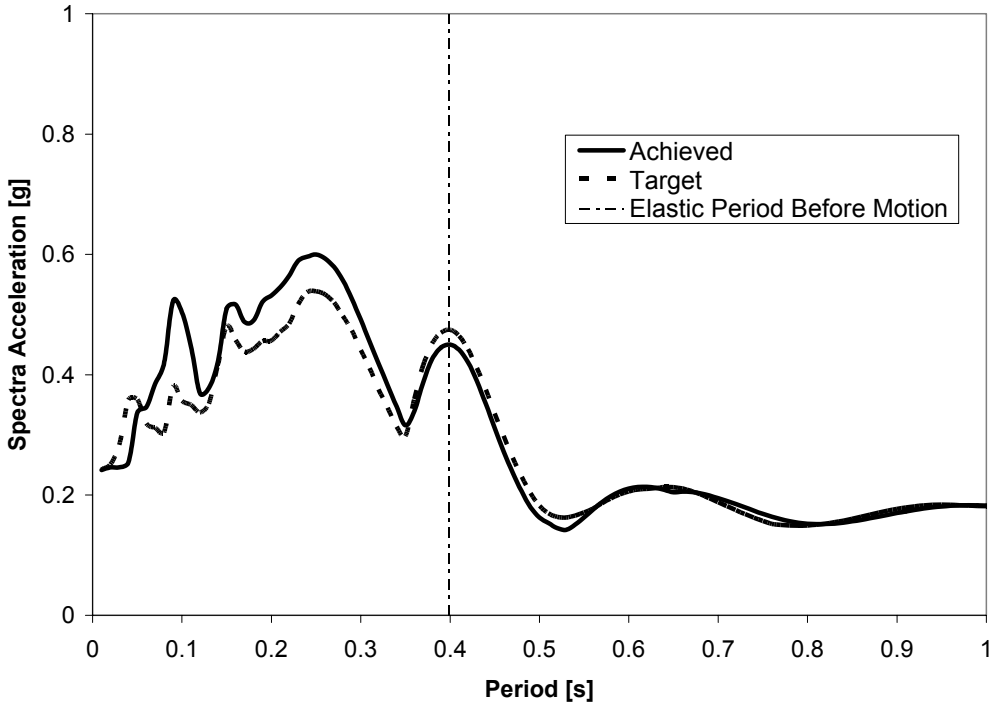

Figure 5-51 Comparison of Achieved and Target Response Spectra for 0.4 x Sylmar Specimen ISH1.5

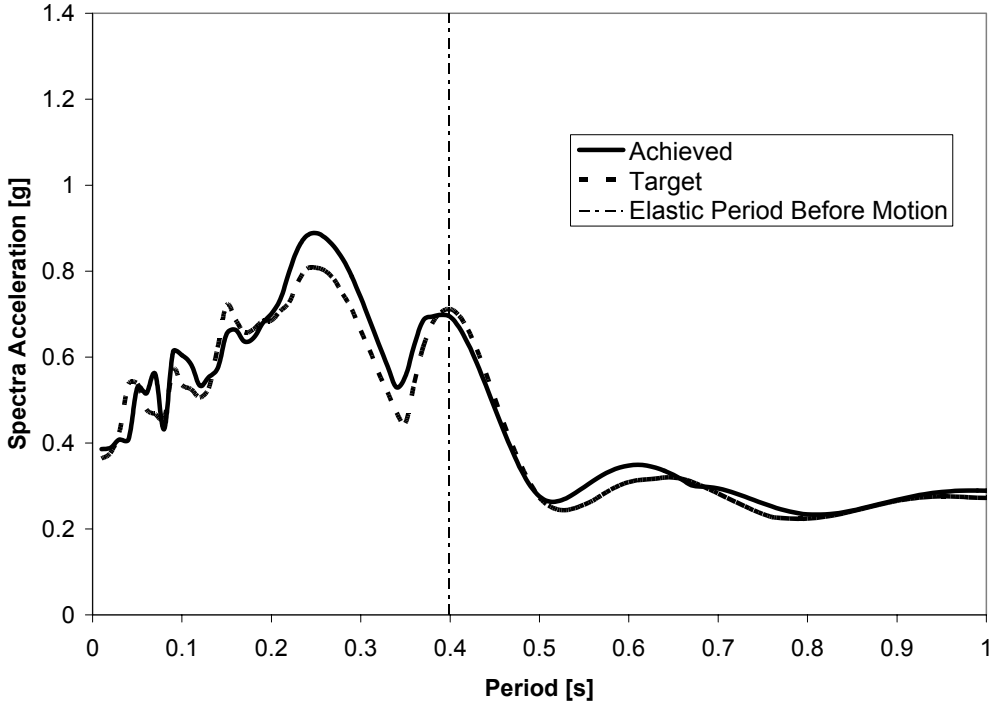

Figure 5-52 Comparison of Achieved and Target Response Spectra for 0.6 x Sylmar Specimen ISH1.5

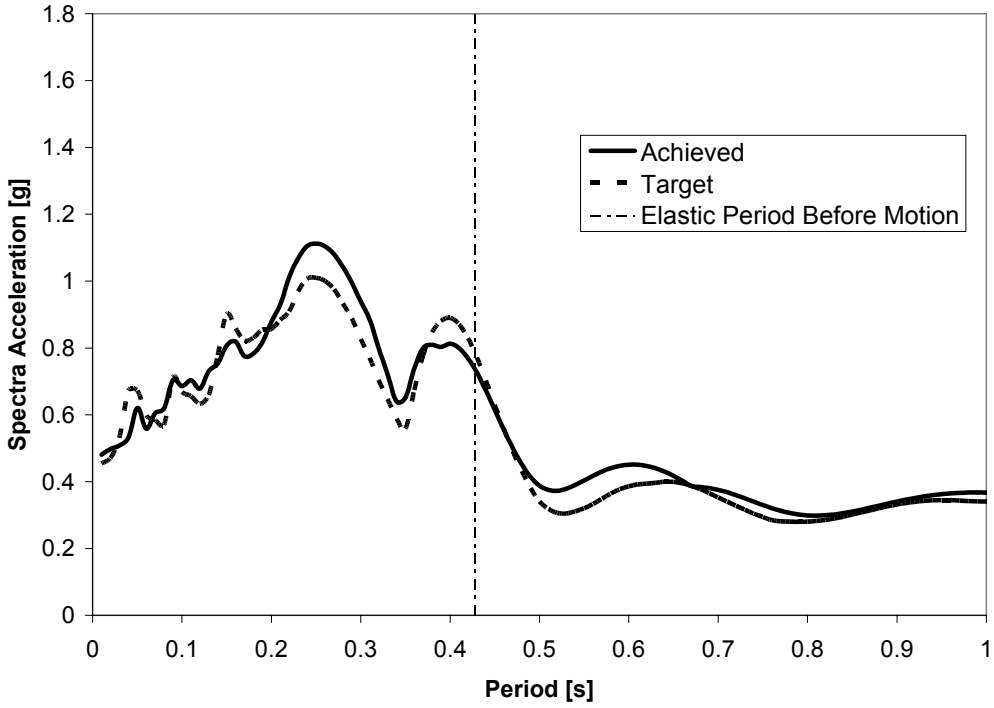

Figure 5-53 Comparison of Achieved and Target Response Spectra for 0.75 x Sylmar Specimen ISH1.5

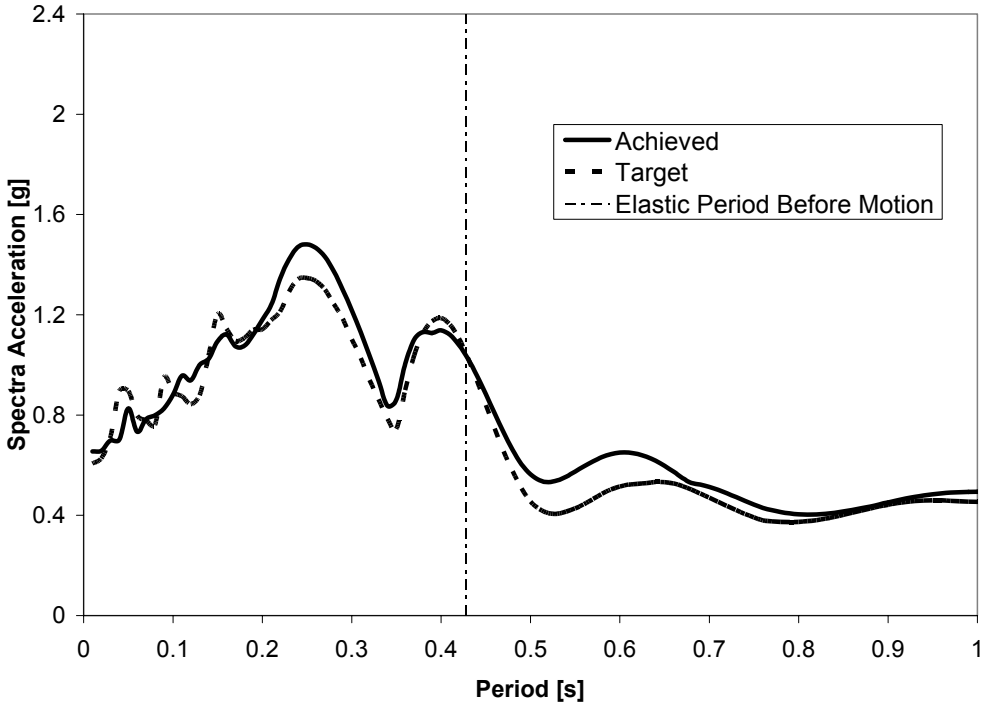

Figure 5-54 Comparison of Achieved and Target Response Spectra for 1.0 x Sylmar Specimen ISH1.5

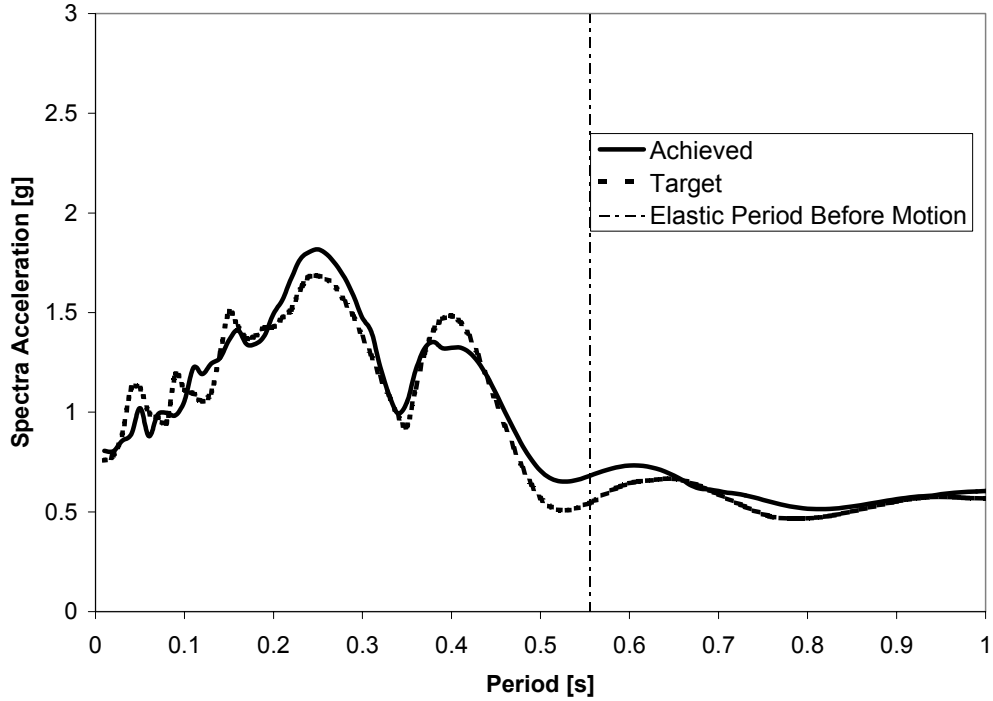

Figure 5-55 Comparison of Achieved and Target Response Spectra for 1.25 x Sylmar Specimen ISH1.5

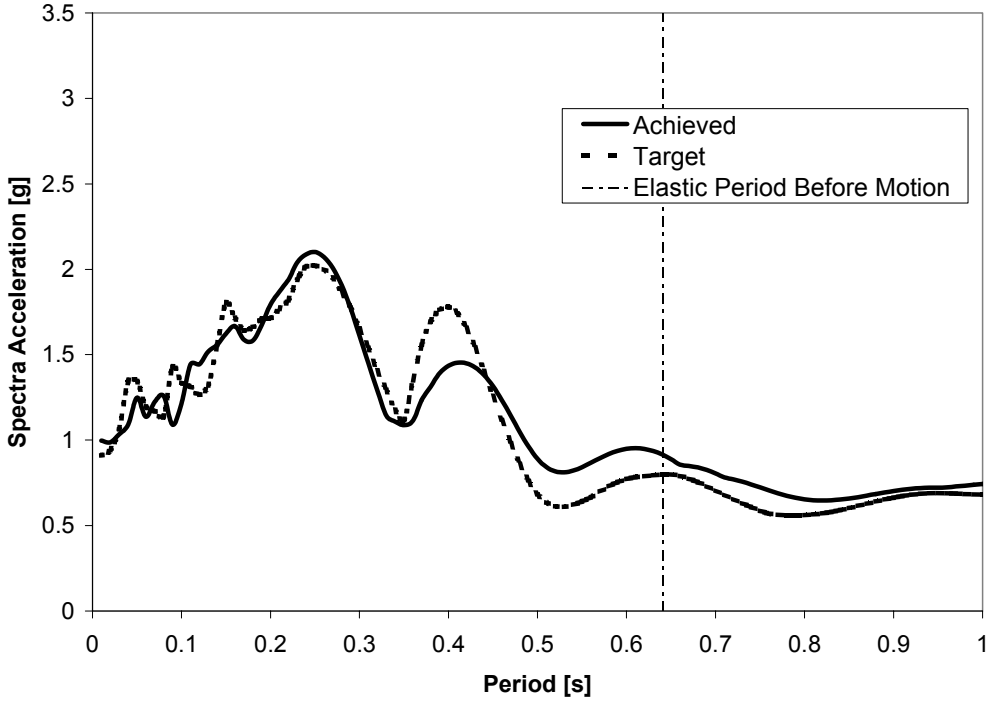

Figure 5-56 Comparison of Achieved and Target Response Spectra for 1.5 x Sylmar Specimen ISH1.5

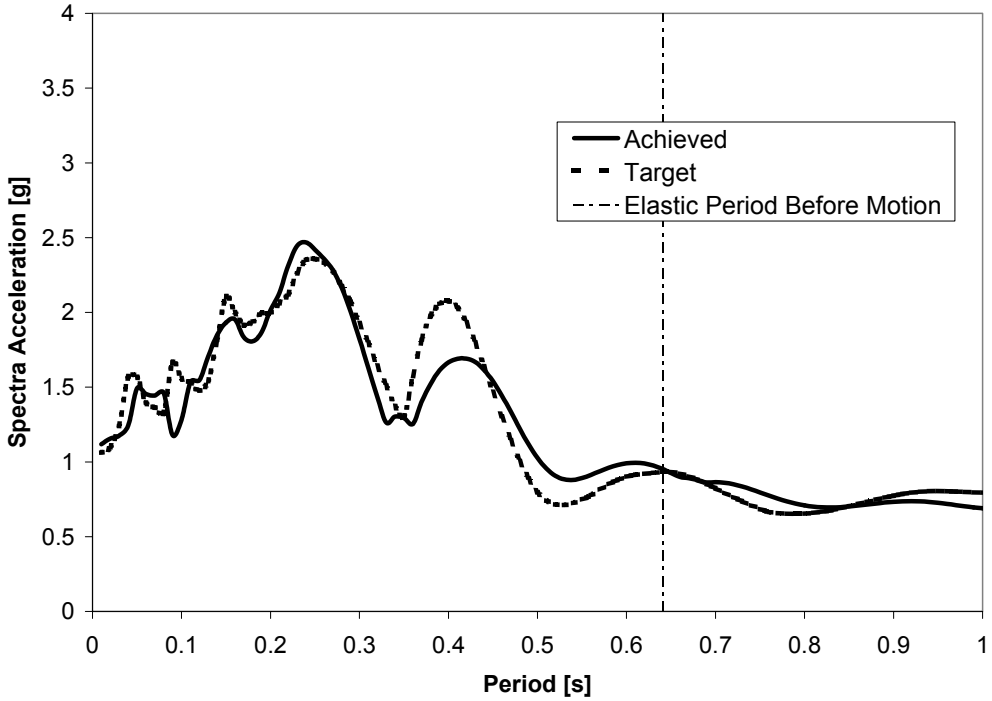

Figure 5-57 Comparison of Achieved and Target Response Spectra for 1.75 x Sylmar Specimen ISH1.5

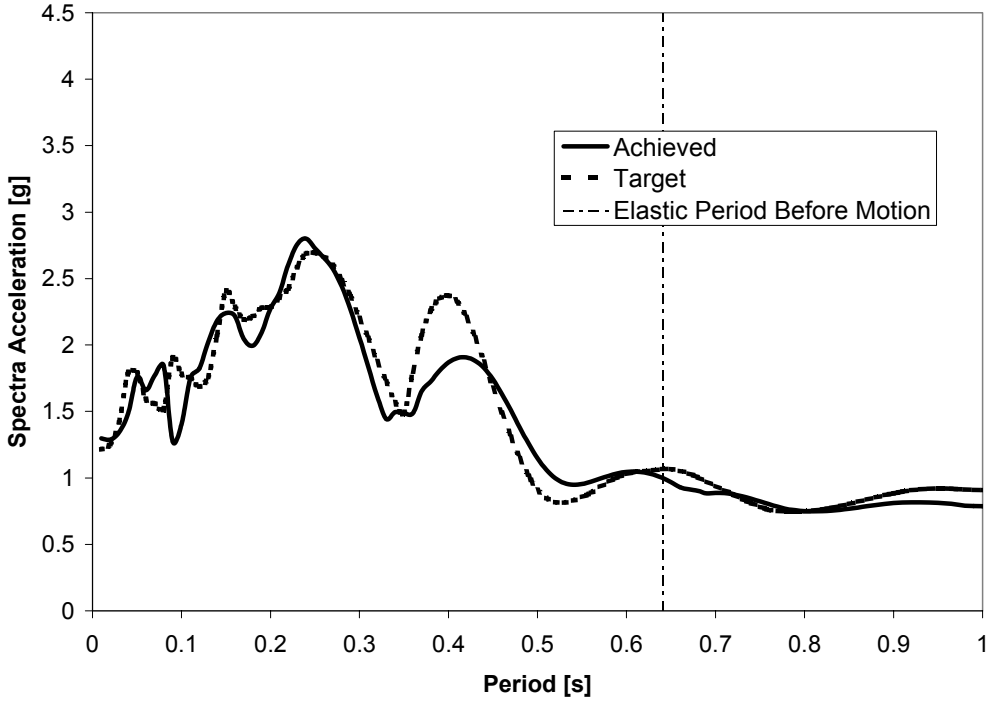

Figure 5-58 Comparison of Achieved and Target Response Spectra for 2.0 x Sylmar Specimen ISH1.5

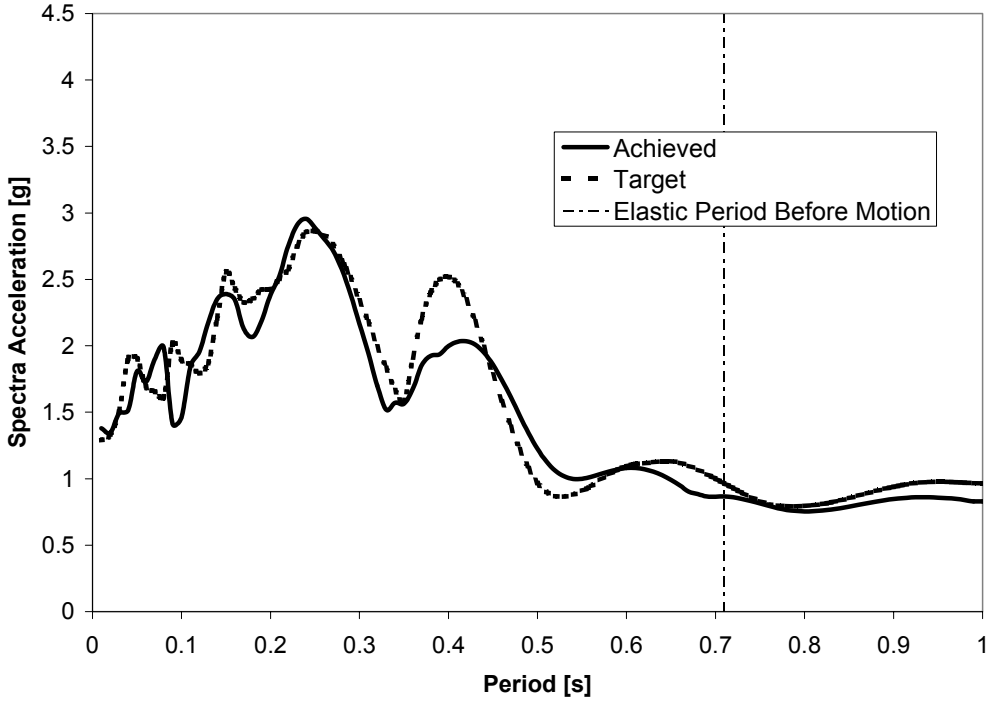

Figure 5-59 Comparison of Achieved and Target Response Spectra for 2.125 x Sylmar Specimen ISH1.5

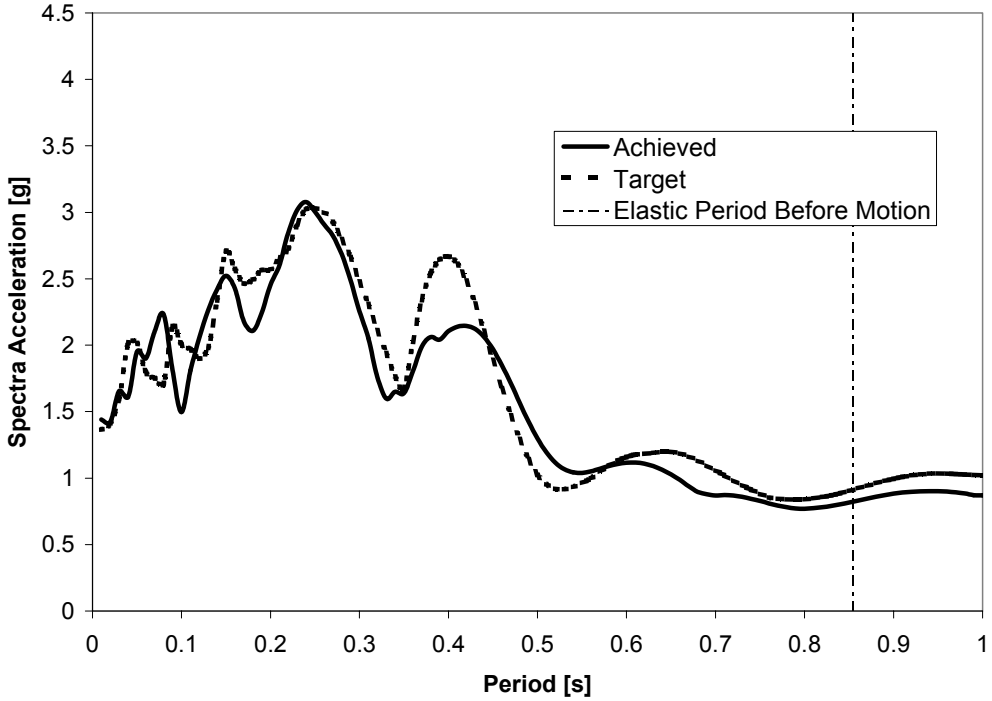

Figure 5-60 Comparison of Achieved and Target Response Spectra for 2.25 x Sylmar Specimen ISH1.5

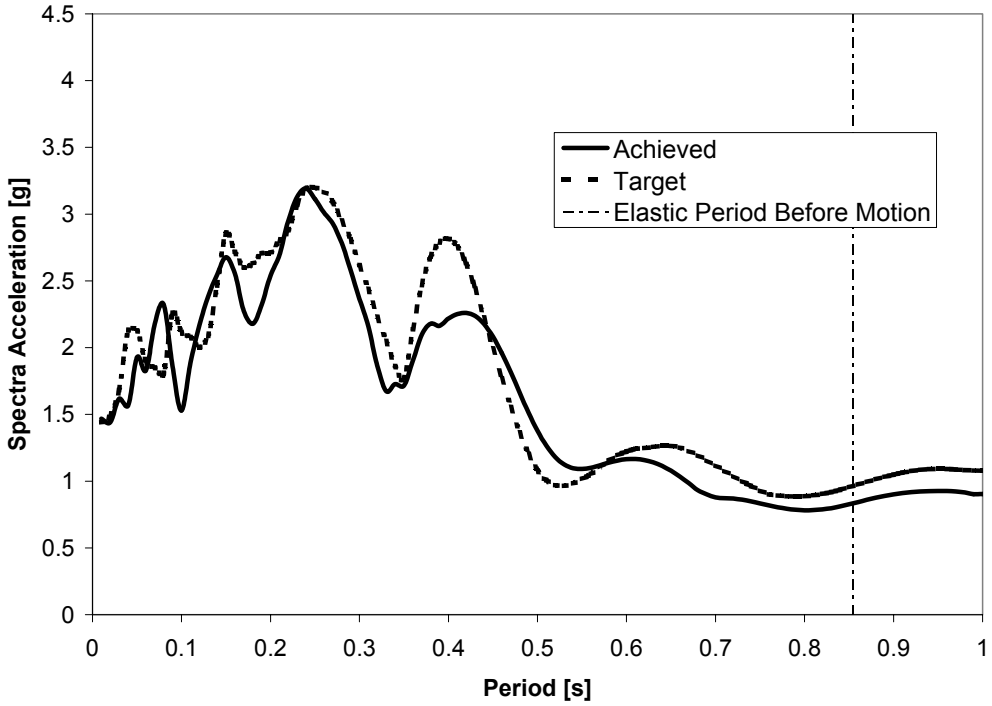

Figure 5-61 Comparison of Achieved and Target Response Spectra for 2.375 x Sylmar Specimen ISH1.5

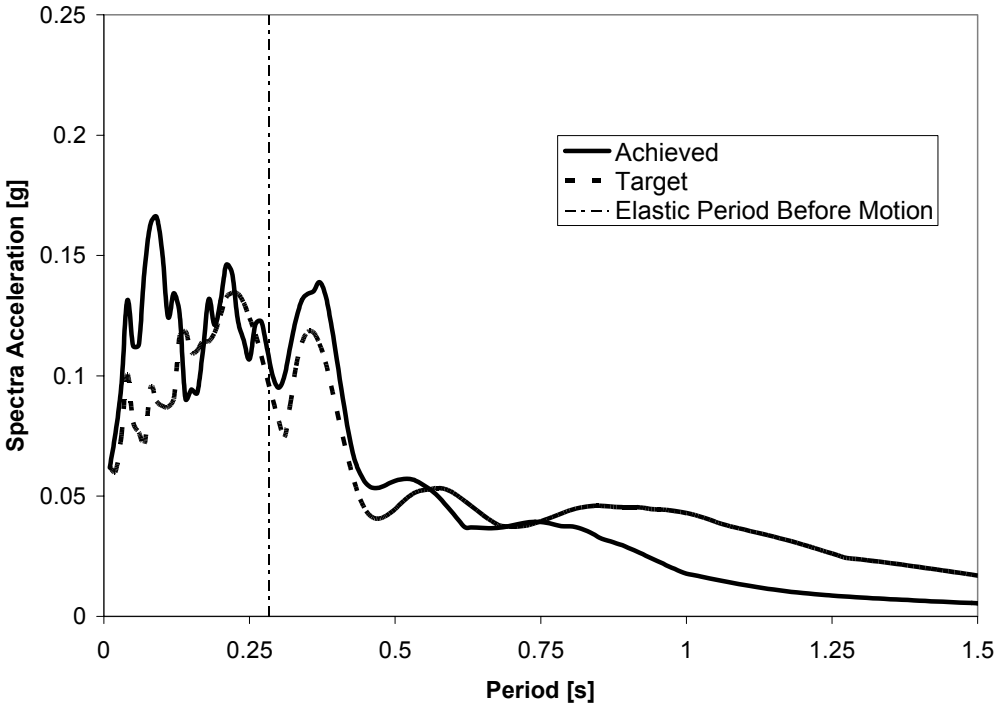

Figure 5-62 Comparison of Achieved and Target Response Spectra for 0.1 x Sylmar Specimen ISH1.5T

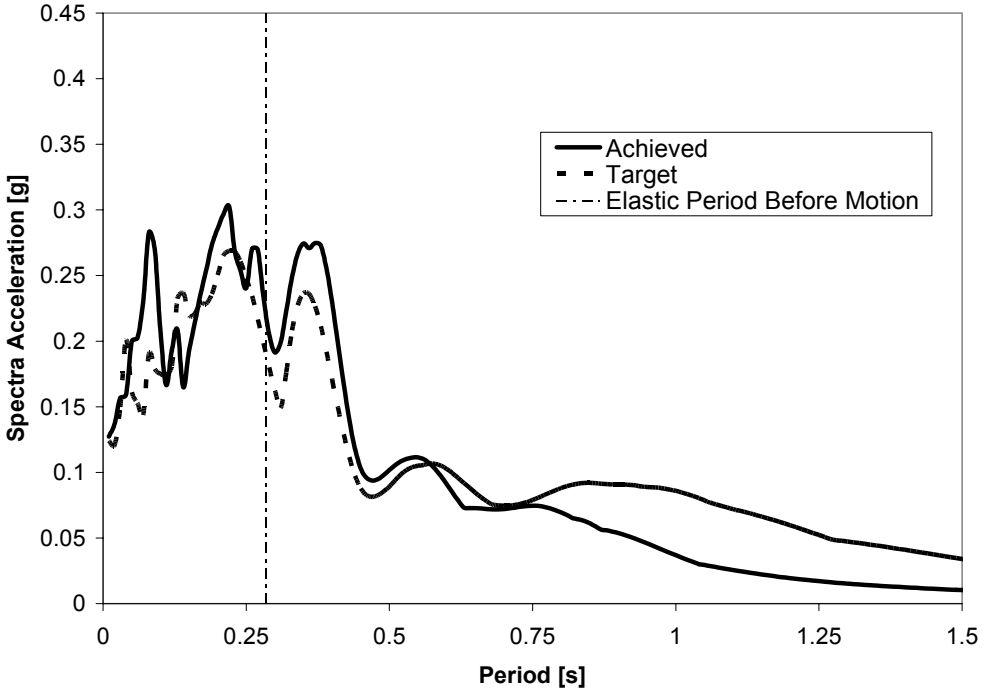

Figure 5-63 Comparison of Achieved and Target Response Spectra for 0.2 x Sylmar Specimen ISH1.5T

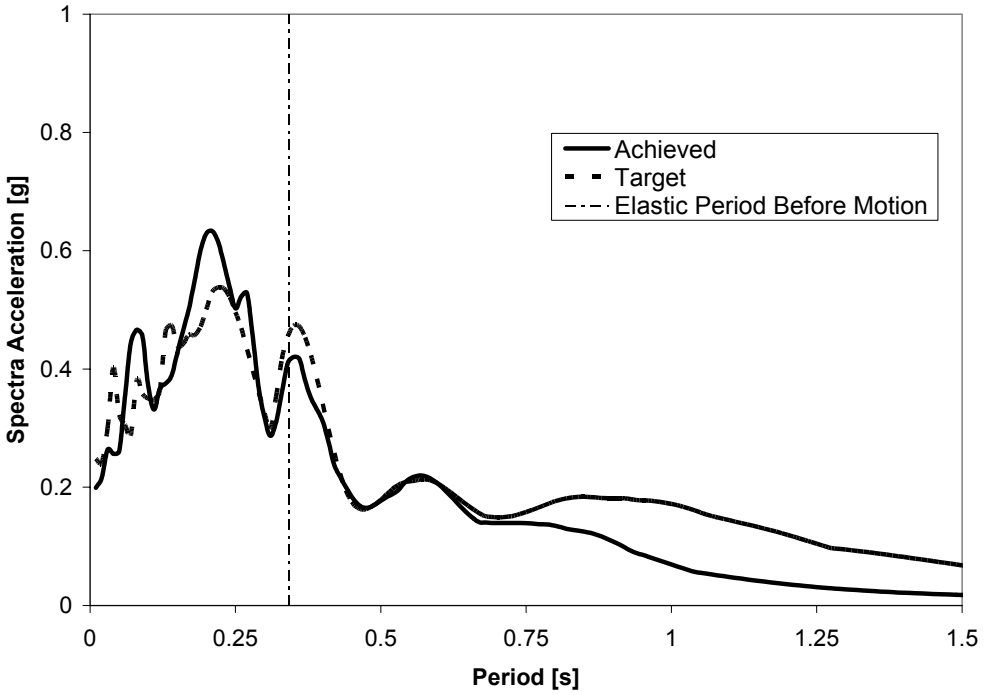

Figure 5-64 Comparison of Achieved and Target Response Spectra for 0.4 x Sylmar Specimen ISH1.5T

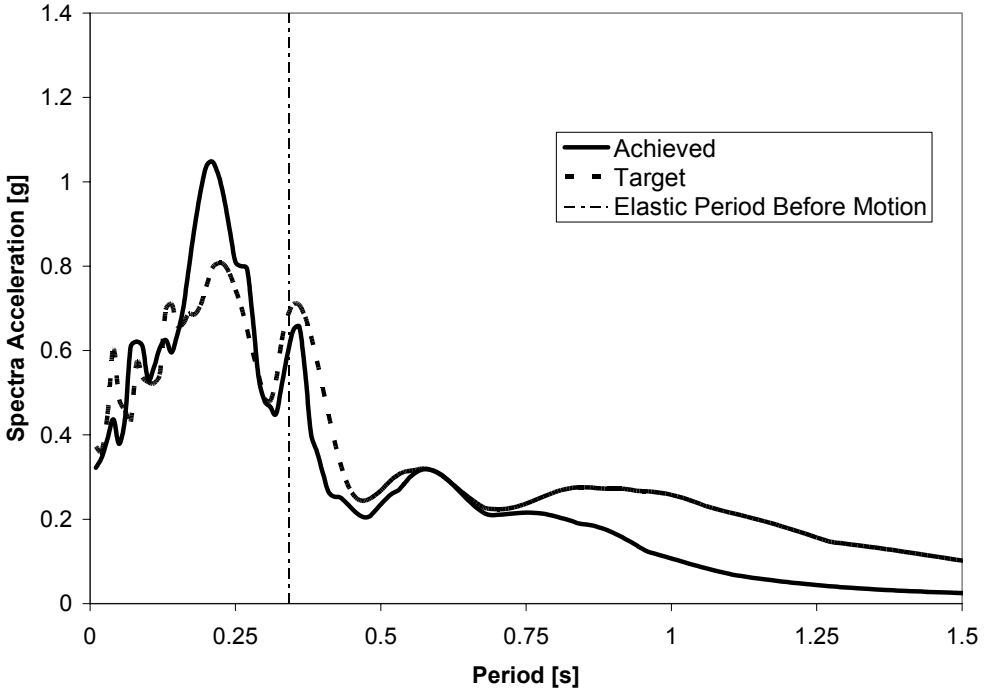

Figure 5-65 Comparison of Achieved and Target Response Spectra for 0.6 x Sylmar Specimen ISH1.5T

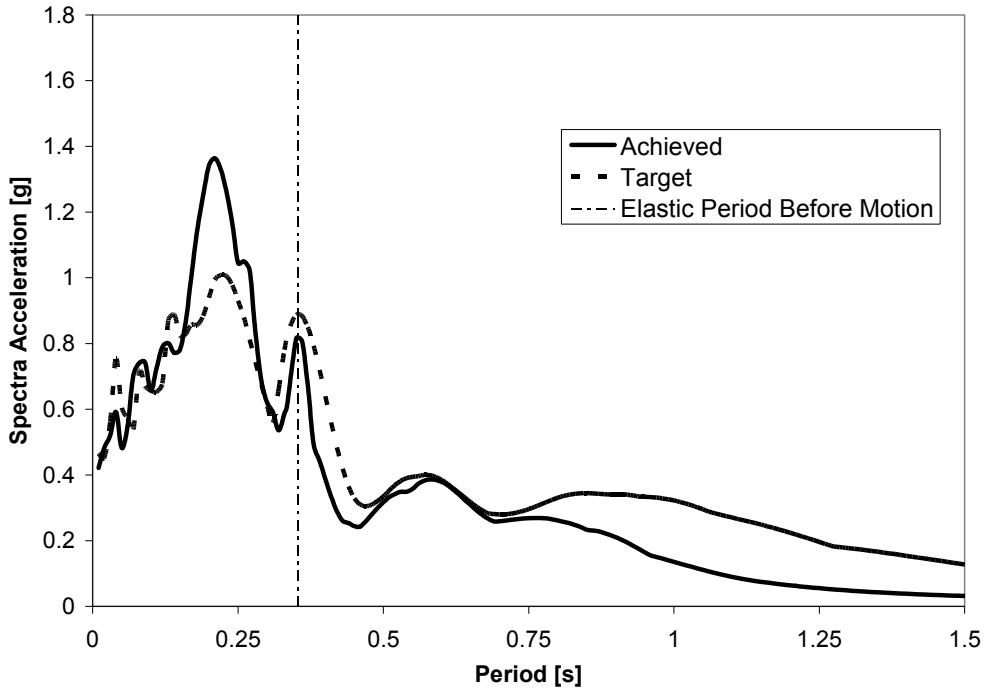

Figure 5-66 Comparison of Achieved and Target Response Spectra for 0.75 x Sylmar Specimen ISH1.5T

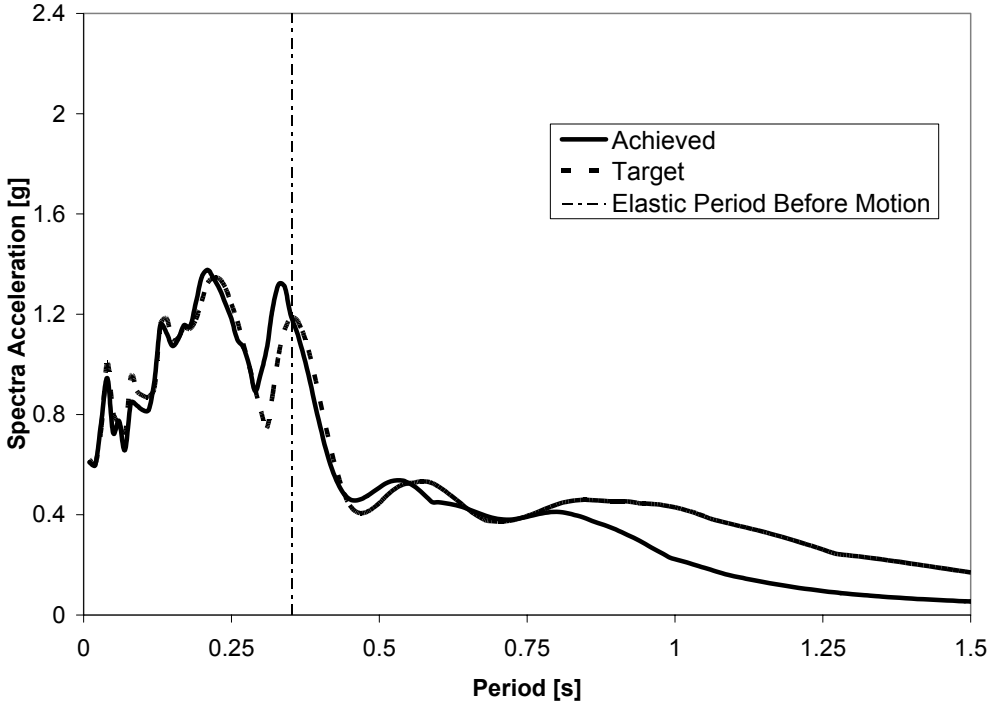

Figure 5-67 Comparison of Achieved and Target Response Spectra for 1.0 x Sylmar Specimen ISH1.5T

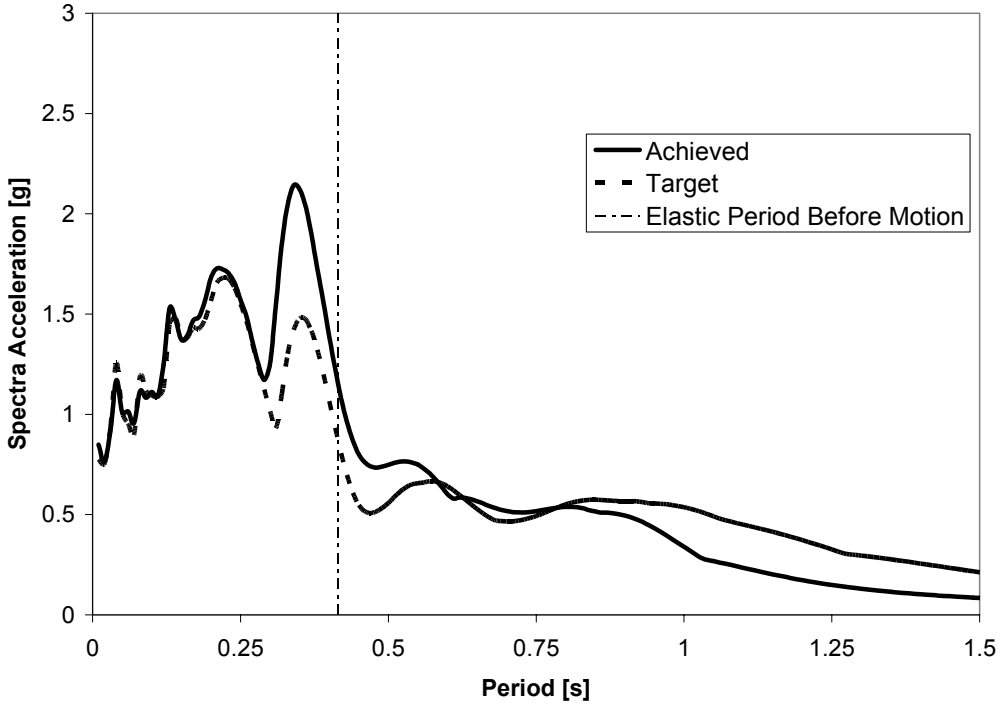

Figure 5-68 Comparison of Achieved and Target Response Spectra for 1.25 x Sylmar Specimen ISH1.5T

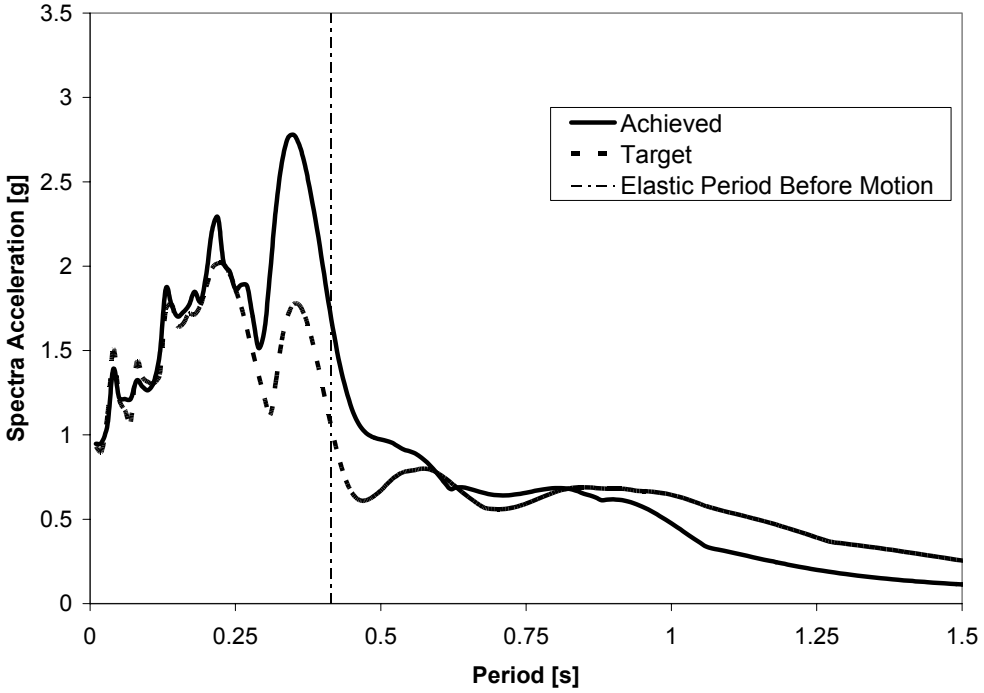

Figure 5-69 Comparison of Achieved and Target Response Spectra for 1.5 x Sylmar Specimen ISH1.5T

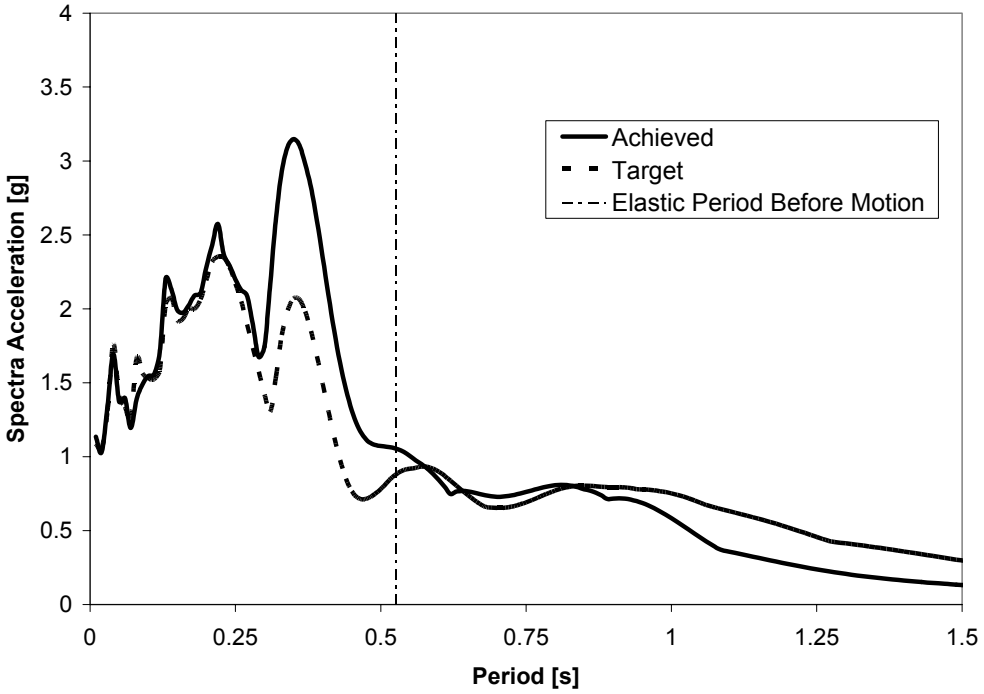

Figure 5-70 Comparison of Achieved and Target Response Spectra for 1.75 x Sylmar Specimen ISH1.5T

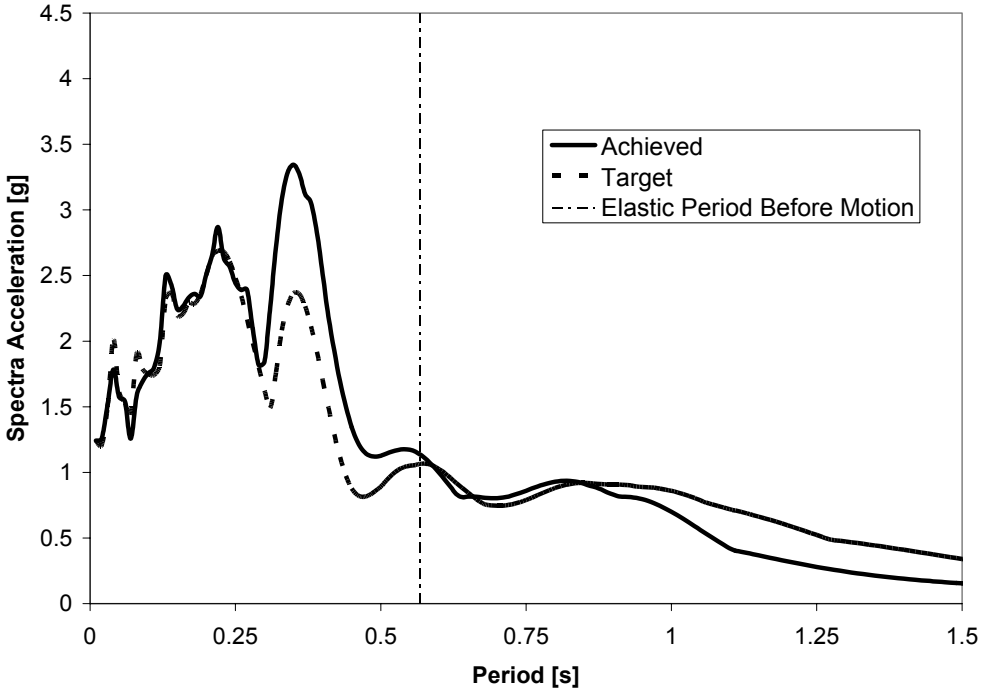

Figure 5-71 Comparison of Achieved and Target Response Spectra for 2.0 x Sylmar Specimen ISH1.5T

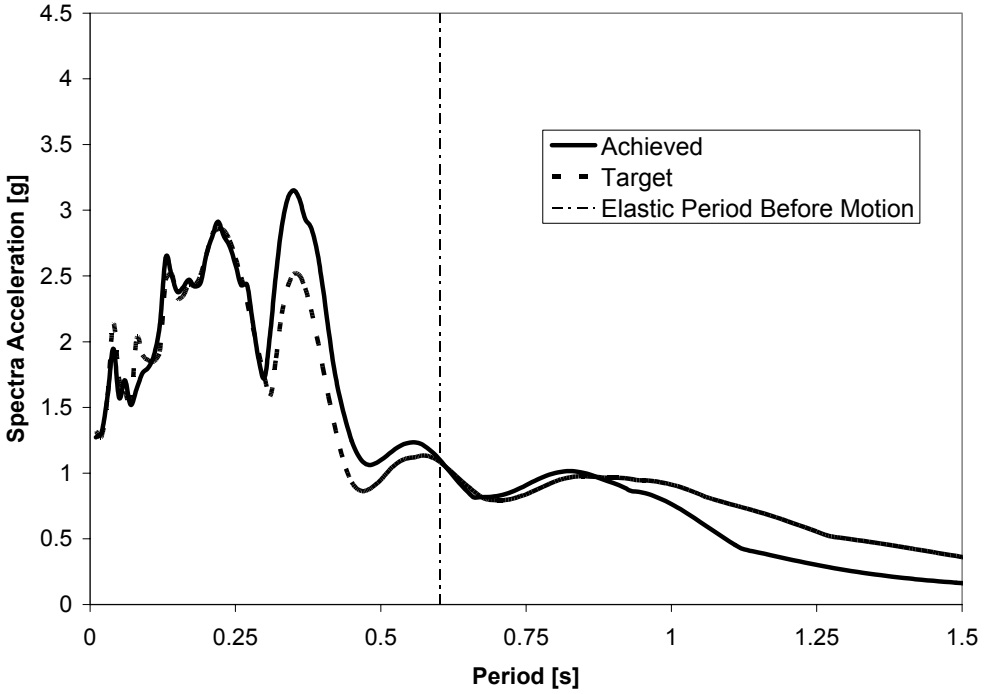

Figure 5-72 Comparison of Achieved and Target Response Spectra for 2.125 x Sylmar Specimen ISH1.5T

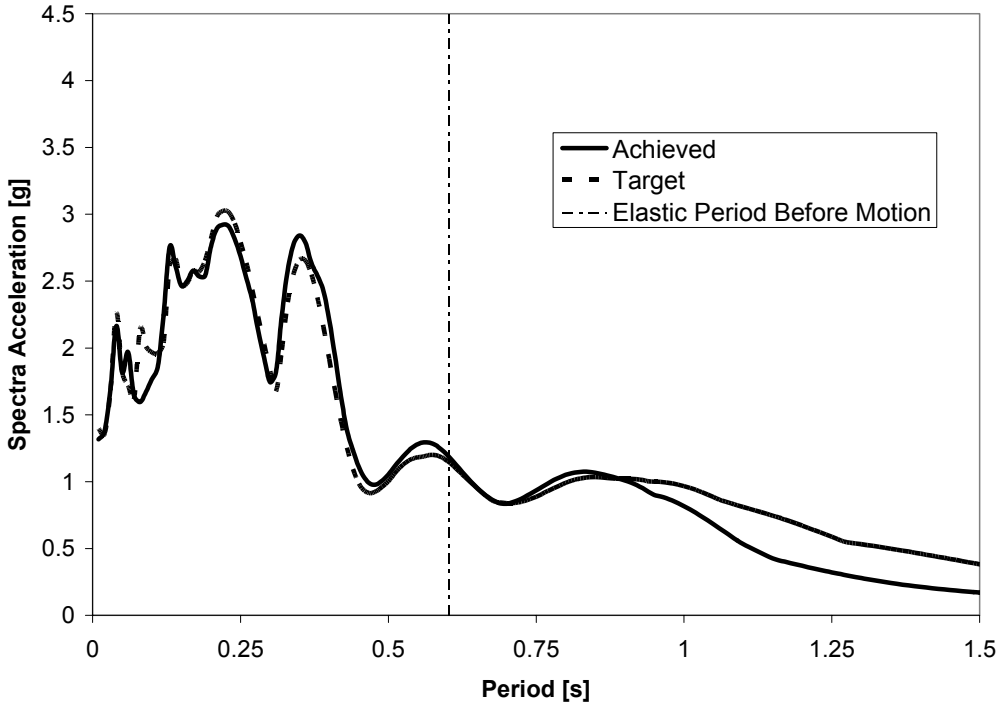

Figure 5-73 Comparison of Achieved and Target Response Spectra for 2.25 x Sylmar Specimen ISH1.5T

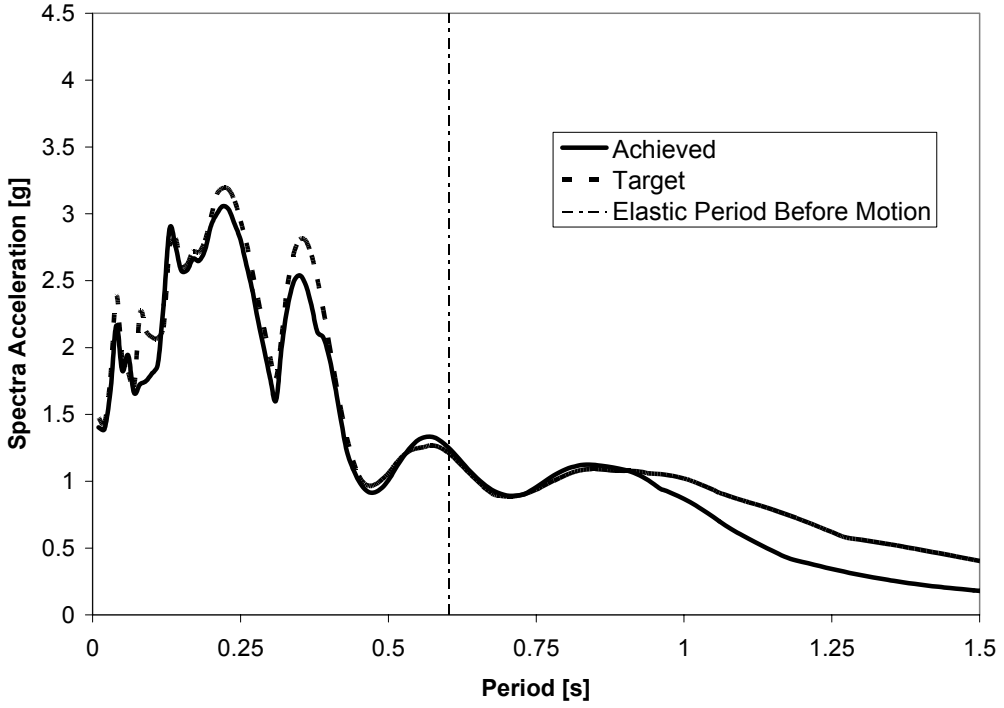

Figure 5-74 Comparison of Achieved and Target Response Spectra for 2.375 x Sylmar Specimen ISH1.5T

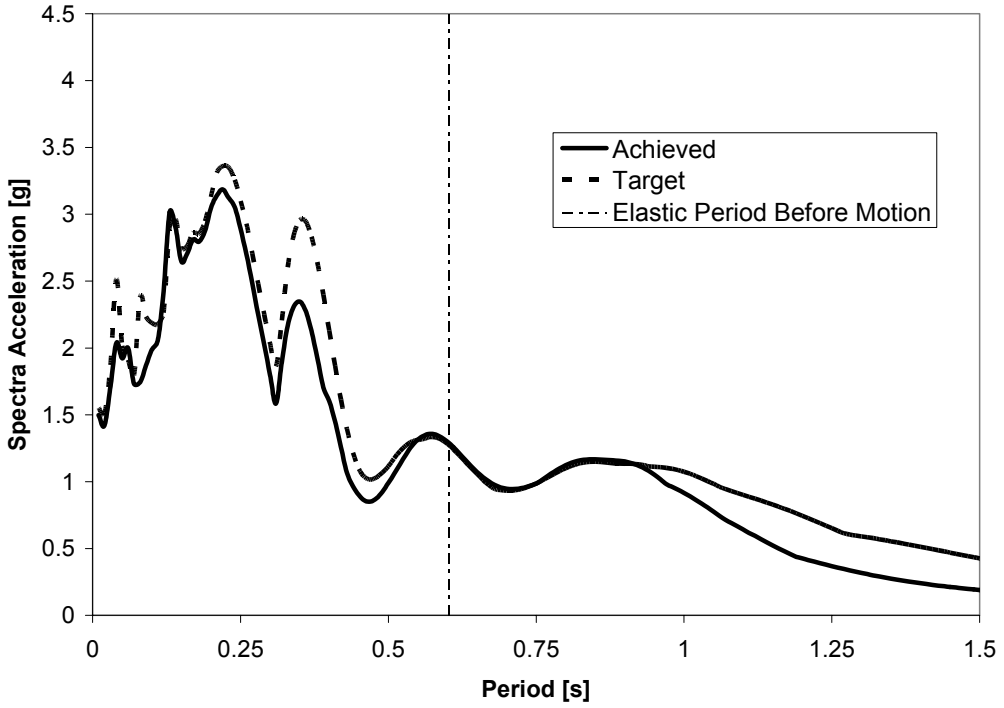

Figure 5-75 Comparison of Achieved and Target Response Spectra for 2.5 x Sylmar Specimen ISH1.5T

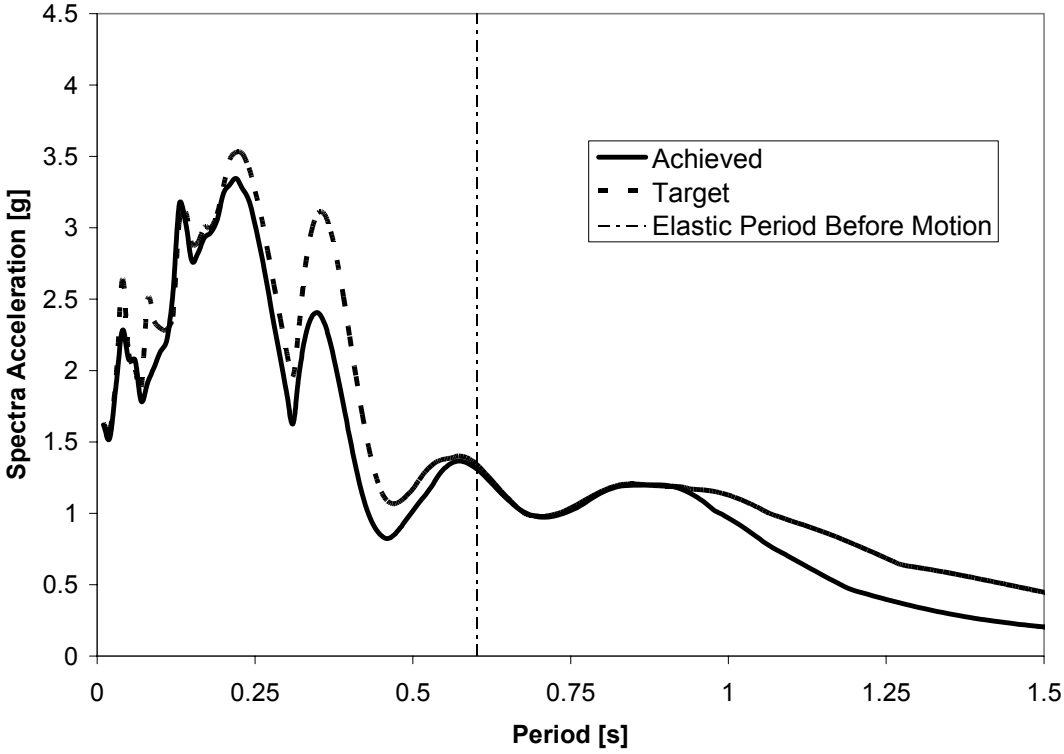

Figure 5-76 Comparison of Achieved and Target Response Spectra for 2.625 x Sylmar Specimen ISH1.5T

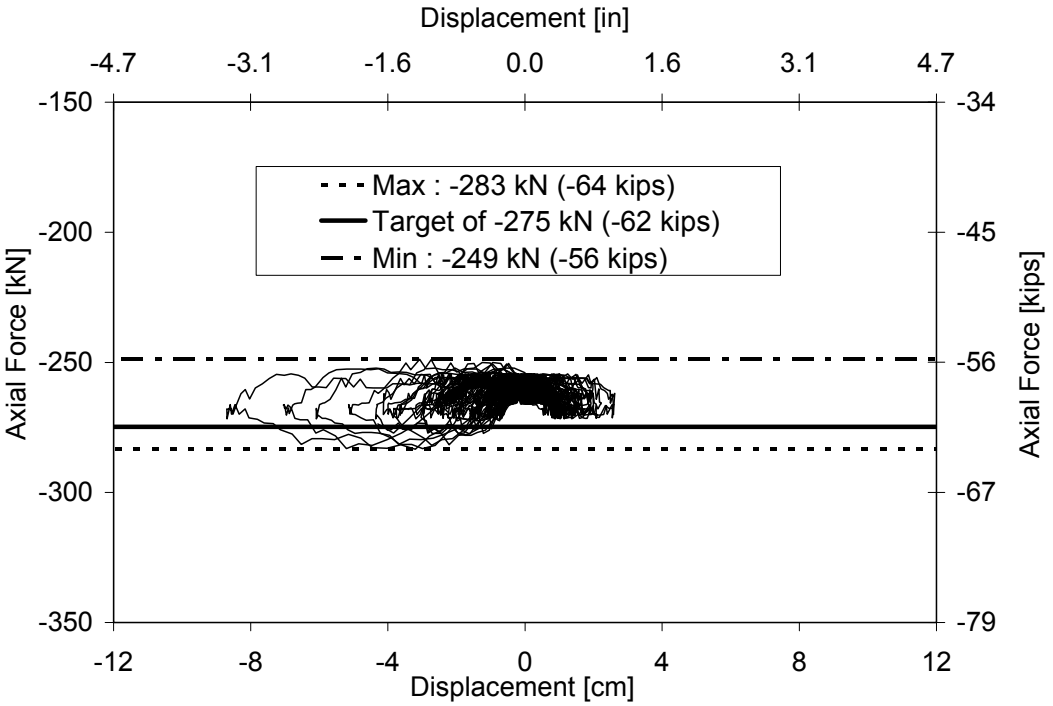

Figure 5-77 Axial Load Variation Specimen ISH1.0

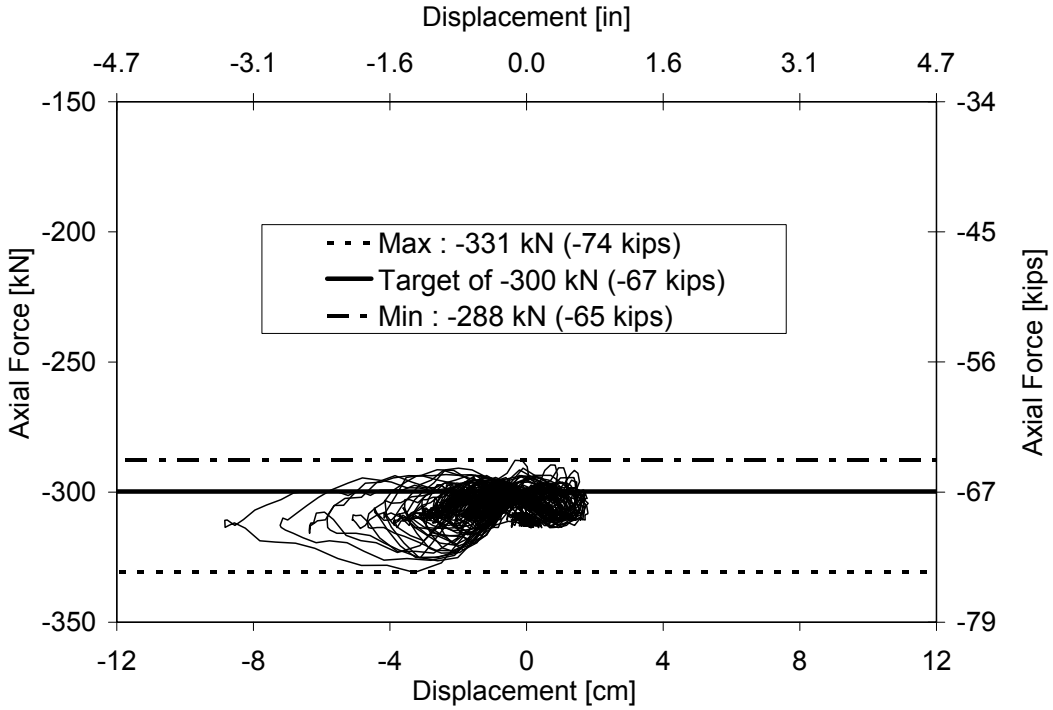

Figure 5-78 Axial Load Variation Specimen ISH1.25

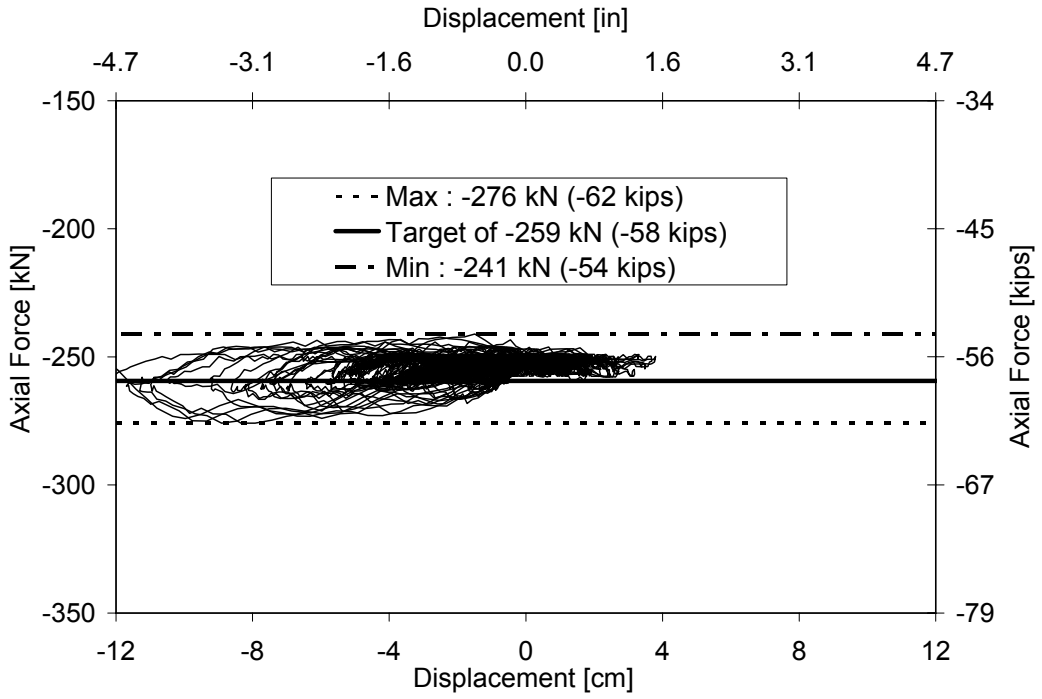

Figure 5-79 Axial Load Variation Specimen ISH1.5

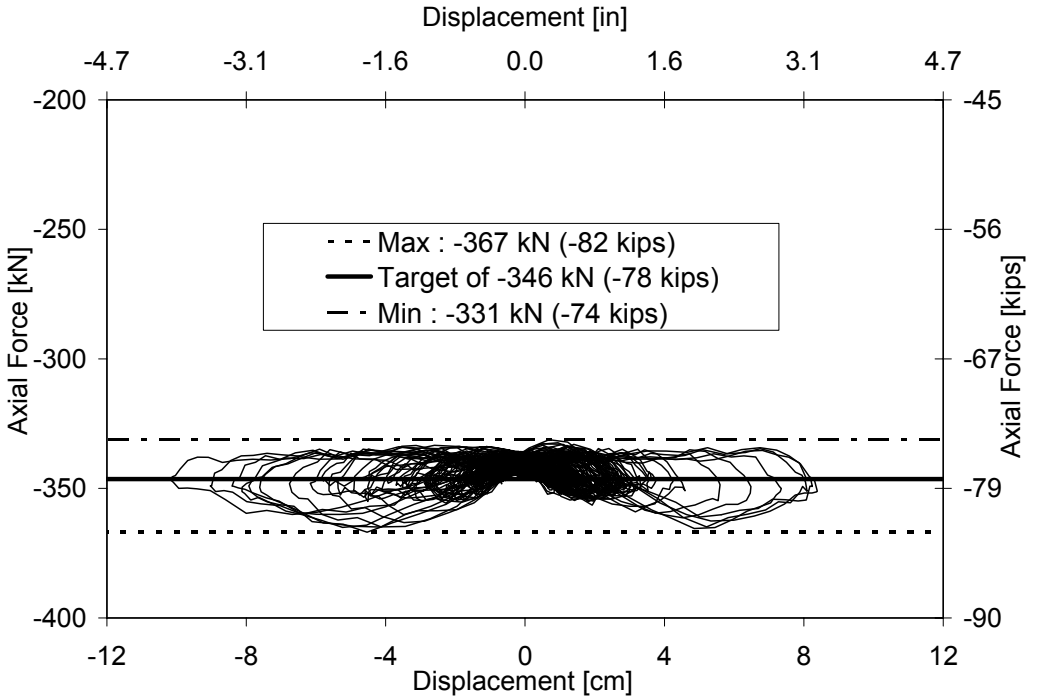

Figure 5-80 Axial Load Variation Specimen ISH1.5T

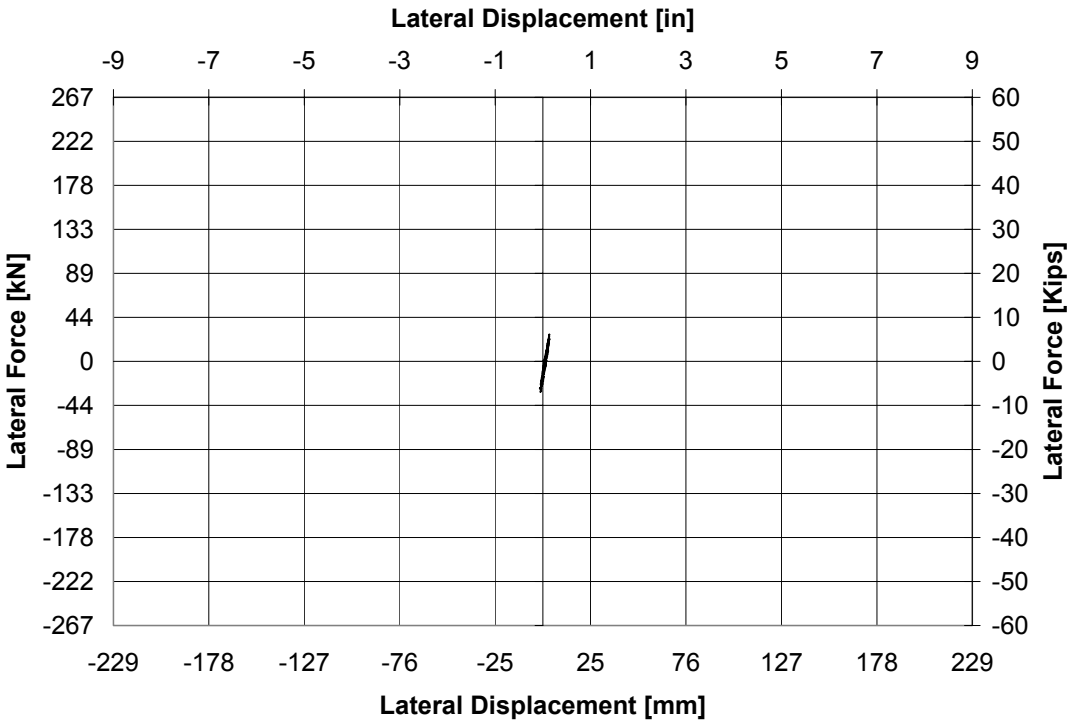

Figure 5-81 Force Displacement Hysteresis Curve for ISH1.0 at 0.1xSlymar

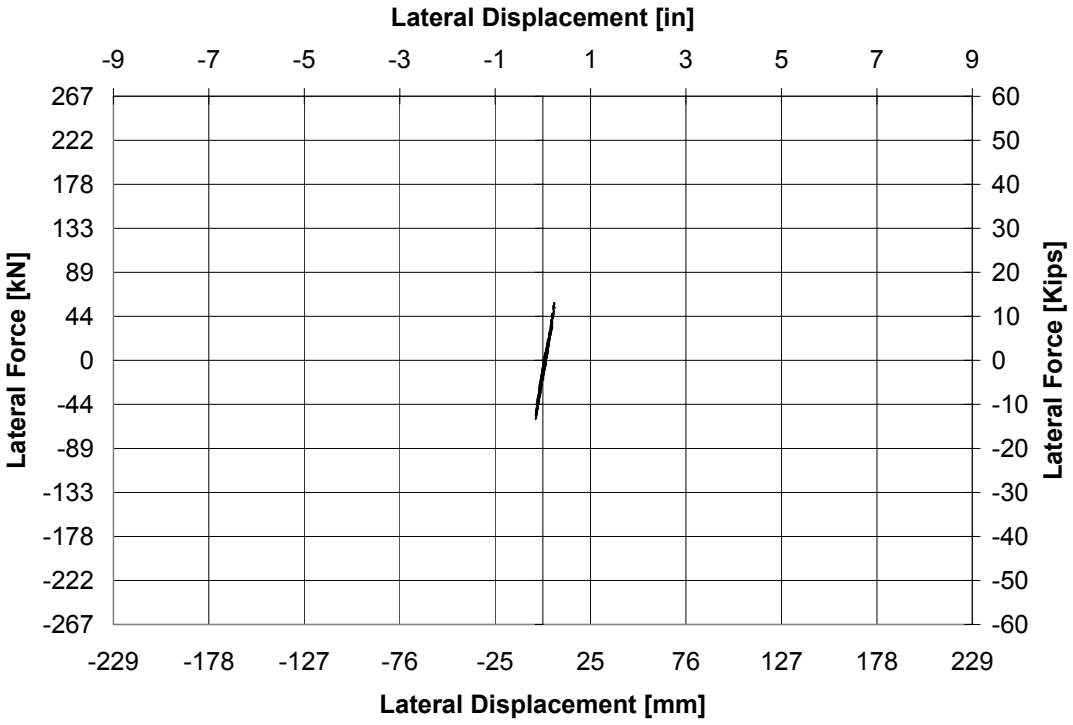

Figure 5-82 Force Displacement Hysteresis Curve for ISH1.0 at 0.2xSlymar

Figure 5-83 Force Displacement Hysteresis Curve for ISL1.0 at 0.4xSlymar

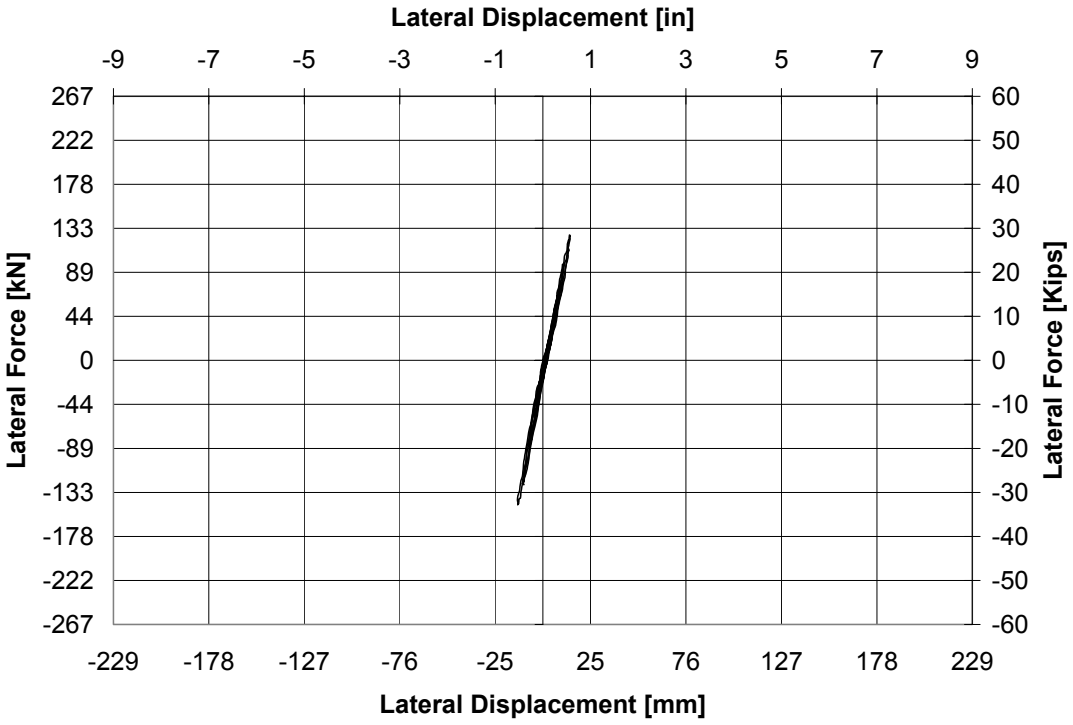

Figure 5-84 Force Displacement Hysteresis Curve for ISL1.0 at 0.5xSlymar

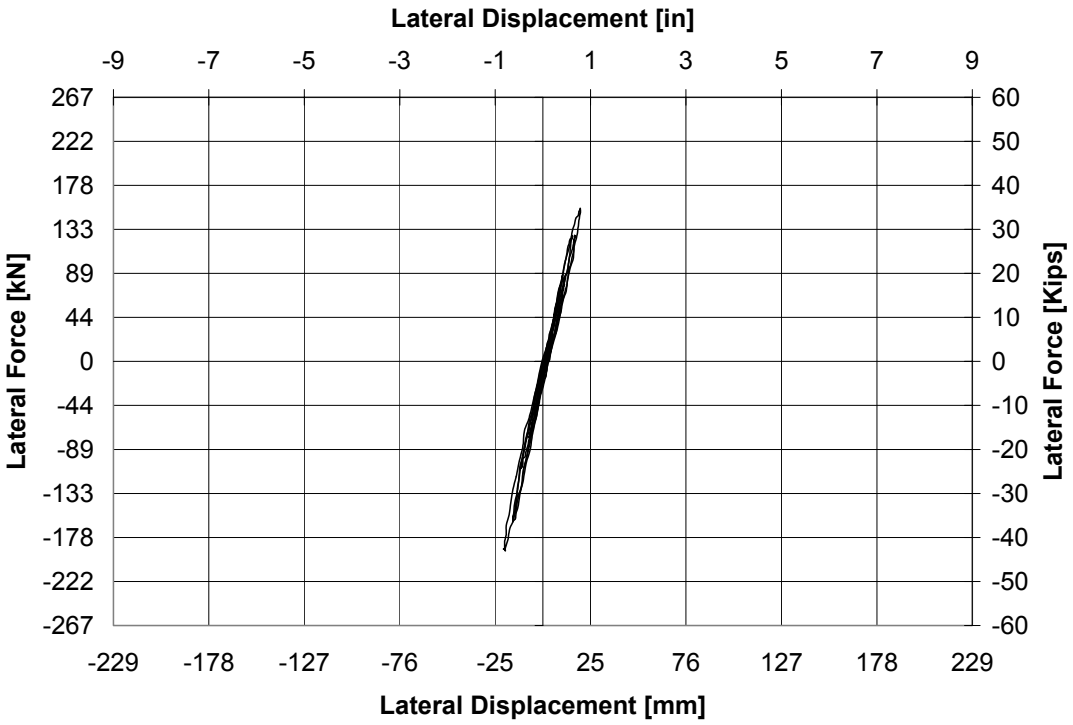

Figure 5-85 Force Displacement Hysteresis Curve for ISH1.0 at 0.75xSlymar

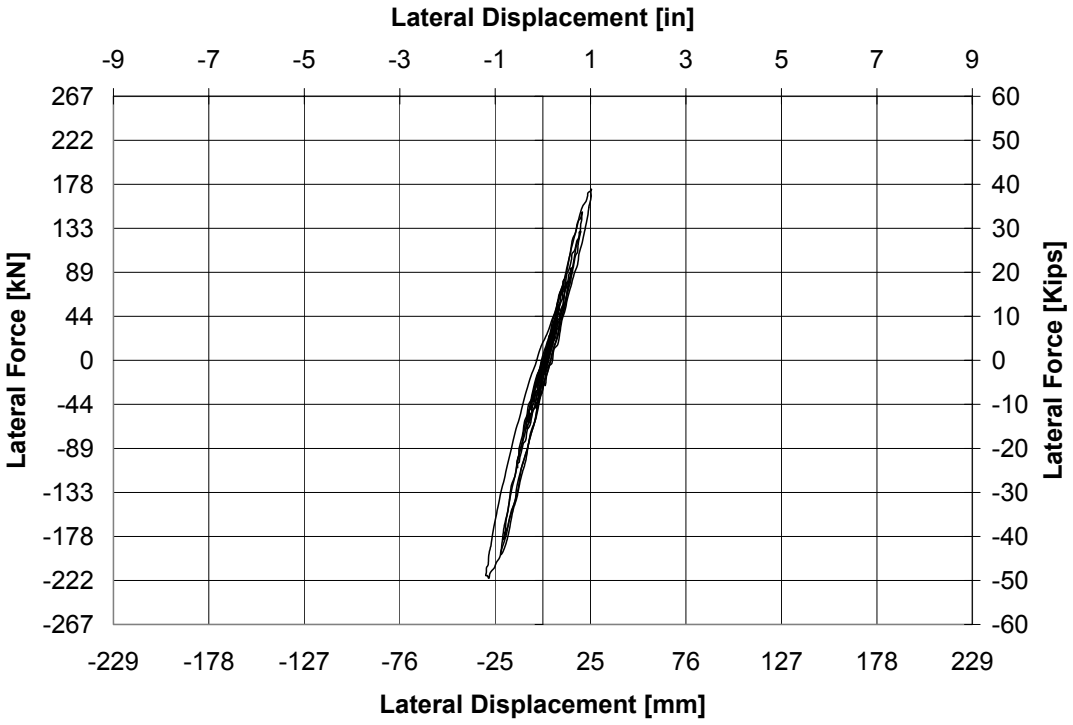

Figure 5-86 Force Displacement Hysteresis Curve for ISH1.0 at 1.0xSlymar

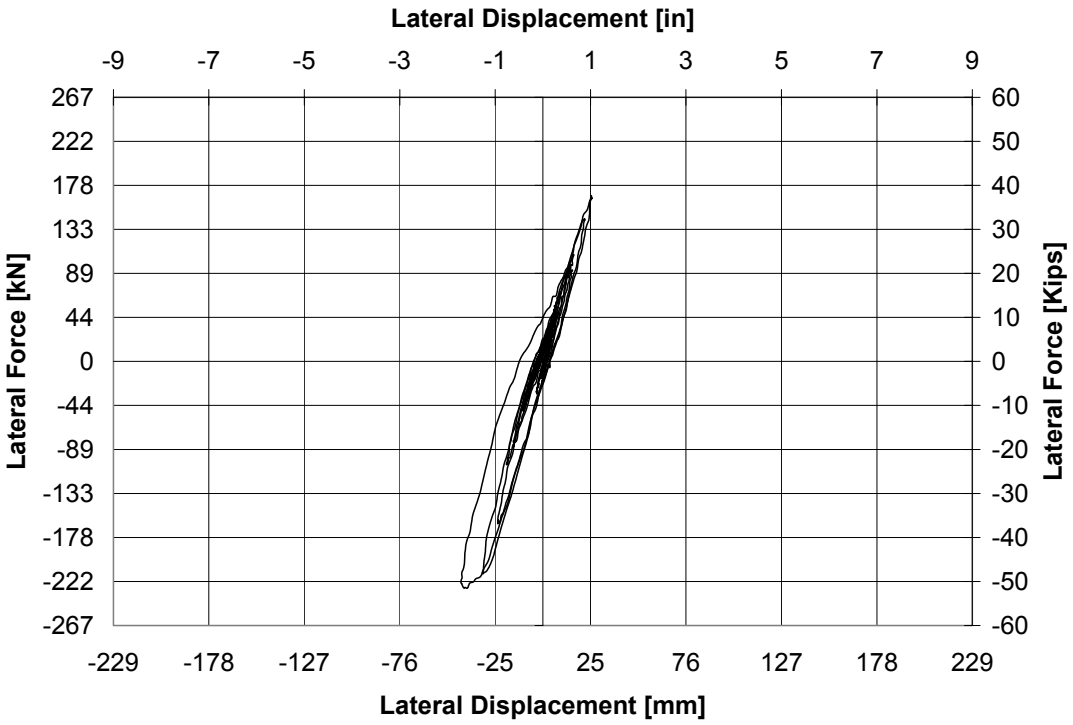

Figure 5-87 Force Displacement Hysteresis Curve for ISH1.0 at 1.25xSlymar

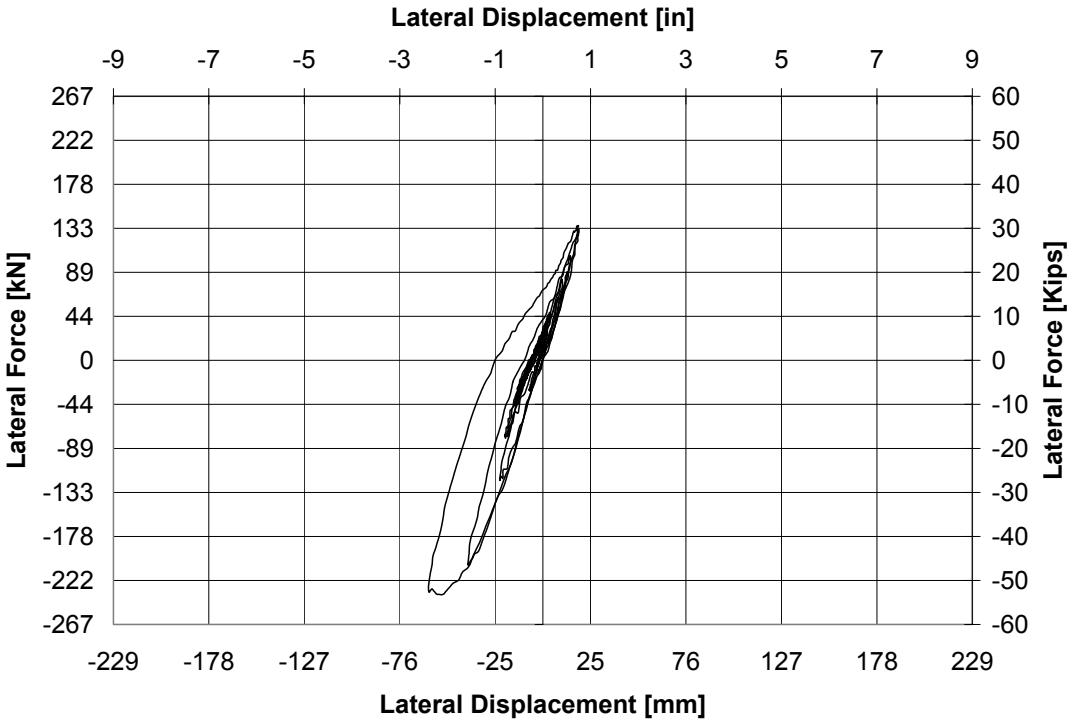

Figure 5-88 Force Displacement Hysteresis Curve for ISH1.0 at 1.5xSlymar

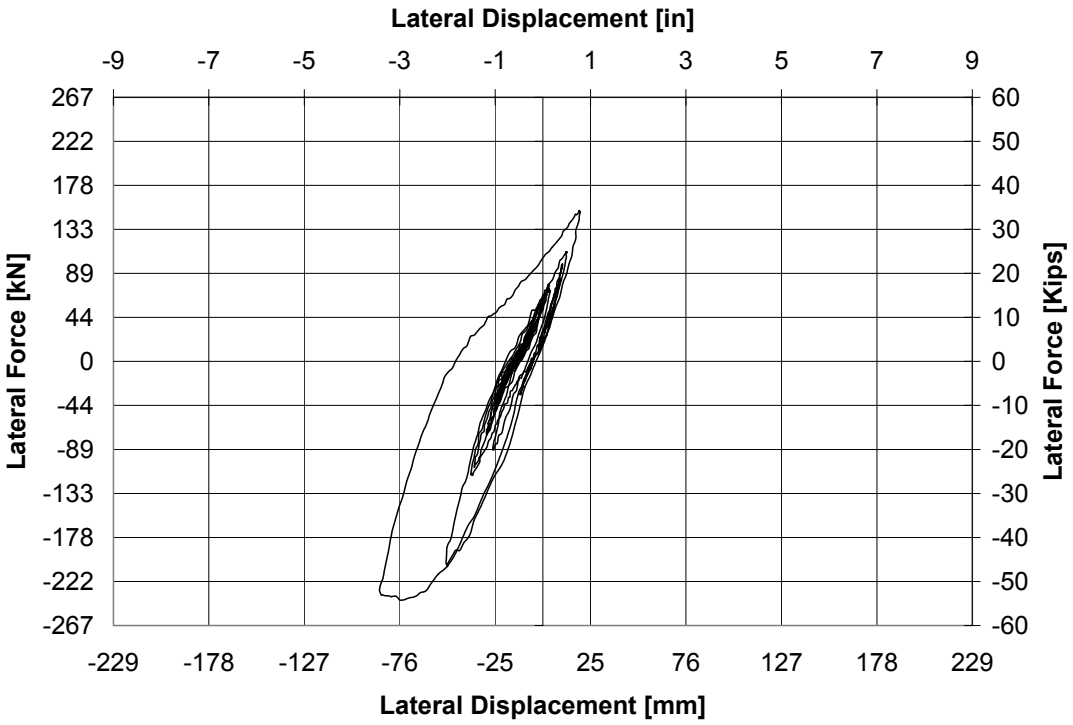

Figure 5-89 Force Displacement Hysteresis Curve for ISH1.0 at 1.75xSlymar

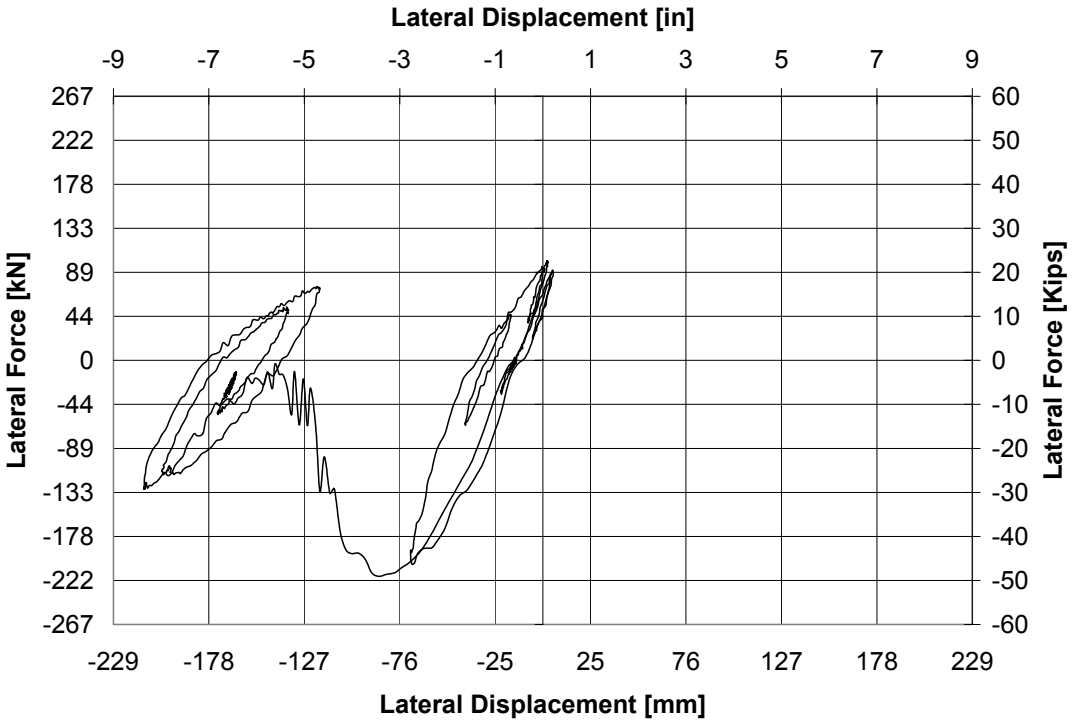

Figure 5-90 Force Displacement Hysteresis Curve for ISH1.0 at 2.0xSlymar

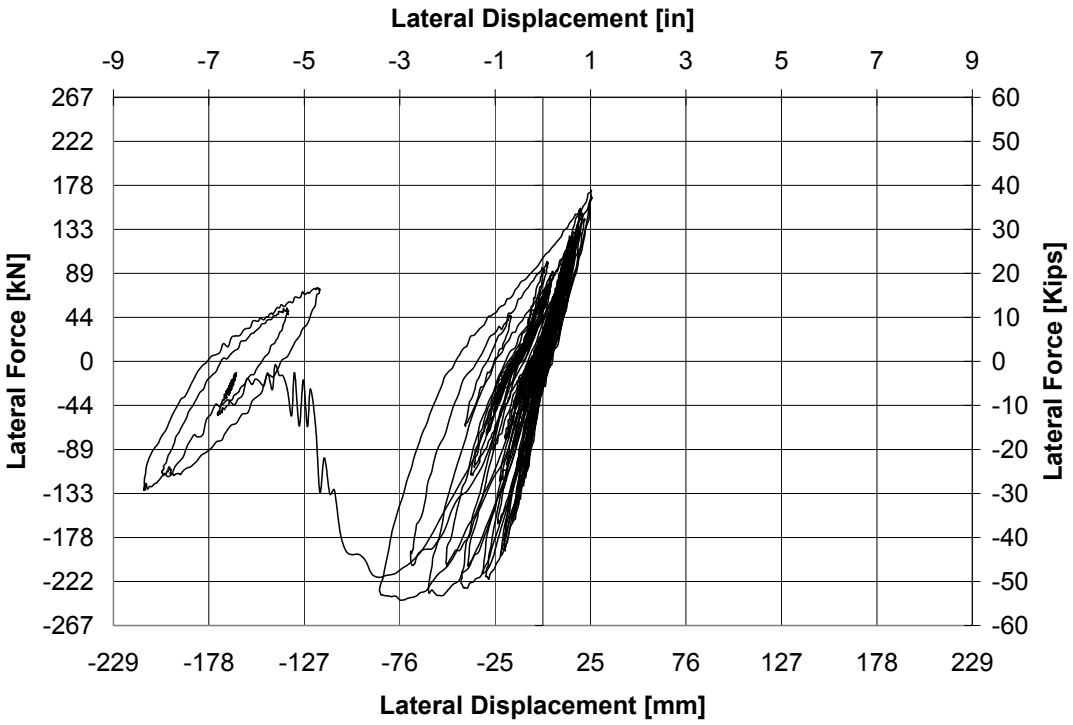

Figure 5-91 Accumulated Force Displacement Hysteresis Curve for ISH1.0

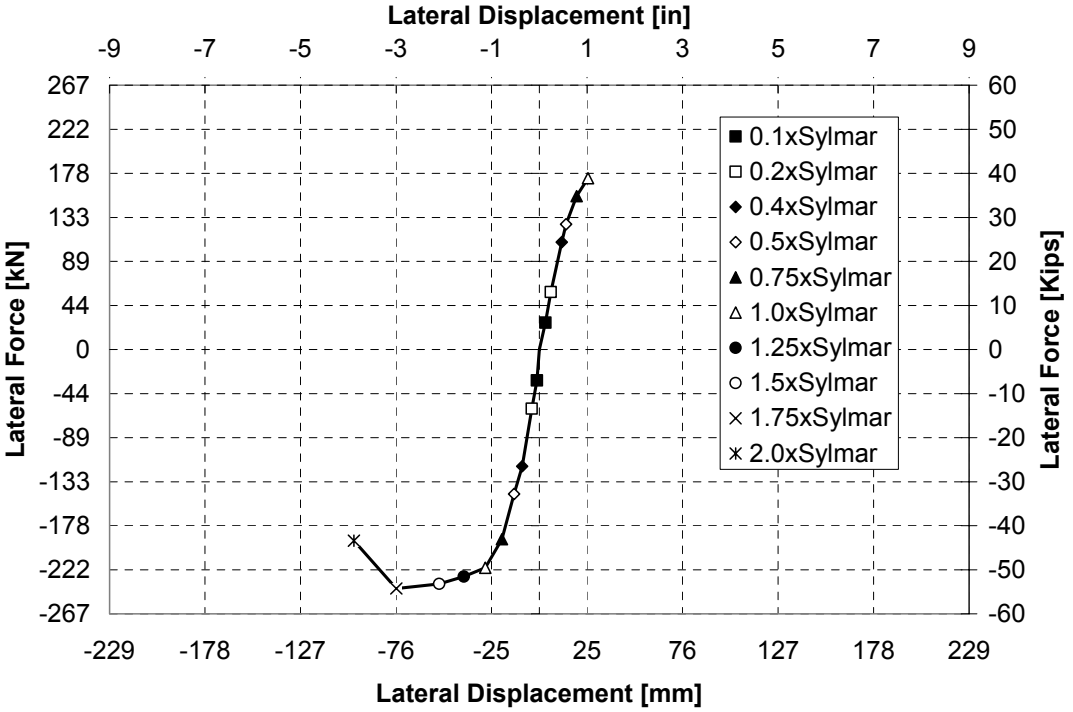

Figure 5-92 Envelope of Accumulated Force Displacement Hysteresis Curve for ISH1.0

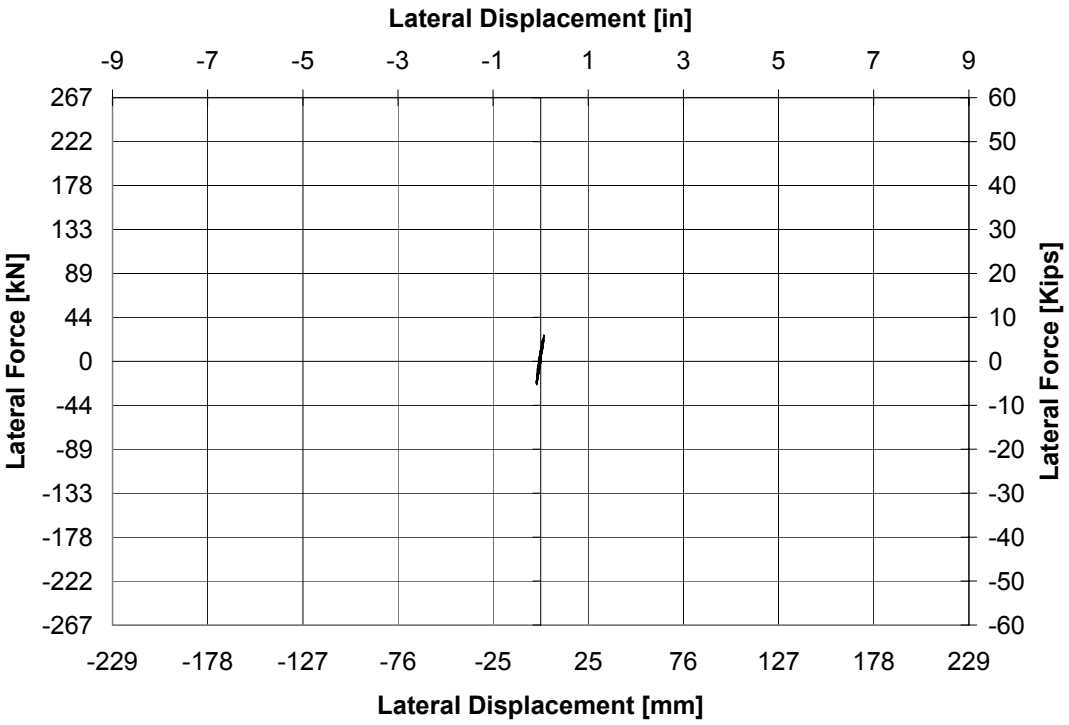

Figure 5-93 Force Displacement Hysteresis Curve for ISH1.25 at 0.1xSlymar

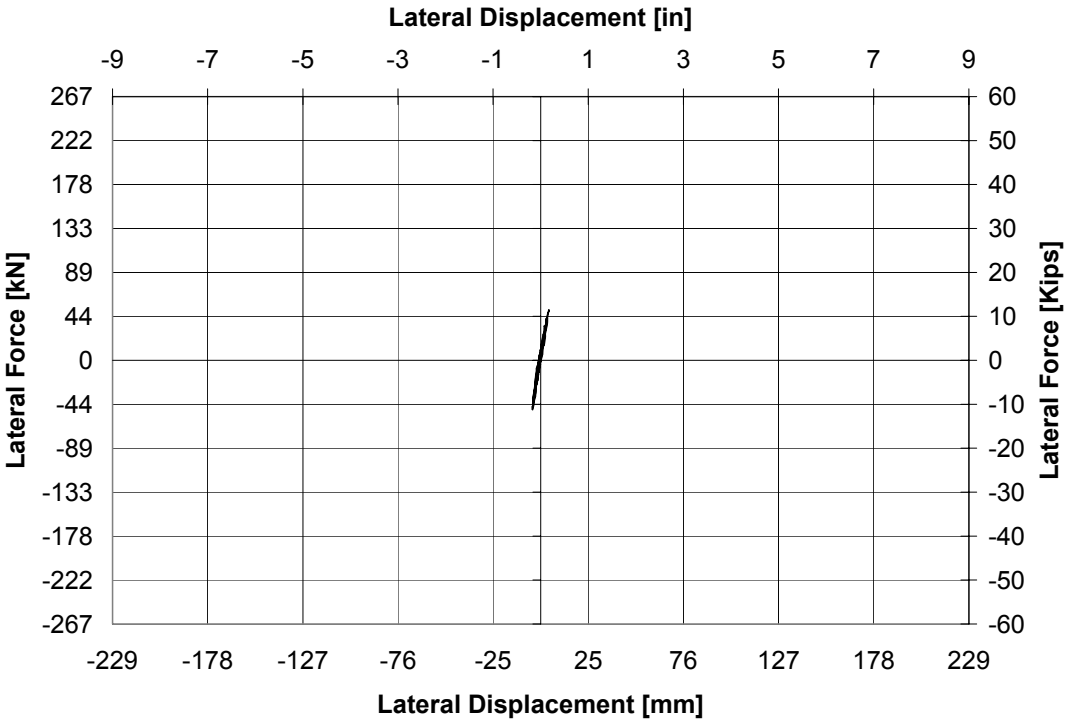

Figure 5-94 Force Displacement Hysteresis Curve for ISH1.25 at 0.2xSlymar

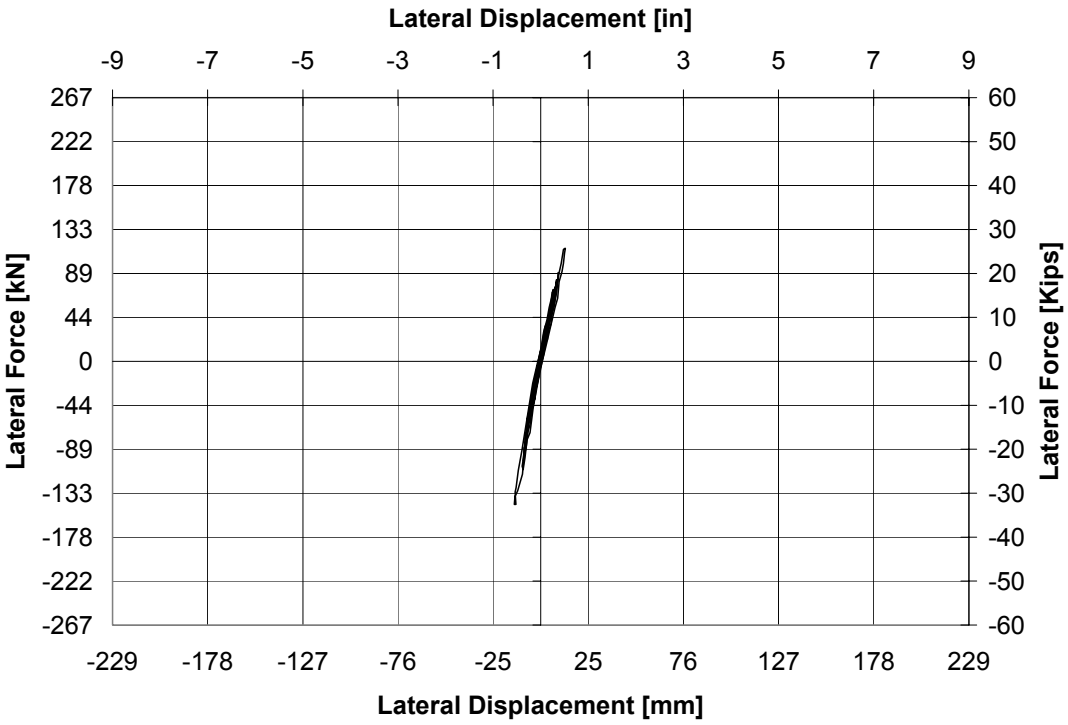

Figure 5-95 Force Displacement Hysteresis Curve for ISH1.25 at 0.5xSlymar

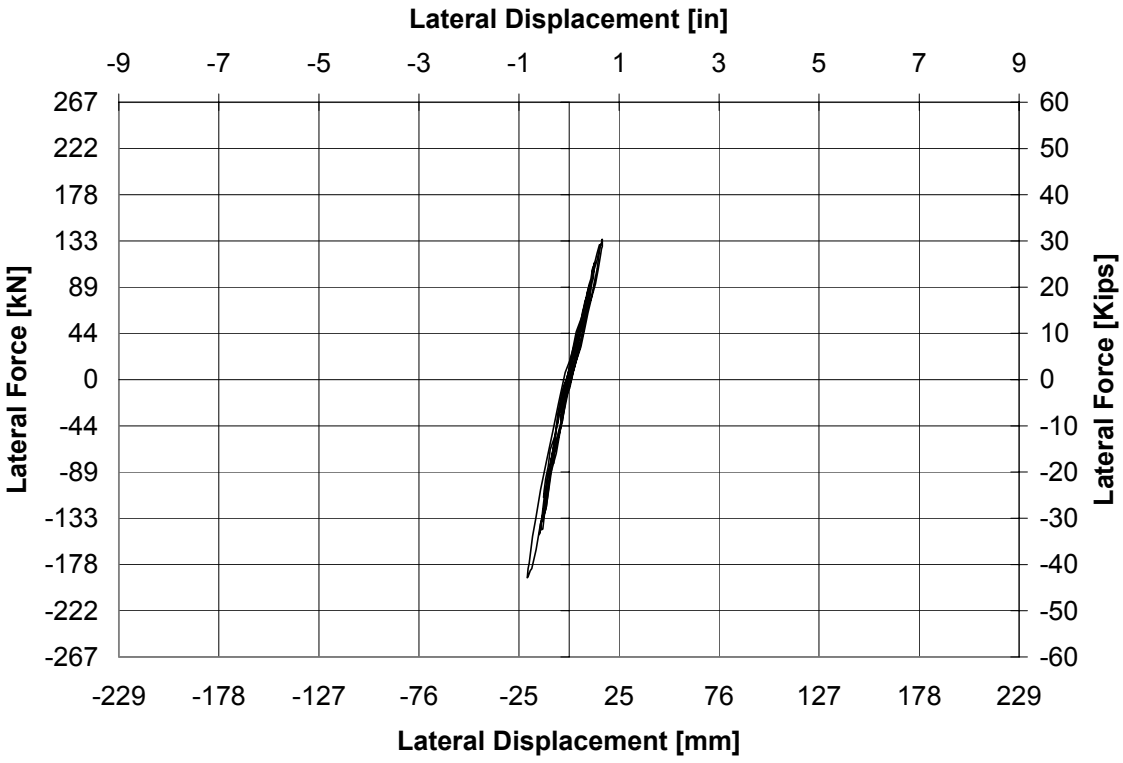

Figure 5-96 Force Displacement Hysteresis Curve for ISH1.25 at 0.75xSlymar

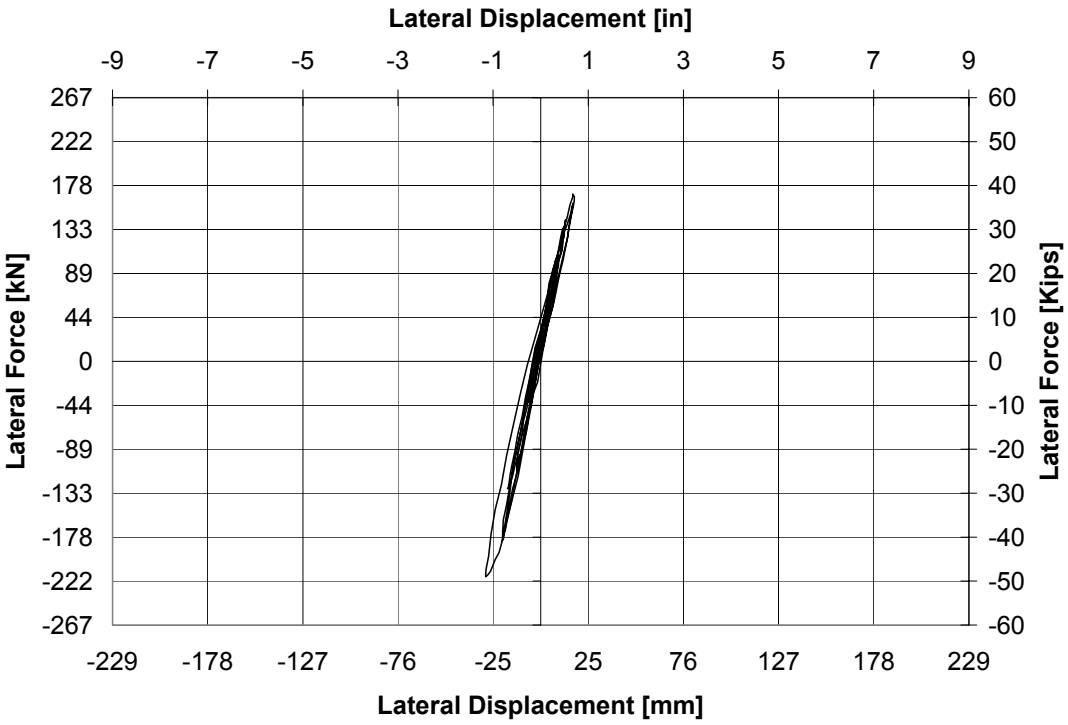

Figure 5-97 Force Displacement Hysteresis Curve for ISH1.25 at 1.0xSlymar

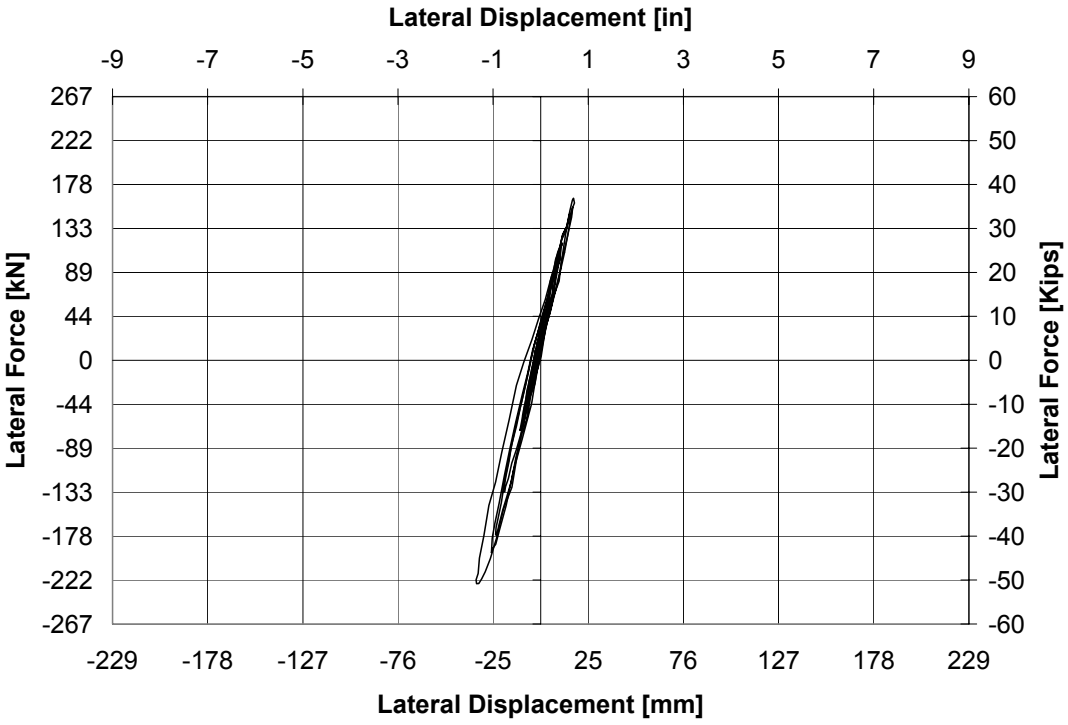

Figure 5-98 Force Displacement Hysteresis Curve for ISH1.25 at 1.25xSlymar

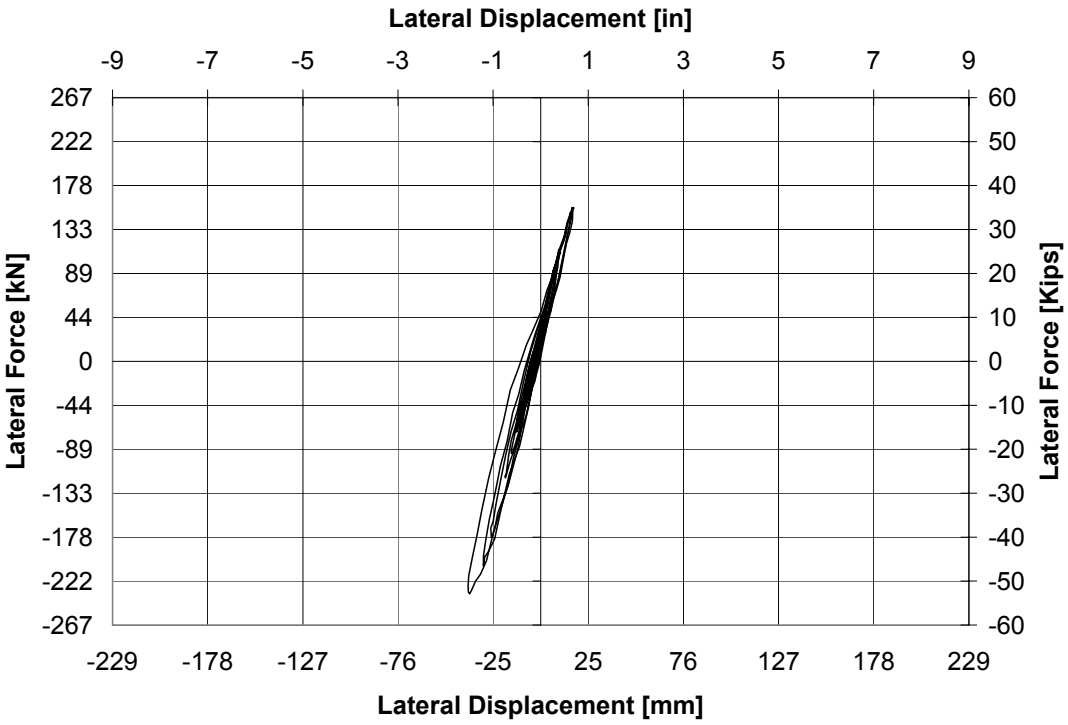

Figure 5-99 Force Displacement Hysteresis Curve for ISH1.25 at 1.5xSlymar

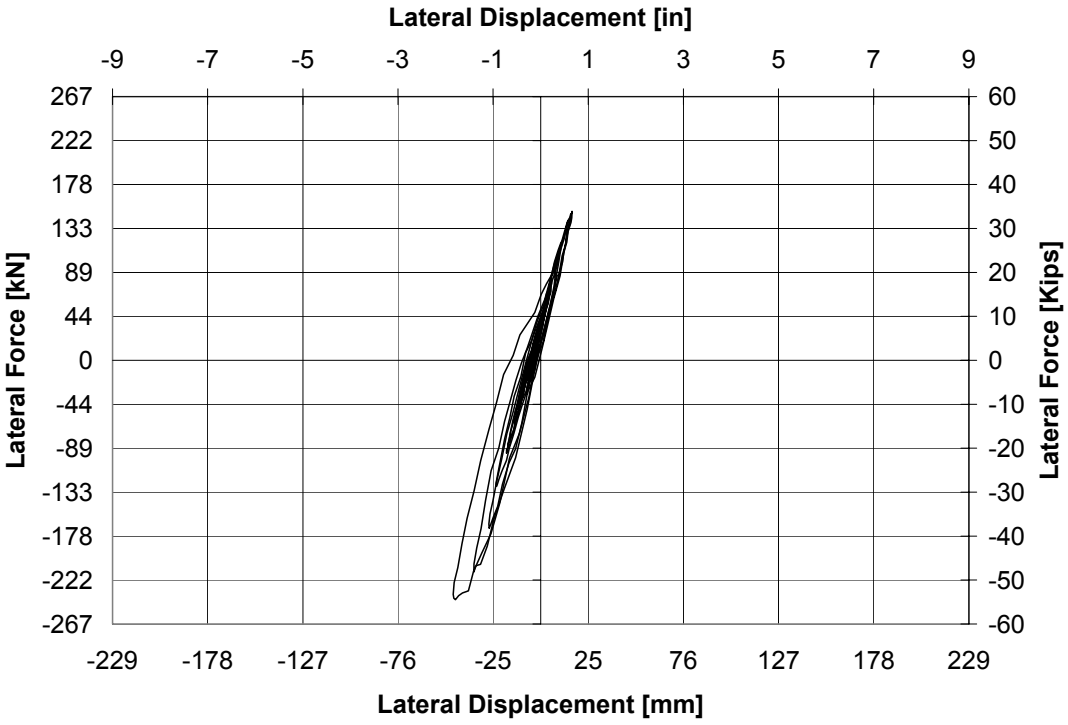

Figure 5-100 Force Displacement Hysteresis Curve for ISH1.25 at 1.75xSlymar

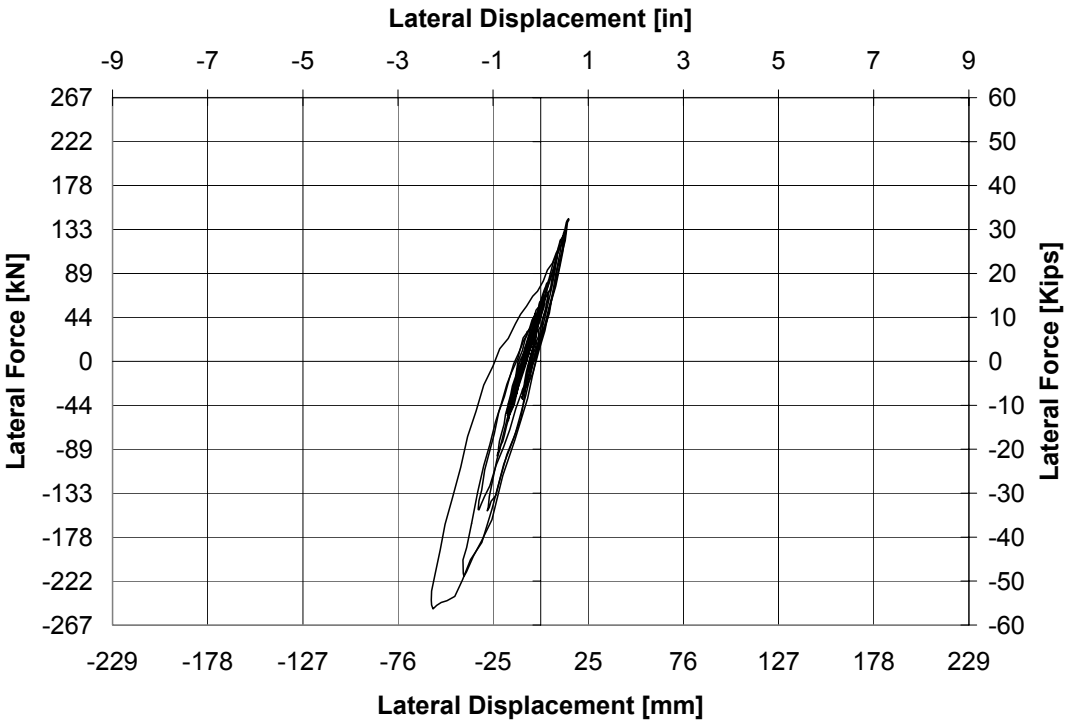

Figure 5-101 Force Displacement Hysteresis Curve for ISH1.25 at 2.0xSlymar

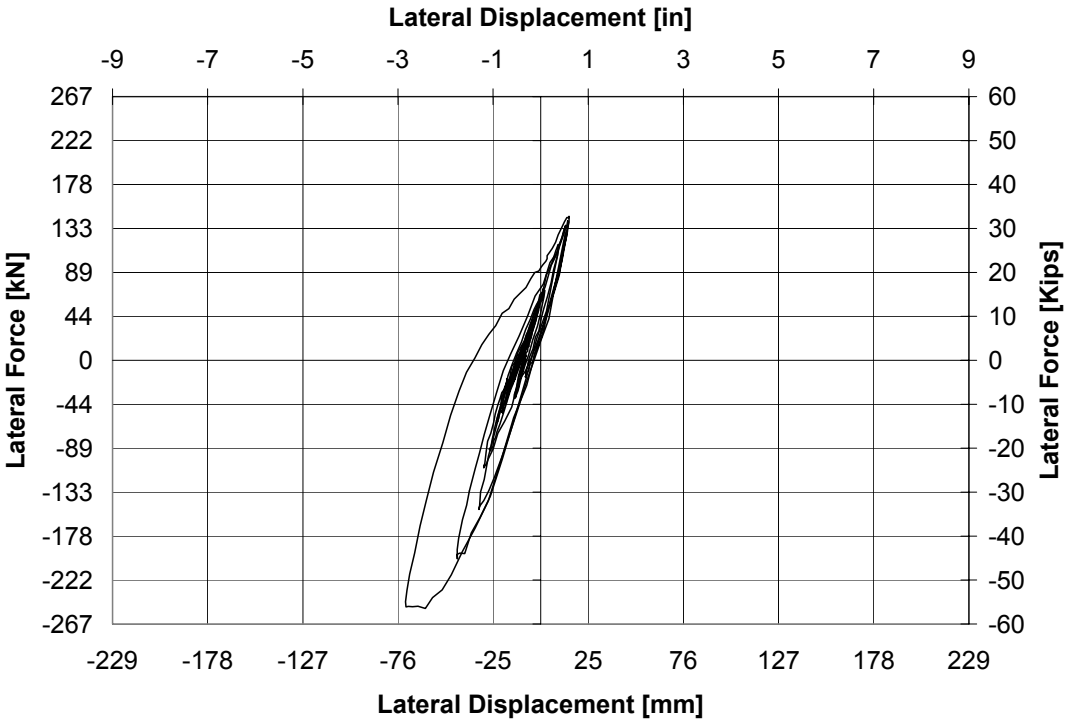

Figure 5-102 Force Displacement Hysteresis Curve for ISH1.25 at 2.125xSlymar

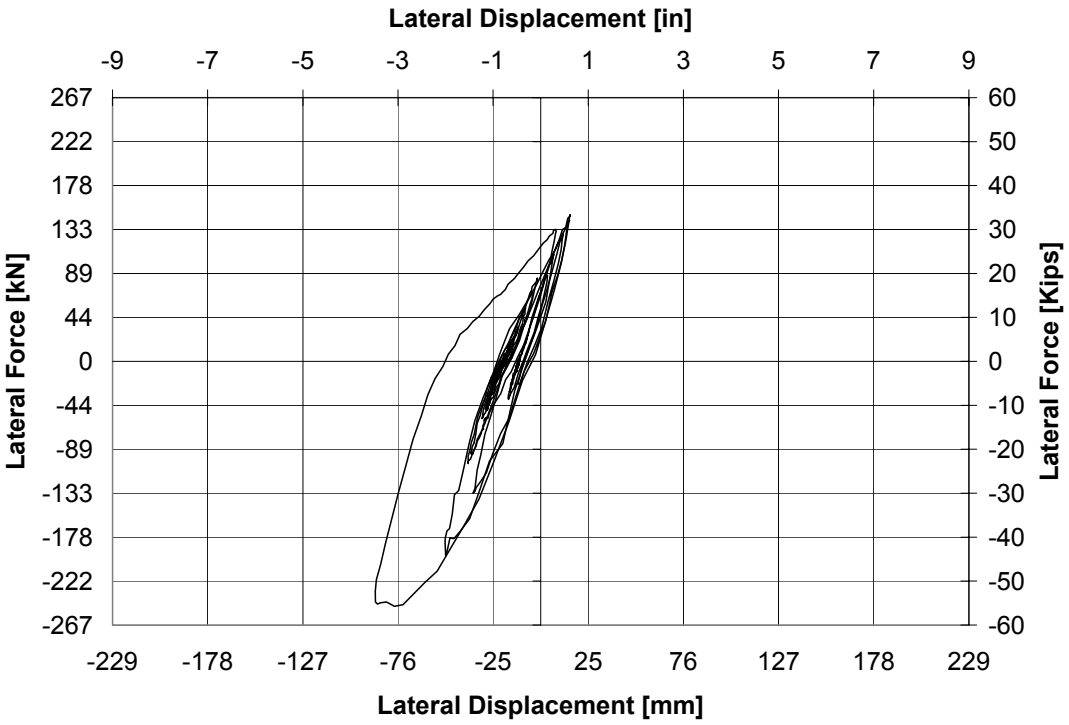

Figure 5-103 Force Displacement Hysteresis Curve for ISH1.25 at 2.25xSlymar

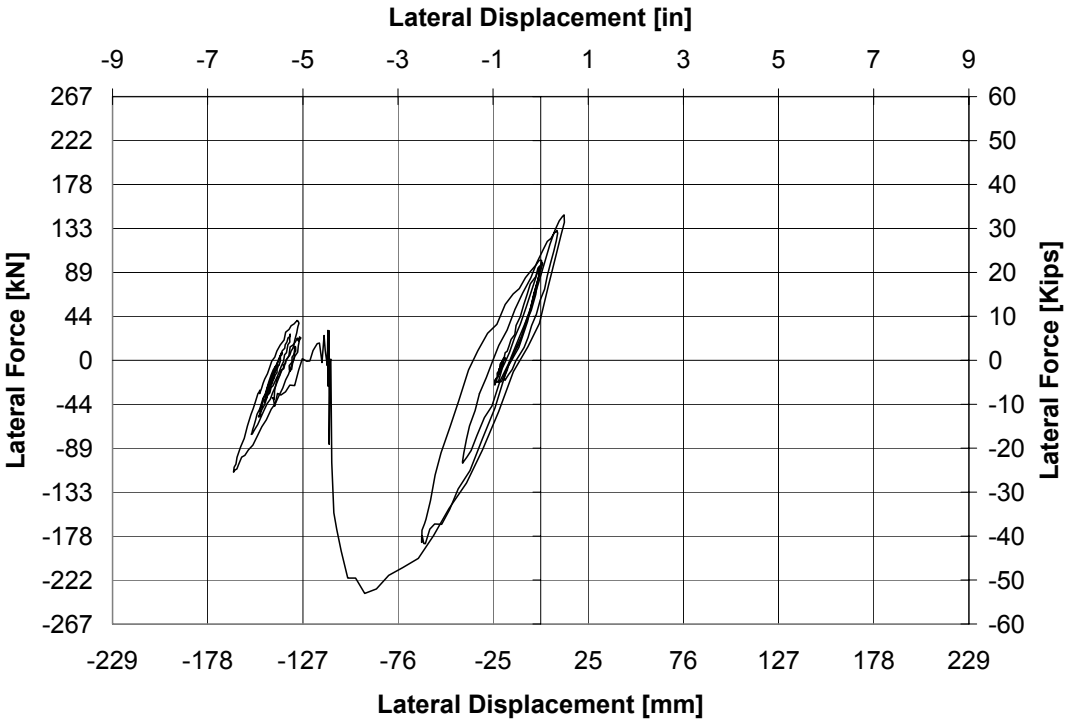

Figure 5-104 Force Displacement Hysteresis Curve for ISH1.25 at 2.375xSlymar

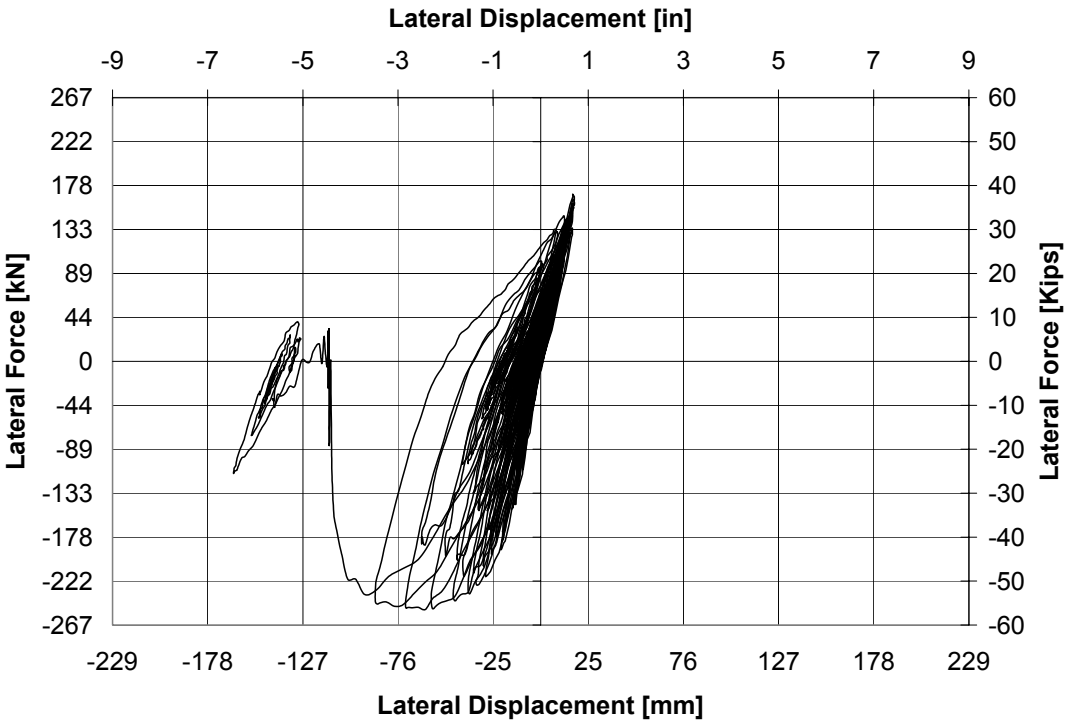

Figure 5-105 Accumulated Force Displacement Hysteresis Curve for ISH1.25

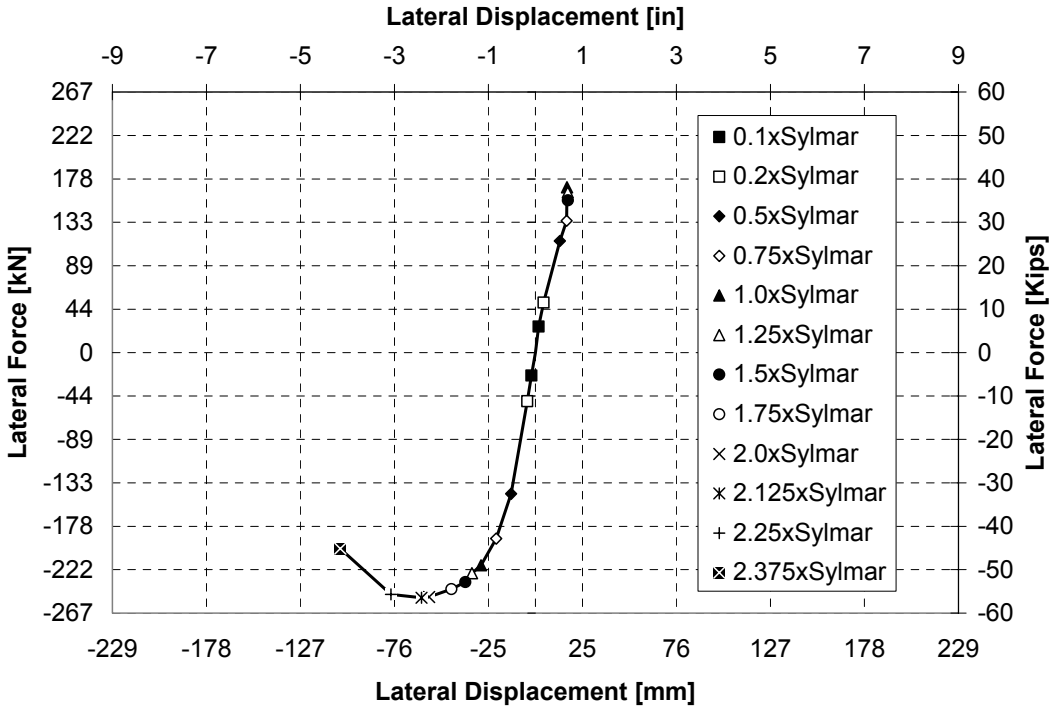

Figure 5-106 Envelope of Accumulated Force Displacement Hysteresis Curve for ISH1.25

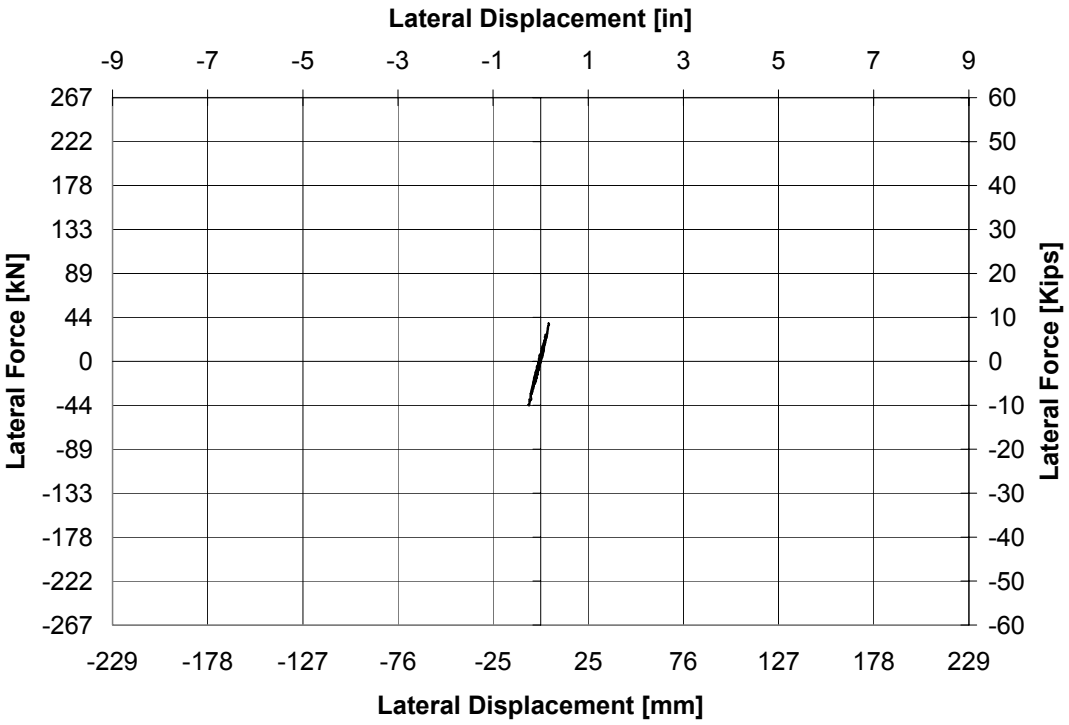

Figure 5-107 Force Displacement Hysteresis Curve for ISH1.5 at 0.1xSlymar

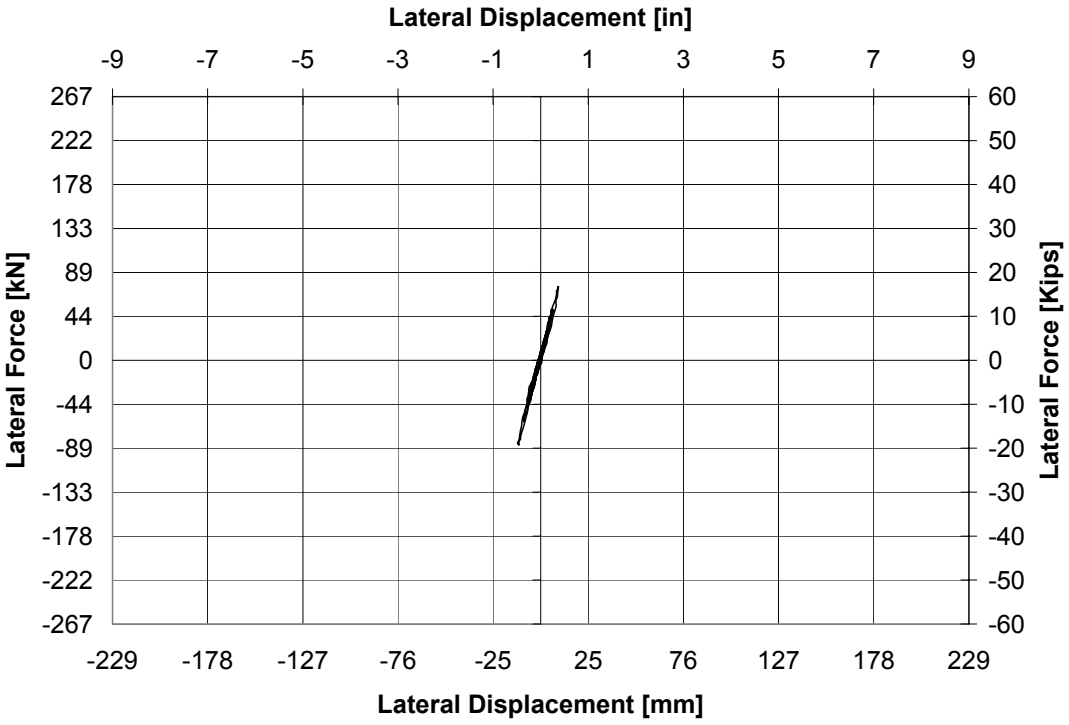

Figure 5-108 Force Displacement Hysteresis Curve for ISH1.5 at 0.2xSlymar

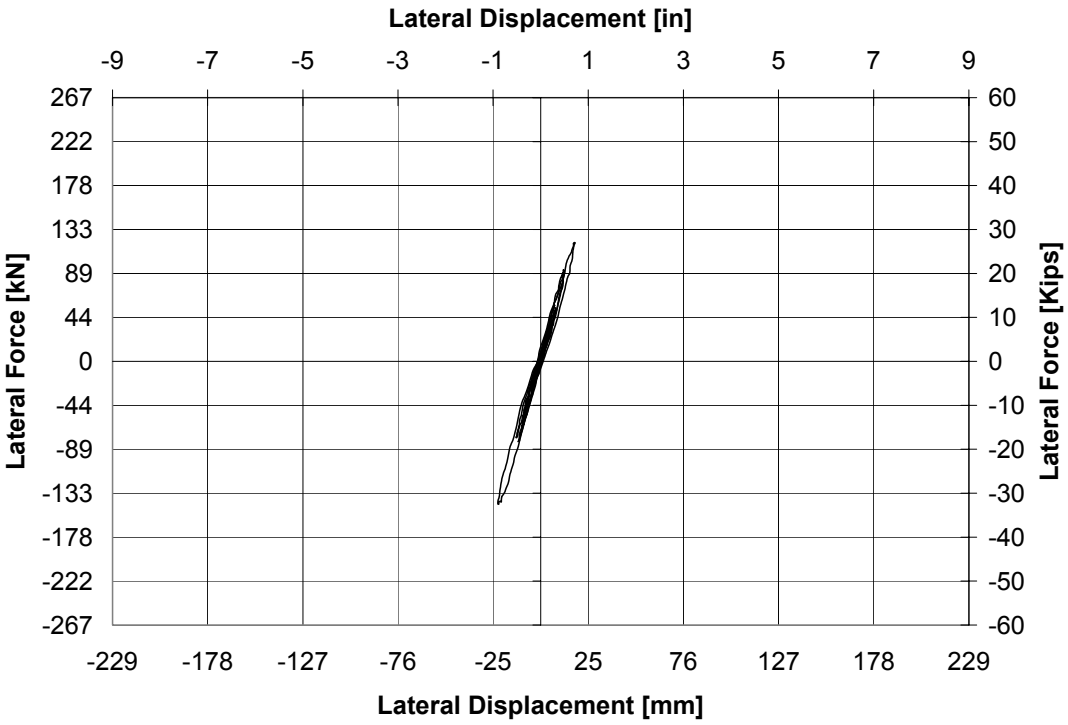

Figure 5-109 Force Displacement Hysteresis Curve for ISH1.5 at 0.4xSlymar

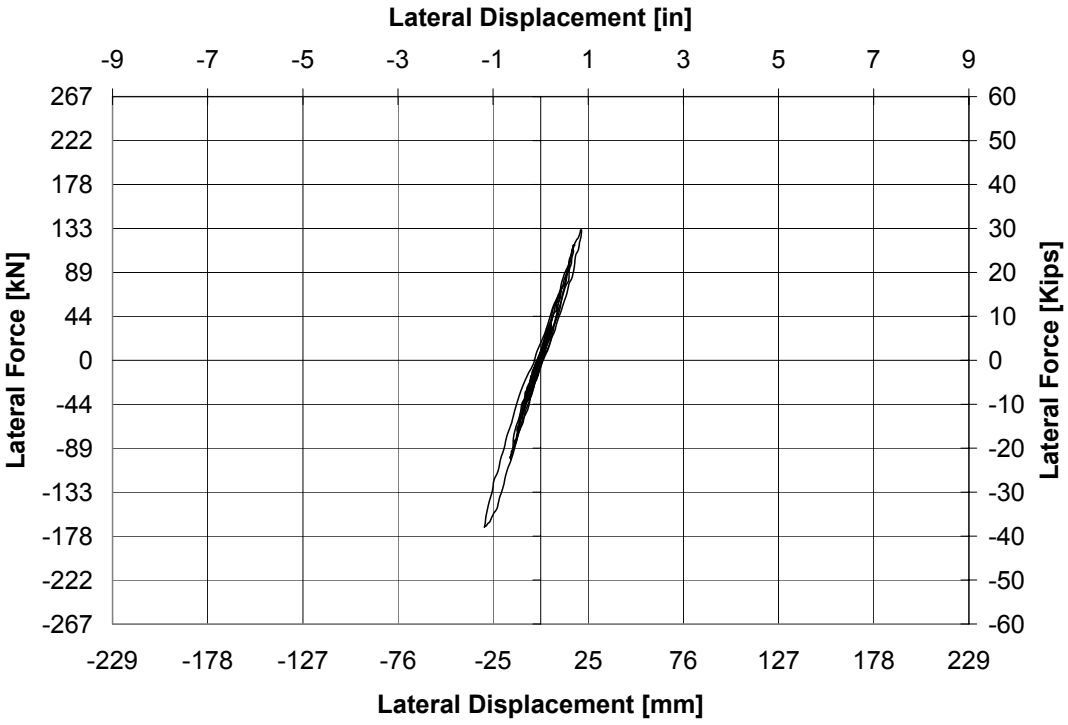

Figure 5-110 Force Displacement Hysteresis Curve for ISH1.5 at 0.6xSlymar

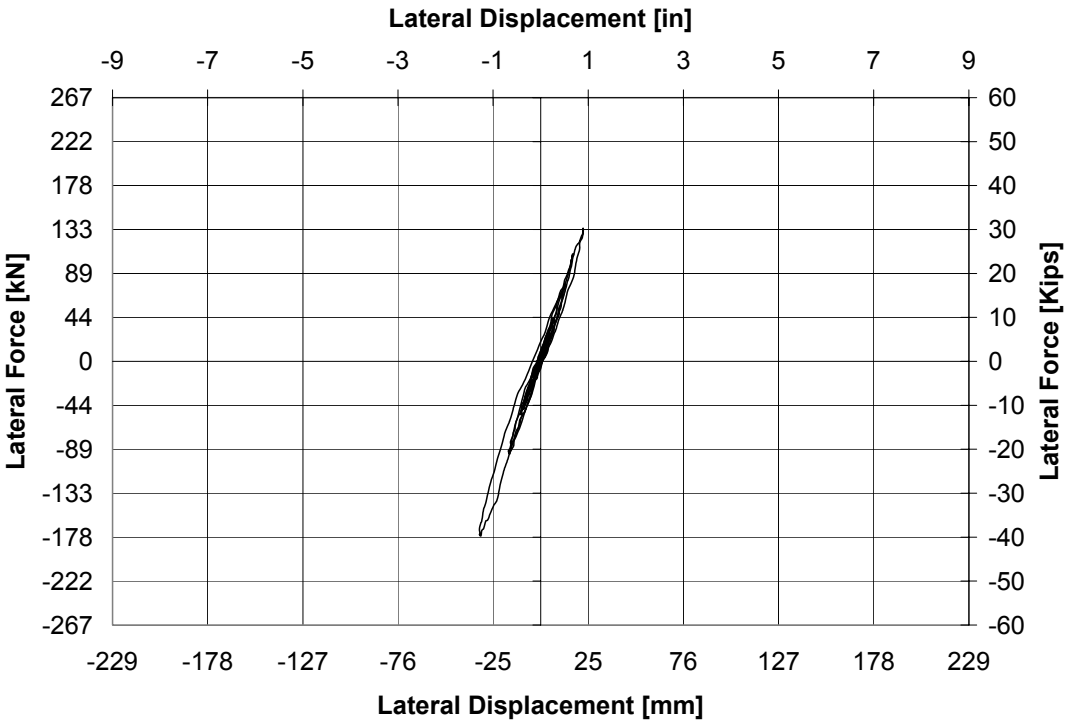

Figure 5-111 Force Displacement Hysteresis Curve for ISH1.5 at 0.75xSlymar

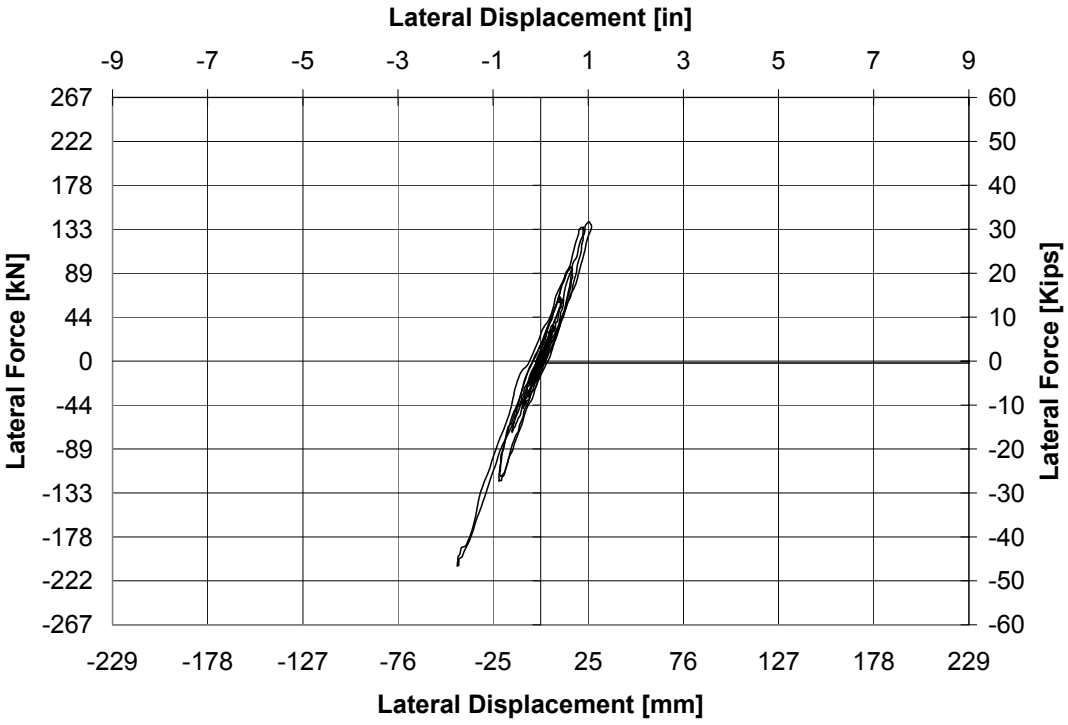

Figure 5-112 Force Displacement Hysteresis Curve for ISH1.5 at 1.0xSlymar

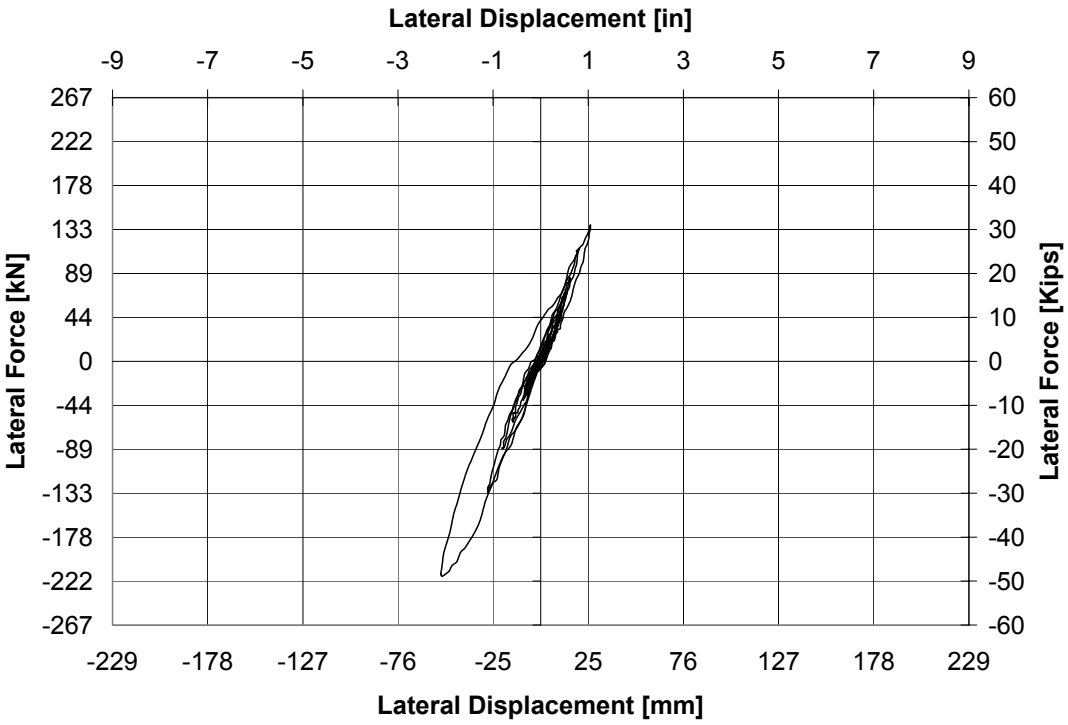

Figure 5-113 Force Displacement Hysteresis Curve for ISH1.5 at 1.25xSlymar

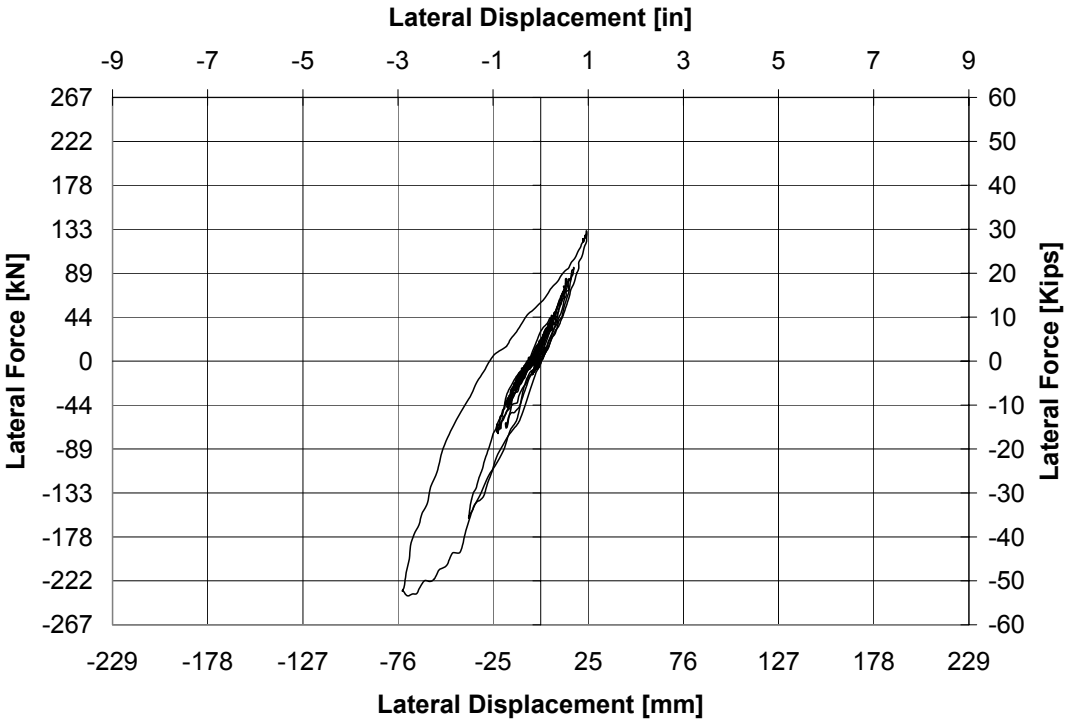

Figure 5-114 Force Displacement Hysteresis Curve for ISH1.5 at 1.5xSlymar

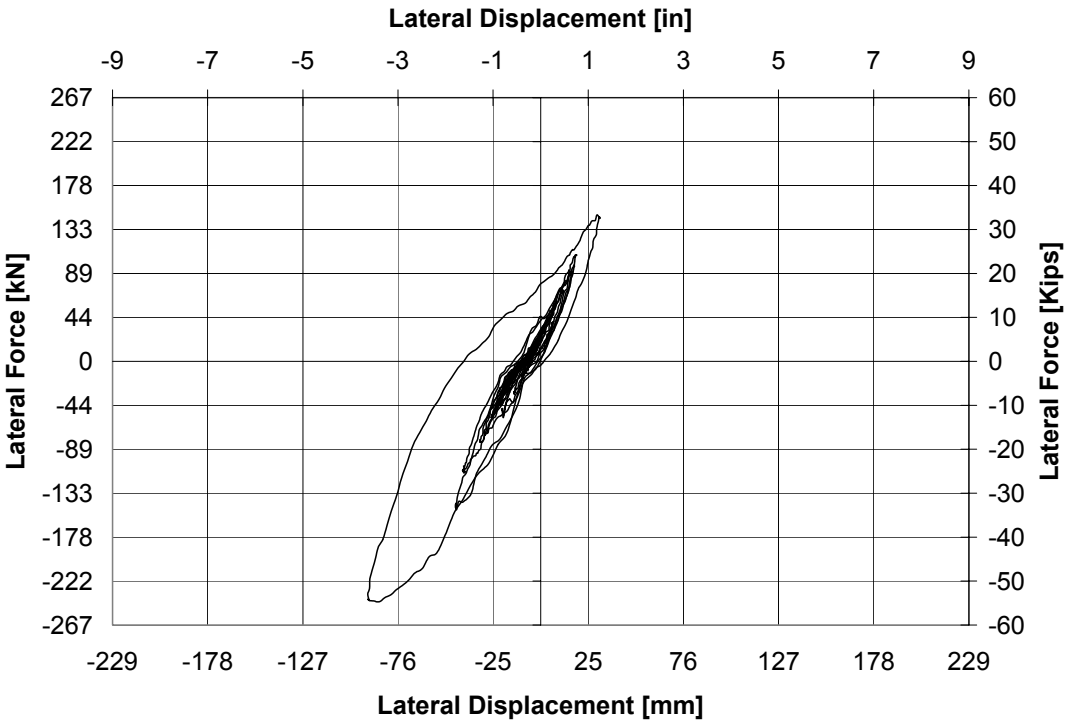

Figure 5-115 Force Displacement Hysteresis Curve for ISH1.5 at 1.75xSlymar

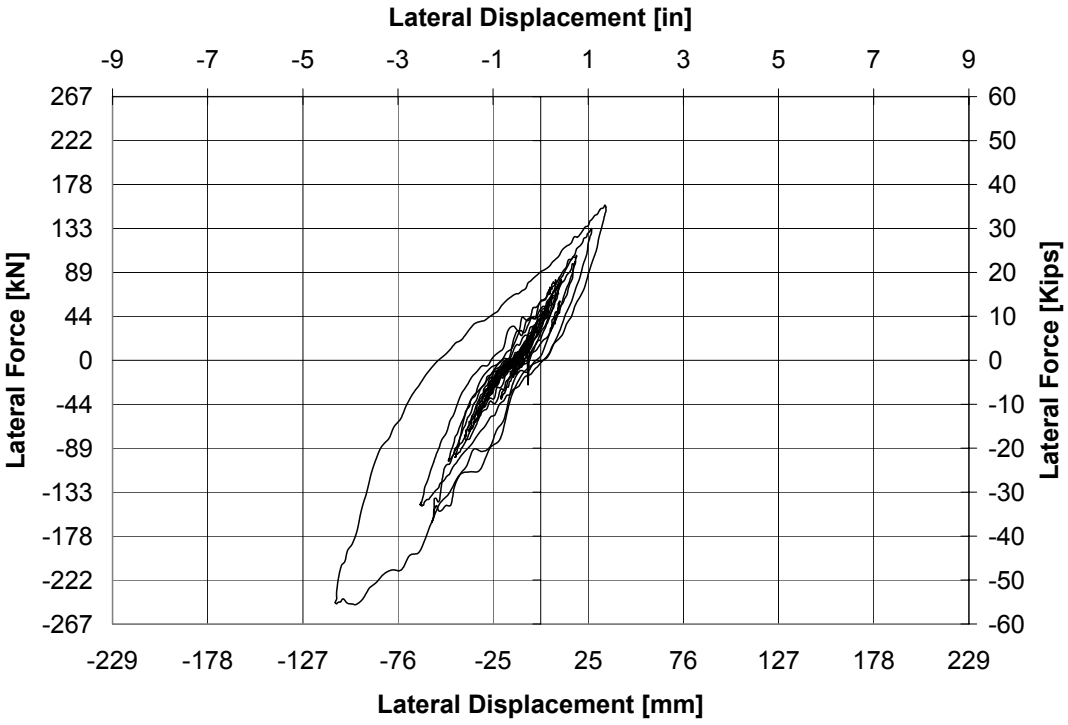

Figure 5-116 Force Displacement Hysteresis Curve for ISH1.5 at 2.0xSlymar

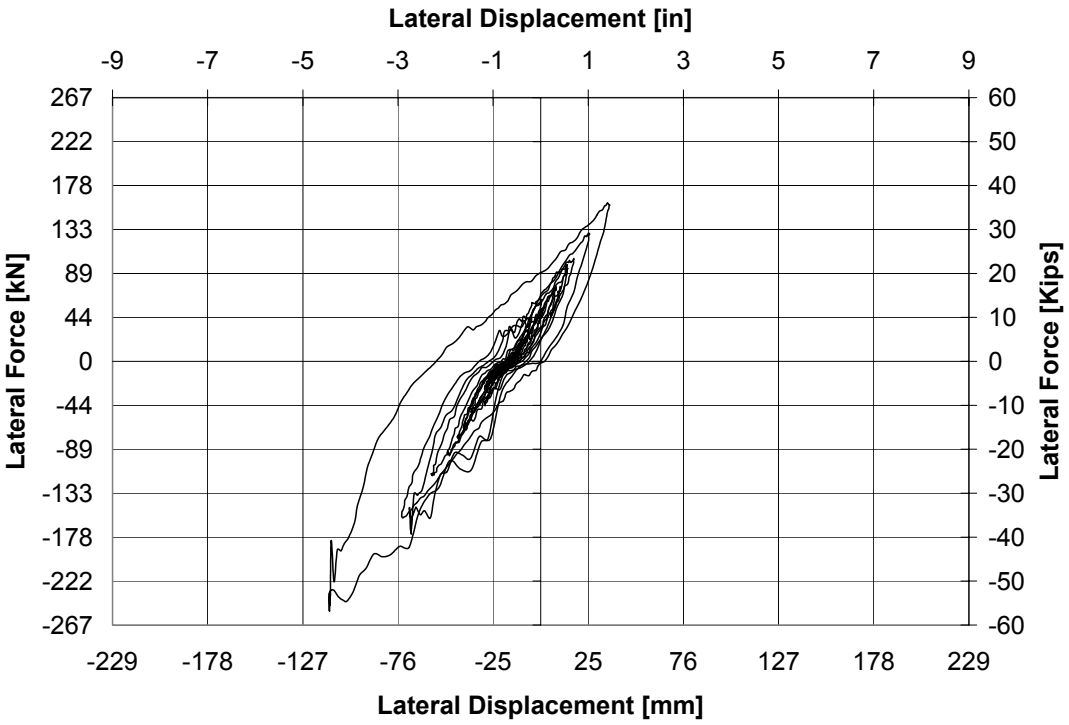

Figure 5-117 Force Displacement Hysteresis Curve for ISH1.5 at 2.125xSlymar

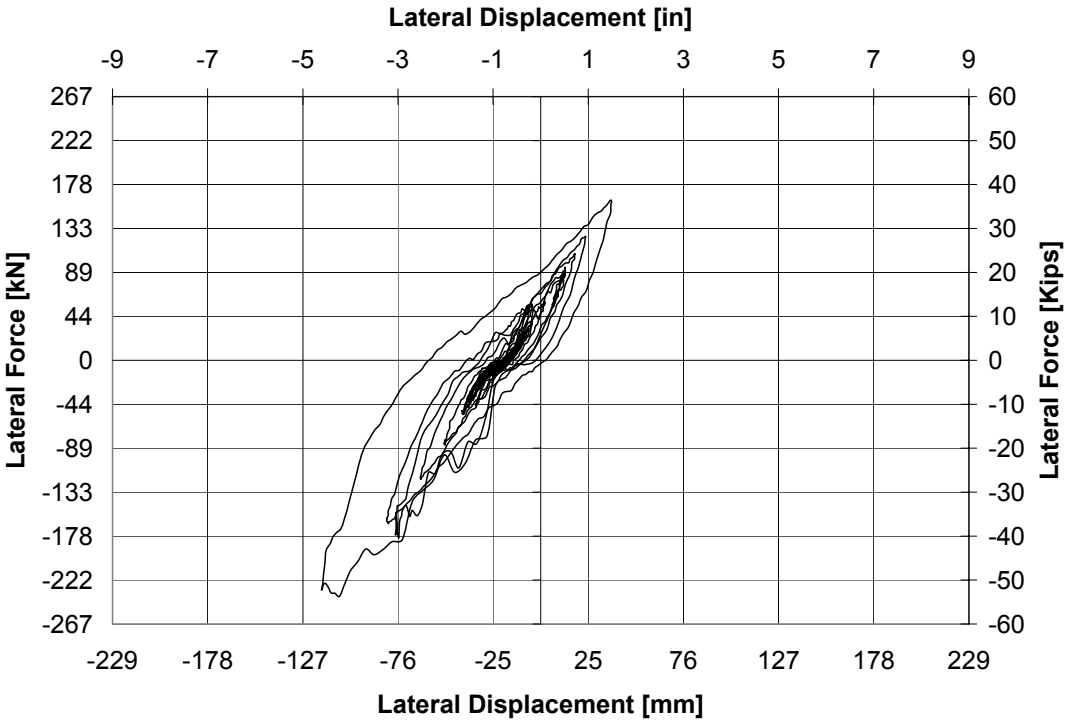

Figure 5-118 Force Displacement Hysteresis Curve for ISH1.5 at 2.25xSlymar

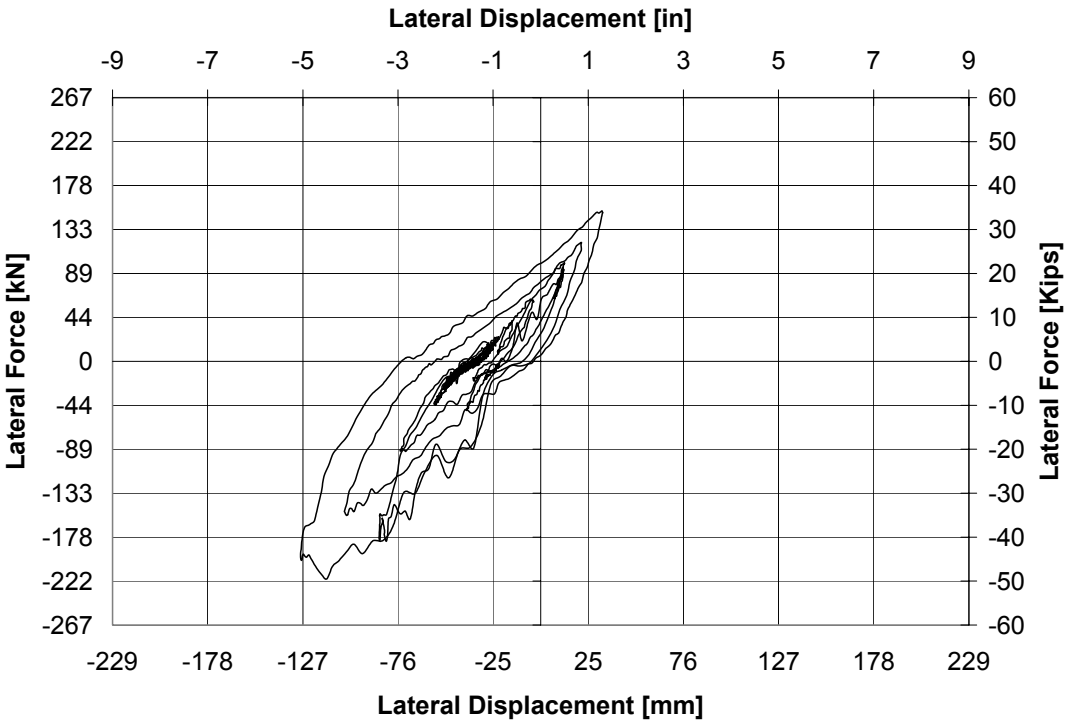

Figure 5-119 Force Displacement Hysteresis Curve for ISH1.5 at 2.375xSlymar

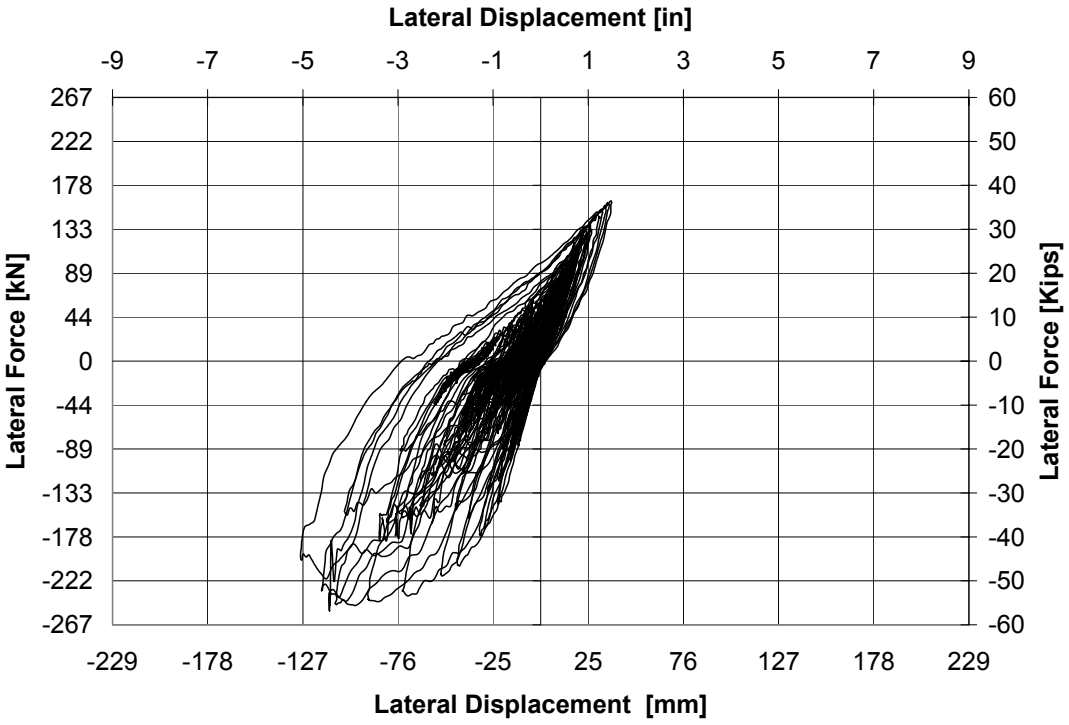

Figure 5-120 Accumulated Force Displacement Hysteresis Curve for ISH1.5

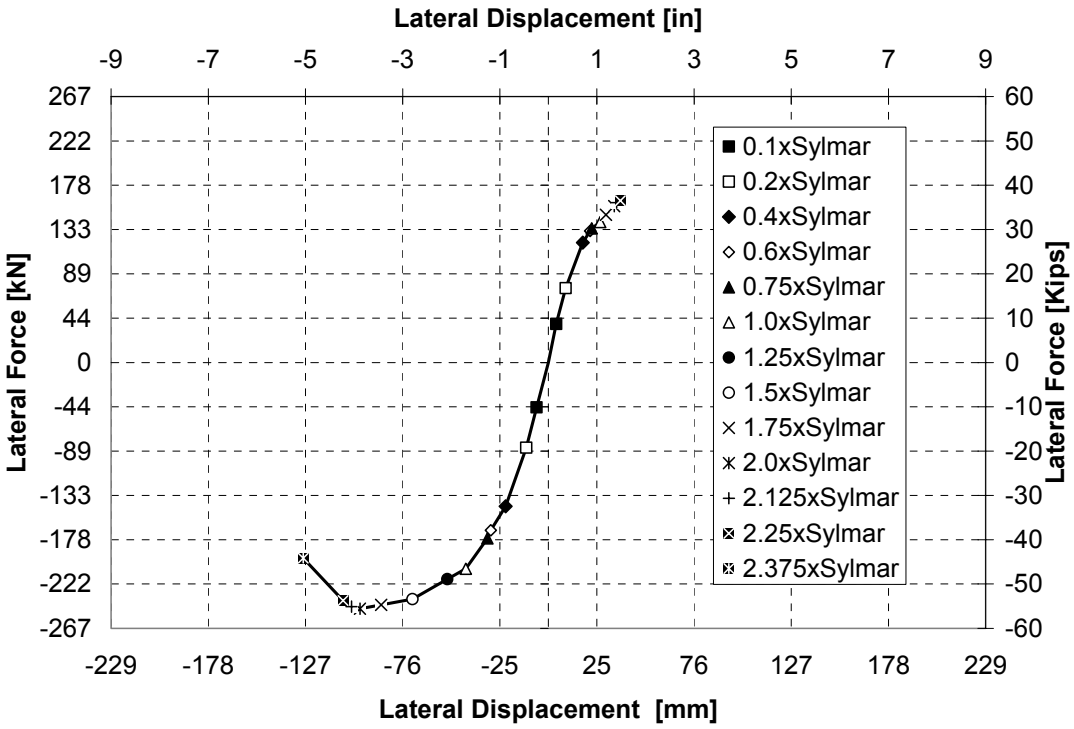

Figure 5-121 Envelope of Accumulated Force Displacement Hysteresis Curve for ISH1.5

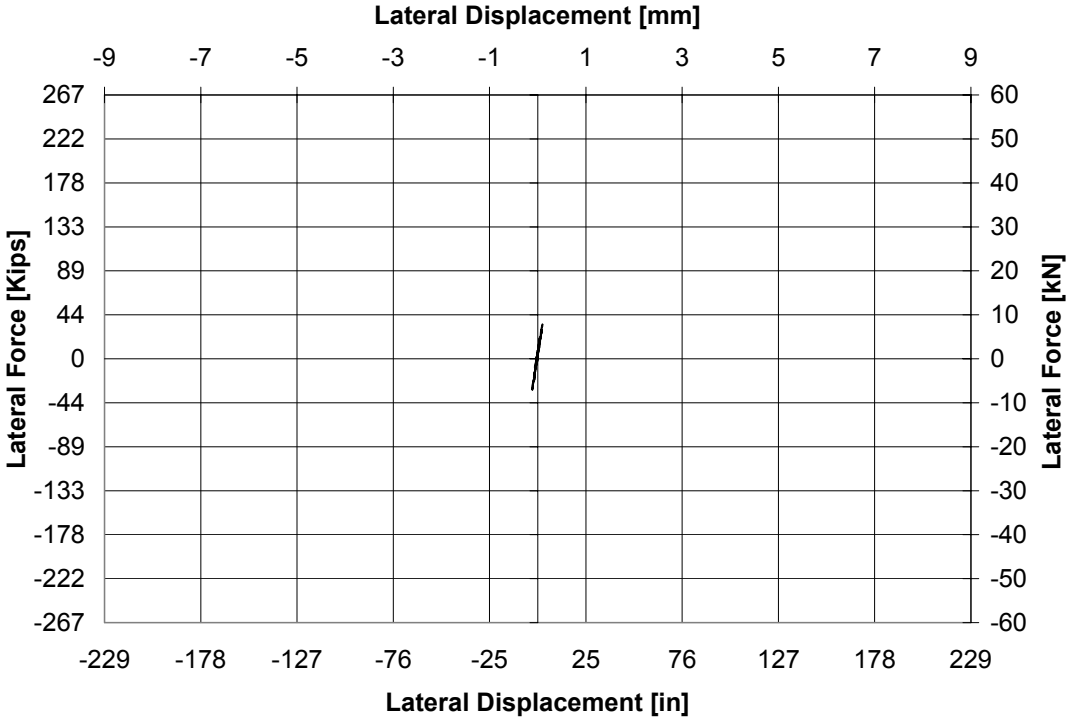

Figure 5-122 Force Displacement Hysteresis Curve for ISH1.5T at 0.1xSlymar

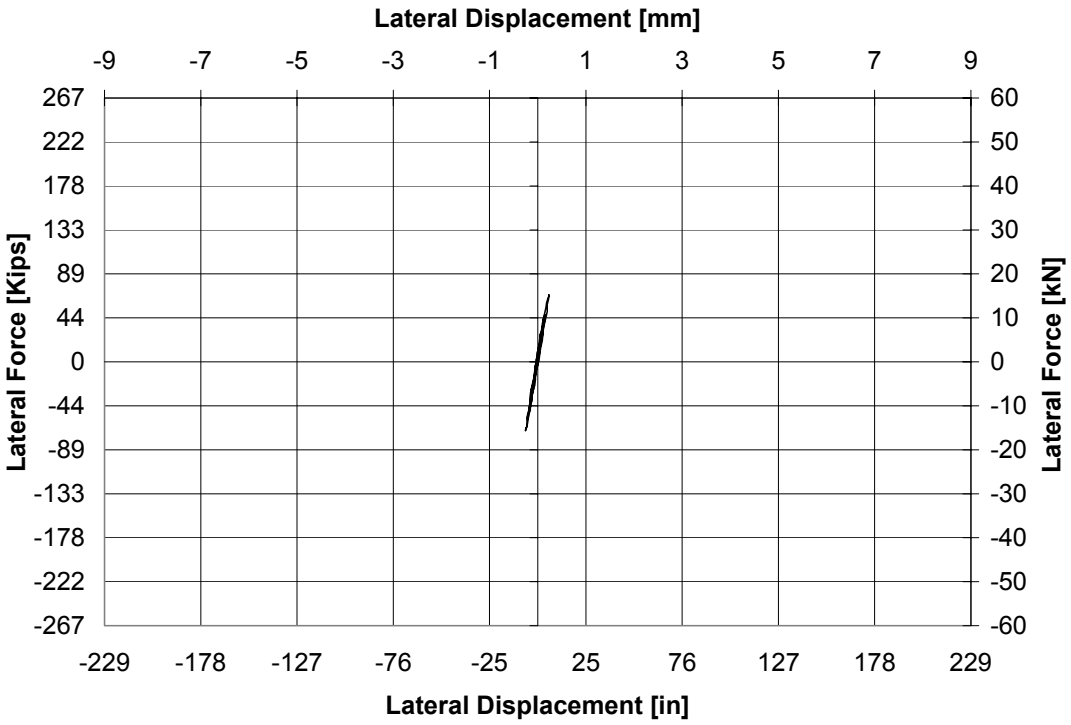

Figure 5-123 Force Displacement Hysteresis Curve for ISH1.5T at 0.2xSlymar

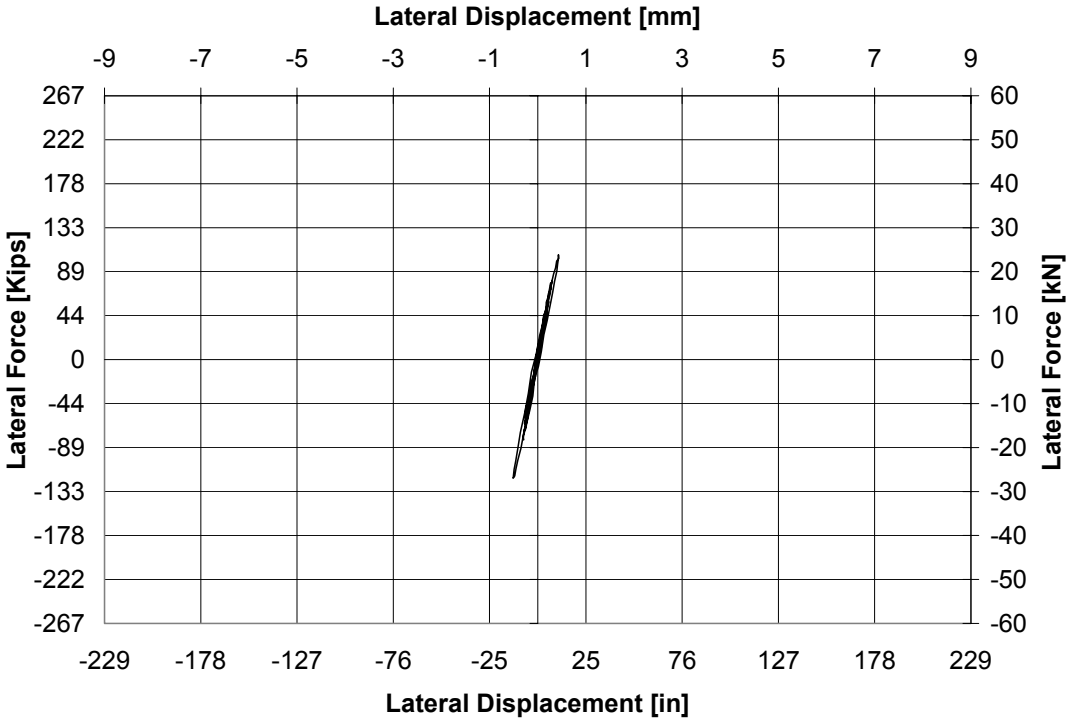

Figure 5-124 Force Displacement Hysteresis Curve for ISH1.5T at 0.4xSlymar

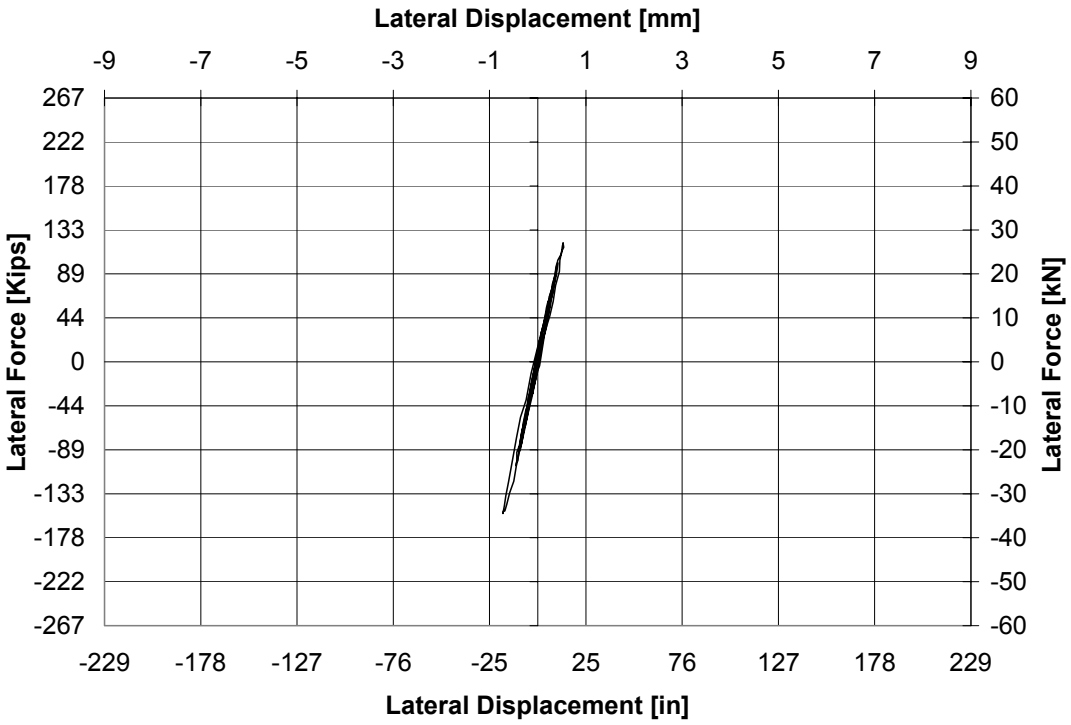

Figure 5-125 Force Displacement Hysteresis Curve for ISH1.5T at 0.6xSlymar

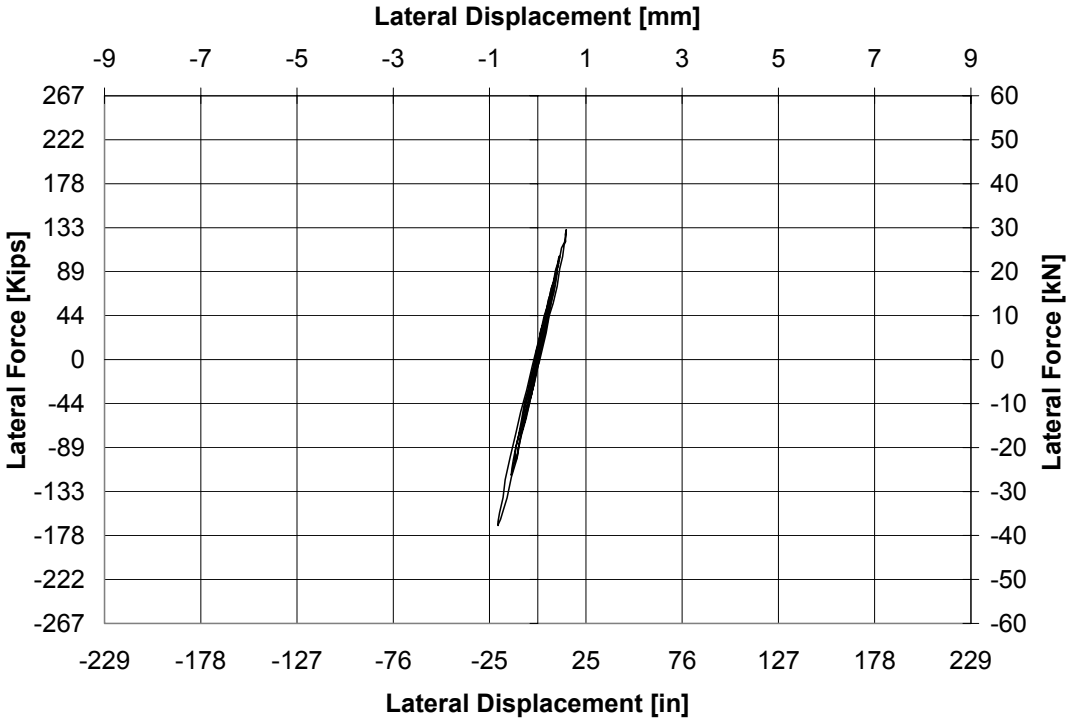

Figure 5-126 Force Displacement Hysteresis Curve for ISH1.5T at 0.75xSlymar

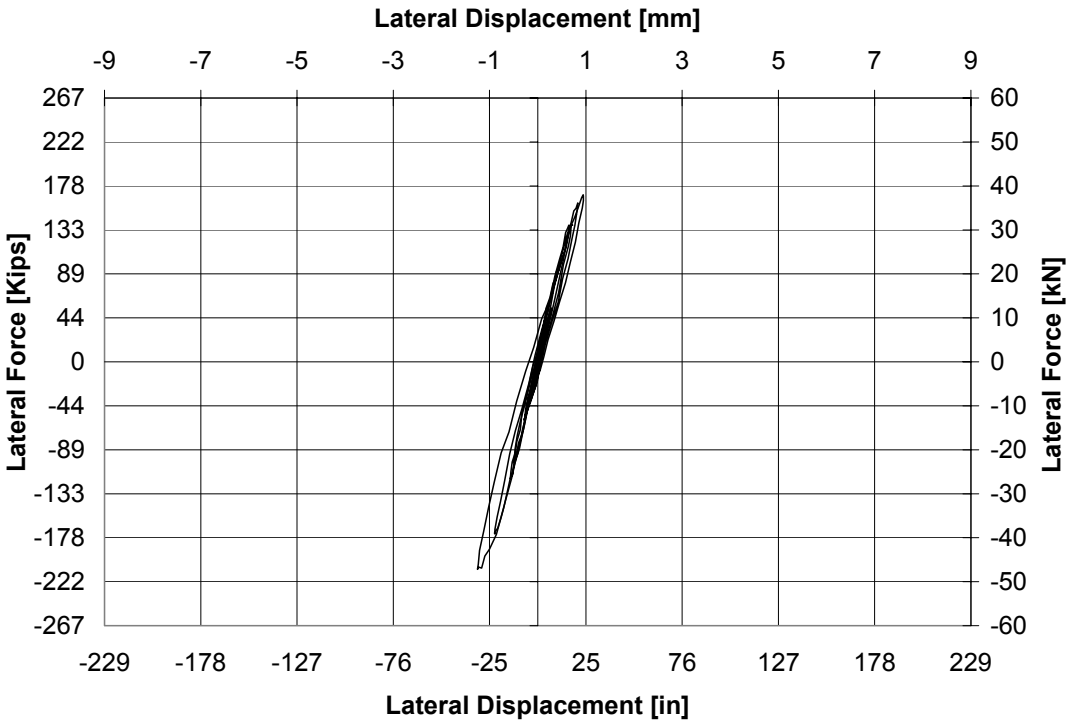

Figure 5-127 Force Displacement Hysteresis Curve for ISH1.5T at 1.0xSlymar

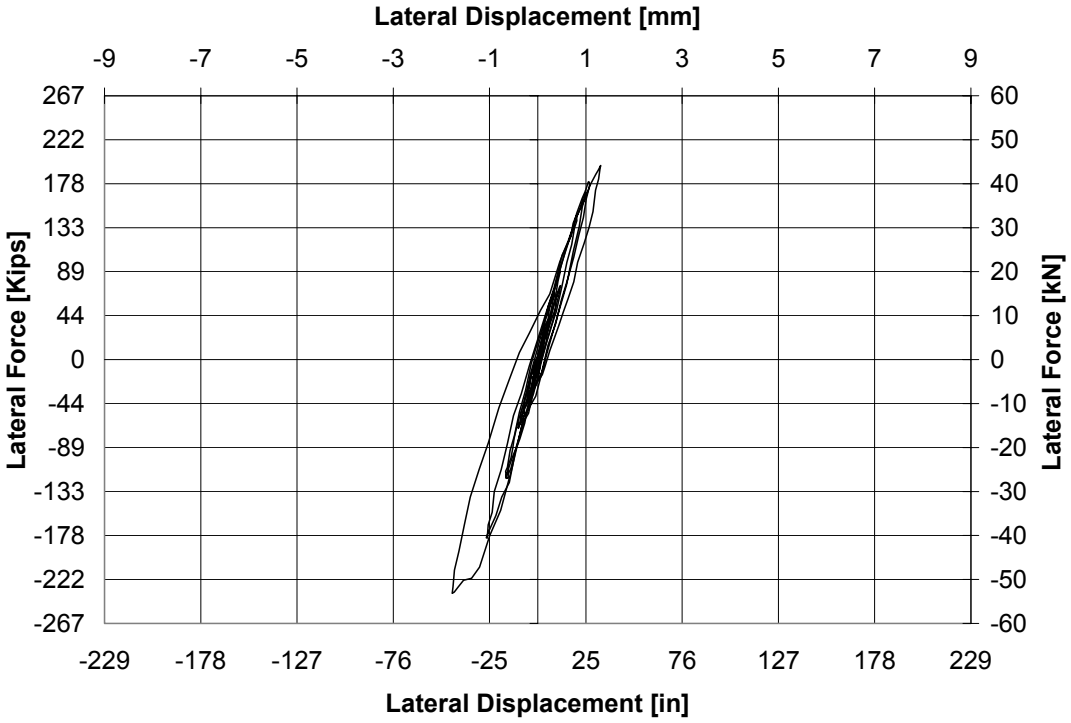

Figure 5-128 Force Displacement Hysteresis Curve for ISH1.5T at 1.25xSlymar

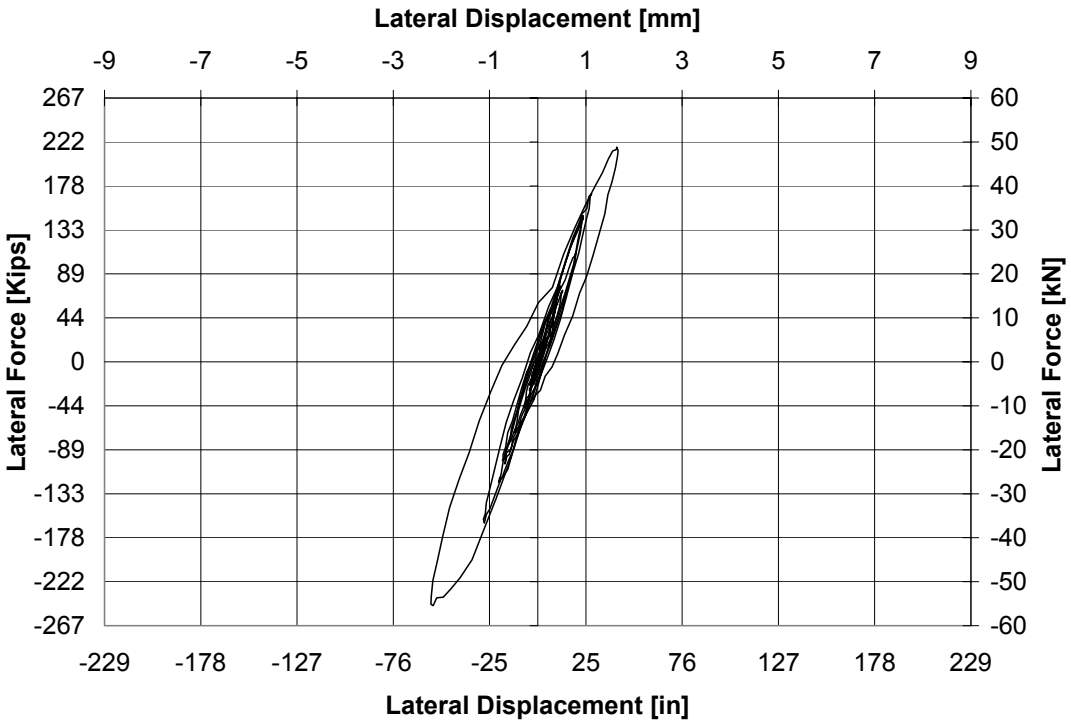

Figure 5-129 Force Displacement Hysteresis Curve for ISH1.5T at 1.5xSlymar

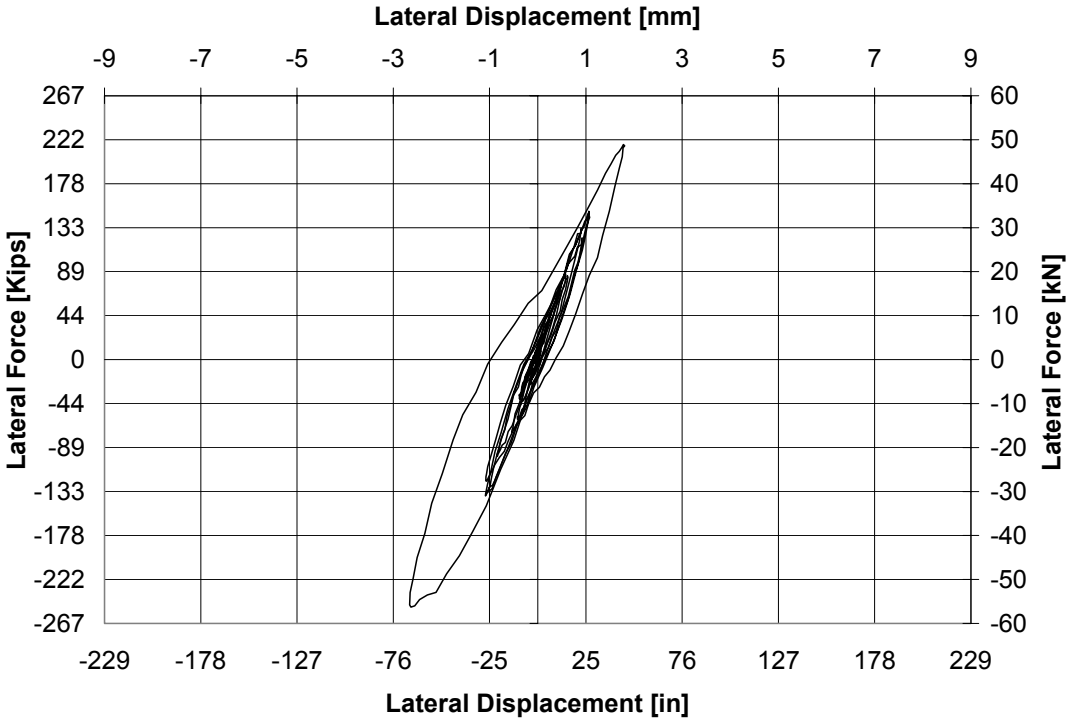

Figure 5-130 Force Displacement Hysteresis Curve for ISH1.5T at 1.75xSlymar

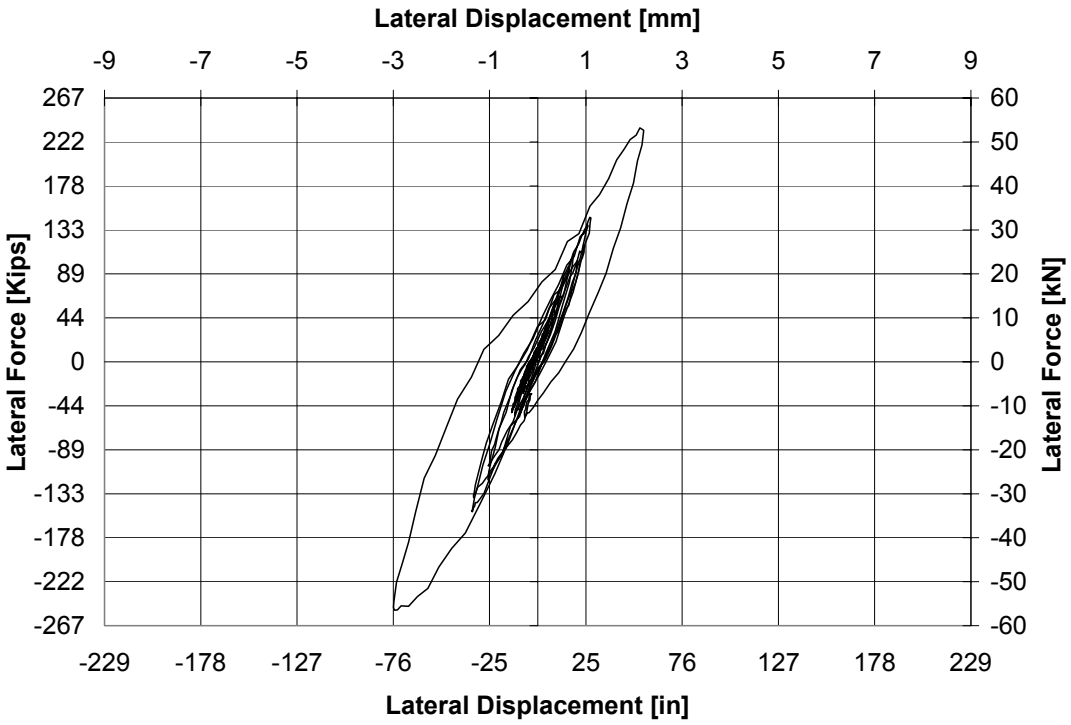

Figure 5-131 Force Displacement Hysteresis Curve for ISH1.5T at 2.0xSlymar

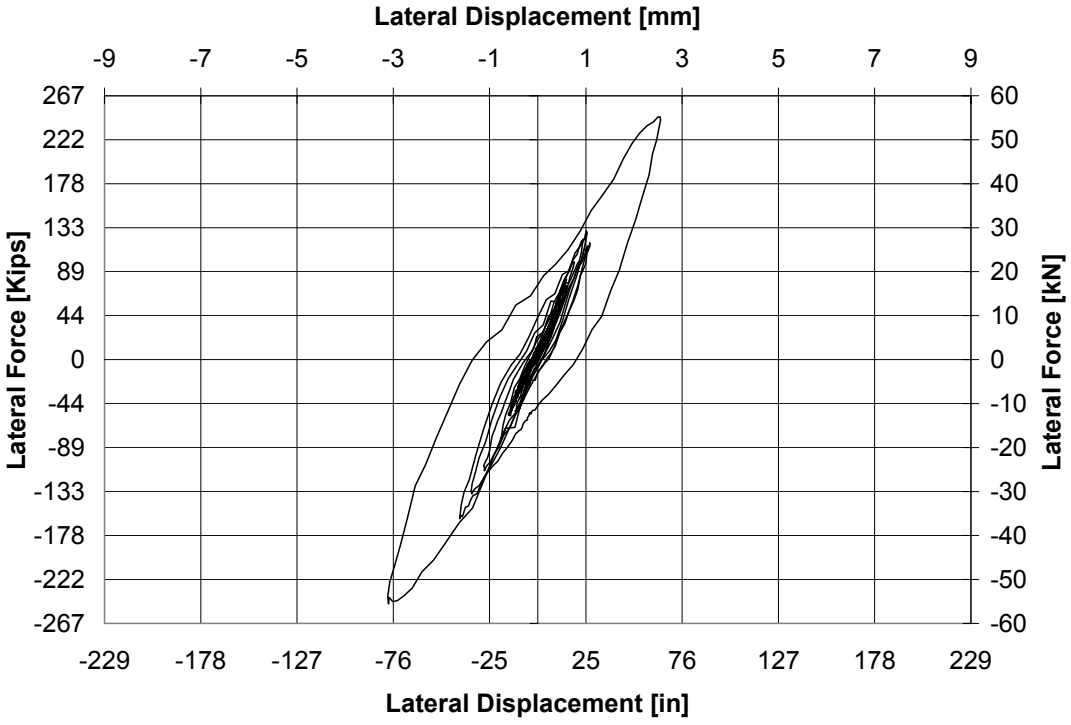

Figure 5-132 Force Displacement Hysteresis Curve for ISH1.5T at 2.125xSlymar

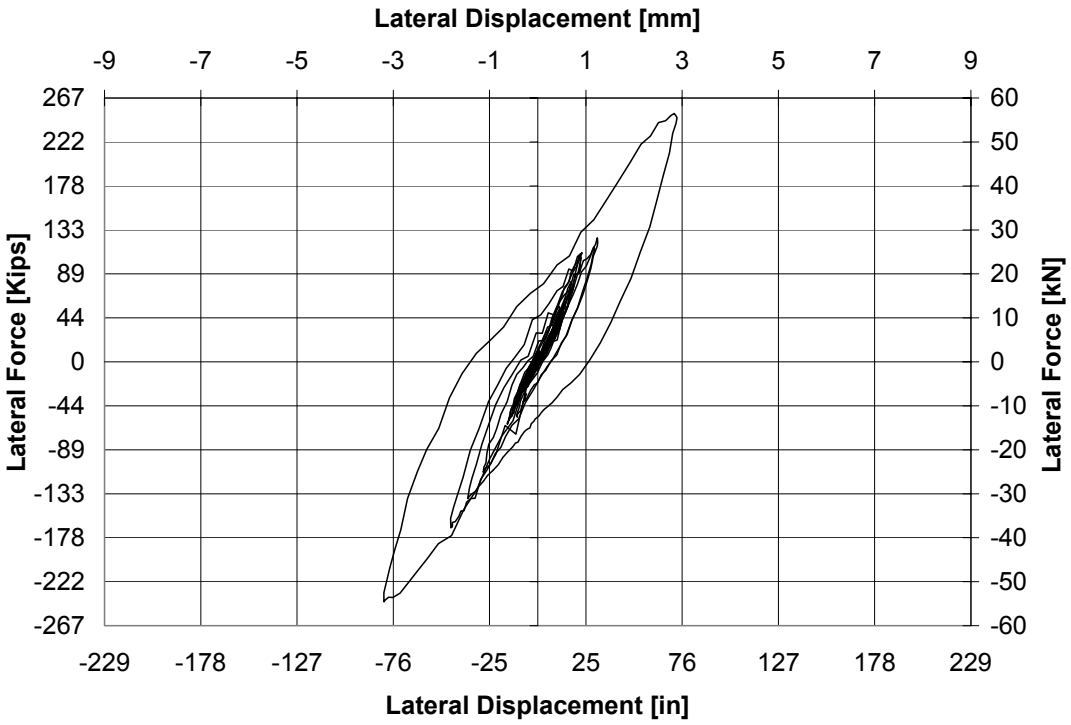

Figure 5-133 Force Displacement Hysteresis Curve for ISH1.5T at 2.25xSlymar

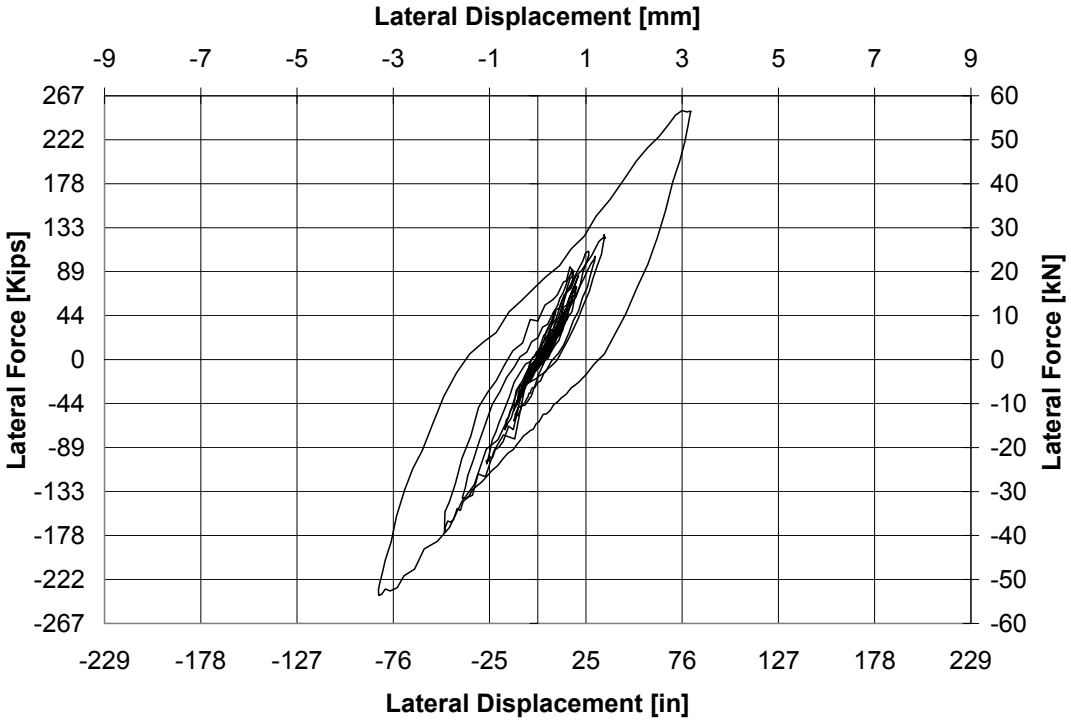

Figure 5-134 Force Displacement Hysteresis Curve for ISH1.5T at 2.375xSlymar

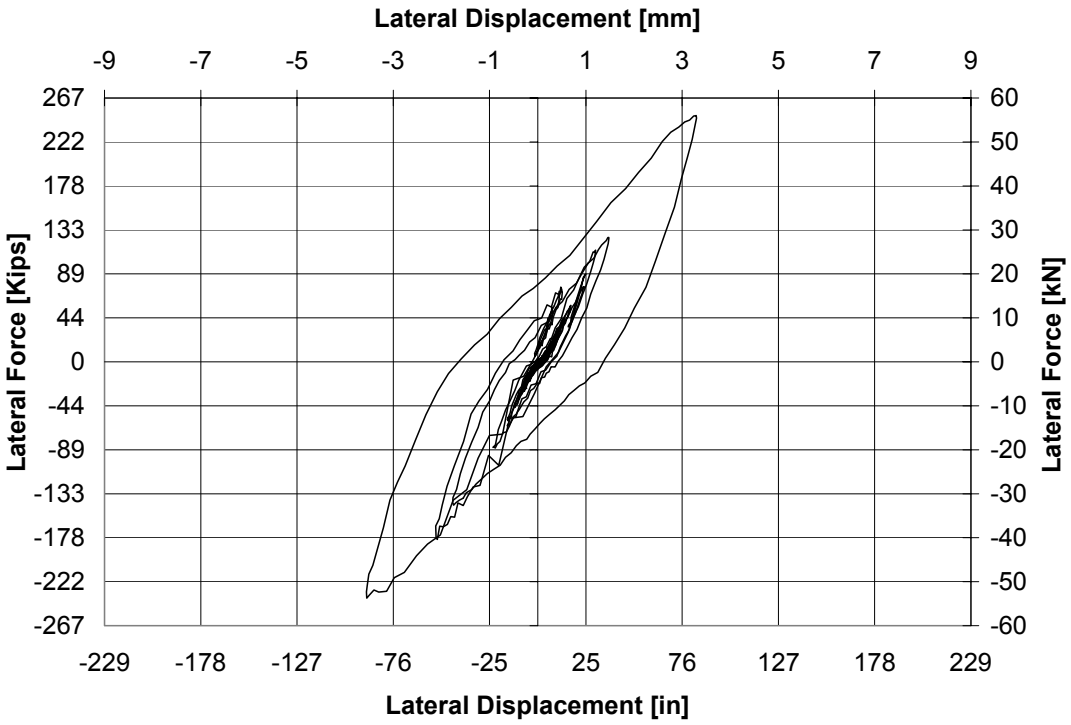

Figure 5-135 Force Displacement Hysteresis Curve for ISH1.5T at 2.5xSlymar

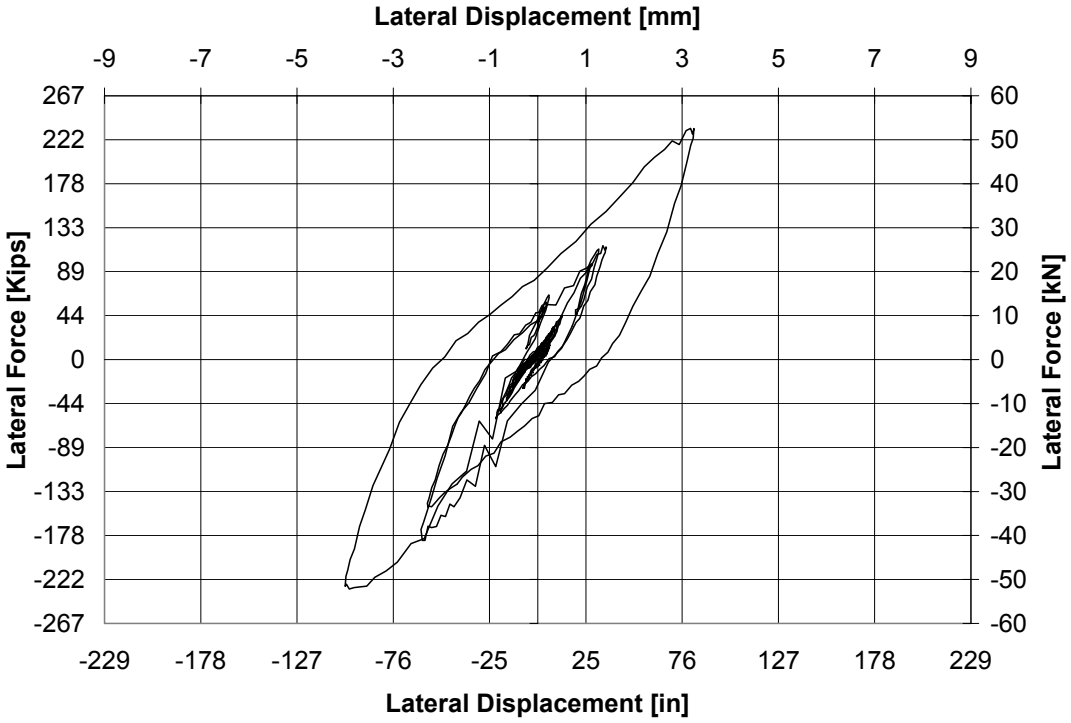

Figure 5-136 Force Displacement Hysteresis Curve for ISH1.5T at 2.625xSlymar

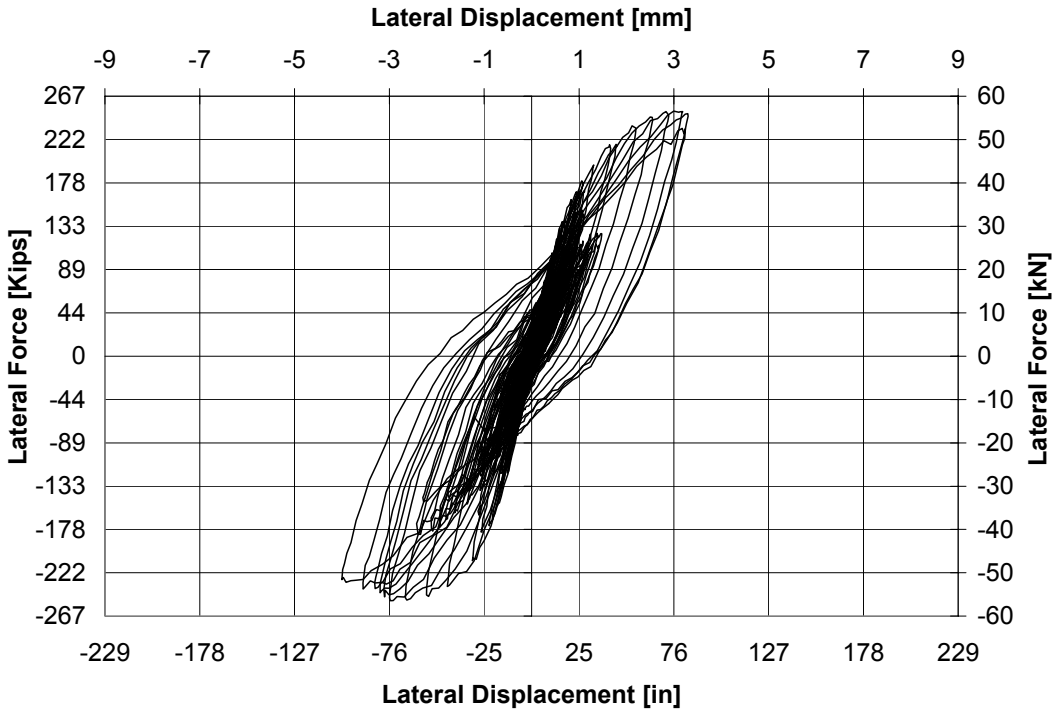

Figure 5-137 Accumulated Force Displacement Hysteresis Curve for ISH1.5T

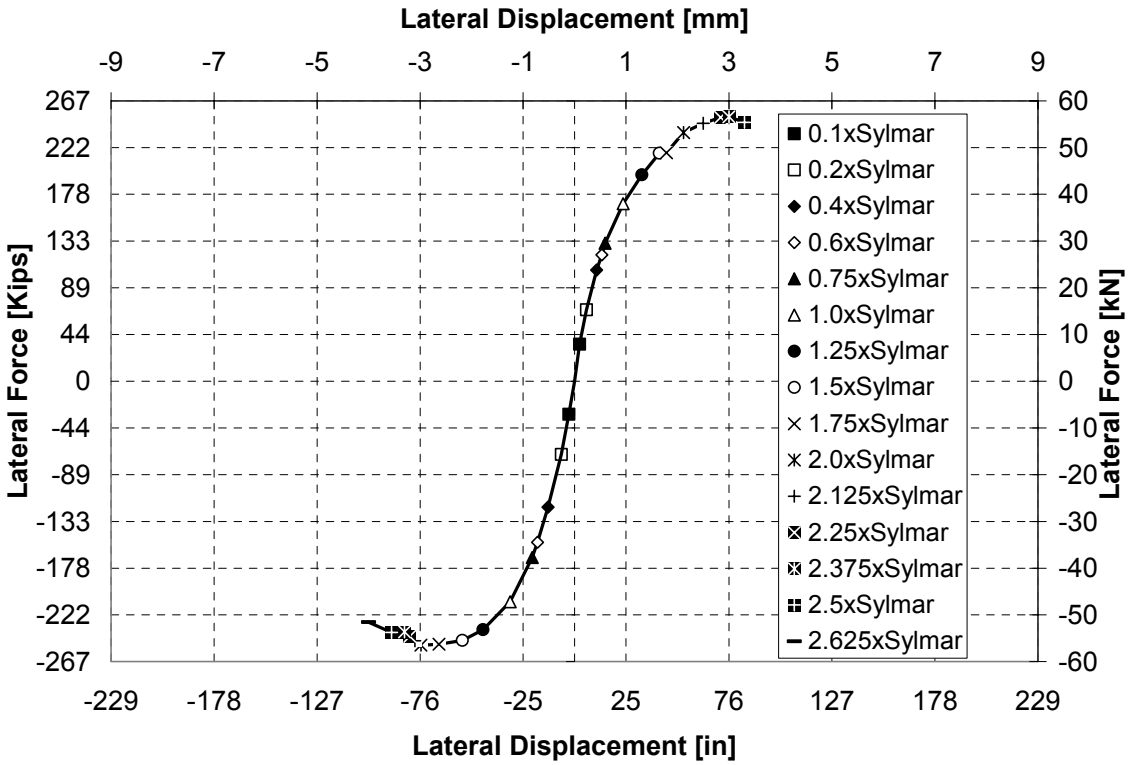

Figure 5-138 Envelope of Accumulated Force Displacement Hysteresis Curve for ISH1.5T

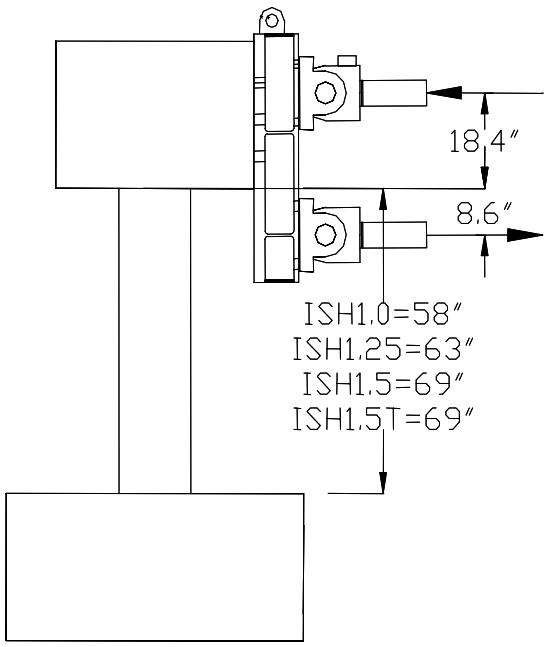

Figure 5-139 Link Forces and Moment Arms to Calculate Moment Demand at the Top and Bottom of the Column

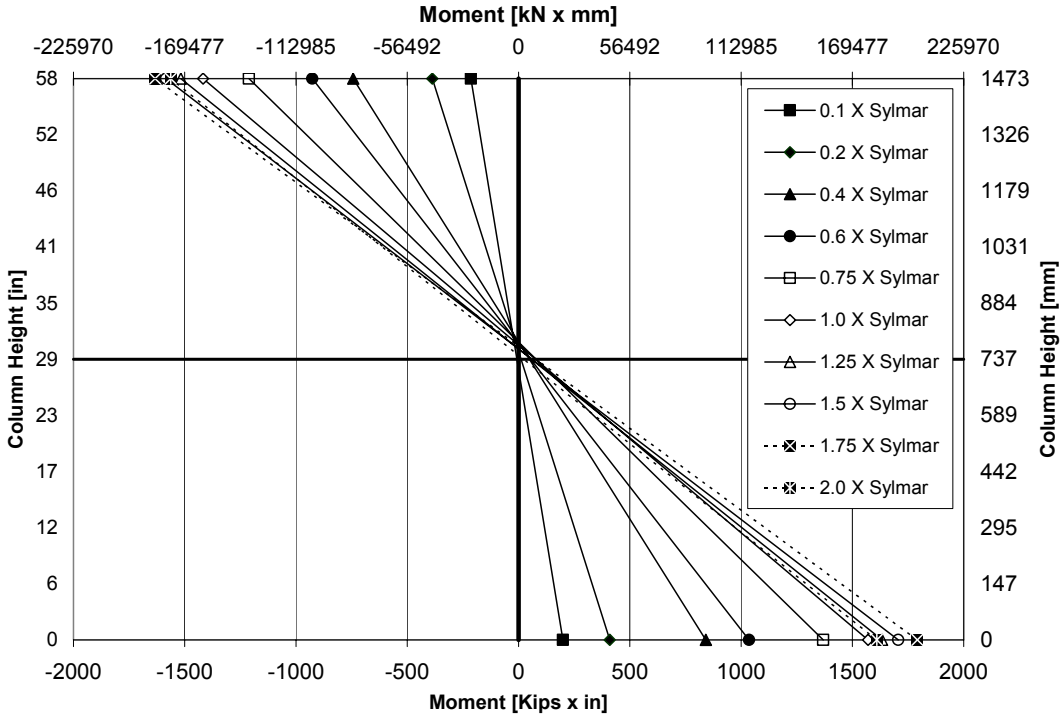

Figure 5-140 Moment Demand Top and Bottom of the Column for the Predominant Direction of Motion Specimen ISH1.0

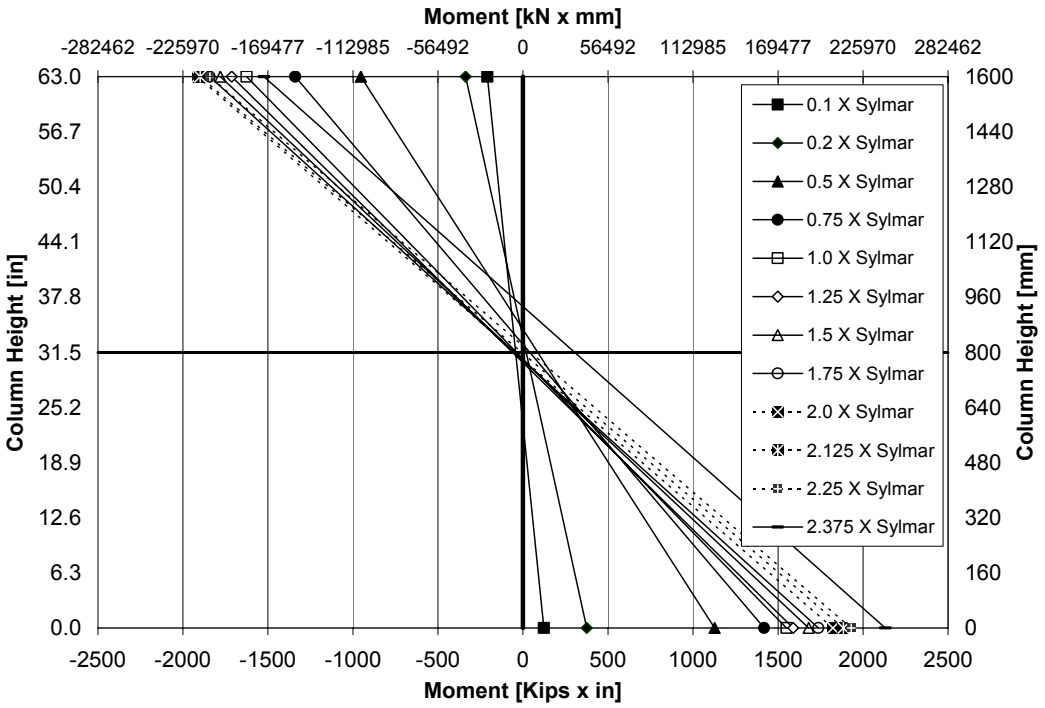

Figure 5-141 Moment Demand Top and Bottom of the Column for the Predominant Direction of Motion Specimen ISH1.25

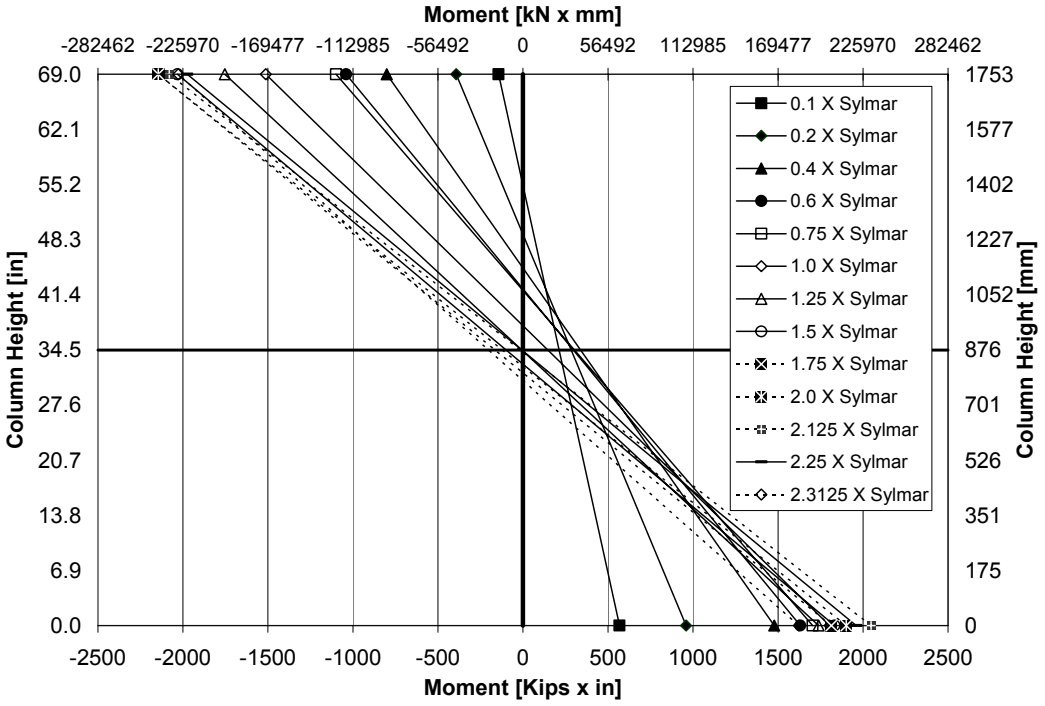

Figure 5-142 Moment Demand Top and Bottom of the Column for the Predominant Direction of Motion Specimen ISH1.5

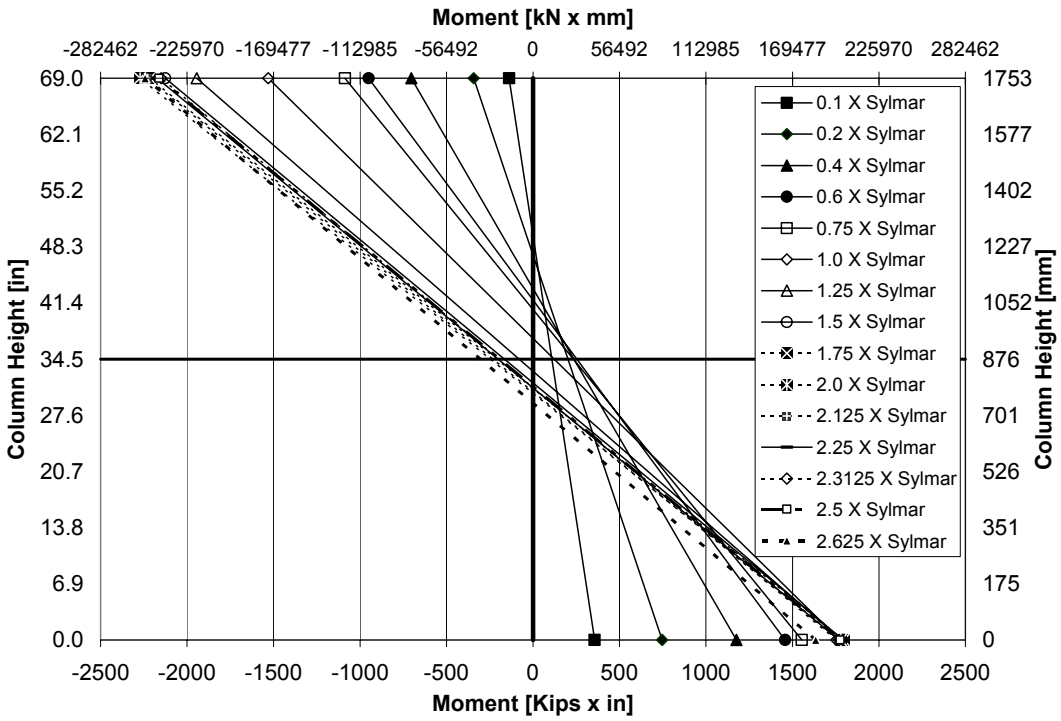

Figure 5-143 Moment Demand Top and Bottom of the Column for the Predominant Direction of Motion Specimen ISH1.5T

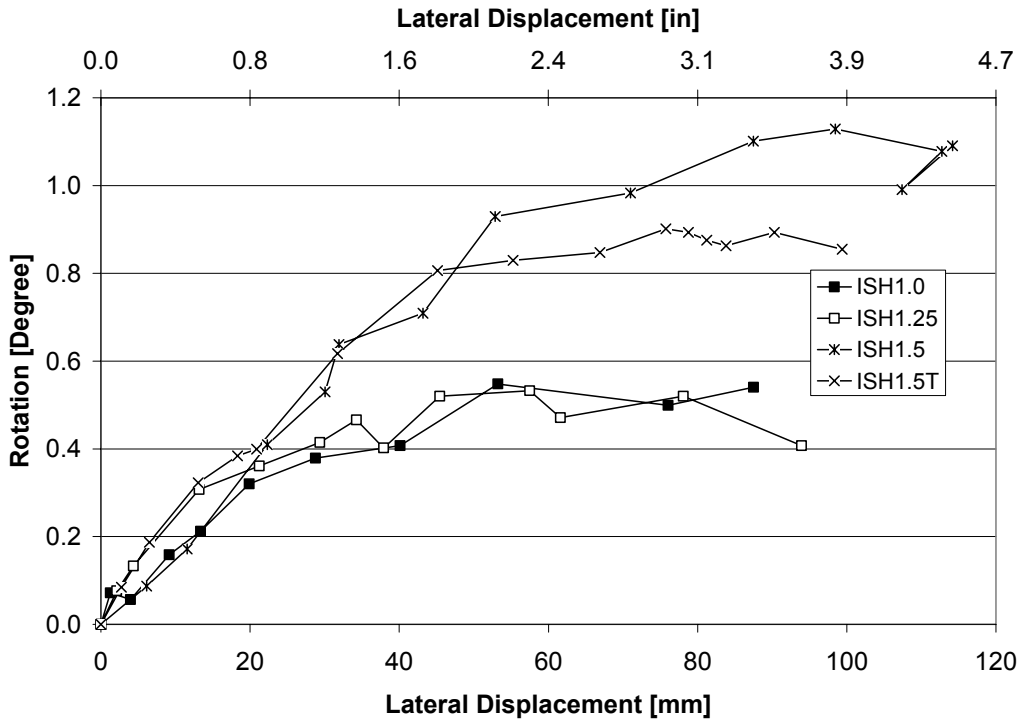

Figure 5-144 Vertical Rotation of the Head versus Lateral Displacement for the Predominant Direction of Motion

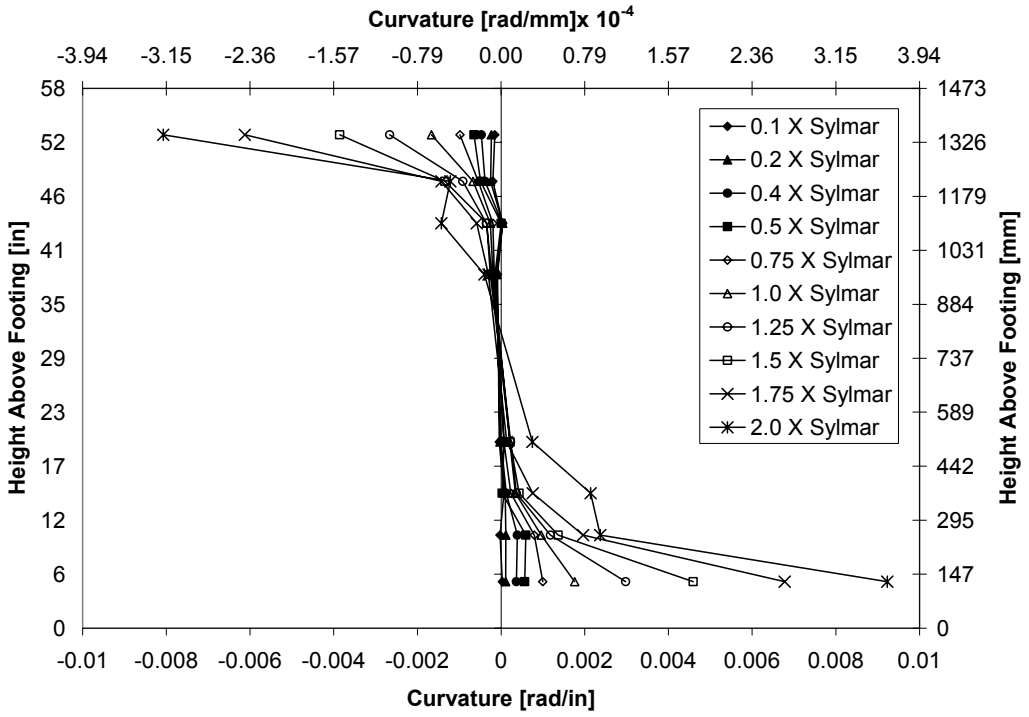

Figure 5-145 Curvature Profile for Predominant Direction of Motion Specimen ISH1.0

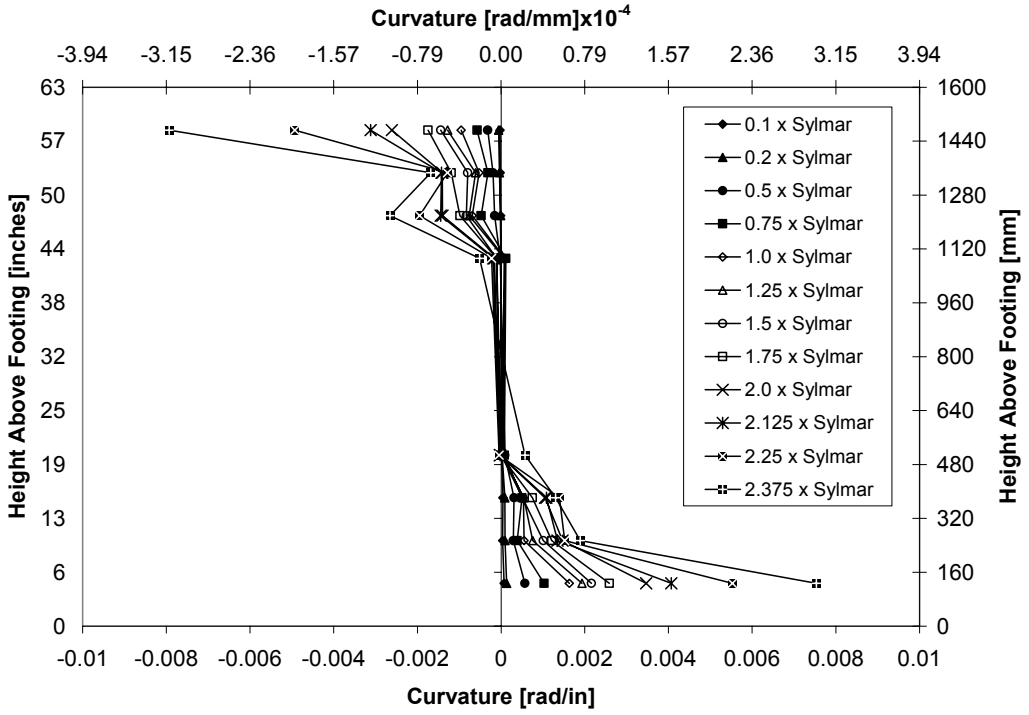

Figure 5-146 Curvature Profile for Predominant Direction of Motion Specimen ISH1.25

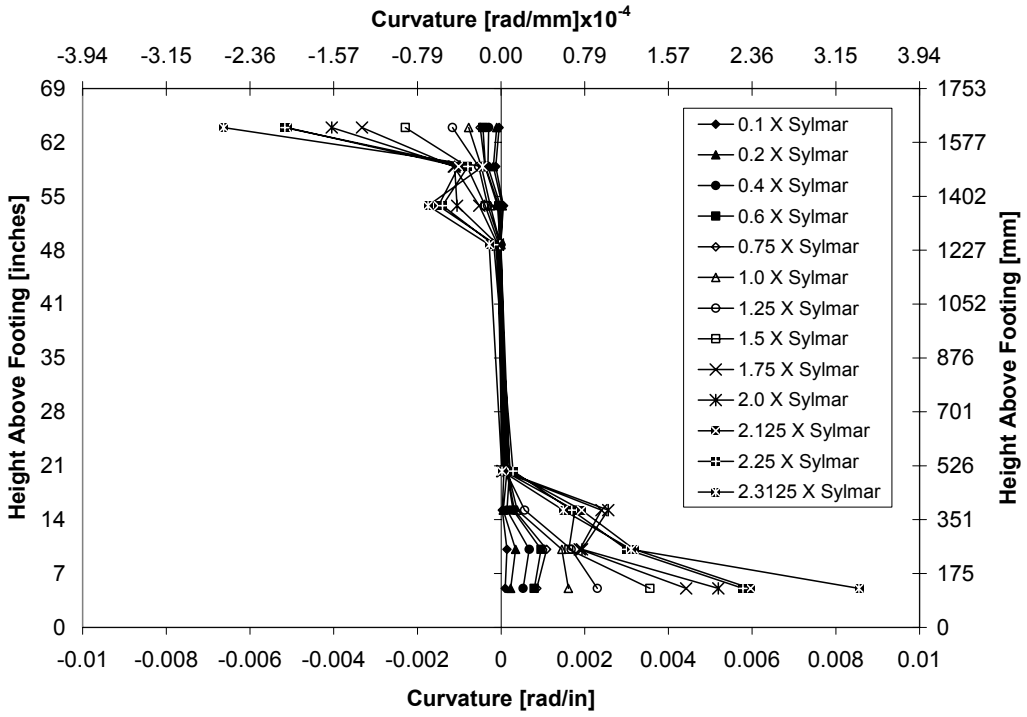

Figure 5-147 Curvature Profile for Predominant Direction of Motion Specimen ISH1.5

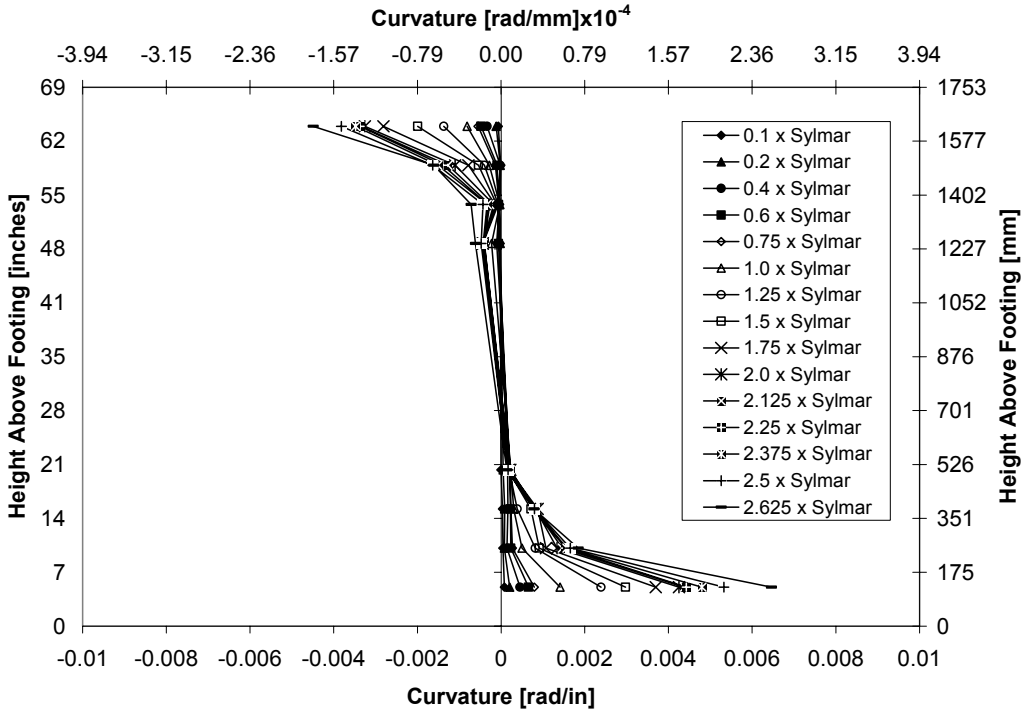

Figure 5-148 Curvature Profile for Predominant Direction of Motion Specimen ISH1.5T

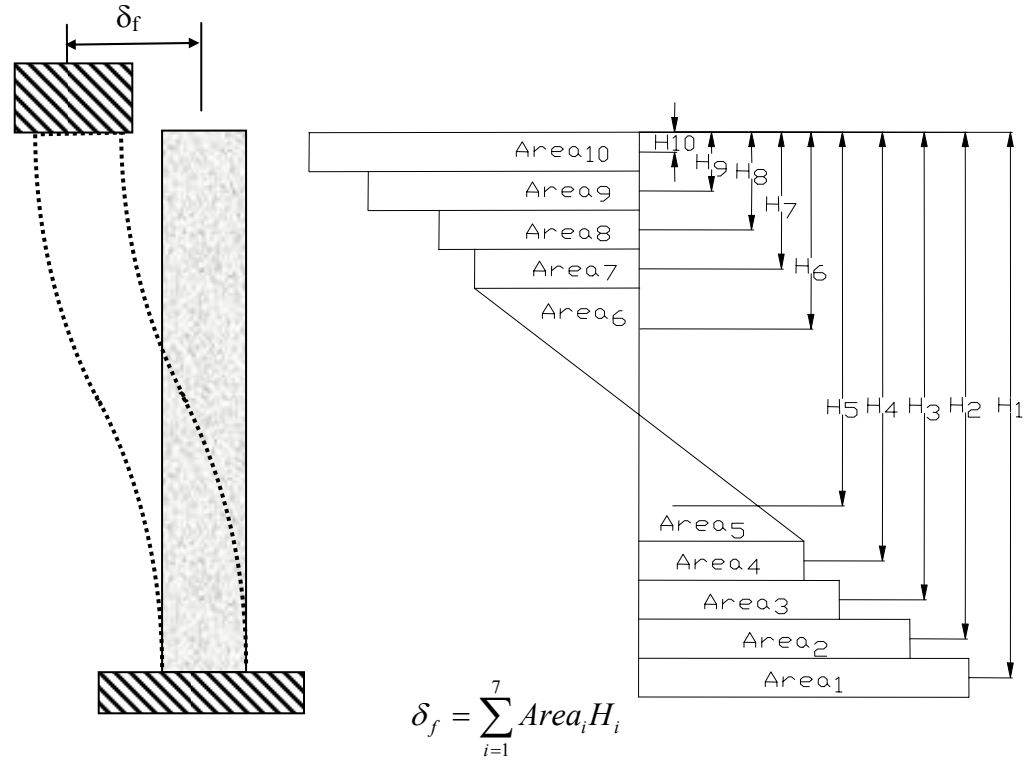

Figure 5-149 Idealized Curvature Used in the Moment Area Analysis

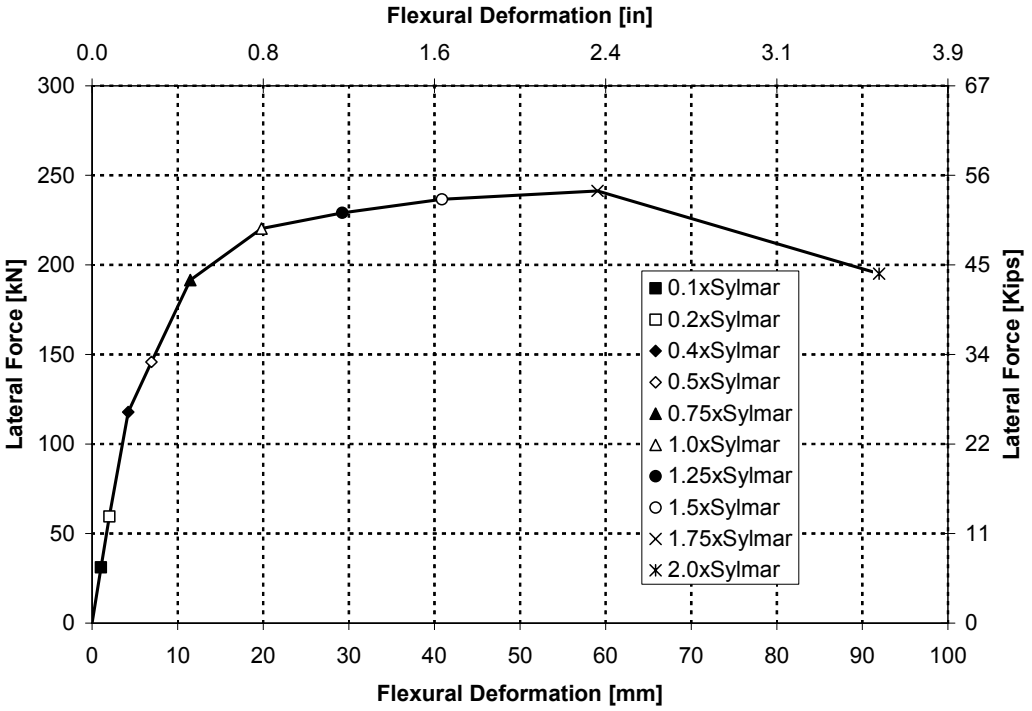

Figure 5-150 Lateral Force versus Flexural Deformation for Specimen ISH1.0

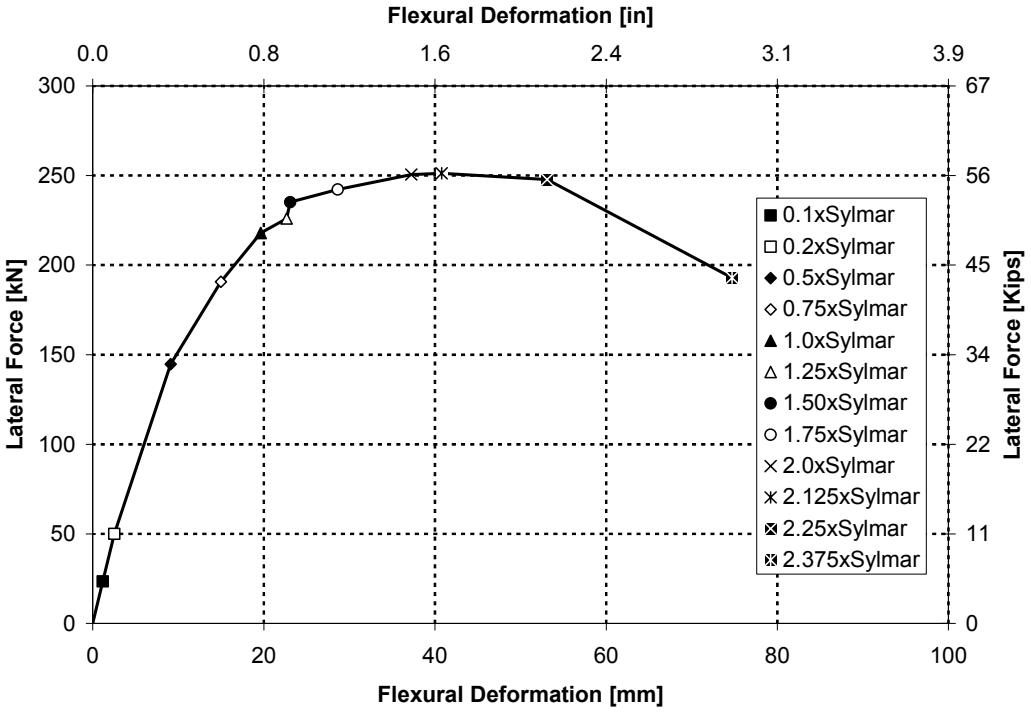

Figure 5-151 Lateral Force versus Flexural Deformation for Specimen ISH1.25

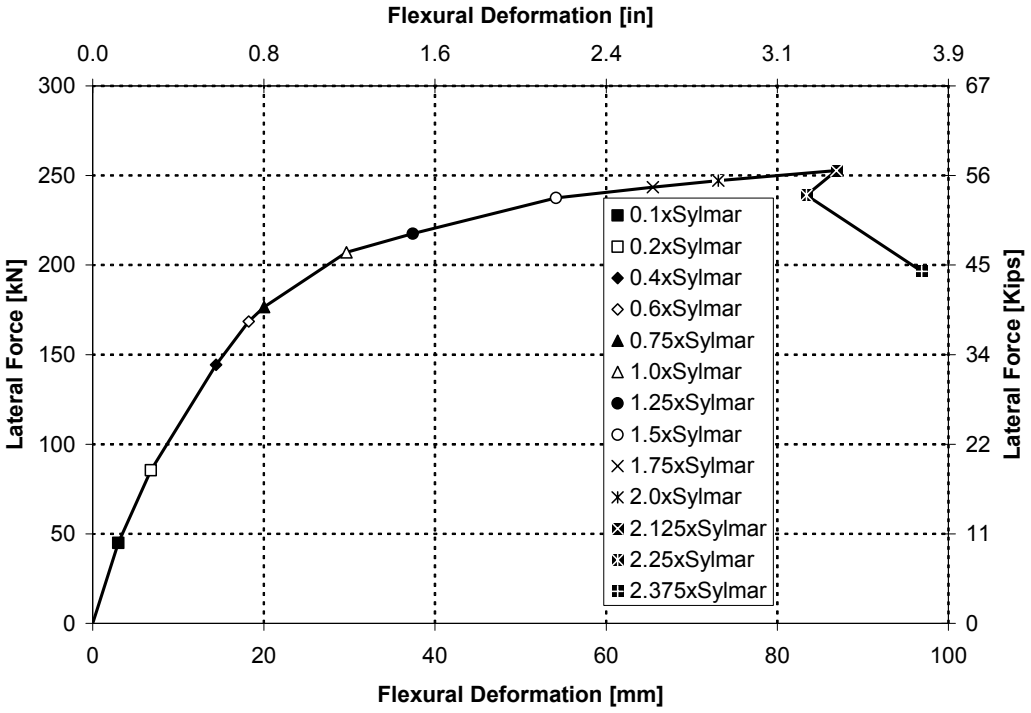

Figure 5-152 Lateral Force versus Flexural Deformation for Specimen ISH1.5

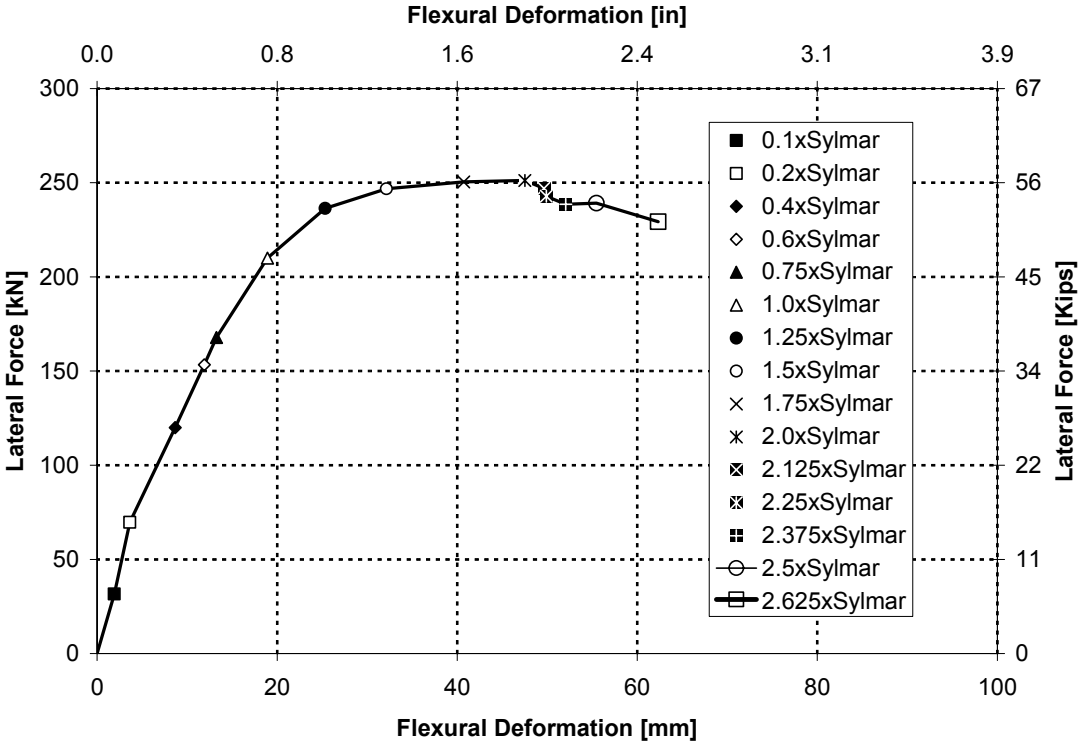

Figure 5-153 Lateral Force versus Flexural Deformation for Specimen ISH1.5T

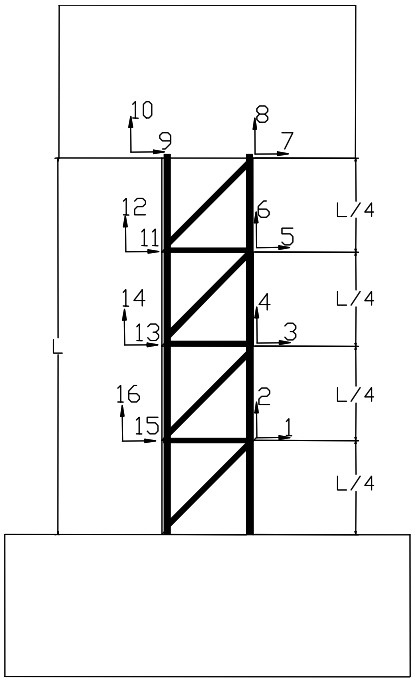

Figure 5-154 Total Displacements Panel Configuration

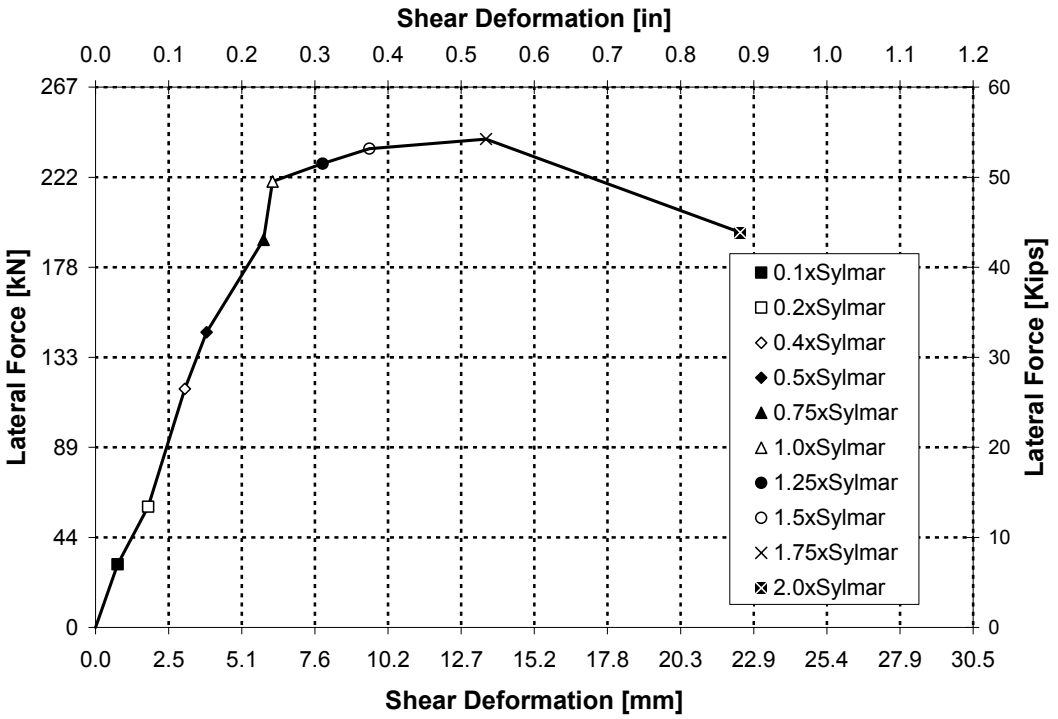

Figure 5-155 Lateral Force versus Shear Deformation for Specimen ISH1.0

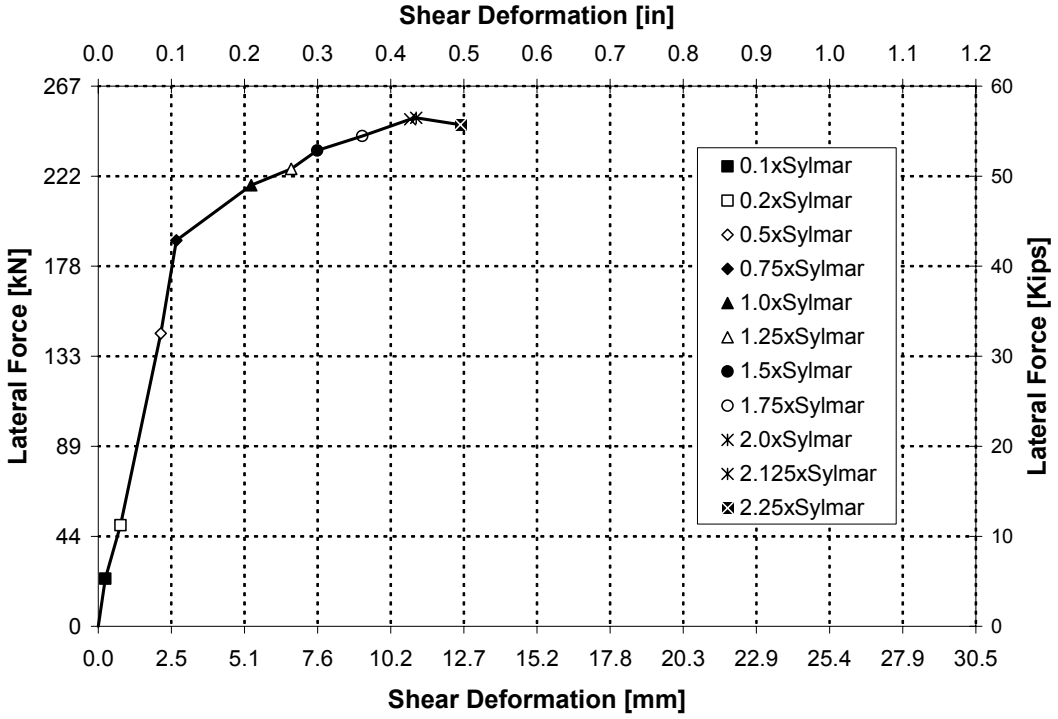

Figure 5-156 Lateral Force versus Shear Deformation for Specimen ISH1.25

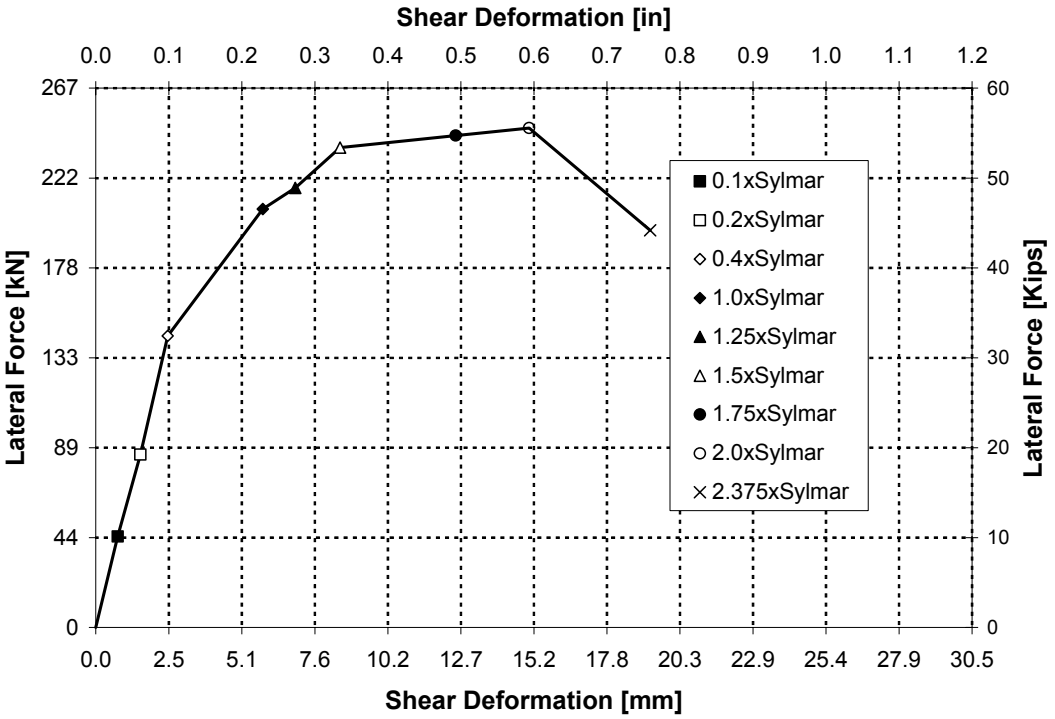

Figure 5-157 Lateral Force versus Shear Deformation for Specimen ISH1.5

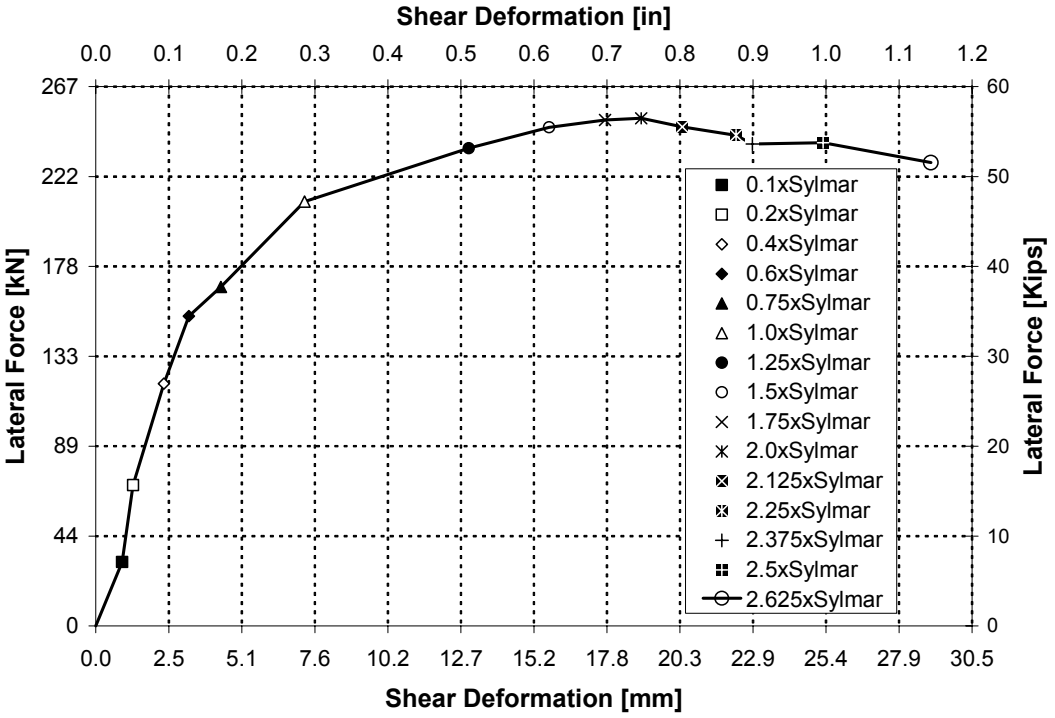

Figure 5-158 Lateral Force versus Shear Deformation for Specimen ISH1.5

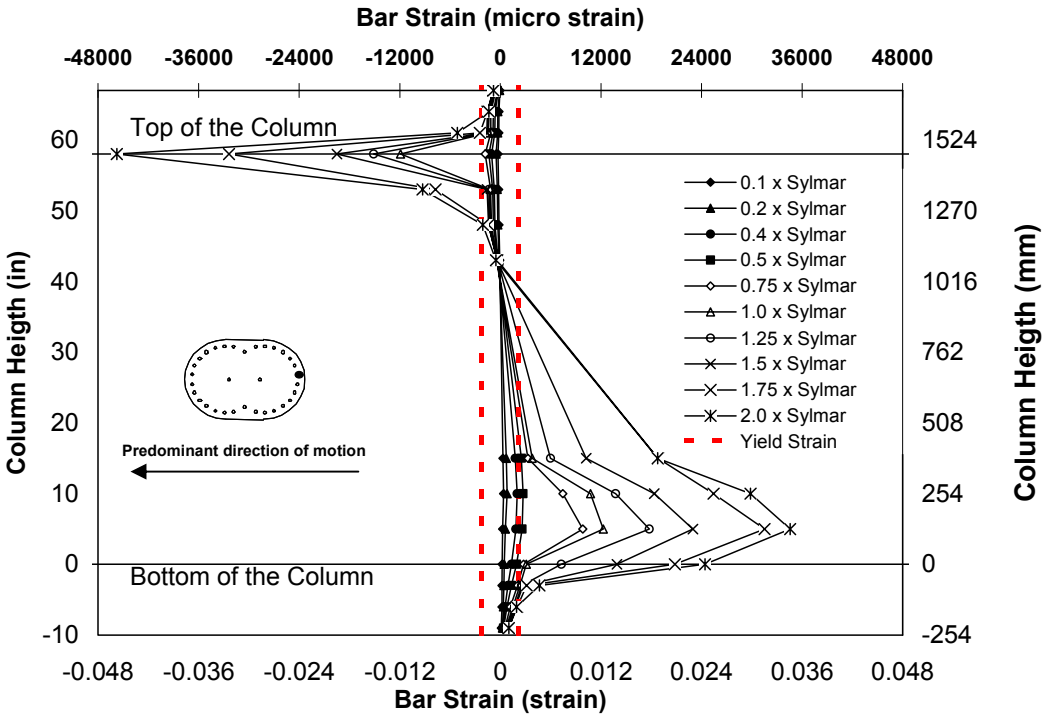

Figure 5-159 Strain Profile Gauge # 6 for Predominant Direction of Motion Specimen ISH1.0

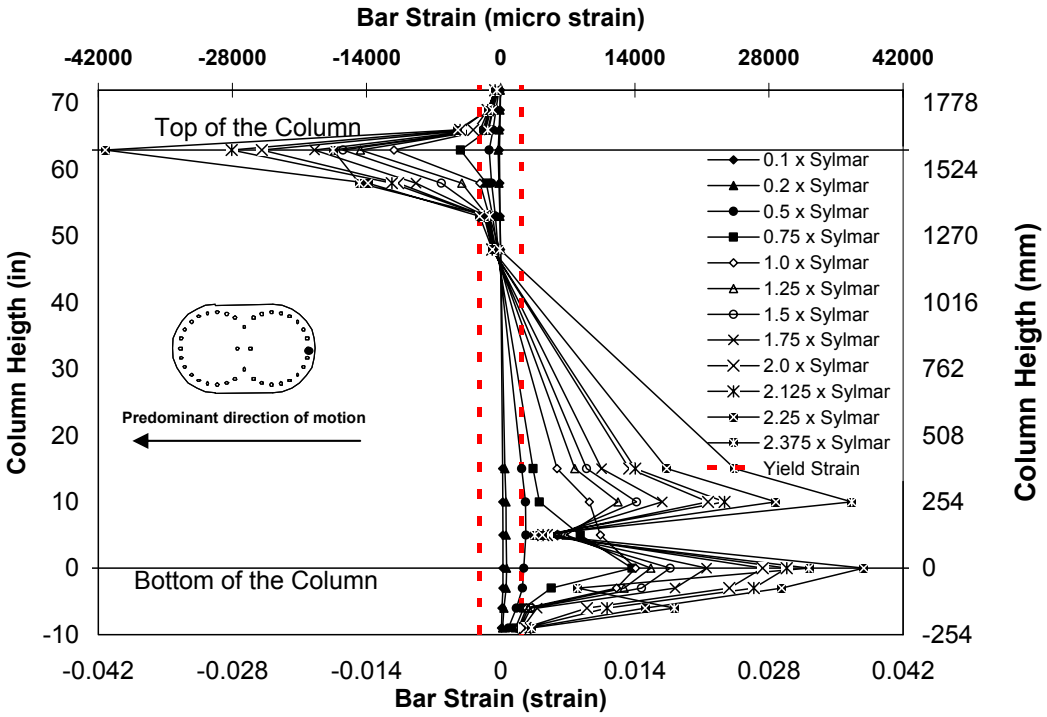

Figure 5-160 Strain Profile Gauge # 6 for Predominant Direction of Motion Specimen ISH1.25

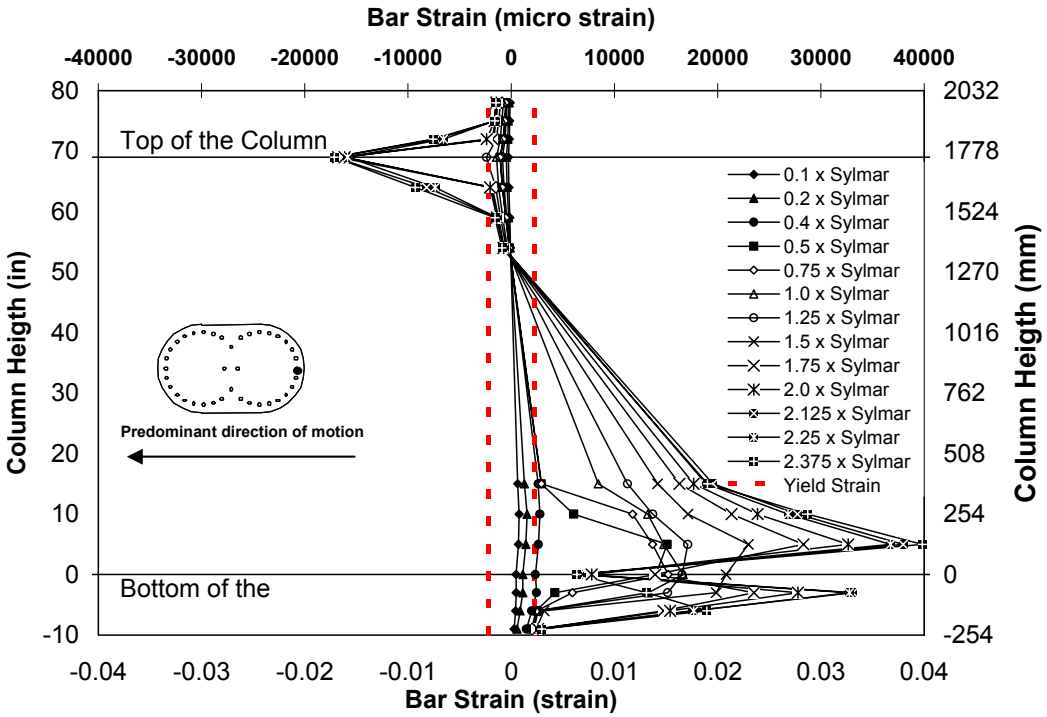

Figure 5-161 Strain Profile Gauge # 6 for Predominant Direction of Motion Specimen ISH1.5

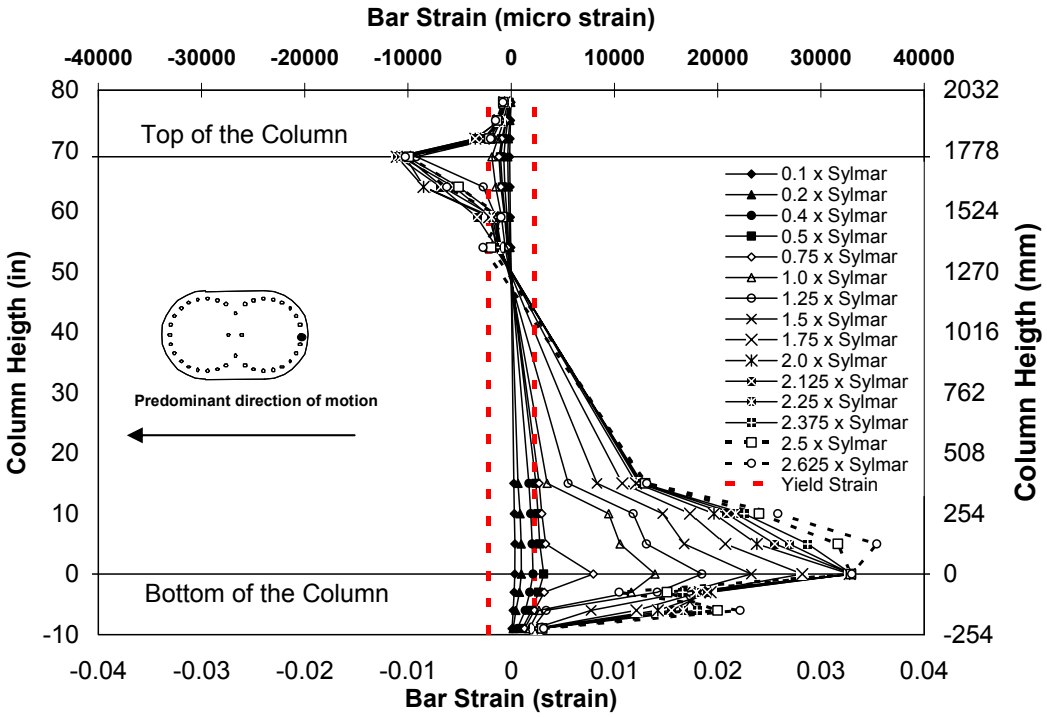

Figure 5-162 Strain Profile Gauge # 6 for Predominant Direction of Motion Specimen ISH1. 5T

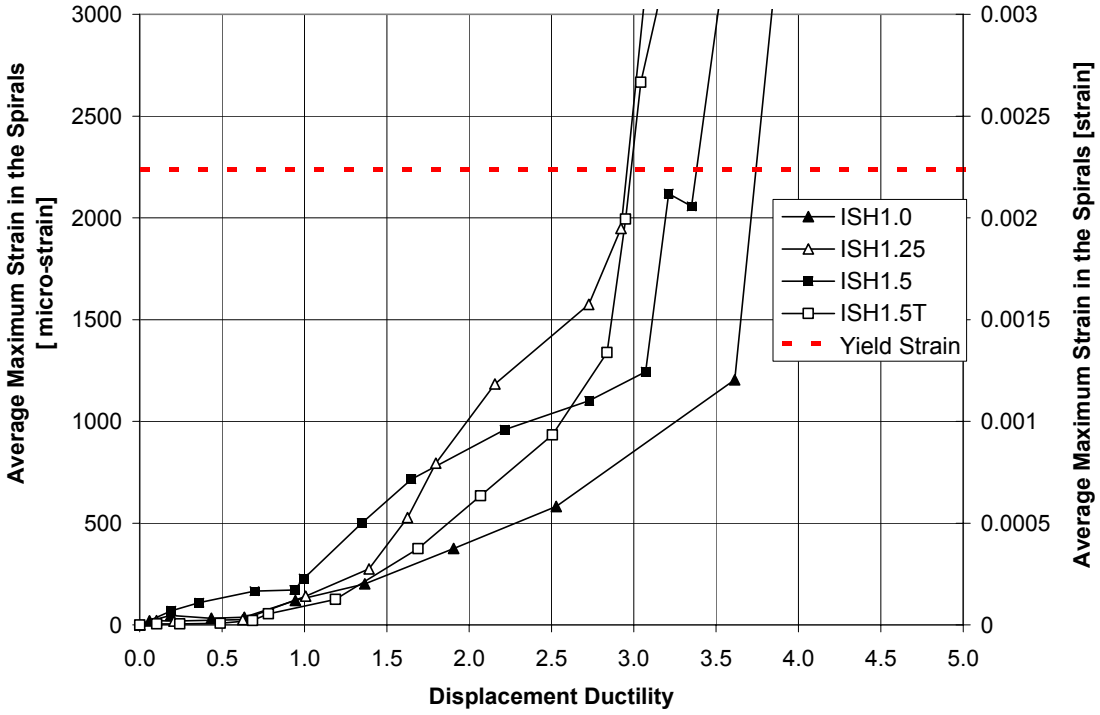

Figure 5-163 Maximum Average Strain in the Spirals for Specimens with High Shear

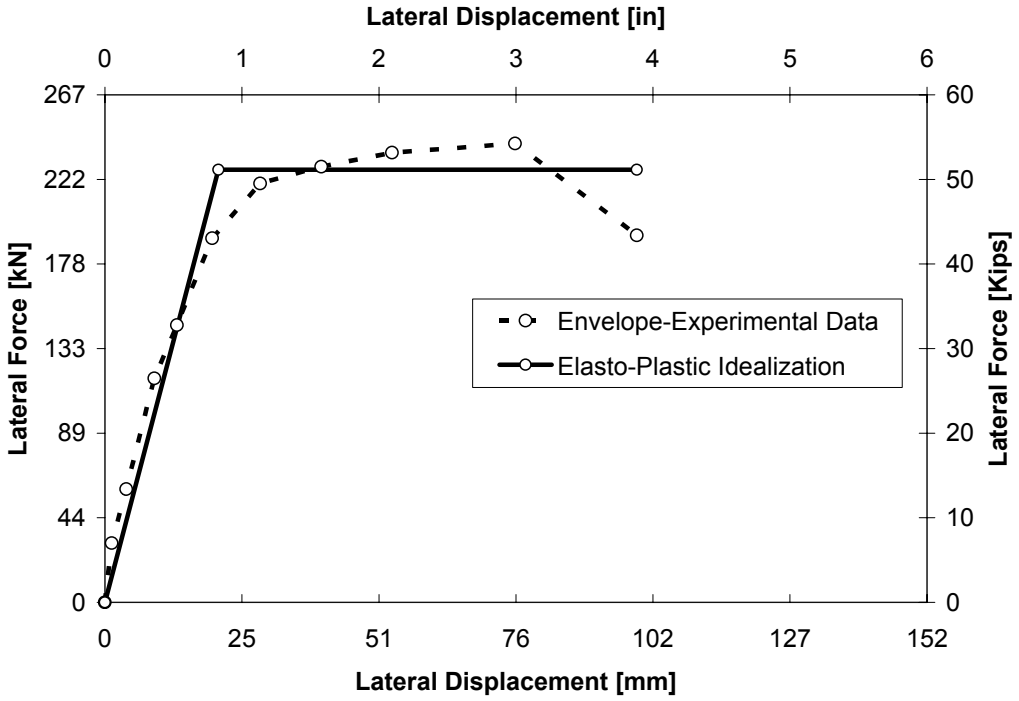

Figure 5-164 Elasto-Plastic Idealized Curve Specimen ISH1.0

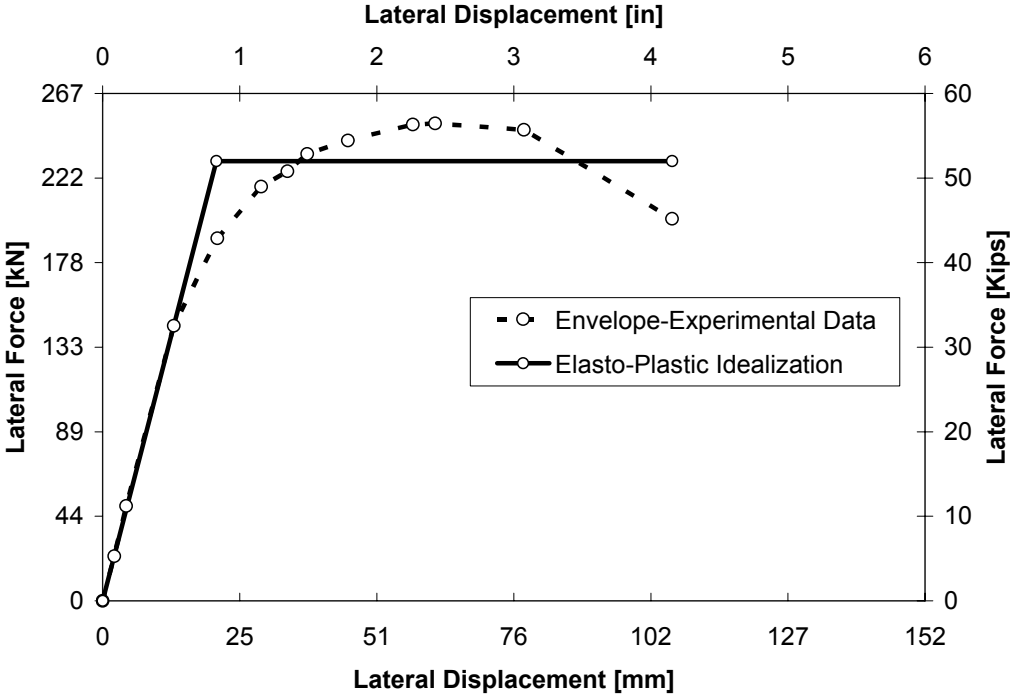

Figure 5-165 Elasto-Plastic Idealized Curve Specimen ISH1.25

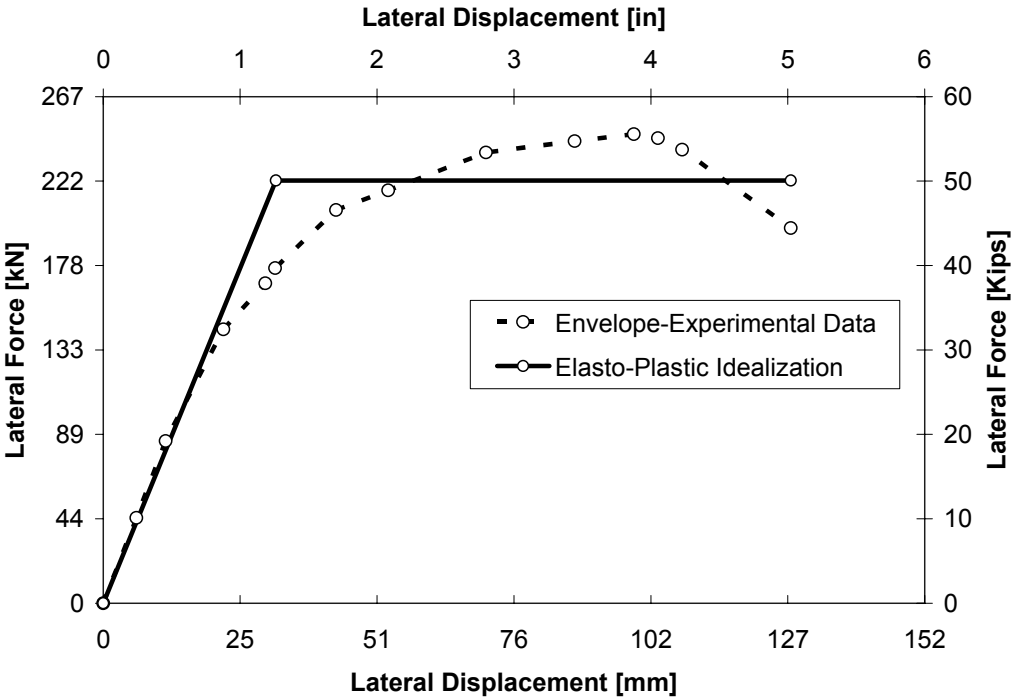

Figure 5-166 Elasto-Plastic Idealized Curve Specimen ISH1.5

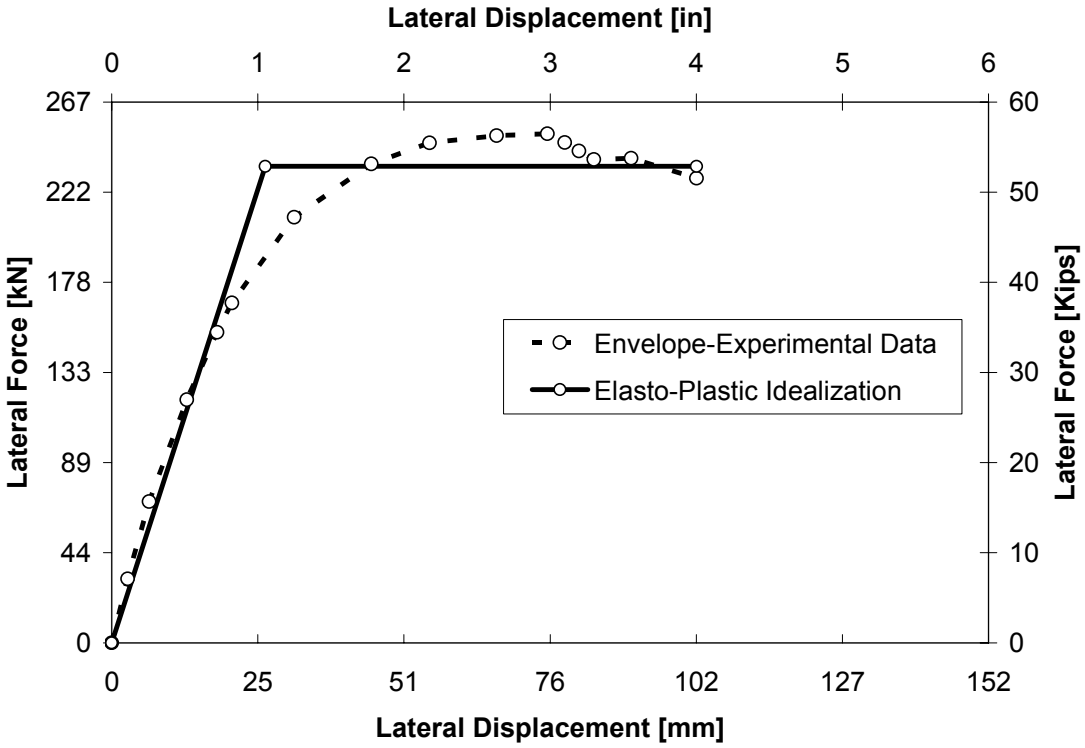

Figure 5-167 Elasto-Plastic Idealized Curve Specimen ISH1.5T

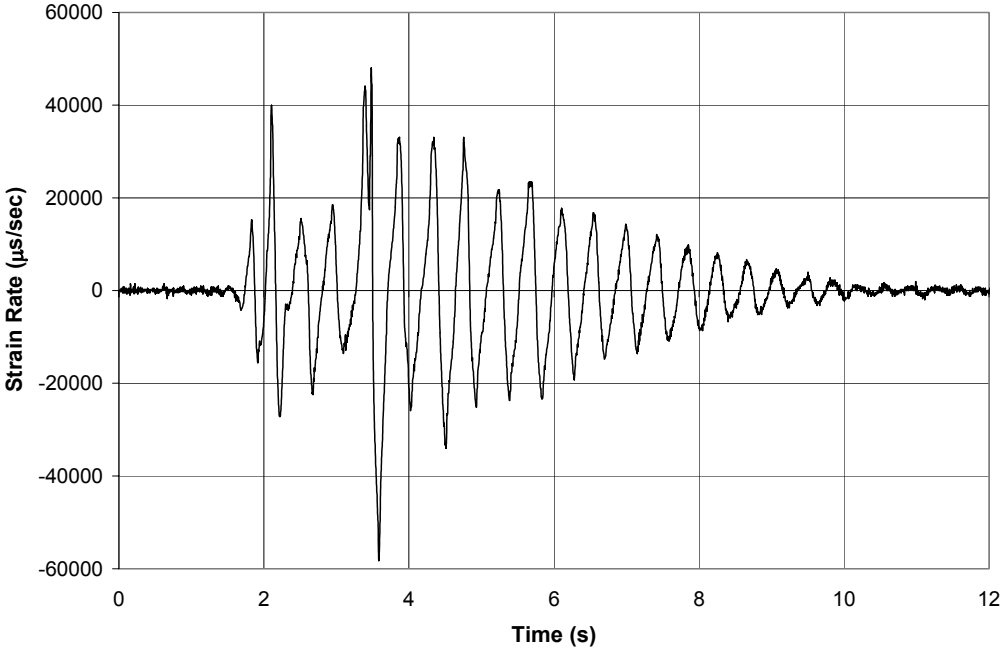

Figure 6-1 Typical Measured Strain Rate History for Steel

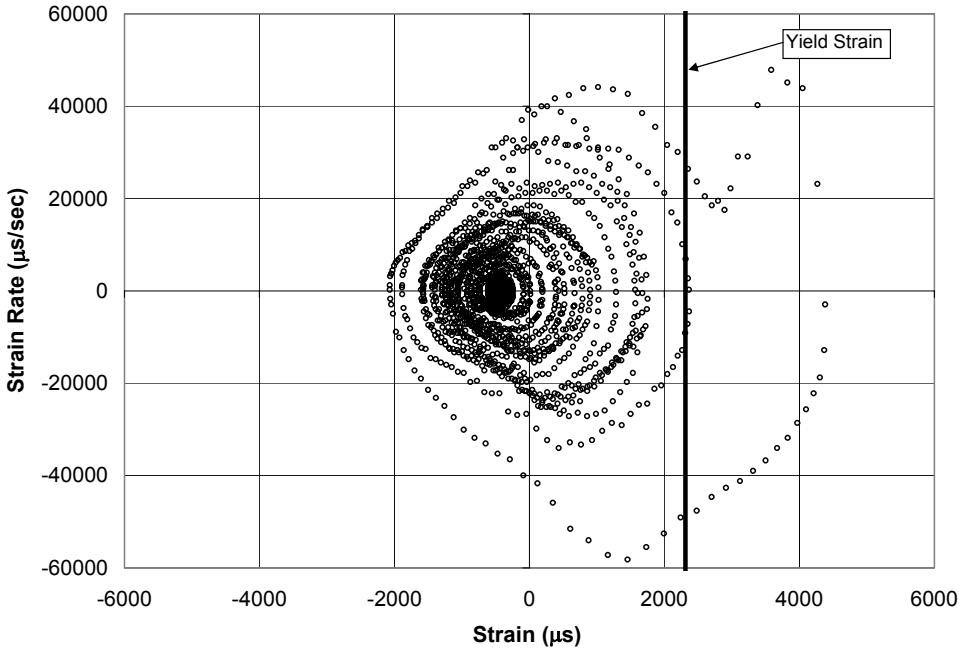

Figure 6-2 Typical Measured Strain Rate versus Strain for Steel

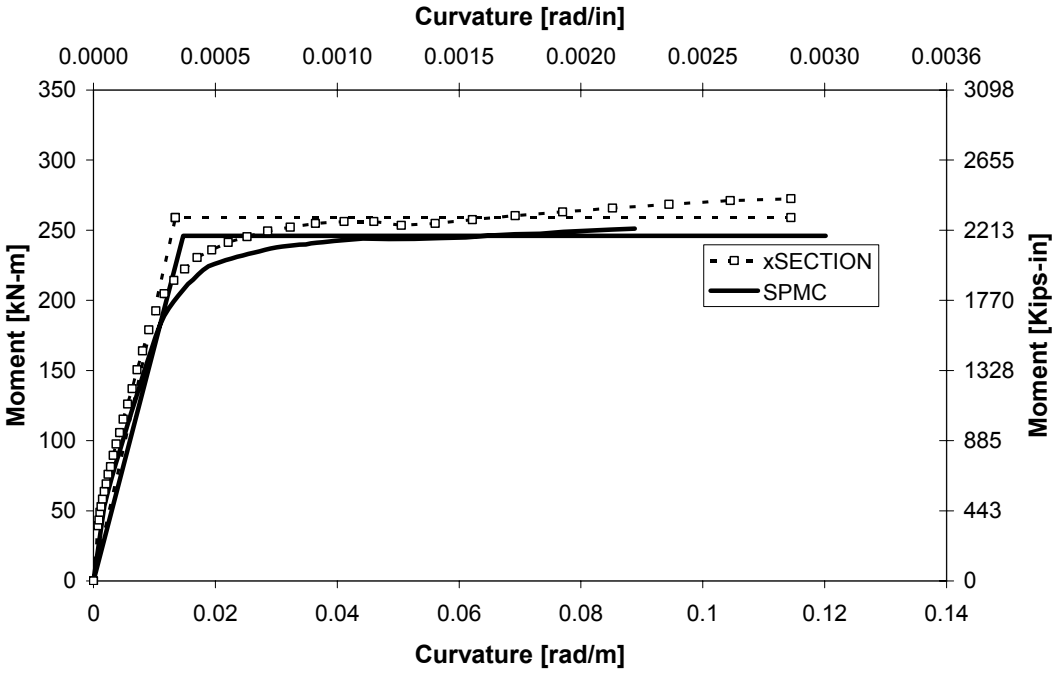

Figure 6-3 Calculated and Idealized M-ϕ Curves using SPMC and xSECTION Specimen ISL1.0

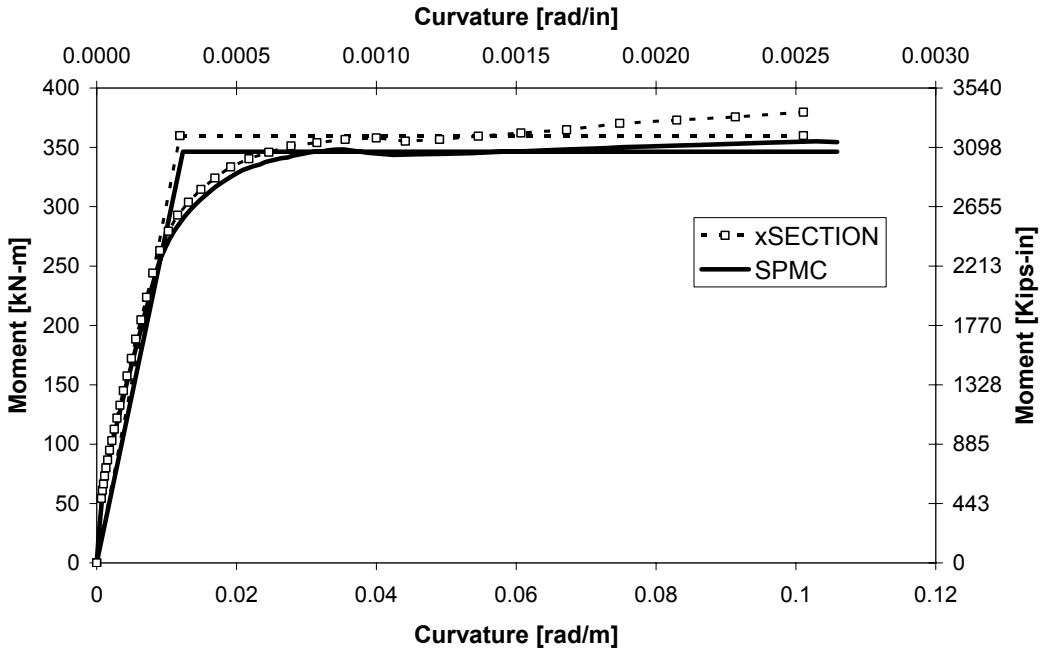

Figure 6-4 Calculated and Idealized M-ϕ Curves using SPMC and xSECTION Specimen ISL1.5

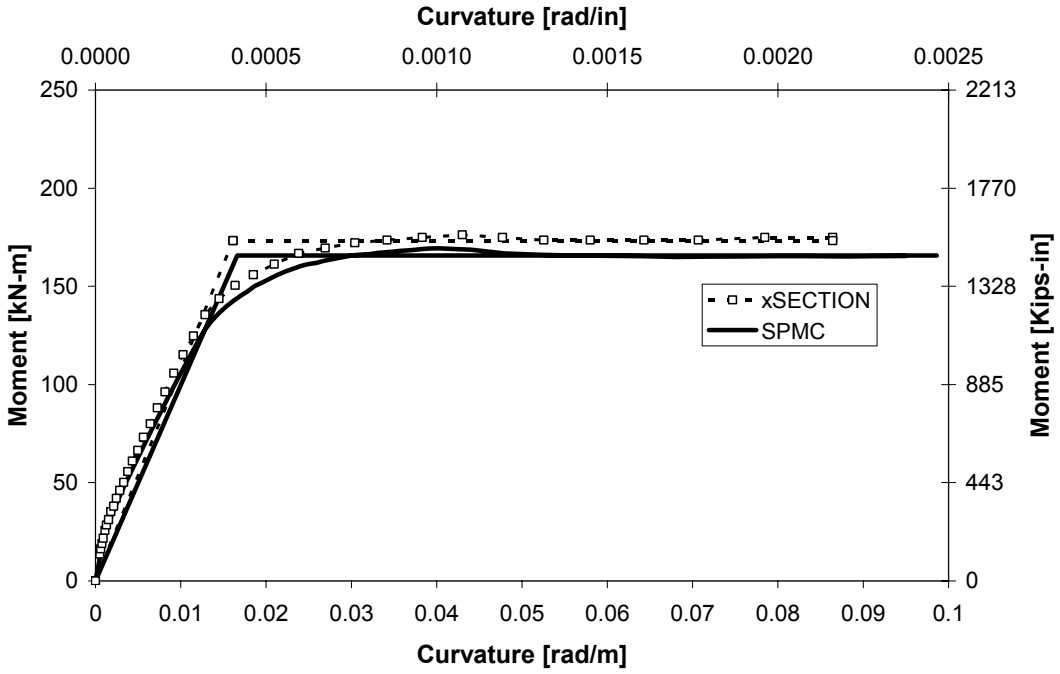

Figure 6-5 Calculated and Idealized M-ϕ Curves using SPMC and xSECTION Specimen ISH1.0

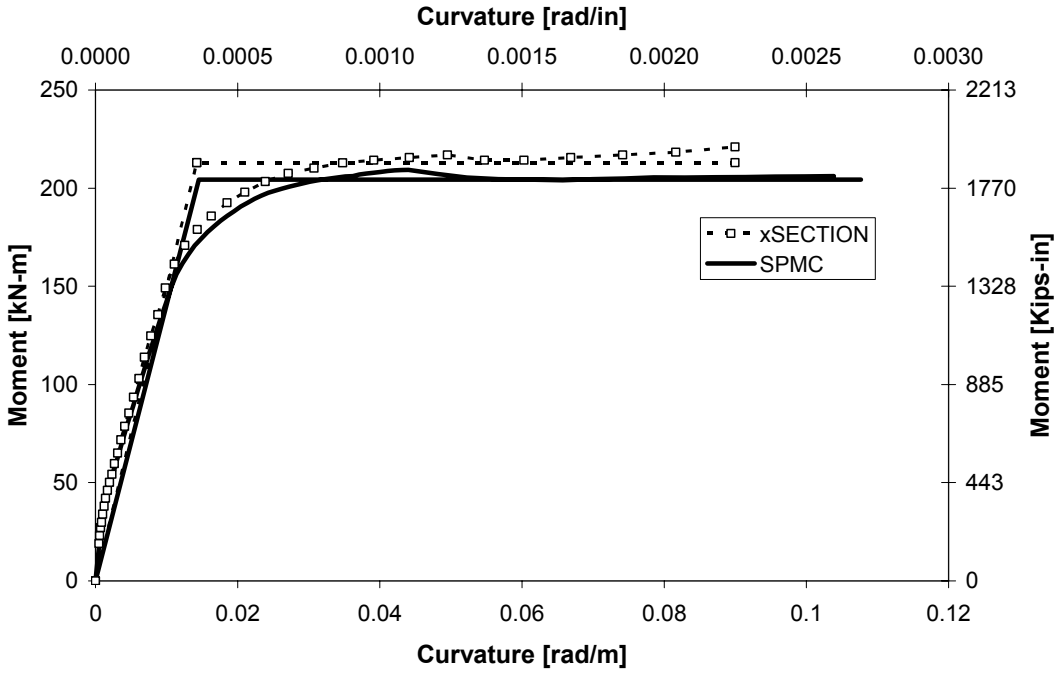

Figure 6-6 Calculated and Idealized M-ϕ Curves using SPMC and xSECTION Specimen ISH1.25

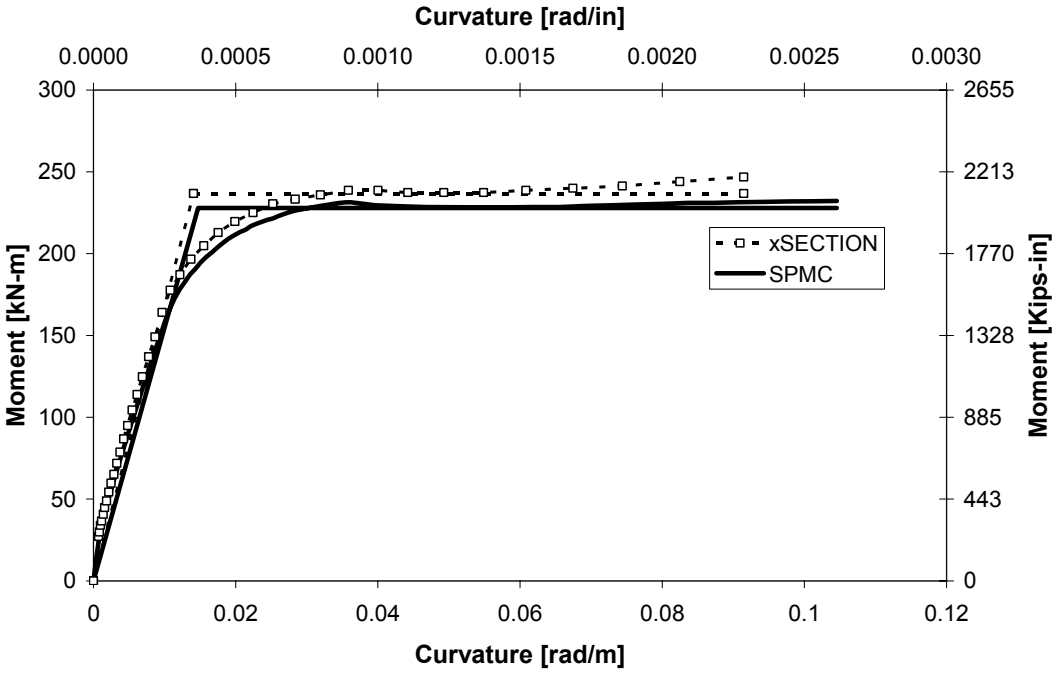

Figure 6-7 Calculated and Idealized M-ϕ Curves using SPMC and xSECTION Specimen ISH1.5

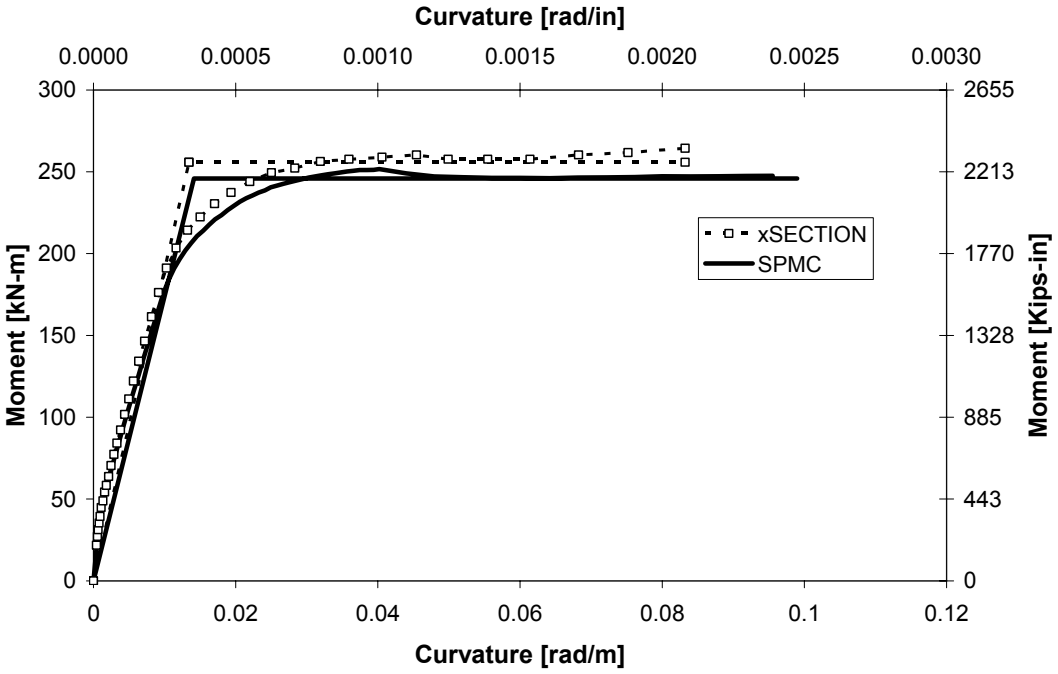

Figure 6-8 Calculated and Idealized M-ϕ Curves using SPMC and xSECTION Specimen ISH1.5T

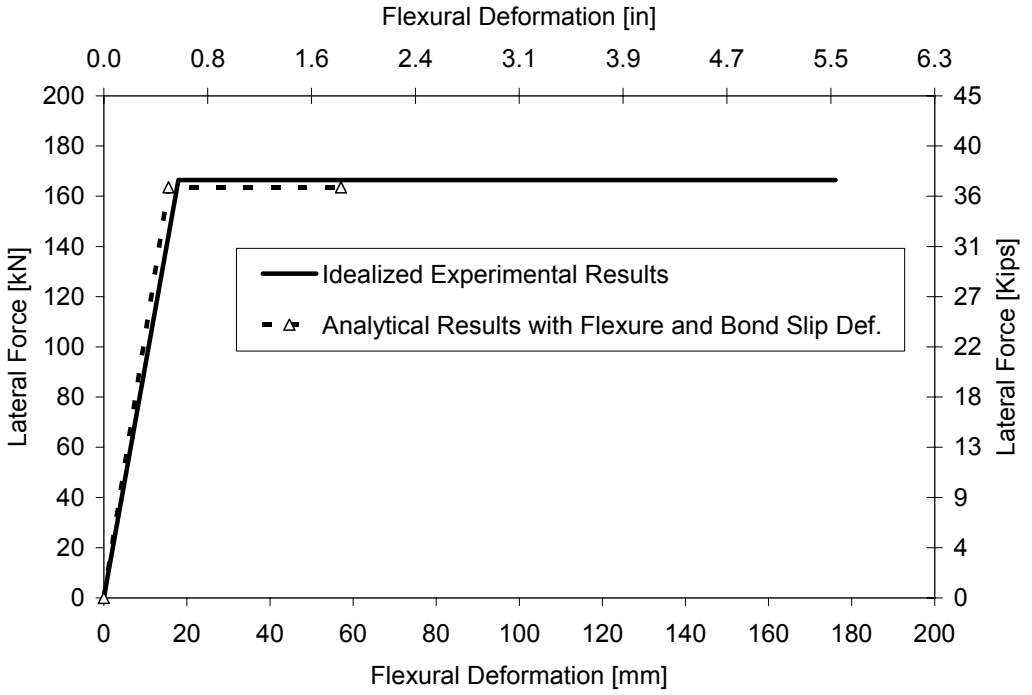

Figure 6-9 Comparison of Analytical and Experimental Force vs. Displacement Including Flexural with Bond Slip Deformations for ISL1.0

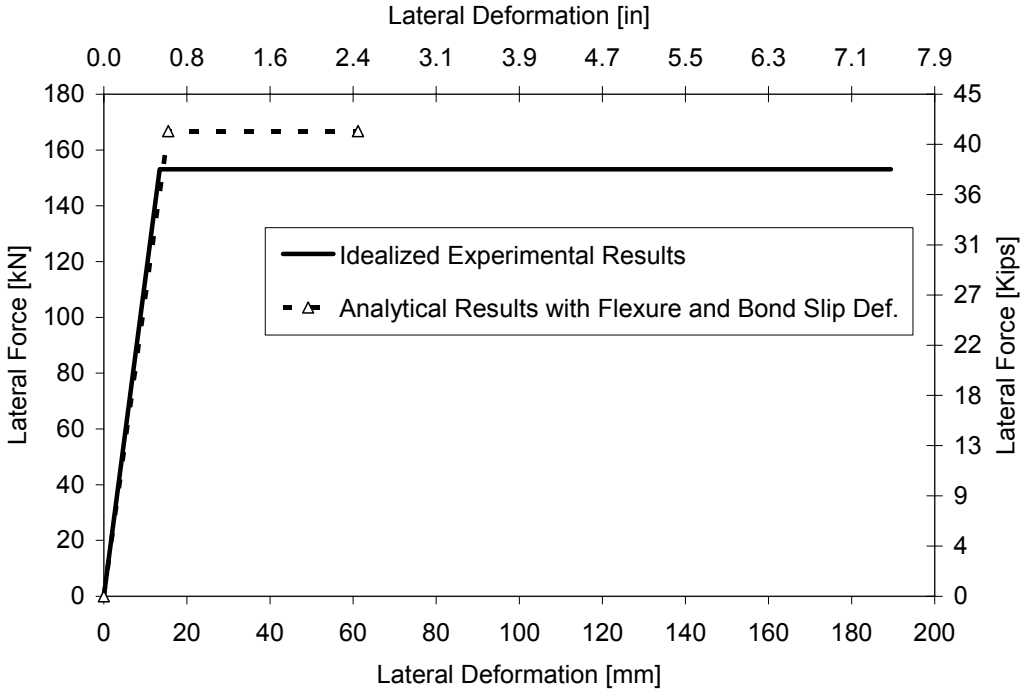

Figure 6-10 Comparison of Analytical and Experimental Force vs. Displacement Including Flexural with Bond Slip Deformations for ISL1.5

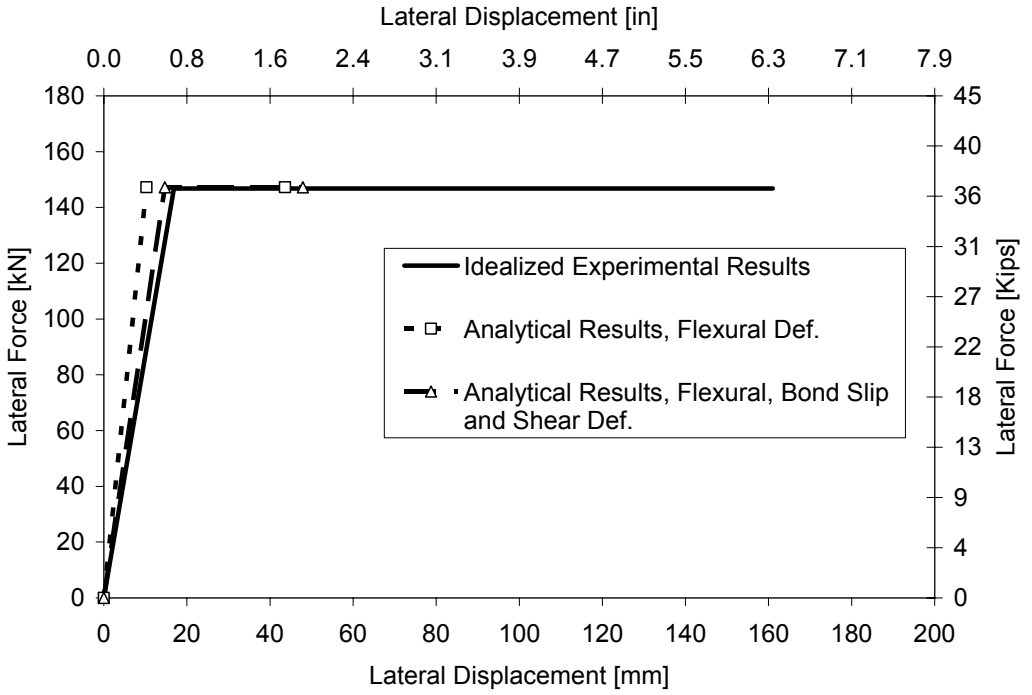

Figure 6-11 Comparison of Analytical and Experimental Force vs. Displacement Including Flexural, Bond Slip and Shear Deformations for ISL1.0

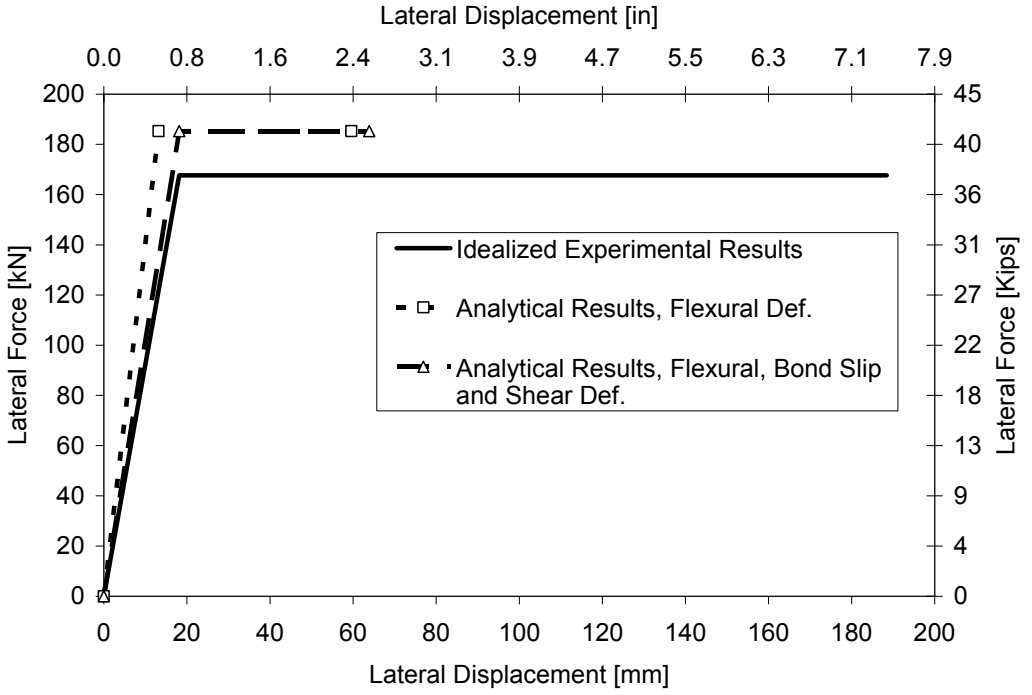

Figure 6-12 Comparison of Analytical and Experimental Force vs. Displacement Including Flexural, Bond Slip and Shear Deformations for ISL1.5

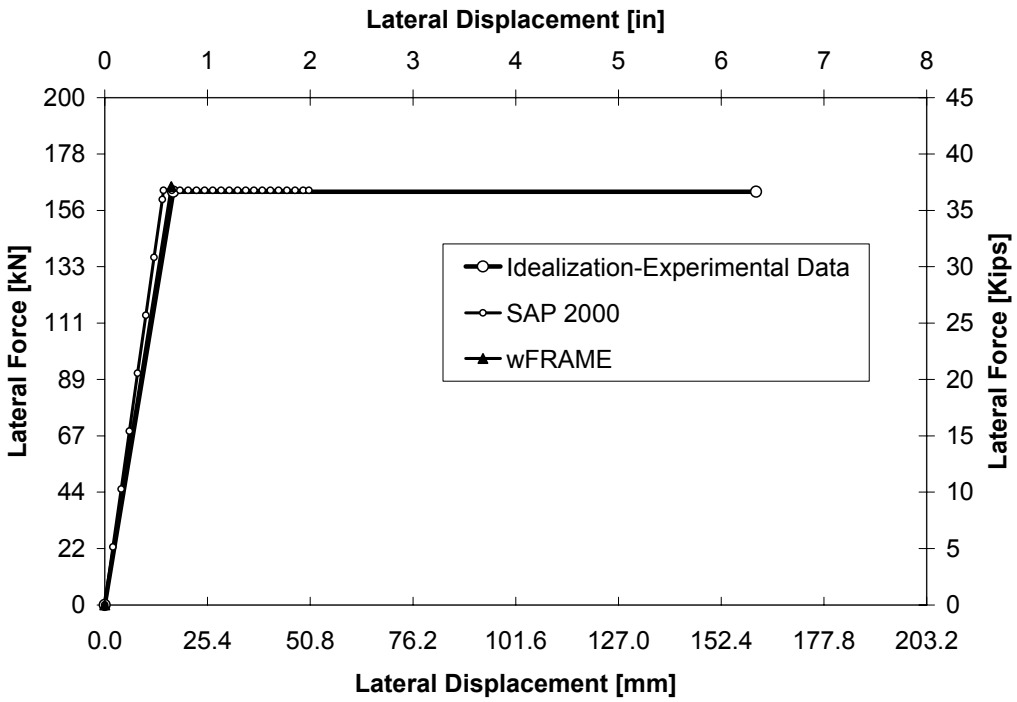

Figure 6-13 Measured and Calculated Force vs. Displacement Curves for ISL1.0

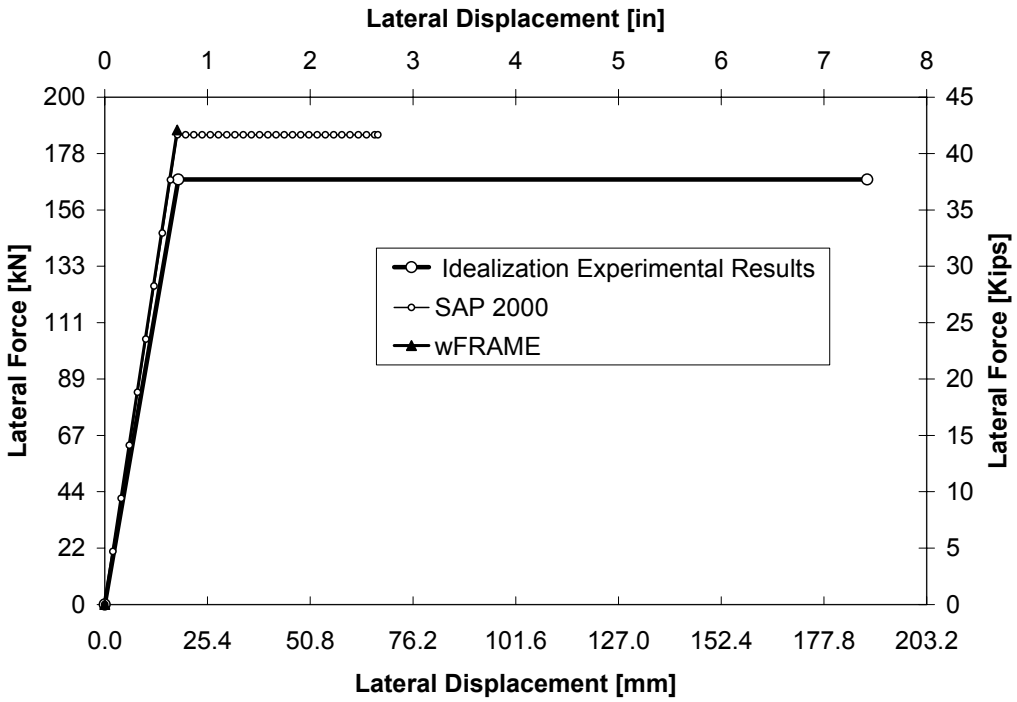

Figure 6-14 Measured and Calculated Force vs. Displacement Curves ISL1.5

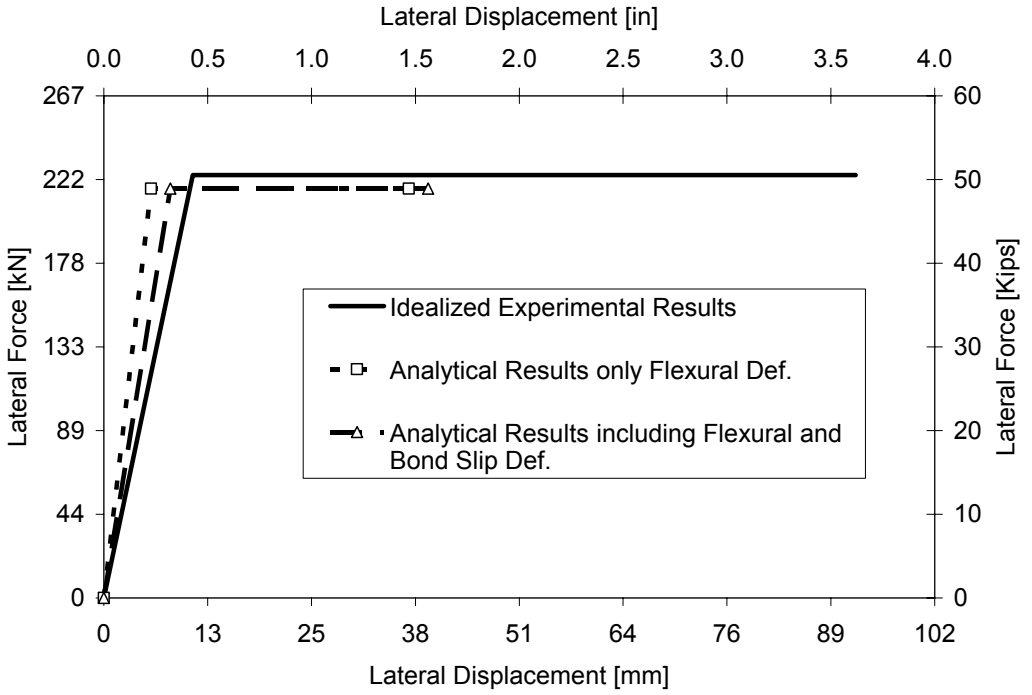

Figure 6-15 Comparison of Analytical and Experimental Force vs. Displacement Including Flexural with Bond Slip Deformations for ISH1.0

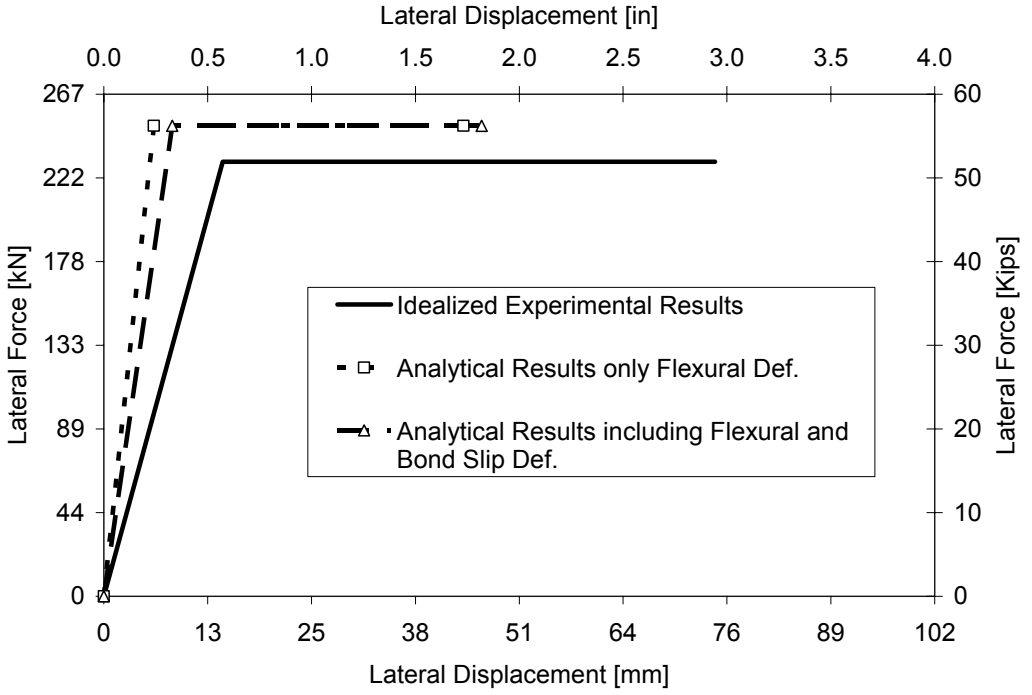

Figure 6-16 Comparison of Analytical and Experimental Force vs. Displacement Including Flexural with Bond Slip Deformations for ISH1.25

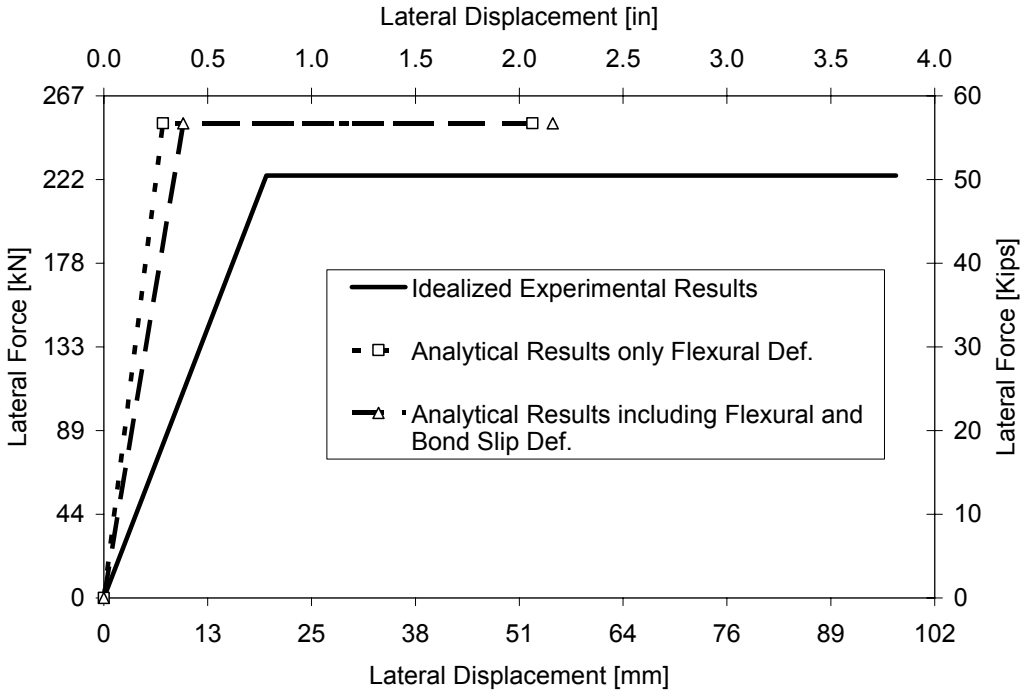

Figure 6-17 Comparison of Analytical and Experimental Force vs. Displacement Including Flexural with Bond Slip Deformations for ISH1.5

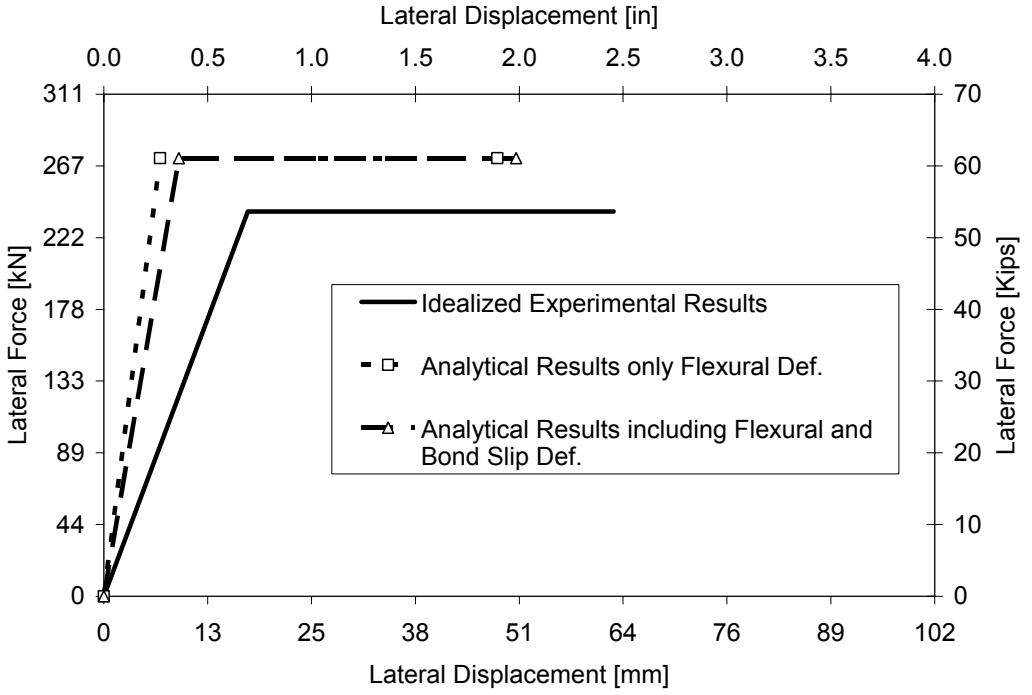

Figure 6-18 Comparison of Analytical and Experimental Force vs. Displacement Including Flexural with Bond Slip Deformations for ISH1.5T

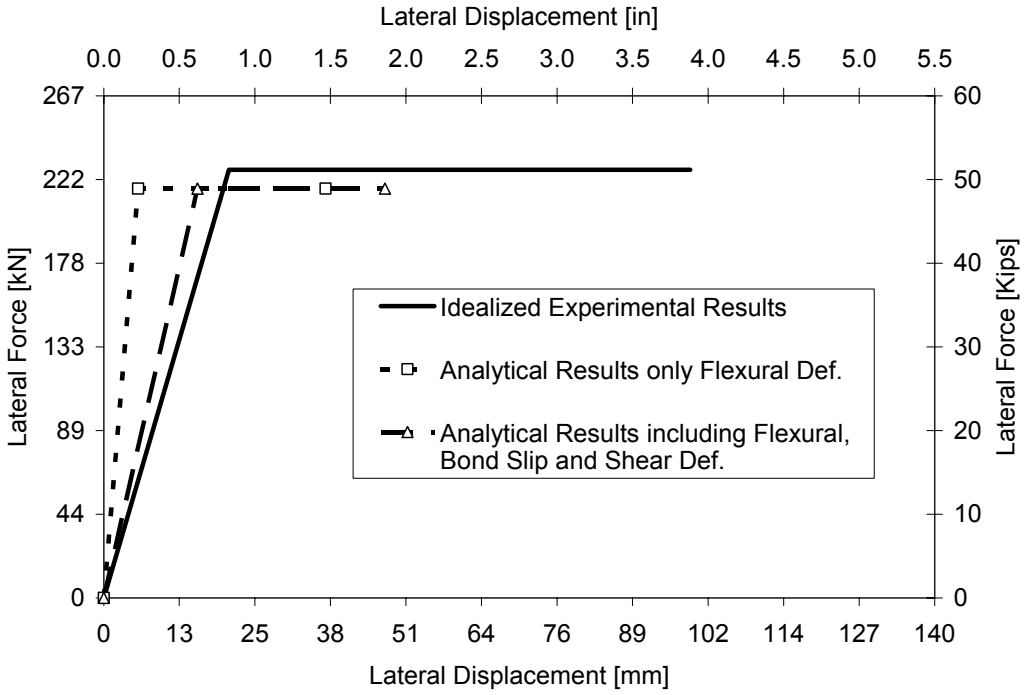

Figure 6-19 Comparison of Analytical and Experimental Force vs. Displacement Including Flexural, Bond Slip and Shear Deformations for ISH1.0

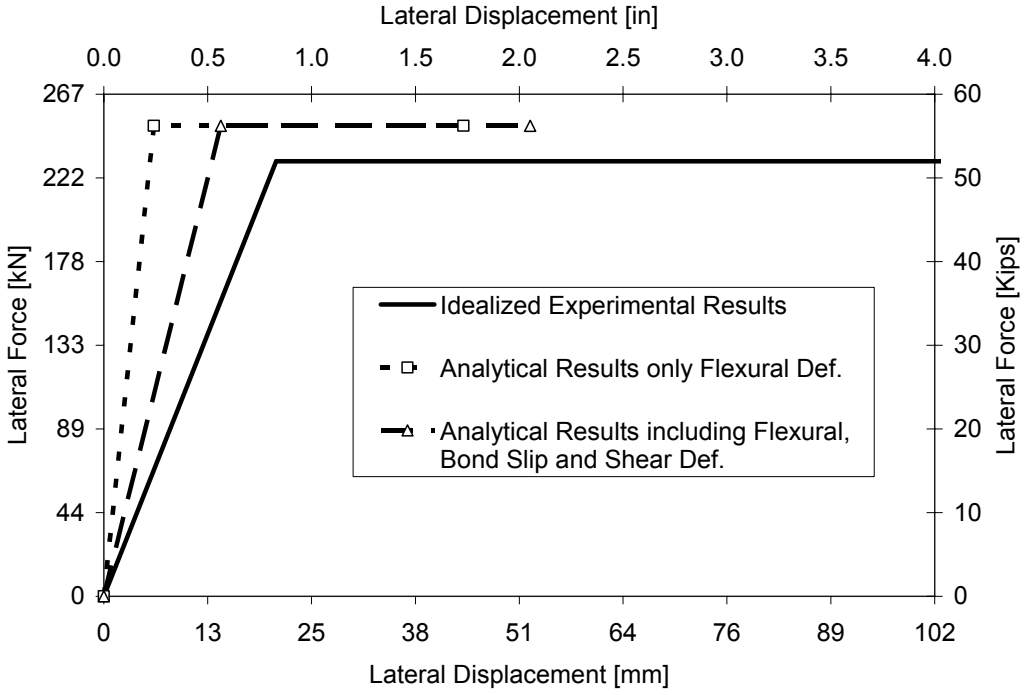

Figure 6-20 Comparison of Analytical and Experimental Force vs. Displacement Including Flexural, Bond Slip and Shear Deformations for ISH1.25

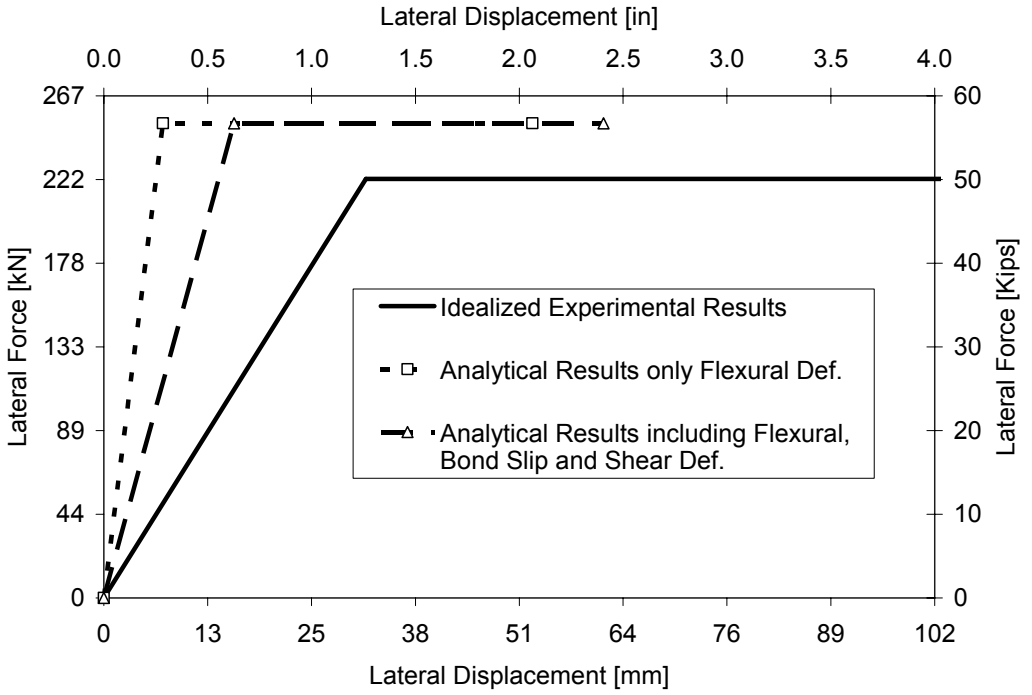

Figure 6-21 Comparison of Analytical and Experimental Force vs. Displacement Including Flexural, Bond Slip and Shear Deformations for ISH1.5

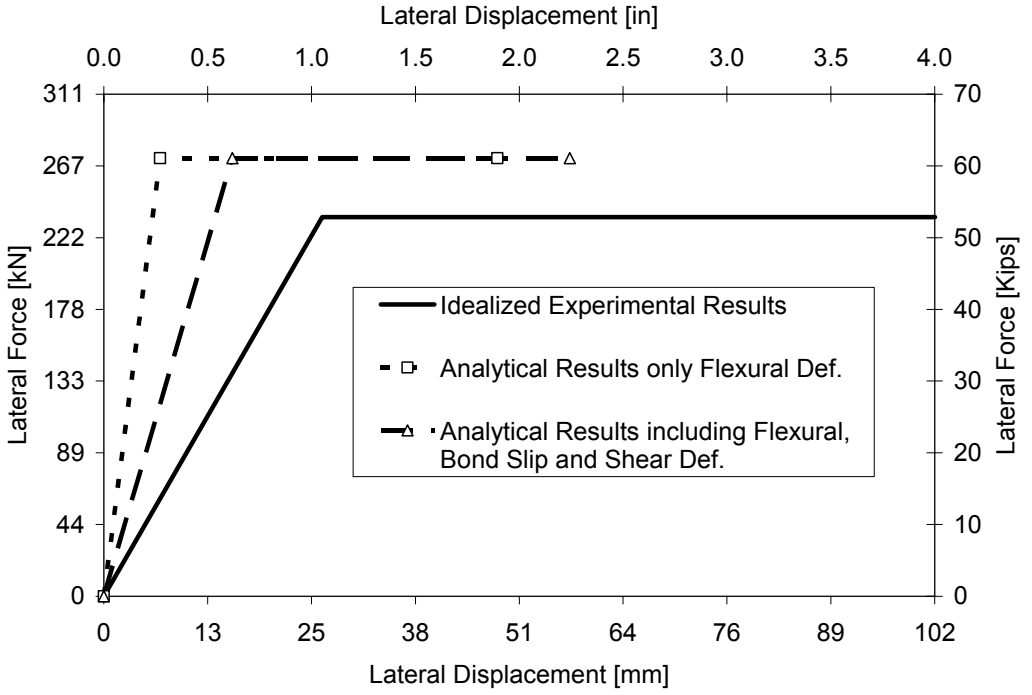

Figure 6-22 Comparison of Analytical and Experimental Force vs. Displacement Including Flexural, Bond Slip and Shear Deformations for ISH1.5T

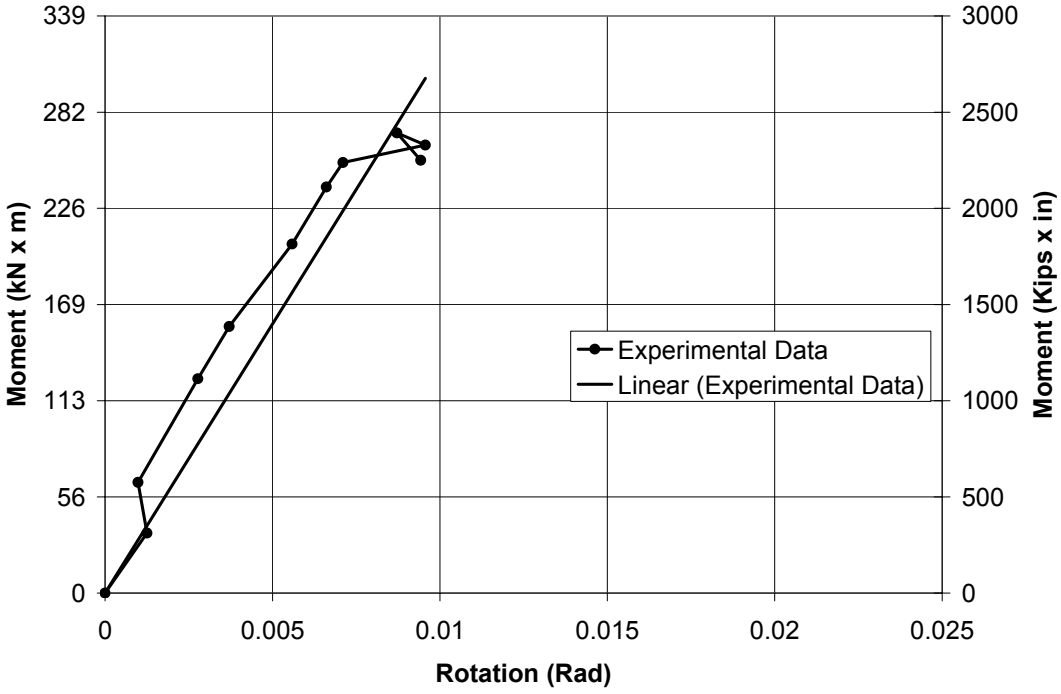

Figure 6-23 Moment vs. Rotation of the Loading Head Specimen ISH1.0

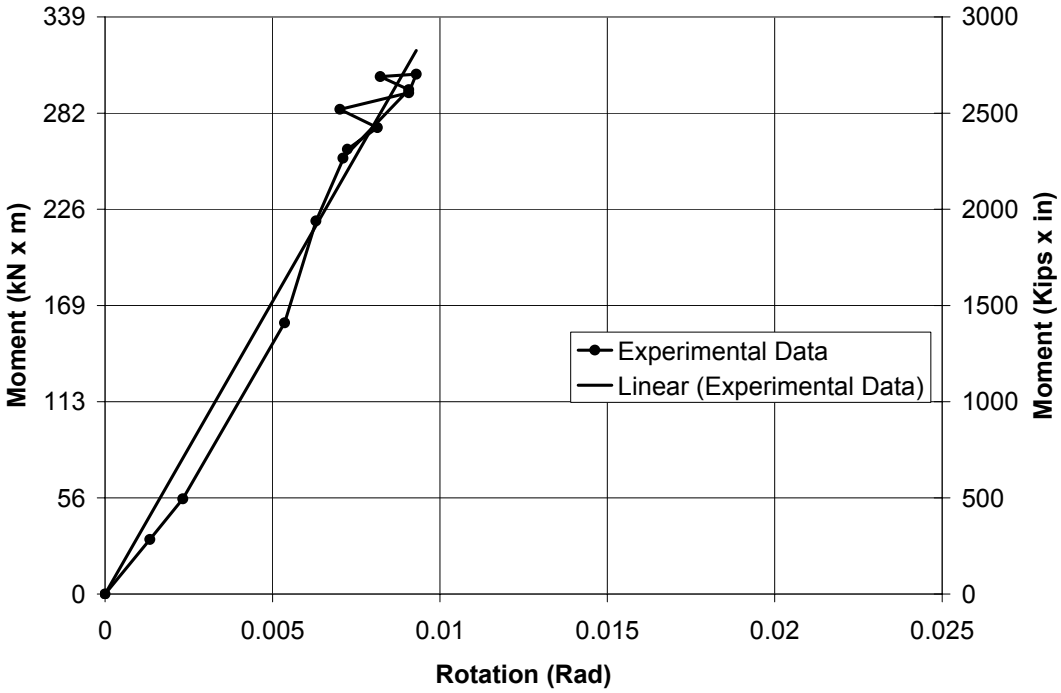

Figure 6-24 Moment vs. Rotation of the Loading Head Specimen ISH1.25

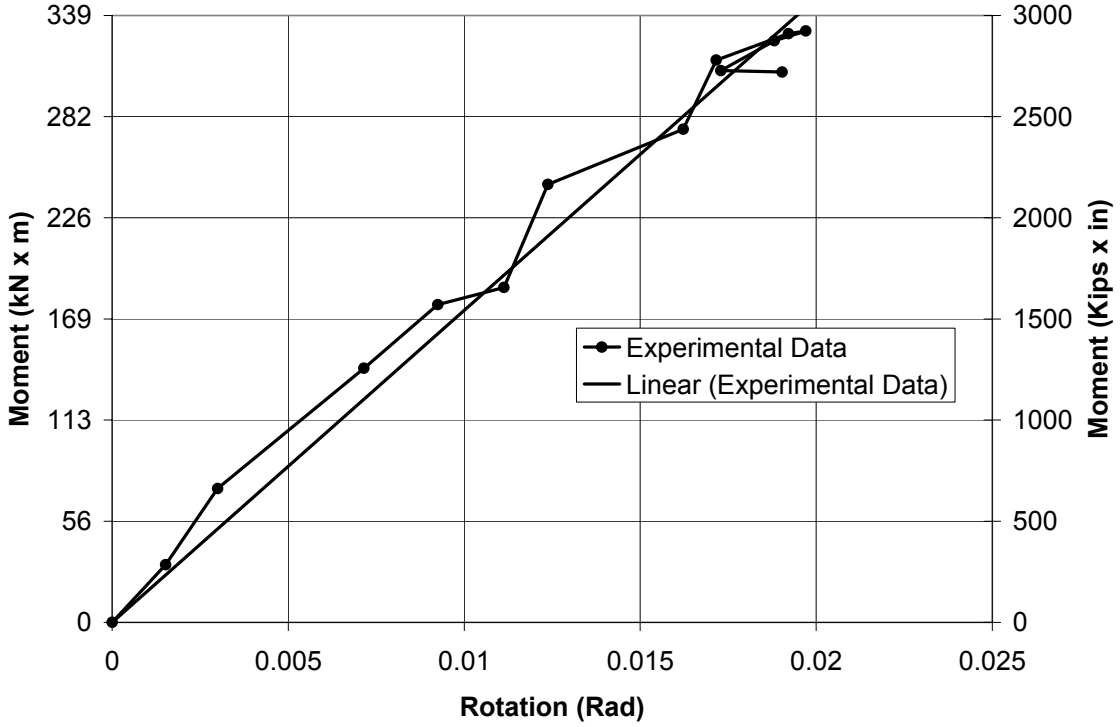

Figure 6-25 Moment vs. Rotation of the Loading Head Specimen ISH1.5

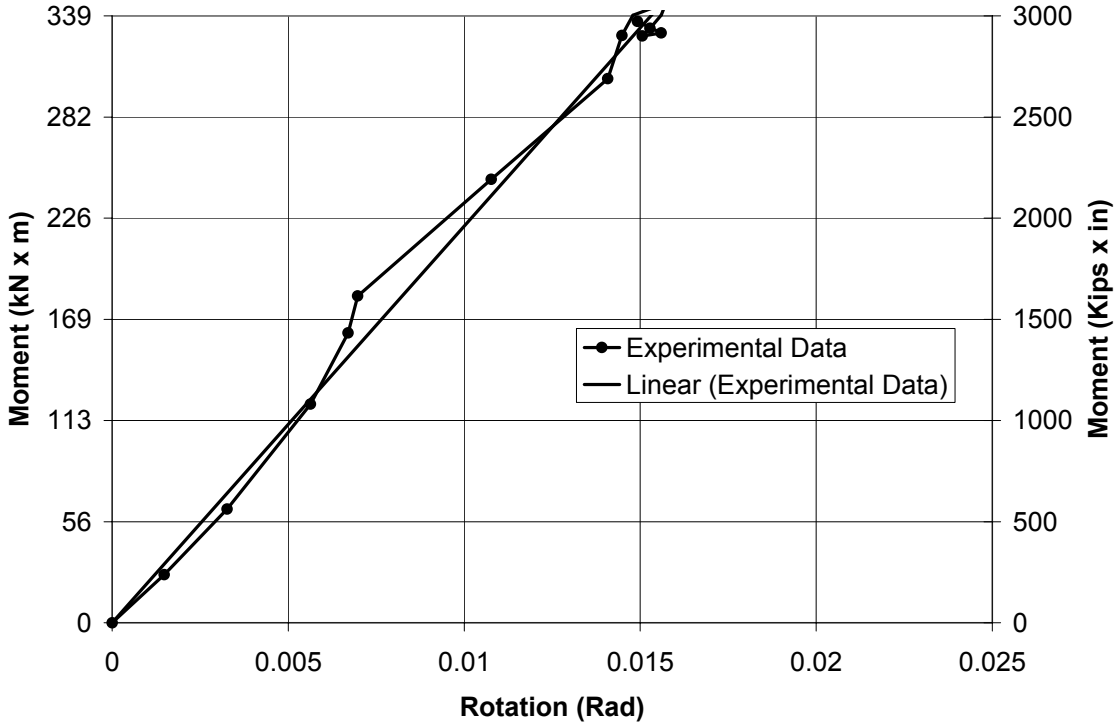

Figure 6-26 Moment vs. Rotation of the Loading Head Specimen ISH1.5T

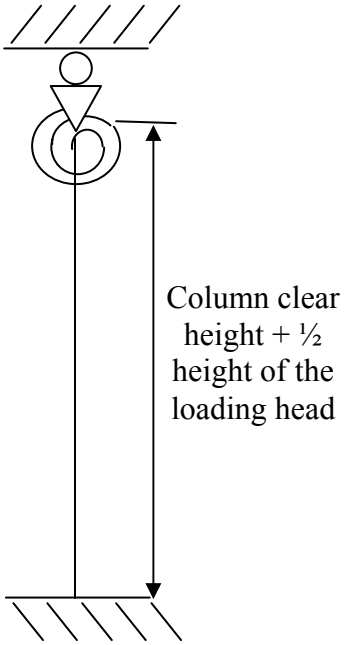

Figure 6-27 SAP 2000 Model

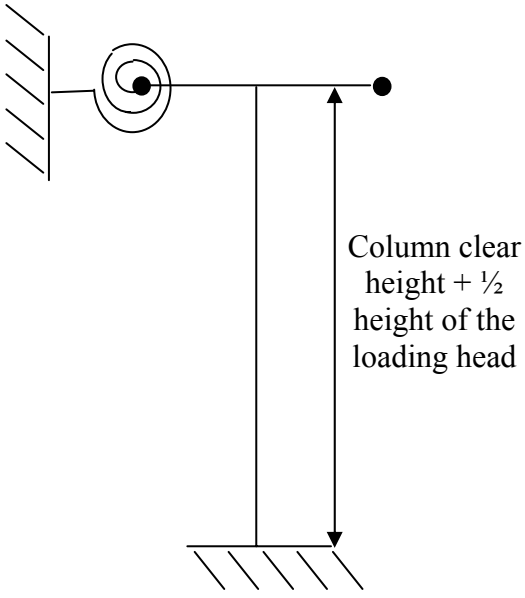

Figure 6-28 wFRAME Model

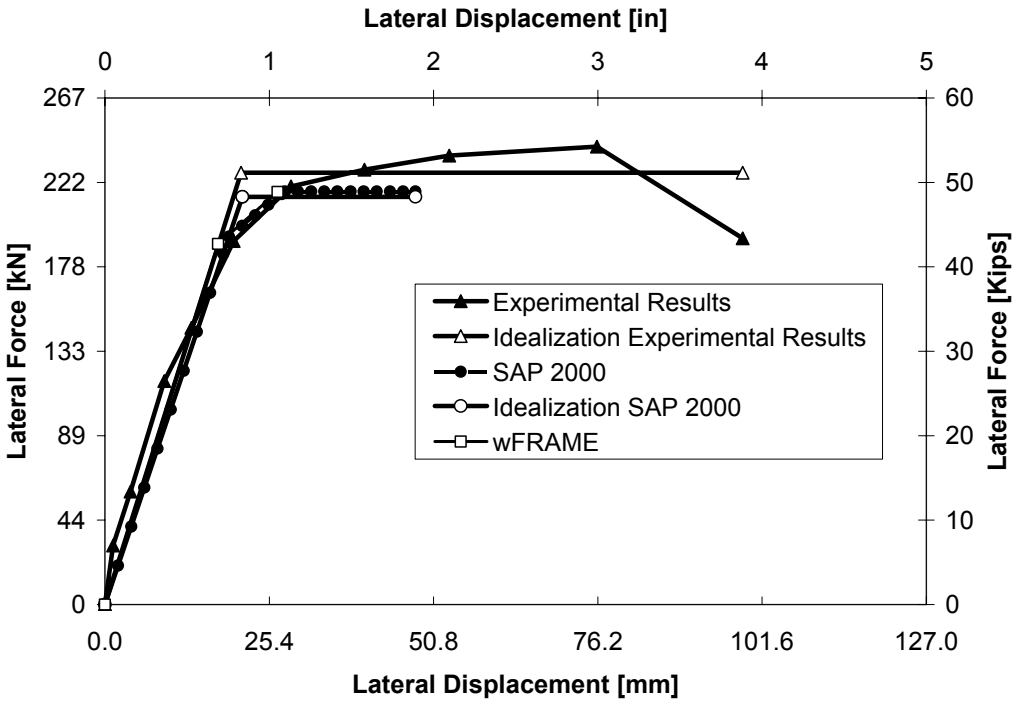

Figure 6-29 Force Displacement Curves for SAP 2000, wFRAME and Experimental Specimen ISH1.0

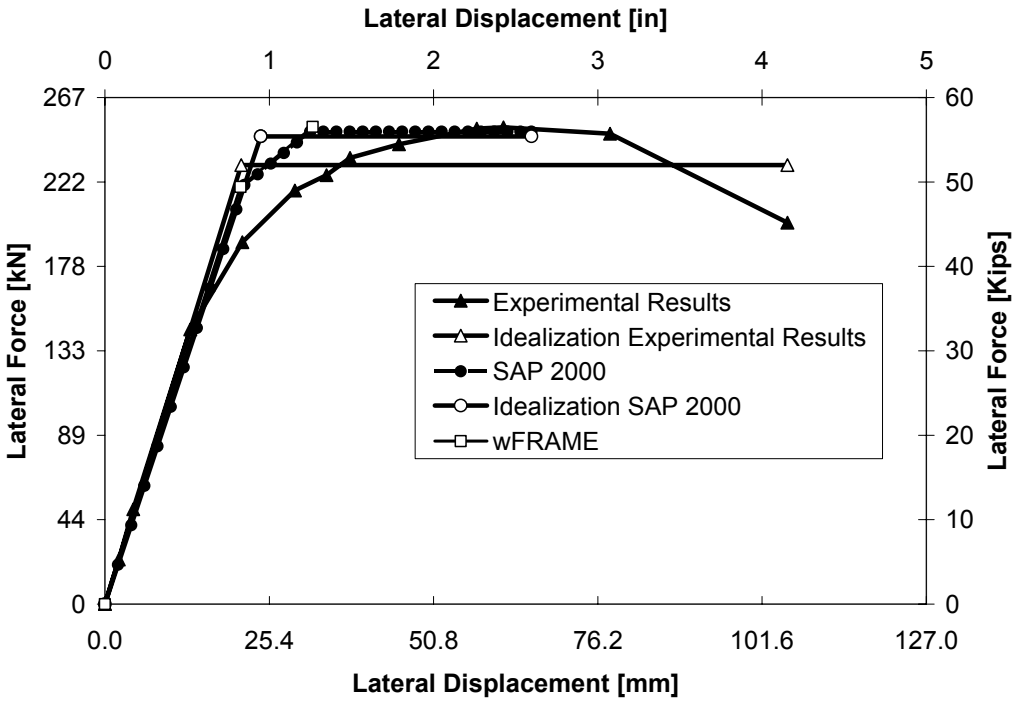

Figure 6-30 Force Displacement Curves for SAP 2000, wFRAME and Experimental Specimen ISH1.25

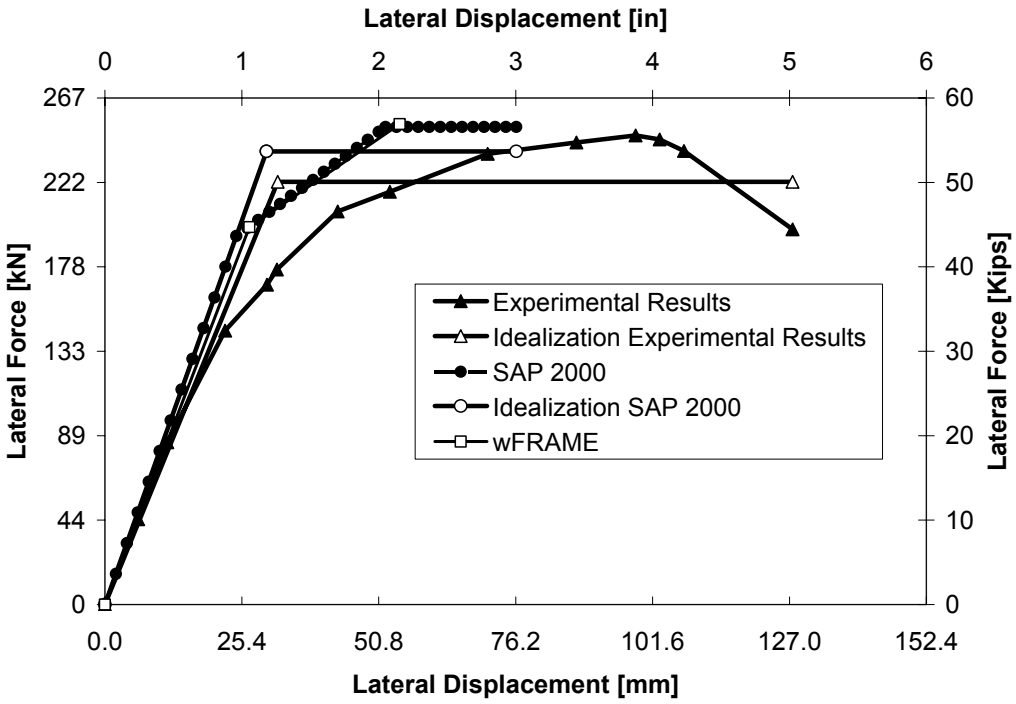

Figure 6-31 Force Displacement Curves for SAP 2000, wFRAME and Experimental Specimen ISH1.5

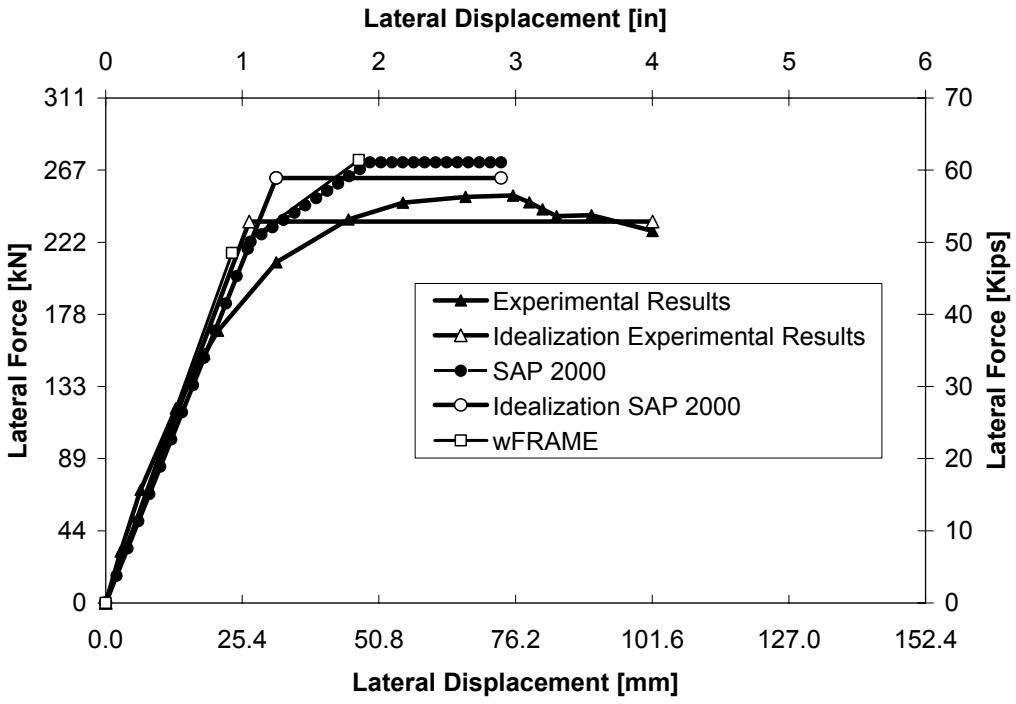

Figure 6-32 Force Displacement Curves for SAP 2000, wFRAME and Experimental Specimen ISH1.5T

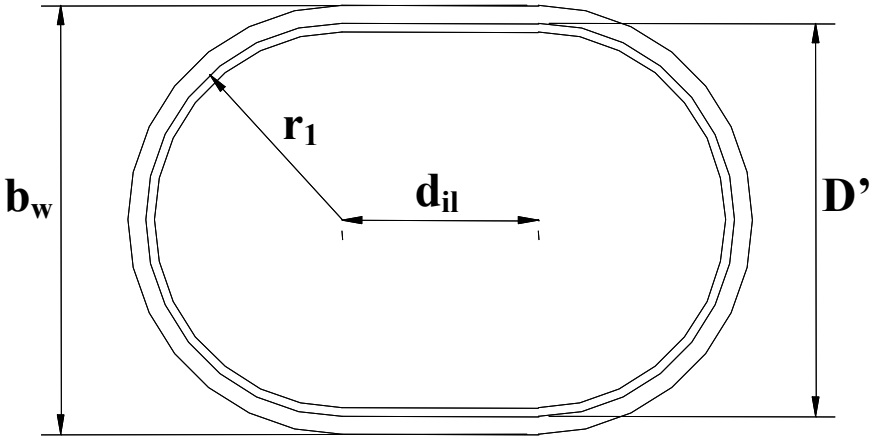

Figure 6-33 Equivalent Transversal Section by Shear Carried by Interlocking Spirals

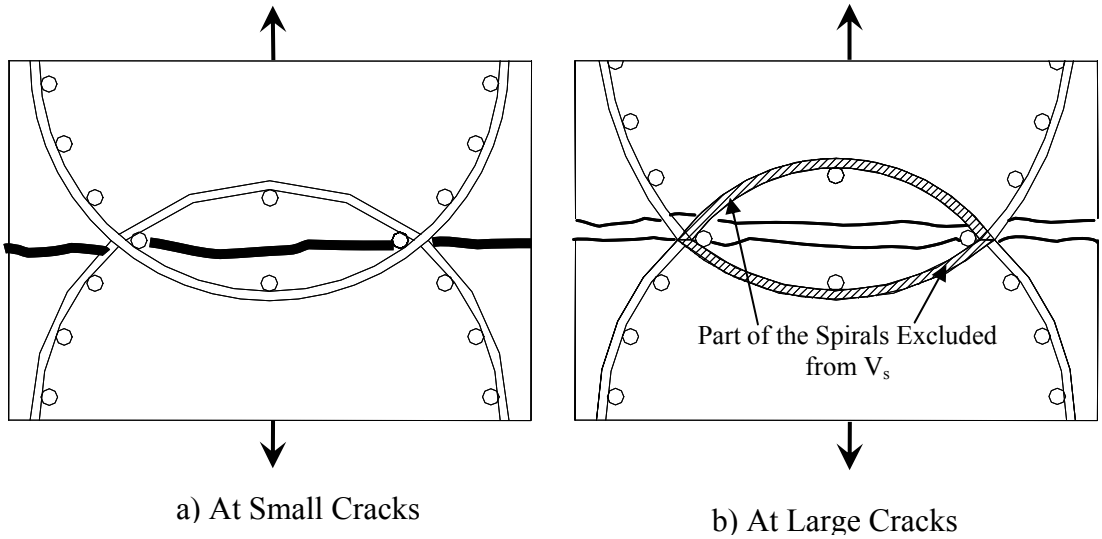

Figure 6-34 Cross Section RC Column with Interlocking Spirals

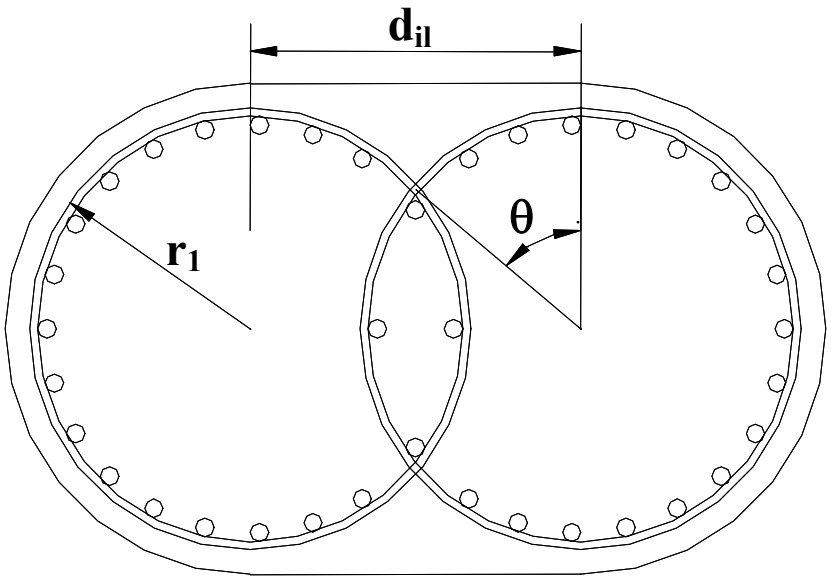

Figure 6-35 Cross Section RC Column with Interlocking Spirals

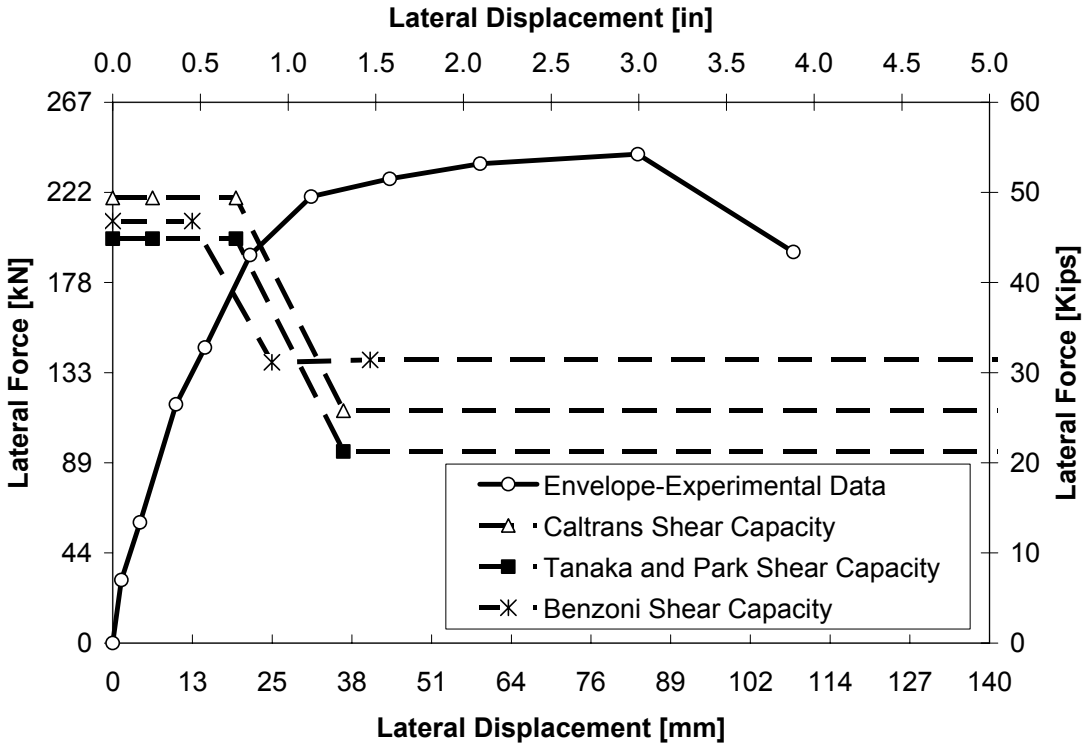

Figure 6-36 Calculated Shear Capacity Based on Flexural Displacement Ductility and Experimental Results for Specimen ISH1.0

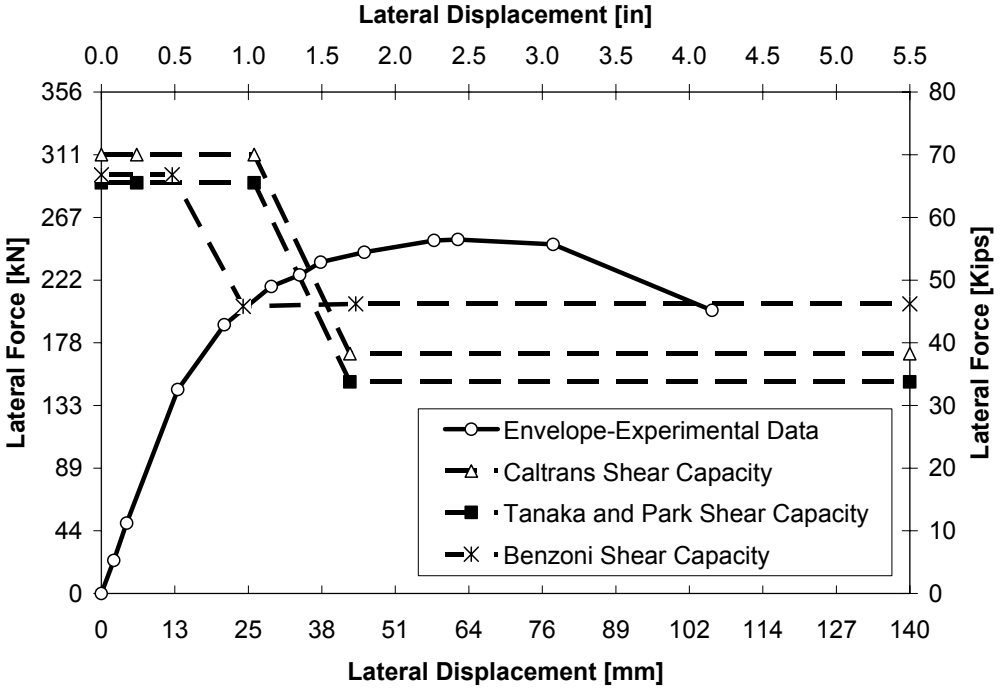

Figure 6-37 Calculated Shear Capacity Based on Flexural Displacement Ductility and Experimental Results for Specimen ISH1.25

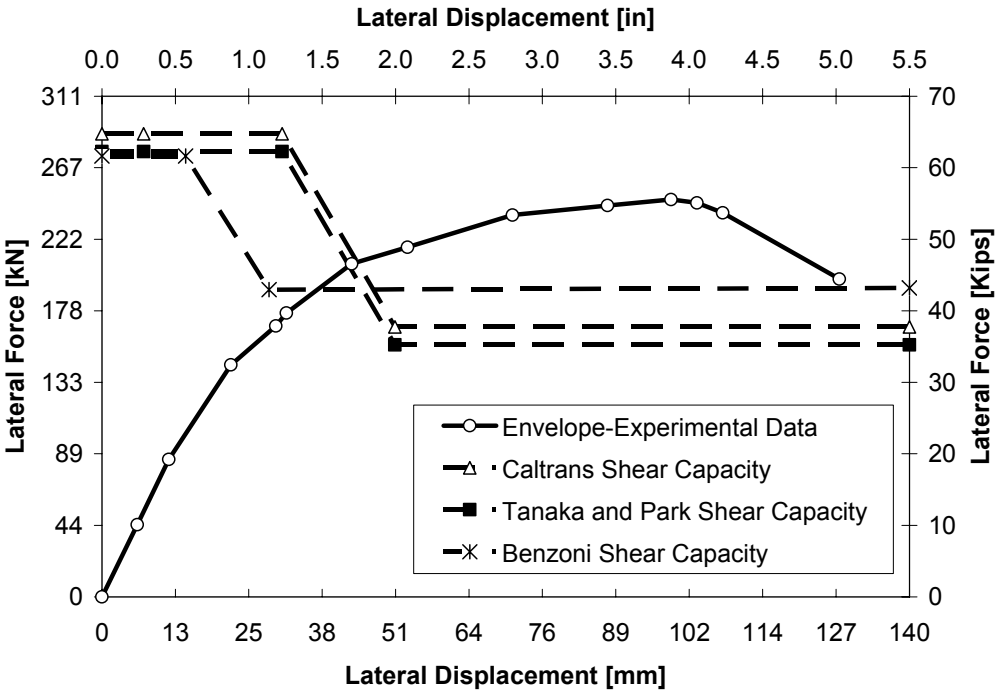

Figure 6-38 Calculated Shear Capacity Based on Flexural Displacement Ductility and Experimental Results for Specimen ISH1.5

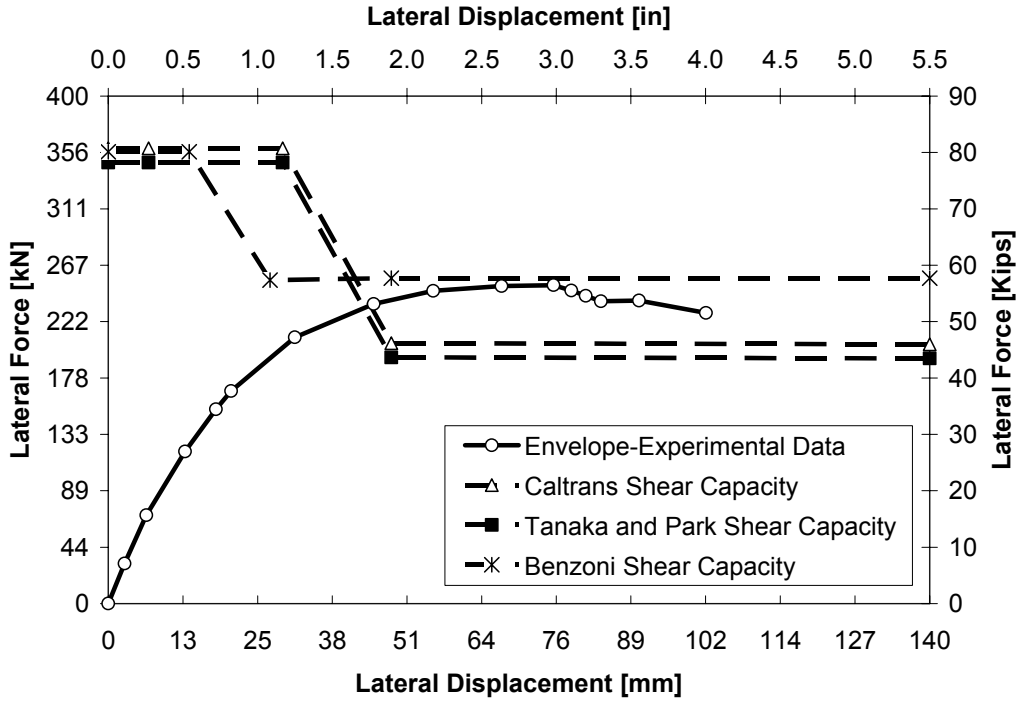

Figure 6-39 Calculated Shear Capacity Based on Flexural Displacement Ductility and Experimental Results for Specimen ISH1.5T

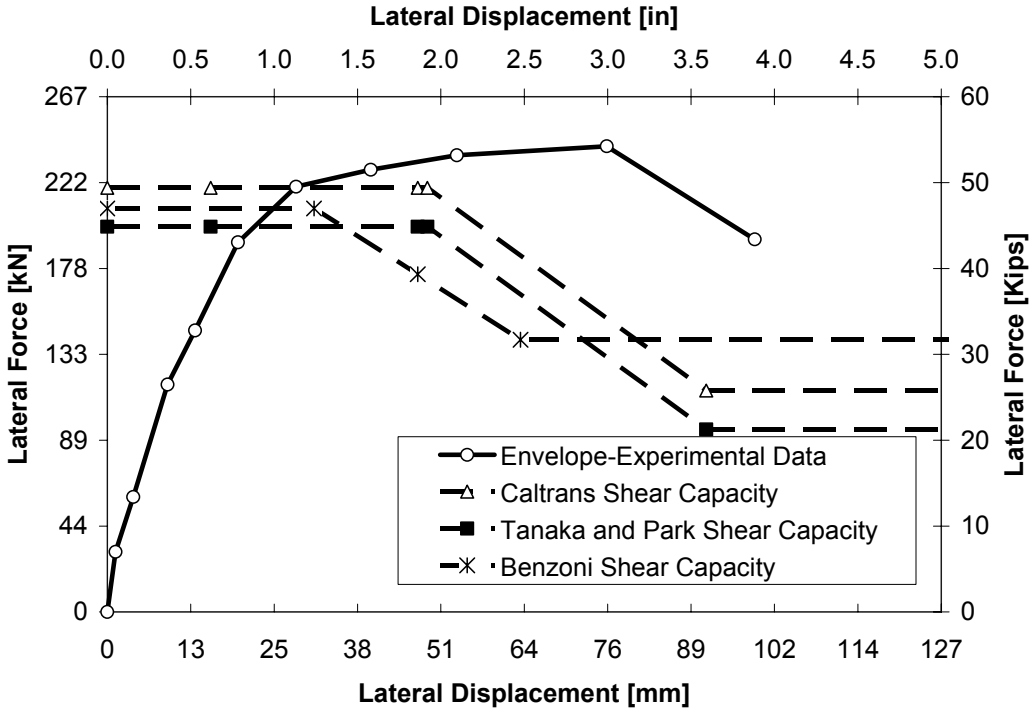

Figure 6-40 Calculated Shear Capacity Based on Flexural, Bond Slip and Shear Displacement Ductility and Experimental Results for Specimen ISH1.0

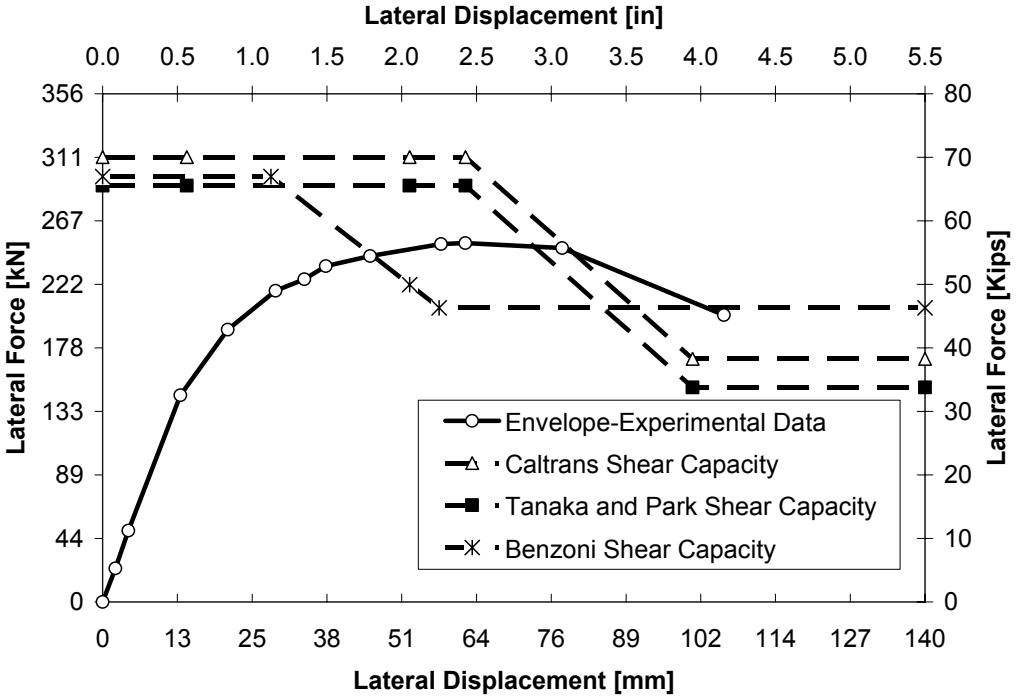

Figure 6-41 Calculated Shear Capacity Based on Flexural, Bond Slip and Shear Displacement Ductility and Experimental Results for Specimen ISH1.25

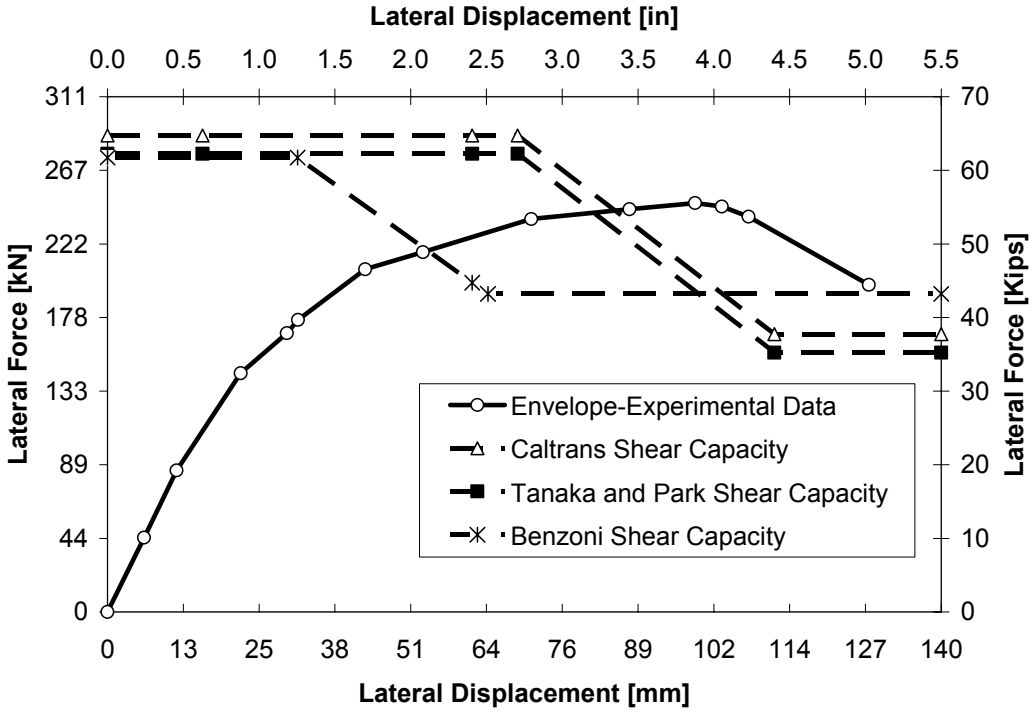

Figure 6-42 Calculated Shear Capacity Based on Flexural, Bond Slip and Shear Displacement Ductility and Experimental Results for Specimen ISH1.5

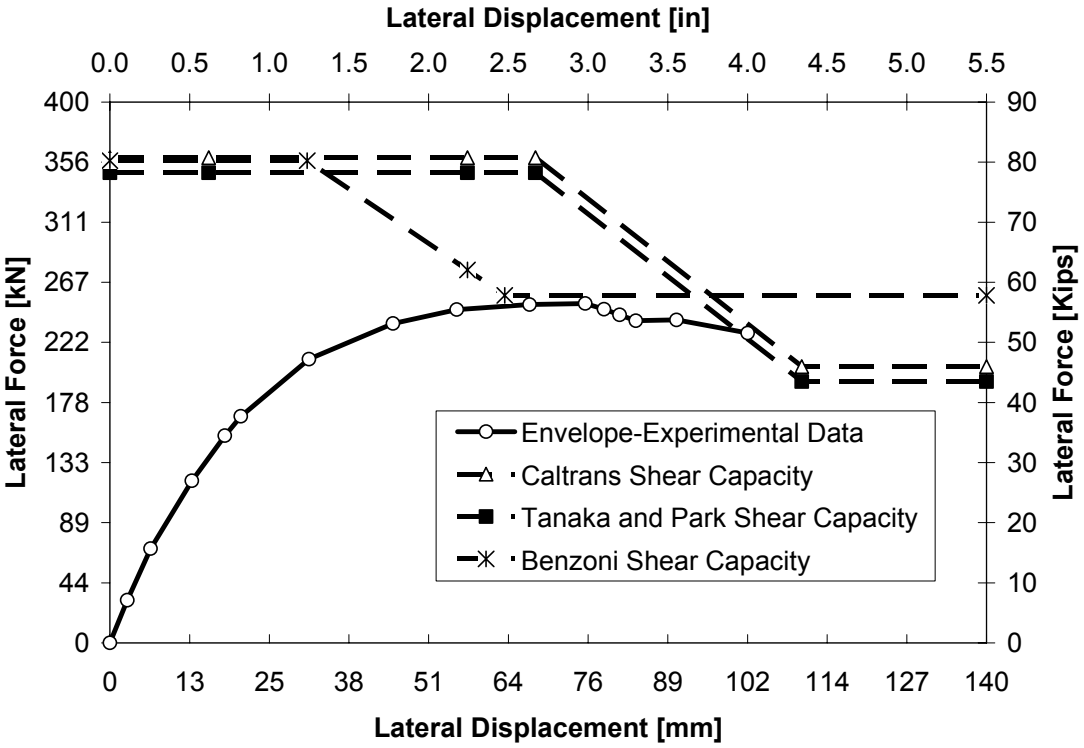

Figure 6-43 Calculated Shear Capacity Based on Flexural, Bond Slip and Shear Displacement Ductility and Experimental Results for Specimen ISH1.5T

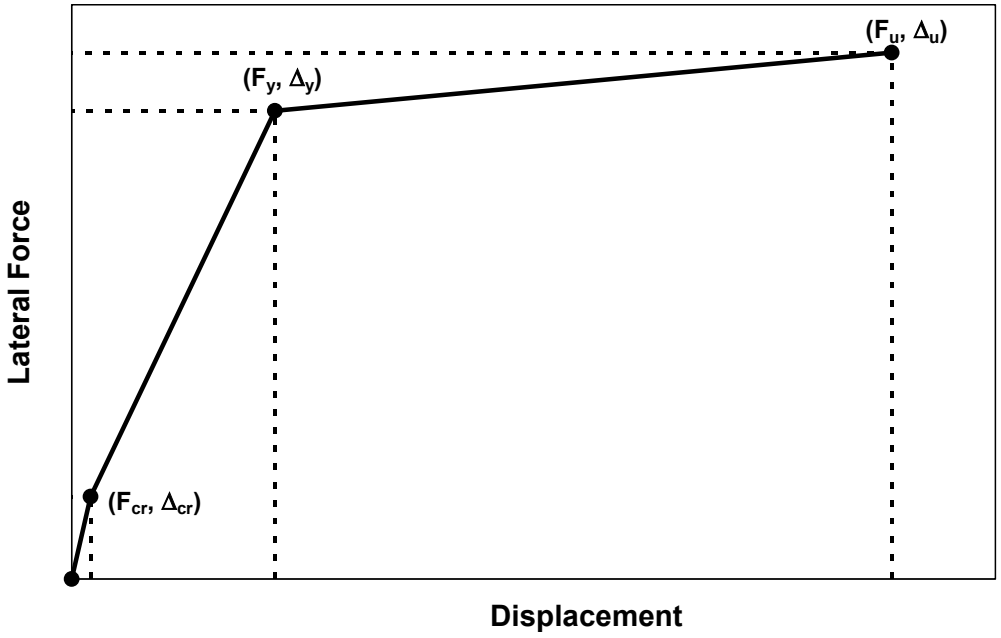

Figure 6-44 Tri- Linear Idealization of Flexural Deformation

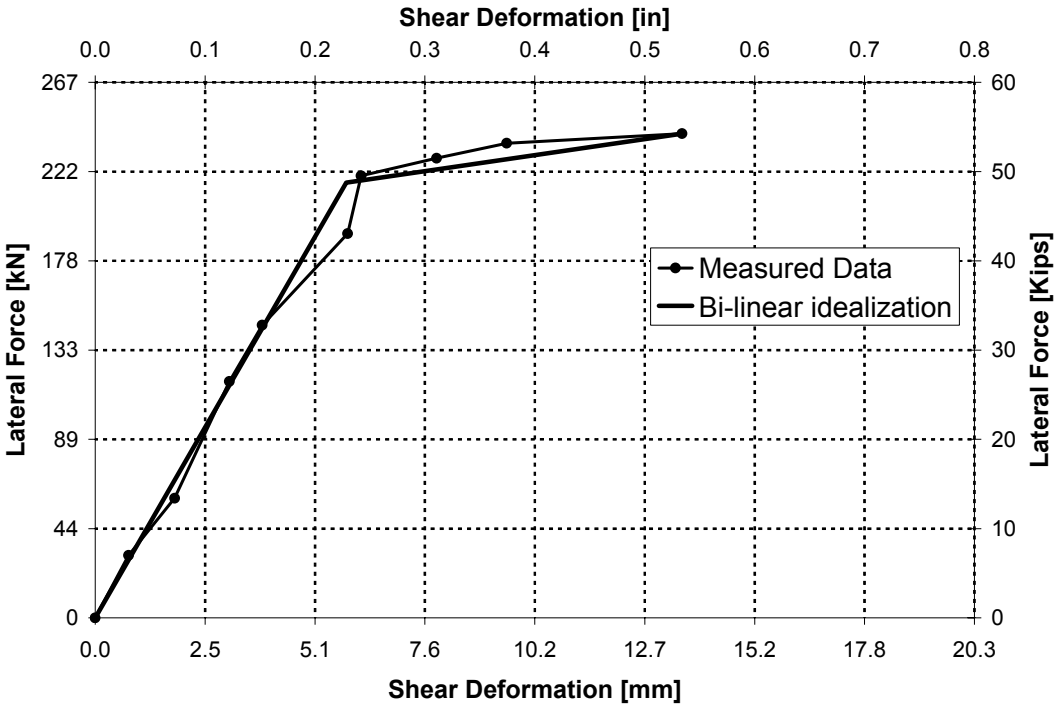

Figure 6-45 Lateral Force vs. Shear Deformation ISH1.0

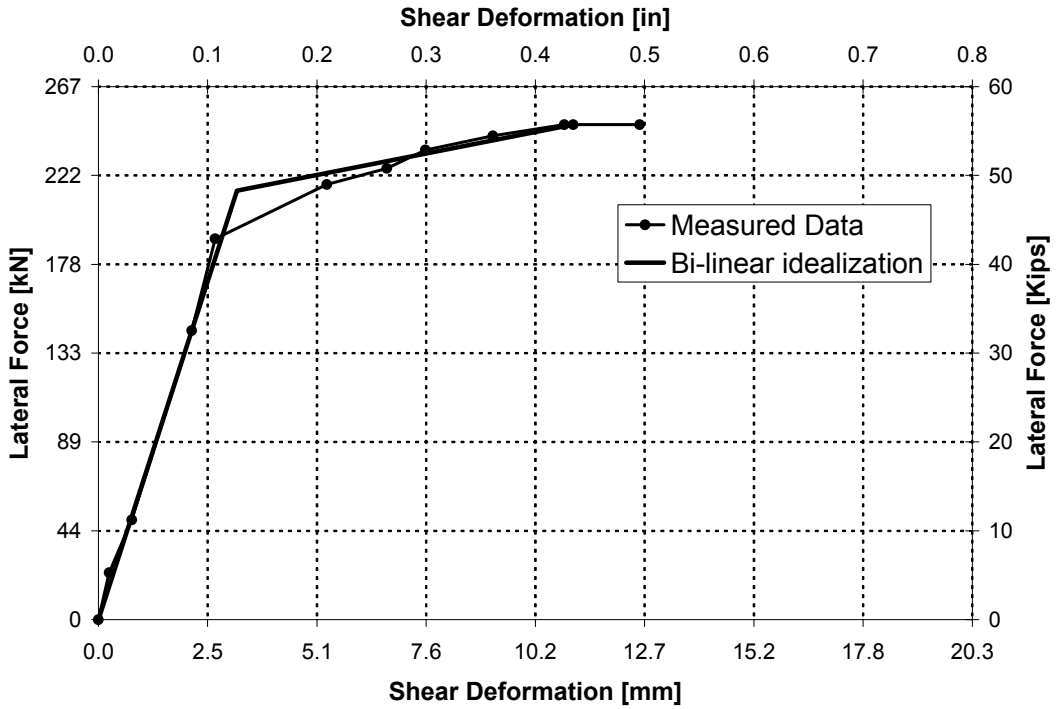

Figure 6-46 Lateral Force vs. Shear Deformation ISH1.25

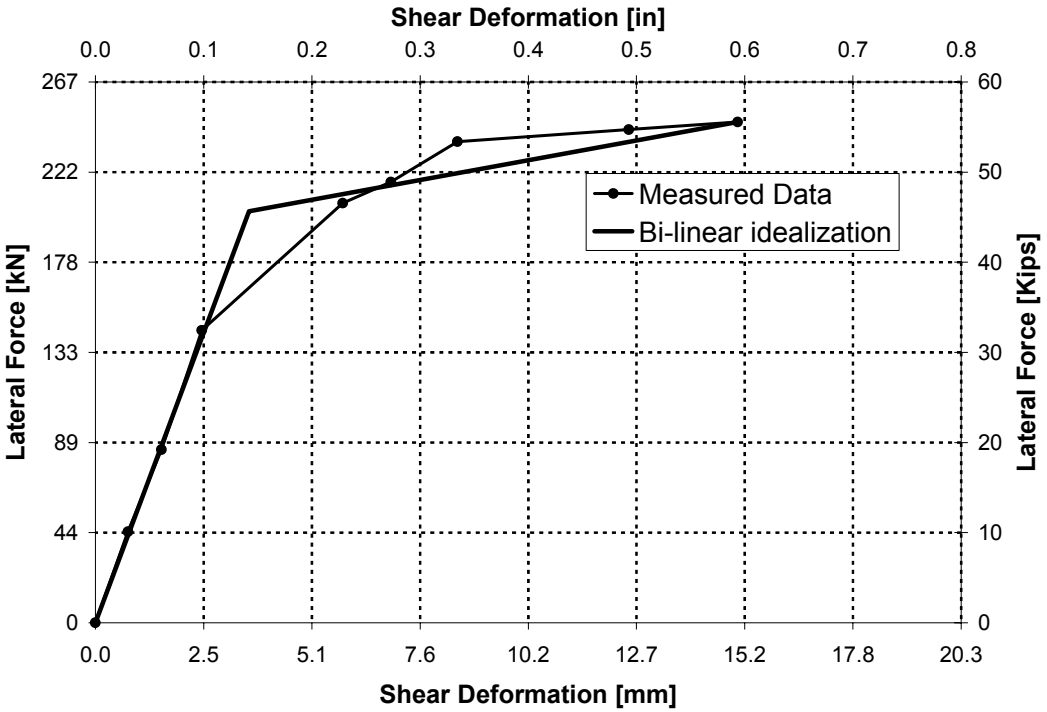

Figure 6-47 Lateral Force vs. Shear Deformation ISH1.5

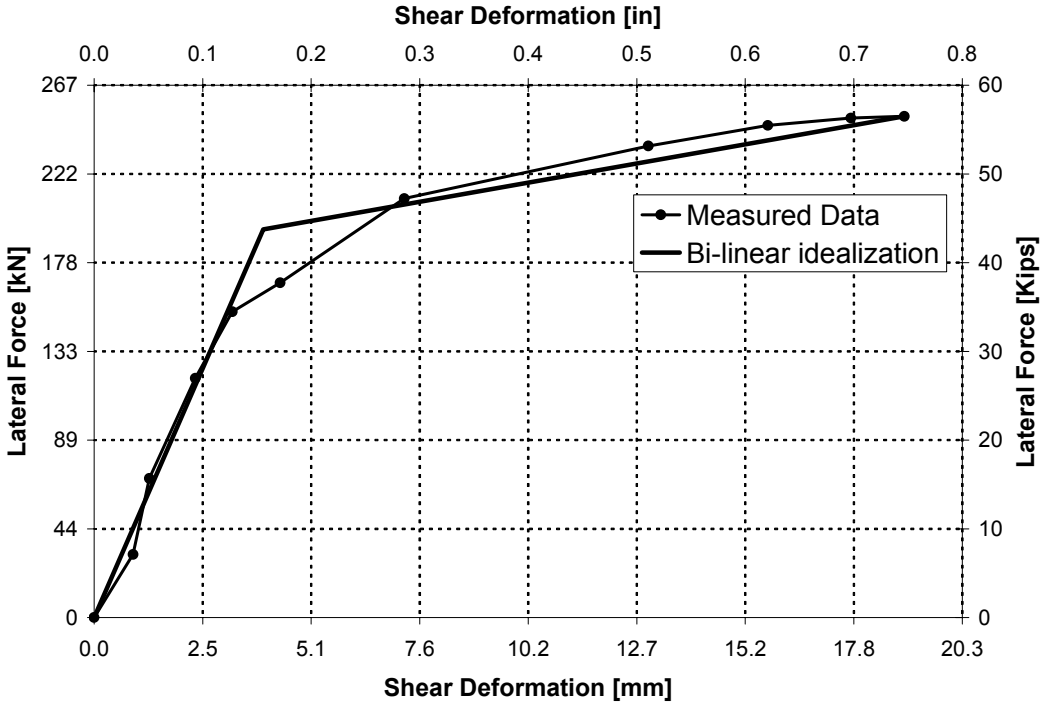

Figure 6-48 Lateral Force vs. Shear Deformation ISH1.5T

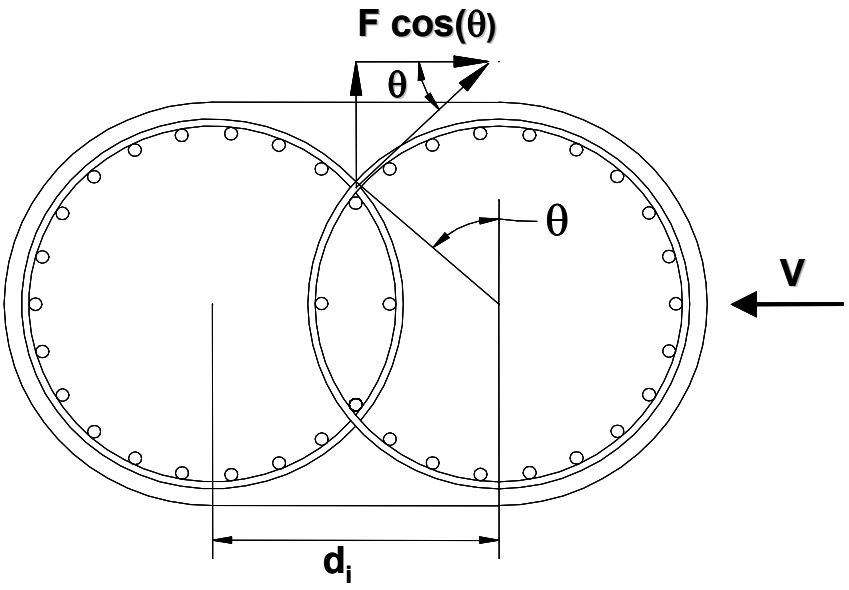

Figure 6-49 Horizontal Component of the Spiral Force at the Middepth of Column Section

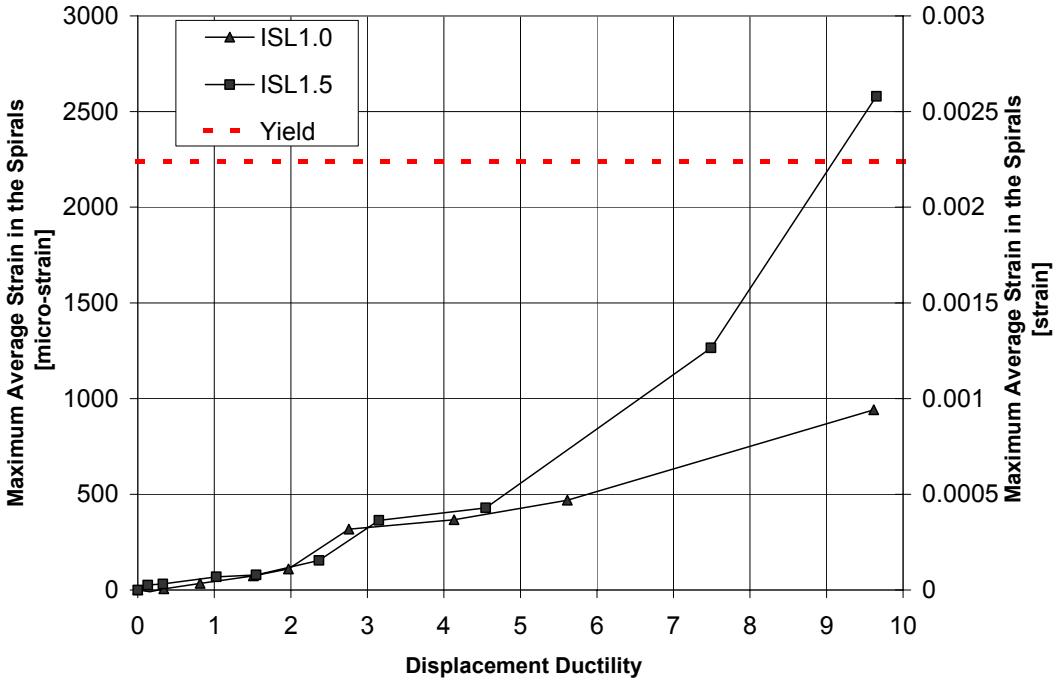

Figure 6-50 Maximum Average Strain in the Spirals Specimens ISL1.0 and ISL1.5

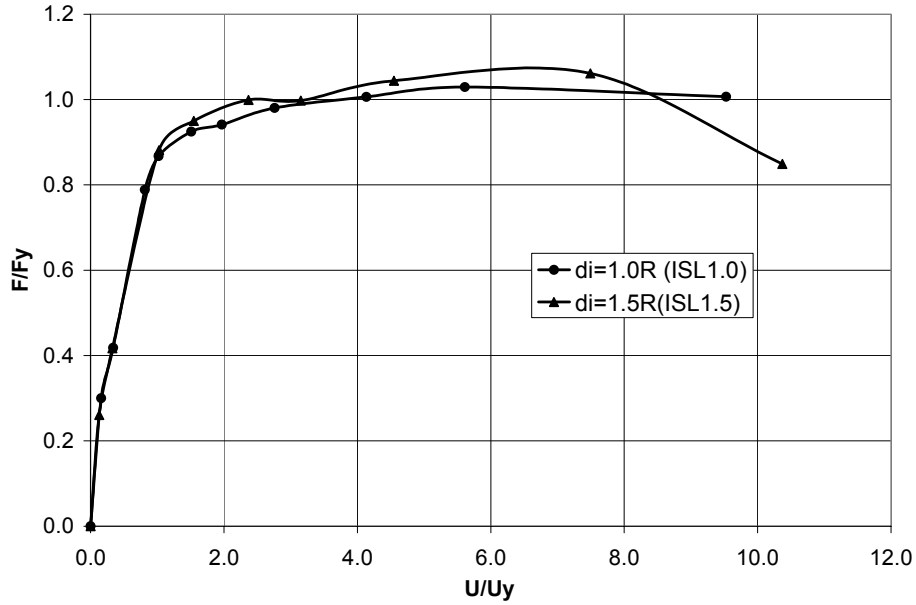

Figure 6-51 Normalized Lateral Force and Displacement for Specimens with Low Shear and d_i of 1.0R and 1.5R

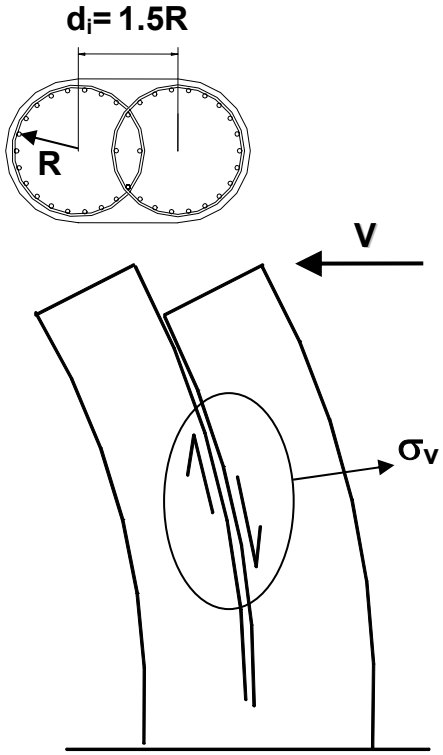

Figure 6-52 Vertical Stress due to the Separate Two Column Action

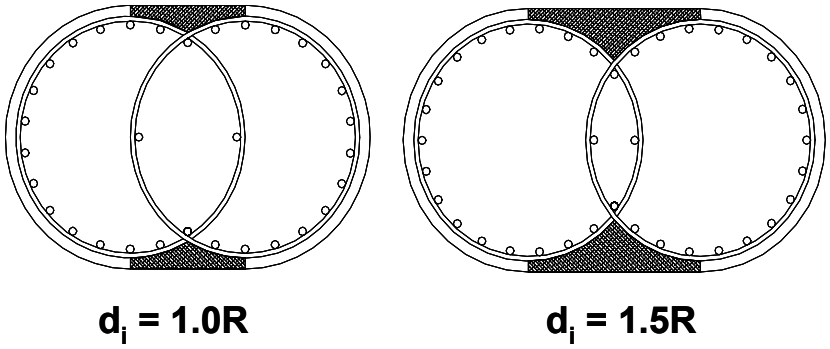

Figure 6-53 Comparison of Plain Concrete at the Interlocking Region for Columns with d_i of 1.0R and 1.5R

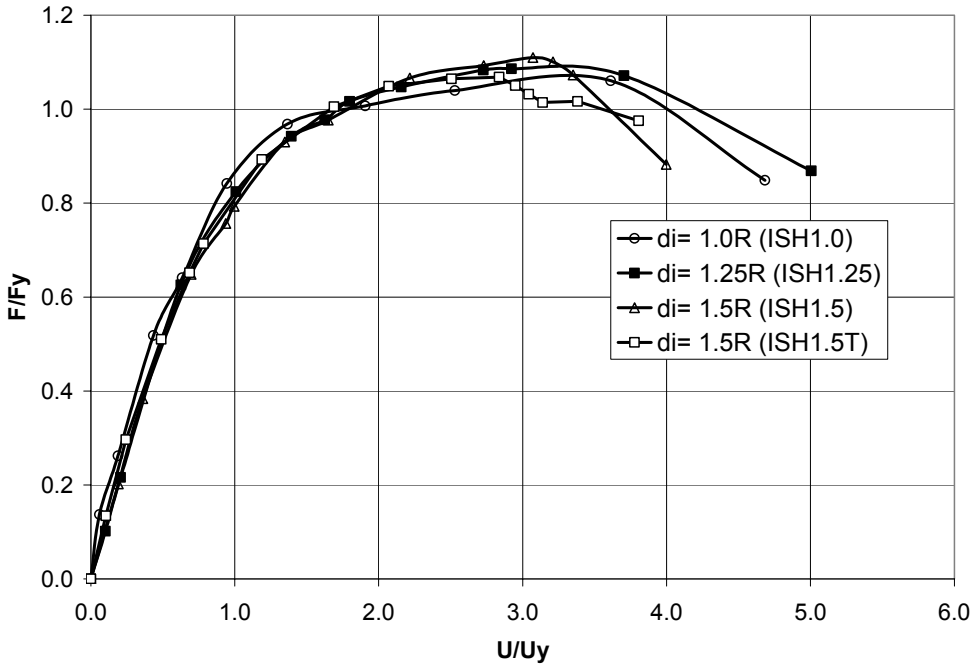

Figure 6-54 Normalized Lateral Force and Displacement for Specimens with High Shear and d_i of 1.0R. 1.25R, 1.5R and 1.5R with Cross Ties

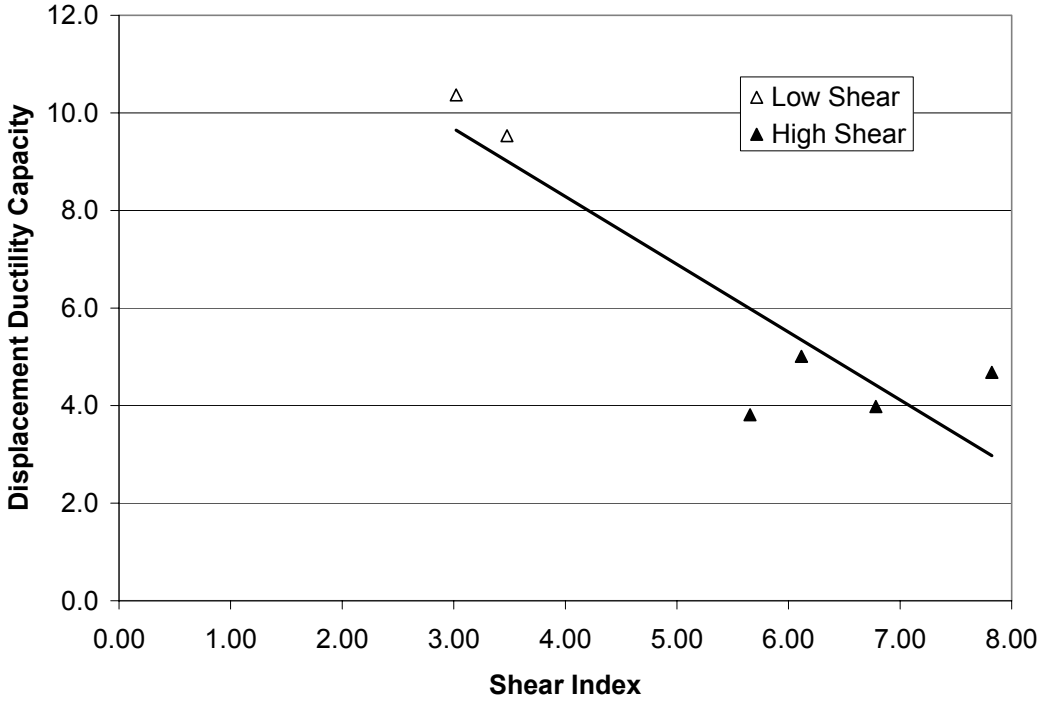

Figure 6-55 Displacement Ductility Capacity vs. Average Shear Stress Index

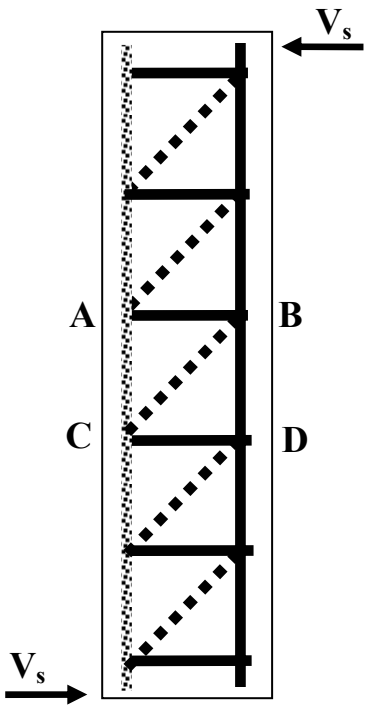

Figure 7-1 Analogous Truss for Shear

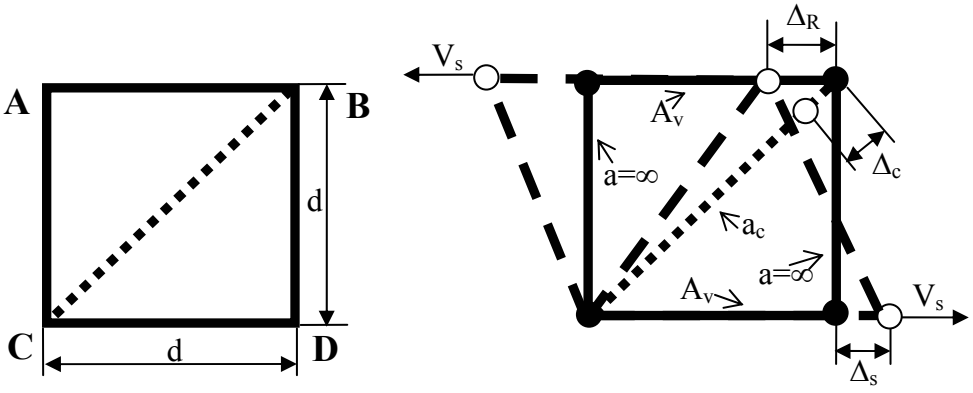

Figure 7-2 Analogous Truss for Shear and Shear Distortion

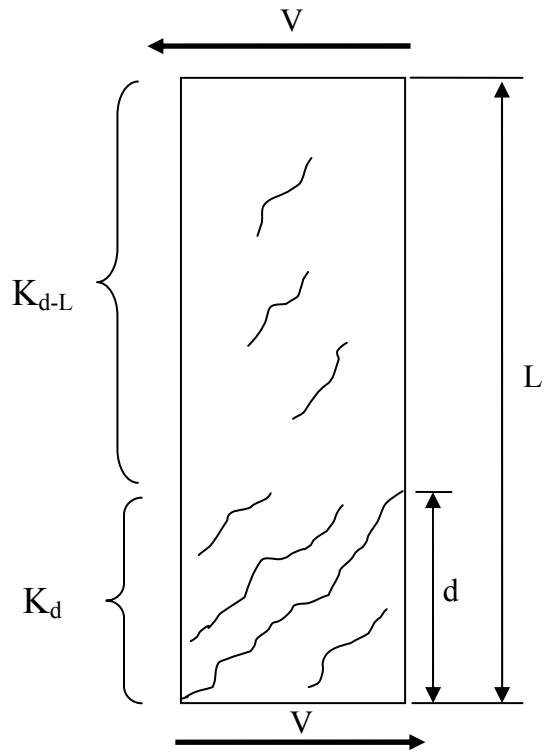

Figure 7-3 Modified Shear Stiffness Model

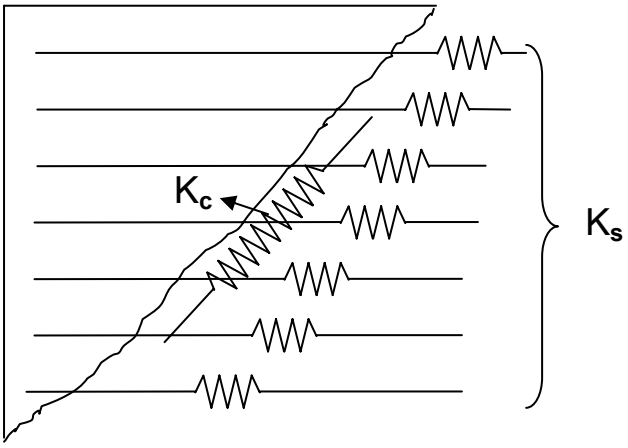

Figure 7-4 Axial Stiffness of the Spirals and Diagonal shear Friction Model

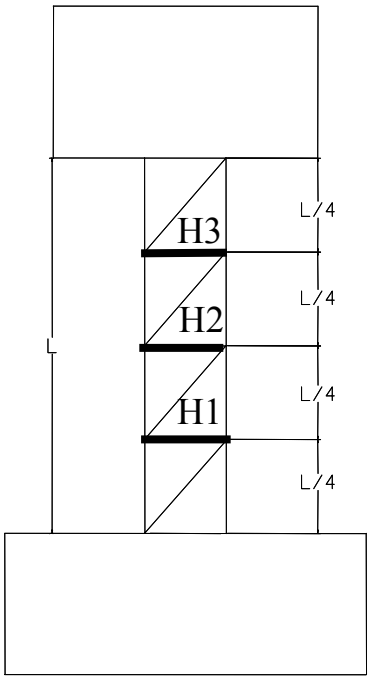

Figure 7-5 Horizontal Transducer of the Panel Instrumentation

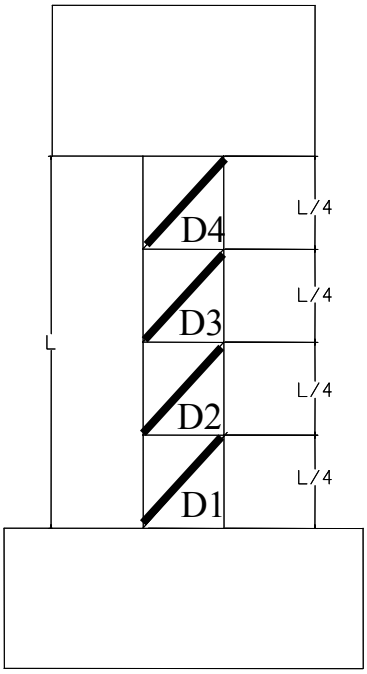

Figure 7-6 Diagonal Transducer of the Panel Instrumentation

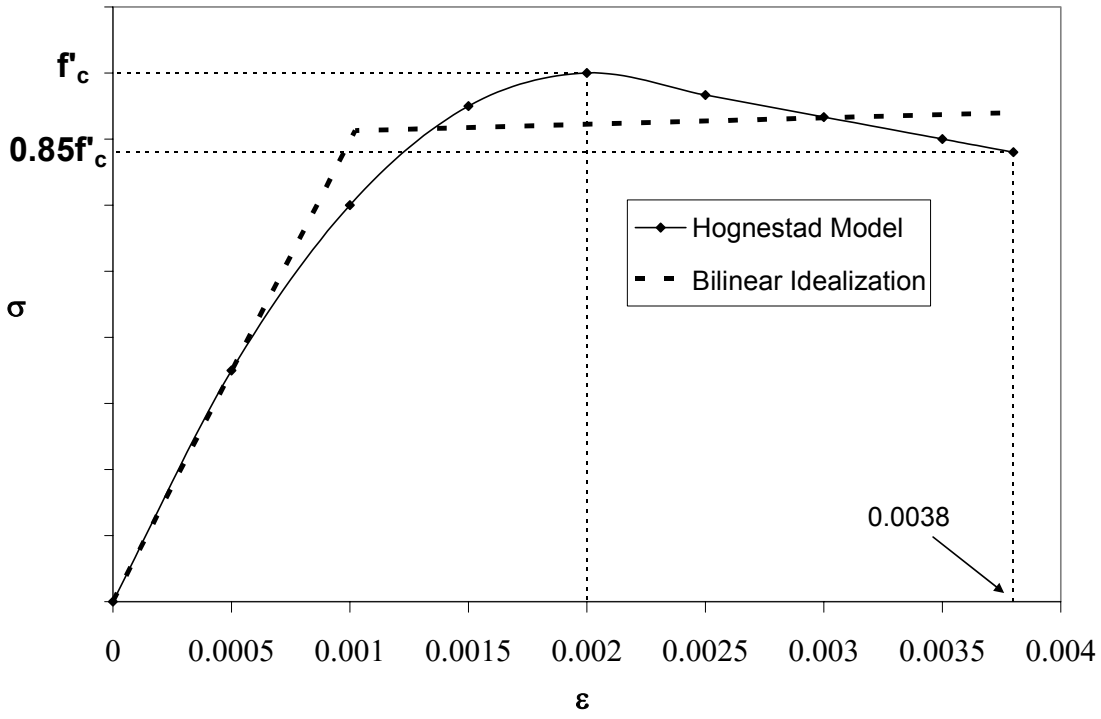

Figure 7-7 Hognestad Model and Idealized Curve

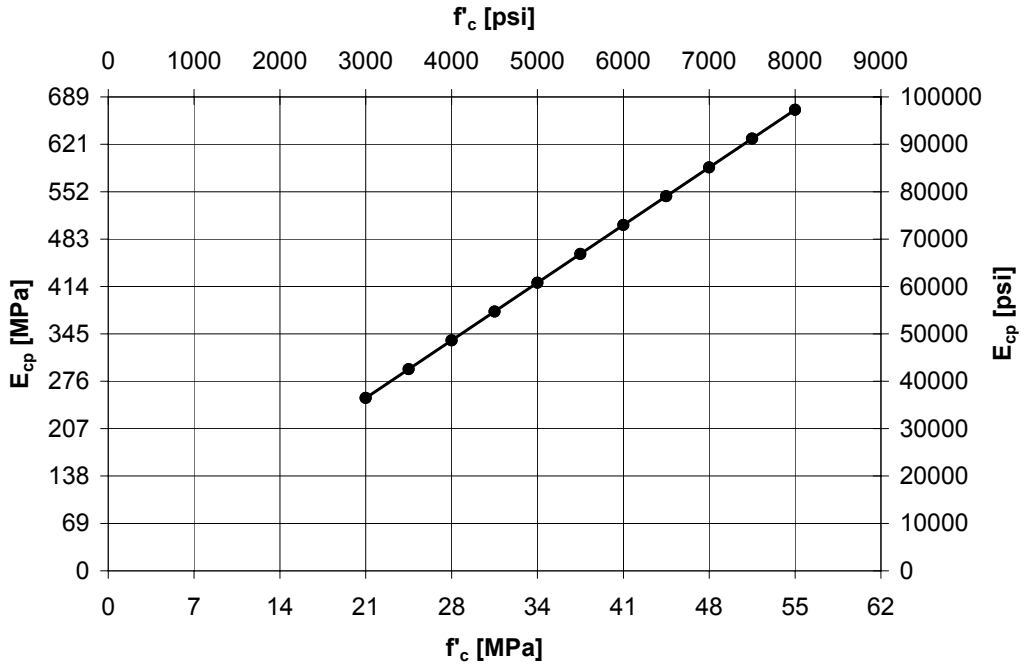

Figure 7-8 Second Slope from the Idealized Hognestad Model, E_{cp}, versus f'_c

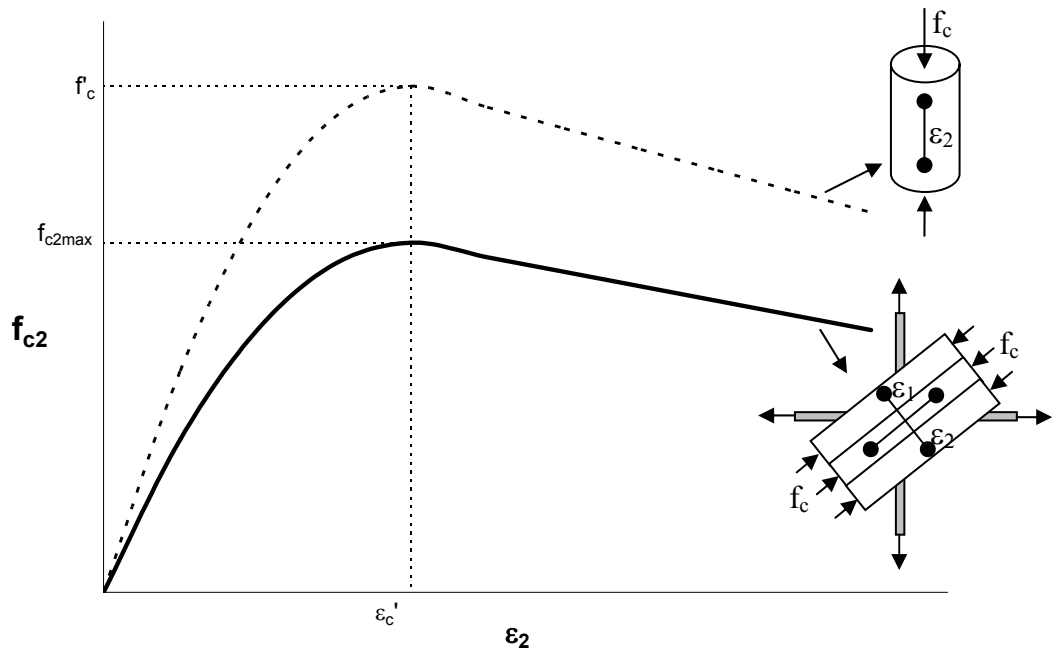

Figure 7-9 Stress-Strain Relationship for Cracked Concrete in Compression

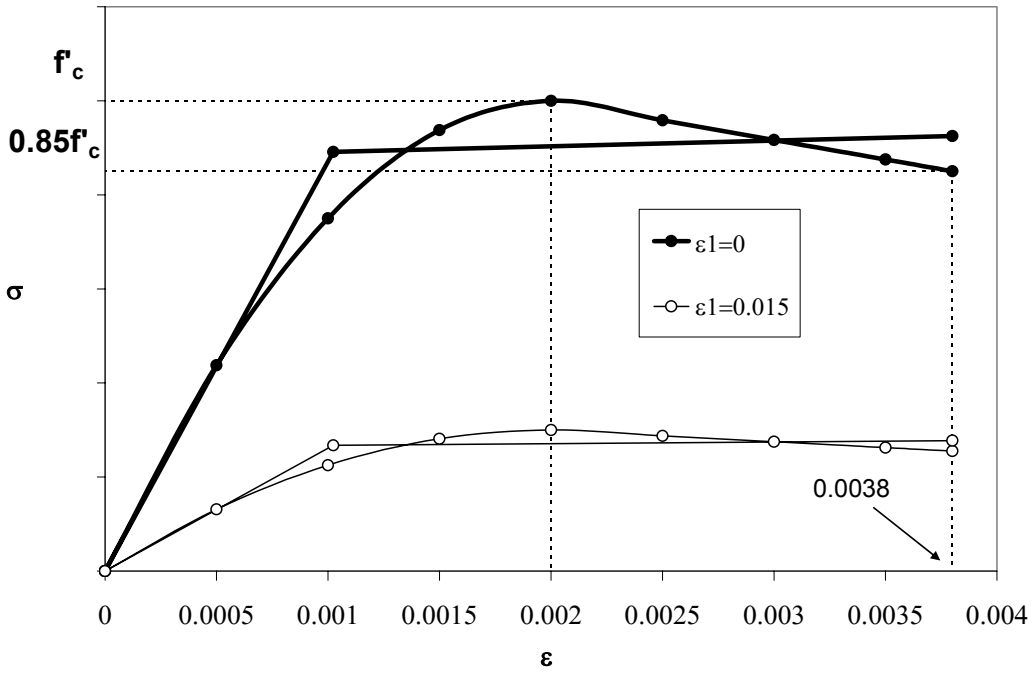

Figure 7-10 Stress-Strain Relationship for Cracked Concrete with Tensile Strain, ε_1 of 0 and 0.015

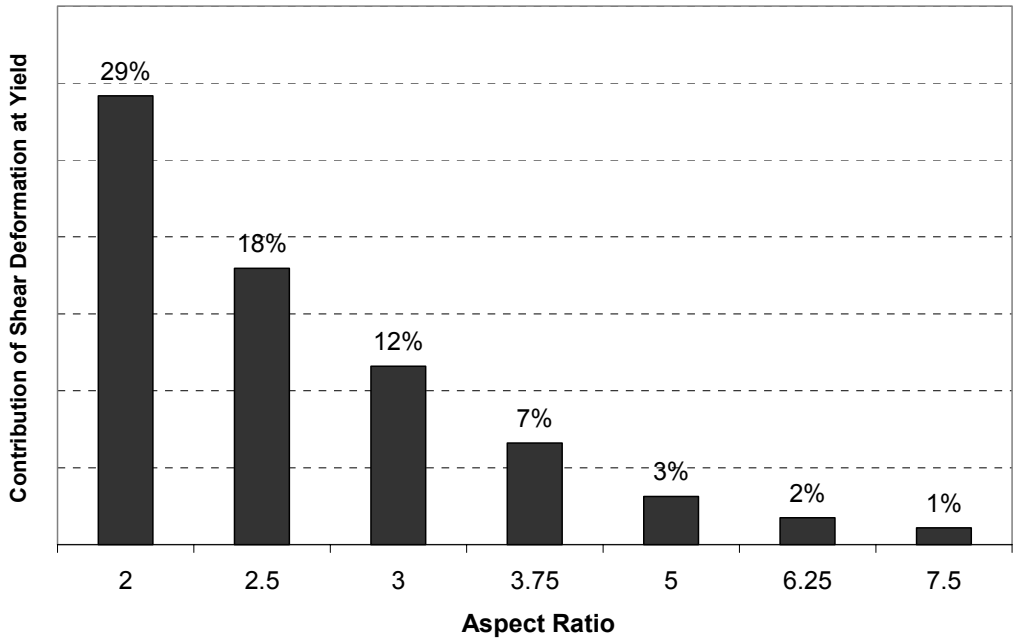

Figure 7-11 Contribution of Yield Deformation Due to Shear to the Total Yield Deformation for Different Aspect Ratios

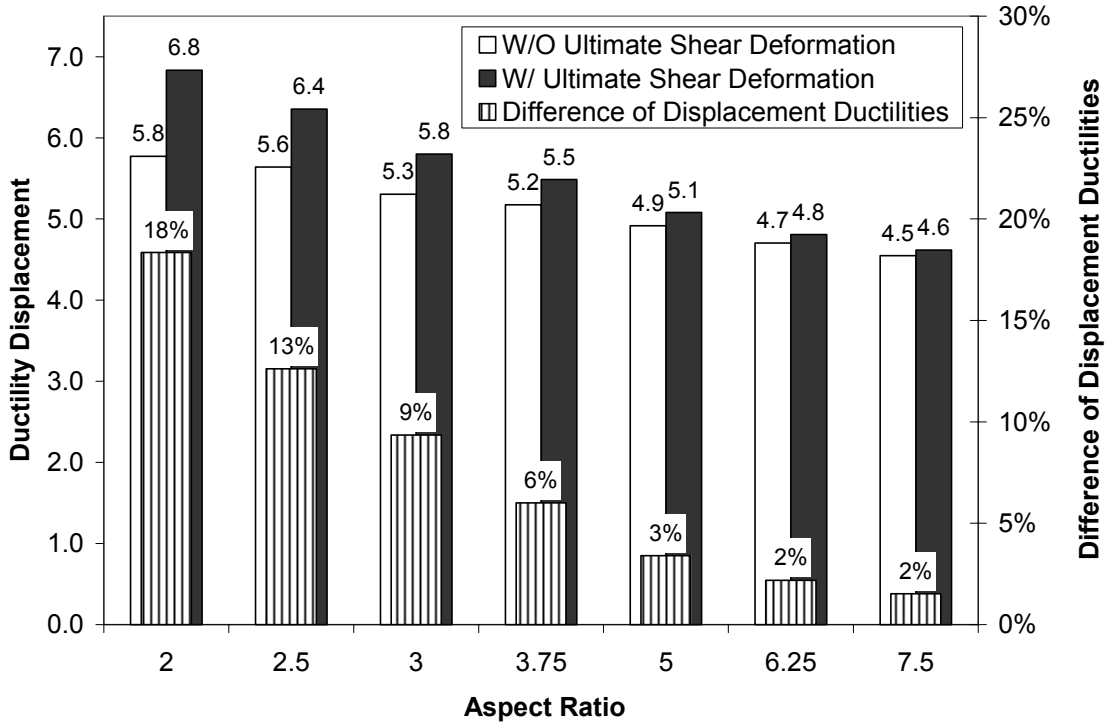

Figure 7-12 Effect of the Ultimate Shear Deformation on the Displacement Ductility Capacity for Different Aspect Ratios

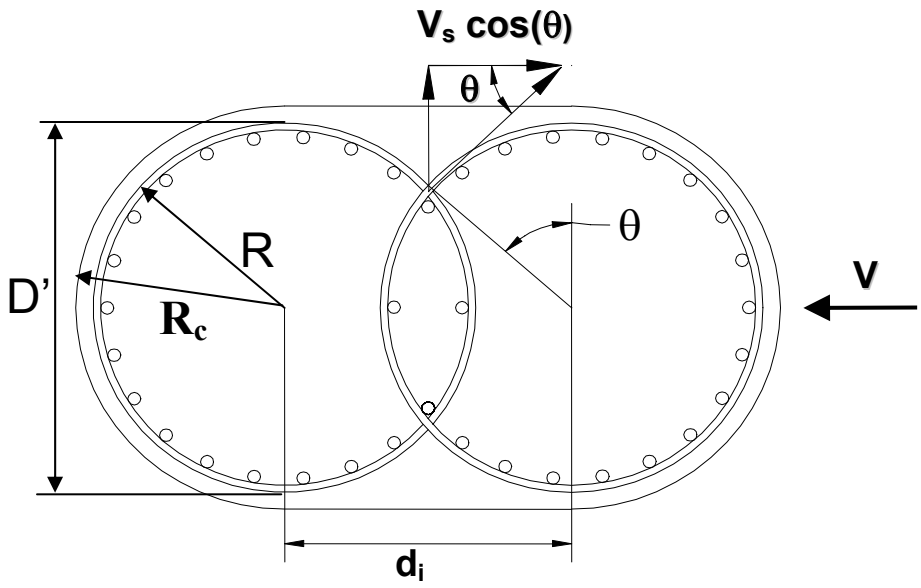

Figure 8-1 Horizontal Component of the Spiral Force at the Middepth of Column Section

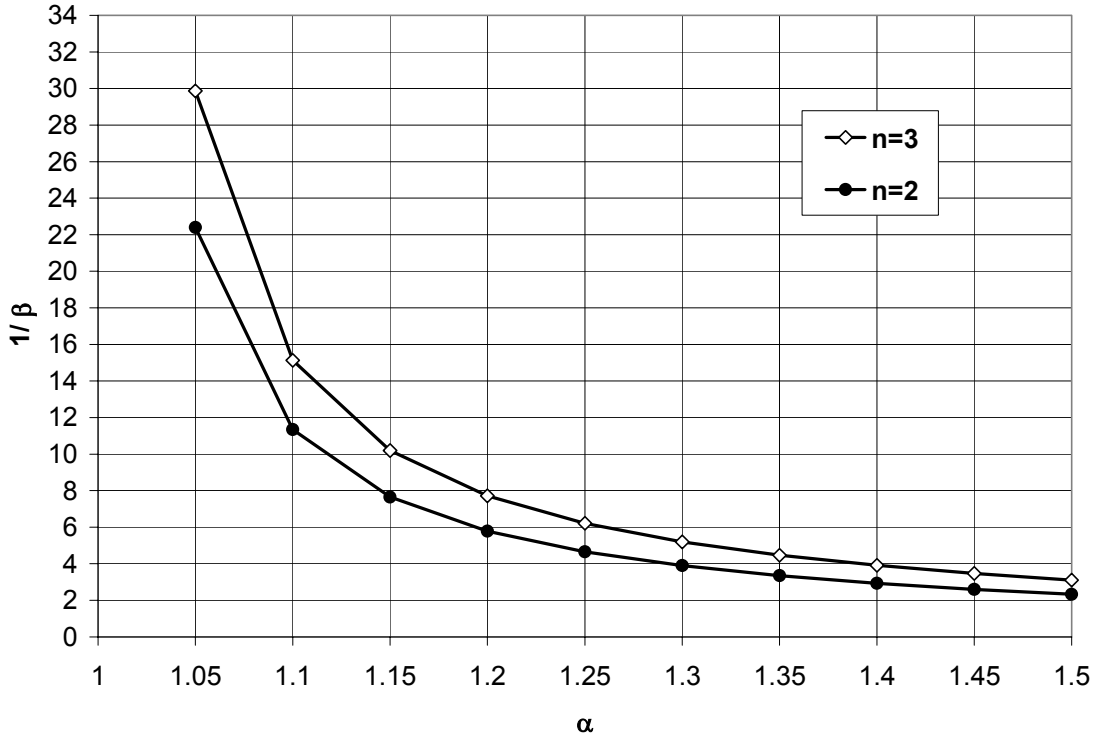

Figure 8-2 Spacing of the Cross Ties as a Function of the Spacing of the Spirals (1/β) versus d_i in terms of the Spiral Radius (α) "Shear Capacity Method"

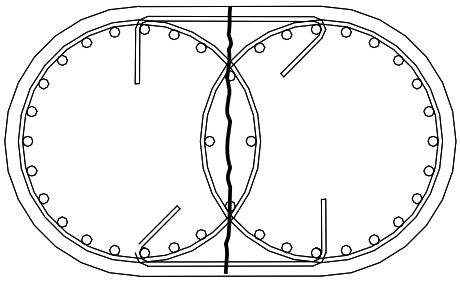

Section A-A

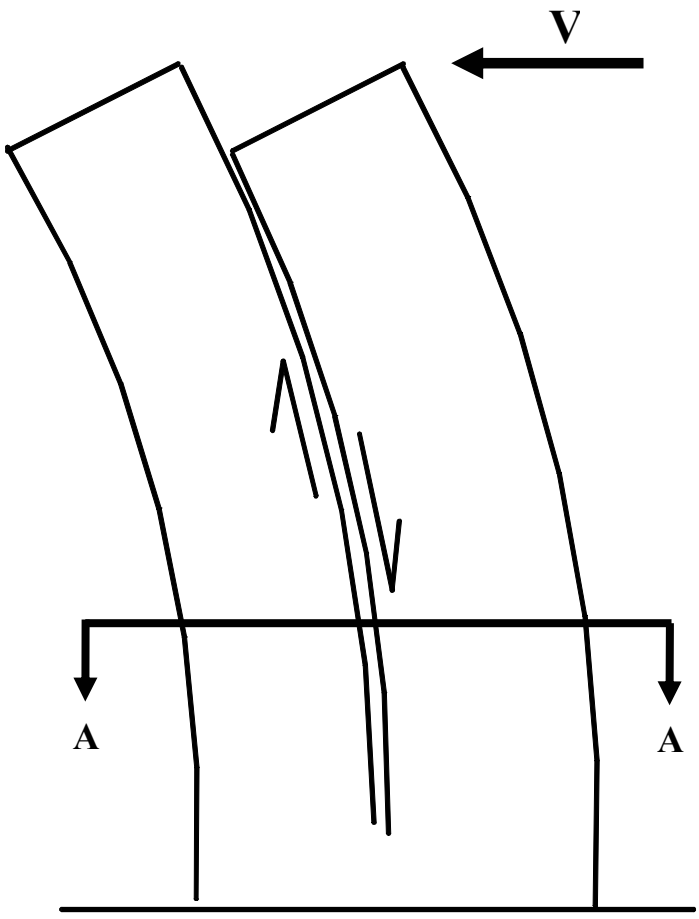

Figure 8-3 Shear Friction Method

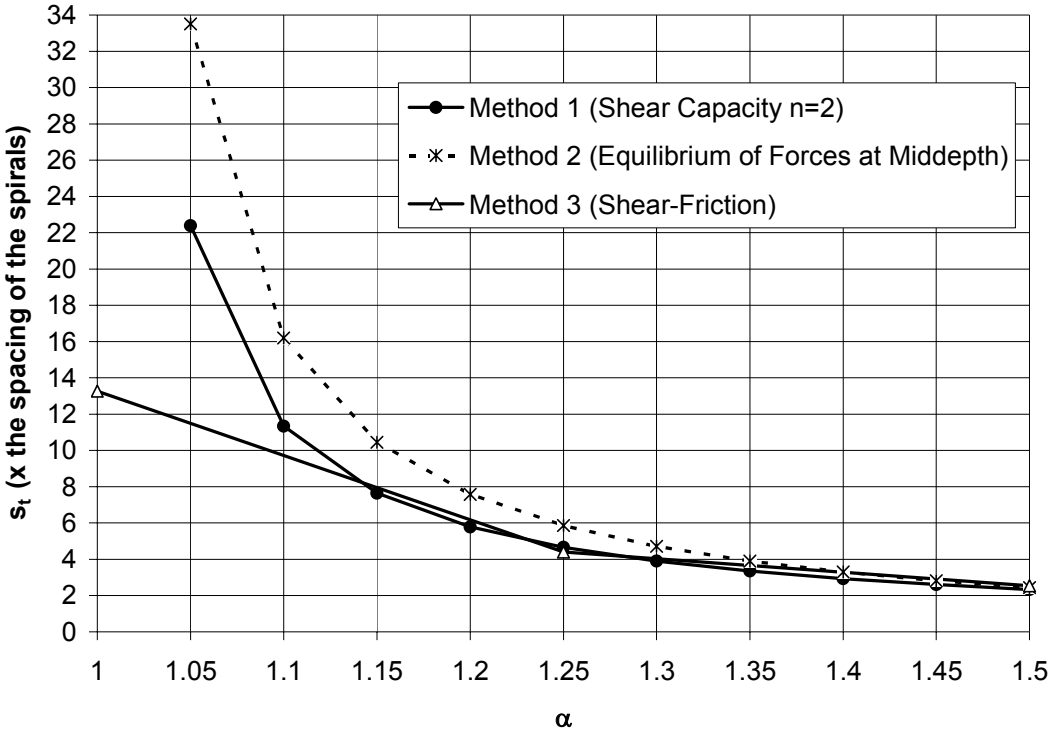

Figure 8-4 Comparison of the Three Methods to Design Horizontal Cross Ties

APPENDIX A: Derivation of the Scaling Factor

APPENDIX A

Derivation of the Scaling Factor

The scaling factor is defined as a transfer coefficient or correlation factor that is multiplied times the scaled member variables to yield the actual prototype variable. Since real concrete and steel are used in the fabrication of the specimens, the stresses are not scaled. Therefore, the forces are scaled in relationship to the cross-sectional areas as follows:

$$F_M = l_r^{\,2} F_P \tag{A-1}$$

$$A_M = l_r^{\,2} A_P \tag{A-2}$$

Where

l_r = scaling factor
F_M = force in the scaled model
F_P = force in the prototype
A_M = area in the scaled model
A_P = area in the prototype

In order to account for the difference between the applied axial load and the effective weight of the inertial system, the time scale for the scaled specimen is determine through the period of the scaled member defined as follows:

$$T_M = 2\pi\sqrt{\frac{M_E}{K_M}} \tag{A-3}$$

Where

T_M = period of the scaled member
M_E = effective mass
K_M = model stiffness = $\dfrac{F_M}{D_M}$
D_M = model displacement

The model displacement is related to prototype displacement as follows:

$$D_M = l_r A_P \tag{A-4}$$

Therefore, the stiffness of the model is related to the stiffness of the prototype as:

$$K_M = \frac{l_r^{\,2} F_P}{l_r D_P} = l_r K_P \tag{A-5}$$

Taking into account the Newton's second law (force equal to mass multiplied by acceleration), and since the accelerations are the same for the model and the prototype, the mass is scaled the same as the force:

$$M_M = l_r^{\,2} M_P \tag{A-6}$$

To account for the differences between inertia and axial load, Eq. A-6 can be modified as follows:

$$M_M = l_r^{\,2} M_P \frac{w_i}{P} \tag{A-7}$$

Where

w_i = weight of the inertia system (including the mass rig)
P = applied axial load

Substituting Eqs. A-5 and A-7 into A-3, period of the scaled member becomes:

$$T_M = 2\pi \sqrt{\frac{M_P}{K_P l_r} \frac{w_i l_r^{\,2}}{P}} = T_P \sqrt{\frac{w_i l_r}{P}} \tag{A-8}$$

Where

T_P = period of the prototype

APPENDIX B: Executive Summary

APPENDIX B

Executive Summary

1. INTRODUCTION

Double or triple interlocking spirals as transverse reinforcement in bridge columns are being used especially in large rectangular cross sections not only because they provide more effective confinement than rectangular hoops but also because interlocking spirals make the column fabrication process easier. The behavior of columns with interlocking spirals has been studied only to a limited extent. In order to revise or possibly refine the current Caltrans design provisions, Caltrans funded a study at the University of Nevada, Reno, on the seismic behavior of interlocking spirals columns. Based on past research and Caltrans seismic design engineers' input, the most critical design parameters of RC columns with interlocking spirals were: the level of average shear stress and the horizontal distance between center to center of the spirals. In addition, effect of horizontal crossties connecting the spirals was studied.

2. OBJECTIVES

The primary objective of this research was to study the seismic performance of bridge columns with double interlocking spirals using shake table simulations. The experimental results were used in order to determine if increasing of the horizontal distance between the centers of the spirals, di, affect the overall performance of the columns when they are subjected to different levels of average shear stress. A further objective was to verify if the addition of horizontal crossties connecting the hoops can improves the overall performance of columns with interlocking spirals.

3. SUMMARY OF RESEARCH

Six large-scale column specimens were tested. The first two were of 1/4-scale with a low level of average shear stress ($3\sqrt{f'c}$, psi unit) and the other four were of 1/5-scale with high level of shear stress ($7\sqrt{f'c}$, psi unit). The models were designed using Caltrans Seismic Design Criteria (SDC-99). A target displacement ductility (μ_c) of 5 was chosen for all the columns. The average shear stress is defined as the maximum plastic shear demand divide by 0.8 times the gross area and expressed as a function of $\sqrt{f'c}$. The overall dimensions of the columns are shown in Figure B-1. The specified concrete compressive strength of the columns was 34.5 Mpa (5000 psi) and the reinforcement was of Grade 60. Table B-I summaries the relevant design parameters for all the columns.

The test setups for single curvature and double curvature columns are shown in Figure B-2. The setup in single curvature was used for the specimens with low average shear stress (ISL1.0, ISL1.5) whereas the setup in double curvature was used for the specimen with high average shear stress (ISH1.0, ISH1.25, ISH1.5 and ISH1.5T). The axial load of $0.1f'_cA_g$ was imposed through a steel spreader beam by prestressed bars to hydraulic jacks. The lateral dynamic load was applied through the inertial mass system off the table for better stability. Strain gages were used to measure the strains in the longitudinal and transverse steel. A series of curvature measurement instruments were installed in the plastic hinge zone. Displacement transducers forming panels were placed along the height of the column in the high-shear models to measure shear deformations. Load cells were used to measure both the axial and lateral forces. An additional measurement of the lateral force was taken by an accelerometer. Displacement transducers measured the lateral displacements of the columns.

Force and displacement capacities were calculated based on the plastic moment capacity of the columns from the M-ϕ analysis, using the program SPMC. The idealized elasto-plastic force and displacements were used to perform a nonlinear response history analysis of the columns with program RCShake. The Sylmar record of the Northridge (0.606 g PGA), California 1994 earthquake, was selected as the input motion based on its high displacement ductility demand. The test motions are shown in Table B-II. A time compression factor was applied to the original Sylmar record (30 seconds) in order to account for the scale factor of the models and adjustment due to inertia mass in specimens. Intermittent free vibration tests were conducted to measure the changes in frequency and damping ratio of the columns.

4. SUMMARY OF RESULTS

The seismic performance of two columns (di=1.0R and di=1.5R) subjected to low average shear stress was similar and satisfactory. The measured displacement ductility capacity in both columns exceeded the target ductility of 5. The larger horizontal distance between the centers of the spirals (di=1.5R) did not lead to excessive shear cracking or a reduction of the shear capacity when the columns are subjected to low level of shear forces. The Caltrans provision of allowing the distance to reach 1.5R is satisfactory at that low level of average shear forces.

The seismic performance of columns with di=1.0R and di=1.25R subjected to high average shear stress was similar. The measured displacement ductility capacities for both specimens were in good agreement with the target ductility of 5. Columns subjected to high average shear stress and di=1.5R did not achieve the target displacement ductility capacities of 5 but exceeded the minimum displacement ductility capacity of 3 specified in SDC. In addition, vertical cracks were observed in this column under small earthquakes. Another specimen, ISH1.5T, was built with horizontal crossties added (Fig. B-1). The crossties connecting the hoops reduced vertical cracks in the interlocking region in columns subjected to high average shear stress with di=1.5R. The spacing of the

additional crossties can be taken as twice the spacing of the spirals. This spacing was calculated based on the difference between tension forces in the spirals at the middepth of the column section for column with di=1.0R and di>1.0R, assuming that the crossties and the spirals have the same bar size.

The force and displacement capacities were calculated based on the plastic moment capacity of the columns obtained from the M-ϕ curves, according to SDC-99. A comparison of the predicted lateral force-displacement and the elasto-plastic idealization of the experimental results are made in Table B-III. The prediction of the lateral force was in good agreement with the experiential results. The analytical model underestimated the yield and ultimate displacements. The addition of bond-slip and shear deformation improved the correlation with the test results.

5. TENTATIVE DESIGN RECOMMENDATIONS

The following design recommendations are for columns reinforced with interlocking spirals and they are based on the experimental results presented above.

- The average shear index should be used be used as a control design parameter to choose the horizontal distance between the centers of the spirals, d_i, and the addition of cross ties in columns reinforced with interlocking spirals.

- The shear index is calculated by dividing the average shear stress by $0.083\sqrt{f'c}$ [MPa] or $\sqrt{f'c}$ [psi]. The average shear stress is found as the ratio between the lateral force capacity and the effective shear area which is defined as the gross area multiplied by 0.8.

- The current Caltrans lower and upper limits on the horizontal distance between the centers of the spirals, d_i, of 1.0R and 1.5R, respectively, are valid subject to the requirements for additional crossties listed below.

- Where needed, horizontal crossties similar to those in ISH1.5T in Fig. B-1, should be used. The crosstie bar should be of the same size as the spiral reinforcement. A maximum spacing of 2 times the spacing of the spirals should be used for the additional horizontal ties. The ties should be detailed with a 135-deg hook in one end and a 90-deg hook at the other end. The 135-deg and 90-deg hooks should alternate in adjacent crossties.

- No cross ties are necessary in columns with shear index equal or less than 3.

- In columns with shear index between 3 and 7, crossties are recommended when d_i exceeds 1.25R.

- In columns with shear index greater than 7, crossties are recommended regardless of d_i.

- Bond slip and shear deformation should be included in the calculation of the idealized yield displacement.

- The ultimate shear deformation needs to be included in the calculation of ultimate displacement for column with aspect ratio of less than 3.0.

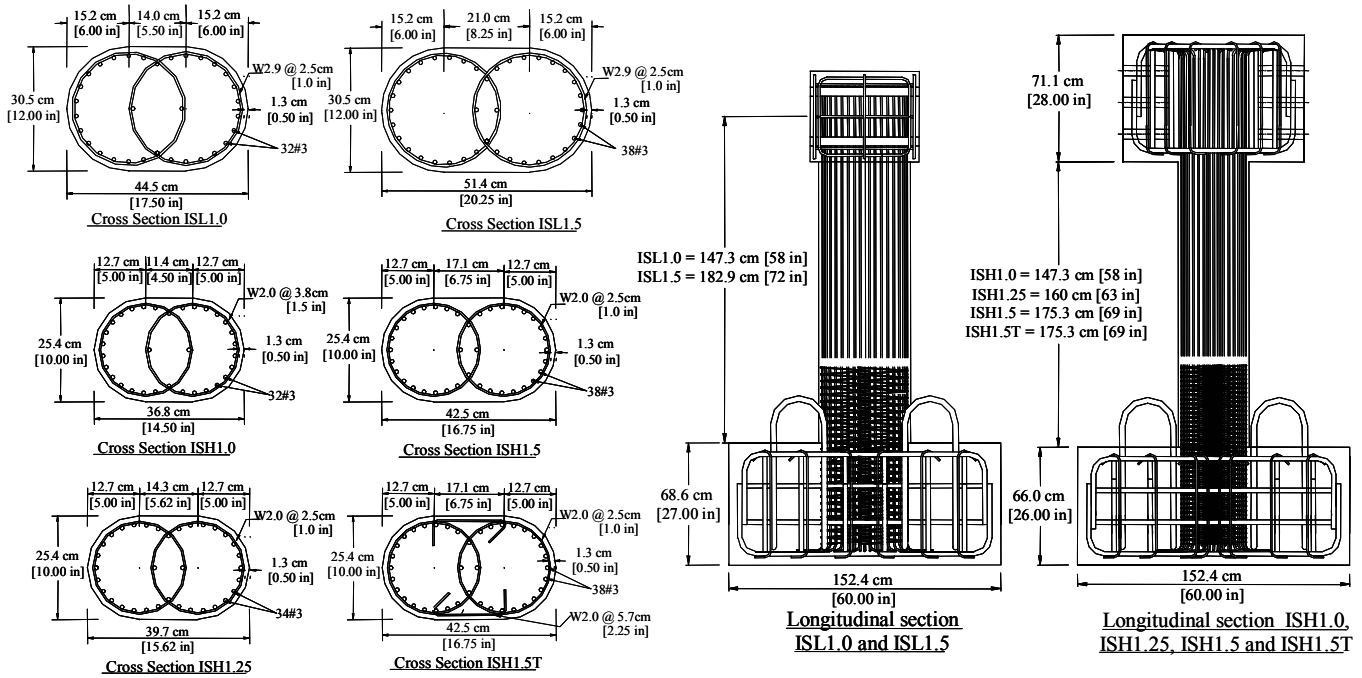

Figure B-1. Test specimens dimensions

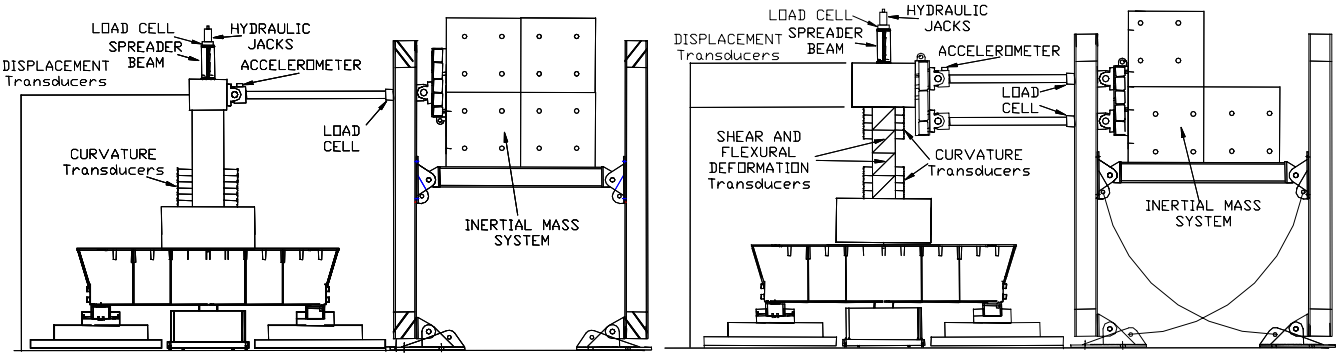

Figure B-2. Single curvature and double curvature test setup

Table B-I Design Parameter for Column Specimens

Specimen No	Aspect Ratio	di	Average shear stress as funtion of √f'c		Steel reinforcement	
					ρl	ρs
		(x R)	[MPa]	[psi]	[%]	[%]
ISL1.0	3.3	1.0	0.25	3.0	1.97	1.05
ISL1.5	3.6	1.5	0.25	3.0	1.98	1.05
ISH1.0	2.0	1.0	0.58	7.0	2.86	0.58
ISH1.25	2.0	1.25	0.58	7.0	2.79	0.87
ISH1.5	2.1	1.5	0.58	7.0	2.87	0.87
ISH1.5T*	2.1	1.5	0.58	7.0	2.87	0.87**

Note: ρl = ratio of longitudinal reinforcement
ρs = ratio of transversal reinforcement to concrete core
* = column with additional cross ties
** = steel ratio from additional cross ties is not included

Table B-II Shake Table Loading Program

	ISL1.0		ISL1.5		ISH1.0		ISH1.25		ISH1.5		ISH1.5T	
	Time compression factor											
	0.51		0.50		0.49		0.46		0.5		0.45	
Run No	[g]	[x slymar]	[g]	[x slymar]	[g]	[x slymar]	[g]	[x slymar]	[g]	[x slymar]	[g]	[x slymar]
1	0.06	0.1	0.06	0.1	0.06	0.1	0.06	0.1	0.06	0.1	0.06	0.1
2	0.12	0.2	0.12	0.2	0.12	0.2	0.12	0.2	0.12	0.2	0.12	0.2
3	0.18	0.3	0.24	0.4	0.24	0.4	0.30	0.5	0.24	0.4	0.24	0.4
4	0.30	0.5	0.36	0.6	0.30	0.5	0.45	0.75	0.36	0.6	0.36	0.6
5	0.45	0.75	0.48	0.8	0.45	0.75	0.61	1	0.45	0.75	0.45	0.75
6	0.61	1	0.61	1	0.61	1	0.76	1.25	0.61	1	0.61	1
7	0.76	1.25	0.76	1.25	0.76	1.25	0.91	1.5	0.76	1.25	0.76	1.25
8	0.91	1.5	0.91	1.5	0.91	1.5	1.06	1.75	0.91	1.5	0.91	1.5
9	1.06	1.75	1.06	1.75	1.06	1.75	1.21	2	1.06	1.75	1.06	1.75
10	1.21	2	1.21	2	1.21	2	1.29	2.125	1.21	2	1.21	2
11			1.29	2.125			1.36	2.25	1.29	2.125	1.29	2.125
12							1.44	2.375	1.36	2.25	1.36	2.25
13									1.44	2.375	1.44	2.375
14											1.52	2.5
15											1.59	2.625

Table B-III Comparison of SDC-Caltrans and Experimental Data

Average Shear Stress/√f'c MPa [psi]	di [R]	Force Kips kN [Kips]		Δy mm [in]		Δu [in]		μ	
		SDC-99 Caltrans	Exp. Results	SDC-99 Caltrans	Exp. Results	SDC-99 Caltrans	Exp. Results	SDC-99 Caltrans	Exp. Results
0.25 [3]	1.0	153 [34]	163 [37]	10 [0.40]	17 [0.67]	43 [1.67]	161 [6.34]	4.2	9.5
	1.5	171 [38]	168 [38]	13 [0.49]	18 [0.72]	56 [2.19]	188 [7.42]	4.4	10.4
0.58 [7]	1.0	202 [45]	228 [51]	6 [0.25]	21 [0.83]	27 [1.06]	99 [3.88]	4.2	4.7
	1.25	217 [49]	231 [52]	6 [0.22]	21 [0.83]	29 [1.16]	106 [4.15]	5.3	5.0
	1.5	199 [45]	223 [50]	10 [0.38]	32 [1.26]	38 [1.48]	128 [5.02]	3.9	4.0
	1.5T	210 [47]	235 [53]	9 [0.35]	27 [1.05]	32 [1.25]	102 [4.00]	3.6	3.8

APPENDIX C: List of CCEER Publications

APPENDIX C

List of CCEER Publications

Report No.	Publication
CCEER-84-1	Saiidi, M., and R. Lawver, "User's Manual for LZAK-C64, A Computer Program to Implement the Q-Model on Commodore 64," Civil Engineering Department, Report No. CCEER-84-1, University of Nevada, Reno, January 1984.
CCEER-84-2	Douglas, B. and T. Iwasaki, "Proceedings of the First USA-Japan Bridge Engineering Workshop," held at the Public Works Research Institute, Tsukuba, Japan, Civil Engineering Department, Report No. CCEER-84-2, University of Nevada, Reno, April 1984.
CCEER-84-3	Saiidi, M., J. Hart, and B. Douglas, "Inelastic Static and Dynamic Analysis of Short R/C Bridges Subjected to Lateral Loads," Civil Engineering Department, Report No. CCEER-84-3, University of Nevada, Reno, July 1984.
CCEER-84-4	Douglas, B., "A Proposed Plan for a National Bridge Engineering Laboratory," Civil Engineering Department, Report No. CCEER-84-4, University of Nevada, Reno, December 1984.
CCEER-85-1	Norris, G. and P. Abdollaholiaee, "Laterally Loaded Pile Response: Studies with the Strain Wedge Model," Civil Engineering Department, Report No. CCEER-85-1, University of Nevada, Reno, April 1985.
CCEER-86-1	Ghusn, G. and M. Saiidi, "A Simple Hysteretic Element for Biaxial Bending of R/C in NEABS-86," Civil Engineering Department, Report No. CCEER-86-1, University of Nevada, Reno, July 1986.
CCEER-86-2	Saiidi, M., R. Lawver, and J. Hart, "User's Manual of ISADAB and SIBA, Computer Programs for Nonlinear Transverse Analysis of Highway Bridges Subjected to Static and Dynamic Lateral Loads," Civil Engineering Department, Report No. CCEER-86-2, University of Nevada, Reno, September 1986.
CCEER-87-1	Siddharthan, R., "Dynamic Effective Stress Response of Surface and Embedded Footings in Sand," Civil engineering Department, Report No. CCEER-86-2, University of Nevada, Reno, June 1987.
CCEER-87-2	Norris, G. and R. Sack, "Lateral and Rotational Stiffness of Pile Groups for Seismic Analysis of Highway Bridges," Civil Engineering Department, Report No. CCEER-87-2, University of Nevada, Reno, June 1987.
CCEER-88-1	Orie, J. and M. Saiidi, "A Preliminary Study of One-Way Reinforced Concrete Pier Hinges Subjected to Shear and Flexure," Civil Engineering Department, Report No. CCEER-88-1, University of Nevada, Reno, January 1988.
CCEER-88-2	Orie, D., M. Saiidi, and B. Douglas, "A Micro-CAD System for Seismic Design of Regular Highway Bridges," Civil Engineering Department, Report No. CCEER-88-2, University of Nevada, Reno, June 1988.

CCEER-88-3 Orie, D. and M. Saiidi, "User's Manual for Micro-SARB, a Microcomputer Program for Seismic Analysis of Regular Highway Bridges," Civil Engineering Department, Report No. CCEER-88-3, University of Nevada, Reno, October 1988.

CCEER-89-1 Douglas, B., M. Saiidi, R. Hayes, and G. Holcomb, "A Comprehensive Study of the Loads and Pressures Exerted on Wall Forms by the Placement of Concrete," Civil Engineering Department, Report No. CCEER-89-1, University of Nevada, Reno, February 1989.

CCEER-89-2 Richardson, J. and B. Douglas, "Dynamic Response Analysis of the Dominion Road Bridge Test Data," Civil Engineering Department, Report No. CCEER-89-2, University of Nevada, Reno, March 1989.

CCEER-89-2 Vrontinos, S., M. Saiidi, and B. Douglas, "A Simple Model to Predict the Ultimate Response of R/C Beams with Concrete Overlays," Civil Engineering Department, Report NO. CCEER-89-2, University of Nevada, Reno, June 1989.

CCEER-89-3 Ebrahimpour, A. and P. Jagadish, "Statistical Modeling of Bridge Traffic Loads - A Case Study," Civil Engineering Department, Report No. CCEER-89-3, University of Nevada, Reno, December 1989.

CCEER-89-4 Shields, J. and M. Saiidi, "Direct Field Measurement of Prestress Losses in Box Girder Bridges," Civil Engineering Department, Report No. CCEER-89-4, University of Nevada, Reno, December 1989.

CCEER-90-1 Saiidi, M., E. Maragakis, G. Ghusn, Y. Jiang, and D. Schwartz, "Survey and Evaluation of Nevada's Transportation Infrastructure, Task 7.2 - Highway Bridges, Final Report," Civil Engineering Department, Report No. CCEER 90-1, University of Nevada, Reno, October 1990.

CCEER-90-2 Abdel-Ghaffar, S., E. Maragakis, and M. Saiidi, "Analysis of the Response of Reinforced Concrete Structures During the Whittier Earthquake 1987," Civil Engineering Department, Report No. CCEER 90-2, University of Nevada, Reno, October 1990.

CCEER-91-1 Saiidi, M., E. Hwang, E. Maragakis, and B. Douglas, "Dynamic Testing and the Analysis of the Flamingo Road Interchange," Civil Engineering Department, Report No. CCEER-91-1, University of Nevada, Reno, February 1991.

CCEER-91-2 Norris, G., R. Siddharthan, Z. Zafir, S. Abdel-Ghaffar, and P. Gowda, "Soil-Foundation-Structure Behavior at the Oakland Outer Harbor Wharf," Civil Engineering Department, Report No. CCEER-91-2, University of Nevada, Reno, July 1991.

CCEER-91-3 Norris, G., "Seismic Lateral and Rotational Pile Foundation Stiffnesses at Cypress," Civil Engineering Department, Report No. CCEER-91-3, University of Nevada, Reno, August 1991.

CCEER-91-4 O'Connor, D. and M. Saiidi, "A Study of Protective Overlays for Highway Bridge Decks in Nevada, with Emphasis on Polyester-Styrene Polymer Concrete," Civil Engineering Department, Report No. CCEER-91-4, University of Nevada, Reno, October 1991.

CCEER-91-5 O'Connor, D.N. and M. Saiidi, "Laboratory Studies of Polyester-Styrene Polymer Concrete Engineering Properties," Civil Engineering Department, Report No. CCEER-91-5, University of Nevada, Reno, November 1991.

CCEER-92-1 Straw, D.L. and M. Saiidi, "Scale Model Testing of One-Way Reinforced Concrete Pier Hinges Subject to Combined Axial Force, Shear and Flexure," edited by D.N. O'Connor, Civil Engineering Department, Report No. CCEER-92-1, University of Nevada, Reno, March 1992.

CCEER-92-2 Wehbe, N., M. Saiidi, and F. Gordaninejad, "Basic Behavior of Composite Sections Made of Concrete Slabs and Graphite Epoxy Beams," Civil Engineering Department, Report No. CCEER-92-2, University of Nevada, Reno, August 1992.

CCEER-92-3 Saiidi, M. and E. Hutchens, "A Study of Prestress Changes in A Post-Tensioned Bridge During the First 30 Months," Civil Engineering Department, Report No. CCEER-92-3, University of Nevada, Reno, April 1992.

CCEER-92-4 Saiidi, M., B. Douglas, S. Feng, E. Hwang, and E. Maragakis, "Effects of Axial Force on Frequency of Prestressed Concrete Bridges," Civil Engineering Department, Report No. CCEER-92-4, University of Nevada, Reno, August 1992.

CCEER-92-5 Siddharthan, R., and Z. Zafir, "Response of Layered Deposits to Traveling Surface Pressure Waves," Civil Engineering Department, Report No. CCEER-92-5, University of Nevada, Reno, September 1992.

CCEER-92-6 Norris, G., and Z. Zafir, "Liquefaction and Residual Strength of Loose Sands from Drained Triaxial Tests," Civil Engineering Department, Report No. CCEER-92-6, University of Nevada, Reno, September 1992.

CCEER-92-7 Douglas, B., "Some Thoughts Regarding the Improvement of the University of Nevada, Reno's National Academic Standing," Civil Engineering Department, Report No. CCEER-92-7, University of Nevada, Reno, September 1992.

CCEER-92-8 Saiidi, M., E. Maragakis, and S. Feng, "An Evaluation of the Current Caltrans Seismic Restrainer Design Method," Civil Engineering Department, Report No. CCEER-92-8, University of Nevada, Reno, October 1992.

CCEER-92-9 O'Connor, D., M. Saiidi, and E. Maragakis, "Effect of Hinge Restrainers on the Response of the Madrone Drive Undercrossing During the Loma Prieta Earthquake," Civil Engineering Department, Report No. CCEER-92-9, University of Nevada, Reno, February 1993.

CCEER-92-10 O'Connor, D., and M. Saiidi, "Laboratory Studies of Polyester Concrete: Compressive Strength at Elevated Temperatures and Following Temperature Cycling, Bond Strength to Portland Cement Concrete, and Modulus of Elasticity," Civil Engineering Department, Report No. CCEER-92-10, University of Nevada, Reno, February 1993.

CCEER-92-11 Wehbe, N., M. Saiidi, and D. O'Connor, "Economic Impact of Passage of Spent Fuel Traffic on Two Bridges in Northeast Nevada," Civil Engineering Department, Report No. CCEER-92-11, University of Nevada, Reno, December 1992.

CCEER-93-1 Jiang, Y., and M. Saiidi, "Behavior, Design, and Retrofit of Reinforced Concrete One-way Bridge Column Hinges," edited by D. O'Connor, Civil Engineering Department, Report No. CCEER-93-1, University of Nevada, Reno, March 1993.

CCEER-93-2 Abdel-Ghaffar, S., E. Maragakis, and M. Saiidi, "Evaluation of the Response of the Aptos Creek Bridge During the 1989 Loma Prieta Earthquake," Civil Engineering Department, Report No. CCEER-93-2, University of Nevada, Reno, June 1993.

CCEER-93-3 Sanders, D.H., B.M. Douglas, and T.L. Martin, "Seismic Retrofit Prioritization of Nevada Bridges," Civil Engineering Department, Report No. CCEER-93-3, University of Nevada, Reno, July 1993.

CCEER-93-4 Abdel-Ghaffar, S., E. Maragakis, and M. Saiidi, "Performance of Hinge Restrainers in the Huntington Avenue Overhead During the 1989 Loma Prieta Earthquake," Civil Engineering Department, Report No. CCEER-93-4, University of Nevada, Reno, June 1993 (in final preparation).

CCEER-93-5 Maragakis, E., M. Saiidi, S. Feng, and L. Flournoy, "Effects of Hinge Restrainers on the Response of the San Gregorio Bridge During the Loma Prieta Earthquake," (in final preparation) Civil Engineering Department, Report No. CCEER-93-5, University of Nevada, Reno.

CCEER-93-6 Saiidi, M., E. Maragakis, S. Abdel-Ghaffar, S. Feng, and D. O'Connor, "Response of Bridge Hinge Restrainers During Earthquakes -Field Performance, Analysis, and Design," Civil Engineering Department, Report No. CCEER-93-6, University of Nevada, Reno, May 1993.

CCEER-93-7 Wehbe, N., Saiidi, M., Maragakis, E., and Sanders, D., "Adequacy of Three Highway Structures in Southern Nevada for Spent Fuel Transportion, Civil Engineering Department, Report No. CCEER-93-7, University of Nevada, Reno, August 1993.

CCEER-93-8 Roybal, J., Sanders, D.H., and Maragakis, E., "Vulnerability Assessment of Masonry in the Reno-Carson City Urban Corridor," Civil Engineering Department, Report No. CCEER-93-8, University of Nevada, Reno, May 1993.

CCEER-93-9 Zafir, Z. and Siddharthan, R., "MOVLOAD: A Program to Determine the Behavior of Nonlinear Horizontally Layered Medium Under Moving Load," Civil Engineering Department, Report No. CCEER-93-9, University of Nevada, Reno, August 1993.

CCEER-93-10 O'Connor, D.N., Saiidi, M., and Maragakis, E.A., "A Study of Bridge Column Seismic Damage Susceptibility at the Interstate 80/U.S. 395 Interchange in Reno, Nevada," Civil Engineering Department, Report No. CCEER-93-10, University of Nevada, Reno, October 1993.

CCEER-94-1 Maragakis, E., B. Douglas, and E. Abdelwahed, "Preliminary Dynamic Analysis of a Railroad Bridge," Report CCEER-94-1, January 1994.

CCEER-94-2 Douglas, B.M., Maragakis, E.A., and Feng, S., "Stiffness Evaluation of Pile Foundation of Cazenovia Creek Overpass," Civil Engineering Department, Report No. CCEER-94-2, University of Nevada, Reno, March 1994.

CCEER-94-3 Douglas, B.M., Maragakis, E.A., and Feng, S., "Summary of Pretest Analysis of Cazenovia Creek Bridge," Civil Engineering Department, Report No. CCEER-94-3, University of Nevada, Reno, April 1994.

CCEER-94-4 Norris, G.M. and Madhu, R., "Liquefaction and Residual Strength of Sands from Drained Triaxial Tests, Report 2," Civil Engineering Department, CCEER-94-4, University of Nevada, Reno, August 1994.

CCEER-94-5 Saiidi, M., Hutchens, E., and Gardella, D., "Prestress Losses in a Post-Tensioned R/C

Box Girder Bridge in Southern Nevada," Civil Engineering Department, CCEER-94-5, University of Nevada, Reno, August 1994.

CCEER-95-1 Siddharthan, R., El-Gamal, M., and Maragakis, E.A., "Nonlinear Bridge Abutment , Verification, and Design Curves," Civil Engineering Department, CCEER-95-1, University of Nevada, Reno, January 1995.

CCEER-95-2 Norris, G.M., Madhu, R., Valceschini, R., and Ashour, M., "Liquefaction and Residual Strength of Loose Sands from Drained Triaxial Tests," Report 2, Civil Engineering Department, Report No. CCEER-95-2, University of Nevada, Reno, February 1995.

CCEER-95-3 Wehbe, N., Saiidi, M., Sanders, D., and Douglas, B., "Ductility of Rectangular Reinforced Concrete Bridge Columns with Moderate Confinement,"Civil Engineering Department, Report No. CCEER-95-3, University of Nevada, Reno, July 1995.

CCEER-95-4 Martin, T., Saiidi, M., and Sanders, D., "Seismic Retrofit of Column-Pier Cap Connections in Bridges in Northern Nevada," Civil Engineering Department, Report No. CCEER-95-4, University of Nevada, Reno, August 1995.

CCEER-95-5 Darwish, I., Saiidi, M., and Sanders, D., "Experimental Study of Seismic Susceptibility Column-Footing Connections," Civil Engineering Department, Report No. CCEER-95-5, University of Nevada, Reno, September 1995.

CCEER-95-6 Griffin, G., Saiidi, M., and Maragakis, E., "Nonlinear Seismic Response of Isolated Bridges and Effects of Pier Ductility Demand," Civil Engineering Department, Report No. CCEER-95-6, University of Nevada, Reno, November 1995.

CCEER-95-7 Acharya, S., Saiidi, M., and Sanders, D., "Seismic Retrofit of Bridge Footings and Column-Footing Connections," Report for the Nevada Department of Transportation, Civil Engineering Department, Report No. CCEER-95-7, University of Nevada, Reno, November 1995.

CCEER-95-8 Maragakis, E., Douglas, B., and Sandirasegaram, U., "Full-Scale Field Resonance Tests of a Railway Bridge," A Report to the Association of American Railroads, Civil Engineering Department, Report No. CCEER-95-8, University of Nevada, Reno, December 1995.

CCEER-95-9 Douglas, B., Maragakis, E., and Feng, S., "System Identification Studies on Cazenovia Creek Overpass," Report for the National Center for Earthquake Engineering Research, Civil Engineering Department, Report No. CCEER-95-9, University of Nevada, Reno, October 1995.

CCEER-96-1 El-Gamal, M.E. and Siddharthan, R.V., "Programs to Computer Translational Stiffness of Seat-Type Bridge Abutment," Civil Engineering Department, Report No. CCEER-96-1, University of Nevada, Reno, March 1996.

CCEER-96-2 Labia, Y., Saiidi, M., and Douglas, B., "Evaluation and Repair of Full-Scale Prestressed Concrete Box Girders," A Report to the National Science Foundation, Research Grant CMS-9201908, Civil Engineering Department, Report No. CCEER-96-2, University of Nevada, Reno, May 1996.

CCEER-96-3 Darwish, I., Saiidi, M., and Sanders, D., "Seismic Retrofit of R/C Oblong Tapered Bridge Columns with Inadequate Bar Anchorage in Columns and Footings," A Report to the Nevada Department of Transportation, Civil Engineering Department, Report No.

CCEER-96-3, University of Nevada, Reno, May 1996.

CCEER-96-4 Ashour, M., Pilling, P., Norris, G., and Perez, H., "The Prediction of Lateral Load Behavior of Single Piles and Pile Groups Using the Strain Wedge Model," A Report to the California Department of Transportation, Civil Engineering Department, Report No. CCEER-96-4, University of Nevada, Reno, June, 1996.

CCEER-97-1-A Rimal, P. and Itani, A. "Sensitivity Analysis of Fatigue Evaluations of Steel Bridges", Center for Earthquake Research, Department of Civil Engineering, University of Nevada, Reno, Nevada Report No. CCEER-97-1-A, September, 1997.

CCEER-97-1-B Maragakis, E., Douglas, B., and Sandirasegaram, U. "Full-Scale Field Resonance Tests of a Railway Bridge," A Report to the Association of American Railroads, Civil Engineering Department, University of Nevada, Reno, May, 1996.

CCEER-97-2 Wehbe, N., Saiidi, M., and D. Sanders, "Effect of Confinement and Flares on the Seismic Performance of Reinforced Concrete Bridge Columns," Civil Engineering Department, Report No. CCEER-97-2, University of Nevada, Reno, September 1997.

CCEER-97-3 Darwish, I., M. Saiidi, G. Norris, and E. Maragakis, "Determination of In-Situ Footing Stiffness Using Full-Scale Dynamic Field Testing," A Report to the Nevada Department of Transportation, Structural Design Division, Carson City, Nevada, Report No. CCEER-97-3, University of Nevada, Reno, October 1997.

CCEER-97-4 Wehbe, N., and M. Saiidi, "User's manual for RCMC v. 1.2 : A Computer Program for Moment-Curvature Analysis of Confined and Unconfined Reinforced Concrete Sections," Center for Civil Engineering Earthquake Research, Department of Civil Engineering, University of Nevada, Reno, Nevada, Report No. CCEER-97-4, November, 1997.

CCEER-97-5 Isakovic, T., M. Saiidi, and A. Itani, "Influence of new Bridge Configurations on Seismic Performance," Department of Civil Engineering, University of Nevada, Reno, Report No. CCEER-97-5, September, 1997.

CCEER-98-1 Itani, A., Vesco, T. and Dietrich, A., "Cyclic Behavior of "as Built" Laced Members With End Gusset Plates on the San Francisco Bay Bridge" Center for Civil Engineering Earthquake Research, Department of Civil Engineering, University of Nevada, Reno, Nevada Report No. CCEER-98-1, March, 1998.

CCEER-98-2 G. Norris and M. Ashour, "Liqueficiation and Undraned response evaluation of Sands from Drained Formulation." Center for Civil Engineering Earthquake Research, Department of Civil Engineering, University of Nevada, Reno, Nevada, Report No. CCEER-98-2, May, 1998.

CCEER-98-3 Qingbin, Chen, B. M. Douglas, E. Maragakis, and I. G. Buckle, "Extraction of Nonlinear Hysteretic Properties of Seismically Isolated Bridges from Quick-Release Field Tests", Center for Civil Engineering Earthquake Research, Department of Civil Engineering, University of Nevada, Reno, Nevada, Report No. CCEER-98-3, June, 1998.

CCEER-98-4 Maragakis, E., B. M. Douglas, and C. Qingbin, "Full-Scale Field Capacity Tests of a Railway Bridge", Center for Civil Engineering Earthquake Research, Department of Civil Engineering, University of Nevada, Reno, Nevada, Report No. CCEER-98-4, June, 1998.

CCEER-98-5 Itani, A., Douglas, B., and Woodgate, J., "Cyclic Behavior of Richmond-San Rafael Retrofitted Tower Leg". Center for Civil Engineering Earthquake Research, Department of Civil Engineering, University of Nevada, Reno. Report No. CCEER-98-5, June 1998

CCEER-98-6 Moore, R., Saiidi, M., and Itani, A., "Seismic Behavior of New Bridges with Skew and Curvature". Center for Civil Engineering Earthquake Research, Department of Civil Engineering, University of Nevada, Reno. Report No. CCEER-98-6, October, 1998.

CCEER-98-7 Itani, A and Dietrich, A, "Cyclic Behavior of Double Gusset Plate Connections", Center for Civil Engineering Earthquake Research, Department of Civil Engineering, University of Nevada, Reno, Nevada, Report No. CCEER-98-5, December, 1998.

CCEER-99-1 Caywood, C., M. Saiidi, and D. Sanders, " Seismic Retrofit of Flared Bridge Columns With Steel Jackets," Civil Engineering Department, University of Nevada, Reno, Report No. CCEER-99-1, February 1999.

CCEER-99-2 Mangoba, N., M. Mayberry, and M. Saiidi, "Prestress Loss in Four Box Girder Bridges in Northern Nevada," Civil Engineering Department, University of Nevada, Reno, Report No. CCEER-99-2, March 1999.

CCEER-99-3 Abo-Shadi, N., M. Saiidi, and D. Sanders, "Seismic Response of Bridge Pier Walls in the Weak Direction", Civil Engineering Department, University of Nevada, Reno, Report No. CCEER-99-3, April 1999.

CCEER-99-4 Buzick, A., and M. Saiidi, "Shear Strength and Shear Fatigue Behavior of Full-Scale Prestressed Concrete Box Girders", Civil Engineering Department, University of Nevada, Reno, Report No. CCEER-99-4, April 1999.

CCEER-99-5 Randall, M., M. Saiidi, E. Maragakis and T. Isakovic, "Restrainer Design Procedures For Multi-Span Simply-Supported Bridges", Civil Engineering Department, University of Nevada, Reno, Report No. CCEER-99-5, April 1999.

CCEER-99-6 Wehbe, N. and M. Saiidi, "User's Manual for RCMC v. 1.2, A Computer Program for Moment-Curvature Analysis of Confined and Unconfined Reinforced Concrete Sections", Civil Engineering Department, University of Nevada, Reno, Report No. CCEER-99-6, May 1999.

CCEER-99-7 Burda, J. and A. Itani, "Studies of Seismic Behavior of Steel Base Plates," Civil Engineering Department, University of Nevada, Reno, Report No. CCEER-99-7, May 1999.

CCEER-99-8 Ashour, M., and G. Norris, "Refinement of the Strain Wedge Model Program," Civil Engineering Department, University of Nevada, Reno, Report No. CCEER-99-8, March 1999.

CCEER-99-9 Dietrich, A., and A. Itani, "Cyclic Behavior of Laced and Perforated Steel Members on the San Francisco-Oakland Bay Bridge," Civil Engineering Department, University, Reno. December 1999.

CCEER 99-10 Itani, A., A. Dietrich, "Cyclic Behavior of Built Up Steel Members and their Connections," Civil Engineering Department, University of Nevada, Reno. December 1999.

CCEER 99-11 Itani, A., J. Woodgate, "Axial and Rotational Ductility of BuiltUp Structural Steel

Members," Civil Engineering Department, University of Nevada, Reno December 1999.

CCEER-99-12 Sgambelluri, M., Sanders, D.H., and Saiidi, M.S., Behavior of One-Way Reinforced Concrete Bridge Column Hinges in the Weak Direction, Report No. Department of Civil Engineering, University of Nevada, Reno, December 1999.

CCEER-99-13 Laplace, P., Sanders, D.H., Douglas, B, and Saiidi, M, Shake Table Testing of Flexure Dominated Reinforced Concrete Bridge Columns, Report No. Department of Civil Engineering, University of Nevada, Reno, December 1999.

CCEER-99-14 Ahmad M. Itani, Jose A. Zepeda, and Elizabeth A. Ware "Cyclic Behavior of Steel Moment Frame Connections for the Moscone Center Expansion," December 1999.

CCEER 00-1 Ashour, M., and Norris, G. "Undrained Lateral Pile and Pile Group Response in Saturated Sand", Civil Engineering Department, University of Nevada, Reno, Report No. CCEER-00-1, May 1999. January 2000.

CCEER 00-2 Saiidi, M. and Wehbe, N., "A Comparison of Confinement Requirements in Different Codes for Rectangular, Circular, and Double-Spiral RC Bridge Columns," Civil Engineering Department, University of Nevada, Reno, Report No. CCEER-00-2, January 2000.

CCEER 00-3 McElhaney, B., M. Saiidi, and D. Sanders, "Shake Table Testing of Flared Bridge Columns With Steel Jacket Retrofit," Civil Engineering Department, University of Nevada, Reno, Report No. CCEER-00-3, January 2000.

CCEER 00-4 Martinovic, F., M. Saiidi, D. Sanders, and F. Gordaninejad, "Dynamic Testing of Non-Prismatic Reinforced Concrete Bridge Columns Retrofitted with FRP Jackets," Civil Engineering Department, University of Nevada, Reno, Report No. CCEER-00-4, January 2000.

CCEER 00-5 Itani, A., and M. Saiidi, "Seismic Evaluation of Steel Joints for UCLA Center for Health Science Westwood Replacement Hospital," Civil Engineering Department, University of Nevada, Reno, Report No. CCEER-00-5, February 2000.

CCEER 00-6 Will, J. and D. Sanders, "High Performance Concrete Using Nevada Aggregates," Civil Engineering Department, University of Nevada, Reno, Report No. CCEER-00-6, May 2000.

CCEER 00-7 French, C., and M. Saiidi, "A Comparison of Static and Dynamic Performance of Models of Flared Bridge Columns ," Civil Engineering Department, University of Nevada, Reno, Report No. CCEER-00-7, October 2000.

CCEER 00-8 Itani, A., H. Sedarat, "Seismic Analysis of the AISI LRFD Design Example of Steel Highway Bridges," Civil Engineering Department, University of Nevada, Reno, Report No. CCEER 00-08, November 2000.

CCEER 00-9 Moore, J., D. Sanders, and M. Saiidi, "Shake Table Testing of 1960's Two Column Bent with Hinges Bases," Civil Engineering Department, University of Nevada, Reno, Report No. CCEER 00-09, December 2000.

CCEER 00-10 Asthana, M., D. Sanders, and M. Saiidi, "One-Way Reinforced Concrete Bridge Column Hinges in the Weak Direction," Civil Engineering Department, University of Nevada, Reno, Report No. CCEER 00-10, April 2001.

CCEER 01-1 Ah Sha, H., D. Sanders, M. Saiidi, "Early Age Shrinkage and Cracking of Nevada Concrete Bridge Decks, "Civil Engineering Department, University of Nevada, Reno, Report No. CCEER 01-01, May 2001.

CCEER 01-2 Ashour, M. and G. Norris, "Pile Group program for Full Material Modeling an Progressive Failure." Civil Engineering Department, University of Nevada, Reno, Report No. CCEER 01-02, July 2001.

CCEER 01-3 Itani, A., C. Lanaud, and P. Dusicka, "Non-Linear Finite Element Analysis of Built-Up Shear Links." Civil Engineering Department, University of Nevada, Reno, Report No. CCEER 01-03, July 2001.

CCEER 01-4 Saiidi, M., J. Mortensen, and F. Martinovic, "Analysis and Retrofit of Fixed Flared Columns with Glass Fiber-Reinforced Plastic Jacketing," Civil Engineering Department, University of Nevada, Reno, Report No. CCEER 01-4, August 2001

CCEER 01-5 Saiidi, M., A. Itani, I. Buckle, and Z. Cheng," Performance of A Full-Scale Two-Story Wood Frame Structure Supported on Ever-Level Isolators," Civil Engineering Department, University of Nevada, Reno, Report No. CCEER 01-5, October 2001

CCEER 01-6 Laplace, P., D. Sanders, and M. Saiidi, "Experimental Study and Analysis of Retrofitted Flexure and Shear Dominated Circular Reinforced Concrete Bridge Columns Subjected to Shake Table Excitation, "Civil Engineering Department, University of Nevada, Reno, Report No. CCEER 01-6, June 2001.

CCEER 01-7 Reppi, F., and D. Sanders, "Removal and Replacement of Cast-in-Place, Post-tensioned, Box Girder Bridge," Civil Engineering Department, University of Nevada, Reno, Report No. CCEER 01-7, December 2001.

CCEER 02-1 Pulido, C., M. Saiidi, D. Sanders, and A. Itani, "Seismic Performance and Retrofitting of Reinforced Concrete Bridge Bents," Civil Engineering Department, University of Nevada, Reno, Report No. CCEER 02-1, January 2002.

CCEER 02-2 Yang, Q., M. Saiidi, H. Wang, and A. Itani, "Influence of Ground Motion Incoherency on Earthquake Response of Multi-Support Structures," Civil Engineering Department, University of Nevada, Reno, Report No. CCEER 02-2, May 2002.

CCEER 02-3 M. Saiidi, B. Gopalakrishnan, E. Reinhardt, and R. Siddharthan, A "Preliminary Study of Shake Table Response of A Two-Column Bridge Bent on Flexible Footings," Civil Engineering Department, University of Nevada, Reno, Report No. CCEER 02-03, June 2002.

CCEER 02-4 Not Published

CCEER 02-5 Banghart, A., Sanders, D., Saiidi, M., "Evaluation of Concrete Mixes for Filling the Steel Arches in the Galena Creek Bridge," Civil Engineering Department, University of Nevada, Reno, Report No. CCEER 02-05, June 2002.

CCEER 02-6 Dusicka, P., Itani, A., Buckle, I. G., "Cyclic Behavior of Shear Links and Tower Shaft Assembley of San Francisco – Oakland Bay Bridge Tower" Civil Engineering

Department, University of Nevada, Reno, Report No. CCEER 02-06, July 2002.

CCEER 02-7 Mortensen, J., and M. Saiidi, " A Performance-Based Design Method for Confinement in Circular Columns," Civil Engineering Department, University of Nevada, Reno, Report No. CCEER 02-07, November 2002.

CCEER 03-1 Wehbe, N., and M. Saiidi, "User's manual for SPMC v. 1.0 : A Computer Program for Moment-Curvature Analysis of Reinforced Concrete Sections with Interlocking Spirals," Center for Civil Engineering Earthquake Research, Department of Civil Engineering, University of Nevada, Reno, Nevada, Report No. CCEER-03-1, May, 2003.

CCEER 03-2 Wehbe, N., and M. Saiidi, "User's manual for RCMC v. 2.0 : A Computer Program for Moment-Curvature Analysis of Confined and Unconfined Reinforced Concrete Sections," Center for Civil Engineering Earthquake Research, Department of Civil Engineering, University of Nevada, Reno, Nevada, Report No. CCEER-03-2, June, 2003.

CCEER 03-3 Nada, H., D. Sanders, and M. Saiidi, " Seismic Performance of RC Bridge Frames with Architectural-Flared Columns," Civil Engineering Department, University of Nevada, Reno, Report No. CCEER 03-3, January 2003.

CCEER 03-4 Reinhardt, E., M. Saiidi, and R. Siddharthan, " Seismic Performance of a CFRP/ Concrete Bridge Bent on Flexible Footings." Civil Engineering Department, University of Nevada, Reno. Report No. CCEER 03-4, August 2003.

CCEER 03-5 Johnson, N., M. Saiidi, A. Itani, and S. Ladkany, "Seismic Retrofit of Octagonal Columns with Pedestal and One-Way Hinge at the Base," Center for Civil Engineering Earthquake Research, Department of Civil Engineering, University of Nevada, Reno, Nevada, Report No. CCEER-03-5, August 2003.

CCEER 03-06 Mortensen, C., M. Saiidi, and S. Ladkany, "Creep and Shrinkage Losses in Highly Variable Climates," Center for Civil Engineering Earthquake Research, Department of Civil Engineering, University of Nevada, Reno, Nevada, Report No. CCEER-03-6, September 2003.

CCEER 03- 07 Ayoub, C., M. Saiidi, and A. Itani, "A Study of Shape-Memory-Alloy-Reinforced Beams and Cubes," Center for Civil Engineering Earthquake Research, Department of Civil Engineering, University of Nevada, Reno, Nevada, Report No. CCEER-03-7, October 2003.

CCEER 03-08 Chandane, S., D. Sanders, and M. Saiidi, "Static and Dynamic Performance of RC Bridge Bents with Architectural-Flared Columns," Center for Civil Engineering Earthquake Research, Department of Civil Engineering, University of Nevada, Reno, Nevada, Report No. CCEER-03-8, November 2003.

CCEER 04-01 Olaegbe, C., and Saiidi, M., "Effect of Loading History on Shake Table Performance of A Two-Column Bent with Infill Wall," Center for Civil Engineering Earthquake Research, Department of Civil Engineering, University of Nevada, Reno, Nevada, Report No. CCEER-04-1, January 2004.

CCEER 04-02 Johnson, R., Maragakis, E., Saiidi, M., and DesRoches, R., "Experimental Evaluation of Seismic Performance of SMA Bridge Restrainers," Center for Civil Engineering Earthquake Research, Department of Civil Engineering, University of Nevada, Reno, Nevada, Report No. CCEER-04-2, February 2004.

CCEER 04-03 Moustafa, K., Sanders, D., and Saiidi, M., "Impact of Aspect Ratio on Two-Column Bent Seismic Performance," Center for Civil Engineering Earthquake Research, Department of Civil Engineering, University of Nevada, Reno, Nevada, Report No. CCEER-04-3, February 2004.

CCEER 04-04 Maragakis, E., Saiidi, M., Sanchez-Camargo, F., and Elfass, S., "Seismic Performance of Bridge Restrainers At In-Span Hinges," Center for Civil Engineering Earthquake Research, Department of Civil Engineering, University of Nevada, Reno, Nevada, Report No. CCEER-04-4, March 2004.

CCEER 04-05 Ashour, M., Norris, G. and Elfass, S., "Analysis of Laterally Loaded Long or Intermediate Drilled Shafts of Small or Large Diameter in Layered Soil," Center for Civil Engineering Earthquake Research, Department of Civil Engineering, University of Nevada, Reno, Nevada, Report No. CCEER-04-5, June 2004.

CCEER 04-06 Correal,J., Saiidi, M., and Sanders, D., "Seismic Performance of RC Bridge Columns Reinforced with Two Interlocking Spirals," Center for Civil Engineering Earthquake Research, Department of Civil Engineering, University of Nevada, Reno, Nevada, Report No. CCEER-04-6, August 2004.